VDI Wissensforum

VDI-Berichte 2381

Dritev

21st International VDI Congress
Dritev

October 13 and 14, 2021, Bonn, Germany

7th International VDI Conference
Drivetrain Solutions for Commercial Vehicles

October 13-14, 2021, World Conference Center Bonn (WCCB)

Image credits: ©ZF Friedrichshafen AG

VDI-BERICHTE
Herausgeber:
VDI Wissensforum GmbH

Bibliographische Information der Deutschen Nationalbibliothek
Die Deutsche Nationalbibliothek verzeichnet diese Publikation in der Deutschen Nationalbibliographie; detaillierte bibliographische Daten sind im Internet unter www.dnb.de abrufbar.

Bibliographic information published by the Deutsche Nationalbibliothek (German National Library)
The Deutsche Nationalbibliothek lists this publication in the Deutsche Nationalbibliographie (German National Bibliography); detailed bibliographic data is available via Internet at www.dnb.de.

Der VDI-Bericht, der die Vorträge der Tagung enthält, erscheint als nichtredigierter Manuskriptdruck.
Die einzelnen Beiträge geben die auf persönlichen Erkenntnissen beruhenden Ansichten und Erfahrungen der jeweiligen Vortragenden bzw. Autoren wieder. Printed in Germany.

ISSN 0083-5560
ISBN 978-3-18-092381-9

VDI Wissensforum

VDI-Berichte 2381

21st International VDI Congress

Dritev

Main topics:

- Design of electric drives
- Optimised mechanical components for hybrids and e-drives
- Simulation and AI-supported design in development
- Plenary speeches: Concepts and ideas for the automotive industry on the way to climate-neutral mobility
- Concepts for conventional and electrifi ed drives
- Latest test methods for the validation of components
- Expectations of the younger generations towards mobility

Content

Drive Architecture

Electric Drive

Simulation

E-axles and Electrified AWD

Hybrid Concepts

Dedicated Hybrid Transmission

Actuation Systems

Shifting Elements and Dampers

AI and Multi-Objective Optimization

Testing

Tribological Systems

Construction and Design of Components

VDI Wissensforum

VDI-Berichte 2381

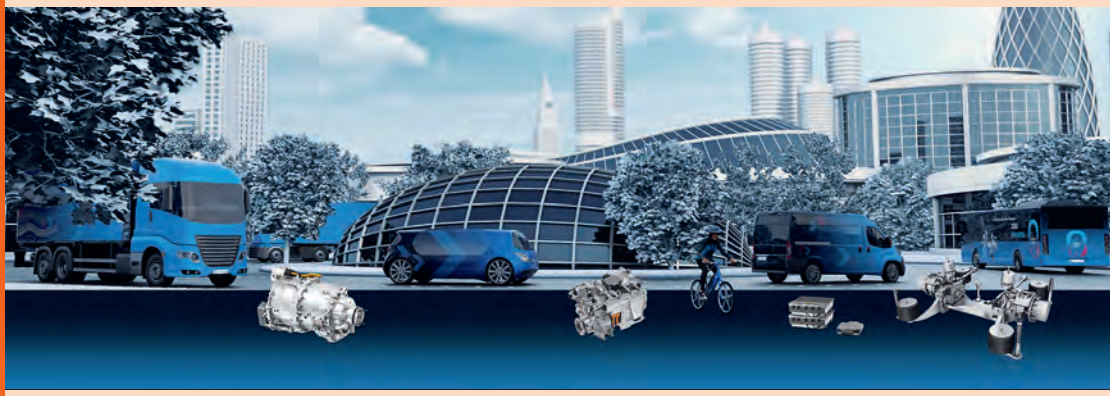

7th International VDI Conference

Drivetrain Solutions for Commercial Vehicles

October 13-14, 2021, World Conference Center Bonn (WCCB)

Image credits: ©ZF Friedrichshafen AG

On the way to zero emission

Future of conventional powertrains

Hybrid powertrain

E-axles

BEV and fuell cell drivetrains

E/E architecture and cyber security

OHNE PROTOTYP GEHT NICHTS IN SERIE.

Unser Podcast ist das Werkzeug, mit dem Sie Ihre Karriere in allen Phasen entwickeln – vom Studium bis zum Chefsessel. Egal, ob Sie Ingenieur*in, Mechatroniker*in oder Wissenschaftler*in sind: Prototyp begleitet Sie. Alle 14 Tage hören Sie die Redaktion von INGENIEUR.de und VDI nachrichten im Gespräch mit prominenten Gästen.

INGENIEUR.de
TECHNIK - KARRIERE - NEWS

PROTOTYP

Karriere-Podcast

JETZT REINHÖREN UND KOSTENFREI ABONNIEREN:
WWW.INGENIEUR.DE/PODCAST

IN KOOPERATION MIT VDI NACHRICHTEN

Many thanks to the Gold-Sponsors of the Congress:

www.castrol.com

www.gknautomotive.com

Sustainable Powertrain Solutions – the new role of the powertrain at Magna

Die veränderte Rolle des Powertrains aus Sicht von Magna

Walter Sackl, Magna Powertrain, Lannach, Austria

Zusammenfassung

Neben der schieren Vielfalt von Varianten elektrifizierter Antriebe sind Antriebsentwickler mit Rahmenbedingungen konfrontiert, die sich jederzeit ändern können. Beispielsweise ist schwer abzusehen, inwieweit und wann die heutige Tank-to-Wheel-Bilanzierung in der EU von CO2 zukünftig durch Well-to-Tank, Produktion oder Recycling ergänzt wird.

Dazu kommen nicht minder herausfordernde technische Trends. Getrieben durch die Digitalisierung unterliegt die Antriebsentwicklung immer kürzeren Entwicklungszyklen. Die Funktionalität verlagert sich in Richtung übergeordneter Software. Dies und die zunehmende Elektrifizierung bewirken, dass die Antriebshardware zunehmend der Systemfunktionalität folgen muss. Schließlich erwarten Autofahrer immer selbstverständlicher vernetzte und personalisierbare Zusatzfunktionen.

Für elektrifizierte Antriebe bedeutet dies einerseits mehr Standardisierung auf Hardwareebene. Es bedeutet andererseits, dass die Antriebe flexibel skalierbar sein müssen, um mit neuen Rahmenbedingungen und Systemmöglichkeiten mitwachsen zu können. Diese Lernfähigkeit wird zukünftig selbst innerhalb des Lebenszyklus einer Fahrzeugplattform erwartet werden.

Der Vortrag zeigt nicht nur, wie ein Portfolio standardisierter elektrifizierter Antriebskomponenten diesen Anforderungen gerecht werden kann. Denn die veränderte Rollenverteilung zwischen Hardware und Software schafft auch große Chancen für Effizienz, Sicherheit, Dynamik sowie neuen Nutzwert und somit mehr Komfort. Das Fahrzeug der Zukunft ist „always new“ und wächst mit volatilen Rahmenbedingungen und neuen Kundenwünschen mit.

Abstract

In addition to the increasing diversification of electrified powertrain solutions, engineers are faced with volatile boundary condition's that might change with little notice: e.g. there is uncertainty how the regulations for tank-to-wheel greenhouse gas targets will incorporate well-to-tank as well as production and recycling in the future.

Driven by digitalization and the fast pace of introducing new technologies, development cycles are reduced. Main functions are increasingly tied to high level software and controls – following system requirements where electrification is an enabler to reflect consumer values and benefits. The end consumer is expecting end-to-end functionality to operate his vehicle according to his needs – connected and individualized.

This means electric powertrains will need to have a high level of hardware standardization, in addition to the ability to be updated, as the availability of data sources, analysis, and functional updates increases during the lifecycle of the product's hardware."

The lecture reflects on how a standardized portfolio of electrified powertrain building blocks is able to support that transition and opens opportunities to improve efficiency, safety, dynamics and convenience, supporting the idea of an "always new" powertrain solution.

Market Forecasts - Reliable vs. Volatile

The powertrain is gaining a new role in passenger cars and light commercial vehicles, driven by a fundamentally changing world. What are these changes? Almost everything– the environment, human needs, and the way the economy works, are all evolving.

This results in new and many changed requirements, which we - as the automotive industry - must take into account.

One main focus is on the environment – the biggest challenge being greenhouse gases. This challenge does indeed require stricter legislative regulation.

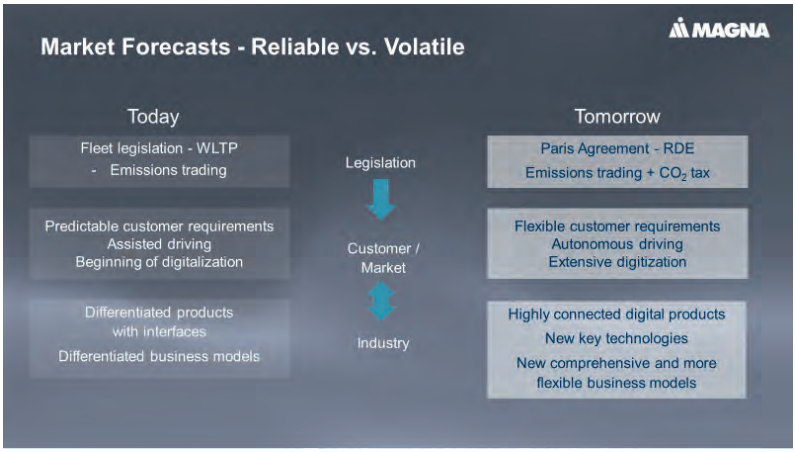

Where the Emissions are Generated

As legislative bodies regulate greenhouse gases, we are faced with a huge impact on, and changes to, global markets and the economy. Many sectors of the industry are severely affected by these changes – and new business models are emerging.

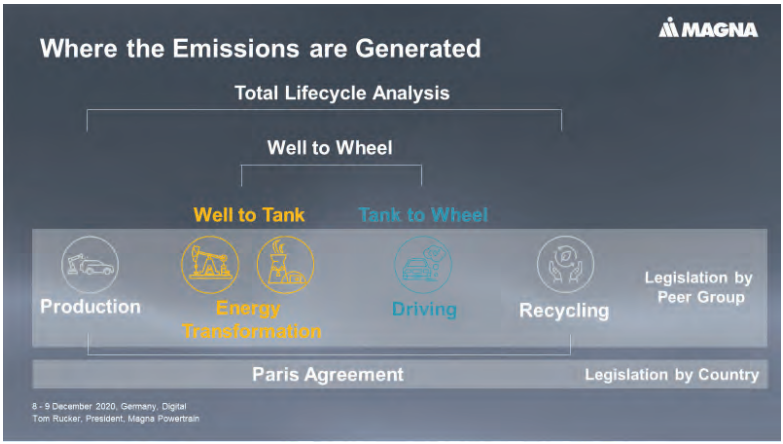

Let´s compare "today“ and "tomorrow“:
Today we are already facing fleet consumption regulations that require a considerable amount of powertrain electrification. Some of these include:
- new and ambitious EU regulations suggesting a green house gas reduction of 55% instead of 40%.
- changes to the emissions trading system, which is planned to be extended to buildings and traffic
- and finally, Real Drive Emission and CO2 taxes are new further measures that drive this development.
- Consumers and the market are responding to new possibilities through digitalization by quickly developing new demands on new products. We expect a clear and rapid trend towards more advanced driver assistance systems (ADAS) and the first steps towards automated driving.
Reacting on this digitalization trend, consumers expect more options for personalized solutions – even after purchase.

- What does that mean for OEMs and their suppliers?
    1.) “self-contained/closed“ products become part of a larger connected product
    2.) digitalization enables new key technologies
    3.) business models may shift from ownership to “usership“

In view of these fundamental changes “no stone will be left unturned“ as we look to the future.

Total Life Cycle Analysis 2020 – 2030
Volatile legislation and the Tank-to-Wheel analysis (?) change the CO2 balance of different powertrain architectures impacting the OEM‘s portfolio.
Consideration of Well-to-Tank changes the assessment criteria of the propulsion system considering the Paris Agreement.
Production and recycling reveal significant CO2 emissions for producing and recycling the architectures which are dominated by electrification. The battery is a significant factor in this consideration.
Today we are limited to a tank-to-wheel assessment – clearly favoring BEVs, but when we include production and recycling using current technology, there is an advantage to shift from BEV to PHEV, primarily due to the CO2 contribution of the battery.

Combining the efforts of electrified propulsion systems and the expected shift towards 100% renewable energy within 30 years, we see a clear carbon footprint advantage of the BEV – within as little as 10 years from now!

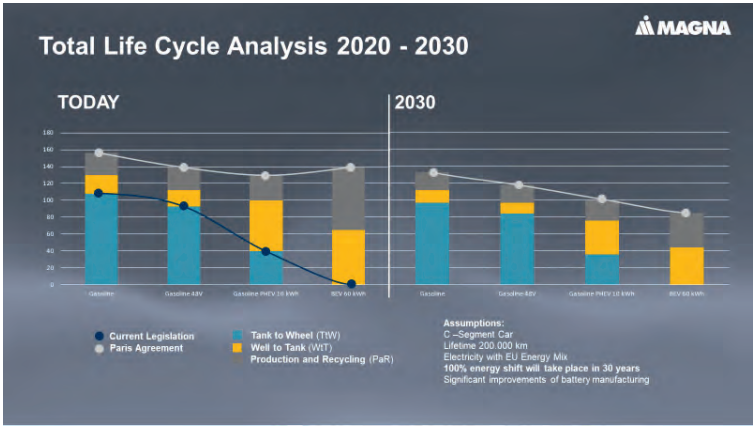

Expected / Unexpected Developments Change the Rules of the Game

However, we are confronted with huge challenges and rapid changes in other areas as well: Today, we can obtain an overview of the expected changes by using fairly accurate models which is difficult enough. However, there are developments, which we simply cannot predict, for example:

The COVID pandemic – changing economic boundary conditions, including a new way of thinking about global supply chains.

Political changes may cause new legislative boundary conditions (CO2 goals etc.)

Changing values of end consumers transferring from ownership to lease.

As we reflect on the increasing dynamics of changing market and consumer demands, the industry must react with more flexibility. In order to safely get through these rapidly changing times we need to have various product and technology paths available.

What the Future Powertrain must Deliver

Which role does the powertrain play – and where must it get better?

1.) **Best-in-Class Efficiency** requires a vehicle to use as little energy as possible within its complete lifecycle. It also means that it should not only be affordable for the consumer to purchase but for daily use too.

2.) **Best-in-Class Safety** stands for a new level of control and active safety through increasingly automated driving and e-mobility.

3.) **Best-in-Class Dynamics** enables a new kind of “fun-to-drive“ without compromising safety.

For example, by electrifying both front and rear axles, we achieve very fast and reproducible controllability of lateral dynamics, as well as better traction and longitudinal dynamics.

When we electrify, dynamics and safety don´t contradict each other – on the contrary they complement each other!

4.) **Best-in-Class Convenience** simply enables more relaxed driving. This includes not having to worry about when, where and what to re-charge your car with; it includes the simplest control of the vehicle, lowest possible acoustic intrusion of the powertrain, and so on....

The Shift to ‘Intelligent’ Powertrains

Achieving best-in-class standards will require more than just good hardware; we must also shift to "intelligent" powertrains. The future of system intelligence is in the software – as functionality shifts from numerous control units to a centralized system. This goes along with a new system architecture:

First, a High-Level-Approach:

In future vehicles and within their powertrains, a comprehensive system approach is crucial, and vehicle intelligence will increasingly include the ability to communicate with the infrastructure environment.

A new Software Architecture is achieved with the software combining all facets of communication in and outside of the vehicle.

No doubt, the challenge in securing functional domains should not be underestimated.

A new E/E-Architecture will result in a reduction of the number of decentralized control units.

Increasingly, only sensors and actuators remain, which are being controlled by a central, learning and communicating intelligence.

Finally, a modular and scalable powertrain approach is needed, which will cover in following slides. In summary we are seeing a fundamental shift from hardware to software.

Intelligent and Connected Powertrain

As we have seen there are a lot of new, challenging requirements. However – and fortunately – there are many new opportunities. Currently we see that Car-2-X and drive electrification profit from each other. Here are some examples of how new technologies allow for further improvements to efficiency, safety/dynamics and comfort:

ADAS increasingly relies on data from Car-2-Car, Car-2-Infrastructure, and from the cloud, making the vehicle act predictively. Traffic-optimized routing has become common already – and we are used to Google telling us that there is congestion one kilometer ahead.

Today, we already have automatically optimized operation strategies. They will be standard quite soon and make electrified drives even more efficient. Another function to quickly emerge is the predictive use of charging and fueling infrastructures, intelligent parking space searches or combining different mobility systems within metropolitan areas.

Connecting vehicle sensors and connectivity enables improved traffic flow. It may start with automated platooning or just provide driving recommendations to the driver.

Further benefit is possible through Over-The-Air functions, when sharing data with the OEMs or a repair shop. Troubleshooting and avoiding malfunctions will be much easier.

Data from the “field“ improves product quality, reliability and operation strategies via persistent optimization loops.

Software functionality will enable vehicles to learn and improve during its lifecycle. The owner will be able to functionally update his or her car and always keep it up-to-date.

Changing Role of the Powertrain

The more software dominates the function, the more it makes sense to define corresponding hardware building blocks. The building blocks we define are interchangeable and scalable where functionality or performance requires. The red building blocks represent Magna‘s “traditional“ products. They were developed based on the success we´ve had, and by exploiting our knowledge and experience with a large variety of drive systems. We basically pursued the exact same strategy to access new e-mobility fields by still using our traditional building blocks – and adding the blue blocks to develop electrified products and systems for 48V and High Voltage applications.

These 3 blue building blocks are the core elements of electrification and allow for a wide range of scalable power and functionality.

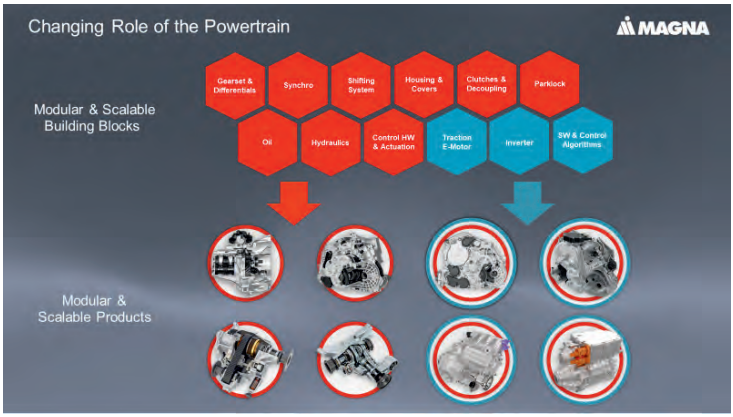

Requirements for Interchangeable Functional Modules

Using our scalable building blocks, we are able to assemble products that achieve best-in-class standards while also tackling the diverse spectrum of global requirements.

Our DHD Eco for example, is a cost-efficient Dedicated Hybrid Drive with boost capability up to 300 Nm and 120 kW peak power. Furthermore, the DHD Plus is a Dedicated Hybrid Drive featuring electric powershift and boost capacity up to 500 Nm, with Best-in-Class efficiency.

Another example is the combination of our eDS HV mid+ and eDS HV mid+ TV with proven Best-in-Class dynamics.

Both together - the DHD Plus and eDS HV mid+ produce Best-in-Class drivability.

Based on the building blocks, various powertrains/drivetrains can be scaled with a manageable effort., and functionality and performance will be increasingly scaled by the e-machines and power electronics. (and software??)

What´s more, new functions can be implemented quite short-term in existing vehicle platforms, be it more power, additional AWD capacities etc.

This addresses the new dynamics of rapidly changing customer requirements mentioned earlier.

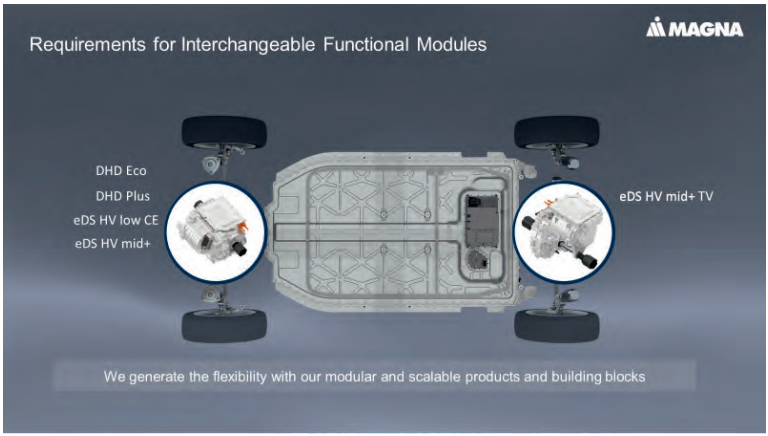

Summary and Conclusion: The Changing Role of the Powertrain

So what are we seeing on our journey to 2030 and beyond?

An always-new vehicle (where the vehicles function will always be "new") based on a scalable electrified kit of powertrain and drivetrain components, where functionality shifts towards software, which enables functional "renewal" during platform lifecycle at any time.

New customer values with the connected powertrain and 35% operating cost reduction and corresponding efficiency improvements: From fossil fuels to electrified powertrains and from Selling Components to Selling Functions.

The business transformation from a focus on efficient drives to management of energy consumption in all driving functions is the way to go for the Powertrain of the next decade.

Modular transmission systems for future BEV platform applications

René Kockisch, Dr. **Jörg Müller**, **Erik Schneider**, IAV GmbH

Zusammenfassung

Um die Emissionsziele für 2030+ zu erreichen, wird die Marktnachfrage nach reinen Elektrofahrzeugflotten kontinuierlich steigen müssen und damit ein wichtiger Bestandteil zukünftiger Antriebsstränge sein. Die systematische Generierung und Optimierung auf Flottenebene zur Entwicklung von Plattformlösungen ist das Hauptziel der hier beschriebenen Entwicklung. Darüber hinaus werden für jeden Teil des Antriebsstrangs untereinander kompatible Subplattformsysteme entwickelt. Die hier im Detail betrachtete Getriebeteilplattform wird mit ihren Technologien, Zusatzsystemen und Modulen, welche zur Abdeckung einer gesamten Fahrzeugflotte mit einem Minimum an Systembestandteilen erforderlich sind, dargestellt.

Abstract

In order to achieve emission targets for 2030+, the market demand for pure electrical vehicle fleets will increase continuously and will be an important part of future powertrains. The systematic generation and optimization on the fleet level to develop platform solutions is the main objective of the development described here. Furthermore, sub-platform systems, which are compatible across each other for every part of the powertrain, will be developed. The transmission sub-platform considered here in detail is shown with its technologies, additional systems and modules, which are required to cover an entire vehicle fleet with a minimum of system components.

1. INTRODUCTION

The Responsibility for sustainable mobility and visions like the green deal pushing the market to a circular economy. This pretension is translated in automotive fleet targets for 2030+ in terms of emissions, performance, comfort, weight and costs, vehicle manufacturer are looking for their optimal powertrain configuration for a certain vehicle fleet with high modularity and

efficiency, low costs and superior performance. An advantageous scalability and highly integrated components are required as well. Changing boundaries for products like a lower environmental impact open the field of ECO-Design for all components starting with a special material selection and an enormous grade of disassembly.

Over the past years, IAV has introduced tool chains and their applications that can be used to represent the modular systems of an entire vehicle fleet consisting of conventional, hybrid and all-electric powertrains. With lower levels of emission targets for 2030+, the market demand for pure electrical vehicle fleets will increase continuously and will be an important part of future powertrains. How the share will be depends on many effects like Legislation, infrastructure for charging, possible incentives and of course on the source of electricity. These are all factors, we cannot influence from the development point of view. What we are able to control are issues like driving range, performance, comfort aspects, etc. (Fig. 1).

Fig. 1: Overview e-mobility changes

As response to this demand, IAV generated a modular, pure electrical powertrain platform to cover vehicles from A-Class up to D-Class SUV. The paper will show the definition of requirements for a representative vehicle fleet. Using the IAV Powertrain Synthesis methodology to generate the powertrain properties for the battery, power electronics, the electric machine and the transmission to achieve the elected vehicle performance targets with simultaneous high grade of modularity and low costs.

2. SYSTEMATIC CONCEPT DEVELOPMENT

Optimizing these powertrain components, topologies and functions requires a development process on the system level for powertrain and vehicles, as well as a long-term product strategy for the whole vehicle fleet. IAV offers unique methods and tools for proceeding systematically the whole development process, from the end user requirement through to the system release recommendation.

The systematic process (Fig. 2) starts by recording all the requirements made by the end user, legislation, the target markets, the vehicle manufacturer, suppliers and energy providers. IAV then uses mobility synthesis to describe the influence of market and environmental conditions on the user behavior, thus developing future mobility scenarios that can be described in terms of their technical requirements and customer acceptance. Based on these mobility scenarios, IAV systematically ascertains and optimizes powertrain concepts that are expedient solutions for the specific vehicle and primary energy source in order to achieve carbon-neutral mobility.

Powertrain synthesis systematically collates the large number of all possible powertrain components to obtain powertrain variants that are optimized in terms of cost, efficiency and driving performance. The main powertrain parameters are defined as the basis for then developing the structures of the respective components, using the proven synthesis methods among others for transmission, electric motor and actuation. The result consists in a powertrain concept with specific individual components. At the same time, the vehicle-specific powertrain variants form the basis for optimization on fleet level. Platform synthesis collates the vehicle-specific optimized powertrain variants in modular systems for systematic minimization of diversity, emissions and costs on fleet level (Fig. 2). This extensive approach thus permits a dedicated and sustainable development of the future mobility.

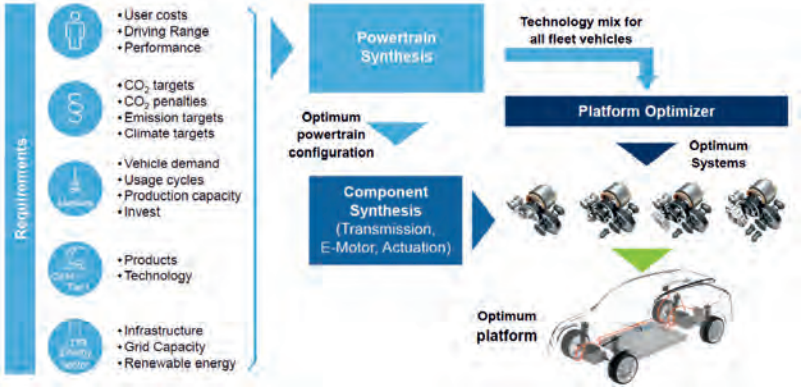

Fig. 2: IAV fleet optimization process

3. BEV FLEET REQUIREMENTS AND POWERTRAIN VARIATION STUDY

As a starting point for the evaluation of a modular powertrain for a complete fleet, the main vehicle segments with its requirements need to be defined. Fig. 3 show the vehicles segments small car (A-class), compact car (C-class), compact SUV (C-SUV-class), mid-size (D-class), full-size SUV (J-class) and light commercial vehicle including their vehicle requirements which are the boundaries for the later powertrain variation study. The focus during the requirement-setting phase was the balancing act between a realistic and of course, pure BEV concentrated fleet without a limitation for the user at the same time. Due to this the vehicles are able to operate at higher velocities or with high acceleration values with peak power, feature a high grade ability and are able to pull a trailer.

Vehicle fleet with common platform		Small car (A)	Compact (C)	Compact SUV	Mid-size car (D)	Full-size SUV (J)	LCV
Vehicle configuration							
Powered axle		FWD	RWD	RWD	RWD / AWD	RWD / AWD	RWD
Estimated curb weight*	[kg]	1200	1500	1700	1700	2200	2500
Vehicle requirements							
Cruising range	[km]	250 – 380	350 – 500	350 – 400	450 – 500	350 – 500	250 – 400
Max. velocity (continuous)	[km/h]	130 – 150	150 – 170	150 – 170	160 – 200	160 – 200	150 – 160
Max. velocity (peak)	[km/h]	160 – 180	160 – 200	170 – 190	180 – 225	180 – 225	–
Acceleration 0-100 km/h (peak)	[s]	8.5 – 14	6 – 10	7 – 9	5 – 9	6 – 10	9 – 11
Gradeability (continuous)	[%]	> 15	> 15	> 15	> 15	> 15	> 15
Gradeability (peak)	[%]	> 25	> 25	> 25	> 25	> 25	> 25
Trailer mass	[kg]	–	1,500	1,500	1,800	2,200	2,500

Fig. 3: Exemplary BEV fleet requirements

For the following powertrain variation study (Fig. 4) the systematic variation of the main powertrain parameters and technologies are performed. The simulation is executed for the vehicle itself with six segments including three different powertrain topologies (FWD, RWD and AWD) for each vehicle. The transmissions are simulated with one and two speeds up to an spread of two and a maximum ratio of 14 based on common packages. A feature for two speeds is the zero drag loss for the second gear justified to a normally closed second gear while dog clutch of the first gear is open without drag losses. The variation for the electric machine is based on generated characteristic maps with a variation of power, torque, speed and air gap diameters for different kind of electric machines like a synchronous or induction machine. In combination with the inverter, the number of phases is another parameter for the simulation. Furthermore,

the chip technology of the inverter is variated between SiC-MOSFET and Si-IGBT to investigate also the effect on the drive system itself and of course the input on the fleet. In the end, the drivetrain including the battery is simulated at the 400 V and 800 V level while using vehicle specific battery capacities based on the target cruising range of each vehicle. Fig. 4 summarizes the parameter of the variation study.

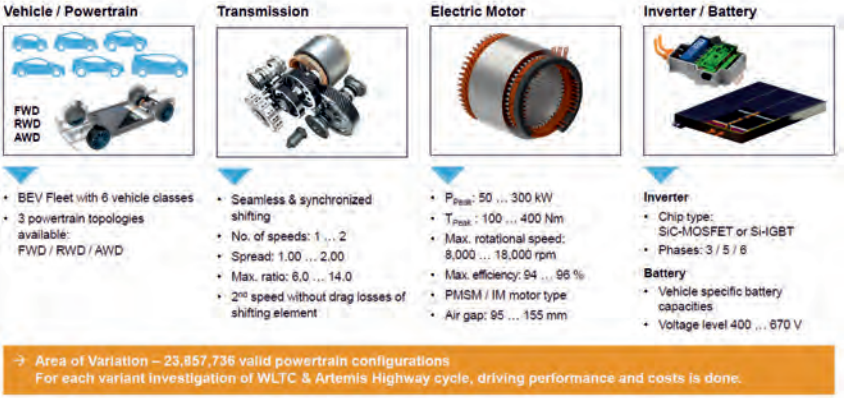

Fig. 4: Variation ranges of powertrain parameters and technologies

By simulating all the possible and of course valid powertrain configurations within the requirements, a huge number of configurations needs to simulate. In our powertrain study round about 24 million valid powertrain configuration have been the result. Each of them investigated with a cycle simulation for WLTP and Artemis cycle, the driving performance values and a cost calculation. Out of these data and an evaluation based on a weighting analysis, a final scenario for the powertrain platform has been selected by targeting minimal costs including battery scaled costs for the whole powertrain. With the selection of a dedicated powertrain configuration for each vehicle segment, the necessary range of the sub-platforms gets more precise. Additional it will be covered by component synthesis simulations for the transmission and the electric machine as well as component development for the inverter and the battery.

5. MODULAR BEV PLATFORM

Fig. 5 shows a basic result of the preferred fleet scenario which is a plain overview coming out of a complex procedure. The tendency is of course entry technology for smaller vehicle segments that are strongly optimized regarding costs and the pure need for function while higher vehicle segments are offering also cost optimized powertrain technology but also offer an option for higher technologies. Considering the entire fleet, we see just 1-speed transmission systems for the small cars (A-class) and from compact cars (C-class) up, we see 1- and 2-speed transmissions due to higher efficiencies at the same or more performance for the vehicles. The result for the electric machine was just focusing on the permanent synchronous machine type with different power and torque level. The induction motor type was not able to play the advantage of costs while fixing the power and torque in combination with the limitation of available package. The inverter was also focusing on one technology, the Si-IGBT, but due to higher efficiencies of SiC-MOSFET chipsets, in some applications that are not only focusing on costs, the possibility of implementation should be existing. The battery and of course the entire platform show the entry voltage level of 400 V, the mid of the segments offer the voltage level of 400 V and 800- V and the upper segments offer the voltage level with 800 V. The battery sizes are defined from 27 kWh up to 115 kWh in five different capacities.

Vehicle fleet with common platform			Small (A)	Compact car (C)	Compact SUV	Mid-size car (D)	Full-size SUV (J)	LCV
Technology range								
Transmission	Number of speeds	[-]	1 speed	1 speed / 2 speed				
E-motor	Peak power	[kW]	100	100		-	220	
	Peak torque	[Nm]	200	200		-	350	
	Type	-	PMSM					
Inverter	Phases	-	3	3 / (5)				
	Chip type	-	Si – IGBT	Si - IGBT / SiC - MOSFET				
Battery	Capacity	[kWh]	27 / 42	42 / 62 / 70	62 / 70	62 / 70	70 / 115	70 / 115
	Voltage level	ca. [V]	400	400 / 670	400 / 670	400 / 670	670	670

Fig. 5: Basic results of a preferred fleet scenario

6. Modular platform for transmissions

The hence development to detail the electric drive unit hardware, especially the transmission, and create a high modular and customizable drive unit is the focus of the sub-platform investigation. The electric drive unit´s modularity is based on different types and size of electric machines as well as a highly integrated power electronics. The transmission platform itself (Fig. 6) is characterized by a 1-speed system and different 2-speed systems, which offer an AMT-, a single-clutch- and a dual-clutch version to provide different prospects of comfort based on the same base layout with a maximum usage of common parts and manufacturing tools for the overall transmission platform.

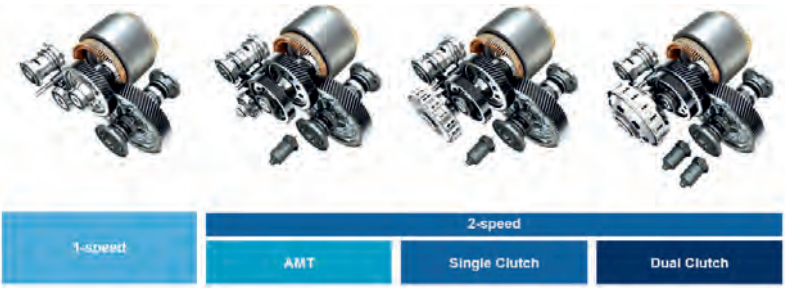

Fig. 6: Modular transmission platform - overview

During the concept phase of the electric drive unit the wide range of technologies, subsystems and components including their later placement has been investigated in detail based on common vehicle packages to suit in average applications. Concerning the transmission concept the center distances, the max outer limits for the gears and interfaces for all different version are defined. Within certain limits, the later ratios could be adapted to adjust the outputs to the demand without changing the basics transmission system. Further, the different coupling technologies of the 2-speed applications (single-clutch and dual-clutch) considered with common parts as well.

Fig. 7: Modular transmission platform - subsystems

The transmission platform also integrates an optional parking-lock module or a gear-and-parking-lock module, which can be combined with every transmission system and uses almost the identical layout and components in every application. In addition the platform allows to combine every transmission with a torque vectoring system or a disconnect system to allow the application in sportive vehicles or hybrids applications. Fig 7 shows the transmission subsystems.

As a summary of the transmission platform, Fig. 8 shows the available transmission system including their technical key parameters – the specification overview. The platform offers a 1-speed with the input torque of 200 Nm and two 2-speed transmissions with 250 Nm and 350 Nm input torque to cover the entire fleet.

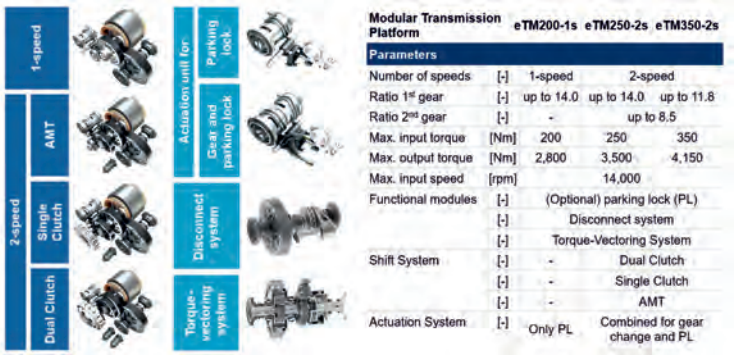

Modular Transmission Platform		eTM200-1s	eTM250-2s	eTM350-2s
Parameters				
Number of speeds	[-]	1-speed	2-speed	
Ratio 1st gear	[-]	up to 14.0	up to 14.0	up to 11.8
Ratio 2nd gear	[-]	-	up to 8.5	
Max. input torque	[Nm]	200	250	350
Max. output torque	[Nm]	2,800	3,500	4,150
Max. input speed	[rpm]	14,000		
Functional modules	[-]	(Optional) parking lock (PL)		
	[-]	Disconnect system		
	[-]	Torque-Vectoring System		
Shift System	[-]	-	Dual Clutch	
	[-]	-	Single Clutch	
	[-]	-	AMT	
Actuation System	[-]	Only PL	Combined for gear change and PL	

Fig. 8: Transmission platform specification overview

The choice for the need of multispeed transmissions, especially the 2-speed systems of our platform, is a multilayer discussion and have been investigated from all perspectives in the past. To show one of these perspectives we are focusing the RWD application for the full-size

SUV (J-class). We created a pure RWD powertrain setting as a low cost version for a SUV and investigated the properties of the powertrain in detail. Fig. 9 shows all valid powertrain configurations for 1- and 2-speed systems for the energy consumption versus powertrain costs and versus the acceleration time as one example parameter. The main message was clear to understand: If battery scaled costs are considered, more efficient powertrains will be promoted and allow spending higher component costs therefore. In our case, this will be possible until very cheap costs for battery capacities are reached. Today's estimations assuming that this will be mid to end of the 2030s.

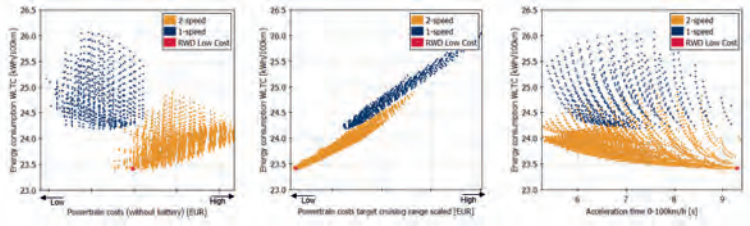

Fig. 9: Spread of 1- and 2-speed configurations for the RWD application of the J-class

The detailed development of the transmission systems focused to overall package, efficiency and costs in combination with different technologies for a wide range of vehicle applications from small A-class vehicles up to heavy light commercial vehicles. Fig. 10 shows our single-clutch transmission system with the gear and parking lock actuation system in detail. The actuation of the power-shift clutch is electro-hydraulic actuated and the gear and parking lock option is electro-mechanic actuated. The cooling and lubrication is realized as a passive system. With 4150 Nm as maximum output torque, the 2-speed system is ready for most of the vehicle applications of our platform.

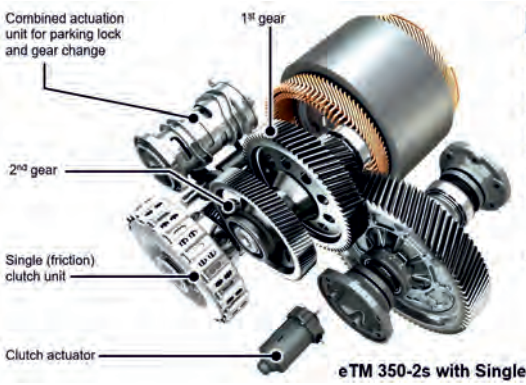

Characteristic EDU properties		
Ratio 1st gear	[-]	11.8
Ratio 2nd gear	[-]	6.1
Max. TM input torque	[Nm]	350
Max. TM output torque	[Nm]	4,150
Max. input speed	[rpm]	14,000
Shift System	[-]	Single clutch with power-upshift
Actuation System	[-]	Combined for gear change and PL

Fig. 10: IAV 2-speed single-clutch transmission design

While offering different technologies, performance level and additional subsystem of the modular platform, the range of powertrain settings allows a wide range from low-cost, to high efficiency up to high performance. Using the example of a full-size SUV (class J) the spread if individual optimized powertrain settings shown in Fig. 11. The different settings allow aligning the powertrain properties like performance, towing capacity, energy consumption and cruising range to the demand of each costumer. The characteristics of the transmission like number of gears and especially the different ratios show a small needed and realizable variation to cover the different settings while using as less as possible number of variations.

Full Size SUV		Low Cost		AWD – Low Cost		High Efficiency		High Performance	
Axle	-	FWD	RWD	FWD	RWD	FWD	RWD	FWD	RWD
EM torque (peak) (front/rear)	[Nm]	-	350	200	200	200	350	350	350
EM power (peak) (front/rear)	[kW]	-	150	100	130	100	150	150	150
EM type / Number of phases	-	PMSM / 3		PMSM / 3		PMSM / 3		PMSM / 3	
Number of speeds (front/rear)	-	-	2	1	1	1	2	1	2
Ratio 1st (front/rear)	-	-	11.5	14.0	10.25	4.5	11.5	11.5	11.5
Ratio 2nd (front/rear)	-	-	5.75	-	-	-	5.75	-	5.75
Power electronics chip	-	Si - IGBT		Si - IGBT		SiC - MOSFET		Si - IGBT	
Battery capacity	[kWh]	115		115		115		115	
Towing capacity (continuous, gradeability > 12%)	[kg]	1,840		2,260		2,270		6,160	
	[lbs]	4,050		4,990		5,000		13,580	
Max. velocity (continuous)	[kph]	160		151		180		182	
	[mph]	99		94		112		113	
Acceleration time 0-60 mph (Acceleration time 0-100 kph)	[s]	9.30		7.01		7.07		4.78	
Energy consumption WLTP	[kWh/100km]	23.42		25.20		23.10		25.11	
	[mi/kWh]	2.65		2.47		2.69		2.47	
Δ powertrain costs incl. battery	[€] [US-$]	Reference		+2,020 +2,224		+1,645 +1,974		+2,510 +3,012	

Fig. 11: Spread of individual optimized powertrain settings for a Full-Size SUV

7. CONCLUSION

The future electric powertrain is characterized by dedicated powertrains for each vehicle but fleet optimized as a platform due to cost optimization and reduced number of systems. Therefore, the IAV fleet synthesis and optimization tools can be used to allocate the overall powertrain system as well as the subsystems with its characteristics. The results of the variation study and the connected development processes show an exemplary powertrain platform including the definitions and a first design for the transmission, the electric machine, the inverter and the battery, each with their own subsystem platform to cover the entire vehicle fleet.

Our advanced development process with a detailed analyzation and optimization process at the beginning of the powertrain definition permitted a limitation of the transmission subsystems to only three base versions to cover the entire vehicle fleet from small segments up to light commercial vehicles. A 1-speed with 200 Nm and two 2-speed transmissions with 250 Nm and 350 Nm input torque have been the result. All transmission derivate are based on a modular architecture with a maximum of common parts, shared manufacturing tools and assembling lines to achieve the best scaling effect. The multispeed transmissions offer optionally a single-clutch or dual-clutch architecture due to aspects of comfort. With additional add-on systems like a parking-lock-, gear-shift-, disconnect- or torque-vectoring-module, the drive unit can be equipped to the needs of each application without changes on the base structure. With this approach, IAV generated a flexible and saleable transmission subsystem platform.

Analysis of propulsion system architectures across vehicle segments and markets

John Shutty, BorgWarner Inc, Auburn Hills, Michigan, USA;
Alexander Moser, BorgWarner Drivetrain Engineering GmbH, Ketsch;
Daniel Gajowski,
BorgWarner Drivetrain Engineering GmbH, Ludwigsburg

Abstract

Tightening GHG and emissions legislation along with the constant drive for improved performance and energy efficiency has significantly increased requirements for vehicle propulsion systems. These demands have driven OEMs to pursue a variety of solutions for their different applications including advanced combustion, FCEV, electrified boosting, hybrid, plug-in, and full battery electric systems. Within each of these larger categories are multiple configuration options. These include voltage level (48V, 400V, 800V), eMotor position (P0, P1, P2, P3, P4, PS, RWD/AWD EV), multi-motor solutions (dual axle, P0/P3, DHT, AWD EV), eTurbo™, eBooster® electrically driven compressor, variations in battery size and type, power electronics (Si, SiC), transmissions (single speed, multi-speed) and other major subsystems (Thermal, HVAC, motor type).

To study this wide field of possibility and answer the types of questions listed later in Table 1, tools are required to understand the trade-offs and performance of the various combinations in different vehicle segments and markets, and to create customer solutions that are optimized for those applications.

One such tool is a state of the art simulation framework that BorgWarner has developed which embodies its global experience in all aspects of propulsion system development (eMotors, thermal systems, power electronics, battery systems, control systems, engine components, drivetrain systems, charging systems, and others).

This paper introduces the structure of the modelling environment as well as the organization of the various control elements used to manage it. Results from a recent survey of different propulsion system types are shared as an example. Drive cycle results showing the efficiency effects of temperature isolated to individual components are also shown to demonstrate the type of testing possible in this simulation environment which is impossible to do on actual hardware.

1. Introduction

Systems analysis through the aid of computer simulation has been ongoing in the automotive industry for decades. Like other areas of development, the requirements placed on simulation engineers have been changing, and continually increasing. Factors contributing to this include:

- Greater dependency on simulation (vs. physical prototypes and testing)
- Faster development cycles
- Tighter tolerances driving the need for increased fidelity
- Higher level of interactions between major sub-systems
- Evolution of the propulsion system from internal combustion to EV

In response to these drivers, the simulation tools from CAE suppliers used to support this activity have continued to improve and expand [1], [2]. At BorgWarner, we have taken advantage of these advanced tools, but we recognized that to continue developing optimized components and systems for our customers, we also needed to evolve the way in which these simulation tools are used. In response, we created a development environment which we refer to as the xEV Propulsion Simulation Framework.

2. Challenges targeted

There are several challenges we have worked to address with our xEV Framework. Some are new and driven by recent industry developments. Other challenges are not new but are intensified by these changes.

- Valid but inconsistent results between models
    - different assumptions
    - different levels of detail
- Intermittent simulation activity
    - Hard to justify significant automation
    - Re-use is not automatic
    - Difficult maintaining critical mass of people
- Controls are more important and more complicated
- Connections to key organizations hard to maintain
- Having physical hardware for model correlation is less common

3. Response and xEV Propulsion Simulation Framework overview

Figure 1 shows an overview of the xEV Framework that we have built up at BorgWarner to address the challenges listed above. While all issues are not eliminated, this capability has allowed us to provide faster, consistent, higher fidelity results than we have been able to in the past. It is used throughout our organization to support the design and optimization of components and systems.

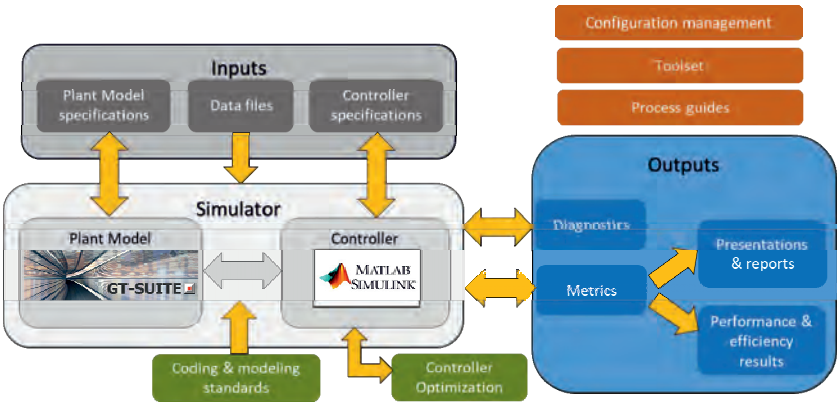

Fig. 1: xEV Propulsion Simulation Framework

The first thing to note about the figure is that while the plant model is at the center, it is only one part of a much bigger overall system. In many cases, the advantages gained with the xEV Framework are the results of these other elements.

Simulator

Plant Model: Primarily developed using Gamma Technologies suite of simulation tools. The model is structured in a modular fashion so that different combinations of components can be configured to represent various propulsion architectures. This modularity greatly reduces duplication and maintenance. Clean and consistent interfaces and data structures are developed to enable this

Controller: Developed in Mathworks' Simulink® environment. Simulink provides advanced control blocks which are utilized for controlling complex propulsion architectures. By using Simulink, the controls used in the simulation environment can also be transferred directly to electronic control units for real-time control of physical systems (e.g. vehicles). The controller is model based and capable of controlling any configured plant model.

Inputs

Specifications: While the development of formal specifications is a standard operating procedure for production software (e.g. embedded controls), it has not been as common for simulation activity. However, because our xEV Framework is a more permanent asset, it is necessary that it be documented and understood by a larger, growing and changing group of people. Coding / modelling standards are also in place to allow ease of integration and common understanding. Process guides are used to generate consistent results and to allow new engineers to quickly come up to speed. They also specify a workflow which includes design reviews, testing and approval of major changes.

Data files: Standard formats for the critical data that populates the various component models have been developed and a database of these files has been created. The data is used by the plant model and, in most cases the model based controller. While this sharing allows the controller to be a little smarter about the system that it is controlling than it would in the real world (since the exact same data is used in the plant model), it does enable the controller to be used without modification on various vehicle configuration models. In addition, most of the simulation activity is carried out to understand and optimize different propulsion hardware configurations. In this case it is desirable that the controller performs in a consistent optimized fashion to avoid penalizing one hardware configuration because of controller performance differences. By having the controller use actual model data, this consistent optimized performance objective is more feasible to achieve.

An example data file is an electric motor loss map:

Power loss = f(speed, torque, voltage, temperatures)

Outputs

Measures, metrics, reports:

The primary goal of simulation is the measured results. For system simulation the results can be quite extensive and involve hundreds of variables – for example: efficiencies, energy, power, temperature, SOC, time in various modes, losses, speed, torque. In order to reduce the time required to compile all of this information we have developed tools which automatically take the raw data and create a clear, consistent, comprehensive report containing tables, plots, graphs and diagrams which provide the insight necessary to make intelligent decisions about the design and application of our products. Examples from these reports can be seen in Section 5.

Diagnostics

When running a vehicle drive cycle model, a necessary step is making sure the simulation ran successfully. Some errors are obvious, but many potential problems are difficult to see and require an expert to do a careful examination of the signals. To address this, a set of diagnostics was developed which automatically runs at the end of each simulated drive cycle and checks for a host of potential problems. Examples include battery SOC limits, shift times, torque split times, excessive vehicle jerk, speed errors, torque mismatch and others. While the diagnostics cannot anticipate every error that may occur, it can catch the majority and free up the engineers to focus on the interpretation of the results. An example page from the diagnostics output is given in Figure 2.

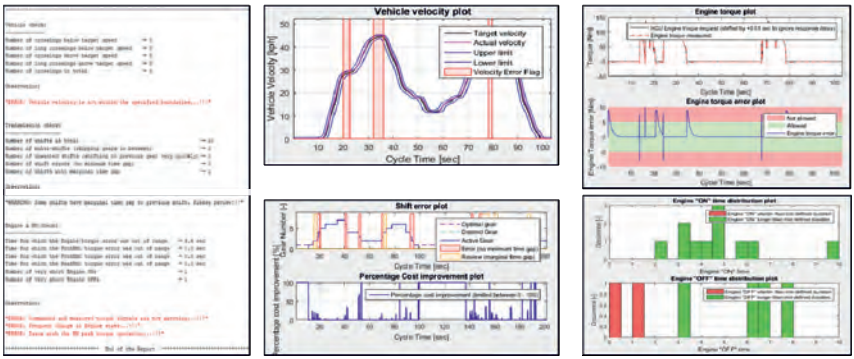

Fig. 2: Portion of diagnostics output

Other

Controller and design optimization: The controller is model based and so most of its parameters are automatically adjusted when the data for a new configuration is populated into the model. However, there are several parameters that require tuning to achieve optimal performance. To accomplish this step, 100's to 1000's of drive cycles are performed while varying the control parameters. Optimization methods are used, such as genetic algorithms, to allow quicker convergence to the most energy efficient settings. This same approach is used to optimize various parameters for the modelled physical components in order to support component design work. Examples include varying eMotor design choices, gear ratios and power electronics control strategies.

Toolset: Along with the commercial tools from Gamma and Mathworks, several custom tools have been developed to accelerate development and improve the quality of results. One example is a vehicle design tool which allows an engineer to specify vehicle requirements

(e.g. top speed, gradeability, range, etc.) and determine which propulsion related components can be used to meet these specifications (e.g. battery size, engine, gear ratio, eMotor, etc.). Another is an off-line optimizer which determines optimal speed / torque points for a series hybrid configuration. A final example is a battery pack design tool which takes the output of the vehicle design and creates a battery pack based on the propulsion components, vehicle requirements and battery cell models.

Configuration Management: Because many engineers contribute to and utilize the xEV environment, it is necessary that a comprehensive configuration management system be used to control all elements. This includes plant model files, controller source code, data files, scripts, spreadsheets, templates, macros, and other critical items that are part of the system.

4. Development philosophy

Whenever an organization becomes involved in simulation the question as to the width and depth of the models is an important one. That is, how many aspects of the system are included (e.g. combustion, HVAC, cornering and other drive dynamics, etc.) and to what extent each is modelled (e.g. efficiency multiplier or speed and torque-based map or detailed electro-magnetics). The choices are not only affected by what questions the system is beind asked to answer, but by what level of complexity can be reasonably managed, what level of supporting data is available to populate the models, and finally, compute power and execution time limits. Our current strategy is shown in Figure 3.

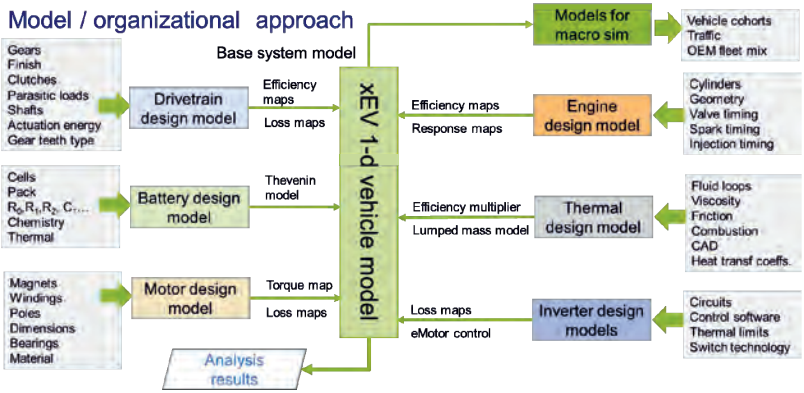

Fig. 3: Model / organizational approach

For most of the major components, loss maps are used within the model. These maps come from component testing as well as more complex mechanical, electrical, magnetic, and chemical models of the components. An example was given in Section 2, where electric motor loss maps can be based on up to 4 variables.

Through the modularity built into the system it is also possible to reduce the number of independent variables used to calculate losses when the question being investigated does not require that axis and/or that data is not available (e.g., temperature of some components is held constant for many studies; where those effects are not important to the result). In a similar way, a more complex model can replace a simple map based model. An example is the use of a full 1-d engine model with flow, temperature, combustion all captured, to replace a map based fuel flow map.

Figure 3 does a very good job of describing the model philosophy, but it is also an accurate representation of the organizational design approach. The outside boxes can be seen as the groups responsible for the development of the individual components. The engineers in these groups understand the design, testing and operation and create detailed models of their component. Their expertise and the output of their work is then encapsulated into system level models within the xEV Framework. In this way the collective system level knowledge of the company is captured in a format (a system simulation) that can be exercised to answer key questions from the organization.

4. Results

The xEV Framework has been used at BorgWarner to support a variety of investigation types. These include:

Table 1: xEV Propulsion Simulation Framework investigation types and examples

Objective	Examples
Corporate level strategic questions	How do different propulsion architectures compare in terms of performance, efficiency, and cost? How is this influenced by vehicle segment/class and market?
Business unit strategic questions	When isolating thermal effects, which components have the biggest impact on drive cycle efficiency?
Customer support and design optimization	What are the performance, efficiency and cost trade-offs associated with various IDM (integrated drive module) configurations (lubrication, PE technology, thermal management) for a customer application?

Although testing of vehicles with actual hardware would theoretically provide the most reliable results to answer some of these questions, in practice it is usually not feasible. Besides the issues with testing uncertainty, the potential costs can exceed yearly budgets and the associated time scales can be orders of magnitude longer than what the program allows. In addition to these barriers, some investigations are simply not possible with physical hardware and can only be carried out in simulation.

Thermal

A case in point is the example in row two from the above table. It was desirable to understand how individual component temperatures affect an EV's overall drive cycle efficiency. This question cannot be answered by testing a vehicle. It is not possible to hold an active component (such as an eMotor) temperature constant during a drive cycle. And it is impossible to even consider holding all other components at some nominal temperature (e.g. 20 C) while the target component temperature is at some more extreme value (eMotor @ 140 C).

However, using simulation this is a trivial exercise and is something we have done for a mid-sized SUV with an electric propulsion system. The drive cycle was run while holding components to fixed temperatures. Some of the results are shared in Figures 4 and 5.

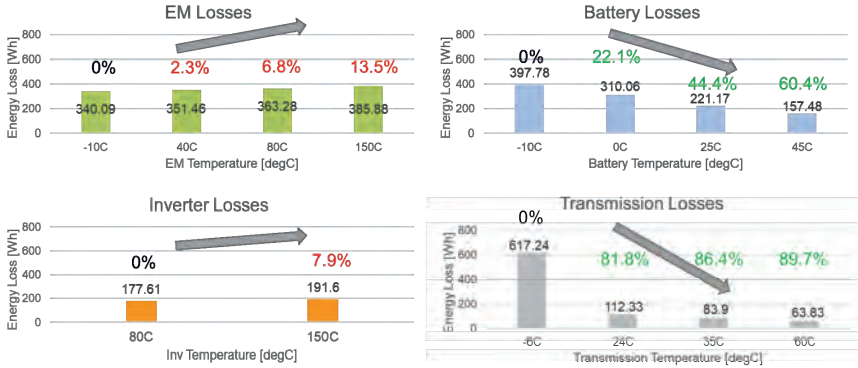

Note: Temperature ranges not the same for all components

Fig. 4: Thermal impact WLTC - individual component losses

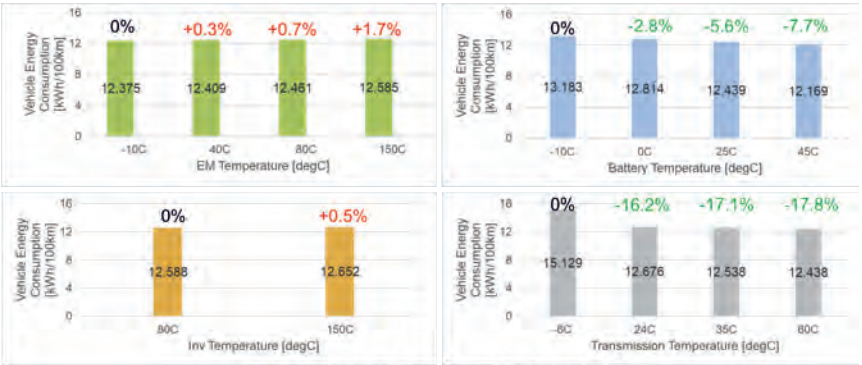

Note: Temperature ranges are not same for all components

Fig. 5: Thermal impact WLTC - vehicle energy consumption

As can be seen from Figure 4, the impact on the losses of each component due to temperature changes is significant and ranges from 8% on the power electronics to 90% on the transmission. In Figure 5 the percent net impact to the drive cycle energy is much less. For instance, the temperature-based changes in efficiency in the power electronics only impacts the total drive cycle energy by 0.5%. For high voltage SiC based PE, this effect is even smaller.

Of course, engineers working on BEV systems need to consider many other thermal effects beyond efficiency (e.g., component degradation, power limits, HVAC, etc.) and our xEV tool is used to understand these as well.

Battery Electric Commercial Vehicles

In another study we conducted, Class 8 trucks (~40 metric tons) with different electric propulsion system architectures were analyzed. Two of the configurations studied are shown below in Figure 6.

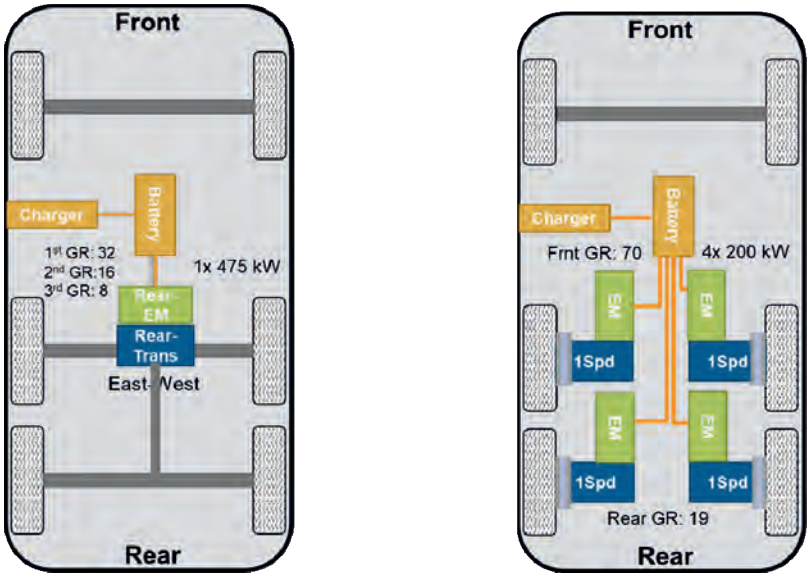

Fig. 6: CV propulsion configurations

The configurations shown represent 2 boundary case design approaches for this type of vehicle. For the single speed transmission case, it was necessary to use 4 of the selected motors to have sufficient torque for low speed hill climbing maneuvers and still have a low enough gear ratio to meet top speed requirements. For the other configuration, a larger single motor combined with the 3 speed transmission was able to meet the vehicle requirements.

A breakdown of energy losses over the World Harmonized Vehicle Cycle (WHVC) is shown in Figure 7. These plots are one page of the report that is automatically generated from the

results of drive cycle simulations. Four configurations can be combined into a single report to allow relative comparisons between different vehicles, propulsion architectures and/or component selections.

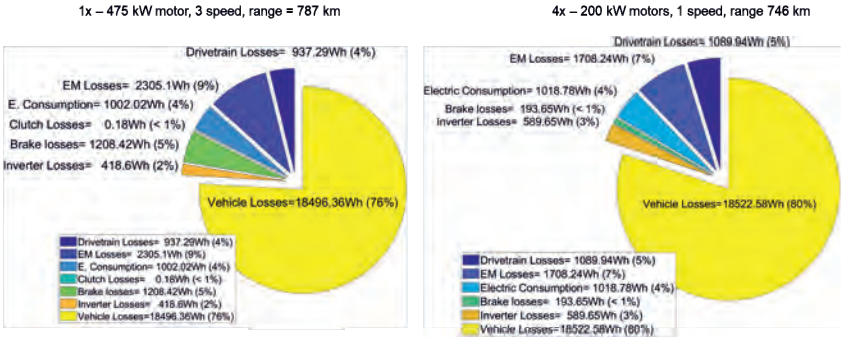

Fig. 7: Energy losses over the WHVC

With these configurations, the 3 speed vehicle has higher drivetrain losses but the reduced motor loss and increased regeneration efficiency more than compensates and the result is increased range over the 4 motor configuration.

6. Conclusions

In today's environment, to successfully develop world class propulsion system products, it is necessary to have a world class simulation and analysis capability. To do this requires more than only focusing on getting the equations correct. Standards, workflows, configuration management, component databases, advanced controls, optimization, automation, data visualization, and connections to key organizations and individuals are all necessary for a propulsion systems global product leader to be successful.

References

[1] Emerging Powertrain Technologies and Future Challenges & Opportunities for Simulation, Professor Federico Millo, Politecnico di Torino, 2019 GT EU Users Conference

[2] A Virtual Journey Home Through Time, Mike Anderson, General Motors, 2020 GT Global Users Conference

Glossary

AWD:	All Wheel Drive
BEV:	Battery Electric Vehicle
CAE:	Computer Aided Engineering
CV:	Commercial Vehicle
DHT:	Dedicated Hybrid Transmission
EM:	Electric Motor
EV:	Electric Vehicle
FCEV:	Fuel Cell Electric Vehicle
GHG:	Green House Gas
GR:	Gear Ratio
HVAC:	Heating, Ventilation and Air Conditioning
IDM:	Integrated Drive Module
km:	Kilometers
kW:	Kilowatt
kWh:	Kilowatt-Hours
OEM:	Original Equipment Manufacturer
PE:	Power Electronics
PS:	Powersplit
RWD:	Rear Wheel Drive
Si:	Silicon
SiC	Silicon Carbide
SOC:	State of Charge (of a battery)
SUV:	Sports Utility Vehicle
Wh:	Watt-Hours
WHVC:	World Harmonized Vehicle Cycle
WLTC:	Worldwide Harmonized Light Vehicles Test Cycle

BorgWarner P2 Modules – from HV to 48V

A Modular Kit for P2 Architectures – full coverage of all applications (PHEV HEV and MHEV)

Dipl.-Ing. (TH) **Martin Dilzer**,
BorgWarner Drivetrain Engineering GmbH, Ketsch

Abstract

P2 hybrid architectures are well established solutions to achieve CO_2 targets at reasonable costs. BorgWarner's innovative and high performing P2 Modules for PHEV applications are successfully in the market. Nevertheless, there is increasing high pressure on cost and strong competition with various alternative solutions. 48V Technologies are showing considerable increase in performance and are getting more and more attention since they offer attractive fuel efficiencies at comparably low efforts.

Therefore BorgWarner is extending its P2 module family portfolio to cover and account for 48V applications. The approach is not just simply to replace the HV e-motor with 48V active parts but to rethink the corresponding functionality and extend scope of supply.

This article will highlight how BorgWarner's new 48V P2 Module combines synergies with existing HV Solutions and consequently covers accompanying potential streamlining due to adapted requirements and ongoing evolution.

Zusammenfassung

Unter den vielfältigen Hybrid Varianten haben sich P2 Architekturen einen breiten Anwendungsraum erschlossen. Insbesondere das hervorragende Kosten-Nutzen Verhältnis ist hierbei mit ausschlaggebend. Mit innovativen und leistungsstarken P2 Modulen für Plugin Hybride konnte sich BorgWarner erfolgreich auf dem Markt etablieren und wird sich auch künftig weitere Marktanteile erschließen. Das Marktumfeld ist jedoch durch einen stetig steigenden Kostendruck und einen starken Wettbewerb mit alternativen Lösungskonzepten geprägt. Aufgrund der mittlerweile realisierbaren hohen Systemleistungen rücken 48V Lösungen zusehends in den Vordergrund. Sie ermöglichen die Darstellung von attraktiven Verbrauchseinsparungen, bei einem vergleichsweise geringem Aufwand bzw. niedrigen

Systemkosten. Folgerichtig entwickelt BorgWarner auch 48V Varianten als Erweiterung des bestehenden Produktportfolios innerhalb der P2 Produktfamilie. Die Herangehensweise beschränkt sich nicht auf die erforderliche Anpassung der Aktivteile des Elektromotors, sondern fokussiert sich auch auf die Grundfunktionen des P2 Moduls.

Dieser Beitrag beleuchtet wie BorgWarner hierbei sowohl die Synergien zu bestehenden HV Lösungen ausnutzt und gleichzeitig eine konsequente Adaption an geänderte Anforderungen und die Implementierung von Optimierungsmaßnahmen umsetzt.

Introduction

The transformation of mobility has gained unexpected dynamics since the begin of 2020. CO_2 legislation boundary conditions and the increased awareness about the required measures to slow down or stop global climatic warming has already put a lot of pressure on the automotive industry. But the way electric mobility demonstrated to be resilient during the Covid-19 crisis intensified this change even further. Today there is little doubt that purely combustion engine driven vehicles will further lose their high market shares and will be pushed back and finally more or less disappear completely.

However there are as well strong arguments about the readiness of required boundary conditions for purely electrical mobility – concerns like charging infrastructure and the availability of sustainable electric power generation. Today both are not yet in place and they will not be in place in the short run.

In total any kind of electrification can be regarded as a vaccine against the threats of dramatic changes in automotive industry.

This is where other technologies like hybrids still gain momentum and enable OEMs to specifically balance their portfolio and control fleet emissions which are strongly dependent on local markets and local legislative boundary conditions.

***BorgWarner* – Positioning for the future**

To account for this change, BorgWarner is continuously reinforcing its leadership within electrified Propulsion Systems – e.g. the recent acquisition and integration of Delphi Technologies and AKASOL AG. This results in a comprehensive and competitive portfolio for electrification technologies and corresponding competencies.

Diversity of HV/EV Architectures

Driven by these disrupting boundary conditions and huge engagement of the automotive industry countless different solutions, with different focus for levels of electrification, have been developed and are available for applications. The following picture illustrates this complexity – although not intending to give the complete picture.

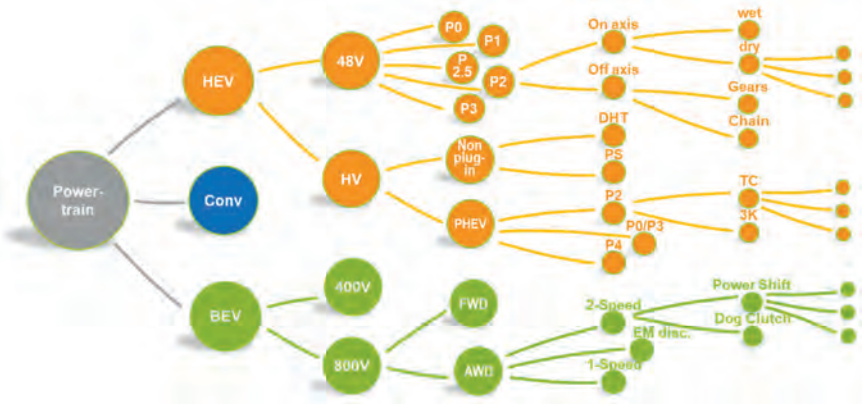

So far there is no consolidation about which and how many of these various opportunities will be the most successful ones in the end. On the contrary, more and more different solutions are showing up and entering the market. One of the most important decisions for the OEMs will be how to spend their available resources in order to cover the market needs and opportunities and how to minimize the corresponding threats. Each OEM will have to carefully pick and balance its solutions to achieve the fleet emission targets, throughout the next 15 years.

P2 Hybrid

This is where P2 Hybrids are very much in focus. Within the branch for the HEV's P2 do and will play a major role. It's the well-known advantages that are providing a solid baseline for supporting adjustable electrification strategies and offering short term availabilities.

Benefits of P2 Hybrid Architectures

- **Scalability** – wide range of applications MHEV to PHEV
- **Performance** – full e-Drive capability with regeneration
- **Flexibility** – high reuse of invested base transmission and engine content
- **Efficiency** – widely adjustable operation points & seamless change thereof
- **High Value** – reasonable integration and application efforts

As illustrated in the following figure BorgWarner has investigated the impacts on costs and efficiency for different P2 electrification levels and compared this with a BEV Reference. The Analysis is shown for a C-Segment vehicle with perspective of a short term SOP in 2024.
The lower section of the chart shows the assumptions about the electrification details like voltage level, peak performance and size of the energy storage system. The bar diagrams on the top do indicate the CO_2 Potential and the specific vehicle on costs to achieve this potential.

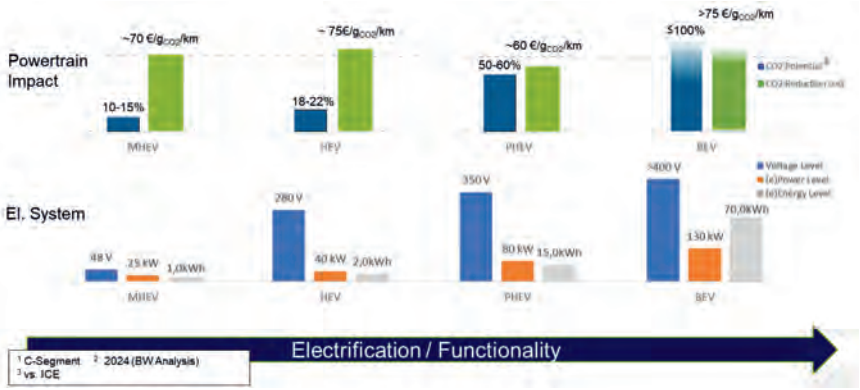

The P2 PHEV gives the best economic value and typically offers up to 60% CO_2 reduction in comparison with combustion Engine. Still with superior specific CO_2 – avoidance cost (in comparison with BEV) of approximately 70€/g_{CO2}/km follows the P2 48V solution.
Due to the strong dependency on the local CO_2 production for electrical power generation PHEV and particularly BEV will potentially not achieve the indicated values in a short term.
In such cases 48V P2 obviously becomes attractive and competitive to achieve targets.

This translates directly to the market analysis as shown in the following figure (IHS/BorgWarner). The 5 years perspective indicates

- strong growth in hybridization (38 Million hybrids in 2026),
- P2 growth nearly doubles the hybrid market growth,
- P2 48V Modules could significantly be part of this growth.

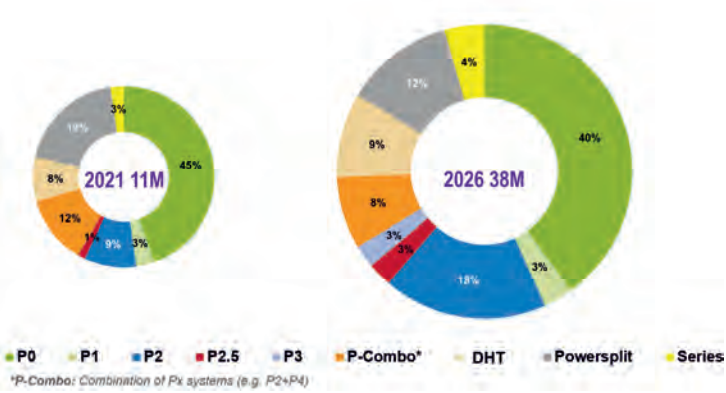

To make this happen it is key to cover for

- very high pressure on cost,
- strong need for continuous improvement of efficiency,
- and the need for short development timelines.

Or in other words: you need to be fast and innovative.

P2 48V Hybrid approach

BorgWarner defined a way to face this promising but as well challenging market environment. The fundamentals are given by the Triple Clutch HV P2 Modules as they are successfully launched to the market in 2021. Taking this and the corresponding experiences made we asked ourselves about how to increase the value for a 48V derivative solution.

The main objectives are the reconsidering of the system functionalities and the customer requirements and to evolutionary improve the system performance. Thus consequently solving the puzzle of “legacy building blocks” and putting them together with the 48V technology specific “new building blocks”.

P2 48V Hybrid Building Blocks – The E-motor

For the highly integrated solutions like P2 Modules the E-Motor plays a dominant role in defining packaging and system performance. Therefore BorgWarner used the proven S-Wind technologies and developed a 48V E-Motor variant accordingly. The key characteristics and performance data are given as shown. The information is based on qualified simulation toolchains.

Description	48V SW270-30mm
DC Bus Voltage	48V
Phase Current – Peak	550Arms
Phase Current – Continuous	400Arms
Power – Peak	>22 kW
Power – Continuous	> 18 kW
Torque – Peak	165 Nm
Torque – Continuous	120 Nm
Efficiency - Peak	94%
Temperature for peak and rated	90°C
Max Operational Speed	7000 rpm
Cooling	Oil, 90°C, 6LPM
BEMF@1000rpm, 25°C	18.5Vrms
ASC Current (Steady State)	< 410Arms @105°C < 470Arms @25°C

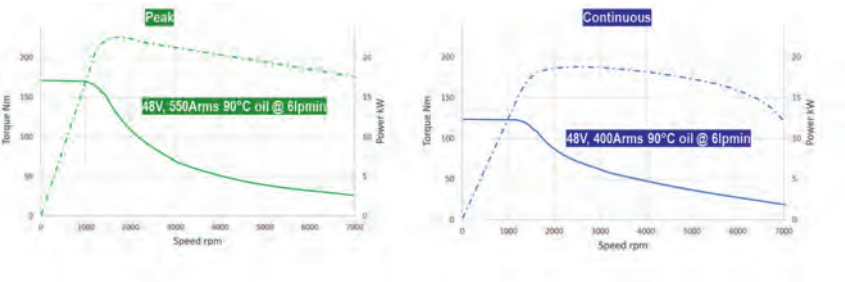

The Stator outer diameter remains with 270mm while an active length of 30mm is defined to fulfill the targets for a peak power beyond 22kW and to achieve sufficient torque characteristics for the different vehicle functionalities. The focus was not only to achieve high peak efficiencies but as well to adjust the sweet operation area to typical speed ranges used in the drive cycles.

Due to the specific load collectives and corresponding low levels of dissipated energy it is possible the reduce complexity and remove the water coolant channel. A carefully balanced oil cooling configuration allows for synergetic cooling of the E-Motor active parts and the embedded clutch system simultaneously.

P2 48V Hybrid Building Blocks – The Inverter

Regarding all the aspects of a combined specification and optimization of the electrical drive system BorgWarner has developed a best fit inverter solution. The precondition to this was to base on and extend the existing 48V Inverter platform. The Inverter includes a 130A DCDC converter to supply the base 14V board net. In current concept status there are both opportunities available “attached or standalone”.

Electrical Specifications	
Operating Voltage Range:	24VDC~54VDC
Inverter Peak AC Current:	550Arms (10 sec.) / 600Arms(1 sec.)
Inverter Cont. AC Current:	350 Arms
DC/DC Cont. 14V Current:	130 amps
Microprocessor:	Infineon TC265
ASIL Rating (Inv./DCDC)	B/B

Mechanical Specifications	
Dimensions (mm):	270 x 158 x 104
Mass (kg):	<4
Mounting Environment:	Motor bolted / Under hood
Thermal System: Coolant Coolant Temperature Flow rate	 50%glycol -40 to 65°C Max. 8 L/min Max.
Operating Ambient Temp.:	-40°C to 105°C
48V Voltage Connections:	Pluggable DC/Bolted AC

Software Specifications				
ASIL Level (Inv./DCDC)	B/B		BSW	ETAS
AutoSAR (ETAS)	4.0.3		APP SW (HCU)	BorgWarner
ASPICE Level	N/A		MCAL	BorgWarner
Cybersecurity	N/A		APP SW	BorgWarner

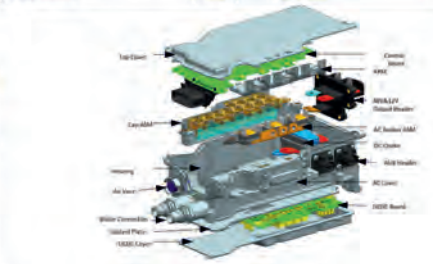

Along with the generic HW go the advantages due to application of mature SW and Control algorithms.

P2 48V Hybrid Building Blocks – The PES (Permanently Engaged Starter)

48V systems with its general idea of small and cost efficient electrical system tend to provide only borderline performance. This limits the availability and fuel efficiency impact of the mild hybrid solutions. As known, the need to reserve restart torque for combustion cranking practically is a major drawback for providing at least a minimum electrical driving feature. While accounting for this by using a belt alternator starter adds a lot of cost to the driveline. Alternatively, it is possible to realize cranking via a highly integrated permanently engaged starter. This offers direct cost potential by replacing the BAS and indirectly offering potential

for further cost down and fuel efficiency improvements by fully removing the complete belt drive. For a detailed insight there is a specific BorgWarner conference contribution about the PES by T. Kaufhold.

P2 48V Hybrid Building Blocks – The Integration

Finally, there are many further aspects and integration details that need to be identified as opportunities and subject for optimization. This is where a systematic approach and vehicle/driveline level comprehension enable for enhanced value. In the following paragraphs some of these points are listed and highlighted.

Advanced Sensor Technologies – the rotor position Sensor is very much in focus due to the comparably high impact on cost and on efficiency. Therefore the replacement of the resolver with an inductive sensor has been developed and integrated into the P2 48V Module. At unrelieved performance the new sensor offers high robustness against EMC impacts and allows for reduced axial packaging.

Cooling Configuration – based on extensive CFD analysis the cooling concept for rotor and stator has been optimized. Thus it was achieved not only to omit the expensive water cooling channel within the hybrid module but as well to realize the required oil cooling at a minimum coolant flow rate. Keeping oil flow rate significantly below 5lpmin for the majority of operation points has positive secondary effects on the level of drag torque within the rotating parts of the module.

K0 Requirements – in combination with PES less stringent requirements do apply for K0 with respect to restart torque precision and restart torque dynamics. Dependent on the application strategy for combustion engine restart – more precisely dependent on the share of restart via the PES further potential for package optimization and cost does show up.

Axial Packaging – on vehicle level, the application of PES frees the combustion engine from the need for belt drive. If all functionalities like water pump, AC etc. are consequently electrified, associated losses and packaging space can be dropped. This offers additional packaging opportunities, e.g. for critical 4-cylinder applications.

Electrical Traction System – as mentioned before, the in house definition and harmonization of specifications and interfaces of inverter, e-motor, sensor system and control SW tweaks the

optimization thereof. By this comprehensive approach it has been achieved to find an attractive solution between the poles of cost and performance and efficiency.

Besides these selected key points there are many evolutionary (small) efficiency measures to cut down the friction losses – like in bearings, sealings, residual clutch torques, oil drag etc..

Status

The shown developments are in a functional sample status stage. P2 modules are build, integration test and performance tests are ongoing. The technology is prepared to start joint development.

Summary

BorgWarner has extended its portfolio for P2 hybrid modules with a dedicated 48V solution. The presented mature technology is accounting for the primary market needs and demands for:

- cost optimzation
- superior efficiency
- short time to market
- reasonable invests

References

[1] Kaufhold T: Modular Starting and Damping System integrated in 48V Hybrid Architectures, Int. VDI Congress Dritev - Drivetrain for Vehicles; Bonn; 2021.

[2] Fulton Dave.: Keynotes, International Conference on Electrical Machines (ICEM) Conference 2020.

[3] Spangler Ch.: A Family of Modular, Scalable, and Integrated Hybrid Drive Modules; CTI Symposium Berlin 2019.

[4] Diemer, P., A Market Segment Approach for Optimizing Hybrid Propulsion Systems, CTI Symposium USA 2020

[5] Steinmair G., Modular and Scalable 48V Platform eDrive Solutions for CO2 Reduction and Traction Assist, CTI Symposium USA 2020

[6] Bondards, A., Mohon, S., Semenov, D., Wenzel, W.: Comparing 48 V Mild Hybrid Concepts using a Hybrid Simulation Toolkit; Stuttgart Symposium 2019.

[7] Eglinger, M.; Hengst, J.; Kücükay, F.; Li, M.; Sieg, C.; Wenzel, W.: Next Generation 48V MHEV, Int. VDI Congress Dritev - Drivetrain for Vehicles; Bonn; 2019.

Finite element approach for analyzing noise and vibration in electric drives

Dr.-Ing. **A. Fröhlcke**, Dr.-Ing. **M. Felbermaier**, Dipl.-Ing. **A. Britten**, Dr.-Ing. **P. Fietkau**, Dr. Ing. h.c. F. Porsche AG, Weissach

Zusammenfassung

In diesem Paper wird am Beispiel des charakteristischen Geräuschs „Brummen“ eine neue Simulationsmethode zur Analyse der Einflussfaktoren für innere mechanische Anregung bei elektrischen Antrieben vorgestellt. Es handelt sich um eine Weiterentwicklung einer etablierten Finite Elemente (FE)-basierten Drehwegfehleranalyse zur akustischen Beurteilung von Verzahnungen. Die Simulationsmethode basiert auf einem quasistatischen FE-Modell, das alle relevanten Komponenten wie die Antriebswellen, Verzahnungen und Lager umfasst. Dies ermöglicht die gesamtheitliche und realitätsnahe Abbildung der elastischen Eigenschaften und der wechselseitigen Einflüsse des E-Maschinen-Getriebeverbunds. Mithilfe des FE-Modells werden Drehwegfehler ermittelt, aus denen sich zur akustischen Analyse Körperschall-Schnellepegel abschätzen lassen.

Aufgrund des sehr hohen Detaillierungsgrads des FE-Modells liefert das Verfahren sehr realitätsnahe Ergebnisse. Die Ermittlung von Drehwegfehlern auf Basis von FE-Modellen benötigt relativ wenig Rechenzeit, wodurch aufwendige Untersuchungen zu den akustischen Auswirkungen beliebiger Fertigungsfehler und Bauteiltoleranzen im System in kurzer Zeit durchgeführt und entsprechende Maßnahmen abgeleitet werden können. Anhand eines aktuellen elektrischen Serienantriebs werden Ergebnisse der Simulationsmethode für verschiedene Einflussfaktoren vorgestellt und mit Messergebnissen von vergleichbaren Versuchen am Prüfstand bestätigt. Der Einsatz der Simulationsmethode ermöglicht von Entwicklungsbeginn an, kostengünstig und frühzeitig einen hohen Reifegrad im Entwicklungsprozess zu erzielen.

Abstract

This paper uses the example of the characteristic humming noise to present a new simulation method for analyzing the factors influencing internal mechanical excitation in electric drives. This method is a further development of an established finite element (FE)-based transmission error analysis for the acoustic evaluation of gears. The simulation method uses a quasi-static FE model, which incorporates all the relevant components, such as drive shafts, gears and bearings. This enables a holistic and realistic representation of the elastic properties and

mutual influences of the electric motor and transmission. The FE model is used to determine transmission errors, which in turn provide the basis for the estimation of structure-borne sound levels for the acoustic analysis.

Using a contemporary standard electric drive, this paper presents the results of the simulation method for various impact factors and confirms them with results from comparable experiments on the test stand. The presented method delivers very realistic results due to the FE model's high level of detail. It nevertheless needs relatively little computing time to determine transmission errors. This enables performing complex and comprehensive analyses of the acoustic effects of all kinds of production faults and component tolerances in the system in a short timeframe. As a result, the method allows for timely improvement measures in the development process of the electric motor and transmission and supports the cost-efficient achievement of a high maturity level from the beginning of and throughout the development process.

1. Introduction

The sweeping technological transition toward electric drives is throwing up new challenges in powertrain development. Acoustic requirements are becoming more relevant, for example, as electric drives mostly have lower noise emissions and the previous concealment of other sounds by the noise of the combustion engine is lacking. With electric drives, increased attention must be paid to noises that are now experienced as a disturbance by vehicle occupants and were not or only dimly perceived with conventional powertrains. See, for example, Krause et al. [1] who describe the increased challenges of acoustic requirements for electromagnetically induced noise in a hybrid gearbox, whereas Möser et al. [2] discuss the general acoustic properties of a hybrid gearbox.

Next to electromagnetically and gear-induced noise, the characteristic humming noise has become increasingly important in the development of electric drives. It is characterized by the higher levels of the rotational frequency of the rotor and input shafts and their multiples (excitation with first engine order and its harmonic orders). The higher levels are caused by internal mechanical excitation.

The novel simulation method presented in this paper enables a comprehensive analysis of the factors behind this excitation. This method is a further development on an established FE-based transmission error analysis that has been standard practice for many years in the acoustic evaluation of gears. With the aid of a quasi-static FE model of the electric drive, transmission errors on the rotor shaft are determined and used to calculate structure-borne sound levels for acoustic analysis.

The characteristic humming noise is described in more detail in section 2, by means of a contemporary electric drive. Section 3 introduces the FE model used to calculate the transmission errors. Section 4 presents the transmission error analysis and structure-borne sound levels based on this. Section 5 explains the calculation results of the individual acoustic influencing factors and test results from comparable test stand experiments for the humming noise.

2. The characteristic humming noise and its possible causes

Vehicle occupants perceive drive noises as airborne sound. This airborne sound primarily results from structure-borne sound emitted by the drive to the body and transferred into the passenger compartment [3]. It is primarily caused by force-induced structure-borne sound excitation, which can be measured by acceleration sensors on component and end-of-line (EOL) test stands. Fig. 1 contains a Campbell diagram showing the increased acceleration levels of the rotational frequency of the rotor and input shafts and their multiples. It is primarily the first three orders of the rotational frequency (referred to as engine orders in the following) that have high levels. These increased levels produce the humming noise that vehicle occupants perceive as a disturbance, especially in low load ranges.

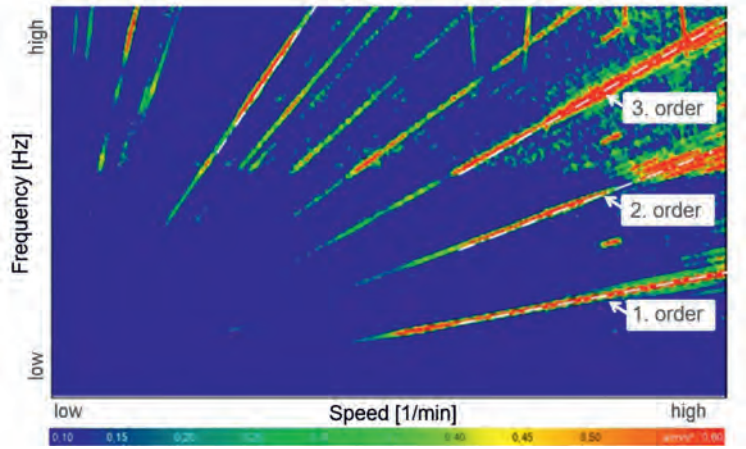

Fig. 1: Campbell diagram of a standard electric drive with increased acceleration levels of the first three engine orders

Furthermore, the electric drives tested on the test stand and the EOL do not show any dynamic abnormalities in the form of resonance in the first engine orders, except for specific test stand resonances. Fig. 2 illustrates the acceleration levels of the first engine order of a speed run-up on the test stand for a defined constant torque. The different colored lines represent the acceleration levels of different drive units at the same design level. The levels increase in a trajectory that is roughly linear to the frequency. The resonance shown in the lower frequency range is caused by the test stand construction and is therefore not considered relevant in the vehicle. The significant differences in the amplitudes of the acceleration levels are caused by the different internal mechanical excitation of the system.

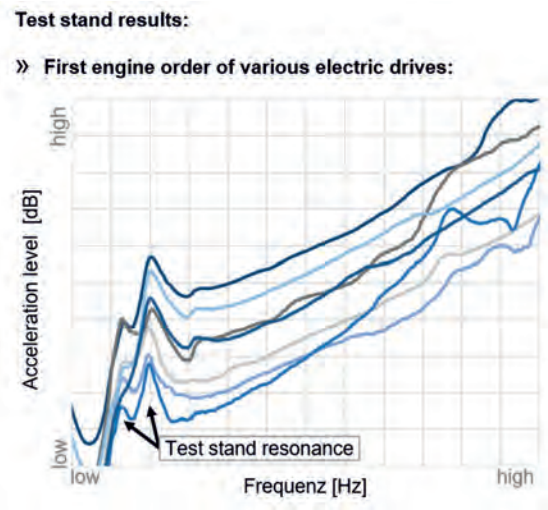

Fig. 2: Acceleration levels of the first engine order of various electric drives during a speed run-up on the test stand

The observed frequencies are well below the system's first natural frequency and are, so to speak, in the quasi-static range of the electric drive. It is therefore feasible to calculate the structure-borne sound levels based on quasi-static transmission errors, as described below.
Possible causes of the differences in internal excitation are (see Fig. 3): (i) production deviations in the rotor shaft/input shaft connection (e.g. splines), (ii) rotor unbalance, and (iii) manufacturing or assembly misalignments of drive components in the immediate vicinity of the rotor and input shafts. The presented simulation method can be employed to determine the

causes of the humming noise and their relative impact, and to devise suggestions for improvement in the development process.

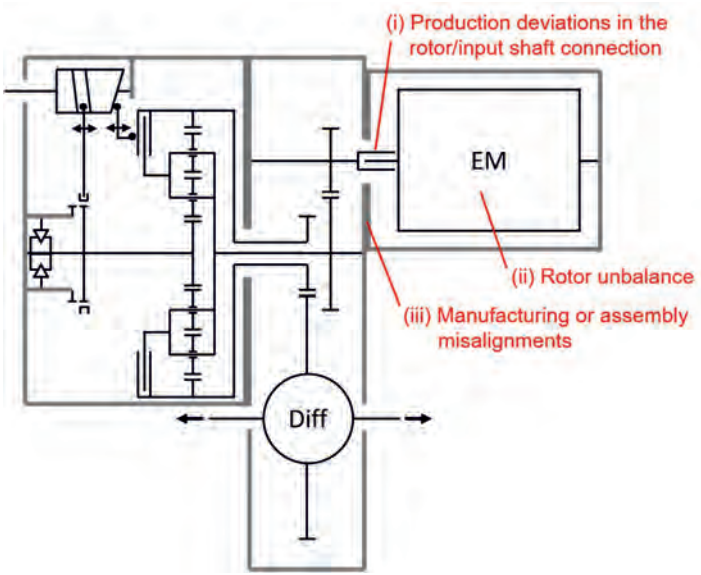

Fig. 3: Outline of a standard electric drive. The main influencing factors of the humming noise are illustrated in red: (i) production deviations in the rotor/input shaft connection, (ii) rotor unbalance, (iii) manufacturing or assembly misalignments

3. The FE model

To estimate the structure-borne sound excitation of an electric drive as accurately as possible, a very detailed FE model is required that contains all the components of relevance for an acoustic evaluation of the humming noise. This FE model features both the electric motor and the transmission to achieve the most realistic analysis possible of the interactions in the motor/transmission system. The FE-based approach has the major advantage in that a drive's elastic behavior under load can be precisely determined accounting for all relevant elastic material characteristics. Fig. 4 shows an exemplary FE model of an electric drive for transmission error analysis. It portrays a sectional view from the front of the rotor and input shaft together with the first-stage spur gears.

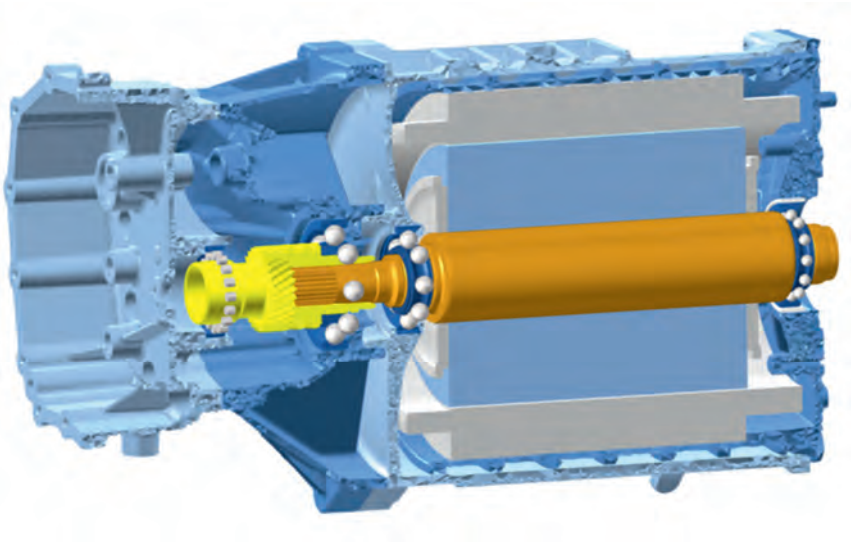

Fig. 4: Sectional view of the FE model for transmission error analysis of a standard electric drive

To determine the force-induced structure-borne sound as realistically as possible, the bearings with bearing clearance, gear teeth and housing components that are part of the power flow are reproduced true-to-life in the FE model. Moreover, the rotor/input shaft connection is a significant acoustic influencing factor, which in modern designs was achieved by means of splines. These splines were modeled in very detail in the FE model in accordance with their parameters to properly capture their influence on the system.

It is furthermore essential to include the rotor unbalance to accurately represent the dynamic forces on the bearings [3,4]. In the quasi-static FE model, the rotor unbalance is presented as a rotating force-pair on the balance disks. The centrifugal force formula

$$F = U \cdot \omega^2 \qquad (1)$$

enables the rotating force-pair on the balancing disks to be calculated from the rotational speed and unbalance U on the balance disks [4], under consideration of the angular velocity ω. The model also accounts for the weight of the rotor which is reproduced at the center of gravity of the FE model.

It is important to note that only the influencing factors and components relevant to the humming noise feature in the model. Components with a negligible influence on the humming noise were

purposefully omitted. This enables the development of a highly accurate FE model with short computing times due to the manageable number of degrees of freedom. This allows performing complex parameter analyses on the acoustic effects of all kinds of production faults and component tolerances in the system in short time.

4. Transmission error analysis and determination of the structure-borne sound level

In digital transmission development, a method presented in Fietkau et al. [5] based on quasi-static transmission error analysis has been standard practice for years in evaluating gears in their transmission environment. In the following, this paper presents a novel and highly accurate transmission error analysis applied to the rotor and input shafts that builds on the work presented in [5].

As described in section 2, internal mechanical excitation due to faulty splines, rotor unbalance, and manufacturing and assembly misalignments are the main cause of the increased levels of the lowest engine orders. These excitation factors lead to small changes in the system's load based elastic deformation during a revolution of the rotor and input shafts. Therefore, the "force-induced" internal excitation can be determined for one revolution by means of a changing displacement transmission (transmission deviation) of the rotor shaft. The transmission deviation and resulting calculated transmission error are used to determine the elastic behavior of the above-mentioned FE model. To illustrate this, Fig. 5 presents the transmission errors of a rotor shaft revolution for various torques, determined using the FE model.

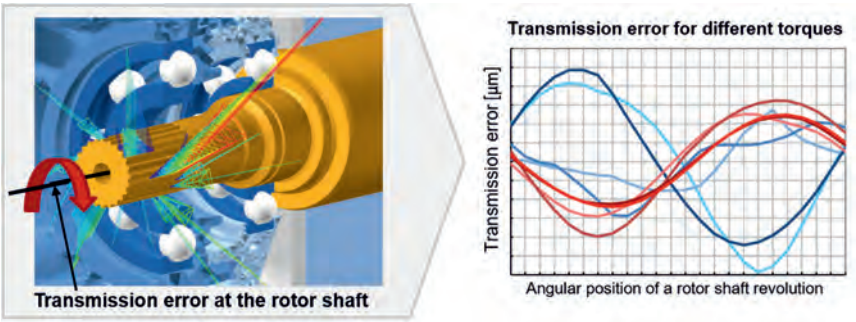

Fig. 5: Transmission error in µm for different torques based on the FE model of an electric drive. The colored lines on the right image represent the transmission errors for different torques.

Based on the transmission errors, a structure-borne sound level can be estimated for any rotational speeds. With the aid of the estimated structure-borne sound level, we can now investigate the acoustic influence of a large variety of production tolerances and variations in component geometry and parameters.

5. Simulation and test results

This section presents simulation and test results from test stand experiments for the three acoustic impact factors mentioned in section 2.

Rotor shaft/input shaft connection

The shaft connection between the electric motor and the transmission took the form of splines in a contemporary standard electric drive. Deviation-prone splines increase the internal mechanical excitation of the system, resulting in higher structure-borne sound levels, making this interface a potentially significant impact factor for the humming noise.

The results of the simulation method are set out below, taking the run-out of splines as an example. The splines of the rotor and input shaft feature run-out deviations, among other production-based faults, which can intensify when the two shafts are connected. Fig. 6 shows the influence of a spline run-out on the contact force distribution on the rotor shaft. In the left-hand illustration, we can see the contact forces of the FE model for an electric drive with error-free splines. The right-hand illustration shows the contact forces of the FE model for an electric drive with splines that have a high run-out. Due to this high run-out, the contact force distribution on the rotor shaft splines is considerably more irregular and the contact forces noticeably higher. The irregularity of and partial increase in contact forces lead to a rise in structure-borne sound levels.

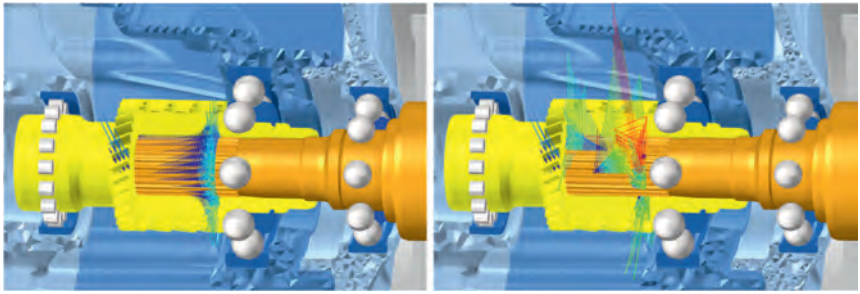

Fig. 6: FE contact forces on a rotor shaft with error-free splines (left image) and a spline pair with high run-out (right image)

Fig. 7 shows the structure-borne sound levels calculated using the simulation method for an electric drive with splines featuring a low run-out and a high run-out. The structure-borne sound levels shown are based on a constant speed and a constant torque on the rotor shaft. The right-hand graph in Fig. 7 illustrates the increased structure-borne sound levels due to the high run-out of the splines.

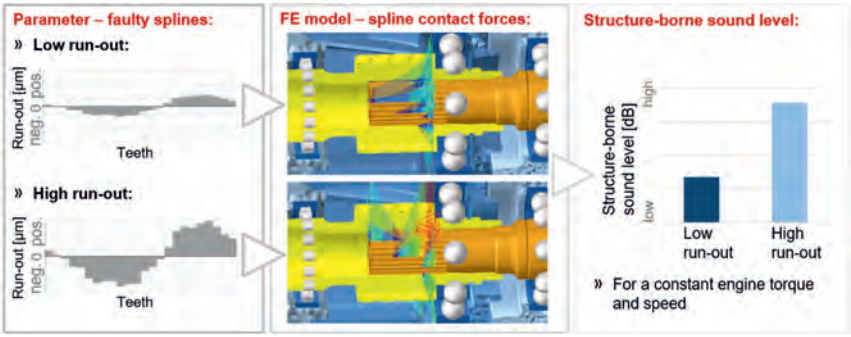

Fig. 7: Exemplary presentation of a low and high run-out (left). Contact force distribution on the rotor shaft splines (center). Calculated structure-borne sound levels in dB (right).

The results of the simulation method shown in Fig. 7 were confirmed through a comparable experiment on the test stand. This experiment aimed to measure acoustic differences for splines with a relatively low and relatively high run-out. The test results from the test stand experiment are shown in Fig. 8. They indicate the acceleration levels of the first engine order over frequency for a constant torque. The splines with the low run-out produce considerably

lower levels than the drives with the high run-out of the splines. In addition, the difference in levels at the chosen constant speed concurs very well with the difference in levels from the simulation.

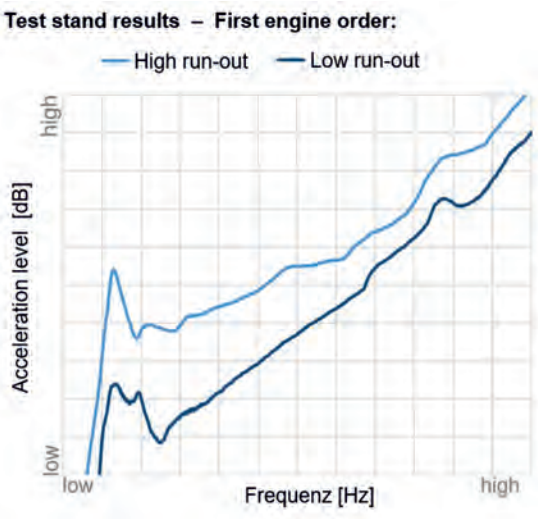

Fig. 8: Acceleration levels of the first engine order during a speed run-up on the test stand at a constant torque. The light blue and dark blue line represent the results of splines with a high and low run-out.

Next to analyzing the influence of production deviations, the simulation method presented here is also suitable for determining geometric influences due to component modifications. For example, the method can be used to analyze whether certain modifications of the spline width result in a reduction in structure-borne sound levels. Fig. 9 illustrates the structure-borne sound levels deduced from the FE model for two different spline widths. The decreased spline width causes a reduction in structure-borne sound levels. On the right, we see the test stand results for the two spline versions. Test stand experiments confirmed the reduction in structure-borne sound due to a smaller spline width. Even with shorter splines, sufficient strength for transferring the maximum engine torque was still available.

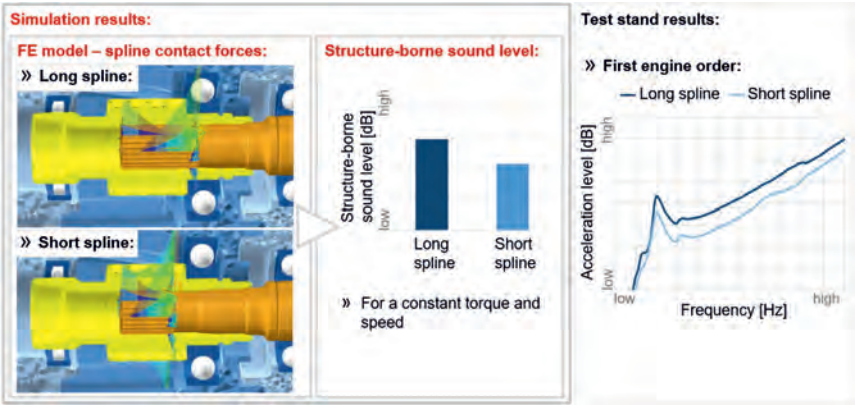

Fig. 9: Contact forces on the rotor shaft splines (left). Calculated structure-borne sound levels for different spline widths (center). Test results from a comparable experiment on the test stand (right).

Rotor unbalance

The simulation method allows also to analyze the impact of the rotor unbalance, another significant factor impacting the humming noise. The findings clearly show that greater rotor unbalance in the FE model leads to an increase in calculated structure-borne sound levels. This relationship was also confirmed in comparable experiments on the test stand.

Fig. 10 illustrates the major influence of rotor unbalance and the rotor shaft/input shaft connection. It shows the results of a test stand experiment for two different rotor shafts of an electric drive. The lines indicate the acceleration levels of the first order for a constant torque. The dark blue line represents the levels for an electric drive with a rotor shaft that has both a high rotor unbalance and splines with a high run-out. The second experiment used a rotor shaft with low rotor unbalance and splines with a very low run-out. The light blue line represents the measured acceleration levels of the drive with the newly installed rotor shaft. As expected, using a rotor shaft with low unbalance and a low run-out can considerably reduce the acceleration levels. The test stand reduction in levels correlates very well with the results obtained using the simulation method.

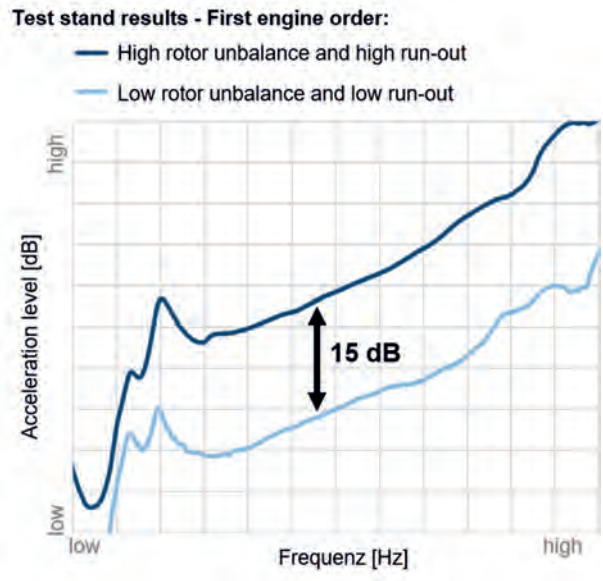

Fig. 10: Acceleration levels of the first order of a speed run-up on the test stand for the same electric drive with two different rotor shafts.

Production or assembly misalignment

Structure-borne sound is also influenced by production and assembly factors that cause misalignments of the rotor or input shaft. The left-hand side of Fig. 11 shows structure-borne sound levels for a constant torque and speed, which were computed using the FE-based simulation method. We can see the results with and without production or assembly misalignment on the positive and negative vertical and longitudinal axes of the rotor shaft. Moreover, the splines in the FE model feature a moderate run-out. The right-hand side contains test results for an experiment on the test stand using a centered and an offset rotor shaft.

Fig. 11 clearly shows that a misaligned rotor shaft leads to increased acceleration levels. The impact of this kind of misalignment is additionally influenced by a run-out. Simulating these influencing parameters in the early stages of the development process enables component and installation tolerances to be defined in combination with other parameters.

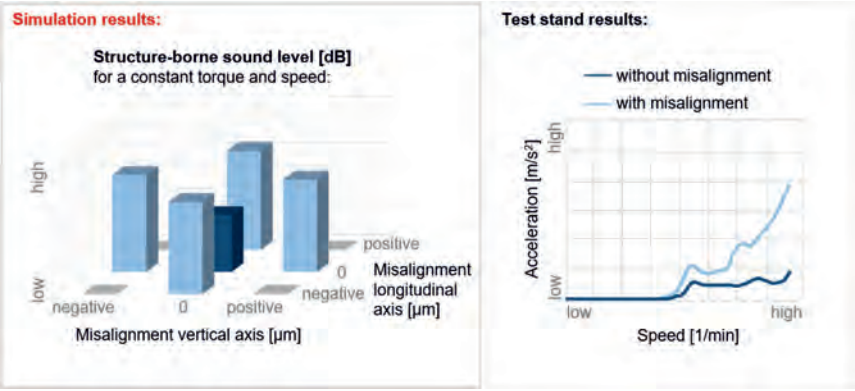

Fig. 11: Calculated structure-borne sound levels for a production or assembly misalignment of the rotor shaft in different directions (left). Test results from a comparable experiment on a test stand (right).

6. Conclusion

The FE-based simulation method presented in this paper enables a detailed analysis of the acoustic influencing factors of the characteristic humming noise. The increased levels of the lowest engine orders related to the humming noise are due to increased internal mechanical excitation. Regarding the influencing factors rotor/input shaft connection, rotor unbalance and production or assembly misalignments, it has been demonstrated that the simulation results concur very well with comparable test results on the test stand. The FE-based simulation method has the additional advantage that parameters and components can be changed quickly and flexibly. Furthermore, the manageable size of the FE model and the simple determination of transmission errors and structure-borne sound levels allow for extensive parameter analyses in relatively short time. The presented analysis shows that using the simulation method allows to significantly increase the maturity level of an electric drive from the start of the development process. At any point during this process, the method can help to ensure that the levels of the lowest engine orders do not exceed the defined limit curves and therefore the humming noise will not be perceived as a disturbance by vehicle occupants. Consequently, the number of acoustic experiments on the test stand and in the vehicle can be reduced and component tolerances be established early on, therefore lowering development costs.

[1] Kruse, M., Decker, H., Eulert, S.: Optimisation of electric motor acoustics of a hybrid dual clutch gearbox using virtual methods. International Conference EDrive, Dritev (VDI-Berichte Nr. 2354), Bonn, 2019

[2] Möser, C., Märkle, T., Hornung, K.: Effective acoustic development of electrified powertrains. International VDI Congress Dritev (VDI-Berichte Nr. 2354), Bonn, 2019

[3] Linke, H.: Stirnradverzahnung. Berechnung, Werkstoffe, Fertigung. München Wien: Carl Hanser Verlag, 2010

[4] Dresig, H., Holzweißig, F.: Maschinendynamik. Berlin Heidelberg: Springer-Verlag 2016

[5] Fietkau, P., Lamparsky, N., Felbermaier, M., Fröhlcke, A., Conze, T: Holistic Design Approach for Electric Drives. International VDI Congress Dritev (VDI-Berichte Nr. 2354), Bonn, 2019

Thermal Simulation according to Maturity Level in E-Drive Development

Dr. **R. Rohith Kasibhatla**, **Philipp Neidhardt**, Dr. **Kemal Caliskan**,
ZF Friedrichshafen AG, Schweinfurt

1. Zusammenfassung

Zur Erfüllung der Leistungs- und Bauraumanforderungen in E-Antrieben, ist ein effektives Kühlungssystem essenziell. Das Kühlungssystem wirkt sich nicht nur auf das thermische Verhalten des E-Antriebs aus, sondern auch auf dessen Effizienz, Funktionalität und Robustheit. Daher sind, für eine umfassende Gesamtsystemanalyse, die Ergebnisse der thermischen Simulation ausschlaggebend.

Entsprechend dem Reifegrad im Entwicklungsprozess, unterscheiden sich die Anforderungen an die Verfügbarkeit und Güte der thermischen Simulationsergebnisse. Zudem erfordern die verschiedenen System- und Kühlungskonzepte unterschiedliche Simulationsverfahren. Ein systematischer reifegradbezogener Ansatz für die thermische Simulation, basierend auf der gekoppelten Systemsimulation, 3D-CFD/CHT-Simulation und Validierungstests, ist zur effizienten Unterstützung des Entwicklungsprozesses notwendig.

2. Abstract

Effective cooling system is essential for e-drives to meet performance and installation requirements. The coiling system effects not only the thermal behavior of the e-drive but also its efficiency, functionality, and robustness. Therefore, for a comprehensive overall system analysis, the outcomes of thermal simulation are crucial.

At different maturity levels of the development process, time and accuracy requirements from thermal simulation differs. Additionally, the variety of system concepts and cooling methods requires special simulation methodologies. A maturity level oriented systematic approach for thermal simulation, based on coupled system simulation, 3D-CFD/CHT simulations as well as validation tests, is necessary to support development process efficiently.

3. Thermal simulation of electric motors for vehicle drivetrain applications

Thermal simulation of electric drivetrains can be performed based on two general methods. These are lumped parameter modelling, or 1D-models, and mesh-based 3D simulation approaches. Lumped parameter models require in depth knowledge and quantified

assumptions for all boundaries, interfaces, material properties and heat flow paths. The advantage of 3D simulation approach is significantly reduced number of assumptions along with detailed resolution of the domain. Drawbacks are the dependency on 3D geometry and significantly higher computational effort, especially in the case of transient simulations.

The advantages and disadvantages of different thermal simulation methods make them suitable for different stages of development, in which the availability of input data as well the time and accuracy requirements from thermal simulation change. On the other hand, the harmonization of the simulation tools and their continuous improvement based on experimental validation is necessary to improve the prognosis quality of simulation models. The utilization of thermal simulation methods at different stages of ZF electrified powertrain development is summarized in Figure 1.

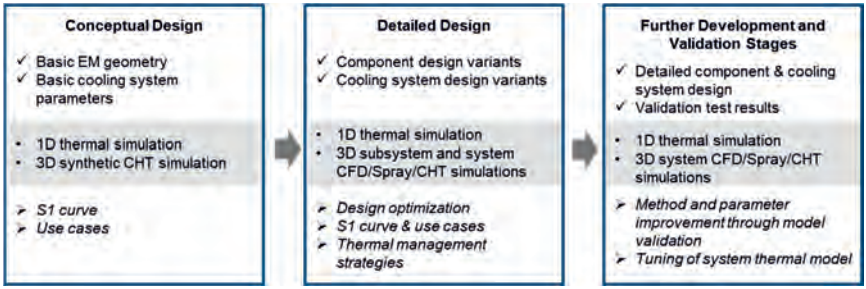

Fig. 1: Utilization of thermal simulation methods at different development stages

a. Detailed 3D CHT Simulation

Detailed 3D Conjugate Heat Transfer (CHT) simulation provides a detailed insight of thermal behaviour of electric drives at different operational points. Consequently, such detailed modelling also demands detailed design of electric drive. Thereby, such detailed modelling and simulation can be executed in matured phase of development.

The detailed representation of electric drive includes not only the active electromagnetic components like stator windings, magnets, stator- and rotor sheet packets but also the mechanical components such as bearings, sealings, gears, stator housing, shaft and lance as shown in Figure 2.

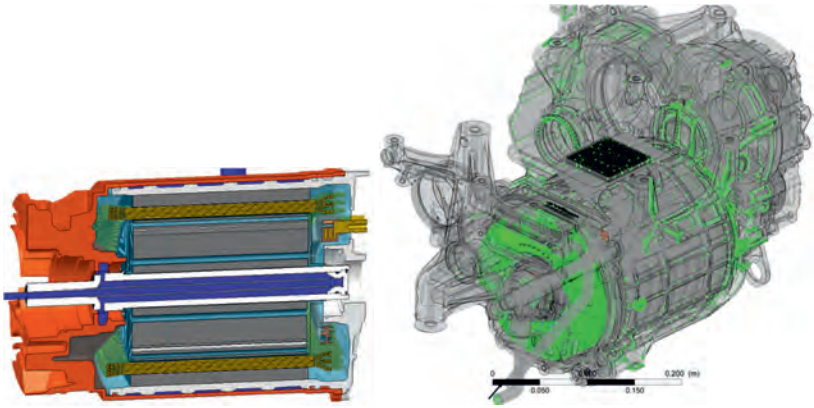

Fig. 2: Detailed geometrical representation of electric motor (left) and electric axle (right)

Detailed 3D CHT model takes both mechanical and electromagnetic losses in electric drives into account to compute the thermal behavior of electric drive. The local thermal losses are implemented in each subdomain continuum, which interacts with the other continuum with or without different material properties. The interaction between different sub-domains enables heat and fluid transfer. Thereby, thermal coupling of such fluid and solid domain is necessary for detailed thermal modeling of electric drives. For a fluid domain i, the governing equations read as (Ferziger, Peric, & Street, 2002):

Continuity of mass in fluid domain:

$$\frac{\mathrm{d}\rho_i \mathbf{u}_i}{\mathrm{dt}} + \rho_i(\nabla \cdot \mathbf{u}_i) = 0 \qquad [1]$$

Continuity of momentum in fluid domain:

$$\frac{\mathrm{d}\rho_i \mathbf{u}_i}{\mathrm{dt}} + \nabla \cdot (\rho_i \mathbf{u}_i \mathbf{u}_i) = -\nabla \mathrm{p} + \nabla \cdot \boldsymbol{\tau} + \rho \mathbf{g} + \mathbf{S_{m,i}} \qquad [2]$$

Continuity of energy in fluid domain:

$$\frac{\mathrm{d}\rho_i \mathrm{e}_i}{\mathrm{dt}} + \nabla \cdot (\rho_i \mathbf{u}_i \mathrm{e}_i) = -\nabla \cdot \ddot{\mathbf{q}} + \frac{\partial \mathrm{p}}{\partial \mathrm{t}} + \nabla \cdot (\tau \cdot \mathbf{u}) + \mathbf{S_{e,i}} \qquad [3]$$

where, ρ_i is the density of fluid, $\boldsymbol{u}_i$ is the velocity, p is the pressure, e_i is the internal energy, $\ddot{\boldsymbol{q}}$ is the heat flux vector, τ is the stress tensor, $\boldsymbol{S_{m,i}}$ is the momentum source term and $\boldsymbol{S_{e,i}}$ is the fluid energy source term. Whereas for the solid domain j, the governing equations read as:

Continuity of energy in solid domain:

$$\frac{\mathrm{d}\rho_\mathrm{j}\mathrm{e}_\mathrm{j}}{\mathrm{dt}} = \nabla \cdot (\mathrm{k}_\mathrm{j}\nabla \mathrm{T}_\mathrm{j}) + \mathbf{S_{e,j}} \qquad [4]$$

where, ρ_j is the density of solid, e_j is the internal energy of solid domain, k_j is thermal conductivity of solid, T_j is the temperature of the solid and $\boldsymbol{S_{e,j}}$ is the solid energy source term. Local thermal equilibrium is maintained between the solid and the fluid domains. At every computed time step, the heat flux is adjusted over the interface, leading to the temperature change in the domains either side of the interface. For an interface between the solid domain j and fluid domain i, the heat transfer source term from thermal equilibrium is defined as (Chesshire & Henshaw, 1990):

$$\mathbf{S_e} = \iint \mathbf{n} \cdot \mathrm{k}_\mathrm{j}\nabla \mathrm{T}_\mathrm{j}\mathrm{dA}_\mathrm{ij} = \iint \mathbf{n} \cdot \mathrm{k}_i\nabla \mathrm{T}_i\mathrm{dA}_\mathrm{ij} \qquad [5]$$

Besides the fluid-solid coupling, a thermal contact is also ensured between solid domains through a thermal contact conductance over the surface contacts like press-fit contact, adhesive contact etc. For a solid-solid contact, thermal equilibrium between solid j and solid k is assured by

$$\mathbf{S_e} = \iint \mathbf{n} \cdot \mathrm{k}_\mathrm{j}\nabla \mathrm{T}_\mathrm{j}\mathrm{dA}_\mathrm{jk} = \iint \mathbf{n} \cdot (\mathrm{h_{jk}}^\mathrm{c}\mathrm{A}_\mathrm{jk})\nabla \mathrm{T}_\mathrm{j}\mathrm{dA}_\mathrm{jk} \qquad [6]$$

where, A_{jk} is the interfacial contact area between the two solids j and k and $h_{jk}{}^c$ is the thermal contact conductance for contacts from press-fit, contact material, or contact gap realized (Patankar, 1980).

Based on the adapted mathematical model in a CFD simulation software, the thermal behavior of electric drive at different operational points can be evaluated via numerical simulation. As simulation input the electro-magnetic losses from electric machine, splash and frictional losses from the transmission, bearings and sealings, and power electronics losses are required. The losses at different operational points are implemented locally in the respective subcomponents of the detailed 3D CHT model. As the simulation output, 3D component temperature

distribution in the system, heat transfer paths and pressure drop in the cooling circuitry can be evaluated.

To achieve continuous steady powers, the cooling system must transport the losses from power electronics, copper windings, magnets, laminations stacks, gearbox, bearings and sealings to the coolant. The thermal performance of an electric drive is not only rated by body-averaged temperatures of its components, but also by local hotpots which might result in thermal degradation. The local hotpots can be only evaluated accurately using 3D detailed simulation models.

In dry electric machines with water cooling, the fluid and air domains can be analysed via single phase CFD simulation. Generally, the coolant flows in the cooling channels of the power electronics and later in stator housing. Optionally the rotor shaft can also be cooled through same coolant as shown in Fig. 1. Higher turbulent velocities can be achieved via design optimization of the cooling channels for available flow rates. The higher turbulent flow in stator, power electronics and rotor result in higher heat transfer coefficients and proportionally higher cooling powers. In ZF electric axle applications, with the mentioned water-based cooling system, 50 % peak to continuous power ratio can be achieved.

Fig. 1: Streamlines of cooling circuit in an ZF electric axle

Alongside high cooling power, homogenous temperature distribution in an electric drive is also a main topic of interest. The temperature homogeneity in sub-components of an electric drive contributes to the durability and NVH behavior of the electric drive. To prevent thermal degradation of an electric drive, temperature levels and homogeneity is not just important in copper isolation but also in magnets.

Fig. 2: Temperature distribution in a series production ZF electric axle

b. Multiphase simulations

Cooling of an electric drive over a stator jacket or a rotor shaft is not always sufficient to achieve high continuous powers in a compact installation space due long thermal bridge to active components. A direct cooling is thereby necessary to remove the losses directly from active components. Due to its electrical conductivity, water-glycol cannot be used as a coolant for direct cooling concepts. Therefore, oil is used to cool the electric motor components directly. Different electric machines, from synchronous to asynchronous motors, may use direct cooling with oil to achieve higher continuous power besides achieving thermal safety. Design and evaluation of thermal performance of oil cooled machines just based on the measurements is an expensive process. Measurement techniques to study the oil flow distribution in electric drives involves laser interferometry, particle imaging and high-speed camera technique. Therefore, in ZF multiphase numerical simulations of oil and air mixture are extensively used to analyse direct oil cooling at winding heads, rotor and stator parts. Multiphase simulations extend from mesh-based Volume of Fluid (VOF) methods to particle based Smoothed Particle Hydrodynamics (SPH) and Moving Particle Simulation (MPS) methods. Coupled multi-physical simulation including fluid dynamics and thermodynamics can be optimally performed using the VOF method, whereas the SPH and MPS methods can be implemented for a fast analysis of the multiphase flow mainly.

In VOF method, the phase advection from one cell to another is computed to obtain the oil transport in each cell of the meshed fluid domain by solving the volume of fluid equation, which can be read as

$$\frac{\mathrm{d}\gamma_i \rho_\mathrm{i} \mathbf{u}_\mathrm{i}}{\mathrm{dt}} + \rho_\mathrm{i}(\nabla \cdot \gamma_i \mathbf{u}_\mathrm{i}) + \rho_\mathrm{i}(\nabla \cdot \gamma_i (1-\gamma_i)\mathbf{u}_c) = 0 \cdot \qquad [7]$$

where, $\mathbf{u}_c$ is the interfacial compressional velocity and γ_i is the volume fraction of a fluid phase like oil, which is computed in every time step and every cell as

$$\gamma_i = \lim_{V \to \infty} \frac{1}{V} \iint \gamma_i \, dV = 0 \cdot \qquad [8]$$

where, V is the volume of a computing cell. In the same ways as in Eq. 2, Eq.3 the momentum and energy of the individual phases are conserved using the VOF approach. The interaction between the two phases, like velocity difference between the independent phases i.e. interfacial compression velocity, surface tension and wetting forces are implemented as source terms in the mixture momentum equation.

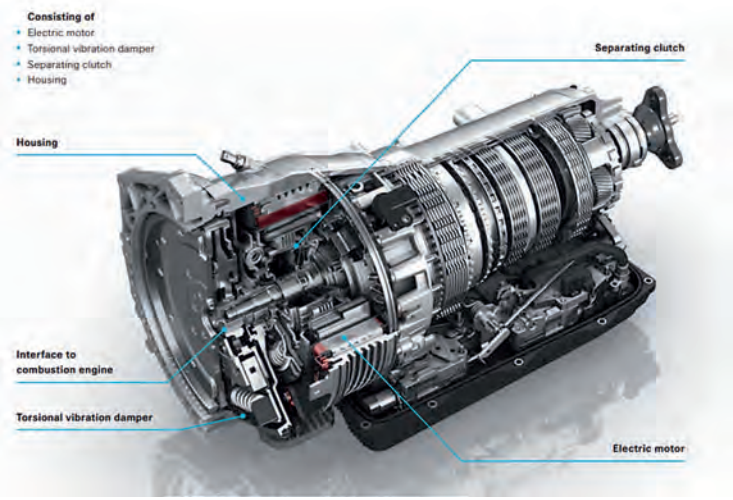

Fig. 3: Oil cooled electric drive in ZF 8HP Automatic transmission (ZF Friedrichshafen AG, 2021)

The oil distribution inside the electric motor is strongly influenced by the rotational speed and oil injection flow rate. To model the oil spray under rotation, generally a sliding mesh approach is employed in VOF method. Whereas, the particle-based methods employ the multi rotational framework system.

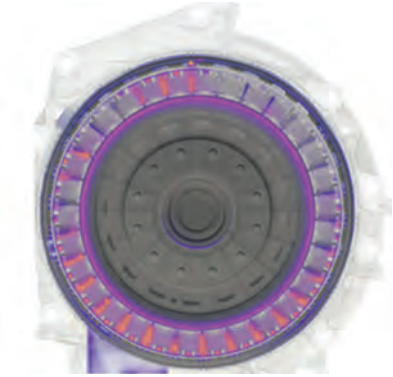

Fig. 4: Oil distribution in a ZF hybrid electric drive based on particle-based simulations

Based on the simulated oil distribution and velocity field via particle-based methods (as shown in Fig. 4: Oil distribution in a ZF hybrid electric drive based on particle-based simulationsconvective heat transfer coefficients on the stator coils, rotor and stator etc. can be evaluated and coupled with the CHT simulations. The local heat transfer coefficient in particle-based methods is evaluated from the selected oil reference temperature and component temperature. As mentioned above, it should be noted that, the VOF method is superior to the particle-based simulation regarding the analysis of the heat transfer.

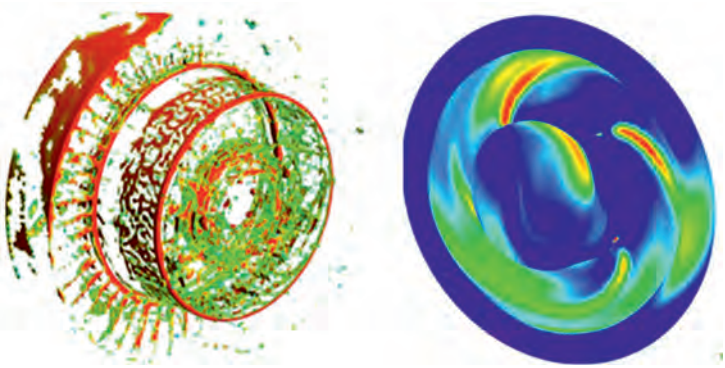

Fig. 5: Oil distribution in a ZF hybrid electric drive based on volume of fluid simulations

In the volume of fluid based multiphase simulations, the solid and fluid domains of the electric drive are initially computed together to solve the VOF and momentum equations in the fluid

domains, and the oil distribution on the fluid-solid walls is also established in this unsteady simulation phase. Later, only the energy equation is solved for the established velocity, pressure, and volume fraction fields. For this later phase, where the temperatures of the components are computed, a steady state computation is preferred to understand the influence of the cooling in reference to the desired continuous powers. Such a temperature field and the oil distribution in an ZF electric drive is shown in Fig. 6. The oil spray from the rotor shaft influencing the temperature field is displayed on the right-hand side of the picture, whereas the oil sticked on the rotor carrier of the electric drive is displayed on the left side. The rotor carrier is extensively cooled to reduce the magnet temperatures and hotspots.

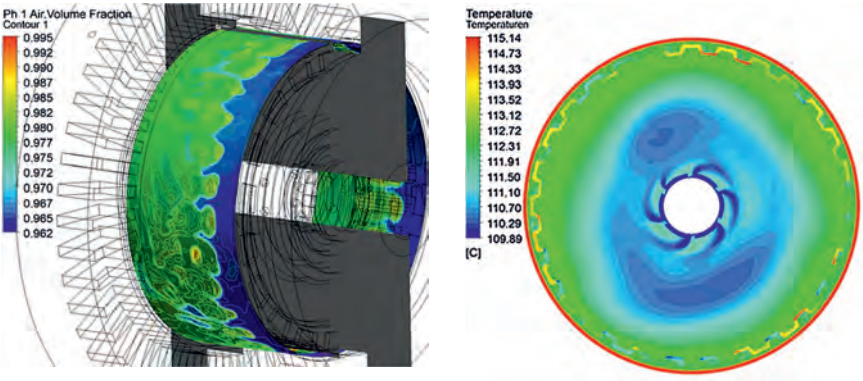

Fig. 6: Oil wetting and oil temperature distribution in rotor space in ZF hybrid electric drive

c. Synthetic modelling for 3D-simulation in early design stages

The 3D-synthetic CHT simulation is closely related to the detailed 3D-simulation. It aims to mitigate the disadvantages of detailed 3D-models by providing a simplified, parameter-based geometry as a base for the simulation. This opens the possibility for several workflow adaptions to make the simulation process as efficient as possible.

The geometry can be constructed in a way that the thermal behaviour is represented as accurately as possible while making the meshing process easier and reducing the required number of elements significantly. The geometry can be setup in a way, that contacts can be defined automatically, making a manual model generation obsolete. The results are that from geometry regeneration to remeshing to model setup, the process can run fully automatized with high efficiency.

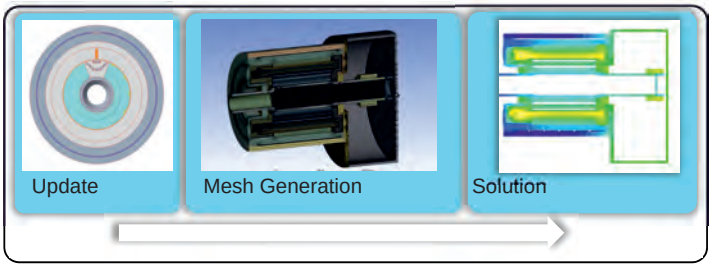

Fig. 7: Automatization Process for the synthetic modelling approach

The loss in geometrical precision is opposed by a major reduction in element count, an automated model-setup process, and the ability to investigate physical effects of electromagnetic loss distribution as well as contact and interface behaviour in more detail. The reduced model size also opens the possibility for transient simulation. The early availability and the quick model setup make it possible to do design studies on a small scale but with greater precision and accountability of the impact of physical effects that cannot be obtained by a 1D-simulation in the needed details.

d. 1D-lumped parameter model

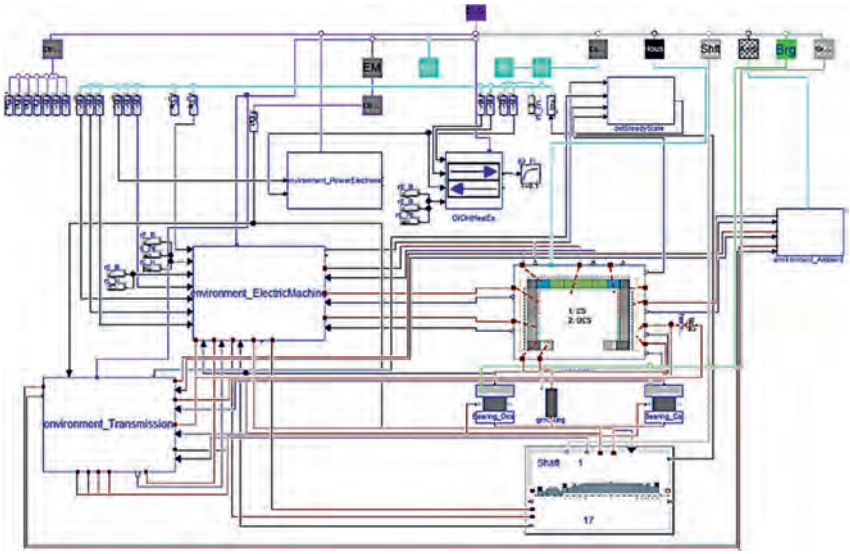

Fig. 8: Thermal 1D Model of an electric axle drive

System simulations find application in different stages of the development process. Thereby the thermal simulation is often part of a multi-physics approach. Combining thermal simulation with electromagnetics, longitudinal dynamics, and electrics the overall system behaviour can be analysed comprehensively. In an early phase of the development project the 1D simulation can be used for concept studies. Fig. 8 shows an example for a thermal model of an electric axle drive.

As an example, the influence of different cooling concepts onto the component, but also on the system behaviour can be investigated in a very efficient way. Another application of 1D thermal models is the integration into further development processes, for instance implementation into route simulation. There different aspects as driveability, energy consumption or the evaluation of specific customer use case must be investigated. By integrating thermal models, interactions with the thermal system behaviour can be considered. In Fig. 9 an example for the temperature time history in an electric axle during a drive cycle is shown. The influence of torque reduction due to high component temperatures onto the driveability can be observed.

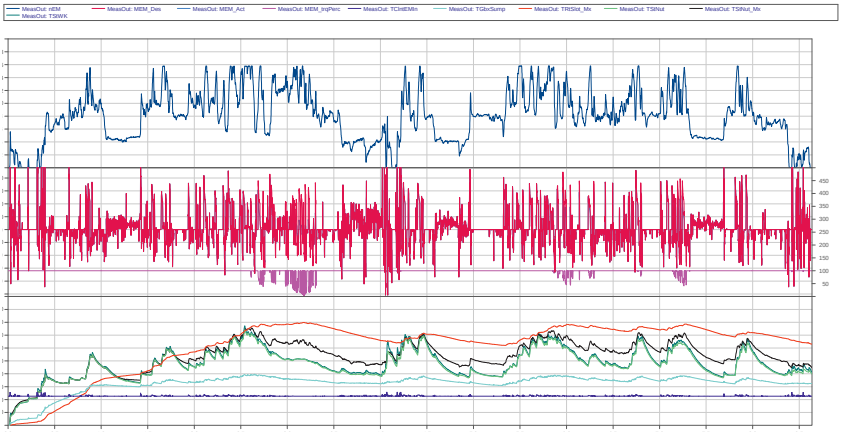

Fig. 9: Temperature curves as output of the thermal lumped parameter model

Based on different applications several requirements to the simulation models can be derived. To be able to investigate different design alternatives, a high flexibility concerning design, concept and parameter variations is necessary. To ensure a straightforward product development process, a high level of maturity is needed, even in early project phase when no test data are available to calibrate the simulation models. One way to reach this target is an

established frontloading process. Thereby knowledge and test results from existing products are used to validate the simulation models. In this case, the models need to be based on physical approaches, which offer the possibility to apply parameter changes in a certain range. The combination of 1D and 3D simulation may also help to ensure a continuity in the product development process. This can be achieved by a permanent alignment process between different simulation models or by implementing reduced order models into the system simulation. The reduced order models (ROM) are derived from 3D simulations. To be able to integrate the 1D system models into different simulation environments standardised processes must be established.

Approaches to meet the demands to the system models is for example a modular concept with scalable level of detail. Depending on the specific simulation target an appropriate system simulation model can be chosen. Hereby the required results and involved physics, but also the desired simulation speed plays an important role. A physical modelling approach helps to achieve scalable models where the model parameters can be adapted to design changes or different boundary conditions in a certain range. In early project phase when only rough CAD data is available, a physical model could be helpful. Using reduced order models, detailed 3D component models can also be implemented into the system simulation. One advantage of this method is, that the same models with known accuracy can be used for component and system simulation.

The lumped parameter model is well-suited for design studies in the early design phase, as well as for the analysis of overall system behaviour considering multi-physics interactions. The 1D-models can be further integrated into the development process to provide a base for route simulation covering driveability, energy consumption and customer use case evaluation, and to support development of software functions.

A modular system model with scalable levels of detail can be achieved through physical modelling approach, a close collaboration between 3D-simulation and testing, and integration of high-fidelity models as reduced-order-models (ROM) into the lumped parameter model.

The basic requirement for this approach is the high maturity level of model, especially in the early design phase to ensure a consistent product development process. The advantages are a high flexibility concerning design-, concept- and parameter variations. Established processes for integration into different development environments can further raise the value of the 1D-simulation models.

e. FMU-Based Multiphysics Simulation

The physical domain of the electric drivetrain consists of multiple coupled physical effects. This is shown in Fig. 10. To create a correct model with these effects, it is required to account for at least all significant couplings to restrain the error margin of simulation results. One main coupling effect is that of electromagnetic motor losses. As the electric motor is a fine balanced thermal system, a relatively small offset of the heat input can lead to large temperature changes. The losses are themselves strongly dependent on the temperature level inside the motor, as well as the actual mechanical power demand, which itself is dependent on the load and temperature.

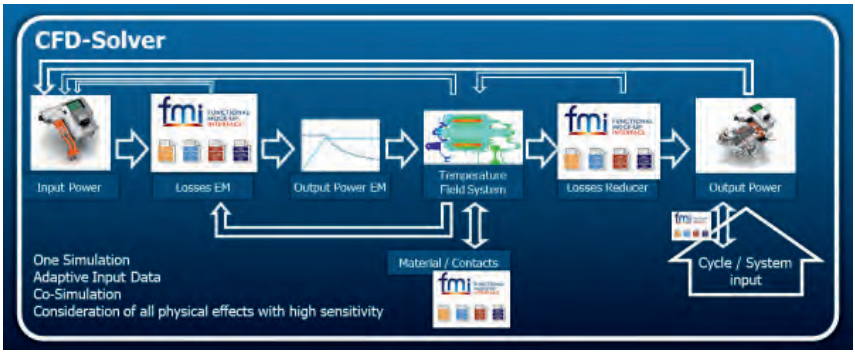

Fig. 10: Co-Simulation Process for thermal CAE-Simulation (Neidhardt, 2021)

To be able to model these effects, it is necessary to have models that can describe these effects individually with all necessary data exchange ports. This leads to the possibility to create reduced order models for all effects that have a significant impact on the thermal behaviour of the motor but are not calculated within the thermal simulation. Among these are the electromagnetic losses, thermal contact behaviour dependent on mechanical contact parameters, reducer losses, non-fluidic mechanical losses (bearing losses, auxiliary component losses) and subsystems, that would add too much complexity to the model. An example is the multiphase coolant flow inside the rotor shaft in case of a rotor shaft cooling setup.

Fig. 11: FMU Sub model integration in thermal simulation process (Neidhardt, 2021)

The flow parameters, heat transfer capabilities and drag losses can be put into correlation to temperature, rotation speed, volume flow and fluid parameters creating a reduced order model (ROM) of this subsystem. Intelligent choice in parameters makes the re-usability of the ROM for a broad variety of applications possible. Integrating reduced order models as FMU in the thermal simulation opens the possibility to directly simulate the thermal behaviour in a single solver environment. The general process, shown in Fig. 11, consists of the creation of simulation input data, coupled CHT-FMU-simulation and subsequent system performance analysis. Other advantages include but are not limited to re-use of the FMU for other purposes and multiple projects as well as for multiple stages in the development process.

f. Verification and Validation

The accuracy level of thermal simulation models does not only depend on the applied simulation methodology but also on the accuracy of input data (i.e., electromagnetic and mechanical losses), boundary conditions and model parameters. The simulation models should be validated regarding all these aspects and harmonized with each other to ensure high credibility level within development process. The validation process covers a broad range of tests, such as material tests for the identification of the thermal characteristics of materials and contact interfaces (Figure 14, left), subsystem tests for coolant flow behaviour (Figure 14, middle), and system performance tests with component temperature measurements (Figure 14, right).

Fig. 14: Material, subsystem and system tests for model verification and validation

4. Conclusion

The utilization of thermal simulation approaches with tailored depth and fidelity in the respective stage of electric drive development enables effective use of simulation models to make right and timely decisions during development process. This requires alignment of thermal simulation models of different complexities in terms of input data, model parameters and boundary conditions, as well as cross-validation of simulation results. Comprehensive validation and calibration of thermal simulation models through testing data is essential to ensure high credibility level of models.

5. Bibliography

Chesshire, G., & Henshaw, W. D. (1990). Composite overlapping meshes for the solution of partial differential equations. *Journal of Computational Physics*, 1-64.

Ferziger, J. H., Peric, M., & Street, R. L. (2002). *Computational methods for fluid dynamics.* Berlin: Springer.

Neidhardt, P. (2021, 03 24). *ANSYS automotive Webinar Series*. Retrieved from https://www.ansys.com/de-de/resource-center/webinar/improvement-of-thermal-cfd-emmodels-by-introduction-of-fmu-submodels

Patankar, S. V. (1980). *Numerical heat transfer and fluid flow.* Taylor & Francis Inc.

ZF Friedrichshafen AG. (2021, 06 20). *ZF Powertrain modules*. Retrieved from https://www.zf.com/products/media/product_media/cars_5/cars_powerttrain_modules_dynastart/pdf_12/ZF_PKW_E-Mobility_2017_DE_Web.pdf

Advanced Design of Dedicated Hybrid Drivetrains

Dipl.-Ing. **Marco Giannantonio**, Dr.-Ing. **Steffen Henzler**,
Mercedes-Benz AG, Stuttgart;
Prof. Dr.-Ing. **Stephan Rinderknecht**,
Institute for Mechatronic Systems in Mechanical Engineering (IMS),
Technical University of Darmstadt

Zusammenfassung

Die Entwicklung von elektrifizierten Antriebssträngen wird in der frühen Phase des Produktentstehungsprozesses verstärkt von einem Zielkonflikt dominiert. Die Vielzahl unterschiedlicher Topologien kombiniert mit neuen Technologietrends und Anforderungen der Fahrzeugplattformen sowie Varianz in der Dimensionierung und Anordnung der Komponenten führt zu einem multidimensionalen Lösungsraum. Dieser kann bei Einsatz des konventionellen Entwicklungsprozesses und der zunehmend angestrebten Verkürzung der Entwicklungszeit bis zur Serienreife nicht mehr vollständig untersucht werden. Ein Beitrag zur Lösung dieses Zielkonfliktes wird im vorliegenden Paper präsentiert: Ein neuartiger, vollständig automatisierter Ansatz für den Konzeptentwurf von dedizierten Hybridantriebssträngen mit mehreren Leistungsquellen. Der Ansatz zeichnet sich durch eine gesamtheitliche und modulare Methodik zur automatisierten, rechnergestützten Erzeugung und Optimierung von 3D-Konzeptentwürfen für beliebig komplexe Layouts mit Planetenradsätzen, Stirnradsätzen und Schaltelementen aus. Der zentrale Baustein des Ansatzes ist die hier vorgeschlagene Verknüpfung der Algorithmen zur Komponentendimensionierung mit einer prädiktiven Kollisionsanalyse. Hierdurch wird ein dichtest gepacktes und kollisionsfreies Package im zur Verfügung stehenden Fahrzeugbauraum erreicht sowie eine belastungskonforme Auslegung der Komponenten gewährleistet. Die Modularität des Ansatzes ermöglicht es, verschiedene Ablaufsteuerungen unter Einsatz von Optimierungsalgorithmen zu implementieren, die rechenzeiteffizient nach dem bestmöglichen Konzeptdesign für das zugrundeliegende multidimensionale Optimierungsproblem suchen. Die Praxisrelevanz des Ansatzes wird anhand der Ergebnisse für zwei unterschiedliche Layouts unter Verwendung verschiedener Ablaufsteuerungen und Lösungsalgorithmen diskutiert.

Abstract

The primary challenge within the early drivetrain concept design process is the identification of the most beneficial design within the large and multi-dimensional solution space containing a vast variety of different topologies and new technology trends in vehicle platforms. Furthermore, the defined reduction of time-to-market initiates a target conflict with the conventional design approach. One contribution to solve this conflict is presented in this paper: A novel approach for the fully automated concept design of dedicated hybrid drivetrains with multiple power sources. This approach features a holistic and modular method for computerized generation and optimization of 3D design concepts for arbitrarily complex layouts, containing planetary gear sets, gear pair sets and shifting elements. The key element of this approach is the combination of a component-dimensioning algorithm with a predictive collision analysis to achieve a densely packed, load capacity-fulfilling and collision-free design within the installation space of defined vehicle platforms. The modularity of the approach enables the possibility to define different control flows using optimization algorithms striving for the most beneficial design in a resource-optimized manner for this multi-dimensional design problem. As a practical proof, the results of this approach with different control flows and solving algorithms for two different layouts are discussed.

1 Introduction and motivation

The variety of new transmission and drivetrain topologies as well as new technology trends in vehicle platforms are leading to a highly increased solution space for the design problem. Furthermore, the defined reduction of time to market initiates a target conflict with today's conventional design approach as shown in Fig. 1.

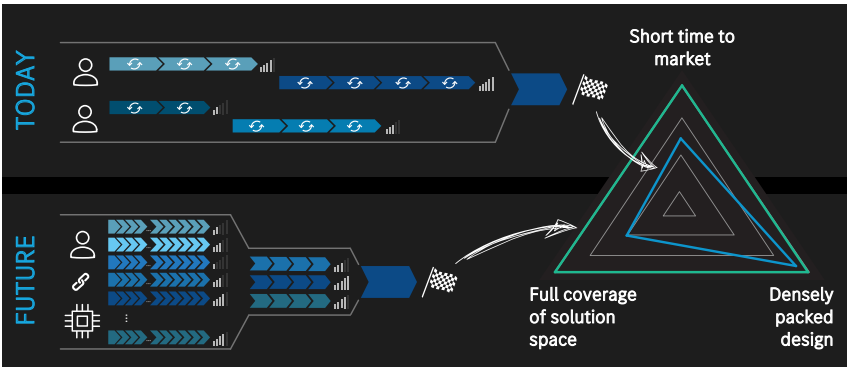

Fig. 1: Today's and tomorrow's concept design process

Engineering teams work out the design for a specific concept until the concept is discarded or finalized. New or changed requirements (e.g. new safety or emission regulations for the vehicle platform) lead to a very time-consuming step back: The concepts must be redesigned considering the new requirements. The main disadvantages are apparent: Limited exploration of the solution space and extended time to market. To solve this conflict, a new approach for the fully automated generation and optimization of arbitrary 3D design concepts of dedicated hybrid drivetrains has been developed and will be presented in this paper (refer Fig. 1 lower part). In general, the approach is suitable for pure electric drive units as well. The main benefit for design teams is the automation of the previously time-consuming steps and the capability to investigate multiple concepts in parallel using computing power. The time saved can be reinvested in a more detailed and densely packed design of the final variant. New requirements or concepts can be easily considered by re-running the process. Therefore, a holistic approach with a seamless and modular tool chain for generating 3D CAD models derived from layout stick diagrams is proposed.

2 Automated 3D design process

The main target of the automated 3D design process is to fully automate the concept design for complex, arbitrary drivetrain layouts with multiple power sources containing planetary gear sets, gear pair sets and clutches (in this paper subsequently referred to as “mixed structures”). Based on a given layout stick diagram including the gear ratios, a fully dimensioned 3D CAD design model considering the vehicle architecture is automatically generated. Furthermore, the approach will strive for (1) exploring the entire multi-dimensional solution space in a time-efficient manner and (2) finding the most densely packed configuration of every design variant with the electrical machine(s) as an integral part of the drivetrain.

2.1 Tool chain

The overall tool chain is represented in Fig. 2. The process is subdivided into five main modules (I to V) with three main inputs (A to C) and two design vector scope sets (DVS 1 and DVS 2). The input A for initialization (I) contains the specifications primarily for the chosen vehicle platform and the customer requirements (e.g. top speed). In Main Module II, a fully object-orientated and relation-based drivetrain model is created.

This model contains all gearbox components (= GBC), electrical machines (= EM), planetary gear sets (= PGS), gear pair sets (= GPS), multi-disc clutches (= MDC) and shaft sections. It also contains the components’ relations (e.g. meshing gear pair) as defined in the layout sketch, in this paper subsequently referred to as “stick diagram”, and its corresponding gear

ratios (input B). This drivetrain model is continuously updated with the data generated by subsequent modules and finally transferred to a CAD model.

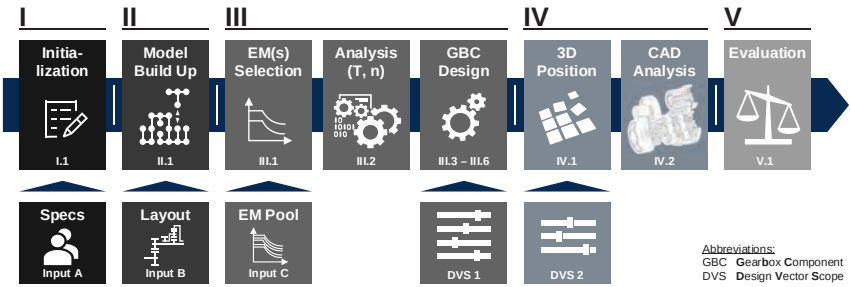

Fig. 2: Automated 3D design process

Main Module III focuses on the component design and will be discussed in detail in the subsequent Section 2.2. First and foremost, an algorithm selects the electrical machines under consideration of the existing modes to fulfill the customer requirements (e.g. top speed, maximum grade) from a given pool (Input C) of predesigned EMs. Then, the maximum torque and speed for every component are calculated for the full-load characteristic by deriving and solving the torque and speed equilibrium equations – the main input for the gearbox component design module. In this module, the dimensioning of all the included components is executed using commercial calculation programs as for example [1].

The next step (= IV) is to solve all remaining internal collisions between the different coaxial shaft packs (= CSPs) and to define the spatial position within the vehicle installation space, which will be discussed in detail in Chapter 3. At the end of this step the drivetrain concept variant is fully specified and ready for the automatic build up and analysis (e.g. collisions, mass) within the CAD system. The final step (V) is to evaluate the calculated variant using a multi-level KO- and multi-criteria analysis transforming these values into a final score – the cost function value.

Both the component design and the 3D positioning module have a wide range of possible variants to investigate; the solution space to explore is determined through design vector scopes 1 and 2. For exploring this multi-dimensional solution space in a resource-optimized manner, a superimposed tool architecture is required and will be introduced in Chapter 4.

2.2 Component design

The traditional component design features many iterative loops to find the most beneficial variant; non-feasible variants are discarded or even not considered using “best engineering judgement”. To automate these loops different design vectors within the scope are investigated by the solving algorithms discussed in Chapter 4. The expert knowledge is partly transferred to the process in consideration of the following major design rules:

- “Design from inside to outside”: Outer components inherit properties from inner ones
- “Restrict the solution space wherever and whenever possible”: Exclude non-feasible design variants as early as possible, but ensure to keep all feasible ones
- “Early action is better than later reaction”: Predict and prevent non-feasible configurations and collisions as early as possible

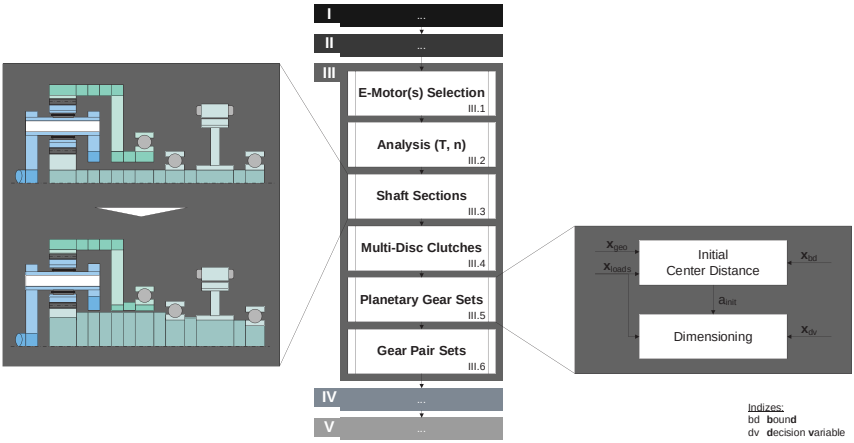

Fig. 3: Component design process

The component design process (refer Fig. 3) starts with selection of the electrical propulsion machines, as briefly described in the preceding section. These algorithms go beyond the scope of this paper. After this step, the speed-torque characteristics of all propulsion machines are ready to use. The analysis module calculates the maximum loads and speeds of every component for every detected mode type (e.g. hybrid parallel, power split) under consideration of the speed-torque characteristics of the previously selected EMs. The torque and speed equilibrium equations for every detected mode are therefore automatically derived as proposed by van Harselaar [2]. For every propulsion machine, all full load torque values are extracted by traversing the torque map with a discrete step width of $n_{step} = 100\ min^{-1}$. Solving the speed and torque equations for every extracted speed and torque data point delivers the corresponding

speed and torque for every gearbox component for the given data point. Data points, which exceed technical restrictions of one component are filtered out. This could happen, for example, if the calculated rotational speed of the 2nd electrical machine exceeds the maximum permissible value in a full electrical mode using two electrical machines for propulsion. The maximum speed and torque values for every component within the remaining data points are the main inputs for the load capacity-based calculations in the following steps.

The dimensioning process distinguishes between components with no design variants at all (shaft sections) and components (multi-disc clutches, planetary gear sets, gear pair sets) that have different design variants to choose from (e.g. number of discs and diameter). The shaft section dimensioning features an algorithm that derives a production- and assembly-ready stepped design in consideration of the maximum load for all solid and hollow shafts, represented schematically in Fig. 3 at the left. The calculated outer diameters of the shaft sections mark a lower geometrical threshold, the minimum inner diameter for their associated components. The component design modules for MDCs, PGSs and GPSs follow the same main scheme as shown by example in Fig. 3 for planetary gear sets. First and foremost, the initial center distance a_{init} is calculated in consideration of three crucial input vectors:

- $\mathbf{x}_{loads}$: Maximum loads for the component as calculated by the analysis module
- $\mathbf{x}_{geo}$: Geometry defined by preceding modules (e.g. sun shaft diameter)
- $\mathbf{x}_{bd}$: Technical bounds to be fulfilled (e.g. root and flank safety)

A load capacity-based minimum center distance is estimated using the equations proposed by Naunheimer et al. [3] with parameters taken from DIN 3990 [4] and ISO 6336 [5]. Geometrical constraints (e.g. minimum planetary gear bolt diameter) are also taken into account. The final initial center distance marks the lower threshold; a smaller center distance is technically not feasible and therefore not worth investigating. The subsequent final dimensioning receives a so-called design vector $\mathbf{x}_{dv}$ and the loads vector $\mathbf{x}_{loads}$. The design vector contains all the decision variables (e.g. helix angle, center distance delta) for the load capacity-based calculation of the respective variant. Determining the gear pair set dimensioning chronologically as the last step is done for a reason: The estimation of the initial center distance considers all outer diameters of the already designed components (e.g. EM, MDC and PGS) and is one main key for achieving a densely packed 3D design and will be discussed in detail in the next chapter.

3 Densely packed 3D concepts

One main target in the current drivetrain design as well as for this automated design approach is to strive for a densely packed, highly integrated design within the given vehicle installation space. The subsequently proposed algorithms are the enabler for densely packed 3D design concepts and EMs as an integral part with regard to the design rule “early action is better than later reaction”. The main contribution to this are a predictive collision analysis and classification and preventing strategies at the right step in the tool chain to achieve a collision-free, densely packed design. Subsequently, a distinction is made between collision types with a single-option solution and multi-option solutions.

3.1 Single-option-solvable constellations

The first type of collisions has a one-and-only solution, in this paper subsequently referred to as single-option-solvable constellations (= SOSC). These constellations usually occur between a gearbox component and a shaft section belonging to another coaxial shaft pack.

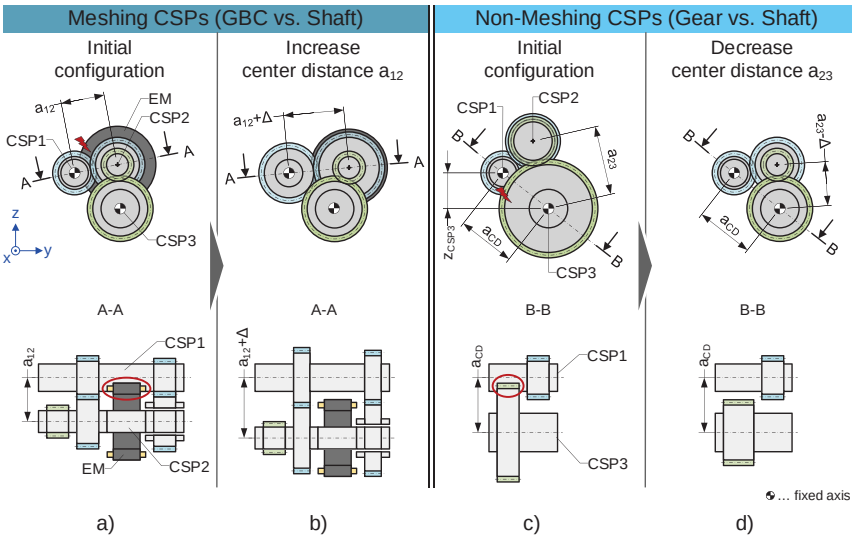

Fig. 4: Single-option-solvable constellations (= SOSC) for meshing and non-meshing coaxial shaft packs (= CSPs)

A typical collision constellation between two CSPs which have at least one meshing gear contact is shown in Fig. 4a. The EM located on CSP2 with a left and right adjacent gear collides with a shaft section from CSP1. The one and only option to solve this conflict is to increase the

center distance a_{12} between these two shaft packs as shown in Fig. 4b. This type of constellation is considered within the estimation of the initial center distance for all gear pair sets and is part of the generalized approach discussed in the subsequent Chapter 3.2.

Another typical collision constellation between two CSPs with no meshing gear pair connection is shown in Fig. 4c: The green-colored gear of CSP3 collides with a shaft section of shaft pack CSP1 – this spatial arrangement often occurs in front wheel-driven architectures between the final drive gear and shaft sections belonging to the gearbox input shaft. The center distance a_{CD} between CSP1 and CSP3 and the z-position z_{CSP3} of CSP3 is defined by the decision vector. Hence, the y-z-position of CSP1 and CSP3 is fixed. The one and only option to solve this conflict is through a reduction of the gear diameter by decreasing the respective center distance a_{23} as shown in Fig. 4d. Such constellations define an upper bound with regard to the predicting and preventing logic of the approach. Imagine the discussed gear being an immutable component like an EM; unfortunately there would be no option at all to solve this collision.

3.2 Multi-option-solvable constellations

In the previously discussed constellations, one of the collision partners is a shaft section. These constellations must be solved via increasing or limiting the respective center distance – there is no other valid option to solve these types of conflict. In contrast, constellations with multiple solving options, in this paper subsequently referred to as multi-option-solvable constellations (= MOSC), are discussed in this section.

Fig. 5a shows an example constellation for such a collision between two GBCs belonging to CSPs with at least one meshing gear pair set. There are three valid options to solve this conflict, compare Fig. 5b to 5d: (1) via an axial shift of the affected component on CSP1, (2) vice versa shifting the component on CSP2 or (3) increasing the center distance as long as no limit has been set by a SOSC (discussed in the preceding section). In this simple example, option 2 (= shift of the EM) should be preferred to option 1 (= shift of the MDC) due to the lower impact on the total axial transmission length – compare axial shifting value Δa_{CSP1} in Fig. 5b with Δa_{CSP2} in Fig. 5c. It is noteworthy that for more complex situations, a combination of axial shift and increasing the center distance is taken into account and will also be considered in the algorithms.

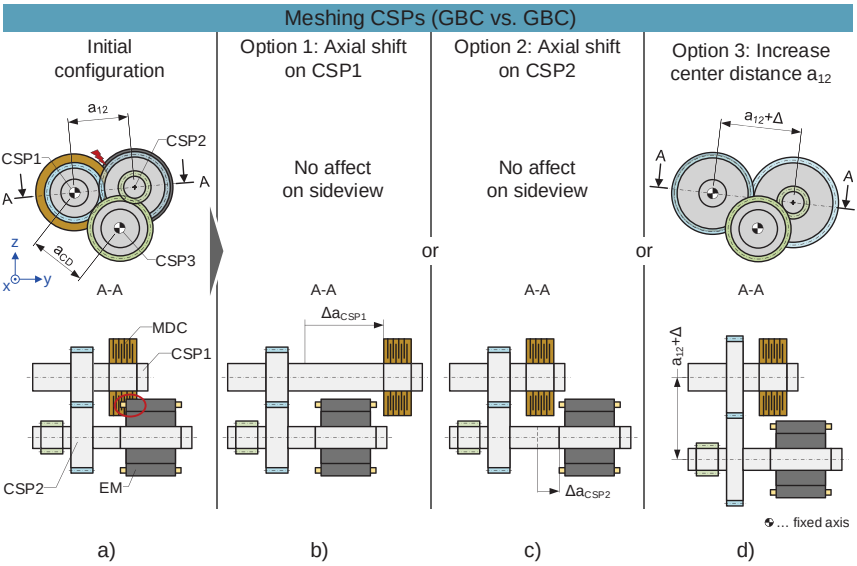

Fig. 5: Multi-option-solvable constellations (= MOSC) for meshing CSPs

For the automated prediction of all collision constellations between two meshing CSPs, thirteen generalized cases can be identified and their possible solutions defined and prioritized. Two example classifications are shown in Fig. 6.

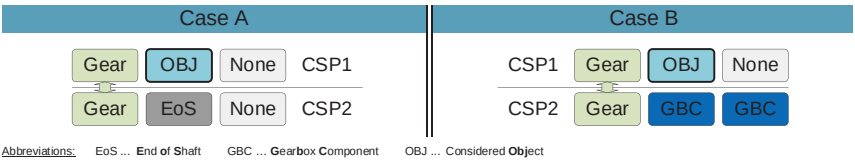

Fig. 6: Generalized collision classification for meshing CSPs

This classification takes advantage of the fact that a gear pair set defines a common axial position for their distinct adjacent components. The detailed deduction of all the cases goes beyond the scope of this paper and is described in detail by Nosch [6]. The decision regarding which option or even which combination of two options is the most beneficial for the distinctive variant can only be made after defining all geometrical parameters and is therefore a part of the gear pair set initial center distance calculation.

3.3 Multi-option-solvable constellations via rotational degree of freedom

A further but clearly different constellation often observed with off-axis EM layouts is shown in Fig. 7: An off-axis EM (= CSP5) meshes with an intermediate shaft (= CSP4), which meshes with a main shaft (= CSP1). In contrast to the prior constellations, an additional mechanism for solving the collision using the rotational degree of freedom (= DOF) exists.

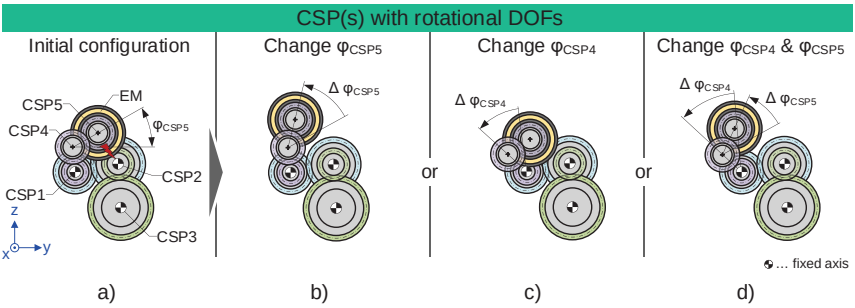

Fig. 7: Multi-option-solvable constellations via rotational degree of freedom

As CSP4 and CSP5 both possess a rotational DOF with respect to the axis of their meshing partner, the collision between EM and the green-colored gear can either be solved by a counter-clockwise rotation of one of the two CSPs (compare Fig. 7b and c) or by rotating both CSPs (see Fig. 7d). Due to the existence of many possible collision-free positions the angular position of these CSPs will become a part of the design vector.

3.4 Integration into the design process

The integration of the previously discussed different collision constellations into the tool chain is shown in Fig. 8. The collision prediction and case classification for every gearbox component is determined directly after the model build up in Main Module II. This generalized surrounding analysis is not dependent on any parameter set later, thus it can be performed once in this early stage of the tool chain. The initial center distance estimation for gear pair sets acquires the classification information as an input. The implemented algorithms decide for or against a center distance increase. One major input for these decision algorithms are the geometrical dimensions of the affected adjacent components, which are defined and are immutable in this step. Furthermore, the algorithms consider the information about any center distance limit due to restrictions from non-meshing constellations (refer Fig. 4d). In the next step, the axial positioning for all meshing CSPs is executed due to the classification and the decision from within the gear pair set dimensioning. Beyond this step, all meshing CSPs are collision-free.

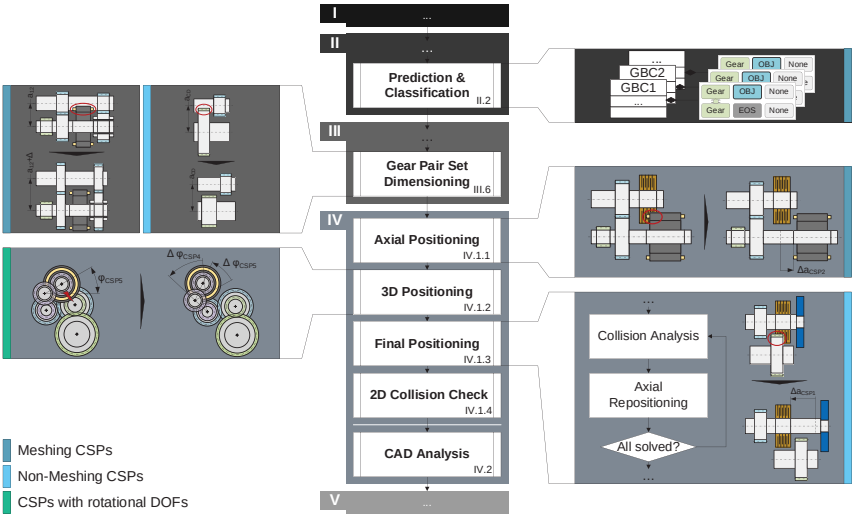

Fig. 8: Integration of the predicting and preventing algorithms into the design process

The subsequent step of 3D positioning calculates the spatial coordinates taking into account the distinct layout and the respective decision variables (e.g. the rotational DOF of an off-axis EM). In the final positioning step, all remaining collisions between non-meshing CSPs are solved via an iterative process: Detect a collision and solve via axial repositioning and repeating until the model is collision-free at all. A fast 2D-based collision check succeeds: This result is one major input for the control of the tool chain to decide if the variant is worth being investigated in detail in the CAD system, discussed in the following chapter.

4 Identification of the optimal design solution

To achieve the main goal of finding the global optimum within the given solution space in a resource-optimized manner, a logic choosing the decision variables in a smart manner is critical. Therefore, a superimposed modular tool architecture is proposed which connects the introduced modules. This architecture features three vertical layers: (1) the **MODEL** layer covering all the previously discussed main modules, (2) the **CONTROL** layer defining the sequential order including possible loops and executing pre- and post-processing of the inputs and outputs of the model layer and (3) the **SOLVER** layer featuring one or more distinct solving algorithms (e.g. an optimization approach) responsible for choosing the decision variables. This architecture provides a fast and easy opportunity to implement and investigate different

solving approaches. In the subsequent sections, three different control flows are presented by examples, their results will be discussed in Chapter 5.

4.1 Backtracking approach

First and foremost, a backtracking-based approach for exploring the full solution space in a discrete step manner is introduced. Backtracking is a problem-solving technique which performs a depth-first traversal through a variants tree and decides in constraint-based fashion after every node whether to traverse deeper. If the output of the current node hits a constraint threshold (also often referred to as KO criterion), the algorithm stops exploring the branches of this node and jumps to the adjacent node of the current level, see Stephens [7]. If in the drivetrain design problem, for example, the gear load capacity hits the root safety threshold, this variant will be discarded and another set of decision variables for this gear will be investigated.

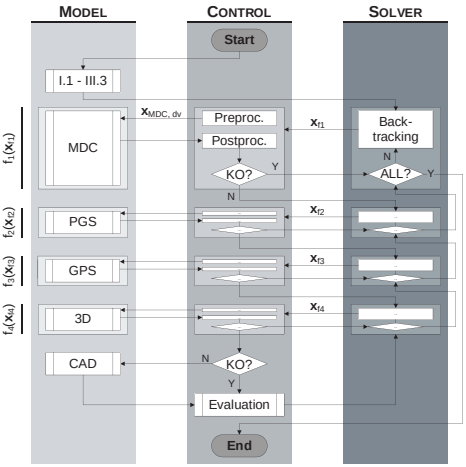

Fig. 9: Backtracking approach (= BTA)

The flow chart of the implemented **BACKTRACKING APPROACH** (= BTA) is shown in Fig. 9. The scope for the iterative approach is determined by the modules featuring decision variables: Component dimensioning and 3D positioning. Each one of these modules is connected to a dedicated backtracking solver taking all possible combinations of decision variables within the given range and discrete steps into account. The solver selects the next variant and hands over the respective design vector ($\mathbf{x}_{f1}$, $\mathbf{x}_{f2}$, $\mathbf{x}_{f3}$ or $\mathbf{x}_{f4}$) to the control layer; the preprocessing routine prepares and triggers the model layer. The post-processing routine evaluates the model results. If none of the KO criteria is hit, the backtracking solver for the subsequent

module is invoked. In the opposite case, one or more KO criteria are hit and the deep-first traversal is stopped – the next design vector variant for this level is chosen by the solver layer. The control flow is absolutely identical for all other affected modules. After passing the 3D module successfully, a final KO criteria check is performed, among others, based on the result of the 2D collision check (see Chapter 3.4). As long as the KO criteria threshold is not hit, a CAD model is created, analyzed and its results are evaluated in the final evaluation step. Generally speaking, the BTA offers a fully deterministic step-based exploration of the solution space. A rerun delivers the exact same results. Therefore, its main purpose is to validate the subsequently introduced optimization approaches and to investigate drivetrain layouts with low complexity and/or a manageable size of the solution space, as discussed in Chapter 5.1.

4.2 Optimization approaches

Due to the extensive number of decision variables, particularly in combination with complex drivetrain layouts, the usage of optimization approaches comes into focus to reduce calculation times. The tool chain introduced for deriving a drivetrain model can be interpreted as a black box model with a non-linear, non-convex, non-continuous and non-derivable behavior with mixed-integer multi-dimensional inputs featuring inequality constraints (= technical restrictions). This type of problem can be classified as a mixed-integer, nonlinear problem (= MINLP), as per Kallrath [8]. The generalized problem can be expressed as proposed by Belotti [9]:

$$\begin{cases} minimize & f(\boldsymbol{x}) & and\ f\colon \mathbb{R}^n \to \mathbb{R}, \\ subject\ to & c(\boldsymbol{x}) \leq 0 & and\ c\colon \mathbb{R}^n \to \mathbb{R}^m, \\ & \boldsymbol{x} \in X \subset \mathbb{R}^n, & \\ & \boldsymbol{x}_i \in \mathbb{Z}\ \forall\ i \in I \subseteq \{1, \dots, n\} & \end{cases} \tag{4-1}$$

Whereby the design vector **x** contains all the decision variables ─ discrete (e.g. number of clutch discs) and continuous ones (e.g. center distance delta) ─ for the defined model f(**x**). The model returns a floating point value; in this paper, subsequently referred to as cost function value (= CFV). The KO criteria (e.g. root safety, collisions) are part of the inequality constraints c(**x**).

An appropriate optimization algorithm for solving these problems must fulfill two crucial requirements: capability of solving a MINLP problem and searching globally for the optimum with regard to a high number of decision variables (up to 100). For the purpose of this paper the Py-BOBYQA algorithm developed by Powell [10] including further improvements, particularly for escaping local minima by using multiple restarts seeking globally for the optimum, proposed by Cartis et al. [11] will be used within the case studies in Chapter 5.

4.2.1 One-shot optimization approach

One obvious approach using optimization algorithms for this problem is to define the entire module scope containing decision variables as function f($\mathbf{x}_f$) to optimize. The flow chart of this **ONE-SHOT OPTIMIZATION APPROACH** (= OSOA) is shown in Fig. 10.

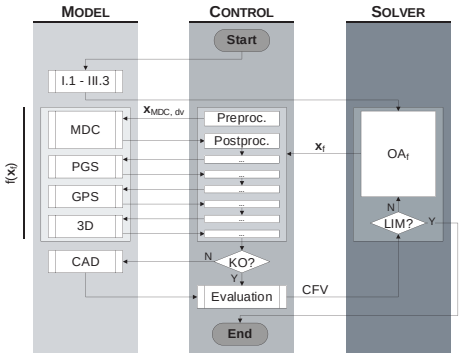

Fig. 10: One-shot optimization approach (= OSOA)

The optimization solver OA_f specifies the design vector $\mathbf{x}_f$ containing all decision variables for the entire scope. The control layer splits this vector into the respective parts for every module, e.g. $\mathbf{x}_{MDC, dv}$ for the MDC dimensioning containing e.g. the number of discs. In contrast to the BTA, the OSOA only executes one final KO criteria check at the end. This is because the optimization solver needs the total cost function value (= CFV) for determining the next variant to investigate. Similar to the BTA, only variants below the final KO criteria threshold are routed to the CAD system to reduce runtime; for details, refer to the case study in Chapter 5.2.

Before calculating the next variant, the solver checks if a limit is hit – either the maximum number of variants to calculate or the global optimum is found within its defined target area. In both cases, the run is terminated, otherwise the iterative process enters the next loop.

4.2.2 Single-nested optimization approach

Another possibility for the control flow is to split the scope into a dimensioning $f_1(\mathbf{x}_{f1})$ and a positioning $f_2(\mathbf{x}_{f2})$ problem; the corresponding flow chart for this **SINGLE-NESTED OPTIMIZATION APPROACH** (= SNOA) is shown in Fig. 11. The primary motivation is to find the most beneficial positioning variant for every dimensioning variant in particular for layouts with many spatial degrees of freedom (e.g. an off-axis EM with an intermediate shaft). The first optimization solver OA_{f1} defines the design vector $\mathbf{x}_{f1}$ only for the three dimensioning modules. After passing the GPS module the control layer starts a second optimization solver OA_{f2} which defines the design vector $\mathbf{x}_{f2}$ only containing the decision variables for the 3D positioning problem. This

inner optimizer OA_{f2} could be viewed as nested within the outer optimizer OA_{f1}. That means for every dimensioning design vector, an inner optimizer determines the most beneficial positioning variant. After reaching the limit, the outer optimizer OA_{f1} determines the next dimensioning variant and the process starts all over again.

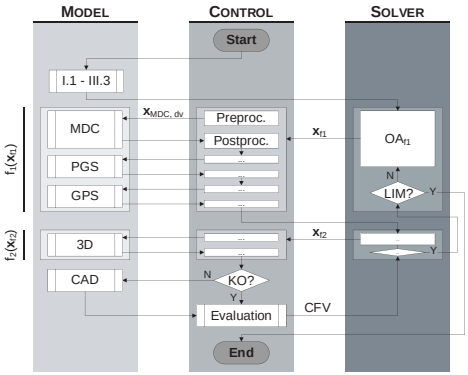

Fig. 11: Single-nested optimization approach (= SNOA)

4.3 Design variant tree traversal

All three discussed approaches perform a traversing through a variant tree with four levels (MDC, PGS, GPS and 3D) as shown in Fig. 12. The trees' shapes depends on the chosen calculation approach. The deterministic step-based exploration of the BTA leads to a tree with a predefined, finite number of nodes on every level due to the fixed step width for every parameter.

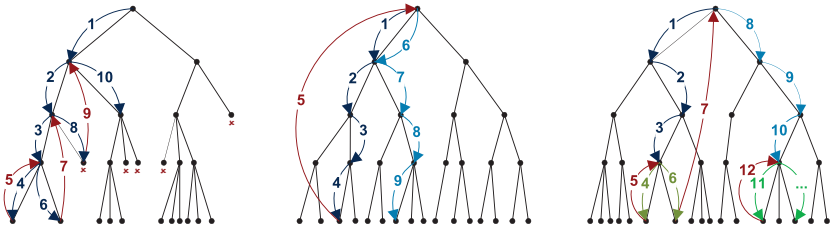

Fig. 12: Branch traversing comparison of the three different approaches

In contrast, the optimizer trees (OSOA and SNOA) theoretically feature an infinite number of nodes and paths, because the non-integer parameters can be chosen along continuous intervals by the optimizer. The algorithms traverse, however, only a finite number of chosen

paths to find the most beneficial variant – Fig. 12 displays exemplarily one possible shape for the one-shot optimization approach and another one for the single-nested-optimization approach. The BTA traverses the given tree with fixed step widths using a full-depth search from left to right. If a threshold is hit, as for example after step 8, the algorithm jumps up one level in this case due to the lack of a further node on this level. The OSOA choses a design vector determining the full path from top to bottom (step 1 to 4). Then, the algorithm jumps back to the top (step 5) and choses a second path from top to bottom of the tree (step 6 to 9). In comparison, the outer optimizer of the SNOA only choses a path from top to one level above the bottom (step 1 to 3). Then, the inner optimizer determines the bottom node (step 4), jumps one level up (step 5) and traverses to a second bottom node (step 6). In this simple example, the limit is hit, the algorithm jumps up to the top node (step 7) and the outer optimizer choses the next variant (step 8 to 10).

5 Case studies

To demonstrate the functionality and effectiveness of the automated design process for dedicated hybrid drivetrains, two different example layouts (see Fig. 13) will be discussed.

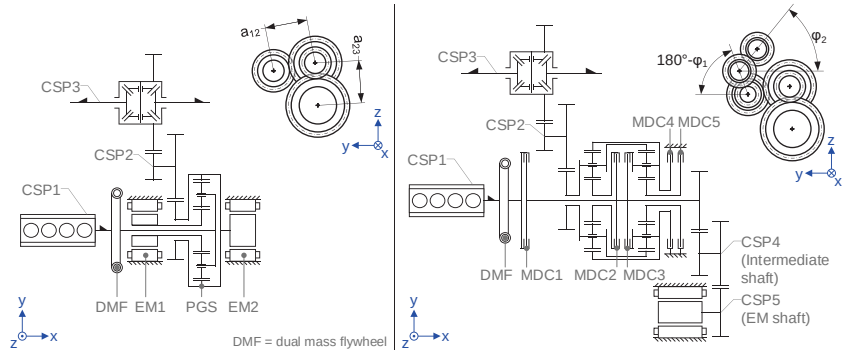

a) Layout A [12] b) Layout B [13]

Fig. 13: Case study layout stick diagrams

Layout A is a well-known series concept slightly modified as an example structure with less mechanical complexity featuring two electrical machines. Layout B is a concept with no series application yet featuring a slightly higher number of components. For the purpose of this paper, the on-axis EM is changed to an off-axis EM meshing with an intermediate shaft.

5.1 Layout A

The objective of this case study is to discuss the capability to handle multiple power sources and the interaction between center distances, transmission length and vehicle package. For this case study, the BTA is a valid option to use due to the fewer amount of decision variables. Due to the non-existence of spatial degrees of freedom the SNOA is not a suitable option for this type of layout – whereas, the OSOA is a valid option. Hence, the BTA and the OSOA will be compared. The equation for calculating the cost function value CFV_1 for this case study is defined as a weighted multi-criteria term:

$$CFV_1 = \underbrace{w_1 M_1(V_{3D,\,int}) + w_2 M_2(V_{3D,\,ext}) + w_3 M_3(l_{ax})}_{weighted\ multi-criteria\ term} \qquad with \quad \sum_{i=1}^{3} w_i = 1 \tag{5-1}$$

Wherein $M_i(\dots)$ is an evaluation function (e. g. a rising linear function), that calculates the sub score for the technical parameters: (1) the internal 3D collision volume $V_{3D,\,int}$, (2) the external 3D collision volume $V_{3D,\,ext}$ and (3) the axial transmission length l_{ax}. Each of these sub scores is multiplied with their respective weighting factor w_i and summed up to the total score CFV_1. The optimization target is to identify the lowest total score.

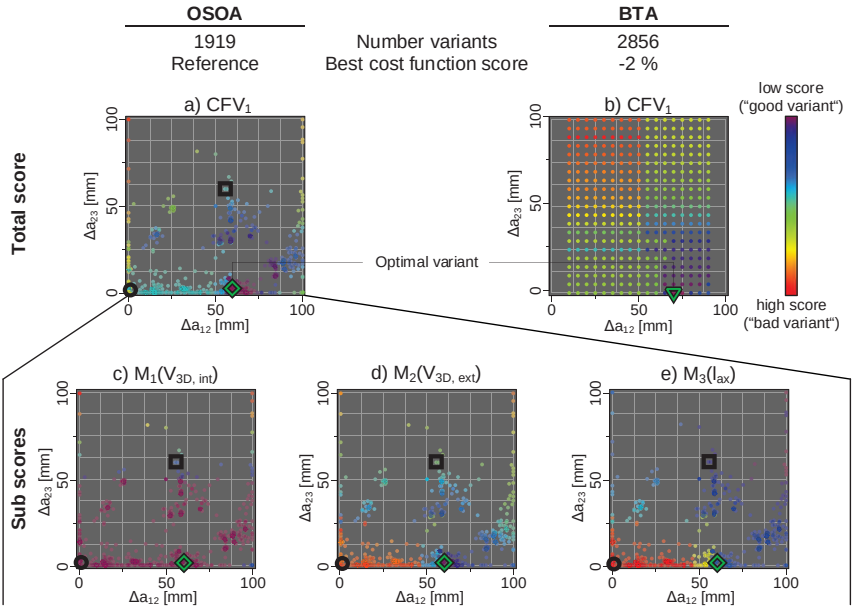

Fig. 14: Case study layout A – Cost function results

Fig. 14 shows the results for the total score CFV_1 in the first row, while the x- and y-axis display the delta from the initial value for both center distances. The most beneficial variant of the OSOA (= ◇) compared to the one of the BTA (= ▽) does not exactly represent the same design variant due to the discrete steps. The BTA overall point value is lower, the approach is only capable finding the optimum within its discrete raster, which does not necessarily represent the global optimum.

The sub scores for internal $M_1(V_{3D,\ int})$ and external collisions $M_2(V_{3D,\ ext})$ as well as the axial length $M_3(l_{ax})$ are shown in the lower part of Fig. 14. It can be seen that nearly every design variant in the lower half of the collision's internal figure is collision-free due to the introduced algorithms. Furthermore, it could be concluded that the overall length of the transmission is highly sensitive to the center distance a_{12} between CSP1 and CSP2 – a high axial length (= red-colored points) leads to a high external collision volume (= orange-colored points).

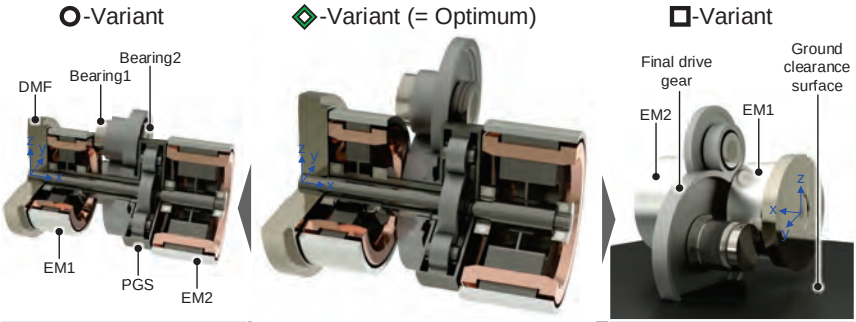

a_{12} ↓	Reference	a_{23} ↑
+10 %	Axial length: Reference	-3 %
+105 %	External collision volume: Reference	+16 %

Fig. 15: Layout A – CAD models for selected variants

The related CAD model of the optimum variant (= ◇) featuring the most beneficial balance between axial length and external collisions is shown in Fig. 15. Reducing the center distance a_{12} leads to a 10% higher axial length and as a result to more than a doubling of the external collision volume caused by a wider gap between EM1 and PGS to prevent the collision between Bearing1 and EM1 as well as between Bearing2 and PGS; refer to left variant (= O). In contrast, increasing the center distance a_{23} leads to a further overall axial length reduction by decreasing the gear width of the affected gear pair. From a collision perspective, this additional axial length reduction is not necessary. This variant fails miserably, however, with regard to the vehicle installation space; the final drive gear in particular vastly violates the ground clearance surface as shown by the variant on the right side (= □). By the way, the

series design of this layout solves the axial length package conflict by replacing the gear pair set between CSP1 to CSP2 with a chain drive. Thus, the gap between EM1 and PGS and consequently the axial length can even be further reduced.

To sum up: The OSOA as well as the BTA are capable of identifying the optimal solution for component dimensioning featuring a densely packed design lacking collisions within the given solution space. Furthermore, the optimization approach identifies the axis distance between CSP1 and CSP2 as the main contributor for reducing the axial length and for solving the package conflict.

5.2 Layout B

Compared to Layout A, this layout features a higher number of gearbox components and coaxial shaft packs. Therefore, a higher number of decision variables has to be considered to determine the optimum variant. For this case study, the OSOA is again a valid option to use. Only a small number of design vectors lead to a beneficial design; many design vectors lead to (a) exceeding of the maximum axial length due to a disadvantageous combination of decision variables or to (b) a position of the EM that causes collisions with other gearbox components and/or the vehicle installation space. The equation for calculating the cost function value CFV_2 for this case study adds a KO criteria term to the prior equation (5-1):

$$CFV_2 = \underbrace{K_1\left(A_{2D,\,int}\right) + K_2\left(A_{2D,\,ext}\right)}_{KO\ criteria\ term} + \underbrace{w_1 M_1\left(V_{3D,\,int}\right) + w_2 M_2\left(V_{3D,\,ext}\right) + w_3 M_3(l_{ax})}_{weighted\ multi-criteria\ term} \quad (5\text{-}2)$$

To save runtime, a fast 2D collision check is performed to detect the intersection area for internal collisions $A_{2D,\,int}$ and collisions $A_{2D,\,ext}$ between the gearbox and a simplified 2D installation space. This simplified 2D installation space is a superset of the far more complex 3D model which is used in the CAD analysis. The sub score for both killer criteria $A_{2D,\,int}$ and $A_{2D,\,ext}$ is calculated by using their respective evaluation function $K_i(\dots)$, a rising linear function. Only variants with a KO criteria term value below the KO criteria threshold are routed to the CAD system. Through this nearly 56% of all variants were classified as not worthy to investigate in detail and therefore filtered out in this run.

Fig. 16 shows the results for the cost function value total score CFV_2 in diagram a in the upper left corner, while the x- and y-axes show the rotational angle φ_2 for the EM shaft (= CSP5) and φ_1 for its intermediate shaft (= CSP4), respectively. The sub-score plots (diagram c and e) on the left side display the 2D collision scores $K_1(A_{2D,\,int})$ and $K_2(A_{2D,\,ext})$. The related 3D collision scores $M_1(V_{3D,\,int})$ and $M_2(V_{3D,\,ext})$ on the right side (diagram d and f) only contain the surviving variants worth being investigated in detail, e.g. the ▽- and □-variants have been filtered out due to their KO criteria term value above the threshold because of their high number

of internal or external collisions. As is frequently observed, a variant with fewer internal collisions (= high point value) has more external collisions and vice versa.

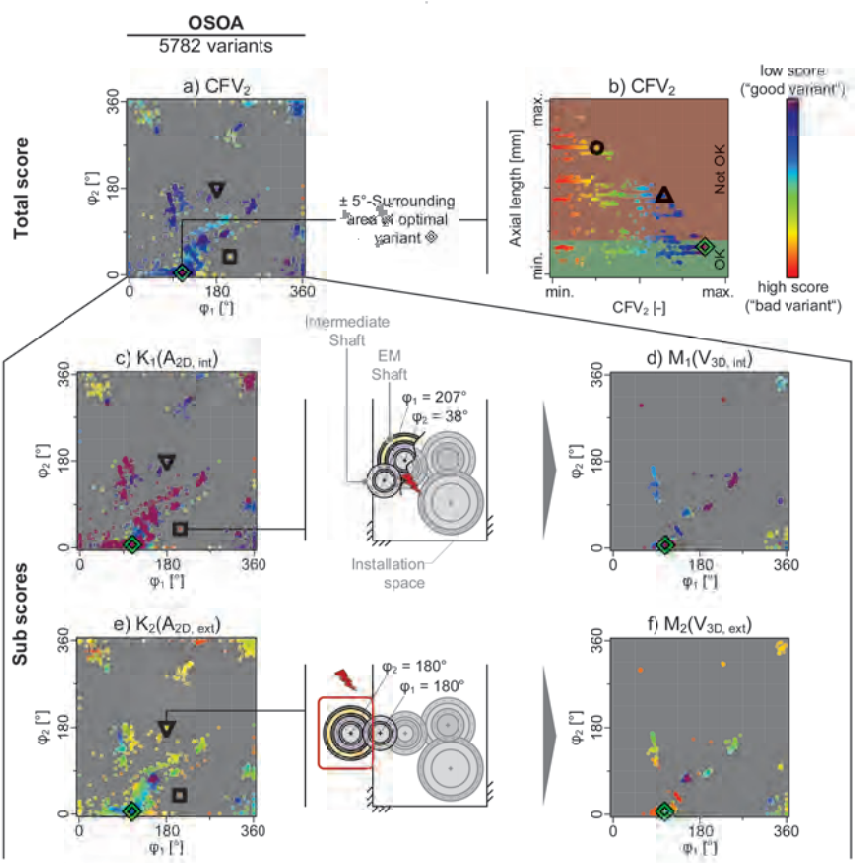

Fig. 16: Case study layout B – Cost function results for the one-shot optimization approach

The axial transmission length and the related cost function score are displayed in diagram b in the upper right corner for all variants featuring rotational angles $\varphi_{1/2} = \pm 5°$ with respect to the optimum variant. It can be seen that even with a given position of the EM, the axial length differs widely – the difference between shortest and longest variant is ca. 100 mm.

CAD models representing the three major steps for reducing the axial length are shown in Fig. 17. The non-nested variant (= O) features a comparatively high axial length due to a clutch package in which all of the clutches are positioned next to each other. The single-nested

variant (= △) achieves a significant length reduction by nesting the clutch pair in the middle (MDC2 and MDC3). The optimum variant (= ◇) features a design vector that additionally leads to a nesting of the other clutch pair (MDC4 and MDC5). Compared to the ○- and △-variants, the clutch diameters of the optimum variant are further increased to reduce the axial length. Furthermore, the optimum variant just passes the break-point for fulfilling the axial length criteria. Although it is within the solution space, reducing the axial length even further by increasing the axis distances is not beneficial, since it would lead to a larger collision volume with the ground clearance surface. Besides this, it is noteworthy that the position of the EM was chosen as close as possible to the ICE shaft pack to achieve a densely packed collision-free design.

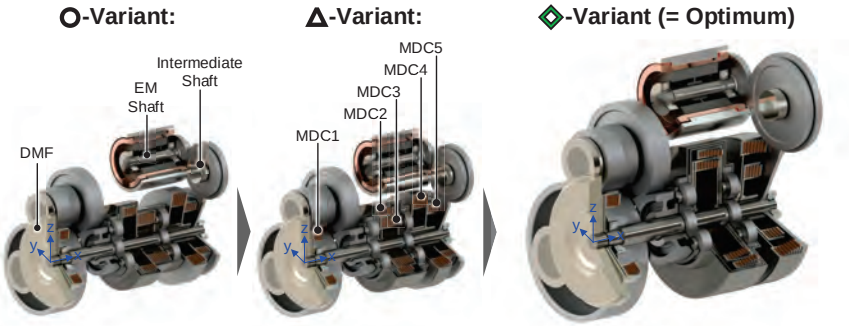

Non-nested	Single-nested	Dual-nested
+20 %	+10 %	Axial length: Reference
+113 %	+37 %	External collision volume: Reference

Fig. 17: Layout B – CAD models for selected variants

To sum up: The algorithms are capable of finding the most beneficial position for the EM within the vehicle installation space and simultaneously reducing the axial length by traversing the multi-dimensional solution space. By filtering out variants that are not valuable based on the 2D collision check, the calculation time can be cut nearly in half.

6 Summary and future works

Main challenges within the early drivetrain concept design process are the vast variety of different layouts/topologies as well as tight available installation space for the drivetrain components due to new regulations (e.g. safety and emission) and improved customer benefits (e.g. decreased turning circle) for the vehicle platform. Furthermore, the defined reduction of time to market initiates a target conflict with the conventional design approach. Hence, a new approach for the automated generation and optimization of 3D design concepts of dedicated hybrid drivetrains and electrical drive units is proposed to solve this conflict.

This holistic approach features a seamless and modular tool chain for computerized 3D CAD models which are derived from layout stick diagrams. The approach is capable of handling arbitrary topologies with multiple power sources containing planetary gear sets, gear pair sets and multi-disc clutches. One key element of this approach is an automated component dimensioning combined with a predictive collision analysis and consideration of the resulting geometrical constraints. Different types of collision are classified, predicted and prevented or solved within the tool chain at the right point to achieve a densely packed, collision-free and load capacity-fulfilling design within the given vehicle installation space.

Different superimposed control flows are proposed to solve this multi-dimensional design problem – benefiting from the modularity of the tool chain: a backtracking approach (= BTA) as fully deterministic and most suitable for less complex layouts with a low number of decision variables, a so-called one-shot optimization approach (= OSOA) as a multi-purpose tool for nearly all types of layout and any number of decision variables and a single-nested optimization approach (= SNOA) best used for layouts with a high number of spatial degrees of freedom and less dimensioning decision variables. To demonstrate the functionality of the approach, the results for two different topologies are discussed using the respectively best fitting control flow approach. Ultimately, the design engineer benefits from a tool identifying the most beneficial design variants in a short period of time. Changed or new requirements can be taken into account very easily and fast results primarily contribute to reducing time to market while at the same time exploring the full solution space.

Future work will focus on increasing the optimization scope, e.g. including the electrical machines, and an algorithm for component nesting will be presented. Furthermore, the performance and results of other optimization algorithms will be investigated.

Acknowledgements

The authors thank Dr. Wolfgang Elser and Martin Dengler for valuable discussions and their feedback. Furthermore, the authors thank all colleagues and students who contributed to the success of this project, especially Anubhav Kumar, Maximilian Schuckert, Paul Bannmüller and Philip Landreh.

References

[1] "KISSsoft Drivetrain Design Solutions", Product Flyer, KISSsoft AG, Bubikon 2021

[2] Van Harselaar, W.; Brouwer, M.; Hofman, T.: A Generic Transmission Model for Hybrid Electrical Drives. Bonn: VDI Dritev Conference 2018

[3] Naunheimer, H.; Bertsche, B.; Ryborz, J.; Novak, W.: Automotive Transmissions - Fundamentals, Selection, Design and Application (2nd Edition). 2011

[4] Tragfähigkeitsberechnung von Stirnrädern, DIN 3990, 1990.

[5] Calculation of load capacity of spur and helical gears, ISO 6336, 2006.

[6] Nosch, J.-L.: Automated Selection of Electric Motors within the Concept Design of dedicated Hybrid Transmissions. Master Thesis (unpublished). University of Stuttgart 2020

[7] Stephens, R.: Essential Algorithms: A Practical Approach to Computer Algorithms Using Python® and C#. Indianapolis: John Wiley & Sons 2019

[8] Kallrath, J.: Gemischt-ganzzahlige Optimierung: Modellierung in der Praxis (2. Auflage). Wiesbaden: Springer Spektrum 2013

[9] Belotti, P., et al.: Mixed-Integer Nonlinear Optimization. 2012

[10] Powell, M. J. D.: The BOBYQA Algorithm for bound constrainted optimization without derivatives. Technical Report University of Cambridge, Vol. 2009/NA06, 2009

[11] Cartis, C.; Fiala, J.; Marteau, B.; Roberts, L.: Improving the Flexibility and Robustness of Modelbased Derivative-Free Optimiziation Solvers. Technical Report University of Oxford, 2018

[12] Meisel, J.: An Analytic Foundation for the Toyota Prius THS-II Powertrain with a Comparison to a Strong Parallel Hybrid-Electric Powertrain. SAE Technical Paper Series, Vol. 2006-01-0666, 2006

[13] Schneider, E.; Müller, J.; Danzer, C.; Liebold, J.: High-performance dedicated hybrid transmission for future plug-in hybrid drives. China: CTI Symposium 2017

Frontloading for (Hybrid-) Transmission Integration at BMW

Andreas Ramsauer, AVL List GmbH, Graz, Austria;
Armin Pujari, BMW Group, München

Zusammenfassung

Steigende Komplexität der Fahrzeuge bei zunehmend kürzeren Entwicklungszyklen erfordert einen nachhaltigeren Gebrauch virtueller Testmethoden sowie Frontloading, um einen hinsichtlich Kosten und Ausnutzung der Ressourcen effizienten Entwicklungsprozess sicherzustellen. Durch die effizientere Nutzung realer Prototypen gewinnt die mathematische Beschreibung des subjektiven Empfindens zur Einbindung in die virtuelle Entwicklung weiter an Bedeutung. Ziel der vorgestellten Methode ist es, die Lücke zwischen der facettenreichen subjektiven Wahrnehmung und der automatisierten mathematischen Beschreibung mit neuen Ansätzen weiter zu schließen, wobei der Fokus auf der Bewertung verschiedenster Manöver hinsichtlich Komfort und Dynamik liegt. Da Gangschaltungen über die gezielte Ausprägung der Schaltcharakteristik und -harmonie eine Betonung des Fahrzeugcharakters über den gesamten Fahrbereich ermöglichen, werden diese in der vorliegenden Arbeit exemplarisch betrachtet. Anhand der Analyse zahlreicher Messdaten unterschiedlichster Fahrzeuge lassen sich bestimmte, immer wiederkehrende Schaltungs-Muster erkennen. Die Vielzahl der Muster ist systembedingt begrenzt, es zeigen sich dennoch deutlich unterschiedlich spürbare Schalt-Ausprägungen bei gleichartigen Getrieben. Mittels Merkmalsextraktion wird gezeigt, dass sich die Vielzahl der vorhandenen Messdaten in eine begrenzte Anzahl an Charaktertypen je Schaltungsart (z.B. Zug-Hochschaltung) einteilen lässt. Diese Typen bilden die Basis für eine möglichst detaillierte objektive Beschreibung des Schaltcharakters. Die Beschreibung des Charakters folgt dabei einem neuartigen Ansatz unter Berücksichtigung der Wechselwirkungen zwischen mehreren objektiven Kennwerten zusätzlich zu in sich abgeschlossenen, bekannten Metriken. Die Erfahrung zeigt, dass die Kombination einzelner Metriken und ihrer Ausprägung einen entscheidenden Einfluss auf das subjektive Empfinden haben. Die Vorteile der Methodik werden durch die Auswertung von Schaltkomfort und -dynamik des BMW Reihensechszylinder-Motors über das BMW-Produktsegment hinweg und durch die Durchführung einer Optimierung des Schaltverhaltens der BMW 4er-Reihe hinsichtlich der gewünschten Produktpositionierung aufgezeigt.

Abstract

Increased vehicle complexity paired with shorter development cycles demands a more intensive use of virtual test methods and frontloading to ensure an efficient development process in terms of costs and utilization of resources. Objective evaluation therefore becomes a central success factor, allowing the derivation of the goal of the current approach, which is to further close the gap between multi-faceted subjective perception and its automated mathematical description with new methods. The focus lies on the evaluation of different driving maneuvers with respect to comfort and dynamics. Since gearshifts allow the vehicle's character to be emphasized over the entire driving range by selectively shaping the gearshift characteristics and harmony, they are exemplarily studied in this paper. Based on the analysis of numerous measurements from various vehicles, certain recurring shift patterns can be identified based on engine speed and longitudinal acceleration. Although the number of patterns being limited by the system layout, shifting characteristics of similar transmissions can still be clearly felt in different ways. By means of feature extraction, the multitude of available measurement data is divided into a limited number of character types per shift type. Combining these types applying an innovative approach, considering the interactions between several objective parameters and their characteristics in addition to self-contained, known metrics, the level of detail in terms of an objective description of shift character raises significantly. The benefits of the methodology are showcased by evaluation of shift comfort and dynamics of the BMW inline 6-cylinder engine across the BMW product segment and by performing an optimization of the shift characteristics of the BMW 4-series with respect to the desired product positioning.

1 Introduction

During the 1990s, a typical OEMs vehicle portfolio consisted of sedans, hatchbacks and coupes propelled either by gasoline or diesel engines. Today, the automotive product portfolio has highly grown in diversity: Apart from newly emerged body styles such as SUVs and crossovers, the number of available propulsion technologies has increased. Powertrain electrification has brought battery and fuel cell electric vehicles as well as hybrid variants to the market. As of now, the main drivers for technology improvement are the reduction of emissions, automation of driving functions and enhanced connectivity of cars and the environment. These factors and constantly rising customer requirements result in an increased development effort, which makes OEMs focus on time to market and cost efficiency without sacrificing the true values of the brand. The resulting shortening of development times and reduction of physical prototype vehicles heralds an increased compulsion of shifting development steps with high maturity requirements, to early development phases with upstream test environments (e.g. chassis dyno, powertrain testbeds, component testbeds, …). BMWs quality claim towards driveability evaluation in automated transmissions must also be guaranteed under these boundary conditions. To achieve this, a detailed and validated objectification of driveability is the key to provide comparable results on different test environments and –above all– reflects the brand specific vehicle character of BMW.

Commercially available state of the art driveability assessment tools focus on individual objective criteria which do not fully leverage the information contained in vehicle related measurement data and do not allow for a detailed description of the multi-faceted subjective impression of driveability. The proposed methodology described in this paper, extends the capabilities of the AVL-DRIVE tool by refining the criteria calculation and the introduction of the superordinate metrics dynamics and comfort, allowing for the mathematical description of complex dependencies matching the subjective impression.

2 Proposed Methodology

The main weak point of the current evaluation methods is the blunt search for individual objective criteria within the measured signals of specific driving events without taking the entire signal progression into account and evaluating it afterwards. As shown in Fig. 1, the presented pattern-based method allows for a targeted calculation of parameters and objective criteria which correlate better with the subjective overall impression than the approaches in the state of the art. The assessment is based on the terms comfort and dynamics, forming the basis of the vehicle character assessment. By consideration of relevance zones for specific operating points, an overall character assessment is performed.

Fig. 1: State of the Art and Enhanced Methodology

The presented methodology is not limited to any specific driving events. However, as the progression of gear changes has a character-building effect on vehicles equipped with stepped transmissions, Power-On-Upshift events were the focus of this work. The following section presents and explains the patterns appearing in the measurement data. Then, the method used for pattern recognition is discussed before the alignment between measurement data and reference patterns is elaborated on. The section concludes with a description of multidimensional models for evaluating the attributes comfort and dynamics for Power-On-Upshifts.

2.1 Power-On-Upshift Patterns

Investigation of measurement data from multiple vehicles confirmed that Power-On-Upshift characteristics can be arranged within different classes – an assumption also consistent with the subjective impression. To achieve the desired behaviour, calibration engineers can make use of three control variables: engine torque M_1 and the torque of the off-going (M_{C1}) and oncoming (M_{C2}) clutches. The influence of each of these variables on the shift characteristic can be derived by investigation of the physical system containing the engine and vehicle inertia (J_{ENG} and J_{VEH}) and the ratios i_i of the corresponding gears depicted in Fig. 2.

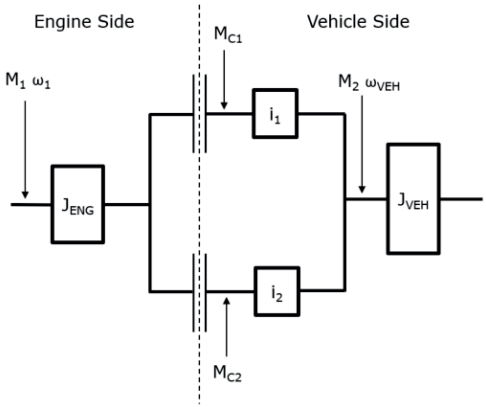

Momentum equilibrium:

Engine side:

$$M_1 - J_{ENG}\dot{\omega}_1 - M_{C1} - M_{C2} = 0$$

Vehicle side:

$$M_{C1}i_1 + M_{C2}i_2 - J_{VEH}\dot{\omega}_{VEH} = 0$$

Fig. 2: Generic Physical Shifting Sequence Model, adapted from

Given this explanation of the system dynamics, the possible clutch control strategies and thus the reference shift characteristics observed within the longitudinal acceleration signal of different measurements can be constructed, compare Fig. 3.

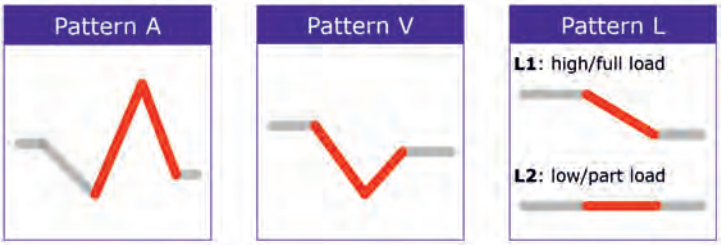

Fig. 3: Power-On-Upshift Patterns

2.2 Pattern Recognition

The aim to find predefined patterns within measured signals is referred to as time series classification task. In order to perform a classification, certain characteristics (i.e. features) have to be extracted from the data. Common features include extreme values, basic statistics of the distribution of the time series, correlations and many others, such as wavelets. Data from several hundred gearshift events were labelled according to the four types from Fig. 3 and used for training a classifier. Using brand-specific training data, emphasizes certain feature ranges, allowing for a detailed description of the different shift types. Based on statistical information, a reduced set of features is selected from the extracted ones aiming for the best distinction of the labelled time series within the training set. When forwarding a test instance to the model, this reduced set of features is calculated for the test data and then compared to the training data. According to the feature values, percentages of affiliation with each class are calculated as shown in Fig. 4.

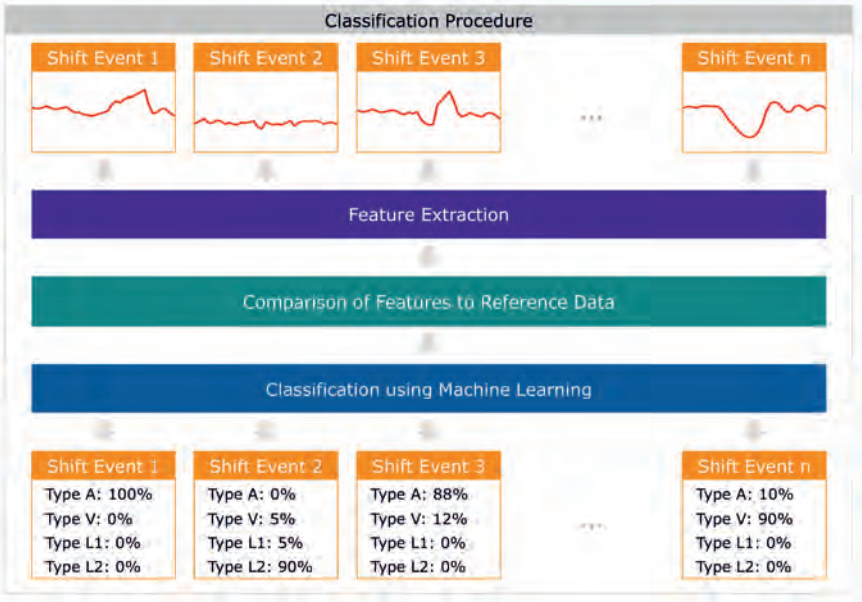

Fig. 4: Classification Procedure

2.3 Alignment with Reference Trajectories & Parameter Calculation

With the classification task completed, the measurement data can be aligned with piecewise linear reference characteristics for each shift type. The number of linear segments varies for each type – for type L1 shifts for example, three piecewise linear segments allow an objective representation of the subjective perception and are therefore used as a basis for the criteria calculation. Type L2 shifts comprise only one segment, type V shifts four segments and type A shifts are represented by five segments, compare Fig. 3. The individual segments are especially important when it comes to the calculation of gradients within the longitudinal acceleration signal: depending on the shift type, the number of gradients varies. For type L1 and L2 shifts only one gradient is assessed, type V shifts contain two characteristic gradients and type A shifts three. Besides the Acceleration Gradients, other objective criteria are calculated: Shock – Largest negative acceleration amplitude after engagement, Kick – First negative amplitude after Shock, Jerks – All negative amplitudes after engagement, Speed Decrease – Maximum negative engine speed gradient during ratio change, Shift Delay (Manual Gearshift Mode) – Delay between the shift request from the driver and start of ratio change, Traction Reduction – Vehicle speed loss during a gearshift, see Fig. 5 for the individual criteria of a type V shift for example.

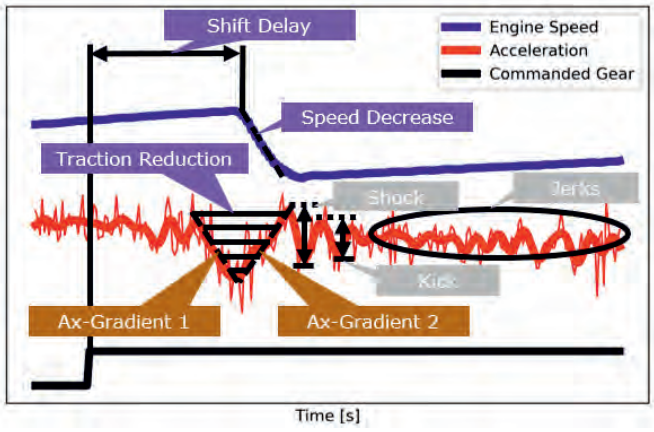

Fig. 5: Type V Shift: Individual Criteria

2.4 Multidimensional Dependencies – Comfort & Dynamics

The individual criteria in Fig. 5 are differently coloured in order to emphasize their relationship with the attributes comfort and dynamics. Whereas the gradients in the longitudinal acceleration are linked to the impression of both comfort and dynamics, the criteria depicted in grey correspond solely to the attribute comfort. Criteria shown in purple are dynamic related. For the exemplary type V shift shown in Fig. 5, the attributes dynamics and comfort describe the dependencies of five individual criteria. Each of these criteria ranges from 1-10 with one digit after the comma, resulting in 90 possible values. A mapping considering all combinations of the five individual criteria would require in 90^5(≈6000 million) data points to be labelled. On the one hand, this would require enormous amounts of data throughout the vast parameter space, on the other hand the calculation of the respective value for the attributes comfort and dynamics would come with the necessity of performing an extensive amount of correlation analyses between the subjective impression and the resulting objective rating. To overcome this challenge, the full factorial design consisting of 90^5 grid points is reduced to a fractional-factorial design using a DOE space filling approach . By maximizing the minimum distance between the DOE design points, good coverage of the design space is achieved. Fig. 6 showcases a space filling design for two exemplary criteria c_1 and c_2.

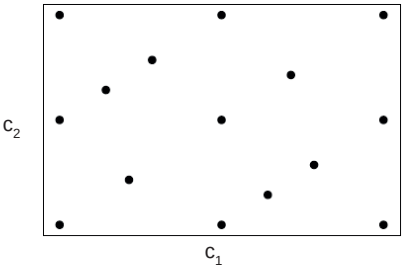

Fig. 6: Space Filling Design

The DOE methodology allows for offline training of the models (one for each attribute) with data from multiple measurements. By following an iterative process of model generation, subjective evaluation and correlation analyses, the final mappings between the individual criteria ratings and the attributes dynamics and comfort are obtained.

2.5 Relevance Weighting of Operating Points & Overall Shift Character

To quantify the overall vehicle characteristics, the ratings of each operating point are condensed into one value for each of the two attributes - comfort and dynamics. The procedure is based on a weighted mean, where the weights of the operating points are determined based on the influence of the operating points on the overall character from a customer's point of view. For the attribute dynamics, this is not necessarily linked to the occurrence within daily driving, compare Fig. 7. With the concept of relevance zones, the ratings of individual operating points (and the respective criteria shown in Fig. 5) are condensed into the overall character rating, allowing for comparison of vehicles at a high level.

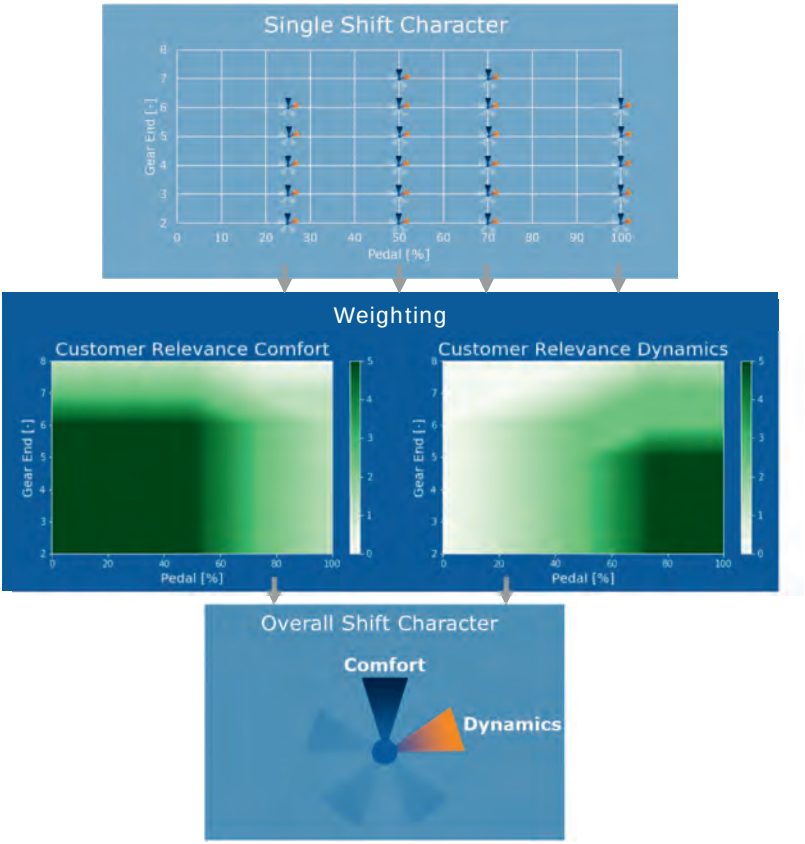

Fig. 7: Relevance Weighting & Overall Shift Character

3 Showcases

3.1 BMW 6-cylinder engine application S-Sport Mode

With the increased number of vehicle variants comes the necessity for adequate product positioning. Over the entire vehicle range, BMW follows the philosophy of a driveability character portfolio based on the experience of dynamics and comfort. During development, the driveability character of each vehicle is shaped according to the class affiliation (e.g. luxury vehicles to the top left in Fig. 8).

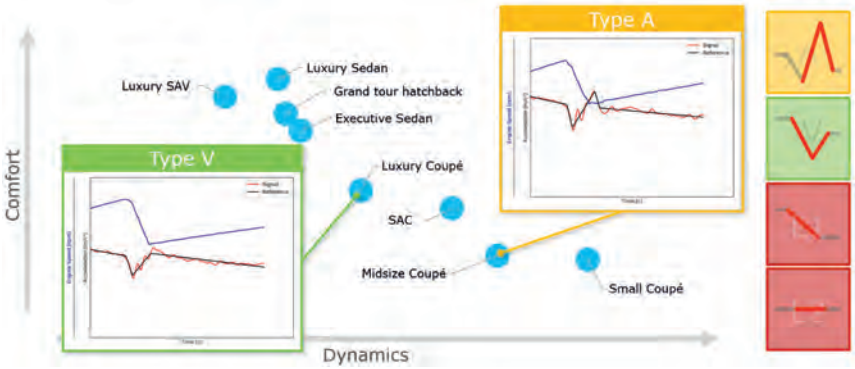

Fig. 8: BMW inline 6-cylinder Engine - Comfort & Dynamics S-Sport Driving Mode

BMWs inline 6-cylinder engine is mated with an 8-speed automatic transmission, the powertrain ensures a setup for pure driving pleasure. Besides giving an overall impression of the driving behavior of vehicles equipped with the BMW inline 6-cylinder engine with transmission set in Sports S mode, Fig. 8 shows two exemplary shift events of a midsize and a luxury coupé. The highlighted upshift from the luxury coupé can be classified as a type V shift with adequate dynamics and balanced comfort. The midsize coupé in comparison is targeted towards more sportiveness by steepening the two gradients adjacent to the V-shaped acceleration phase. Additionally, the overshoot in the longitudinal acceleration (assessed within the Shock criterion) is increased in comparison to the luxury coupé, resulting in a type A shift behavior. Overall, Fig. 8 shows BMWs successful efforts in adjusting the engine's characteristics according to the vehicle class.

3.2 BMW 4 Series S-Sport Mode: Comparison of Performance Levels

Within the 4-series family, BMW offers various engine options. Gasoline propelled vehicles come with either 4- (base & mid performance level) or 6-cylinder engines (high and top performance level). Depending on the engine, balancing of the attributes comfort and dynamics is required for adequate positioning in the market. Fig. 9 shows the procedure of balancing these attributes during the development process. The initial state of the mid performance level is targeted more towards high comfort and low dynamics when compared to the base level, which is expressed by the type V shifts for low gears and high pedal positions. However, for adequate market positioning, the mid performance level is required to deliver an increased dynamic impression with slightly reduced comfort when compared to the base model. To achieve this, the shift types of the final calibration of the mid performance level are approximated towards the characteristics of the high-performance class, showing type A behavior for high pedal positions and low gears. By relying on the criteria derived in Fig. 5, the positioning in terms of comfort and dynamics can be expressed based on objective metrics allowing for reproducible and unambiguous target setting.

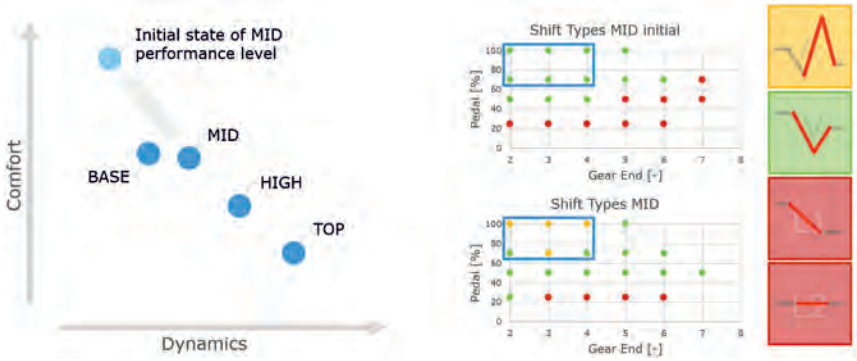

Fig. 9: BMW 4-Series Performance Levels

4 Outlook

The transmission as a central component for torque coordination – especially in P1- and P2-parallel hybrid concepts – needs a high effort regarding adjustment and validation. An increase of automatization raises the efficiency in development.

Basic premises are:

- Enablement of test bed hardware and software.

  The BMW group invested for the last couple of years in modern, highly dynamic test beds. With good models of vehicle and tires it is possible to simulate realistic longitudinal acceleration in dynamic maneuvers, like gear shifting in automatic transmissions. The test bed capacity and the precision of the simulation models gets continuously improved in the virtualization program at BMW Group.

- Automated driving manoeuvres on a test bed

  The different departments in powertrain development have different requirements on driving maneuvers for application and validation driven on test roads. These vary from a simple 0 to 100 km/h acceleration to complex skidding turns or drives on surfaces with alternating frictions. All basic maneuvers can already be driven freely and automatically on the test bench. This saves time in coordination due to the 24/7 use and enables working with fewer test vehicles. Due to the further automation of special maneuvers, additional expensive trials or risky driving maneuvers can be substituted by the test bench.

- Correlation between road and test bed

  Accurate comparison between road and test bench measurements is mandatory to avoid artificial errors in coordination or protection. All automated maneuvers are verified by a match before use. Simulated vehicle acceleration plays a special role here, as it is the central factor for objective assessment of comfort and dynamics. Comparisons between road and test bed measurements show very good consistency with good tire and vehicle simulations. In addition to the direct comparison of the measurements, the small deviations in AVL-DRIVE evaluations also confirm the correct transferability of driving maneuvers to the test bench.

- Objectified maneuver evaluation

  For the processing of driving and comfort issues on the test bench, objectification is a central component. There are maneuvers with easily measurable, objective criteria,

such as a 0-100km/h acceleration or the response time after a load addition. There are quantitative targets for such maneuvers at the BMW Group. Comfort issues are much harder to assess. Objectification tools such as AVL-DRIVE are suitable for this purpose. This means that gearshift events and start-up processes with automatic transmissions can also be evaluated. Also, this topic is being continuously further developed in order to be able to drive and evaluate driving maneuvers effectively on the test bench. In the context of this article, it was described how sporty gearshift events with specific BMW characteristics can be objectified in the shifting sequence.

5 Summary

Future mobility concepts, future emission regulations in addition to future customer requirements, present new challenges and lead to more complex powertrain layouts. In order to handle the increasing complexity of hybrid powertrains, the development process must be adapted accordingly – meaning that development steps with high maturity requirements need to be shifted to early development phases with upstream test environments. This change is accompanied by the challenge of transferring the subjective perception by the driver to the increasingly virtual development and testing environment. The need for objective metrics - in addition to the enhancement of the test bench landscape - represents one of the key elements in a successful transformation of the development process. The challenge for objective evaluation is to offer a uniform methodology for all relevant test environments (road tests, test beds and simulation models). On the one hand, the evaluation must deliver consistent results between all environments in order to be able to establish an efficient development process with a high level of automation. On the other hand, the objective evaluation must reflect the subjective perception of the driver as precisely as possible in order to create a high level of acceptance among users (engineers). Against this background, the existing evaluation approaches at AVL - starting with shift quality - were fundamentally revised to offer a methodology that is as detailed as possible, easy to understand, and based on the subjective assessment. The analysis and classification of the individual AVL-DRIVE criteria into the two central evaluation attributes - comfort and dynamics presented in this paper, allows both an evaluation of individual gearshift events and the evaluation of a large number of gearshifts over the entire speed and load range and thus the characterization of a vehicle. The differentiated view opens the way to combine the global product view with the engineer's view of individual events/causes. The new evaluation methodology makes it possible to position the large number of product and drive variants in the market according to their product orientation and

to derive (quality) target values for development in order to ensure the highest customer satisfaction time and brand experience in an efficient development process.

The upgrading of the test bench landscape already allows BMW to shift a large proportion of the driving maneuvers for validating shift quality from the road to the test bench. Future challenges lie in extending the presented methodology for objective evaluation to other driving maneuvers and shift types, integrating further evaluation attributes in order to ultimately draw as holistic an evaluation picture of the vehicle as possible. Objective evaluation thereby not only covers comfort/dynamic related issues, but also includes a second dimension in the form of strategy topics, particularly with the hybridization of the powertrain, topics such as operating strategy, are becoming increasingly important in addition to shift strategy and must be taken into account in the development process. While an evaluation of the basic shift characteristics is already possible today with AVL SPA, an evaluation of the dynamic adaptation of the shift points or operating strategy based on the individual driving styles of the customers as well as the respective route characteristics is significantly more complex and challenging. However, since strategy topics have a decisive influence on the quality and brand experience in addition to comfort and dynamics, AVL is working on a tool-based objectification of such strategy topics with the VIORE product.

With the overall detailed objective evaluation of comfort, dynamics and strategy, the full potential of an increasingly virtualized development process in an increasingly complex drivetrain landscape can ultimately be realized.

References

[1] AVL List GmbH, AVL-DRIVE Product Guide, 2020.

[2] R. Fischer, F. Kücükay, G. Jürgens and B. Pollak, Das Getriebebuch, Wiesbaden: Springer Vieweg, 2016.

[3] M. Johnson, L. M. Moore and D. Ylvisaker, "Minimax and maximin distance designs," *Journal of Statistical Planning and Inference,* vol. 26, no. 2, pp. 131-148, 1990.

Power to the Wheels – Challenges and Benefits of Electrified AWD for EVs and Hybrid vehicles

Simon Kaimer,
Magna Powertrain GmbH & Co. KG, Lannach, Austria

Since the 1950s, all-wheel drive technology has evolved from a traction aid to a means for greatly improved driving dynamics, including torque vectoring. In the future, AWD electrification enables further improved controllability and eliminates any additional fuel consumption from mechanical losses. But which e-drive axle technology is favorable in terms of driving dynamics and efficiency? Magna Powertrain has compared four different axle drives with torque vectoring function to answer this question.

Electrification – challenge and opportunity

There is a consensus that future CO_2 targets and local requirements of zero-emission driving require powertrain electrification. But electrification or hybridization on many different scales leads to a huge variety of drivetrain configurations, due to the combination of internal combustion engine and electric motors, possibly via two axles.

In order to make this diversity manageable, Magna has developed a modular system of ‘building blocks’ that allows variants to be based on common standard components. In addition to lower costs for the OEM, this approach allows for offering end customer-specific variants at manageable costs. Another advantage is that innovation at building block level is immediately available to all variants.

However, electrification is not just about reducing emissions; it can also help improve drivability, active safety and performance. Electric motors can be controlled easier and more precisely than internal combustion engines. And the peak power of e-motors, being instantly available, allows for very effectively and accurately controlling lateral dynamics.

AWD and torque vectoring history

Magna has a long history of developing and producing AWD and 4WD systems, on its own and in cooperation with several renowned OEMs. Originally being an aid for more traction, the technology has evolved to systems that enable substantial longitudinal and lateral dynamic improvements and improved active safety.

In 1959, former Steyr-Puch started production of the ‘Haflinger’, an off-road vehicle whose main task was off-road capacity through improved traction. Transverse dynamics via longitudinal or lateral distribution of torque were not in focus, fuel efficiency not too much either. The Mercedes G-Class, manufactured by Steyr-Daimler-Puch and Magna Steyr from 1979, represented one step forward: Although it was also consistently designed for off-road use, for the first time a further focus was placed on lateral dynamics in order to improve driving safety on the road. In 1987, Mercedes-Benz launched the W124, with the 4Matic all-wheel drive system developed by Magna Steyr. Similar to the G-Class, a mechanical center differential was used to split drive torque between the two driven axles.

From 2003 on, the BMW X3 was manufactured at Magna Steyr. A controlled multi-plate clutch made it possible to vary axle torque from 100 percent on the rear axle up to a 50:50 distribution. This allowed for basic torque vectoring by distributing torque longitudinally and improved drivetrain efficiency.

In 2016, with the introduction of an additional drivetrain decoupling, Audi´s quattro-ultra system enabled fuel consumption values close to a front-wheel drive, utilizing a Magna clutch and rear axle module. Beside that, the quattro-ultra system also demonstrates that modern all-wheel drive systems require a lot of system integration know-how to exploit expected state-of-the-art drivability.

The next step: electrified all-wheel drive systems

Electrification enables all-wheel drive systems with further improved longitudinal and lateral dynamics through individual torque control of both propulsion sources on front and rear axle as well as, depending on the degree of electrification, significant fuel consumption improvements. Key differences to conventional all-wheel drive systems are the elimination of the longitudinal propeller shaft and hypoids with related drag losses.

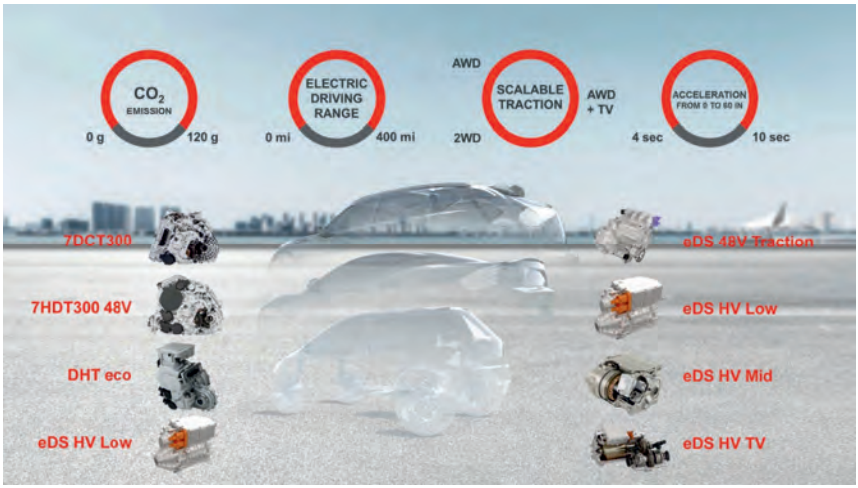

Fig. 1: Magna hybrid transmissions and e-axle drives overview

Magna Powertrain has a portfolio of hybrid transmissions and axle drives to build differently scaled, electrified powertrain architectures, Fig. 1. The axle drives are compatible with BEV usage. For example, even a 48 V hybrid in P2.5/P4 setup with mere 2x25 kW added power improves longitudinal and to some extent lateral dynamics. High voltage ‘mid’ and ‘high’ axle drives will improve dynamics and CO_2 reduction further, the high voltage ‘TV’ drive allowing for active torque vectoring between the rear wheels.

In principle, there are different ways to provide a torque vectoring function. The question is: Which one can offer the best combination of lateral dynamics, complexity, cost and energy consumption?

Evaluating different torque vectoring concepts

Magna Powertrain went into a detailed comparison to evaluate four different axle drive system architectures with mechanical and electric torque vectoring.

The comparison base was an electrified axle with a simple differential (standard eDrive). It is the benchmark in terms of lowest possible losses due to clutches etc. as well as low weight and low costs. Here, the torque vectoring potential is obviously limited to longitudinal distribution between front and rear axle.

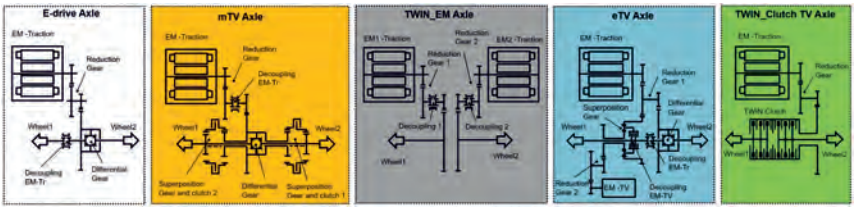

Fig. 2: Five rear axle units compared in the analysis, the colored variants including active torque vectoring systems

Differing from the ‘standard eDrive’, the four architectures described below each feature a lateral torque vectoring function that enables active torque distribution between the rear wheels, Fig. 2. In each case, the target was torque vectoring capacity of 1800 Nm between the wheels. In the illustrations for each solution, the lateral torque distribution is represented on the y-axis, the longitudinal torque or drive torque on the x-axis respectively. The bold lines envelope the lateral torque capacity that is available throughout the whole range of longitudinal drive torque.

mTV

As can be seen in Fig. 3, the mechanical torque vectoring solution is characterized by constant availability of lateral torque, being fully independent from drive torque. A speed difference of 12 % can be imposed on the left or right wheel, which is available at constant speed as well as under full load. This solution offers the full benefit of torque vectoring but is relatively complex. It comes with relevant drag losses in the clutches, otherwise shows good response times, representing state-of-the-art clutch technology.

Twin-EM

The ‘opposite’ concept to mTV includes two wheel-individual electric motors that enable adjusting wheel torque directly. Again, a difference of 1800 Nm can be achieved, however only up to about 60 percent of the maximum drive torque. That is because when approaching maximum load, little or no additional left torque is left for lateral distribution. This is no problem at low to moderate torque requirements. In very dynamic situations however, this means that the torque vectoring capacity is not constant, resulting in poor predictability. For example, torque will be limited at the point where you are most likely to accelerate – at the exit of a corner. In theory, this could be compensated by overdimensioning the e-machines, but that

would conflict with costs, weight and package – and thus efficiency. Generally, this solution needs more electrical power, and a decoupling device is required to avoid drag losses.

eTV

The eTV drive type, like the mTV, generates the torque difference by raising the effective value above the nominal torque of the single e-machine. Here, this is not done mechanically but using an additional e-machine as a servo motor. Besides full torque vectoring capability over the entire longitudinal torque range, eTV needs no clutch and lateral torque distribution can be controlled very precisely and responsively. On the downside, there is more complexity due to the e-machines and power electronics, a decoupling element is also required and the package is relatively large.

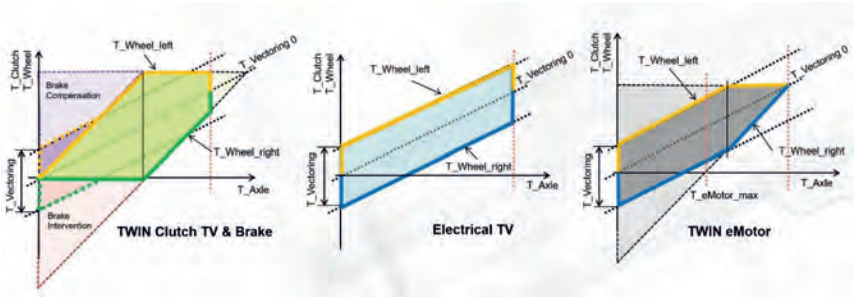

Fig. 3: Lateral torque comparison of Twin-Clutch TV, eTV and Twin-EM (the mTV result corresponds to eTV)

Twin-Clutch-TV

After all, Magna looked at the Twin-Clutch TV, representing the best compromise in this comparison, as it turned out, Fig. 4. Active torque vectoring is achieved by closing one of the two clutches while the other is partially or fully opened. Here too, the full torque vectoring capacity is available, albeit with limitations at very low and very high drive torques. Compared to Twin-EM however, this restriction is a small one. The little low-range restriction is uncritical, because brake intervention is appropriate at low loads to substitute the system functionality, like at constant speed driving through a bend. In the medium an upper range, available lateral torque distribution exceeds all other examples shown above.

The clutches may generate certain drag losses and system integration on the software level is challenging. The benefits prevail however: a disconnect function is available by design.

Provided that torque and brake interventions are integrated, torque vectoring is available in any driving situation up to near maximum torque. Energy consumption in WLTP is low. After all, the system is clearly superior in terms of mechanical complexity, package and costs.

	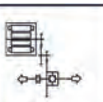 E_Drive	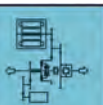 eTV	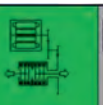 TWIN_TV	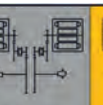 TWIN_EM	 mTV
Torque Vectoring Capability	n/a	++	+	o	++
TV Response time	n/a	+	o	+	o
Dynamic driving manoeuvre (representative – shown in simulation)	--	++	++	o	++
Power Consumption WLTC (RA decoupled)	++	+	+	o	--
Power Consumption Handling Track (TV active)	n/a	+	-	++	--
System drag loss (TV passive)	++	-	+	o	--
ABS/ ESP compatibility	o	--	o	-	o
Functional Safety	o	--	-	-	--
System Complexity	++	--	+	o	-
Package	++	--	+	--	-
Costs	++	-	+	--	o

Fig. 4: Comparison results overview

Summary

‘Classic’ all-wheel drive systems were primarily used to improve traction, for example off-road or in poor friction conditions such as snow. Through the last decades, major advances have been made in reducing drag losses and with regard to improving lateral vehicle dynamics. Yet, even latest technology is on cost of fuel consumption, if only little.

Electrification eliminates the mechanical longitudinal connection and adds new dynamic options through independent operation of the front and rear wheel drive units, notably much improved lateral dynamics. With regard to CO_2, electrified all-wheel drive systems offer all the advantages of hybridization or electrification, and a high degree of flexibility in designing the drivetrain to suit specific brands and customers.

Magna Powertrain has compared four electrified axle drives with torque vectoring function, evaluating them in terms of longitudinal and lateral dynamics, fuel consumption and cost. The best solution proved to be the Twin Clutch TV module with one electric machine and two clutches. It combines full torque vectoring capability in all driving situations with low fuel consumption in the WLTP. The solution also reflects the progress being made in terms of system integration: Mastering the functional blending of torque and brake interventions is essential indeed, but in turn allows for lowest mechanical complexity and thus cost.

TREMEC HYbrid DRive Axle - HYDRA

Hybridization enables RWD dynamics in a FWD car

Ir. **Jannick De Landtsheere**, TREMEC, Zedelgem, Belgium

Abstract

Analyzing the options for hybridization of fun-to-drive, performance-oriented vehicles, TREMEC has identified that electrifying the main vehicle transmission is not always possible or favourable. Some vehicles benefit more from a hybridized axle, resulting in improved performance, highly efficient electric driving, and enhanced vehicle dynamics. A hybrid axle concept is realized that combines a power dense electric motor with a mechanical on-demand torque vectoring AWD system, for which simulations show that performance and fun-to-drive are stepped up significantly compared to pure ICE powered vehicles on the market today. Initially designed as an AWD+P4 axle for FWD platforms, architectural derivatives are possible for RWD+P3 applications or pure e-axles.

TREMEC introduction

TREMEC is a global transmission and driveline solutions company, headquartered in Queretaro, Mexico, and with facilities in Wixom, Michigan (US) and Zedelgem, Belgium (EU). Historically a leading manufacturer in the North American market for manual transmissions for high performance passenger cars and commercial vehicles, TREMEC has established itself as number one full-system supplier for high performance DCT's in recent years, with applications in C8 Corvette, Ford Mustang GT500 and Maserati MC20. Key attribute to the TREMEC development approach is vertical integration from component design and manufacturing to full transmission system assembly and electronic control unit development including SW and calibration. Confronted with a rapidly changing market under the impulse towards electrification, TREMEC has entered advanced development programs to build on the DCT experience and move towards electrified drivetrain solutions. Aside from the development of hybrid DCT's [1], this paper focusses on the development of electrified axle solutions.

Background of project HYDRA

Passenger cars continue to become more powerful generation after generation. Especially for the performance versions of mainstream vehicles, engine power and torque levels are often surpassing what can be transferred effectively to the road with a two-wheel drive layout. In

recent years, more and more powerful FWD vehicle platforms turn to AWD for their most powerful version. Typically, the AWD system is an on-demand system, only sending power to the rear wheels when the vehicle controls system decides it is required. Additionally, to increase the agility of those performance versions, torque vectoring in some form is utilized. While some manufacturers remain with brake-system based torque vectoring only, others are turning to mechanical torque vectoring systems with clutch packs on the rear axle to divert torque left or right. Table 1 shows the driveline layout, engine power and acceleration performance for a few well-known “hot hatchbacks”. Clearly the addition of AWD cuts around 1 s of acceleration time by virtue of improved traction. Some vehicles are now producing around 300 kW resulting in 4 s 0-100 kph acceleration, which was supercar territory only a few years ago.

Table 1: Comparison of high-performance hatchbacks

Model	Power (kW)	Acc 0-100 (s)	Driveline
Mercedes A45S AMG	310	4,0	AWD+TV
Audi RS3	294	4,1	AWD
VW Golf 8 R	235	4,7	AWD+TV
BMW M135i	225	4,8	AWD
Honda Civic Type-R	235	5,8	FWD
Ford Focus ST	205	5,7	FWD
VW Golf 7 TCR	213	5,6	FWD

Along with increasing targets for performance and driving dynamics, there is a rapid movement to some form of electrification in view of the global requirements to severely cut CO2 emissions. While full electric BEV platforms are on the rise, mainstream passenger cars are still mainly ICE powered, with a rapidly increasing the number of hybrid versions. Focussing on the full-hybrid or PHEV variants, meaning those that can propel the vehicle in a purely electric mode, two primary options are available: addition of an electric machine in the transmission, typically a P2 layout, or addition of an electric machine on one of the vehicle axles (P3 or P4 layout). CO2 emissions of the PHEV variants are typically in order of 20-25 % of their pure ICE counterpart, with many hybrids being rated less than 50 g/km in WLTP. Several vehicles are combining hybridization and AWD needs in one solution, using an e-axle at the rear in addition to a pure FWD ICE powertrain.

Staying close to our typical market segment of fun-to-drive, high performance vehicles, TREMEC has been looking for ways to use electrification as means to increase performance and driving dynamics, in addition to its benefits in terms of fuel economy and emissions.

P3 and P4 hybridization

Zooming in on the hot hatchback type vehicle and the available options for hybridization, TREMEC concludes that electrifying the rear axle is the only viable way to take benefit of the performance increase offered by the electric machine. While P2 transmissions for FWD layout exist and could theoretically be mated to the typical high-torque turbocharged ICE in the segment, in practice, the FWD transmission simply cannot handle the combined torque input of the EM and the ICE. Especially in the lower gears, torque limits are often already applied with the ICE engine alone. No such problem exists when electrifying the rear axle.

Table 2 shows a simulated performance comparison for different hybridization options, with identical power levels for each hybrid option. P2 hybridization is clearly unfavourable, because the main gearbox torque limits prevent exploiting the additional performance on offer, while the weight of the vehicles is increasing with hybridization. A pure eAWD system brings a significant performance gain, while the addition of the mechanical AWD prop shaft brings a further improvement, resulting in performance gains over todays highest power output ICE vehicles. A 1.5 s reduction in acceleration time is achieved without any modification to the ICE.

Simulated vehicle:

- Front engined hatchback
- 235 kW ICE
- FWD DCT with 4500 Nm output torque limit
- On-demand AWD
- All hybrid options are equipped with a 150 kW peak power e-machine
- Vehicle weight is increased according to the hybrid layout

While non-performance versions may delete the front-back prop shaft in favour of a pure eAWD architecture, maximum performance and driving dynamics can only be realized by combining the virtues of the mechanical on-demand AWD system with an electric machine added to the rear axle. The rear axle is essentially the most suited to transfer tractive effort due to weight transfer under acceleration. Without the prop shaft, the front axle is still easily overwhelmed by

the torque and power of a powerful ICE, even more so when weather conditions are less than perfect.

Table 2: simulated performance of different hybrid architectures

Configuration	Acceleration 0-100 kph (s)
Base vehicle (non-hybrid)	4,7
P2 hybrid	5,1
P4 rear axle, pure eAWD	3,4
P4 rear axle, with mech AWD = TREMEC HYDRA P4	3,2

Fig. 1 shows the total front and rear axle torque levels realized with the different powertrain layouts during full throttle acceleration, compared to the max transferable torque level for each axle. In the eAWD version (FWD+P4), acceleration is still limited by front wheel grip, but perhaps more important, the front-rear torque split remains front-biased under full acceleration. In the case of the combined mechanical AWD+P4 layout, the distribution is heavily rear biased, resulting in superior acceleration. In dynamic cornering conditions, the reduced torque load on the front axle improves the driving experience in terms of lateral grip and steering. This natural benefit can be enhanced further with the addition of torque vectoring capability.

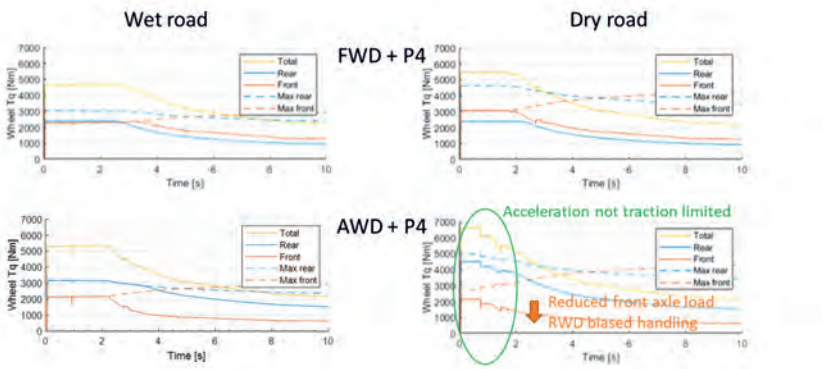

Fig. 1: Axle torque during full throttle acceleration for eAWD and mech-AWD+P4

In the case of a front-engine RWD sports car architecture, hybridization of the rear axle is also considered favourable, with as benefits, amongst others, improved weight distribution, more efficient electric driving (no main TM losses), direct response of the electric assistance in hybrid mode regardless of ICE drivetrain gear selection, and reduced load profile of the ICE transmission.

Based on the above, TREMEC has developed a hybrid drive axle concept (HYDRA), initially as P4 design but with spin-off possibilities towards a P3 version as well as pure electric versions.

Hybrid axle concept, features and specification

Fig. 2 shows a schematic layout of the hybrid axle concept. At the heart of HYDRA is a planetary, open differential. The differential transmits the driving torque from the electric drivetrain only to the wheels. This allows maximum pure electric driving efficiency (no power transfer over slipping clutches). Further, the electric motor drives the vehicle in pure RWD mode, enhancing the driving experience and maximizing traction potential of the rear axle. The electric drivetrain consists of a compound planetary gear set, with a disconnect tooth clutch between the output of the compound gear set (planet carrier) and the input of the planetary differential (ring gear). The disconnect allows the e-machine to be disengaged when vehicle speed would surpass e-machine max allowed speed, and also allows the (permanent magnet) e-machine to be disconnected during pure ICE driving for improved efficiency. The e-machine is installed concentrically with the output shafts for compact packaging. In addition to receiving electric driving (or braking) torque through the differential, each output shaft can also receive additional torque from the prop shaft input via a double clutch pack on-demand AWD and torque vectoring system. The clutches receive torque input through a combination of a cylindrical final drive gear set and a bevel gear set. The cylindrical gear set allows for flexibility in the choice of the total effective final drive ratio. The chosen gear layout also allows the overall axle to be symmetric to the prop shaft input.

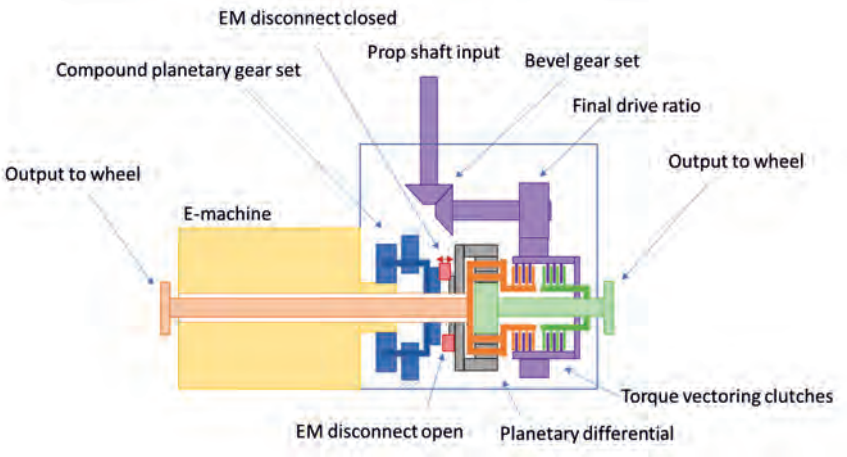

Fig. 2: HYDRA P4 schematic layout

Key specifications of the P4 axle system are listed in Table 3.

Table 3: Key specifications of HYDRA P4 axle

Topic	Specification
Effective final drive ratio	2.46-3.39
Bevel set ratio	1.114
TV clutch capacity	1300 Nm each side
Compound gear ratio	7.93
Planetary differential input torque = pure E-drive output torque	2400 Nm
Total output torque	5000 Nm
Total weight including EM (IPM machine without inverter)	69 kg

Different operating modes of the system are illustrated in Fig. 3 (cylindrical gear set ratio 3).

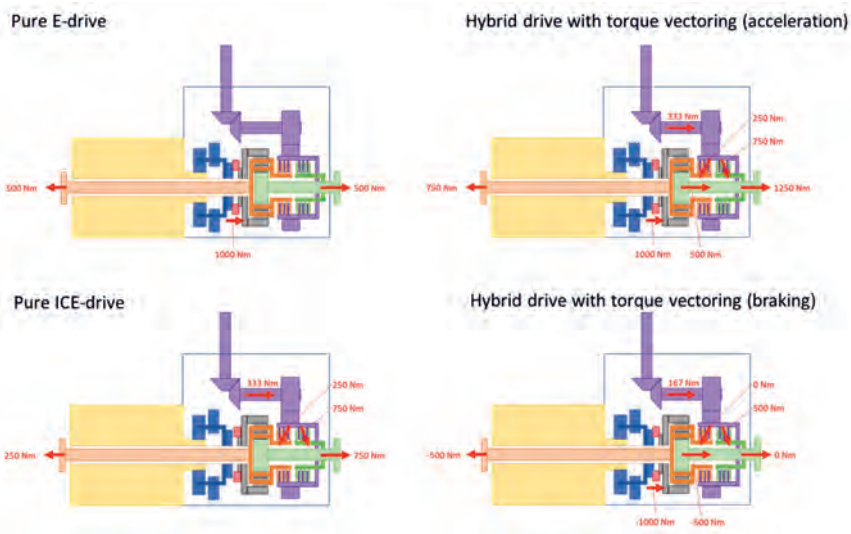

Fig. 3: Operating modes of HYDRA P4 system

In a typical performance application, the effective final drive ratio at the rear axle would differ a small percentage from the final drive ratio at the front, ensuring a positive delta speed across the torque vectoring clutches, allowing positive torque transfer over the clutches in all required vehicle cornering conditions. In the pure mechanical torque vectoring system with twin clutch packs, torque vectoring is limited to positive (driving) torque. By virtue of the electric machine in HYDRA, a negative torque offset can be generated through the e-machine under braking (regenerating). When combined with positive clutch torque, it becomes possible to generate a torque vectoring effect also under braking. The effect of the e-machine on widening the torque vectoring breadth of abilities is illustrated in Fig. 4. Instead of a single quadrant, HYDRA allows for 4 quadrant torque vectoring and as such maximizes the options for vehicle handling optimization while reducing CO2 emissions.

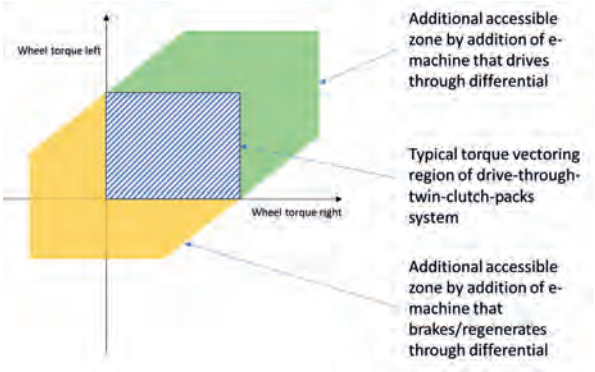

Fig. 4: HYDRA P4 torque vectoring operating range

Last but not least, in an era where “drift” modes are being enabled in many vehicles through powertrain setting calibration, HYDRA also overcomes a key shortcoming of many mechanical AWD systems: their inability to enter a power-oversteer situation, due to torque transfer front to rear being limited to positive speed difference front-rear. Because the shown concept is a real P4 axle, in which the e-machine drives the rear wheels only, there is a much more pronounced rear wheel drive handling characteristic compared to a P3 or pure mechanical AWD system.

Hybrid axle design

Fig. 5 shows a 3D view of HYDRA P4 design. The axle has been designed with strong focus on the compactness to allow for good ground clearance, minimum luggage compartment space intrusion, acceptable width and output shaft flange distance, and low weight.

Fig. 5: 3D view of HYDRA P4

Fig. 6 shows a cross section of HYDRA P4 design. The characteristic layout with open differential at the heart, electric drivetrain on one side, torque vectoring clutches on the other side, and the layshaft design with split final drive ratio is clear. The input bevel gear set is a non-hypoid design to allow for low viscosity oil instead of typical hypoid lubrication oil, improving churning losses and clutch controllability. The offset between input and output shafts is generated purely by location of the cylindrical final drive gears and is as such more flexible for application-specific modification than a hypoid bevel gear set. To aid with space and weight reduction, the e-machine housing also fulfils the function of closing cover of the electric drivetrain. The cooling channels in this shared housing avoid the use of a separate oil cooler for the axle. The torque vectoring clutches are taken from TREMEC's TR-9080 transaxle eLSD (Fig. 7). They incorporate springs between the clutch plates to ensure minimal drag torque with open clutches.

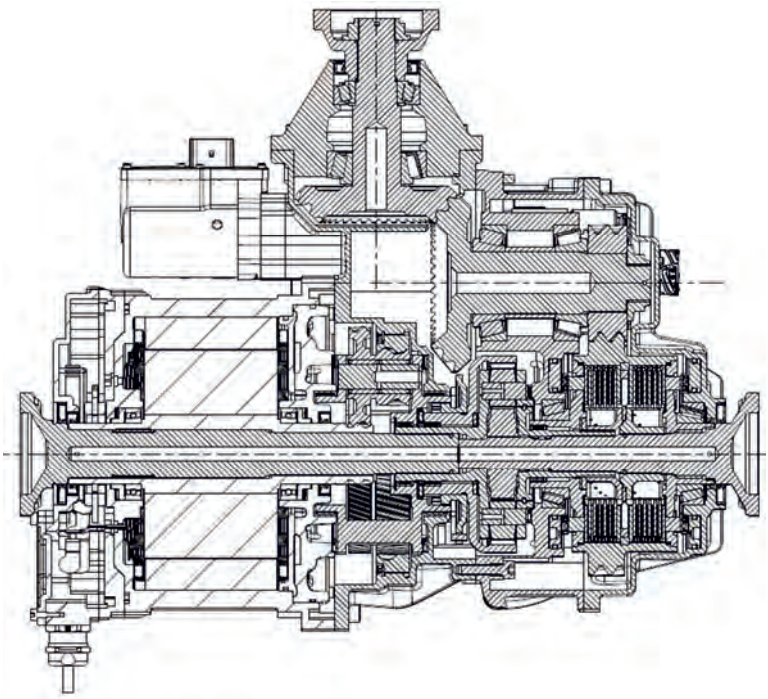

Fig. 6: Cross section of HYDRA P4 design

Fig. 7: TR-9080 eLSD

Electric machine

While the design of HYDRA allows relatively free choice of the e-machine, the concept is worked out with the motor solution as discussed below, specifically for a power dense solution towards a performance-oriented application. The high voltage e-machine is a permanent magnet, radial flux, concentrated wound, fractional slot motor generator unit (MGU) with an outer segmented stator/ inner rotor configuration. Stator outer diameter is 200 mm, stator inner diameter is 154 mm. The high speed enabled by the small diameter results in a light and power dense unit that meets the target constant power speed ratio (CPSR), whilst having a low rotor inertia for optimum dynamic responses. The CPSR is the ratio between the base speed (where peak torque and peak power occur together at the “knee point”) relative to the maximum speed of the e-machine and is 3.67 and 3.56 respectively for the interior permanent magnet IPM and surface mount permanent magnet SPM types shown in the figure below.

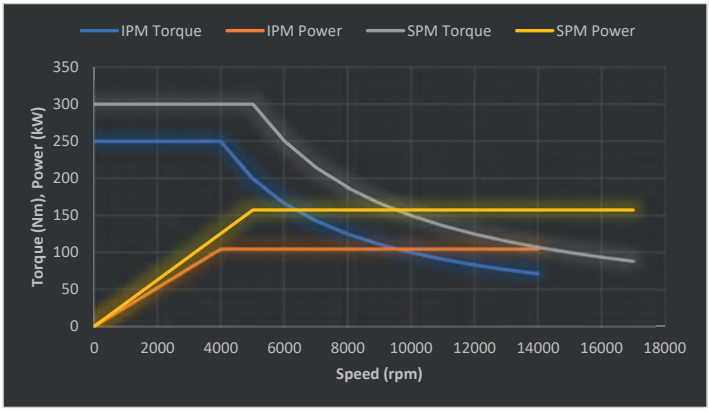

Fig. 8: e-machine performance curves

The concentrated wound e-machine has very short end windings versus the more traditional distributed wound architecture and is favored here to ensure minimum motor packaging space in combination with an integrated overall system design. There are other benefits such as ease of manufacturing, more robust insulation performance and reliability. NVH characteristics (cogging, torque ripple, structure borne noise) and space harmonics (rotor heating), are optimized with multiple solutions with focus on the design-for-manufacturing aspects. The stator is designed to be capable of running with both (IPM) and (SPM) rotors with no changes to geometry, only requiring rewinding for the rotor type and DC bus voltage range. The

segmented design, as shown in Fig. 9, allows industry-standard precision winding methods to be used and provides high net slot fill while minimizing AC losses in an e-machine that operates at higher electrical frequencies.

Table 4: e-machine options

Topic	Version 1 High performance	Version 2 Medium performance
Voltage	800 V	400 V
Peak torque	300 Nm	250 Nm
Peak power	> 150 kW	> 100 kW
Max speed	> 17.000 rpm (>250 kph)	> 14.000 rpm (> 200 kph)
EM type	SPM	IPM
IV integration	Integrated	Not integrated
IV type	SiC	N/A
Weight	20.4 kg total mass including inverter, excluding DC cables and coolant	17.7 kg total mass, excluding phase cables and coolant

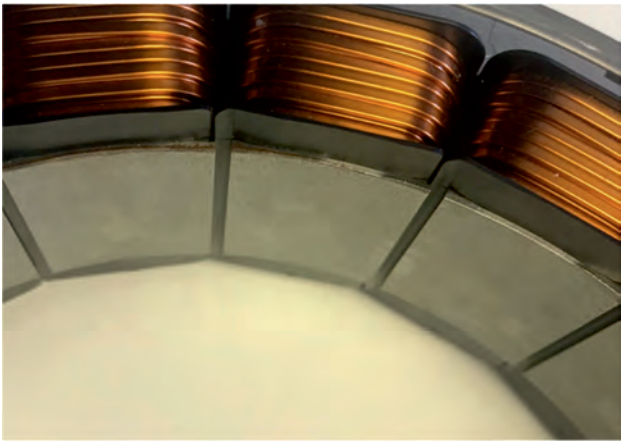

Fig. 9: Segmented stator with precision winding principle

E-machine torque density is 17.6 Nm/kg (referred to the active mass) when using an IPM rotor. Moving to an SPM rotor increases the torque density up to 25.4 Nm/kg, resulting in more performance and/or the ability to reduce the active length of the motor for the same torque level. The shorter stack length for the SPM variant off-sets some of the extra costs for the increased magnet mass and composite retention system of the rotor. Shown performance curves for the SPM version are conservative, and higher power levels can be realized remaining below a target phase current of 300 A rms for the inverter, if the vehicle application demands it and of course if the vehicle battery and cooling system are able to support the power levels. At 150 kW the SPM machine peak power density is 12.7 kW/kg (active mass) and 9.7 kW/kg (total mass). Simulations (Fig. 10, Fig. 11) show that from an electromagnetic point of view, within the 300 A phase current limit and for a bus voltage of 750 V, this could be stretched to 19 kW/kg (active mass) and 14.8 kW/kg (total mass). Predicted efficiency of the motor is over 96 % for a vast area of the working range and can peak to 98 % for its operating sweet spot. These efficiency levels have been validated on similar architecture machine prototypes.

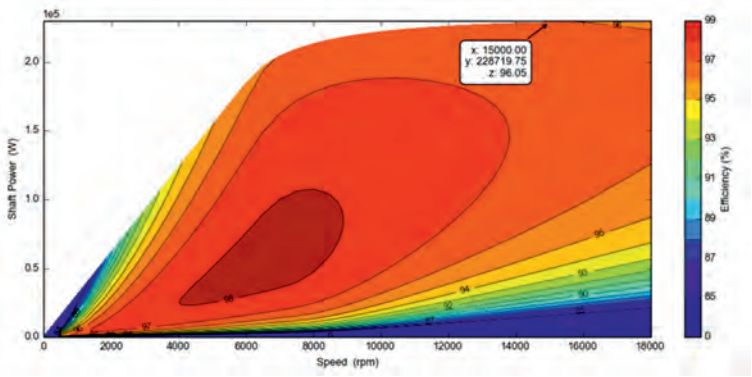

Fig. 10: Power v speed ultimate performance limit for the SPM machine

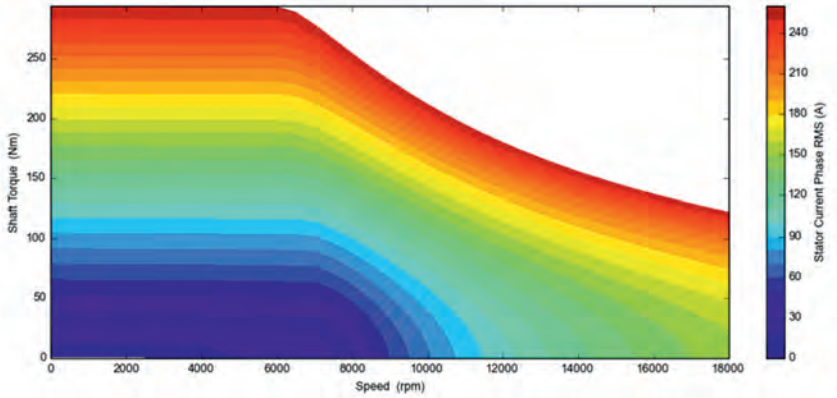

Fig. 11: SPM machine phase current map

The integrated inverter option is based on a SiC mosfet power stage for its superior efficiency both in the WLTP cycle and in high performance drive cycles. Rotor sensing technology suitable for ASIL-D has also been applied. The integrated inverter has many additional benefits over a standalone option, such as a shared cooling system with the e-machine, shared housings with the e-machine for reduced mass and componentry, direct and robust coupling of the inverter to motor phases and lack of phase cables (reduced mass, EMC/EMI, and points of failure) and reduced low voltage connections.

Fig. 12: Integrated inverter layout principle

Actuation, sensors and controller

Building on TREMEC's expertise in development, production and control of hydraulic systems in DCT's, a hydraulic actuation system is selected to actuate the different functions in the axle system. The power density, responsiveness and ability to serve several functions with single power source are key motivators. Fig. 13 shows the hydraulic diagram.

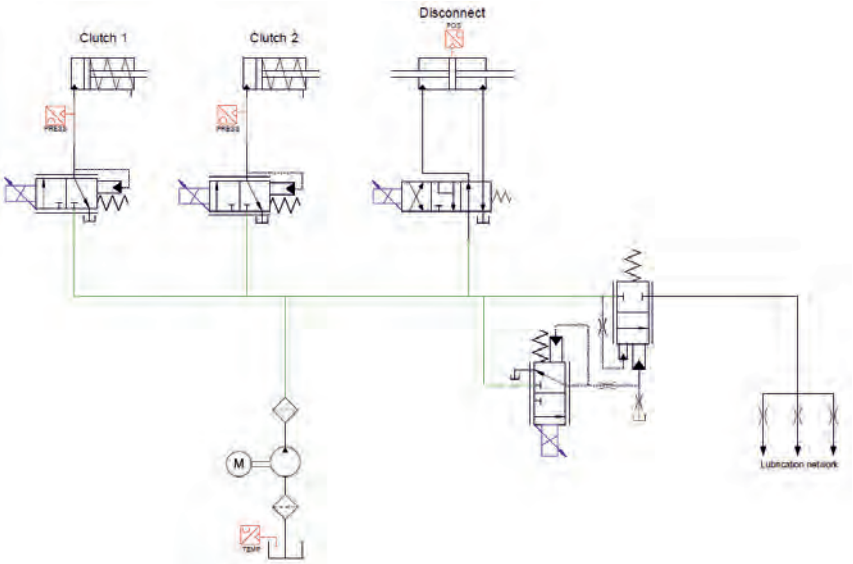

Fig. 13: Hydraulic diagram for HYDRA P4

A 12 V electric pump with BLDC motor directly feeds the actuation system without need the for an accumulator. Each torque vectoring clutch pack is controlled with a proportional pressure control valve. The disconnect clutch is shifted by a hydraulic piston and directional solenoid valve. The pump pressure can be regulated depending on the requirements of the different actuators and is regulated to a minimum in steady driving conditions. Oil that is not consumed for actuation, is used for lubrication of the gears and bearings as well as cooling of the clutch packs. Lubrication oil flow is controlled by the speed of the electric pump, further minimizing energy losses when flow demand is low.

Several sensors are present for control and diagnostics: pressure sensors for each torque vectoring clutch, a disconnect position sensor, a differential input speed sensor, an oil temperature sensor, an e-machine stator temperature sensor and an e-machine rotor position sensor.

To maximize the application flexibility of HYDRA, a dedicated control unit is installed onto the axle, that takes care of all axle control functions as well as inverter communication and

communication to the vehicle controls network. Fig. 14 shows the block architecture of the controller. The BLDC pump motor driver is integrated into the controller together with input/output control of the sensors and actuation valves. This integrated approach allows for optimum controls responsiveness as well as the ability to use the pump as a true redundant shutdown feature for safety reasons (fast removal of operating pressure).

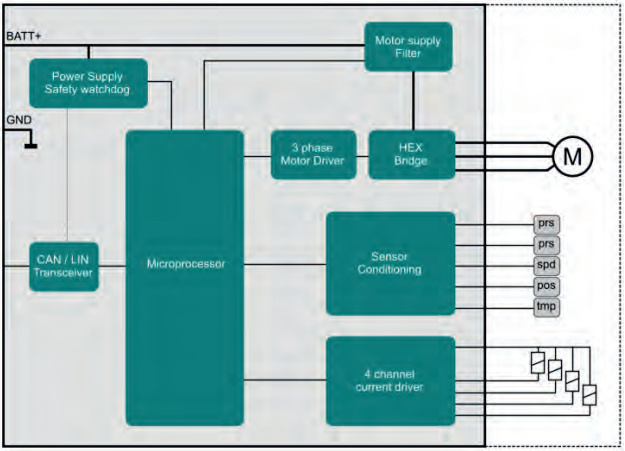

Fig. 14: HYDRA controller block diagram

Other functional variants

Based on the core architecture of concentric e-machine and output shafts, compound planetary gear set and planetary differential, several spin-off versions are possible.

First, a P3 version can be derived, suitable for a RWD sports car application. This can be achieved by adding a cylindrical gear stage connection between layshaft and differential input, as such combining prop shaft input and electric machine input into the differential. The cylindrical gear stage towards the clutch packs is then designed with a percentage difference to the gear stage towards the differential, so that the clutch packs allow torque to be diverted directly to one of the outputs instead of through the differential, resulting in a torque vectoring functionality. For the P3 RWD version, the high torque requirements for the differential are met by the differential of TREMEC's TR-9080 planetary differential (Fig. 7). By omitting the twin

clutch packs and overspeeding gear set in favour of the single clutch pack of the TR-9080 eLSD, a RWD P3 axle with eLSD function is realized.

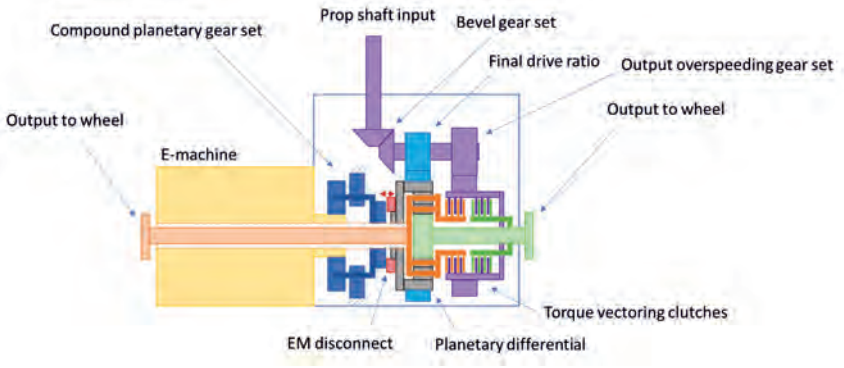

Fig. 15: P3 RWD version of HYDRA

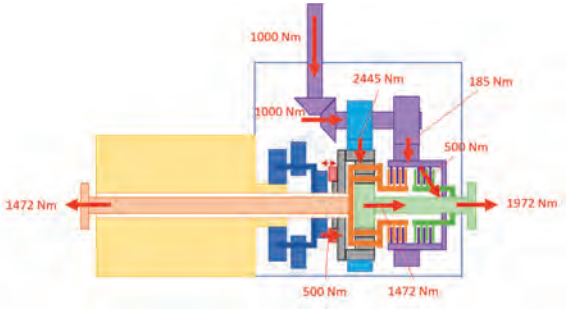

Fig. 16: Example of torque vectoring condition for HYDRA P3 version

Secondly, by removing the input bevel set, a pure e-axle is possible, with a choice of open differential, eLSD or torque vectoring setup.

Conclusion and outlook

After establishing itself as a leading high performance full-system provider for dual clutch transmissions, TREMEC is transitioning along with the entire automotive market into the era of electrified drivetrains. Keeping focus on the fun-to-drive aspects, solutions for hybridized

performance vehicles have been studied and concept designs established. For many vehicles, hybridization through electrifying the main transmission is not considered favourable, instead requiring the electrification to be installed on one of the vehicle axles. With HYDRA, an integrated design concept for a P4 on-demand AWD axle is realized that not only allows for efficient and performant electric driving, but it also utilizes the electrification element to really enhance the driving experience by maximizing usage of the rear axle for traction, as well as offering possibilities for four-quadrant torque vectoring controls to further improve vehicle dynamics. HYDRA also lends itself to generate spin-off architectures towards RWD applications and pure electric axles.

Using HYDRA as a technology showcase and development platform for electric drive system integration, actual prototype hardware is scheduled to be available in the first half of 2022, with vehicle demonstrations being planned before the end of 2022.

References

[1] TREMEC Hybrid Dual Clutch Transmission (HDCT), de Ruijsscher, Dritev Bonn 2021

High Efficient 2 speed e-Axle

Highly efficient and shiftable under load

Christian Schmidt, Henrik Dhejne, AVL List GmbH, Graz, Austria;
Joakim Karlsson, AVL MTC Motortestcenter AB, Trollhättan, Sweden

ABSTRACT:
The vehicle architectures for SUV and LD-BEV's come with higher performance requirements, which can no longer be supported by single speed architecture. A highly efficient 2speed e-Axle featuring single dry-clutch transmission and utilizing high-speed E-machine is the right answer to fulfill future needs for this segment.
By increasing the maximum E-machine speed enables potential for further size reduction. Highly efficient cooling concepts are the key to fulfill the customer expectation on high efficiency and performance repeatability. New simulation methods are required to obtain an optimized overall efficiency, NVH, thermal behavior and durability already in early stage of the e-Axle development

1 Introduction

At the moment, these are demanding and exciting times in the field of powertrain development for passenger cars because of the legislations. The market acceptance for battery electric vehicles has increased significantly the last 5 years and are increasing even more than expected.
The modular AVL 2-speed e-Axle is based on design innovations developed by AVL.
The technical solutions enable state of the art efficiency and affordability by utilizing dry clutch and high speed e-motor as an example. By using a smart and sophisticated power flow architecture, we can guarantee a comfortable power shift with low-loss gear shifting with manageable control effort. With this innovative concept, AVL was already able to develop a dedicated 2speed solution for a customer which combines the high efficienct e-drive of the customer with AVL´s 2speed transmission.

2 AVL e-Axle Concept

2.1 Requirements and Target Setting

Based on the electrification trend, we did see a clear need for a solution in the bigger vehicles segment, such as SUV and Light duty trucks, in order to achieve a good performance, high efficiency and affordability.

The high-level requirements were set accordingly for the 2 speed e-Axle

- Affordable
- Layshaft design
- High integration
- Single Clutch
- High speed e-motor
- Smart actuator
- Power shift

And key performance targets:

Fig. 1: AVL 2speed e-Axle (© AVL)

The targeted system efficiency in WLTC cycle was set to 2-5% higher compared to a single speed solution while keeping performance on the same level.

The overall e-axle concept should be modular in order to minimize the modifications for different applications. Inverter and e-motor could be carried over as modified and improved versions from AVL high speed e-axle [1] which is already benchmark in power density and the right solution for this innovative application.

2.2 Solution and Performance

The development landscape of EDUs is currently shaping itself around high speed, high integration level with compact design and very high power density. In order to satisfy high performance requirements and high efficiency, AVL decided on following technologies on the 2speed e-axle:

- 800V e-Drive System
- Inverter with SiC Technolgoy
- High speed e-Motor
- Multi plate dry clutch as enabler for high efficiency and compact design
- Electromechanic actuation system based on a drum shift to ensure shift under load and easy controllability
- Mechanical park lock as feature of the shift system (“Smart park lock”) to reduce cost and weight. No separate park lock mechanism with additional actuator is needed
- Layshaft transmission layout which is robust and efficient

Table 1: Key Parameters of AVL 2speed EDU

Item	Unit	Value
Power	[kW]	up to 250
Axle Torque	[Nm]	7500
Clutch	-	Dry multi plate
Vehicle Speed	[km/h]	210
System Voltage	[V]	850
Max. Input Speed	[rpm]	20.000
Transmission Layout	-	Layshaft Offset
Configuration	-	Smart Park Lock / Power Shift
Shift System	-	Electro Mechanic / optional: pneumatic/hydraulic
Inverter	-	SiC Powermodules

The e-drive system is defined by the high speed e-motor which is controlled by a state of the art SiC inverter. The system voltage of the e-drive is 800V. The higher voltage is the enabler to reduce weight of conducting materials and reduce chip area in the inverter. Both effects have the potential to lower cost of inverter and wiring.
The e-machine costs can be decreased by reducing size and thus the material costs with the draw back of reduced torque output. To reach the required output, speed needs to be increased. When increasing machine speed, the influence on transmission and inverter must be observed. Shiftable 2 speed transmission offers the possibility to run the e-machine in the most efficient operation points. The challenge during the development is to keep cost and complexity of the transmission system on an affordable level [1].

2.2.1 Performance and Efficiency

As already mentioned in the chapter before, the 2 speed transmission can compensate the trade off between high driving performance versus high efficiency which is a big draw back on single speed EDUs.

But it is not done only by integrating a second gear into the transmission. There needs to be a well balanced optimization between transmission, e-motor and inverter in oder to achieve the best efficiency based on the vehicle boundaries and driving cycles. Advance simulation methods like design of experiments can help to find the best balance in defining the optimal design of the sub systems in order to use the full potential of the 2 speed transmission. The 2 speed gear box offers the option to reduce the e-motor power by keeping same driving performance compared to single speed EDU with higher power.

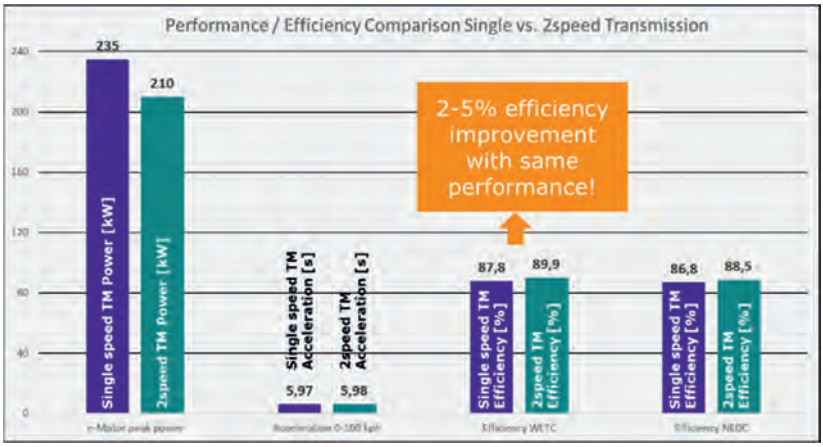

Fig. 2: Performance & Efficiency comparison Single vs. 2speed EDU (© AVL)

The efficieny benefit can reach between 2-5% improvement, depending on the vehicle boundaries. In the shown application, see also Fig 2, AVL could achieve > 2% efficiency in WLTC and NEDC, by keeping the performance of the vehicle on the same level. As target vehicle a 2,5 ton SUV has been used. The two e-axles which have been compared, offer same technology like forced lubrication system, 20.000 rpm high speed e-motor and SiC inverter. The difference is defined by the transmission which offers 4000 Nm at the single speed version and 5000 Nm on the 2 speed solution.

There is more potential to bring the efficiency on a higher level by optimizing the e-motor characteristic, inverter controls and shift map optimization.

2.2.2 e-Drive System – 800V e-Motor and Inverter

The basis for the e-drive system was done by the AVL high speed e-axle solution [1]. Most of the design could be reused and has been optimized for this application.

For the inverter a technical solution had to be defined, to fulfill current and frequency requirements of the e-motor by also enabling highest efficiency and power density. To achieve this, wide bandgap Silicon carbide (SiC) power modules are the perfect solution. These modules have lower switching losses than state of the art IGBT solutions and allows to increase the switching frequency while maintaining high efficiency.

Another key parameter of SiC technology is their smart package by same power specification and better thermal conductivity compared to IGBT.

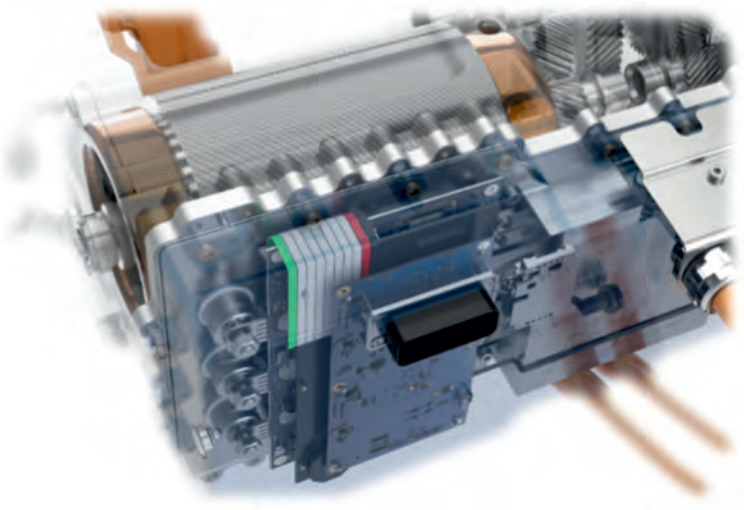

Fig. 3: SiC Power Inverter (© AVL)

The permanent magnet synchronous machine (PMSM) with single layer V-shape magnets has been optimized to match the load points from the 2speed gear box with the optimal efficiency area of the machine. The winding layout is distributed round wires, which has been preferred to hairpin winding. Thin wires are used to prevent skin effect even at the maximum speed.

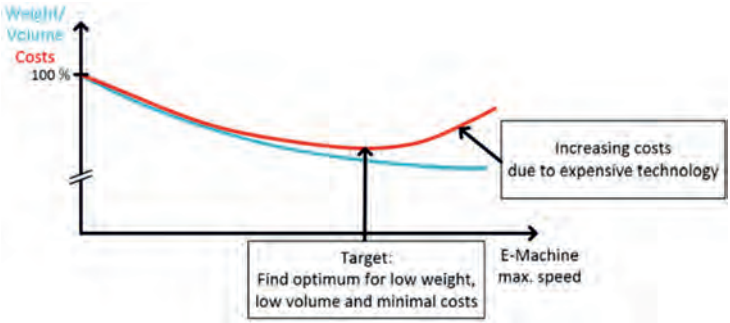

Fig. 4: E-Motor Cost / Volume vs. Speed

The stator is cooled directly via oil on the windings. This concept is introduced several years ago in the AVL COUP-E 800V electric vehicle [4]. The oil flow is in axial direction through the stator slots and allows a direct heat dissipation from the conductors to the fluid. The oil is kept

inside the slator slots due to closed slots. This design saves an additional tube in the air gap and thus avoids an increased air gap. With the direct cooling the continuous power output of the very compact machine can be drastically improved compared to water jacket cooling and improves the efficiency due to lower temperature level of the components.

2.2.3 Transmission Layout and Power Flow

One premise during the development of the transmission was affortable technology, shift under load and highest efficiency. In order to achieve these targets, a layshaft design was chosen as this layout combines low production cost and robust design with highest efficiency.

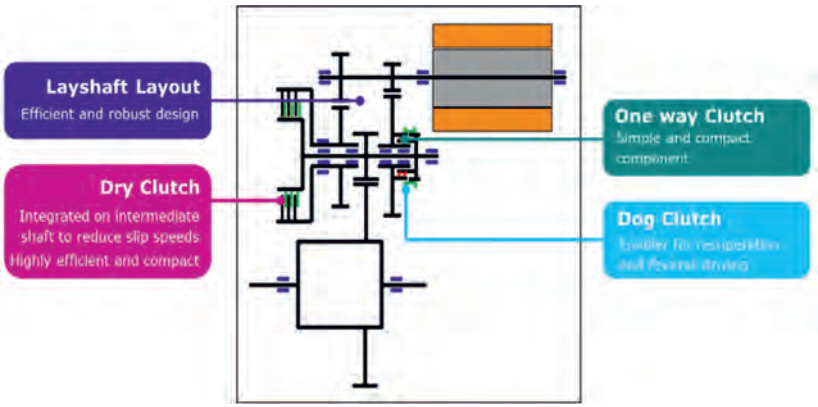

Fig. 5: Transmission Layout (© AVL)

To enable power shift, usally double clutch systems are used. In order to reduce cost and complexity, a single clutch solution was set as target. The friction clutch is transferring the torque on the second gear and is combined with a one way clutch on the first gear, which is freewheeling during driving in second gear. Another reason for the one way clutch is the compact package. A dog clutch is supporting the one way clutch during coast drive and reverse driving, as the component would free wheel during this operation.

The friction clutch is operating in the second gear only, therefore drag losses in first gear need to be avoided as much as possible. This was one of the main drivers for using a multiplate dry clutch. As there is no cooling option like on a wet clutch, the decision was to place the clutch on the intermediate shaft to reduce the maximal speed and the corisponding thermal load on the component during shifting.

The transmission layout allows several operations states which are summarized in the following table 2:

Table 2: Operating States

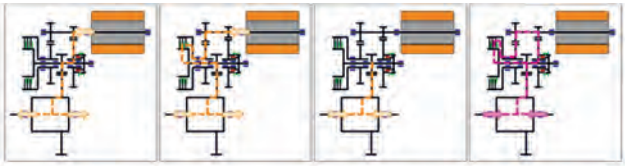

Torque transfer device	1st Gear	2nd Gear	Neutral	Smart Park Lock
Friction clutch	open	closed	open	closed
OWC	blocked	free wheeling	free wheeling	stand still
Dog clutch	closed	open	open	closed

In first gear, the friction clutch is open, the one way clutch is blocked and dog clutch is closed. The torque transfer is done via the one way clutch in motor mode and supported by the dog clutch during recuperation and reverse driving. During shift from first to second gear, the torque is handed over seemless via the friction clutch. The dog clutch is open and the one way clutch starts free wheeling.

The transmission layout provides two additional states for free which are a neutral or eco-mode and the park lock mode. In the neutral mode, both clutches are open and the one way clutch is free wheeling. In this mode, losses from e-motor can be avoided and partially form the transmission too, as differential and intermediate shaft are still rotating.

In the park lock mode both clutches are closed in order to block the system internally. The engagement need to be assessed carefully, as very high loads accur during engagement, especially if park lock is triggered directly from second gear via the dog clutch. On the other hand the integration of this so called “smart park lock function” can reduce package, complexity, weight and cost for a separate system as the shift actuator is used and no additional mechanics are needed.

2.2.4 Shift and Actuation System

The two clutches are mechanically actuated by a shift fork. Depending on the application, the actuation of the forks can either be handled via shift drum, which is driven by an smart actuator, or by a pneumatic or hydraulic system. The base application from AVL uses the electromechanical version as the target vehicle is a high performance SUV where performance and drivability is at least as important as efficiency. This requires good and simple controllability, which can be handled best by this concept. For light duty vehicles there is the option of pneumatic actuation, if the system is available for the vehicle platform.

Looking in more detail on the electromechanics system: The shift forks of the two clutches are guided by one shift drum. The profiles for both clutches are linked via the shaft, so the shift logic is the driver for the profile design – see Fig. 6. The shift drum can rotate in both direction to enable a fast park lock engagement from 2nd gear. At the dedicated positions for 1st and 2nd gear, the drum profile is designed in a way that no energy will be consumed by the actuator. An additional benefit of this system is the reduction to one actuator only, which is used to control the single shift drum.

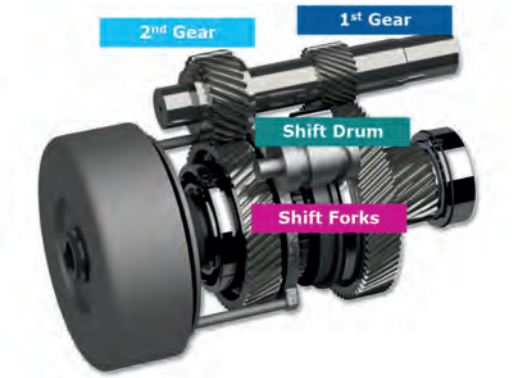

Fig. 6: Transmission gear set and shift concept (© AVL)

The electromechanic shift system is the enabler for an easy and good controllability of the shift event, which is highly influenced by the type of friction clutch as well. As already mentioned in the chapter 2.2, a dry multi plate clutch has been chosen due to benfits on efficiency and package. The dry friction material provides higher friction coefficients compared to wet design, thus lead to lower clamping force and higher torque capacity within the same package. Disadvantage of the dry clutch concept is the lower thermal capacity which is less relevant in

this application, as the chutch is not used as launch element. Furthermore the integraton of the dry cluch at the intermediate shaft reduces the relative speed and therefore the energie input during a shift event. Fig. 7 summarizes the main advandages of the dry friction clutch compared to wet clutch type, in relation to the customer requirement [3].

Fig. 7: Dry Clutch Performance Parameters [3]

The clutch is a normally open type for the current application but can be switched to normally closed concept depending on the application. This depends on the driving strategy of the target vehicle and the usage of second gear. If first gear is defined as a launch gear and the overall driving is done in second gear, a normally closed clutch would be the choice.

2.2.5 Transmission Controller

Dedicated e-axle system with dry clutch, drum, electro-mechanical control requires deep system knowledge, understanding of both conventional and electrified elements. To enable an high quality power shift, the response of the e-machine must follow on a very high level in order to avoid unacceptable torque drops during the shift event. Automated software testing is used to find the best strategy. A front loading calibration approach supports base calibration setting on virtual test bed already.

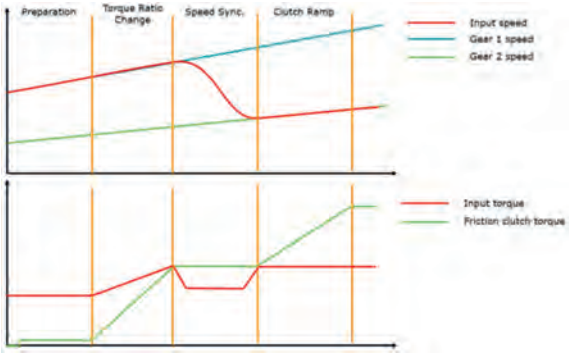

Fig. 8: Powershift sequence first to sescon gear

3 AVL 2 speed e-Axle applications

The AVL 2speed concept is a modular and scalable solution and therefore flexible to use for several applications. As stated in the chapters before, the benefit for 2speed gear box in battery electric vehicles can be gained especially on heavy vehicles, with a high demand of performance and efficiency too. The focus of the EDU design can be set on the one side to increase top speed, acceleration and trailor load or on the other hand to increase efficiency, reduction of the e-motor power by keeping same driveability targets.

In the following a short overview of the current AVL 2speed e-axle applications will be given. The architecture of the transmission is the same on all applications. Also the inverter and e-motor are from same family and can be scaled and adopted based on the application targets. Finally a short summary of one customer application is described.

3.1 2speed Application for SUV

The 2speed e-Axle application for SUV is the base design, which has been developed by AVL. Tue to the modular and scalable design the system can be modified to single speed transmission as well. This application can be the basis for a modular e-axle platform, based on state of the art technologies, high efficiency and affortable design. The key features and parameters can be found below.

Fig. 9: AVL 2speed Application for SUV (© AVL)

3.2 2speed Application for Light Duty

Compared to passenger cars, the light duty applications have a different focus. Trailor load, gradeability, efficiency and especially cost are important targets. The 2speed system is the enabler for better drive- and gradeability by keeping the efficiency and therefore the driving range of the vehicle high. The challenge for LD application is, to keep the complexity low in order to minimize cost and invest. Due to the modular design of the AVL application the EDU can be adopted based on the vehicle requirements very easily. Especially on the actuation system, available interfaces of the vehicle, e. g. a pneumatic system, can be used to minimize cost and weight of the EDU.

Fig. 10: AVL 2speed Application for Light Duty Vehicle (© AVL)

3.3 Customer 2speed Application for SUV

As mentioned in the introduction, the AVL 2speed application has already been further developed for a Asian customer. It is the perfect extension of their product portfolio of high innovative e-axles. The application is designed for a heavy SUV in order to achieve good driving performance with main focus on efficiency. The customer application is using the high efficient inverter and e-motor from an existing high integrated single speed EDU. Mechanical interfaces, lubrication and cooling concept could be taken over from the base application in order to achieve a short time to marked and to have as mutch communality between the products as possible. This application shows very well the modular and flexible approach of the AVL concept as it could be easily adopted to fit to the customers e-drive system.

The transmission controller is integrated in the motor control unit, the software development was done by AVL, challenged by the high shift quality requirements while the integration kept in responsibility of the customer.

The key features and parameters can be found below:

Fig. 11: AVL 2speed Customer Application (© AVL)

4 Conclusion

The AVL 2speed e-axle is a smart and modular concept to improve vehicle efficiency and drivability keeping additional cost in an exceptable range. After outlining the target setting approach based on the given requirements from the market and the customers, an overview of the technical solution has been given, followed by the technical description of the sub-systems.

The 2speed e-axle combines state of the art e-drive technology with highly efficient and cost effective transmission design. The layout of the transmission enables shift under load with very good controllability due to electromechanics shift system. A modular design approach has been used to meet high performance passenger car requirements as well as Light Duty application requirements. The one clutch approach and integrated smart park lock system ensure competitive weight and cost compared to single speed applications.

REFERENCES

(1) Mathias Deiml, AVL Software and Functions Regensburg: High Speed Electric Drive System, A solution for the next generation e-cars, VDI eDrive 2020,

(2) Andreas Volk, Dr. Michael Leighton, AVL List GmbH: Integrated Development Program for Electrified Drivetrains, ATZ 06/2020

(3) Nickel Falk, Miba Frictec Austria: Dry Multi-Plate Clutch, CTI Symposium China 2019

(4) A. Engstle, M. Deiml, M. Schlecker und A. Angermaier, AVL Software and Functions Regensburg: Entwicklung eines hechgetriebenen 800-V-Elektrofahrzeugs, ATZ 2021

TREMEC Hybrid Dual Clutch Transmission (HDCT)

Electrification of TREMEC's high performance dual clutch transmission

Ir. **Leroy de Ruijsscher**, TREMEC, Zedelgem, Belgium

Abstract

For years, dual clutch transmissions (DCT) have been the pinnacle of driveline technology. Combining top class performance with a unique driving sensation, the DCT has been a popular go-to for many vehicle manufacturers. With electrification playing a prominent role in recent driveline design, the DCT needs to find its place amongst several hybrid concepts. Striving to find the right balance between the fuel- and emission-friendly electric drivetrain and fun-to-drive, high-performance DCT, this paper will cover the several hybridization options for TREMEC's TR-9080 DCT and demonstrate its capabilities to serve as high-performance hybrid dual clutch transmission (HDCT) through the development and testing of a P2.5-P3 HDCT prototype.

TREMEC INTRODUCTION

TREMEC is a global transmission and driveline solutions company, headquartered in Queretaro, Mexico, and with facilities in Wixom, Michigan (US) and Zedelgem, Belgium (EU). Historically a leading manufacturer in the North American market for manual transmissions for high performance passenger cars and commercial vehicles, TREMEC has established itself as leading full-system supplier for high performance DCT's in recent years, with applications in the C8 Corvette, Ford Mustang GT500 and Maserati MC20. A key attribute to TREMEC's development approach is vertical integration from component design and manufacturing to full transmission system assembly and electronic control unit development including SW, calibration and vehicle integration. Confronted with a rapidly changing market under the impulse towards electrification, TREMEC has entered advanced development programs to build on the DCT experience and move towards electrified drivetrain solutions.

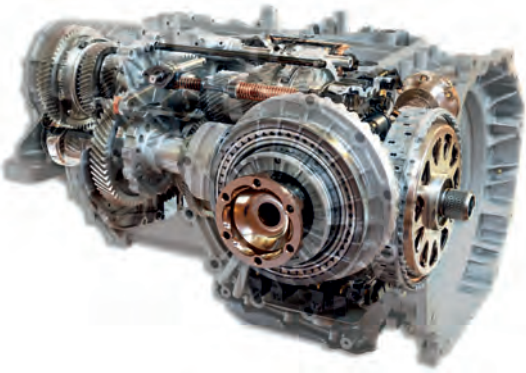

Fig. 1: TREMEC TR-9080 Transaxle DCT

TR-9080 DCT

With the introduction of TREMEC's 8-spd Transaxle DCT in 2020, the TR-9080 [Fig. 1], another high-performance transmission was added to the TREMEC portfolio. Designed with a torque capability up to 1000Nm and with the option to choose between electronic or mechanical Limited Slip Differentials (eLSD or mLSD), the TR-9080 is utilized in several new mid-engine sports car applications. The dual clutch, gear shift system, eLSD and park-by-wire system are controlled electrohydraulically with a TREMEC in-house developed Transmission Control Unit (TCU) and software. Oil pressure to control the transmission is provided by an input driven gear pump or via an integrated electric auxilliary pump for use in hybrid applications.

Unique transmission characteristics:

- Small output shaft distance to front plate: 120mm
- Best in class torque-to-weight ratio of up to 6.5Nm/kg
- High ratio spread up to 8,8
- Dynamic torque up to 1300Nm

TREMEC has explored multiple options to hybridize its dual clutch transmission while maintaining the focus on the high-performance and fun-to-drive character.

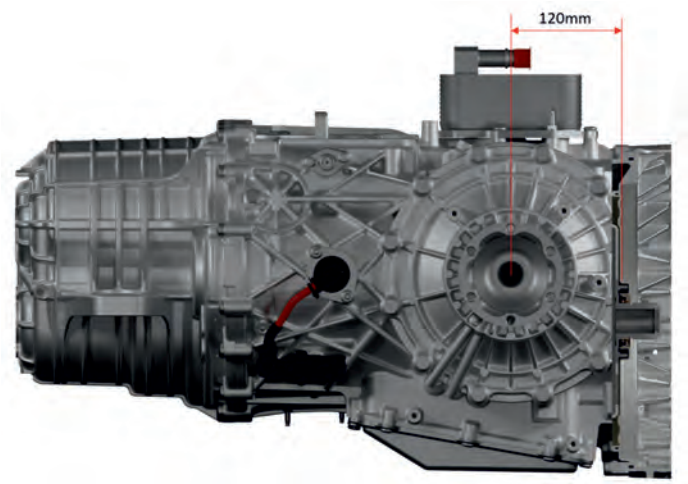

Fig. 2: TR-9080 Output shaft to front plate distance

HYBRID CONFIGURATIONS

Several hybrid configurations [Fig. 3] were reviewed and evaluated in terms of performance, efficiency, cost, weight, and functionality (ICE cranking, standstill battery charging and torque vectoring capabilities). As P0 and P1 hybrid configurations are already compatible with the current transmission, and do not allow for full electric driving, these two configurations are not evaluated further. In Fig. 4, a spider-diagram is showing the results for each hybrid configuration, ranging from 1 being the worst to 4 being the best in a particular category.

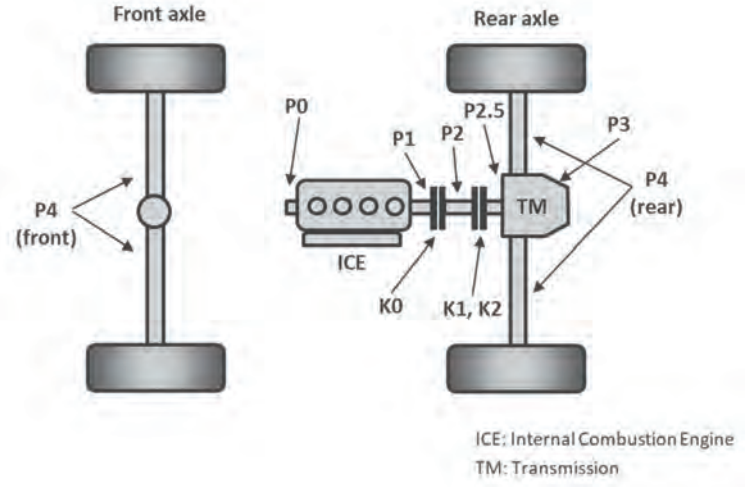

Fig. 3: Hybrid configurations in mid-engine vehicle

With the electric motor between the engine and transmission, the P2 is considered a good all-round option. Being able to boost performance, drive fully electric and provide important features like ICE cranking and battery charging at standstill, the P2 configuration is considered a good option to hybridize while keeping cost & weight low. However, when overall efficiency is important, other configurations perform better. In a P2.5 configuration, the emotor is connected to the odd or even driveshaft of the gearbox, which means electric torque does not pass through the double clutch. This improves fuel economy compared to P2, as clutch and pump spin losses, which are a large contributor to the overall losses in a P2, are reduced. Even higher efficiencies are achieved in a P3 configuration (ref. measurements on P2.5-P3 demonstrator unit) where the emotor is immediately connected to the output of the transmission through the differential. Features like ICE cranking and standstill battery charging are no longer available, as the emotor has a direct connection to the wheels of the vehicle. To benefit from these hybrid features, while maintaining optimal performance and efficiency behaviour, the shiftable P2.5-P3 concept is best suited. Creating the ability to shift between P2.5 and P3 modes, this configuration combines performance, efficiency and functionality, but can be more expensive due to the increase in components and is typically larger in both size and mass, making it more difficult to package.

The P4-rear configuration adds electromotors to the rear axles, one on each output shaft of the transmission. This results in a configuration similar to the P3 setup, but at a higher cost and increased weight/size. An advantage for the P4 configuration is the improved torque vectoring capability. As the motors are directly and independantly connected to the wheels, there is immediate independent control over additional positive or negative torque to each wheel, which will positively affect vehicle track behaviour. The same can be said about the P4-front configuration, where the electromotors are placed on the front axle. With a mid- or rear-engine configuration, this results in an all-wheel drive (AWD) vehicle, which does not only result in an improved torque vectoring capability, but also provides an increase in performance as maximum traction torque is no longer limited by only the rear axle.

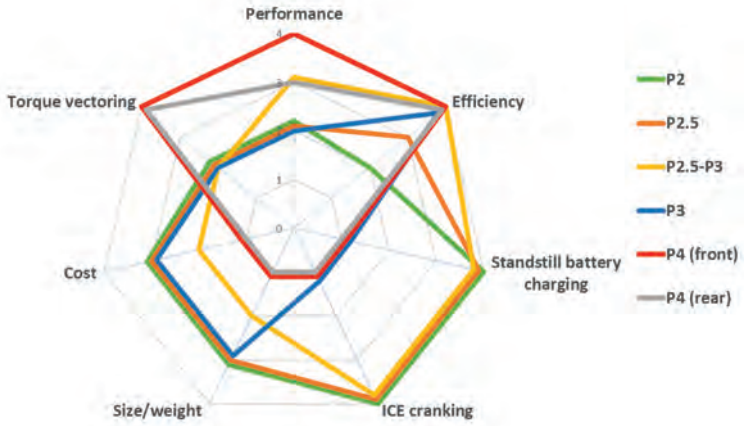

Fig. 4: Evaluation of EV-capable hybrid configurations (1=low score; 4=high score)

Clearly, there is not a single ideal hybrid solution for all vehicles. The decision between each of the configurations, or combination of configurations, will be driven by a variety of factors, which originate from vehicle level demands and targets. Vehicle packaging becomes more challenging as additional electrical systems need to be incorporated: cooling systems, inverter(s), battery pack(s), electronics, … This drives the need to keep component size small or pursue an integrated solution to optimize package space. Overall cost can also influence the selection of a hybrid configuration. Building on existing technology (both hardware and/or software) can help in keeping cost and risk low. Modularity and adaptability become key

characteristics in drivetrain design. Providing a broader choice between various options and allowing future updates to be implemented more easily. Integration complexity becomes a large factor in the overall system design, where a high number of controllers, drivers, actuators and sensors need to function as a whole. This not only brings challenges to hardware packaging and design, but also requires electronics architecture, software and functional safety, to be reviewed from a system level. Finally, the vehicle's character needs to be considered. Hybridization enables adding, removing or even amplifying certain driving characteristics of a vehicle beyond what can be done in an ICE or electric vehicle alone. Based on how these factors are weighed, some hybrid layouts can be favoured above others.

Considering the large amount of influencing factors, and to provide multiple solutions towards the drivetrains of the future, TREMEC has developped several hybrid concepts based on the TR-9080, with the focus on keeping the package compact and having a high level of re-use.

HYBRIDIZATION OF TR-9080

The TR-9080 is considered usable as base for each of the discussed hybrid configurations. While P0 and P1 configurations do not require changes to the current transmission, P2 to P4 result in integrated designs, where the core components of the TR-9080 are carried over. Several hybrid spin-offs of the TR-9080 are under development, as shown in Fig. 5.

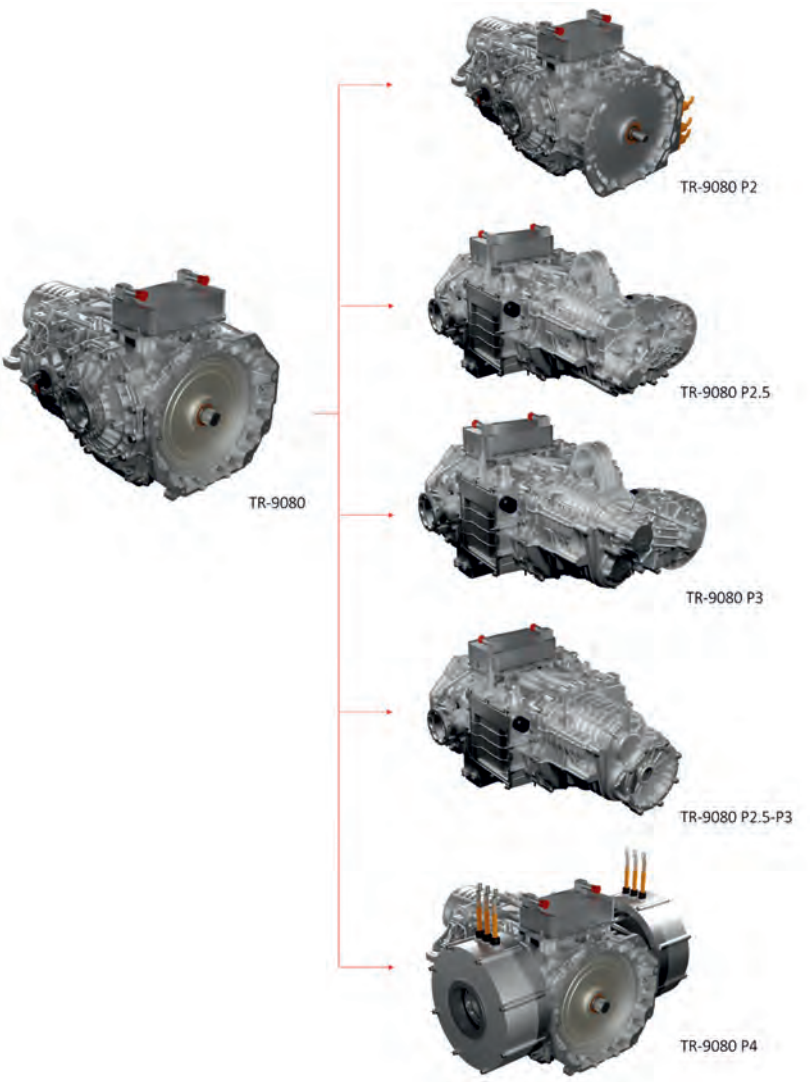

Fig. 5: TR-9080 as base for hybridization

The P2 version of the TR-9080 requires changes to the front section only, where an additional disconnect (K0) clutch, actuation valve and emotor are installed. Other components of the transmission remain untouched. The P2 module makes use of the P2 concept of TREMEC's TR-9070 transmission, which can be seen in Fig. 6. To limit the axial length increase of the transmission, the K0 clutch is nested in the emotor. This results in an axial length increase of only 74mm compared to the base transmission [Fig. 7]. Within this package, the emotor is able to deliver 100kW extra power and would be able to boost ICE torque with 300Nm.

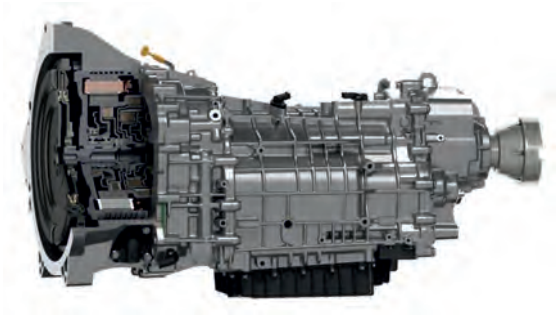

Fig. 6: TR-9070 P2 HDCT

The P2.5 and P3 variant of the TR-9080 are similar in setup. Changes are limited to the rear section of the transmission [Fig. 7]: the rear cover is adapted to be able to install an emotor at the side of the transmission, and provide a geared connection between emotor and carry-over gearbox. This drives an update from sidemounts to a top mount. In case of the P2.5 version, a gear ratio connects the emotor to the odd driveshaft of the transmission, in case of the P3 version, a gear ratio connects the emotor to the countershaft (and therefore output) of the transmission. Gear ratio and emotor selection can be tuned to engine and vehicle specifications.

For the P2.5-P3 variant the gear ratios and additional shift system is placed at the rear side of the transmission, the electric motor is mounted on the back. In this setup, preference goes to an electric motor with small length to limit the total length of the transmission and emotor.

For the P4 variant, a front and rear axle solution are possible. As P4-rear configuration with the transaxle design, the emotors are positioned on each of the outputs of the transmission to immediately drive the wheels. Output flanges are nested inside the emotor to ensure sufficient

halfshaft length. As two motors are added to the transmission, cost and package become critical factors, making the P4-rear more likely suitable for extreme applications which require the extra performance. The P4-front solution would make use of an e-axle in the front [1]. Although a P4-front design is compatible with the current TR-9080, it could also be combined with a hybrid version (P0 to P4) for increased capabilty.

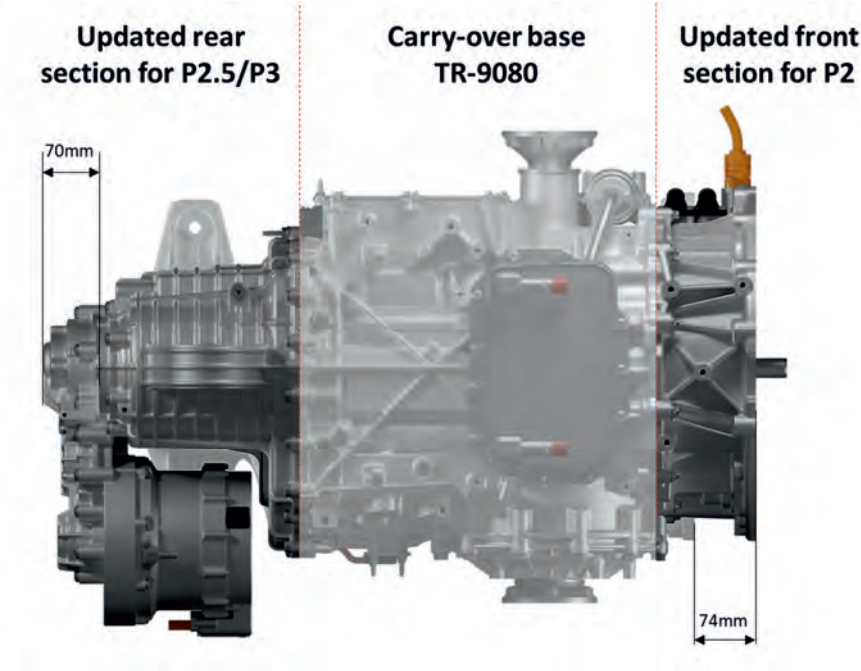

Fig. 7: Front/Rear adaptions to TR-9080

With regards to emotor selection and application, each of the proposals has different specs and features to consider. Within the P2 package, an 100kW Permanent Magnet Synchronous Motor (PMSM) is able to add 300Nm of extra input torque beyond what the ICE can produce. During full electric mode, this results in an available wheel torque of 4800Nm (in 1st gear). In hybrid mode, boosting can happen continuously through all gears up to max vehicle speed. The P2.5 and P3 concept both package the same motor. A 100kW PMSM which is able to provide 150Nm of torque and go up to 20 000rpm. The wheel torque curves for both P2.5 and P3 variants are shown in Fig. 8. For the P2.5 concept, a ratio of 2 is targeted from emotor to

odd driveshaft of the transmission, which would result in a boost of 300Nm at the input shaft of the transmission, similar to the P2. This results in a wheel torque of 4800Nm during full electric driving in 1st gear. Torque from the emotor will always go through one of the odd gears. Therefore, when an odd gear synchronizer needs to be (dis)engaged, for example during a preselect shift, a short emotor torque interrupt is unavoidable to allow the synchronizer shift to happen. As with any P2.5 system, this emotor torque interrupt is present during boosting, when shifting through the gears, but also when a shift needs to happen from one odd gear to the other during full electric driving. A possible mitigation would be to limit full electric driving to one gear only (e.g. 3rd gear), which is able to cover most of the driving conditions: motorway speeds, sufficient gradeability, ... without the need to shift. The P3 system uses a gear ratio of 1.4 from motor to countershaft of the transmission, resulting in 1100Nm wheel torque. Both P2.5 and P3 system allow boosting up to max vehicle speed.

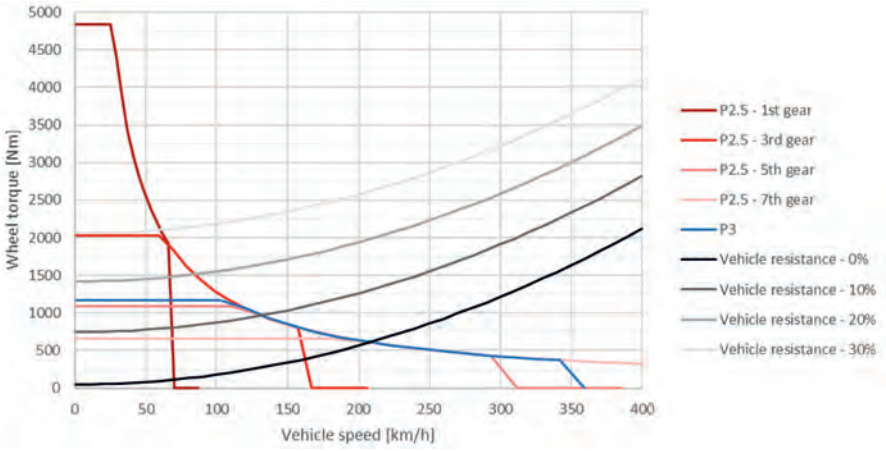

Fig. 8: Wheel torque curves for P2.5 and P3 concept

DEMONSTRATOR P2.5-P3 HDCT

A demonstrator P2.5-P3 TR-9080 HDCT was built [Fig. 9] to use as development platform for hybrid applications. The choice of P2.5-P3 mainly follows from the versatility of this configuration. The transmission is able to demonstrate performance & efficiency gains, as well as hybrid features like ICE cranking and standstill battery charging. Additionally the prototype

will be used to optimize simulation models (e.g. efficiency & NVH models) and will be used to develop and optimize software for hybrid applications.

Fig. 9: Demonstrator P2.5-P3 HDCT

With the focus on maximizing carry-over content of the existing TR-9080 the demonstrator HDCT is designed to be able to demonstrate and compare different hybrid concepts. Aside from showing the applicability of the P2.5-P3 variant of the TR-9080, the transmission allows a direct comparison between P2, P2.5 and P3 in terms of efficiency, performance and NVH. The transmission can act as platform to develop and optimize control software, which can be extended to other hybrid and full electric applications. Specifications of the Demonstrator P2.5-P3 HDCT can be found in Table 1. An off-the-shelf axial flux emotor is used which can provide 160kW of power and 350Nm of torque and was selected to meet the desired performance requirements. This results in sufficient power in both P2.5 and P3 mode for full electric driving or performance boosting in hybrid mode. For production, transmission and emotor will be customized for optimal performance, packaging and other characteristics.

Table 1: Demonstrator P2.5-P3 HDCT Specs

Demonstrator P2.5-P3 HDCT Specs	
Functionality	• 7-spd HDCT (8th gear shift system replaced with P2.5-P3 shifter) • Mechanical reverse gear still present • Battery charging (regeneration & standstill charging) • ICE cranking • Full electric driving • Performance boosting (acceleration boost, top speed increase, ...)
Hybrid driving	• P2.5 – electric boosting up to max speed • P3 – electric boosting up to 180km/h
P2.5 Full electric	• Acc: 0,97g (1st gear) • Max speed: 240km/h
P3 Full electric	• Acc: 0,27g • Max speed: 180km/h • Gradeability: 30%
Performance*	Power • Additional 160kW (from electric motor) 0-100km/h • ICE only: 2.9s • Hybrid: 2,7s Max speed: • ICE only: 320km/h • Hybrid: 350km/h *assumptions based on performance type vehicle

The P2.5-P3 concept allows the selection between P2.5 or P3 operation through an extra shift element, which is operated hydraulically and integrated at the rear of the transmission. This allows the emotor to be connected to the odd input shaft (P2.5 mode) through a gear ratio, or directly connected to the countershaf (P3 mode). The multiple full electric and hybrid torque paths (from ICE and eMotor to output) can be found in Fig. 10 to Fig. 13.

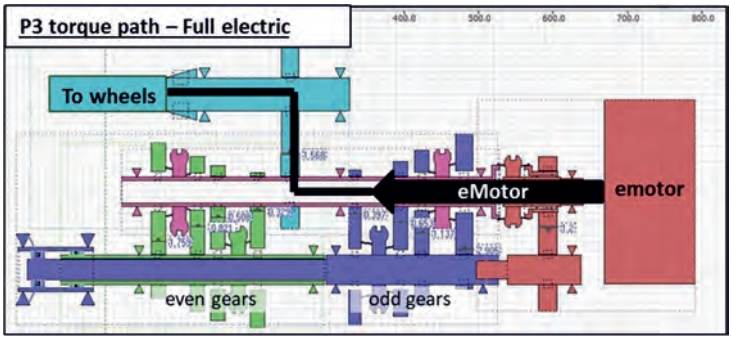

Fig. 10: P3 – Full electric torque path

In the P3 – Full electric torque path [Fig. 10], the emotor is directly connected to the countershaft of the transmission, which results in a direct connection from emotor to the output. Being the most efficient configuration, and also not having to worry about gear shifts up to 180km/h (defined by max emotor speed), P3 is ideal for full electric day-to-day driving.

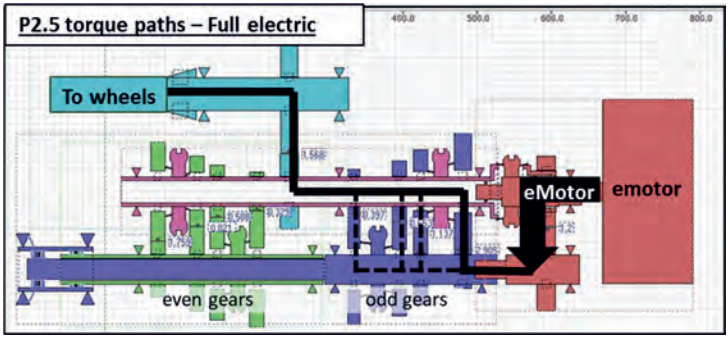

Fig. 11: P2.5 – Full electric torque path

In case there is insufficient wheel torque at low speed in P3-Full electric mode, or to reach max vehicle speed while driving fully electric, P2.5-Full electric mode can be used. The P2.5 - Full electric torque paths [Fig. 11], show the possibility to connect the emotor to the odd input shaft. From the input shaft, torque transfer to the output occurs through one of the odd gears (1st, 3rd, 5th or 7th), depending on the gear selection. When 1st gear is selected, the emotor torque benefits from a large torque amplification over 1st gear, resulting in a wheel torque up to 7000Nm. When 7th gear is selected, the maximum full electric vehicle speed can be achieved of 240km/h.

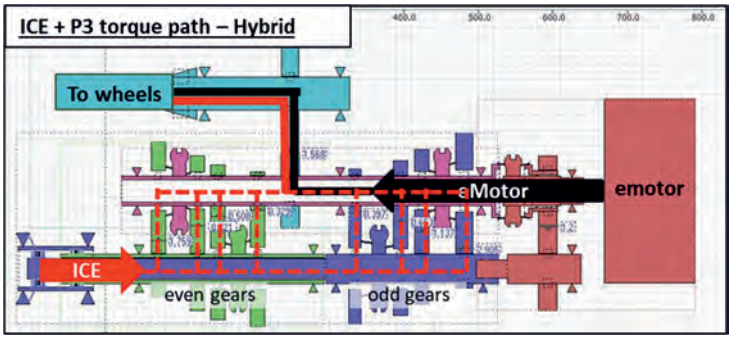

Fig. 12: P3 – Hybrid torque path

In P3 – Hybrid mode, the emotor is still connected to the differential, and additional ICE power is transmitted through one of the gears, as would be the case during conventional DCT operation. Similar to full electric driving, P3 is also favoured in hybrid mode due to its efficiency and absence of torque interrrupts for vehicle speeds up to motorway speeds.

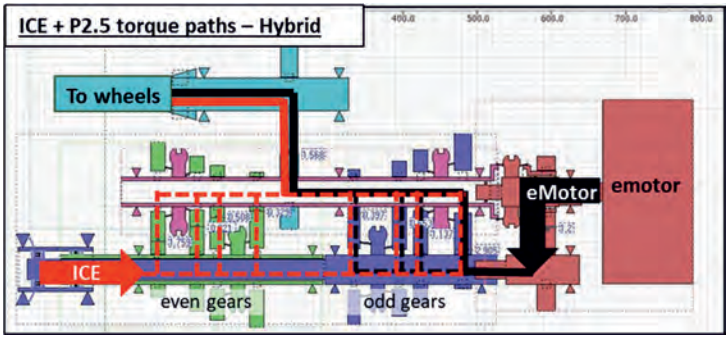

Fig. 13: P2.5 – Hybrid torque path

To boost top speed of the vehicle, P2.5 can be selected as hybrid mode. In this case, torque of the emotor can go through one of the odd gears, while torque of the ICE is able to go through one of the odd or even gears (incl. the same gear through which the emotor is already providing torque to the output).

When no gears are engaged (all synchronizers in neutral position) and P2.5 mode is selected, a direct connection between ICE and emotor can be made when the odd clutch is closed. In this case, the wheels of the vehicle are disconnected from emotor and ICE. This would allow the emotor to be used as starter motor for the engine (driving ICE with emotor) and also allow charging of the battery at standstill (driving emotor with ICE). In P3 mode, the electric motor is always connected to the wheels, which makes regeneration and ICE start through the emotor only possible while the vehicle is moving.

DEMONSTRATOR AS DEVELOPMENT PLATFORM

The demonstrator unit has been subjected to various characterization tests, from basic functionality tests to system efficiency and NVH behaviour. Software has been developed to control the transmission-emotor-inverter combination. A picture of the testbench can be found in Fig. 14, which is showing the tri-axial bench at TREMEC's engineering lab in Zedelgem, Belgium, which allows loaded transaxle transmission testing. Specifically for hybrid transmission testing, the bench was updated with a battery emulator to provide power to the inverter (at 800V DC) and a power analyser to characterize emotor and inverter functionality, efficiency and NVH. [Fig. 15]

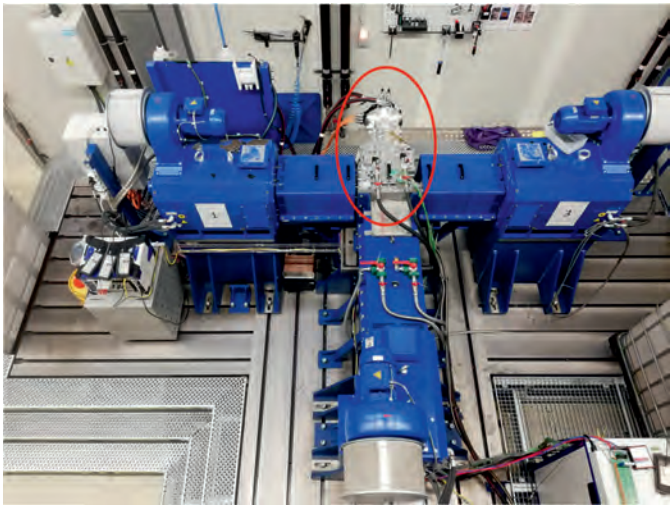

Fig. 14: Tri-axial bench at TREMEC (Zedelgem) with the demonstrator HDCT mounted

Fig. 15: Battery emulator (left) – Power Analyser (right)

As a development platform, the demonstrator has been subjected to various analysis and checks, among which:

- Basic functionality of various modes:
    - P2.5 – full electric
    - P2.5 – hybrid
    - P3 – full electric
    - P3 – hybrid
    - P2 – full electric
- Efficiency comparison
- Drive cycle review
- Hybrid functionality checks
    - Standstill battery charging
    - Regeneration while driving (in combination with positive or negative wheel torque)
    - ICE starter functionality
    - Electric torque response verification

An efficiency comparison was done between P2, P2.5 and P3. First, a correlation study was done between the simulation models of the hybrid configurations and the test data. The results, which can be seen in Fig. 16, show a correlation between measured and simulated cumulative energy smaller than 1%, which validate the hybrid efficiency models. Next, a WLTP cycle [Fig. 17] was performed. Fig. 18 shows the relative energy over the WLTP cycle for all three configurations, comparing the required energy to run a WLTP cycle on the same vehicle with different hybrid architectures. These include transmission, motor and inverter losses during the cycle. As expected, the P2 configuration requires the most energy over the cycle due to its lower efficiency. Due to the smaller torque transfer path for P2.5 and P3, the required energy over the cycle is lower, showing the higher efficiency for these configurations. The difference between P2.5 and P3 cumulative energy is already smaller, but still a higher efficiency can be observed on the P3, being the configuration with the smallest torque transfer path.

The HDCT demonstrator has proven to be a useful tool in hybrid development. Allowing direct comparison between several hybrid configurations, the demonstrator will serve as base for future developments. Several additional investigations are being conducted on the demonstrator, further expanding the knowledge of hybrid systems and control strategies within

TREMEC. These include NVH correlation, in-depth drive cycle evaluation and control software optimizations.

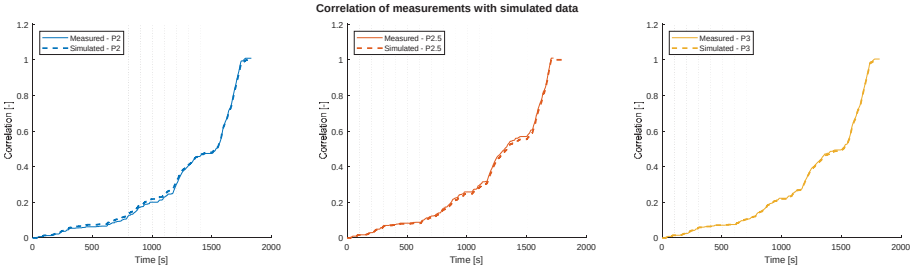

Fig. 16: Correlation simulated data Vs Measured data

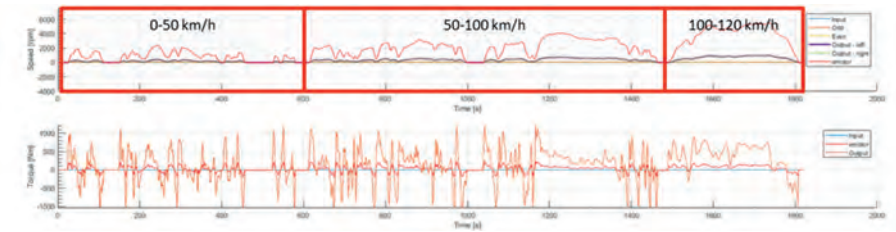

Fig. 17: WLTP Cycle

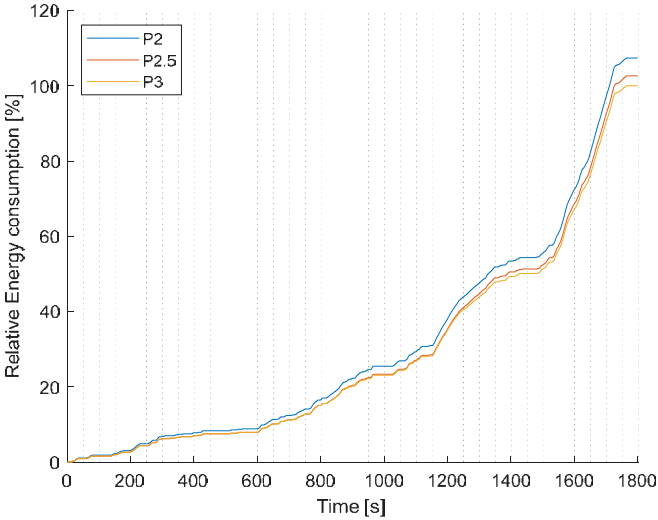

Fig. 18: Relative Energy over WLTP cycle for P2, P2.5 and P3

SUMMARY AND OUTLOOK

The applicability of various hybrid configurations has been reviewed and projected onto the TREMEC TR-9080 high-performance DCT. Considering various factors that impact a hybrid concept, multiple spinoffs from the TR-9080 have been concepted with a high level of carry-over from the current design. This results in several HDCT versions of the TR-9080 which can be used in all hybrid configurations, ranging from P0 to P4. The P2.5-P3 TR-9080 HDCT being the most efficient, performant and feature-rich hybrid configuration, has been built and tested as prototype unit to serve as platform for hybrid hardware and software development. The experience gained during the development and testing of several hybrid configurations, combined with the know-how of producing high-performance transmissions, allows TREMEC to propose several electrified drivetrain solutions to the market.

REFERENCES

[1] TREMEC HYbrid DRive Axle – HYDRA, J. De Landtsheere, Dritev Bonn 2021.

hofer H8-DCT-850 – High Performance Dual Clutch Transmission for transaxle application

Development of an all-new hybrid transmission

A.R. Lowis, **R. Smith**, **A. Tauchmann**, hofer powertrain

Abstract

The new H8-DCT-850 eight-speed dual-clutch transmission has been designed and developed by hofer powertrain, suitable for high performance sportscar applications. The transmission features hybrid technology, enabling EV only driving mode, optimised acceleration and system efficiencies. Alongside hybrid power the transmission also features an e-differential for enhanced driving dynamics alongside high levels of system integration to deliver a compact product with outstanding torque and power capability. Start of series production for the transmission was achieved in Q1 2021, at a brand-new state of the art manufacturing facility.

Key drivers for product development

The first customer for the H8-DCT-850 demanded a set of challenging requirements to be achieved from this transmission. Combined with an all new V6 engine, the transmission had to be made capable of input speeds of up to 8500rpm, with a maximum steady state input torque of up to 850Nm. The desire to have hybrid capability was paramount; permitting EV only driving. Weight and package were also primary objective targets to support the high-performance dynamic attributes from the sportscar application. Despite addition of hybrid technology, transmission mass was optimised, for example, by deletion of mechanical reverse, and taking every opportunity to reduce overall dimensions. A “no compromise” approach was taken during design and development to ensure the requirements were achieved successfully.

Transmission Concept Overview

The H8-DCT-850 is a three-shaft design, incorporating a single split input shaft with two driveshafts for the gearsets. This concept was selected in order to keep overall length to a minimum and to offset the additional length required to incorporate the P2 hybrid motor. The transmission is designed specifically for mid-engined transaxle applications.

Table 1: Overview of the transmission specification

	H8-DCT-850
Number of Speeds	8 forward, e-reverse
Max Input Speed	8500 rpm
Max Input Torque	850 Nm
Max Transient Torque	1150 Nm
Clutch Fill Time	50 ms
Input Shaft to Ground Line	135 mm
Weight (inc. fluids)	175 kg

Detailed evaluation of alternative concepts led to the selection of an 8-speed transmission. This concept demonstrated the best overall solution; providing outstanding levels of acceleration and an exhilarating driving experience; combined with high levels of efficiency and ultimate top speed.

Design Approach: Minimise Mass and Optimise Package

To facilitate a dynamic vehicle handling experience, low mass and CoG are key attributes for any high-performance RWD sports car. This in turn drives a demanding set of requirements for the powertrain, in-particular the transmission. Dual Clutch Transmission systems in the market all comprise of a similar set of sub-systems and components; they all require a gearset, a dual clutch module, and a mechatronic system, as well as various ancillary sub-systems to support automated transmission of the prime mover's power to the wheels. The result is a broadly linear relationship between a transmission's power density and it's mass. Maximising power density whilst minimising overall mass requires an innovative approach to the design and development of a new dual clutch product.

During the early development phases of the hofer H8-DCT-850, challenging attributes of low mass and CoG were highly regarded in the endeavour to produce a competitive, power-dense, high-performance DCT. Ancillary sub-systems such as the lubrication, hydraulic and mechatronic systems became one of many focus areas for innovation and weight saving opportunities, as well as areas requiring significant development effort.

Targeting a low CoG dictated a compact package height between the input centreline of the transmission and the groundline (or lowest point of the transmission). In order to achieve this, hofer pushed the required transmission volume outwards through careful selection and packaging of proprietary components, and ensuring cross-functional systems were designed and developed concurrently for maximum integration.

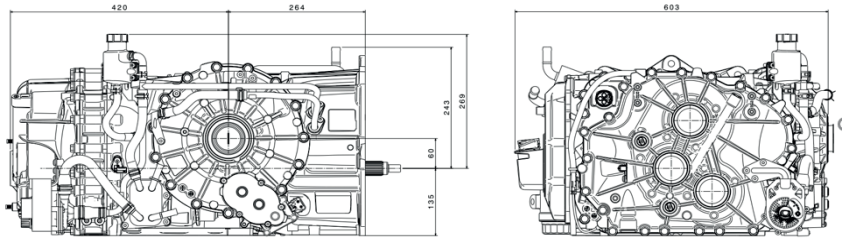

Fig. 1: Compact external dimensions to meet exacting customer package requirement

Design Challenges for the Lubrication and Hydraulic System

A consequence of the overall transmission concept and layout was a large, flat oil sump at the bottom of the transmission, with minimal clearance to the main gearset. This is an unfavourable constraint for any wet sump system and needed careful engineering effort to overcome potential failure modes, for example excessive aeration.

A dry sump concept was evaluated early in the project, but not pursued due to additional mass and complexity.

In addition to the package height restrictions, minimising overall transmission mass was another key requirement for the final product. Development of a new transmission fluid for the H8-DCT-850 allowed hofer to specify a common oil system for all gears, (including bevel stage) and clutch. This solution was taken with the objective to reduce complexity, mass and simplify maintenance.

The DCT concept required a low flow/high pressure hydraulic supply to actuate clutches and select gears. It also required a high flow/low pressure cooling and lubrication supply, to underpin the high-power density design. Finally, the P2 hybrid layout with e-reverse necessitated an electrically controllable pump to cover the low power operation modes of pure electric driving. In response, hofer integrated a single variable vane oil pump to supply the high pressure and high flow demands, with an electro-mechanical oil pump to cover pure electric driving and to boost flow during high power events. The result is a highly integrated pump system capable of supporting all operating modes, whilst minimising mass and package space compared to a conventional fixed pump solution. Similarly, an oil cooler is fully integrated into the clutch housing oil circuit to reduce additional part count and mass that a remote solution would require.

The combination of the variable vane and electro-mechanical oil pumps allows the hydraulic flow and subsequent parasitic losses to be minimised at various operating conditions – offering efficiency savings over more commonly used fixed capacity pumps. However, the stable control, NVH and durability aspects of a variable vane pump are all sensitive to the quality of oil supplied – particularly the level of aeration.

The selection of a common oil, wet sump system with a variable vane oil pump posed a significant development challenge for hofer to overcome. Advanced design and verification techniques were applied to accelerate the development cycle for the hydraulic and oil management components, to optimise the quality of oil available to the pumps and mechatronic systems. This process began with an extensive correlation exercise between lubrication distribution assessments with physical parts on a quasi-static tilt test bench (simulating vehicle g-loading), with a complex CFD simulation package for the complete transmission. The simulation allowed hofer to assess the impact to the oil distribution over numerous input conditions (including gearset speed, hydraulic consumers, and g-loading, for example), in areas of the transmission not practically accessible through physical testing alone. This allowed cross-functional engineering teams to make development changes to their components in advance of physical test results – all with a common goal to improve oil availability at the point of pick-up. Prototype components were rapidly manufactured at the test engineering facility, and trialled on the test bench.

Fig. 2: CFD simulation of lubrication system (left) & physical rig test (right)

Finally, at the end of each programme phase – the optimised design was subjected to a fully dynamic tilt test, capable of operating the transmission under conditions experienced in a high-performance vehicle. The specialist test bench replicated race track levels of vehicle g-loading, by articulating the transmission to a real time acceleration profile of up to 120° of tilt per second (45° = 1g static). The overall approach facilitated numerous development loops in quick succession, and verification of complete system performance in advance of vehicle testing - ultimately lead to a highly optimised and stable oil management system ahead of vehicle testing feedback.

Gearset and Shifting

Fig. 3: Gearset arrangement

The 8 forward ratios within the DCT were carefully selected to optimise acceleration and efficiency. A separate mechanical reverse gear is not required, as the electric motor provides the capability to drive the input in the reverse direction. The split input shaft effectively separates the transmission into two halves, with odd ratios at the rear of the transmission and even at the front. In turn, this split input is connected to two driveshafts, the upper driveshaft comprising gears for ratios 1-4, the lower for ratios 5-8. These driveshafts are then connected to a single output shaft, comprising a helical final ratio and bevel stage to finally transfer torque to the vehicle driveshafts and wheels. An electronically controlled differential is integrated into the transmission. This provides significant benefits from a traction and vehicle dynamics perspective. The e-diff is fully controllable, with locking torque capability of up to 2000 Nm within a fraction of a second.

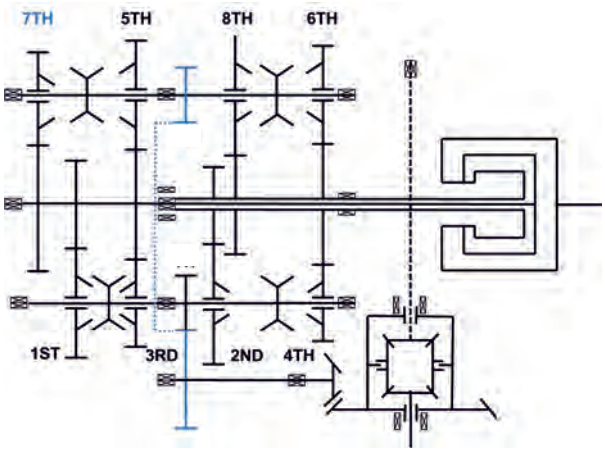

Fig. 4: Schematic Powerflow diagram

Shifting is hydraulically actuated via a shift fork and rod system. Speed synchronisation during shift events is achieved through the use of triple cone synchronisers for all gears. Shift sensor, detent and bearing are combined into a single component, reducing mass, complexity and cost.

Actuation is split across two hydraulic control units. Responsibilities for overall pressure and flow control are managed by the HCU integrated into the base of the clutch housing. The second HCU, located on the side of the transmission, manages clutch pressure and individual valves for shift events. Both HCU's utilise a series of integrated channels in the main casting of the clutch housing.

Optimisation of Gear Set Micro Geometry for Refinement

Reliable torque and power transfer is only part of the story for gearset and holistic transmission development. In addition, stringent NVH (Noise, Vibration and Harshness) targets were set, to ensure a refined driving experience, adding to the challenges faced by the hofer engineering team. During early phase testing, an opportunity to improve refinement was identified, specifically for the 7th gear ratio.

Typically, optimisation of gear micro geometry is a time-consuming process requiring multiple iterations of manual calculation, simulation and assessment. Gear micro geometry can be a significant excitation factor and contributes to audible noise, noticed in vehicle as gear whine. To minimise this, it is necessary to reduce peak to peak transmission error within the gear train.

The hofer NVH team applied a new optimisation tool to resolve this concern. This tool was developed in house by hofer engineers and enables a systematic approach to optimisation of gear micro geometry. This approach considers all relevant design parameters; for example stiffness and geometry of gears, shafts and bearings. The tool utilises proprietary KISSOFT and MATLAB software to evaluate multiple micro geometry candidates and assess corresponding gear contact pattern. The most beneficial geometry for NVH is automatically selected and generated to be utilised in the gear design and manufacturing process.

A successful outcome was achieved in a fraction of the time usually associated with a conventional manual methodology.

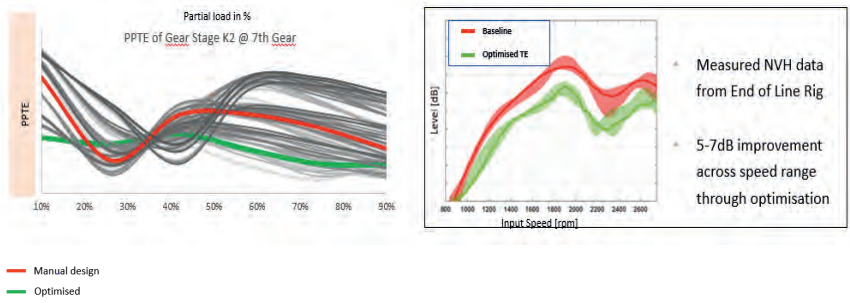

Fig. 5: Output of Transmission Error Optimiser and measured End of Line comparison, post optimisation of all gears

Industrialisation and Manufacturing

An all new, purpose-built facility has been created by hofer powertrain products, located in Solihull UK; for the final assembly and test of the transmission. This is a joint venture between hofer powertrain and ElringKlinger, drawing upon the expertise of both companies.

The manufacturing facility was constructed in parallel to the engineering development activity and achieved the significant milestone of series production in Q1 2021; four years after the project began.

Virtual tools were used extensively to support the manufacturing team evaluate and create an efficient and effective facility layout.

The 4400 m² facility meets all necessary automotive APQP standards, with overall capacity to produce up to 15,000 transmissions per annum.

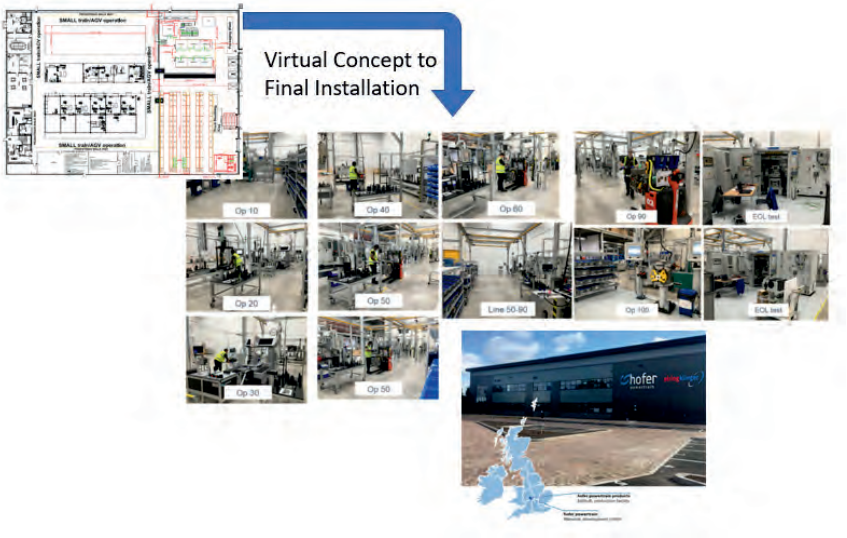

Fig. 6: Production Facility Virtual Concept & Final Installation

Potential Future Developments

Numerous potential adaptations of the transmission are possible for future customer demands. The hofer development team have already evaluated an early phase concept to support ultra-high levels of performance. The motivation to do this is to provide increased levels of e-motor power for high acceleration levels and maximum vehicle speed (in excess of 450 kph). In addition, a requirement was identified to shorten the distance between the front transmission flange and output shaft, to provide greater freedom to the customer to achieve more aggressive vehicle design proportions.

A P2.5 hybrid topology has been designed, moving the motor to the rear of the transmission, connecting drive via 7th gear within the transmission. Performance has been simulated with an e-motor output of 300kW maximum. The P2.5 layout enables a power split to deliver very high combined torque levels from the ICE and EM.

This concept builds on the existing H8-DCT-850 design and highlights the potential flexibility for the future.

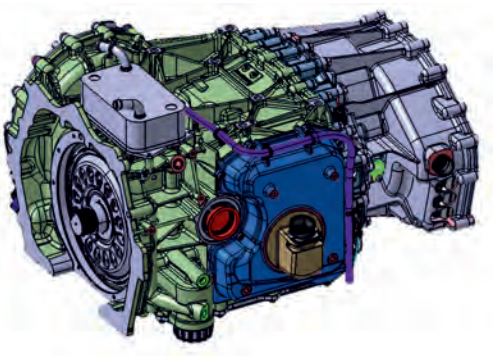

Fig. 7: Concept design with rear mounted P2.5 E-motor

Summary

The hofer H8-DCT-850 provides outstanding levels of performance within a compact package envelope. Hybrid drive capability from the axial flux motor enables EV only propulsion and torque fill capability, coupled with optimised efficiency.

High levels of integrated technology within the transmission have provided the customer with significant benefits to the desired driving attributes. Volume manufacture of the transmission, to the latest quality standards has been achieved.

The hofer H8-DCT-850 is a new hybrid transmission within the sportscar segment and can be adapted for a range of future applications; providing a world class solution in an electrified world.

Modular and highly functional Hybrid Platform for subcompact cars up to full-size SUV

Erik Schneider, Dr. **Christoph Danzer**, **Erik Schreiterer**,
IAV GmbH, Stollberg

Zusammenfassung

Um die Flottenziele für 2030 in Bezug auf Emissionen, Leistung, Komfort, Gewicht und Kosten zu erreichen, suchen Fahrzeughersteller nach der optimalen Antriebsstrangkonfiguration und Technologiekombination für ihre zukünftigen Fahrzeugflotten mit hoher Effizienz und Modularität, erschwinglichen Kosten und überlegener Leistung. Mit niedrigeren Emissionszielen für 2030 in Kombination mit einem ganzheitlichen Ansatz für CO2-Emissionen über die gesamte Fahrzeuglebensdauer wird die Marktnachfrage nach Hybridfahrzeugen kontinuierlich steigen. Vor diesem Hintergrund beschreibt das vorliegende Paper das Konzept eines modularen Hybridbaukasten, um diese Marktnachfrage für ein breites Fahrzeugspektrum mit Frontquer-Antriebsstrang abzudecken.

Abstract

In order to achieve the fleet targets for 2030 in terms of emissions, performance, comfort, weight and costs, vehicle manufacturer are looking for the optimal powertrain configuration and technology combinations for their future vehicle fleets with high efficiency and modularity, affordable costs and superior performance. With lower levels of emission targets for 2030 in combination with a holistic approach to CO2 emissions over the entire vehicle life, the market demand for hybrid vehicle will increase continuously. With this in mind, this paper describes the concept of a modular hybrid platform to meet this market demand for a wide range of vehicles with front-transverse powertrains.

Introduction

CO2 fleet targets in Europe through to 2030 are defined essentially by legislation [1], with target values ranging from 50 to 70 g CO2/km, depending on fleet composition. These targets can only be achieved with considerable electrification measures, which reduce the consumption level in the currently tank-to-wheel balancing (TtW). But carbon-neutral mobility can only be achieved by 2050 if most of the necessary primary energy comes from renewable energy sources. Consequently, carbon balancing should be extended from the wheel at least

to the fuel or energy source (chemical/electrical), known as well-to-wheel (WtW). An honest comparison of the powertrain concepts needs to consider cradle-to-grave balancing (CtG), due to the fact that the various powertrain forms differ in terms of their global warming potential (GWP - ecological footprint for manufacturing, production and recycling) in addition to emissions from their operation.

Another challenge encountered the route to carbon-neutral mobility is that for certain vehicle segments, complete electrification cannot be realized in competitive terms, neither from an economic nor from a technical point of view. Combustion engines are still the expedient solution for vehicles that demand continuously high power like airplanes, heavy commercial vehicles or construction machinery. This kind of mobility needs synthetic fuels (e-fuels) synthesized from ambient CO2 and renewable hydrogen. The demand for renewable primary energy is increased considerably by the relatively low efficiency of these power-to-gas/liquid generation paths of between 45% and 65% (WtT) [2]. Besides CO2 and emission legislation, manufacturing costs and customer acceptance will define which powertrain types are offered in which vehicle segments. This is accompanied by the challenge of defining cost-efficient platforms with modular components so that a wide range of vehicles can be offered with different levels of electrification. Modular powertrain systems must also be highly flexible to withstand possible changes in legislation (WtW, CtG), unclear establishment of renewable energies (renewables) and a volatile purchaser behavior.

Systematic Concept Development

Optimizing these powertrain components, topologies and functions requires a development process on the system level for powertrain and vehicle, as well as a long-term product strategy for the whole vehicle fleet. IAV offers unique methods and tools for proceeding systematically the whole development process, from the end user requirement through to the system release recommendation.

The systematic process (Fig. 1) starts by recording all the requirements made by the end user, legislation, the target markets, the vehicle manufacturer, suppliers and energy providers. IAV then uses mobility synthesis to describe the influence of market and environmental conditions on the user behavior, thus developing future mobility scenarios that can be described in terms of their technical requirements and customer acceptance. Based on these mobility scenarios, IAV systematically ascertains and optimizes powertrain concepts that are expedient solutions for the specific vehicle and primary energy source in order to achieve carbon-neutral mobility.

Powertrain synthesis systematically collates the large number of all possible powertrain components to obtain powertrain variants that are optimized in terms of cost, efficiency and driving performance. The main powertrain parameters are thus defined as the basis for then developing the structures of the respective components, using the proven synthesis methods among others for transmission, electric motor and actuation. The final result consists in a powertrain concept with specific individual components. At the same time, the vehicle-specific powertrain variants form the basis for optimization on fleet level. Platform synthesis collates the vehicle-specific optimized powertrain variants in modular systems for systematic minimization of diversity, emissions and costs on fleet level (Fig. 1). This extensive approach thus permits a dedicated and sustainable development of the future mobility.

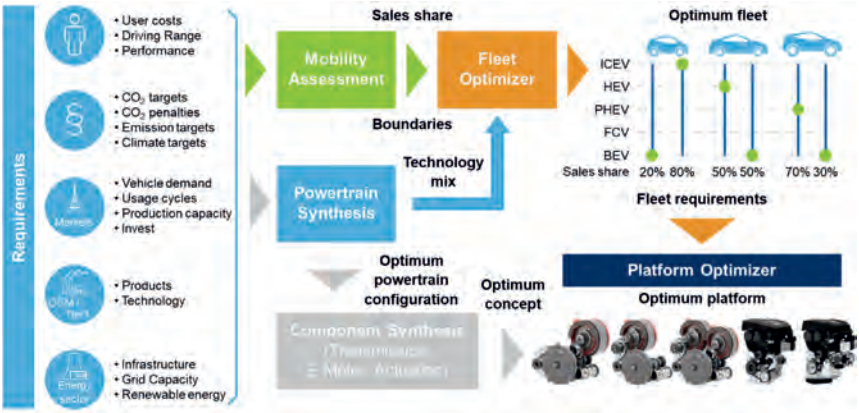

Fig. 1: IAV's Methods for Advanced Development

For an objective comparison of powertrain concepts regarding their impact on the greenhouse gas effects a focus on the vehicle operation is not sufficient. Life cycle assessment (LCA) is one way of extending the scope. Here WtW balancing also considers synthetic fuels with various energy paths. Furthermore, a CO2 assessment of the manufacturing and production process (CtG) is necessary for a neutral comparison of the concepts behind various powertrain types. This paper extends the traditional TtW view by adding the CO2 influences for the WtW and CtG system limits. In particular, this takes account of the CO2-intensive manufacturing process for the battery systems and magnet materials used in electrified powertrains. The LCA properties can be generated for every single powertrain variant in the overall system, with downstream fleet synthesis (Fig. 1) permitting an overall assessment of

all powertrain types in all vehicle segments including CO2-TtW, -WtW and -CtG, primary energy demand and manufacturing costs.

Variation Study for Powertrain Mix 2030

For the following variation study the five key powertrain types - combustion engine, hybrid, plug-in hybrid and pure electric with fuel cells or battery - are assigned to the three main vehicle segments (B, C, D/E segment). The TtW-CO2-emissions for every vehicle/powertrain combination are calculated according to the WLTP, together with the CO2-equivalent for WtT-, WtW- and CtG-balancing. Furthermore, the primary energy demand is ascertained for manufacturing and producing the fuel/electrical energy, the vehicle and the powertrain. The primary energy demand and the manufacturing costs for the powertrain components including the energy storage system are added to the dataset.

The variation study (boundary conditions in Fig. 2) includes a maximum of three powertrains for each vehicle segment. The combination of powertrain types is open and subjected to a fully combinational analysis. It is thus possible to assess how many powertrain types are expedient for which vehicle segments in terms of CO2 fleet targets and manufacturing costs.

At the moment, it is not known how the purchasing acceptance of end users will develop for the new powertrain types. This unknown purchaser acceptance has been quantified by considering all combinations of sales distributions, in order to take account of the production prediction for 2030 and also to view 100 % or mixed scenarios.

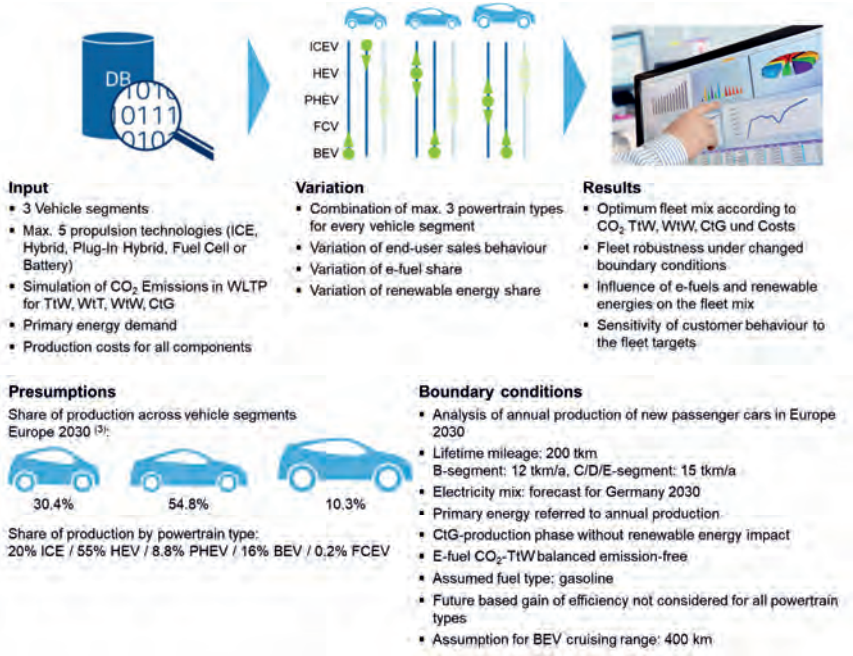

Fig. 2: Boundary Conditions for the Variation Study

Influence of CO2 Legislation

Fig. 3 shows the individual fleet scenarios in the total solution set of approx. 9 million powertrain and fleet variants, thus giving an overview of limits and sensitivities for the key fleet characteristic numbers. It shows the two 100% scenarios ICEV and BEV as well as the predicted fleet forecast for 2030. Color-coding is used to show the share of battery electric vehicles. The third area of the parameter area is marked by a theoretically possible 100% scenario for fuel cell vehicles.

Under current TtW-legislation, average OEM CO2-fleet emissions are reduced primarily by zero-emission vehicles, with an almost linear increase in manufacturing costs on the fleet level. Expanding the CO2-balancing limits, for example to WtW, would result in an absolute increase in emissions as well as greater potential for optimizing costs. Fig. 3 (on the right) also shows a high cost gradient as soon as WtW-emissions are reduced to values below approx. 120 g CO2eq./km with the predicted 2030 electricity mix. It is not possible to bring the WtW-value below approx. 80 g CO2eq./km, even with 100% battery electric vehicles.

CO2-neutrality can only be achieved by further increasing the share of renewable energy compared to the 2030 electricity mix.

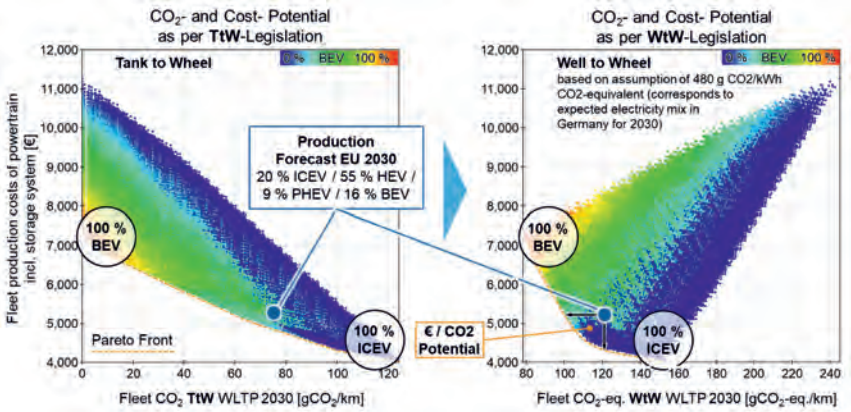

Fig. 3: CO2 and Cost Potential due to Change of Legislation

Influence of Powertrain Types on CO2-Potential

Another challenge consists in the systematic generation of modular powertrain systems to take account of the complete combination of maximum three out of five possible powertrain types (ICEV, HEV, PHEV, FCV, BEV) for every vehicle segment. It is thus possible to ascertain the powertrain types needed for the fleet objectives, and to minimize their quantity. Fig. 4 on the left shows the impact of number of powertrains on TtW-CO2-emissions. There are considerable differences between all the noted scenarios for optimum costs, optimum TtW and optimum WtW, in terms of both CO2-potential and the composition of the power-train types. All three optimization targets exhibit seven different powertrain types for the fleet that achieve the lowest TtW-CO2-emissions overall. Every single fleet configuration (point in the data cloud) includes a segment-specific distribution of the powertrain types with all information about CO2, primary energy and cost values. Furthermore, the powertrain types needed for the WtW-optimum scenario shown in Fig. 4 as well as the vehicle-specific distribution.

The results show that the pure ICE powertrain has a very high share for the B-segment with 40%, due above all to the lower consumption advantage compared to HEV with far lower costs. HEV technology dominates the C-segment with an 80% share. Here the high sales figures make a significant contribution to the CO2-fleet target.

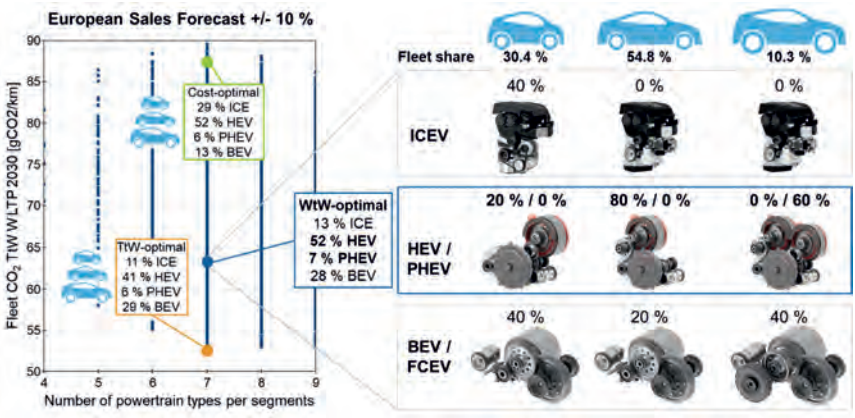

Fig. 4: Powertrain Types optimized in Terms of WtW-CO2, TtW-CO2 and Costs

The use of plug-in hybrids is expedient for the D-segment even after WtW-balancing, as consumption can be clearly reduced by electric driving particularly in urban traffic. The BEV powertrain type accounts for a relatively high share in the B- and D-segment with 40%. The results also show that only in the B-segment a pure combustion engine powertrain is seen as expedient for the fleet targets. All other vehicle segments have combustion engines combined with either HEV or PHEV technology. Summarized this leads to a demand of a widespread applicable powertrain platform for HEV-system in B- and C- segments and for PHEV-application in D- and E-segments. Additionally a BEV-powertrain platform with single- and multispeed transmissions are needed to cover effectively a wide spectrum of vehicle applications.

Platform Approach for Hybrid Systems

How can one modular DHT system cover the divergent boundary conditions of a whole vehicle platform? This is the main question when it comes to the requirements definition of a future hybrid system for a front-transverse vehicle platform. Between a subcompact car, which is mainly used for urban driving, and a full-size SUV, which needs to provide a high load and towing capacity, the main development targets like system costs, package, driving performance and comfort as well as functional aspects can differ in a wide range, even if all these vehicles are based on the same platform. The breakdown of these requirements from the vehicle level to the hybrid system leads to different demands for output torque and power,

range of hybrid functions and the level of driving comfort. A reasonable approach is to define a basic DHT layout for the demands of the smaller vehicle classes, where low system costs, advantageous low fuel consumption, small system package and a decent drivability are important. The enhanced requirements of mid-size passenger cars and full-size SUV can be covered by the smart integration of a second e-motor into the drive train.

In case of the D-segment vehicle, the additional e-motor is installed in the DHT in order to increase the driving performance in electric and hybrid drive and to offer a serial driving mode for very good driving comfort at low and medium vehicle speed, which is on the level of battery-electric vehicles. In addition, the serial driving mode enables a fast battery recharging. The high traction demand of a full-size SUV and the needs for a good off-road capability requires an all-wheel-drive system. Here the second e-motor is mounted at the rear axle. The advantages of a serial driving mode can also be captured with this powertrain con-figuration.

Hybrid System Optimization of the Platform Basis

The next question in the development process of the modular DHT platform is to find the right setup for the basic hybrid system with one e-motor. The pre-mentioned IAV Powertrain Synthesis offers the right methodology for answering this question by varying the general hybrid topology as well as the main parameters of the hybrid system like number of speeds, ratio configuration, performance parameters of the e-motor as well as the kind of the e-motor integration (Fig. 5).

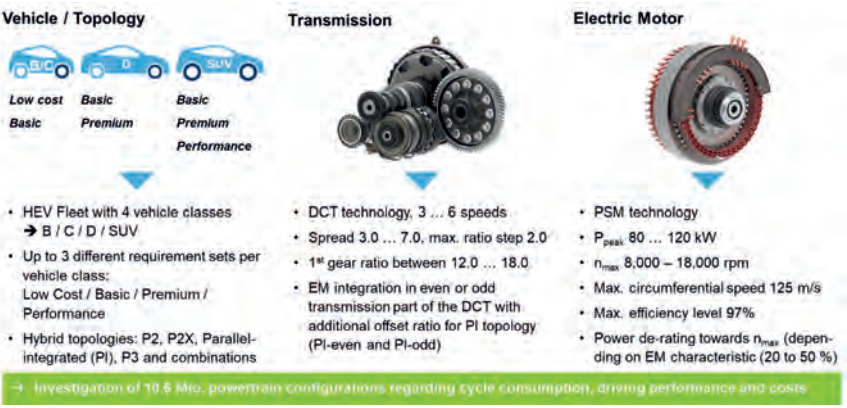

Fig. 5: Investigation of the DHT System with IAV Powertrain Synthesis

The variation study of the hybrid systems, which are all based on a DCT technology, shows a clear tendency towards systems with three or four speeds, since they offer a good compromise between fuel consumption and system costs. A higher number of speeds does not lead to a reduction of the fuel consumption, but the costs increase due to the higher mechanical effort. A comparison of the different hybrid topologies - P2(X), parallel-integrated (PI) and P3 - does not show an obvious trend towards one specific system layout. With an optimized parameter set all investigated topologies can achieve a very good overall compromise in regard to efficiency, performance and powertrain costs. From this reason, an investigation of the rough package situation is added to the system investigation. At this point the P2 configurations show a noticeable disadvantage, because the additional C0 clutch and the arrangement of the e-motor at the input shaft lead to an increased overall transmission length. Furthermore, the shift of the differential position towards the left front wheel can be critical for the length of the left side shaft, especially in smaller vehicle segments. In conclusion, a DCT with a parallel integrated e-motor, which is connected to the hollow input shaft, offers a very good compromise between the properties from the powertrain variation study and the package investigation and was therefore selected for a further detailing of the modular DHT platform.

Gear Structure Definition

An investigation of a suitable gear structure with the IAV Transmission Synthesis methodology ended up with a very compact 4-speed DCT structure, which uses a winding power flow in the first speed for a low mechanical effort and a short gear set with only 3 gear set levels (Fig. 6).

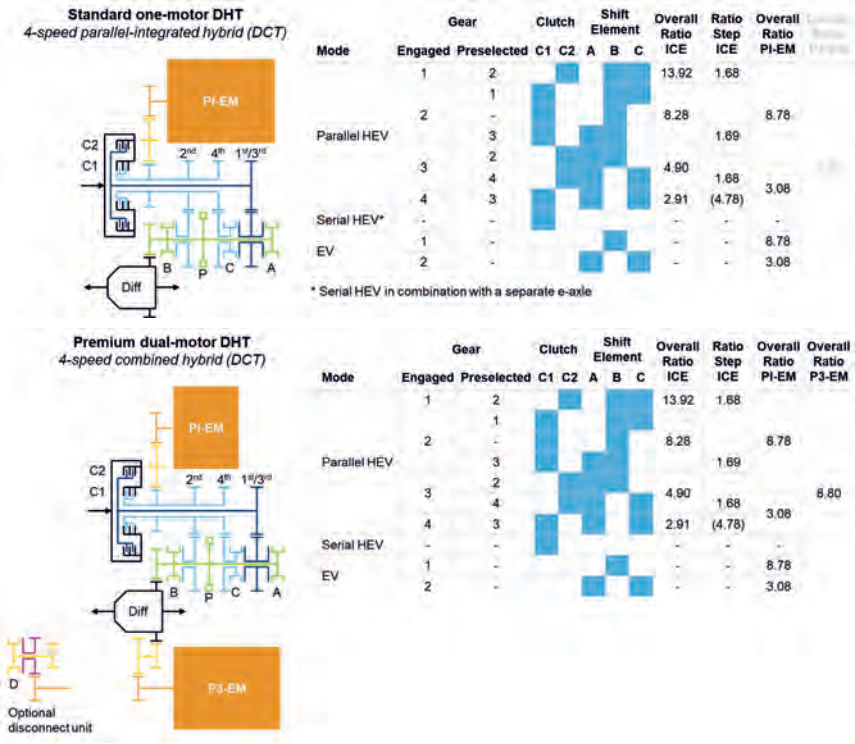

Mode	Gear Engaged	Gear Preselected	Clutch C1	Clutch C2	Shift Element A	Shift Element B	Shift Element C	Overall Ratio ICE	Ratio Step ICE	Overall Ratio PI-EM	Overall Ratio P3-EM
Parallel HEV	1	2	■			■		13.92	1.68		
		1									
	2	-						8.28		8.78	
		3							1.69		
	3	2						4.90			6.80
		4							1.68	3.08	
	4	3						2.91	(4.78)		
Serial HEV*	-	-						-	-	-	
EV	1	-						-	-	8.78	
	2	-						-	-	3.08	

* Serial HEV in combination with a separate e-axle

Mode	Gear Engaged	Gear Preselected	Clutch C1	Clutch C2	Shift Element A	Shift Element B	Shift Element C	Overall Ratio ICE	Ratio Step ICE	Overall Ratio PI-EM	Overall Ratio P3-EM
Parallel HEV	1	2	■			■		13.92	1.68		
		1									
	2	-						8.28		8.78	
		3							1.69		
	3	2						4.90			6.80
		4							1.68	3.08	
	4	3						2.91	(4.78)		
Serial HEV	-	-						-	-	-	
EV	1	-						-	-	8.78	
	2	-						-	-	3.08	

Fig. 6: Transmission Structure and Functionality of the Standard One-Motor and Premium Dual-Motor DHT

The first e-motor (PI-EM) is used in both system configurations and is connected to the hollow input shaft with the second and fourth gear on it. The overall spread of the ICE and HEV speeds is 4.8, as this was identified as the favorable transmission spread in the Powertrain Synthesis. A change of the ratio between the e-motor and the output happens in the third HEV mode by changing the preselection from second to fourth speed. During this shift process, an active torque support from the ICE provides enough output torque to prevent a noticeable vehicle jerk. With this adjustable e-motor ratio, the rotational speed can be lowered at high vehicle velocities, which helps to achieve better operating points of the e-motor and lowers the speed dependent losses. For a good drivability in the EV mode, the first speed with a ratio of 8.78 is optimized for both a sufficient pure electric output torque and a maximum e-drive velocity of 130 kph. A shifting of the e-motor ratio is therefore not mandatory in

a typical EV mode velocity range. However, a second pure electric gear (EV 2) is available. The decision of using this optional speed depends on the driving comfort requirements and can differ across the vehicle fleet. For the extension of the basic DHT to a combined hybrid system, a second e-motor (P3-EM) drives the differential gear over an independent intermediate shaft. The overall ratio of this e-motor is comparable to the first speed ratio of the PI-EM as the output torque demands are on a comparable level. A limitation of the rotational speed of the P3-EM is possible with an optional disconnection device at the intermediate shaft.

Definition of the Gear Actuation System

For the gear actuation in the 4-speed DCT, an electro-mechanical shift drum actuator is favorable as all shift elements and the parking lock are placed on the intermediate shaft. This allows a compact actuator with very short connections. To identify an actuation system which is well-balanced regarding shift performance, package and costs, the fundamental procedure of the Synthesis methodology is used in this context as well (IAV Actuation Synthesis, Fig. 7). In the first step, the variation space for the investigation is defined. In addition to the characteristic of the DC motor, the groove geometry of the drum and the gear set type – helical or planetary – as well as the gear set ratio are varied for the considered gear actuator. For each valid combination of the sub-components, a computer-aided pre-dimensioning is carried out by using a transient 1D simulation of the shift process. Based on the results of this simulation, the main parameters such as shift time, power consumption, size and weight can be assessed for thousands of analyzed actuators. By applying weight-based cost approaches for the main components, even the production costs can be compared in this early development phase. In the final evaluation step, the overall benefit value of the different systems can be displayed in a ranking. This benefit value results from the weighting of the single properties and can be customized for each application. In case of the considered gear actuation for the DCT, a shift drums with an integrated planetary gear set (Wolfrom transmission) prove to be particularly suitable as they gain a significant package advantage. Finally, a design concept of the shift drum and the shift fork assembly is created to check the feasibility and to investigate the integration into the transmission system.

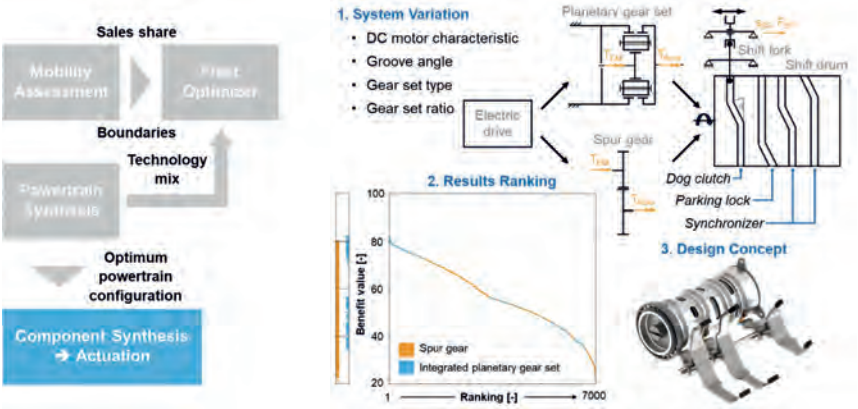

Fig. 7: Gear Actuation Definition with IAV Actuation Synthesis

Modular Electric Motor Design

According to the introduced platform approach, up to two electric motors will be used in the DHT, one with a parallel-integrated position (PI) and the other one in P3-arrangement. Besides, different levels of electrification (e.g. HEV / PHEV) also require a decent power scaling of the electric motors. Despite the different requirements regarding installation, speed limits and power demand, a modular design with a common lamination is to be developed in order to save development and production costs through synergy effects. The basic design of the high power version of the electric motor with 100 kW peak power is already pre-optimized by the variation study with IAV Powertrain Synthesis. The standard power version is to be used primarily as a generator-machine in the combined hybrid systems. For this purpose a continuous power of 40 kW and a resulting peak power of about 60 kW is perfectly sufficient to ensure adequate charging power in serial mode. But even the use of two standard power e-motors, one as generator and one as main traction motor, in a combined hybrid system is possible.

Furthermore, the design approach for the e-motor platform is to maximize the stator outer diameter by pure oil cooling (no radial space for a water jacket required) for high peak torques and to lower the circumferential speeds by low connection ratios. This ensures that a short e-machine can be designed at a typical power density level to meet the challenging length requirements of the overall system.

The result of the concept design of the e-motor family is summarized in Fig. 8. For both installation positions (PI and P3) the same e-motor can be used as the maximum speed re-

quirement can be covered with a common design. The power scaling between the high and the standard power version is mainly based on a length adaption. With a common rotor and stator lamination, the high power version uses 5 sheet metal segments with an individual length of 15 mm, whereas the standard version uses 3 of these segments. In addition, there is a difference in the winding, which can be seen in Fig. 8 at the bottom of the table. This results in different designs of the hairpins, which are necessary anyway due to the length scaling.

In the end, the developed e-motor platform fulfills the different performance and package requirements, thus offers a high degree of modularity to serve the various applications of the DHT family at advantageous development and production costs.

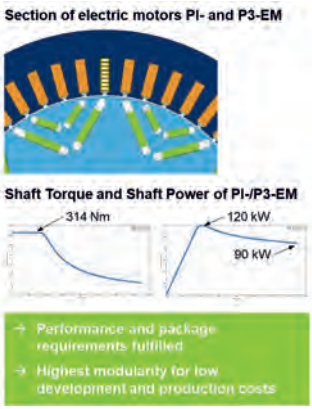

Selected Design Properties		PI- and P3-EM High power	PI- and P3-EM Standard power
Geometry			
Iron core stack length	[mm]	75 (5 x 15)	45 (3 x 15)
Air gap width	[mm]	0.8	
No. of pole pairs	[-]	4	
Stator core			
No. of slots	[-]	48	
Outer diameter	[mm]	248.5	
Inner diameter	[mm]	175.0	
Rotor core			
Outer diameter	[mm]	173.4	
Inner diameter	[mm]	60.0	
Winding			
No. of slots per pole and phase	[-]	2	
Short pitching	[-]	5/6	
No. of parallel paths per phase	[-]	2	1
No. of serial turns per phase	[-]	32	48
No. of conductors per slot	[-]	8	6

Fig. 8: Sizing Results of the E-Motor Family

Introduction of the Hybrid Platform Design for Vehicle Fleets

Besides the introduced 4-speed DCT, the gear set can be simplified to a 2-speed AMT by removing the odd-numbered transmission part while keeping most of the remaining gear set parts unchanged. This 2-speed derivative is very interesting for combined hybrid systems with a serial driving mode at low and medium velocities. Even a very simple 2-speed AMT P3-hybrid can be represented. Fig. 9 shows the complete variant space of the hybrid platform with 16 different derivatives for parallel and combined hybrid powertrains including the option of an electric all-wheel drive (eAWD) by using an electric rear axle. With this modular design approach a complete vehicle fleet from a cost-oriented B-segment vehicle up to a performance-oriented full-size SUV can be served.

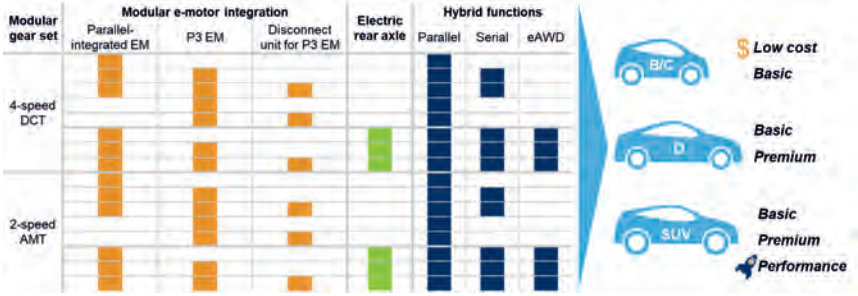

Fig. 9: Modular Design for the exemplary Fleet Application

In order to demonstrate the potential of the DHT system, a design study is implemented. As a result, Fig. 10 shows the digital prototype of the 4-speed DCT in the configuration of a combined hybrid for PHEV applications for the D/E-segment. With an input torque limitation of 430 Nm at a maximum combined system power of 170 kW the transmission has a competitive length of 384 mm.

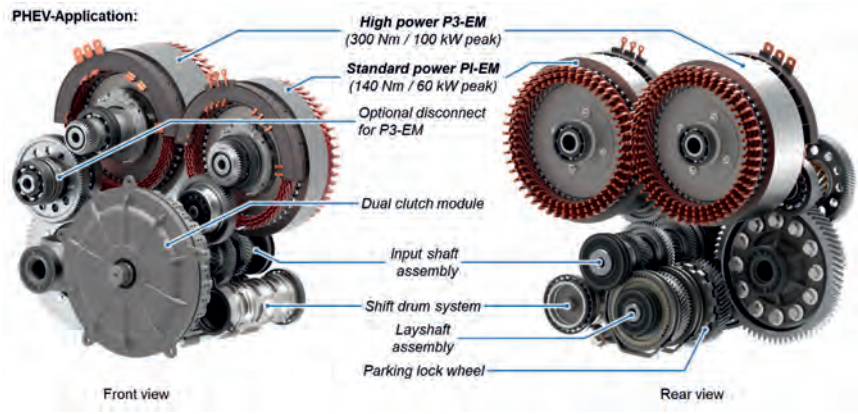

Fig. 10: Digital Prototype of the 4-Speed Combined Hybrid System

Conclusion

The future powertrain mix will be derived above all from the stipulations for a CO2- and emission-optimized vehicle fleet. IAV Fleet Synthesis can be used to allocate the five main powertrain types – internal combustion engine, hybrid (incl. plug-in) and electric with fuel

cells or battery – to the main vehicle segments. The TtW-CO2 emissions for every vehicle/powertrain combination are generated according to the WLTP, together with the CO2 equivalent for WtT, WtW and CtG balancing. Furthermore, the sales distribution is varied for every segment. The results of the variation study show that a scenario with high HEV share in the fleet is robust with regard to the external boundary conditions, particularly the electricity mix and the share of renewables. The high share of combustion engines also makes it easy to reduce CO2 emissions using e-fuels. The low share of PHEV, BEV and FCV also results in reduced manufacturing costs on the powertrain level. Furthermore, the analysis also looked at which powertrain mix would be expedient for WtW-CO2-legislation. The results also show that only in the B-segment a pure combustion engine powertrain is seen as expedient for the fleet targets. All other vehicle segments have combustion engines combined with either HEV or PHEV technology. The BEV powertrain type accounts for a relatively high share in the B- and D-segment with 40%, while the plug-in hybrid share is particularly prominent in the D-segment with 60%. Finally, modular powertrain systems were allocated to the three vehicle segments to allow for a combination of combustion engines with dedicated hybrid transmissions with one or two electric motors, which opens the way to a hybrid platform.

To realize such a modular hybrid platform, a well-balanced arrangement with right-sized systems and technologies needs to be selected. Therefore, the IAV synthesis methodology is used to investigate each of the pre-defined hybrid transmission topologies with a wide parameter variation. The result of this systematic engineering process is a suitable Dedicated Hybrid Transmission (DHT) platform with one and two electrical motors with a good balance between performance, energy consumption and costs. The platform modularity covers a parallel-integrated one-motor DHT as well as an extended dual-motor DHT. With the two motor version the electric performance is increased and the functionality is extended to a combined hybrid including serial hybrid mode. Additionally an electric rear axle can be added to offer electric all-wheel drive functionality.

For the development of a customized, on-demand actuation system for the gear shifting and parking lock actuation inside the DHT platform, a further component of the IAV synthesis methodology is introduced. With the Actuation Synthesis, a wide parameter variation study for different electro-mechanical shift drum actuators is conducted. Based on the results of this systematic investigation, a suitable shift drum actuator using an integrated planetary gear set is selected due to a good balance between shift performance, package and costs.

The paper is supplemented by the presentation of a modular approach for the electric motors. For two different installation positions and two different power levels, a scalable con-

struction kit for the electric motors is introduced. It is based on a uniform rotor and stator lamination and can be adapted to the different requirements via the stack length and the connection of the hairpin winding.

As the main result of the platform development, the exemplary use of the DHT in a vehicle fleet with up to 16 different vehicle applications, ranging from a low-cost B-segment vehicle up to a performance-oriented SUV, is introduced.

References

[1] EU Regulation 2019/631 (20019).

[2] Kratzsch, M.; Wukisiewitsch, W.; Sens M.; Brauer M.: The path to CO2-neutral mobility in 2050, Vienna Engine Symposium (2019)

[3] IHS Market Data Vehicle Production, as of 05/2019

Novel “Two-Drive-Transmission for Long-Range” Powertrain: Ecology and Efficiency meet Driving Comfort

Felix Langhammer, **Aaron Kappes**, Dr.-Ing. **Andreas Viehmann**, Prof. Dr.-Ing. **Stephan Rinderknecht**, Technische Universität Darmstadt

Zusammenfassung

Batterieelektrische Fahrzeuge mit einer langstreckentauglichen Reichweite von mehr als 500 km benötigen große Batteriekapazitäten von über 70 kWh. Diese großen Batterien haben einen hohen Energiebedarf in der Produktionsphase und führen durch ihre große Masse zu einem erhöhten elektrischen Energieverbrauch in der Nutzungsphase. Dagegen zeigt sich ein großes Potential bei dedizierten Hybridantrieben hinsichtlich einer Minimierung der ökologischen Belastung. Mit besonderem Augenmerk auf Effizienz und zugleich Fahr- und Schaltkomfort wurde am IMS der TU Darmstadt der dedizierte Hybridantrieb *DE-REX* entwickelt und untersucht. Darüber hinaus wurden weitere Potenziale hinsichtlich der Reduzierung des elektrischen Energie- und Kraftstoffverbrauchs und der Erhöhung des Schaltkomforts bei hohen Fahranforderungen identifiziert. Im nächsten Schritt werden daher die Erkenntnisse aus dem *DE-REX*-Antrieb auf das neuartige Antriebsstrangkonzept "Two-Drive-Transmission for Long Range (TDT4LR)" übertragen. Der Fokus dieses Beitrags liegt auf dem erstmalig vorgestellten TDT4LR-Antriebsstrangkonzept mit vier Gängen für den Elektro- und Hybridbetrieb. Die technischen Highlights und die Vorteile im Vergleich zum *DE-REX* werden hinsichtlich Package, Effizienz und Schaltqualität diskutiert.

Abstract

Battery electric vehicles with a range of more than 500 km suitable for long distance driving require large battery capacities of more than 70 kWh. These high capacities have a high energy requirement in production phase and, due to their large mass, lead to a higher electrical energy consumption in the use phase. In contrast, dedicated hybrid drives show great potential in terms of minimizing the ecological impact. With focus on efficiency, driving, and shifting comfort at the same time, the dedicated hybrid powertrain *DE-REX* was developed and investigated at the IMS at TU Darmstadt. However, further potential has been identified with regards to reducing electrical energy and fuel consumption and increasing shifting comfort

under high power demands. Therefore, the knowledge gained from the *DE-REX* powertrain will be applied to the new "Two-Drive-Transmission for Long Range (TDT4LR)" powertrain concept. The focus of this paper is on the TDT4LR with four gears for electric and hybrid operation, which is being presented for the first time. The technical highlights and advantages compared with the *DE-REX* are discussed regarding package, efficiency, and shift quality.

Introduction

In context of the mobility turnaround, ongoing electrification has been one of the main topics challenging the automotive industry in recent years. Political and individual rethinking leads to an increasing demand and market shares of plug in hybrid electric vehicles (PHEVs) and battery electric vehicles (BEVs) [1].

Across different brands PHEVs and BEVs are marketed as a substitution of conventional internal combustion engine vehicles providing customer known long range capability of more than 500 km. Commercially available BEVs are mostly based on powertrain layouts with one powerful electric motor (EM) attached to a fixed speed gearbox. As explained in [2] providing only a single speed leads to a design conflict between vehicle top speed and launch torque, which often results in comparatively high powered EM. Furthermore, high battery capacities of 70 kWh or more are common to achieve long rage capability, resulting in high costs and high vehicle weight directly affecting the overall energy consumption of the vehicle negatively. In [3] different powertrain concepts are optimized and evaluated in regard of their greenhouse gas (GHG) emissions over the whole product lifecycle (manufacturing, usage and recycling) for the reference years 2018 and 2030. The results in this scenario show that PHEVs offer higher potentials regarding a reduction of GHG than long-range BEVs (350 km in real driving scenarios) even in 2030, because of their smaller sized batteries. Since the battery is one major factor for the lifetime GHG emission of BEVs, it is expected that the requirement for an even longer range will further increases the GHG potentials of PHEVs over BEVs. Furthermore, [3] has identified that the optimal hybrid powertrains converge to dedicated hybrid powertrains, sizing both energy converters in a way that takes advantage of their synergetic use. This stands in contrast to most recent production of PHEVs, that are often carried out as an add on solution by electrifying an existing powertrain. This is, for example, often carried out by adding an electric motor in a P2 or P3 configuration to a dual clutch transmission (DCT) or automatic transmission (AT) combined with a high power ICE.

At the Institute for Mechatronic Systems (IMS) at TU Darmstadt a different approach to pure electric and hybrid powertrains is pursued. The idea is a dedicated modular powertrain concept

designed for two EM named Two-Drive-Transmission (TDT), aiming for high efficiency while pure electric driving, moderate costs, and high shift comfort. In this context, a new approach for a hybrid TDT was developed, which is discussed in more detail in this paper after a general introduction.

Two-Drive-Transmission (TDT)

Key features of TDTs are using a multi-speed transmission consisting of two parallel subtransmissions (STMs), installing two EMs with lower power instead of one powerful EM, the usage of simplified transmission technology, and functional integration, e.g. electric synchronization and torque supported gearshifts for high shift comfort [4]. For some applications it is useful to hybridize this concept by adding a simplified ICE, enabling different parallel and series hybrid operation modes. Fig. 1 gives an overview over the TDT powertrain family, distinguishing between pure electric and hybrid variants.

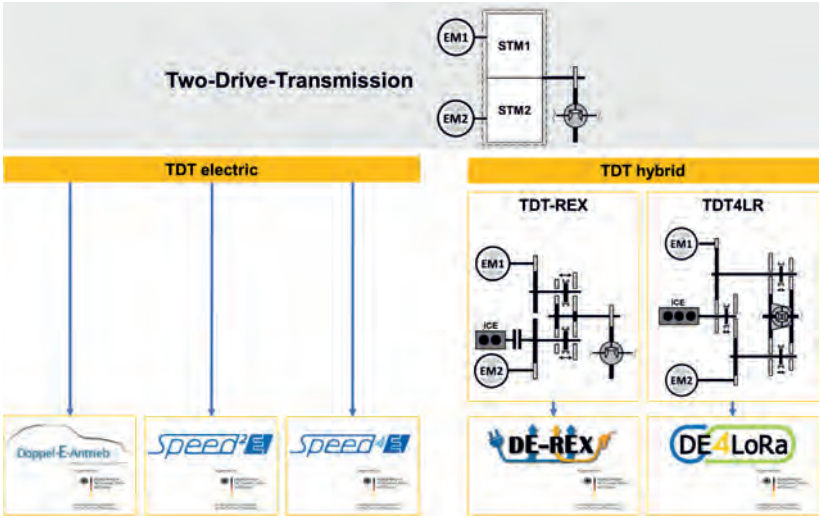

Fig. 1: TDT family

For pure electric TDTs, three publicly funded projects have been carried out with different project objectives, at first the name giving project *Doppel-E-Antrieb*, followed by *Speed2E* and recently *Speed4E*. In this article, focus will be on the hybrid variants, where two general concepts named Two-Drive-Transmission with Range-Extender (TDT-REX) and the novel

Two-Drive-Transmission for Long Range (TDT4LR) have been developed. For the TDT-REX concept one specific configuration hast been designed and realized in the publicly funded project *DE-REX*. This project ended in 2018 and was the first hybrid variant of a TDT put to the test in a demonstrator vehicle. In *DE-REX* the general potentials of hybridized TDTs in regards of efficiency, costs [2] and shift comfort [5] have been shown. The most recent project Doppel-E-Antrieb for Long Range (*DE4LoRa*) aims to realize a specific variant of the TDT4LR. It intends to leverage unused potentials especially concerning efficiency in electric and hybrid operation and shift comfort it will be introduced briefly in the course of this paper.

Scalability of TDTs

The TDT family offers high potentials regarding modularity and scalability. Apart from pure electric or hybrid applications in particular the voltage level, e.g. ranging from 48 volts up to high voltage applications, the power of the drive units and also the number of totally available speeds are scalable. Depending on the boundary conditions of the design, e.g. efficiency, installation space or cost effectiveness, the EMs can be chosen as identical machines for each STMs or as different sized EM in terms of power and/or installation space. As an example, two identical EMs allow for higher quantities in production and reduced costs per unit, but two different sized EMs may offer higher potentials regarding energy efficiency since the EMs can be designed for different operating conditions. Depending on the application, different types of EM might be considered as well, e.g. an asynchronous motors (ASM) for a full hybrid with more percentual usage of the ICE because of ASMs' lower drag losses. For pure electric applications, fuel cell electric vehicles are another feasible use case. Additionally, different levels of functional or geometric integration are possible, e.g. by integrating the EMs and power electronics into the transmission housing. To give some examples, Fig. 2 shows possible configurations for different vehicle classes, ranging from baseline electrification in compact vehicles up to BEVs.

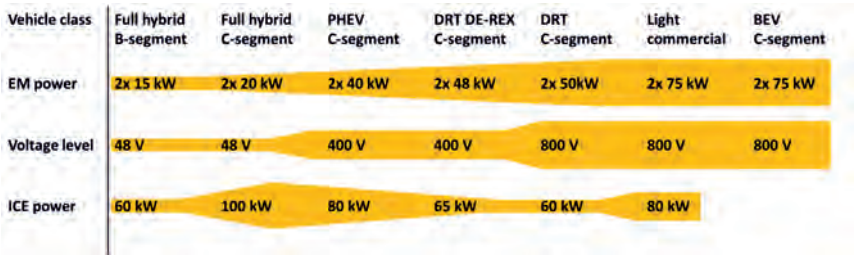

Fig. 2: Example configurations for TDTs in different types of vehicles

TDT4LR concept

The TDT4LR concept is an innovative, modular, and scalable dedicated range-extender transmissions (DRT) based on the TDT idea with focus on high efficiency, high modularity, and cost efficiency. Key attribute of DRTs following an IMS definition is that the EMs function as the main traction machines, enabling full functionality without the ICE running for most scenarios, meeting all driving demands in pure electric mode, and extend its range by coupling the ICE of needed. The overall high level of integration and usage of synergetic potentials leads to a reduction in complexity and costs of the transmission and the ICE. The latter can be simplified and operated phlegmatized since the EMs as the main traction machines reduce its dynamic requirements. Due to the transmission layout, no starter generator is needed, since both EMs can be used to crank the ICE. In addition, the hybrid concept brings further advantages for the user. The flexibility of having two different energy sources brings the advantage, of flexible energy accumulation depending on the available infrastructure. Furthermore, despite a heated passenger cell, the range in winter only reduces slightly. The concept can also be used CO_2-neutral, if renewable fuels or gases are used. Due to the relatively large electric range compared to PHEVs, common everyday trips are emission-free.

The TDT4LR concept itself envelopes several different layouts and configurations. Each TDT4LR consists of two STMs each carrying at least two speeds. To each of these STMs one EM is connected permanently. Furthermore, the ICE can be coupled to each STM individually. Fig. 3 and Fig. 4 show a basic transverse and a basic inline layout, respectively. A remarkable feature of the TDT4LR for transverse applications is, that only two gear stages are needed between all drive units and the wheels.

The shifting elements C1 and C2 (both with three shift positions) as well as the shifting elements connecting the ICE C0 or respectively C01 and C02 (two to three shift positions) are form-locking dog clutches without any frictional elements like synchronizer rings or friction clutches. Dog clutches produce less drag torque, need less actuation force when compared to conventional synchronizer rings and tend to be more cost efficient to manufacture. Additionally, the usage of dog clutches to connect the ICE reduces weight in comparison to friction clutches. Furthermore, it reduces application efforts regarding shift comfort, temperature control and lifetime adaption. To allow fully torque supported gearshifts, the speeds are separated in odd and even speeds between both STMs, e.g. STM1 carrying the odd gears and STM2 carrying the even gears. In doing so, the idler wheels of first and second speed share one cogwheel on the differential cage as well as third and fourth speed do.

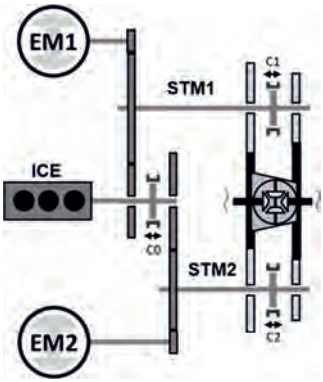

Fig. 3: Schematic layout of a transverse TDT4LR

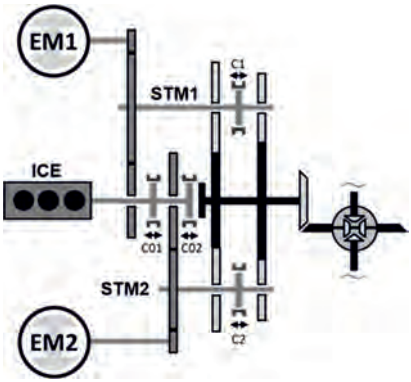

Fig. 4: Schematic layout of an inline TDT4LR

For inline applications two gear stages plus an axle drive are located between all drive units and the wheels. In this specific layout, connecting the ICE input shaft directly to the transmission output is possible by closing clutch C02, offering a direct drive and a fifth gear ratio for the ICE. Additionally, this layout allows connecting the ICE to both SMTs simultaneously, providing more operating modes for series or parallel-series application. Furthermore, this allows the functional integration of a mechanical parking lock by connecting the ICE to both SMTs and engaging a gear in both of them.

Package

In most platforms for conventional or hybrid front-wheel drive passenger cars, the available axial installation space is a limiting factor. The TDT4LR concept was developed to realize a full electric powertrain despite the limited installation space and to use an combustion engine as a dedicated range-extender. The layout concept is designed for a higher efficiency and more functions than in a TDT-REX, realized within a smaller volume. For a real application, the basic layout shown as stick diagram in Fig. 3 can be further optimized by arranging the combustion engine shaft and double differential in a trapezoidal arrangement axially parallel to each other as shown in Fig. 5 on the left. The feasibility of such a transmission with both electric machines on the opposing side of the combustion engine was investigated in a package study shown in Fig. 5 on the right.

In order to evaluate the axial space requirement of a given transmission layout, a comparison of the required functional planes can be useful. This approach assumes that a coupling unit or a spur gear stage have similar axial dimensions and therefore require one functional plane of installation space. One plane can accommodate multiple parallel elements. In a coaxial layout, the planes are lined up one after the other. Fig. 6 compares the gear layout of the *DE4LoRa* transmission, which bases on the layout of the TDT4LR shown in Fig. 5, with that of the *DE-REX*. The coaxially arranged *DE-REX* transmission has eight functional planes, and thus it needs conceptionally more axial installation space than the *DE4LoRa* transmission with five planes only.

Fig. 5: Schematic layout (l) and design study with both EM on one side (r) of a short version of a TDT4LR

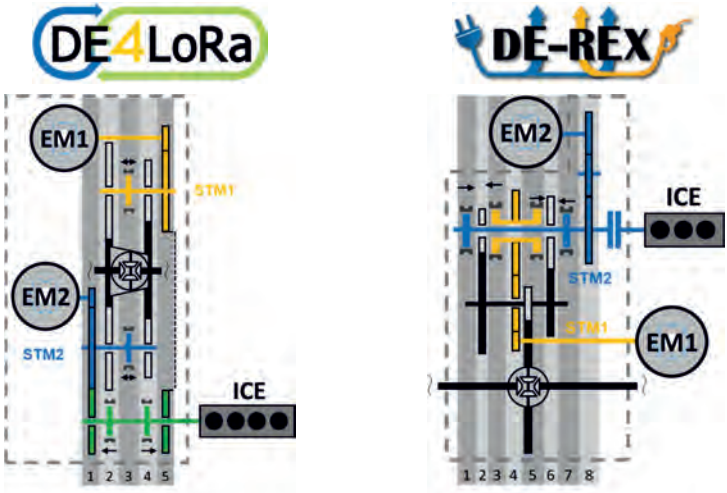

Fig. 6: The specific TDT4LR-Layout “DE4LoRa” (l) vs. the specific TDT-REX-Layout “DE-REX” (r)

Without the separation clutch, the *DE-REX* transmission has an axial length of 360 mm. According to the design study, the *DE4LoRa* transmission will require only about 75 % of this length. Due to its long coaxial main shaft, the electric machines of the *DE-REX* had to be orientated in parallel. The resulting large center distances required intermediate gears to connect the EMs to the associated STMs. However, the compact design of the *DE4LoRa* allows the EM to be mounted coaxially, eliminating the need for intermediate gears. Thus, power losses, costs, and complexity are reduced.

Table 1: Comparison of DE-REX and DE4LoRa

	DE-REX	***DE4LoRa***	**Potential in DE4LoRa**
Number of “functional planes”	8	5	~ 25-30% less axial length
Number of ICE speeds	2	4	More efficient usage of the ICE
Number of electric speeds	2	4	More efficient EV modes
Number of gear stages from EM to the wheel	4	2	Less gear meshing losses
Total number of gears / shifting actuators	12 / 4	12 / 4	Comparable production costs even with higher functionality

To enable a package as shown in Fig. 6 on the left, further measures are being pursued in the *DE4LoRa*-Project to reduce the axial length. This includes saving installation space of the EM-flanges and redundant housings via integrating the electric machines into the transmission housing. In addition, the use of flat roofs and dedicated shift actuators enable a shorter design of the STM-clutches. In contrast to the basic version of the TDT4LR, instead of the double-sided clutch, two single-sided dog clutches are used to enable a connection of the combustion engine in both STMs simultaneously. This modification does not affect the axially required installation space but enables additional shifting functions, e.g. the virtual dual clutch (vDC) as shown in [6], that can be used to phlegmatize the combustion engine and increase shifting and acoustic comfort. Furthermore, it enables an integrated parking lock.

Operation modes

Since all speeds of the TDT4LR can be used for pure electric as well as hybrid operation modes, the powertrain is high flexible regarding operation modes. In general, the operation modes differentiate by the number of active drive units in combination with the dog clutch positions. The shown example in Fig. 3 offers in total 24 different clutch positions, dividing in eight clutch positions for pure electric use and 16 clutch positions for hybrid use. In addition, two clutch positions for charging while standstill are possible. These clutch positions in combination with different drive units active, result in over 30 different operation modes.

Function wise the operation modes can be classified in pure electric, parallel hybrid, series hybrid driving modes, and parallel-series hybrid driving modes as well as charging modes. As examples for pure electric driving Fig. 7 and Fig. 8 show using one or respectively two EMs propelling the vehicle in their respectively lower speed. Therefore, the clutches C1 and respectively C2 are in an engaged position. The driving mode shown in Fig. 8 could be used e.g. for sporty launches or for steep uphill driving.

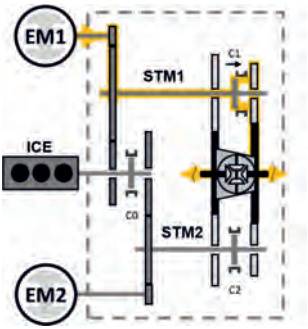

Fig. 7: Pure electric driving in 1st speed

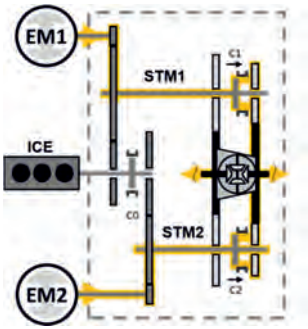

Fig. 8: Pure electric driving in 1st and 2nd speed

An exemplary parallel driving mode is shown in Fig. 8, where both ICE and EM2 propel the vehicle in forth gear, e.g. in highway use. Therefore, the ICE is connected to the second STM by engaging C0. For series hybrid operation, the ICE is coupled to one STM, e.g. STM2 as shown in Fig. 10, while the associated layshaft is not connected to the transmission output. In this case the EM in STM1 propels the vehicle, and the hybrid control unit decides which of the two possible speeds of STM1 is used. An important use case for this series hybrid mode is launching the vehicle at low battery state of charge, since the ICE is coupled to the output with form-locking clutches, and therefore it can not be used for launching the vehicle. Furthermore, with additional virtual gears enabled by the series mode (as explained in [5] and [7]) different trade-offs can be made between efficiency and further optimized acoustic behavior with different control strategies.

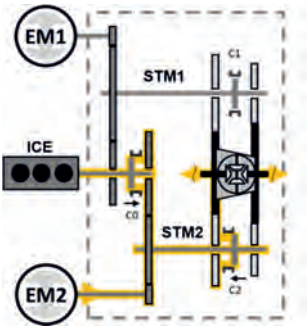

Fig. 9: Parallel hybrid driving in 4th speed

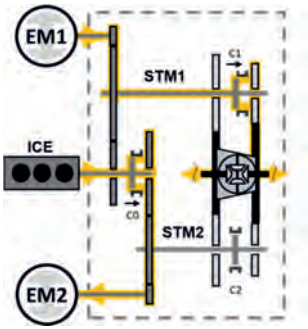

Fig. 10: Series hybrid driving in 1st speed

Efficiency

The efficiency advantages of a two-speed gearbox for electric drives with one electric machine has been shown in [8]. It has been concluded that a multi-speed gearbox can solve the conflict of objectives in designing an efficient and at the same time high-performant electric drivetrain. The TDT concepts allow synchronization processes to be executed electrically, eliminating the need for power-transmitting friction elements such as synchronizer rings, a dual clutch, or power shifters. This eliminates the unwanted losses of friction clutches (friction losses, drag losses and permanent clutch actuation losses) resulting in a higher efficiency of the transmission. The underlying theoretical efficiency benefits of using the advantages of a two speed gearbox, combined with the downsizing effects, drivetrain have already been evaluated in the *DE-REX* project on a powertrain test rig [2]. Further investigations revealed new potentials considered in the development of the new TDT4LR concept including the realization of four different electric speeds, as well as a possibility to connect the ICE in both STMs. The latter enables a much more efficient usage of the ICE via parallel hybrid modes. Furthermore, the number of loss-effected gear stages between input and output is reduced from four for the EM and two for the ICE to two for all drives. The potential for reducing the fuel consumption in a SOC-neutral driven WLTC using a TDT4LR-layout instead of a TDT-REX with the same ICE and EM efficiency maps was estimated at approximately 5 % [7]. For pure electric driving, a possible reduction of over 10 % in WLTC compared to a fixed gear long-range capable BEV (over 500 km range) was estimated based on prior studies from [9].

In order to qualitatively explain the processes leading to these efficiency improvements, an exemplary TDT4LR is discussed in the following with focus on the electric powertrain. The parameters used for the longitudinal driving simulation and the four chosen electric speeds are listed in Table 2. Fig. 11 shows qualitatively the efficiency map of the used permanent-magnet synchronous machine (PSM) with a continuous power of 25 kW and a peak power of 50 kW (30 seconds). The characteristic speed is 4.000 rpm and the maximum speed is assumed as 10.000 rpm. The area of the relatively highest efficiency is called “sweet spot”.

Table 2:
Simulation parameters of the example

Parameter	Value	Unit
Vehicle mass	1700	kg
Rolling friction coefficient	0.01	-
Air drag coefficient	0.26	-
Frontal area	2.432	m^2
Dynamic wheel radius	0.31	m
First electric speed	18	-
Second electric speed	12	-
Third electric speed	7.7	-
Forth electric speed	6.5	-

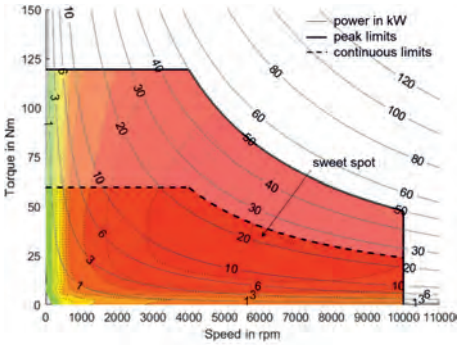

Fig. 11: Exemplary efficiency map of a 50 kW PSM

The fundamental objective of efficiency optimization is to enable the given requirements for speed and torque at the vehicle's wheels with as little effort as possible. To illustrate the different possibilities in realizing the required torques and speeds, the summed torques at the drive shafts are plotted against the velocity of the vehicle in Fig. 12, 13 and 14. The efficiency maps of the two identical PSMs (EM1 in yellow, EM2 in blue) are transformed into this representation depending on the selected speed ratio (higher speed light, lower speed dark). The Fig.s show, how the limits and sweet spots of the engines shift toward lower vehicle speeds and higher torques at higher speed ratios.

In this exemplary design, the fundamental advantage of multiple speeds for electric drives is shown. The high transmission ratio of the lowest speed enables EM1 to fulfill most requested launch torques in series mode. For higher launch torques both EM are used. Although the EMs are neither characterized by a particularly high torque nor a particularly high speed, the multi-speed design allows a maximum electric velocity of 150 km/h using both EM. Higher speeds up to a maximum of 180 km/h can be achieved with a correspondingly powerful combustion

engine by disengaging EM1 and using the combustion engine in fourth speed in the second STM in parallel with EM2. In comparison, a fixed gear BEV must use a more powerful EM to meet the same driving requirements (qualitatively indicated in Fig. 14).

Fig. 12 shows the load requirements of the WLTC for the given vehicle. Many of the operating points can be fulfilled with one EM in its continuous load range, whereby the most efficient of the four possible speeds is selected for each situation. The downsizing effect comes into account, according to which a small EM utilized to a higher degree is more efficient than a large one in its partial load range. However, some of the operating points are above the continuous and the sweet-spot power of one single EM. In such a condition, the operating strategy decides if it is worth executing a mode change and dividing the power between both EMs, enabling a higher combined efficiency. With higher load requirements, such as those caused by the Artemis drive cycles (see Fig. 13) or a cycle representing a sporty driver, the modes with both EMs are used more often.

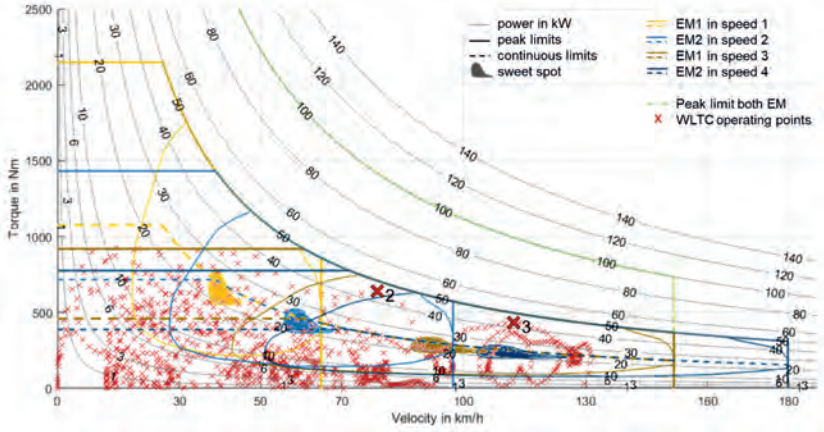

Fig. 12: Torques and speeds at the wheel for WLTC

To explain the effect of power splitting, the changes are illustrated choosing four exemplary load points of the given driving cycles (see Fig. 14). At the load points one to three, splitting increases the efficiency compared to the most efficient realization with one EM. For example, the first operating point with 35 kW load requirement could be realized by EM1 in first speed or by EM2 in second speed. As shown in Fig. 15, EM1 in first speed would be operated in a more efficient area than EM2 in second speed, which demonstrates the efficiency advantages

of a two-speed transmission. By using both EM in the corresponding speeds, the load point in both EMs can be shifted to areas with even higher efficiencies (see Fig. 15).

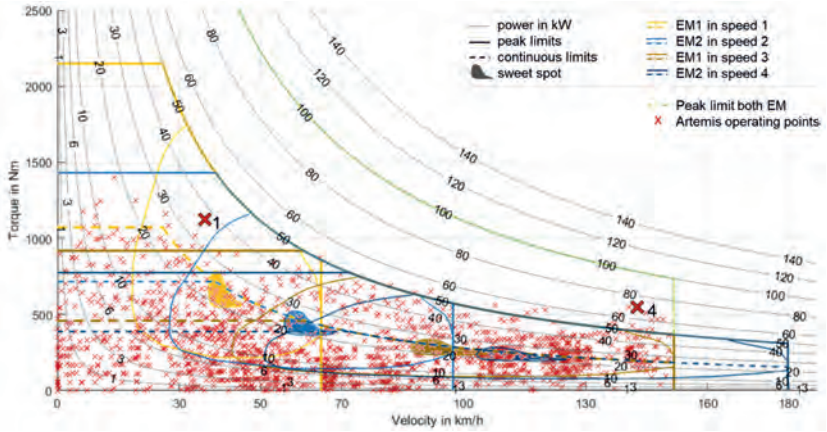

Fig. 13: Torques and speeds at the wheel for the Artemis cycles (Urban, Rural Road and Motorway 150 combined)

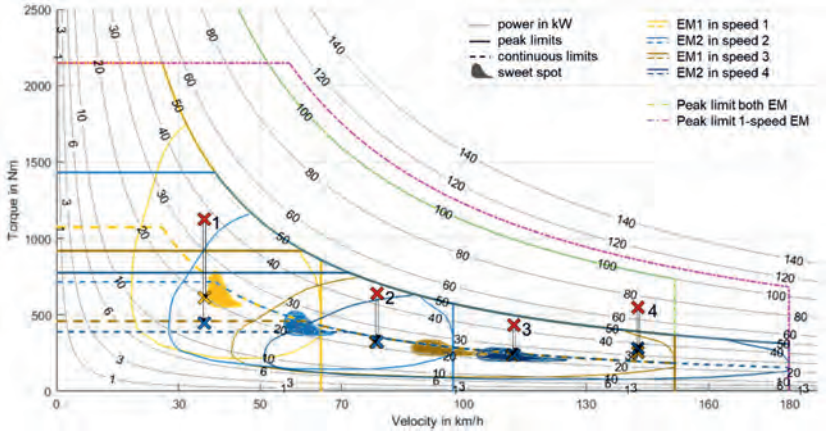

Fig. 14: Efficiency maps of two 50 kW PSM with two different speeds each for an exemplary TDT4LR transition setup transformed to and overlaid at the wheels

Operating point two could be realized by EM1 in third speed or by EM2 in second or fourth speed. Again, higher efficiency is achieved by splitting the load between the two EMs. The decision as to whether EM2 is operated in second (2) or fourth speed (2') depends on the specific characteristics of the used EM and can be influenced by additional boundary conditions such as the efficiency characteristics of the transmission. The third operating point represents a special situation, since at this vehicle speed EM2 can be operated via load sharing in its sweet spot. Due to the high load requirements of the Artemis Motorway 150, operating point four cannot be realized by one single EM. In this case, at least one EM must be operated above its continuous power limits for a short time.

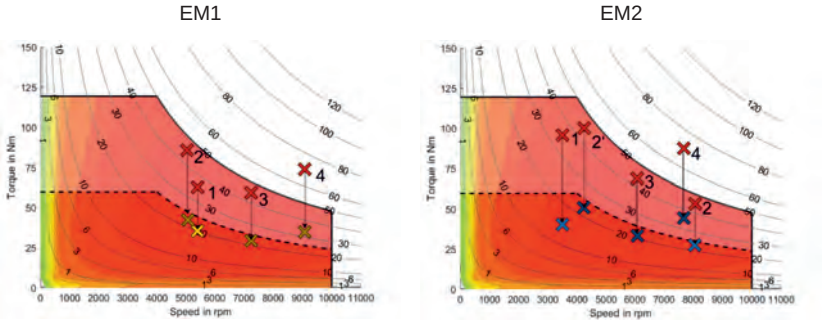

Fig. 15: Exemplary operating points in the corresponding EM efficiency map

The actual used power split for each load point is selected by the optimizer implemented in the operating strategy. The latter must also estimate, whether a gearshift is beneficial in which operating state. This depends to a large extent on the dynamics of the driver's wishes, his requirements for the shift comfort, and the power needed for a shifting process.

Shift Comfort

As already mentioned, the TDT4LR allows for torque supported gearshifts with only form-locking dog clutches. The general principle of torque supported gearshifts with active synchronization in TDT4LR drivetrains resembles the gearshifts of the *DE-REX* powertrain. Hence for a deeper insight in gearshifts, as well as a validation of shift comfort in context *DE-REX,* reference is made to [5] and [6]. Fig. 16 qualitatively illustrates a pure electric power upshift derived from [5] and [6] in STM2 from its first to its second speed while the EM in STM1 torque supports in its respective second speed. A shift event like this happens, for example, when dynamically accelerating to highway speeds. Trajectories are shown for the *DE-REX* as

well as a for a TDT4LR configuration with four different speeds. In *DE-REX* both STMs feature the same gear ratios. In the TDT4LR STM1 is geared lower than STM2, thus torque supporting the gearshift in third electric speed (second STM1-speed).

To understand the basic principles a brief explanation of the shift process will be given at the example of the *DE-REX* curves. Different functional phases of the gearshift are highlighted and named from A to E. At the outset, both EMs propel the vehicle with EM1 in second STM1-speed and EM2 in its first STM2-speed. At the beginning of the gear shift, torque is blended to EM1 so that the dog clutch in STM2 is load free. Therefore, in phase A the torque of EM2 ramps down and EM1 increases its torque to further propel the vehicle. If the overall transmission output torque stays ideally constant in this phase, no oscillations are induced, no matter how fast the torque is blended [6]. In shift phase B the dog clutch of STM2 is actuated and put into neutral position, leading to EM2 running down slowly due to drag losses, since it is not connected to the transmission output any more. Afterwards, in phase C EM2 is actively speed-controlled in order to synchronize its rotational speed to match claw-speed of its desired second STM2-speed. In the following phase D the dog clutch of STM2 is engaging and thus coupling STM2 to the idler wheel of its second speed. To finalize the gearshift between EM1 and EM2 torque is blended in phase E.

As described in [6] the *DE-REX* powertrain is not capable of performing fully torque support gearshifts for accelerator positions of 70 % or higher due to torque limitations of the electric components. This is qualitatively shown in Fig. 16 with EM1 providing its maximum torque, but still resulting in a lower vehicle acceleration in shift phases B to D. It is expected, that both the amplitude of the drop in acceleration, as well as the duration of the gearshift are relevant criteria for the shift comfort. In addition, changes in the drive shaft torque lead to fluctuations, inducing jerking that negatively impacts drive comfort, if not addressed with elaborate application effort. Therefore, minimizing shift time, maximizing torque support, and executing an ideal torque blending are the main objectives for maximizing shift comfort.

Since the amplitude of the drop in acceleration is induced by a lack of torque to compensate the torque of EM2 while shifting gears, on the one hand more powerful power electronics (PE) and EM would be a feasible solution. On the other hand, downsizing of EMs is a key feature to achieve high overall efficiency (as already discussed in the efficiency chapter). To address this design conflict [5] suggests the usage of short time (about one second) highly overloadable PE and EM, which is highly suggested for TDT4LR drivetrains. Due to the non-linear ohmic losses and therefore the need of much higher current during these phases, the possible peak power of PE and EM and related timespan is mainly limited by the thermal design. This leads

to reducing the shift process timespan being beneficial not only for comfort, but for efficiency as well. As shown in [6] for the *DE-REX*, changes in side shaft torque can have a negative effect on shift time and comfort, since the torque blending needs to be slowed down to reduce oscillations in the powertrain. Such effect occurs, if the torque during shifting is not fully supported, for example. Thus, for highly overloadable electric components, it is expected that the torque changes at the side shafts are neglectable, and the torque of the EMs can be ramped with their maximum dynamics, effectively reducing the duration of shift phases A and E.

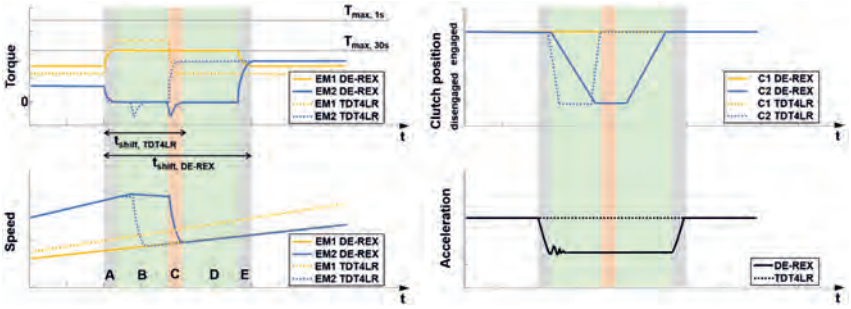

Fig. 16: Qualitative illustration of a power upshift in STM2. For a better comparison, the gear ratio of the TDT4LR STM2 are chosen to exactly match the gear ratios of the DE-REX.

As seen in [5] the shift phases B and D in *DE-REX* are mostly limited by the shift actuators themselves. The shift drum actuators were carryover components of a conventional dual clutch transmission, offering high shift forces to the detriment of actual speed (at least ~140 ms timespan form neutral to engaged). Since high forces are not necessary for form-locking dog clutches, dedicated and smart actuators are expected to be used in a TDT4LR. These actuators (e.g. as shown in [10]) offer the potential to reduce pure (dis-)engaging time by factor five to seven. In addition, application-specific dog clutches matching the respective actuator will be used. To significantly shorten the shift time in *DE-REX*, [6] researches parallelization of shift phases. Measurements out of the *DE-REX* demonstrator vehicle show the high potential, since for an exemplary power upshift the shift time could be reduced from 850 ms in sequence to 650 ms with partial parallelization. [6] expects the potential to further reduce shift times by approximately 100 ms when utilizing full parallelization. Though for the TDT4LR it is expected that due to the already faster dedicated shift actuators the benefit in time gained by

parallelization will be less significant. As further suggested in [6], using an angular position control instead of speed-control could further increase shift comfort when using form-locking dog clutches.

In *DE-REX* the shift comfort was subjectively and objectively rated to be on a high level. For example, for pure electric power upshifts comfort is rated better than ATs up to 70 % accelerator position. Above 70 % accelerator position shift comfort decreases since gearshifts are not fully torque supported, but the overall shift comfort is still rated to be comparable with ATs. [6] Higher overload capability can provide the highest level of comfort for all load requirements leading to imperceptible gearshifts. Concerning all the shown potentials, the TDT4LR concept enables highest shift comfort even with the usage of cost efficient and simplified transmission technology due to a high level of functional integration in combination with an intelligent shift and operating strategy.

Summary

The TDT4LR concept offers overall ecological advantages over current long-distance BEVs. These advantages are based on a better lifetime GHG balance, due to a smaller battery, and especially on the high efficiency in purely electric driving mode due to a highly efficient multi-speed gearbox. Furthermore, its economic potentials result in particular from the reduction of the required battery capacity and, compared to current PHEVs, from the dedicated design and the consistent use of synergy effects, which lead to simplified subsystems. However, despite the simplified transmission, a high shift and driving comfort is realized. In general, the two EMs enable a TDT4LR powertrain shifting gears without any interruption of traction force and is expected to be even better than the current state of the art dual clutch or automatic transmissions. Combined with the flexible energy accumulation, this leads to high user acceptance.

Summarized, the primary goal of the TDT4LR concept is to pursue a powertrain system approach that, compared to the direct reference vehicles, combines better efficiency especially in partial load ranges with a long-range capability thanks to hybridization and high shift comfort, while being economically attractive. Additionally, it enables good performance due to a sufficient combined system power, if needed.

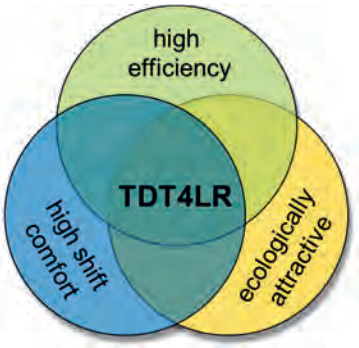

Fig. 17: Main objectives of a TDT4LR powertrain

Outlook

In April 2021 “Doppel-E-Antrieb for Long Range”-project started publicly funded by the German Federal Ministry for Economic Affairs and Energy. The project aims to design and build up the first member of the TDT4LR family in hardware within three years project term. For this purpose, a consortium coordinated by Vitesco Technologies Germany GmbH and consisting out of APS-technology GmbH, AVL Software and Functions GmbH, BMZ Batterien-Montage-Zentrum GmbH, Compredict GmbH, Hyundai Motor Europe Technical Center GmbH, Isar Getriebetechnik GmbH & Co. KG and Windschiegl Maschinenbau GmbH as well as four institutes of the Technical University of Darmstadt was formed. *DE4LoRa* will be designed to meet driving requirements of everyday life (100 km) in pure electric mode and thereby meet highest efficiency requirements. The electric system will operate on a state of the art 800 V voltage level. To achieve long range capability while maintaining low GHG emissions, *DE4LoRa* will feature a monovalent natural gas (CNG) internal combustion engine that will be operated largely phlegmatized. Furthermore, it will be the first powertrain featuring all characteristics of a universal hybrid electric vehicle (UHEV).

Fig. 18: Logo of the DE4LoRa-Project.

References

[1] EUROPEAN ENVIROMENT AGENCY: *New registrations of electric vehicles in Europe*. URL https://www.eea.europa.eu/data-and-maps/indicators/proportion-of-vehicle-fleet-meeting-5/assessment. – Modified: 2021-05-11 – Viewed 2021-07-25

[2] VIEHMANN, A.; SCHLEIFFER, J.-E.; RINDERKNECHT, S.: Evaluation of the Dedicated Range-Extender Transmission Powertrain Concept DE-REX regarding Efficiency, Costs and Complexity. In: VDI Wissensforum (Hrsg.): *Dritev - Drivetrain in Vehicles*: *19th International VDI Congress*, VDI-Berichte 2354. VDI Verlag, Düsseldorf, 2019. pp. 21–48

[3] EßER, A.; SCHLEIFFER, J.-E.; EICHENLAUB, T.; RINDERKNECHT, S.: Development of an Optimization Framework for the Comparative Evaluation of the Ecoimpact of Powertrain Concepts. In: VDI Wissensforum (Hrsg.): *Dritev - Drivetrain in Vehicles*: *19th International VDI Congress*, VDI-Berichte 2354. VDI Verlag, Düsseldorf, 2019. pp. 137–162

[4] RINDERKNECHT, S.; KÖNIG, R.; SCHLEIFFER, J.-E.: Modularity Aspects for Hybrid Electric Powertrains on the Example of the Two-Drive-Transmission. In: VDI Wissensforum (Hrsg.): *Drivetrain for Vehicles 2014*: *International VDI Conference*, VDI-Berichte 2218. VDI Verlag, Düsseldorf, 2014. pp. 147–166

[5] VIEHMANN, A.; KÖNIG, R.; RINDERKNECHT, S.: Investigation of Gear Shifts in a Parallel-Series Hybrid Powertrain with Dog Clutches in a Demonstrator Vehicle (Two-Drive-Transmission with Range-Extender, DE-REX). In: VDI Wissensforum (Hrsg.): *Dritev - Drivetrain in Vehicles*: *International VDI Congress*, VDI-Berichte 2328. VDI Verlag, Düsseldorf, 2018

[6] KÖNIG, R.: *Gang- und Moduswechsel in elektrischen und hybrid-elektrischen Antriebssträngen mit aktiv synchronisierten Klauenkupplungen*. Shaker Verlag, Düren, 2019

[7] VIEHMANN, A.: *Erweiterte Betriebsstrategie für dedizierte parallel-serielle Hybridantriebe zur Berücksichtigung des akustischen Komforts*. Shaker Verlag, Düren, 2020

[8] DEMMERER, S.: Efficiency of Electric Axle Drive Systems. In: VDI Wissensforum (Hrsg.): *Dritev - Drivetrain in Vehicles*: *19th International VDI Congress*, VDI-Berichte 2354. VDI Verlag, Düsseldorf, 2019. pp. 279–286

[9] RINDERKNECHT, S.; SCHEBEK, L.; BEIDL, C.; KUHNIMHOF, T. G.; ESSER, A.; SCHLEIFFER, J.-E.: *Abschlussbericht FahrKLang* : *Verbrauchs- und Emissionsbewertung von Fahrzeugantriebs-konzepten für die Langstreckenmobilität der Zukunft*. Berichtszeitraum: 01.10.2017-30.09.2018

[10] SCHÖNEBERGER, D.; GAO, G.; RINDERKNECHT, S.: Applikation und Test eines dedizierten Schaltungssystems für elektrische Mehrgang-Fahrzeugantriebe. In: BERTRAM, T.; CORVES, B.; JANSCHEK, K.; RINDERKNECHT, S. (Hrsg.): *MECHATRONIK 2021*: *Digital-Fachtagung*, 2021

E-Axle with multi driving modes for BEV & Mild HEV P4

The 3 in 1 e-Axle for EV requiring a wide range of driving force

Kotaro Hirano, UNIVANCE Corporation, Washizu, Japan

ABSTRACT

The “Dual Motor - Multi Driving Mode” e-Axle is a “Two motor - Two speed” eAxle developed to achieve low power consumption and high driving performance at the same time, together with an improvement of vehicle mountability. This paper describes the results of the simulation and actual vehicle experiments for the operating principle and development purpose of this eAxle.

1. INTRODUCTION

Last Mile EVs have begun to be widely used mainly to solve environmental problems in urban areas, and thus a low-cost powertrain with low power consumption is needed. The P0P4 system is also expected to improve the environmental and kinetic performance of the 48V P0 HEV at a minimum cost. Last miles truck EVs for which delivery is the main use are required to reduce environmental impact, ensure optimal driving force according to cargo and vehicle load changes, and provide as much cargo and passenger compartment space as possible. In other words, a package design with lower power consumption, higher driving performance, and better vehicle mountability is required, and in addition, it is mandatory that it can be realized at low cost. With the current mainstream “single motor - single speed” eAxle, it is not possible to achieve low power consumption and high driving performance at the same time in all driving and loading situations. In recent years, single motor eAxles equipped with two-speed transmission for achieving low power consumption at low- and high-speed, have started to appear, pushing the trend to multi-staged or continuously variable transmissions [1, 2, 3]. However, in a vehicle such as a delivery truck in which the required driving force varies greatly depending on the loading conditions of the cargo, or in super sports cars in which completely different driving performance is required for urban driving and racing circuit use, there are limitations to the driving scenes that can be covered in the high efficiency range by a single motor. Moreover, there is the issue that due to the huge investment cost for a new high-output motor, its cost becomes inevitably high. In order to solve the above issues, we have developed the ”Two-motor - Two-speed” 3 in 1 eAxle: Dual Motor Multi Driving Mode e-Axle (hereinafter

referred to as DMM Axle) with 4 driving modes and 2 regenerative modes, which can be produced with low cost motors.

2. MECHANISM

As shown in Fig. 1, the DMM Axle is a three-axis eAxle with an integrated gearbox and inverter. The motor and inverter on the low gear side are arranged symmetrically to the motor and inverter on the high gear side. The LH motor is connected to the low gear and the RH motor is connected to the high gear. The low gear on the second axis has an integrated one-way clutch in its inner circumference to realize seamless gear shift. In addition, the dog clutch on the first axle can directly connect the right and left motors to realize powerful driving when needed. By combining two motors and two gears, four driving modes can be selected. By controlling the switching between the four driving modes according to the driving scenes, power consumption can be saved and high driving performance can be achieved. Regeneration is possible with the high gear torque path without the one-way clutch and is possible in two modes (see Fig. 2). The torque flow and driving scenes for each mode are shown below.

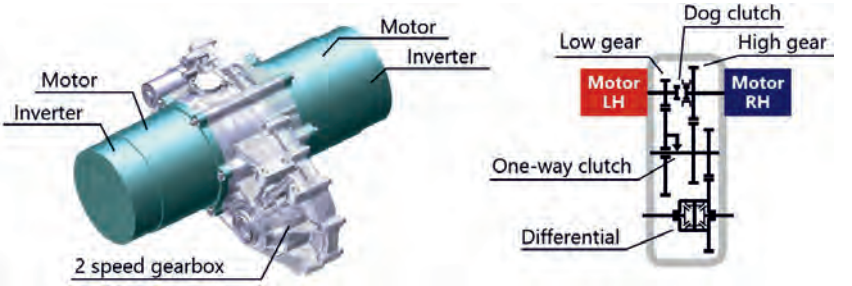

Fig. 1: Dual Motor Multi Driving Mode e-Axle

Fig. 2: Torque/speed range of each mode

2.1. “1-Motor-Low” mode

“1-Motor-Low” mode is used from starting up to low speed driving. Only the LH motor’s torque is transmitted to the tire via the low gear. (see Fig. 3)

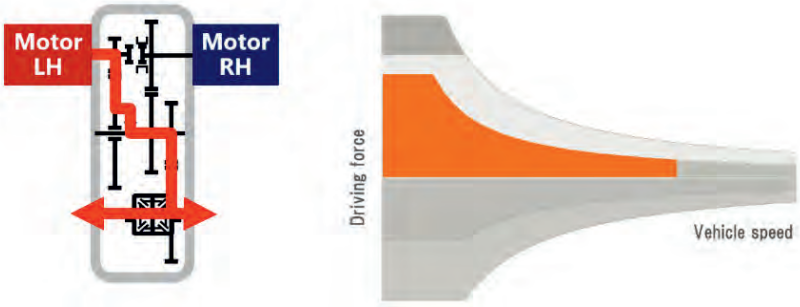

Fig. 3: Torque transmission path of “1-Motor-Low” mode

2.2. “1-Motor-High” mode

“1-Motor-High” mode is used in medium speed to high speed driving situations, where power consumption is to be saved. Only the RH motor’s torque is transmitted to the tire via the high gear (see Fig. 4). Switching between “1-Motor-Low” and “1-Motor-High” mode is performed seamlessly by the one-way clutch built inside the low gear. If the second axis, which is directly connected to the high gear, rotates faster than the low gear, the one-way clutch is unlocked, the low gear becomes free, and the transition to “1-Motor-High” mode is completed.

Fig. 4: Torque transmission path of “1-Motor-High” mode

2.3. “2-Motor-Low/High Combination” mode

The “2-Motor-Low/High Combination” mode is used for driving situations where a high torque is required such as driving uphill. The LH and RH motors are operated simultaneously, their torques are combined on the second axis and the maximum driving force is transmitted to the tire. (see Fig. 5)

Fig. 5: Torque transmission path of “2-Motor-Low/High Combination” mode

2.4. “2-Motor-High” mode

The “2-Motor-High” mode is used in driving situations, where fast and powerful acceleration is required, such as merging onto the highway and overtaking. When the LH and RH motors’ revolutions are synchronized and the dog clutch on the first axis is activated, the LH and RH

motors are connected and their torque is combined. The combined torque is transmitted to the tire through the high gear. (see Fig. 6)

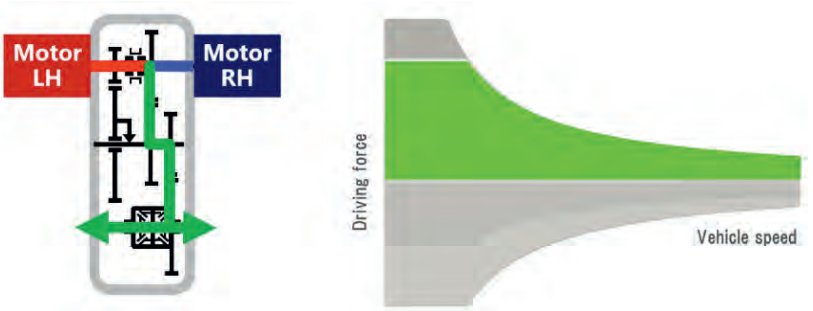

Fig. 6: Torque transmission path of “2-Motor-High” mode

3. FEATURE

DMM Axle is an eAxle, with main characteristics of low power consumption, high driving performance, and compact size. The following is a detailed description of each feature.

3.1. Low power consumption

The driving energy efficiency can be improved by optimally selecting the above described mode in accordance with the vehicle driving load state and the driving scene. With a typical single motor eAxle without transmission mechanism, it is difficult to achieve low power consumption in both low and high speed, because the driving scenes are limited by the motor’s high efficiency range. In DMM Axle, the combination of two motors and a two-stage transmission enables it to switch its mode according to the driving scene, which greatly expands the driving scene range which can be covered with the motors’ high efficiency range as shown in Fig. 7. This makes it possible to drive at low speed or high speed with power savings. In the WLTC driving mode, the system operating points in the prototype vehicle specifications described later can run in almost all areas only in the “1-Motor-High” mode. However, in the real world, where large driving force is required in situations such as hill climbing, high speed driving, and overtaking, a high system efficiency can be realized by switching the number of operating motors and gear ratios. As shown in Fig. 8, in case of the prototype vehicle, the power consumption can be improved by 10% in comparison to the general 1 motor 1 speed eAxle. This is equivalent to a 10% reduction in battery cost and weight supposed that the cruising range is equal.

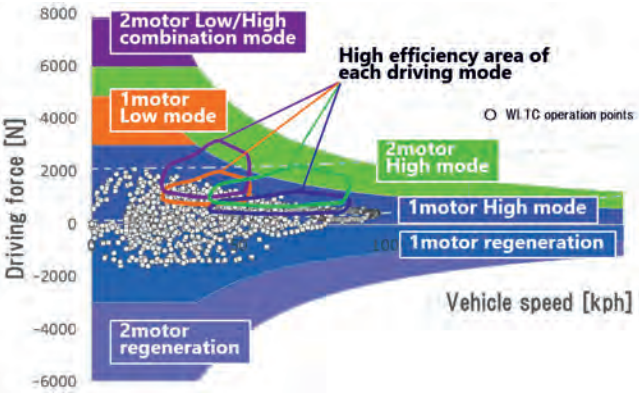

Fig. 7: Multi driving mode

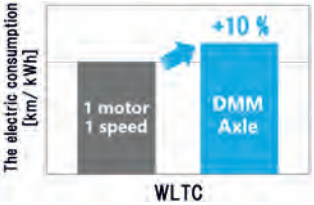

Fig. 8: Improvement of power consumption with DMM Axle

3.2. Flexible installation in a vehicle

The symmetric, flat and compact shape of the DMM Axle can be mounted at a lower position of the vehicle (see Fig. 9). This reduces the center of vehicle gravity, enabling more stable driving and contributing to greater freedom in interior and exterior design. For example, cargo compartments can be expanded in last-miles delivery vehicles. It also contributes to the reduction of torque steers because the length of the right and left shafts can be set to equal.

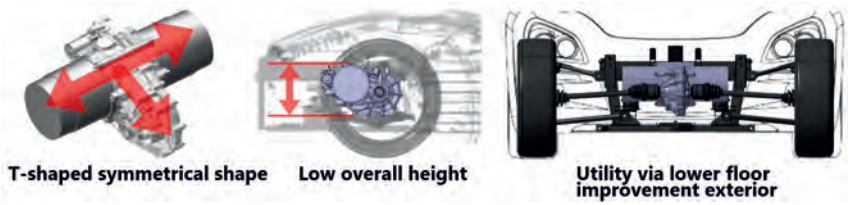

Fig. 9: Package of DMM Axle

3.3. Additional function

In order to provide Hill Assist function with an ordinary eAxle for EV, it is necessary to hold the vehicle by motor operation or brake operation, and this power consumption becomes an issue, as it deteriorates the vehicle's power consumption. The DMM Axle features two sets of built-in clutches, enabling the Hill Assist function without consuming power. In "2-Motor-High" mode, when the vehicle is stopped at uphill and the accelerator pedal is released, the vehicle cannot go backward and stops due to the circulation of the torque inside the unit. Stepping on the accelerator pedal automatically releases the torque circulation and allows the vehicle to advance (see Fig. 10). This simple hill assist function can be implemented without additional components.

Fig. 10: Hill assist start function

4. TEST RESULT

A test vehicle was equipped with a DMM Axle to verify power consumption and driving performance. The test vehicle is a 48V EV with a selectable drive mode of 4WD/FF/FR, which is based on a compact sports car and is equipped with a DMM Axle in the front and one in the rear. Table 1 shows the specifications of the test vehicles.

Table 1: Specifications of the test vehicle

Curb weight	1,000 kg
Battery voltage	48 V
Total motor torque	220 Nm (55Nm×4)
Total motor power	60 kW (15 kW×4)

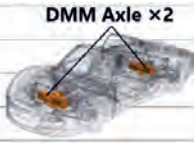

4.1. Low power consumption

Comparison and verification of the simulation in each driving mode and the system efficiency during actual driving were carried out under the conditions of 5 vehicle speeds and 2 types of load condition. As shown in Fig. 11, the difference was observed depending on the driving mode, and it became worse especially under the low load condition of the low mode. Based on the root cause analysis of the deterioration, the adaptation of the system to improve the efficiency is an issue for the future.

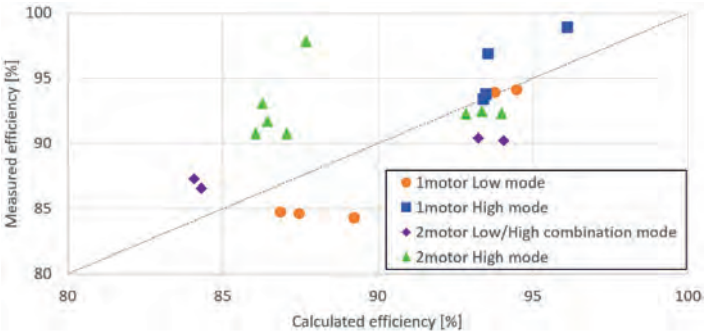

Fig. 11: Comparison of calculated and measured efficiency

4.2. Smooth Mode Changes

Vehicle acceleration at mode switching was measured. A typical mode switching result is shown below.

4.2.1. Mode switching by one-way clutch (“1-Motor-Low” to “1-Motor-High” mode)

By increasing the torque of the RH motor and decreasing the torque of the LH motor at the same time, the mode was switched by passing the torque from the LH to the RH motor. As shown in Fig. 12, there was no change in the acceleration of the vehicle when the torque was handed over from the LH to the RH motor.

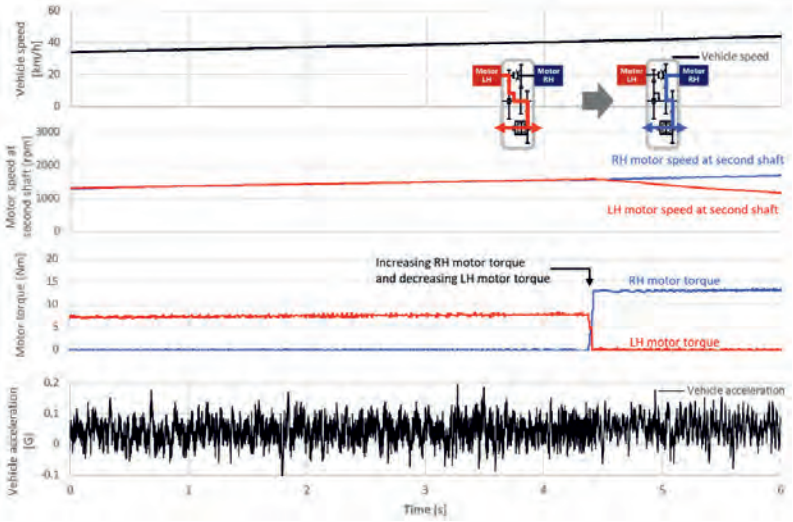

Fig. 12: Test result of mode change from “1-Motor-Low” to “1-Motor-High” mode

4.2.2. Mode switching by dog clutch (from “1-Motor-High” to “2-Motor-High” mode)

When the rotation speed of the LH motor is increased and the difference of rotation speed between the RH and the LH motor is less than the target value, the dog clutch is engaged, and the torques of the LH and RH motor are combined on the first axis to complete the mode switching. As shown in Fig. 13, there was no change in the acceleration of the vehicle when the dog clutch was engaged, indicating that the mode was switched smoothly.

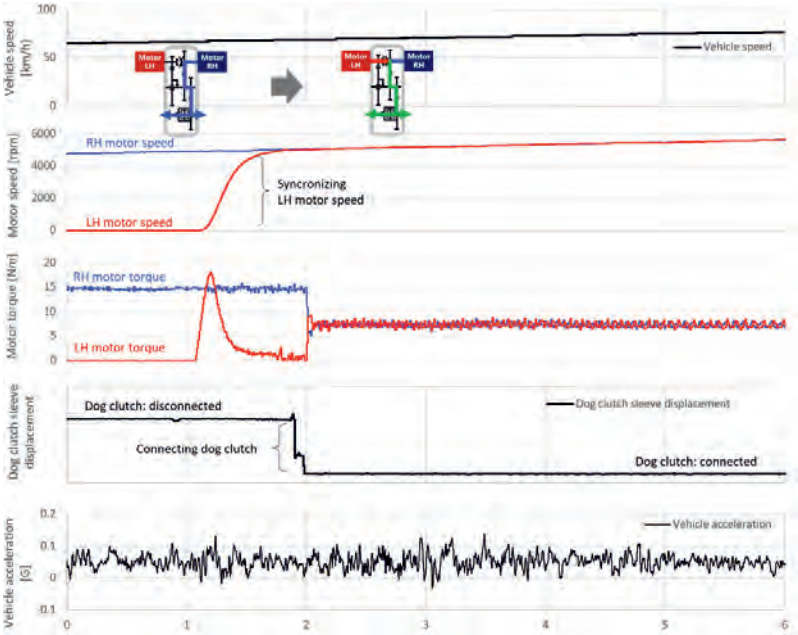

Fig. 13: Test result of mode change from “1-Motor-High” to “2-Motor-High” mode

5. SCALABILITY

DMM Axle has the following scalability by utilizing the components (motors and inverters) of one motor systems, where cost reductions due to mass production effects have already been conducted.

- Expansion to commercial vehicles and sports cars requiring higher output under high voltage
- Expansion to micro-city commuters by further lowering voltage (12 to 24 V)
- Application to HEV P4 at each voltage (simple e4WD)

6. CONCLUSION

We have developed a Dual Motor Multi Driving Mode e-Axle that solves the issues regarding the electrification of the vehicles such as the last mile delivery truck, etc., which have a large change in the required driving force in the actual driving condition, in terms of achieving low

power consumption and driving performance at the same time and providing a wide cargo space.

The combination of two motors and a two-stage transmission to realize four driving modes and two regenerative modes made it possible to achieve low power consumption and high driving performance at the same time.

The flat thin layout of the DMM Axle also allowed the eAxle to be mounted at a lower position on the vehicle, thus contributing to the expansion of the cargo space.

Compared to the current mainstream 1 motor single speed eAxle, the power consumption improvement is expected to be +10% in the WLTC mode, which indicates the possibility of a 10% reduction in battery cost and weight. However, as the result of the verification the measured efficiency was lower than the predicted efficiency in the “1-Motor-Low mode” in the low load range, the cause needs to be investigated and improved.

The issue of shift performance, such as shock and loss of acceleration G during shifting by multi-stage speed shift of the eAxle, was solved mechanically by adopting a one-way clutch structure, and it was confirmed that there was no problem with each mode transition in the test vehicle.

We confirmed that there are no critical problems with the functions and performance of DMM Axle in this 48 V low voltage prototype vehicle, and further detailed verification is necessary for mass production.

REFERENCES

[1] Kaneko, S., Yamada, S., Yamamoto, A., Kishida, H., Urakami, S., Ogawa, K., Aihara, T.: Demonstration of 2-speed Seamless Shifting for EV Using Magnetostrictive Torque Sensor. JSAE Annual Congress, No.20205168. 2020

[2] Mair, A.: Highly Efficient Drivetrains for the Mobility of the Future. 18th International CTI Symposium. 2019

[3] Matsumoto, S., Wada, M.: Effective Drive Control of an Electric Vehicle with DC motor and CVT. JSAE Annual Congress, No.20135834. 2013

Scaling the functionality of a DCT-based DHD to segment-specific requirements

The new high torque DHD Plus

Dr.-Ing. **Sebastian Idler**, Dr.-Ing. **Carsten Bünder**,
Magna PT B.V. & Co. KG, Untergruppenbach

Abstract

The DHD Plus is part of a dedicated hybrid drive (DHD) product family based on dual clutch transmission (DCT) building set. It has five mechanical gears with up to 400 Nm internal combustion engine (ICE) torque and an electric boosting capacity up to 550 Nm equivalent input torque. The electric machine (EM) replaces the launch gear and optionally the reverse gear.

For highest possible efficiency, the new DHD Plus includes a disconnect function for both ICE and EM. Other features include a powershift in electric drive, an electric crawler functionality with approx. 30 % more electric low speed maneuvering torque, a bridged crawler extension, charge during standstill and creeping and the ability to start the ICE at any time.

Finally, detailed solutions that enable best possible efficiency and performance during all-electric, hybrid and ICE driving are presented.

Kurzfassung

Das DHD Plus ist Teil einer Dedicated Hybrid Drive (DHD) Produktfamilie welche auf einem Baukasten von Doppelkupplungsgetrieben (DCT) basiert. Es hat fünf mechanische Vorwärtsgänge für Verbrennungsmotoren (ICE) mit bis zu 400 Nm Drehmoment sowie einer Boost-Fähigkeit bis zu 550 Nm äquivalentem Eingangsdrehmoment. Die elektrische Maschine (EM) ersetzt den Anfahrgang sowie optional den Rückwärtsgang.

Für größtmögliche Effizienz beinhaltet das DHD Plus eine Abkoppel-Funktion sowohl für den Verbrennungsmotor als auch für die elektrische Maschine. Weitere Funktionen stellen eine Powershift im elektrischen Fahren, ein elektrischer Crawler-Gang mit zusätzlich ca. 30 % höherem Manövrier-Drehmoment bei niedrigen Geschwindigkeiten, eine Crawler-Erweiterung mittels Brücke, eine Batterie-Ladefähigkeit im Stillstand und bei niedrigsten Geschwindigkeiten dar sowie die Fähigkeit zum jederzeitigen Start des Verbrennungsmotors dar.

Zuletzt werden detaillierte Lösungen vorgestellt, welche bestmögliche Effizienz und Leistung während elektrischem, hybridischem und konventionellem Fahren ermöglichen.

1. Introduction

Europe is currently facing a rapid ramp up of electric and plug-in hybrid electric vehicle market shares bringing increasing uncertainty and complexity into hybrid passenger vehicle powertrains. In the upscale segment of passenger cars, electrification will substantially increase further in order to fulfil ambitious fleet consumption targets, particularly in Europe. At the same time, we see demanding cost targets and the need to exploit further performance and efficiency potentials of plug-in hybrid technology.

Besides solutions for battery electric vehicles (BEV) Magna is answering to these challenges with its Hybrid Drive Scalability, shown in Figure 1.

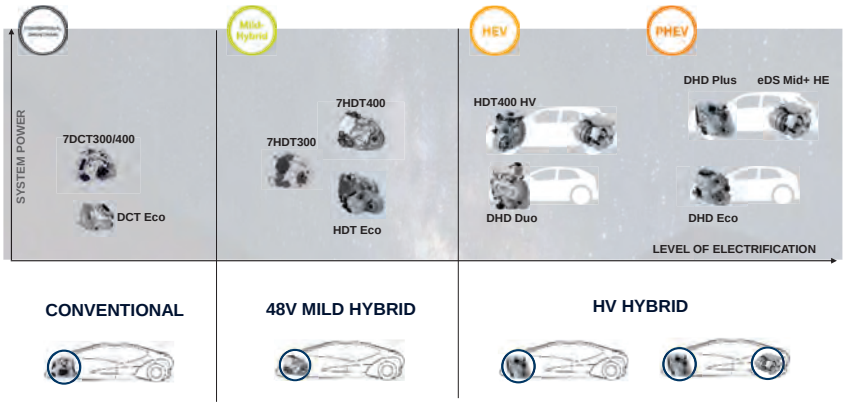

Figure 1: The Magna Hybrid Drive Scalability

Starting with conventional powertrains with a dual clutch transmission (DCT) like the 7DCT300/400 in the front, the approach goes over to 48V mild hybrid solutions like the hybrid dual clutch transmissions (HDT) 7HDT300/400 and ends up at high voltage hybrid powertrains with a dedicated hybrid drive (DHD) either as a front driven solution or in combination with an electric drive system (eDS) on the rear axle.

What distinguishes the new DHD family is a consequent overall system approach based on dual clutch transmission (DCT) building set.

In 2019, Magna introduced the DHD Eco, a dedicated hybrid transmission for applications up to 300 Nm boosted input torque [3]. The DHD Eco is a cost-optimized solution based on a dual-clutch transmission with four physical gears. It relies on a P2.5 architecture with four gears for the ICE and two of these four gears being used for the electric machine within the electric sub-transmission.

The DHD Plus conveys the common underlying concept of the DHD Eco into higher C- to D-segments and adds performance and functional versatility for correspondingly upscaled customer demands. It is thereby based on the 7DCT400 and 7HDT400 transmission family with its proven building blocks and functionalities [4], [5], [6]. This realizes commonality, like having an existing DC400 dual clutch with actuation and control system available, as well as scalability, like having an all-wheel drive ready differential available.

2. DHD Plus architecture meeting highest performance requirements

As the DHD Eco, the DHD Plus is based on a simplified dual-clutch transmission architecture, but with five physical gears. Although the EM acts as a logical launch gear, the five mechanical gears are referred to as 1 to 5 in the following.

While the 2nd and 4th gear transmit both ICE and EM torque, 1st, 3rd and 5th are exclusively intended for ICE and some additional functional features discussed below.

2.1. Conventional Driving Performance

As known from DCT architectures, the mechanical gears are arranged in an even and odd sub-transmission. Thereby the DHD Plus features a full conventional powershift capability with the proven dual clutch technology as shown in Figure 2 [2], [4].

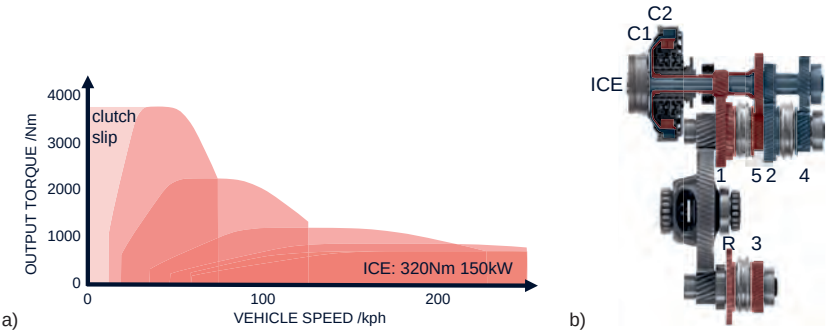

Figure 2: Full powershift capability with five physical gears enabling a) axle torque over vehicle speed close to ICE peak power with b) even and odd sub-transmission

2.2. ePowershift capability of the electric sub-transmission

A scalable eDS electric machine is connected to the 2nd and 4th gear with up to 120 kW electric output power, creating an electric sub-transmission equipped with an NVH optimized dedicated eGear Set.

The ratio of the 2nd gear supports electric drive up to approx. 130 kph with a maximum output torque of almost 3000 Nm, see Figure 3.

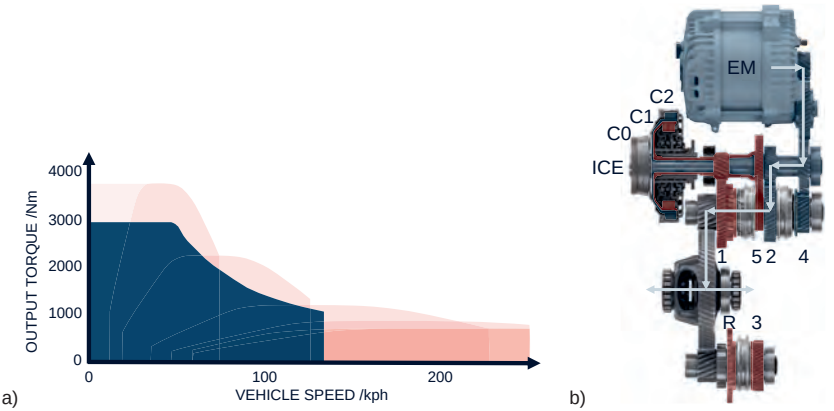

Figure 3: eDrive in gear 2nd with a) axle torque over vehicle speed and b) DHD Plus torque flow path

An important development goal was to enable gearshift during electric drive without torque interrupts: This is where the Magna C0 comes into play, in addition to its usual task to decouple the ICE from the transmission. The ePowershift works as follows: While the C0 is open, the 5th gear of the conventional sub-transmission is preselected. By redirecting the EM torque path through the slipping clutches C1 and C2 and thus the conventional sub-transmission, the electric sub-transmission can be disengaged to neutral and the EM can adjust its speed to the target speed of the 4th gear. During this shift operation of the electric sub-transmission the dual clutch adjusts the output torque and thus maintains the tractive force at the wheels.

Once the target speed is reached, the 4th gear can be engaged and the torque is retransferred to the electric sub-transmission, again without having a torque interrupt.

The described sequence of a powered upshift is illustrated in Figure 4.

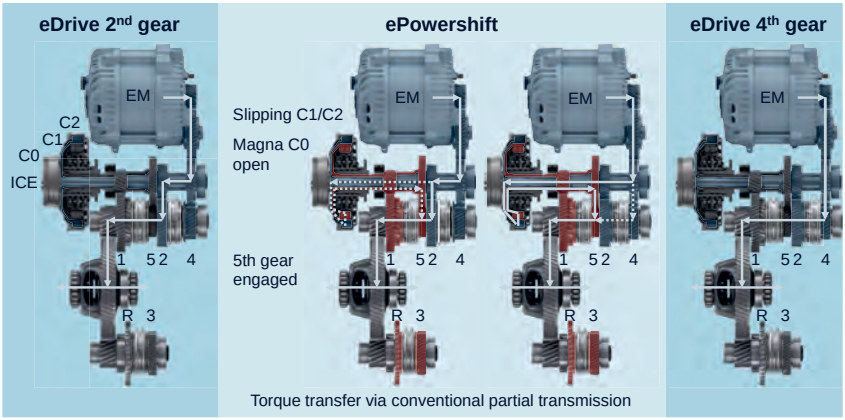

Figure 4: ePowershift with torque transfer via conventional sub-transmission

Once the ePowershift is completed, the EM is again directly connected to the wheels via the 4th gear, enabling an output torque of up to around 1000 Nm and thanks to its ratio the 4th gear reaches up to maximum vehicle speed, see Figure 5.

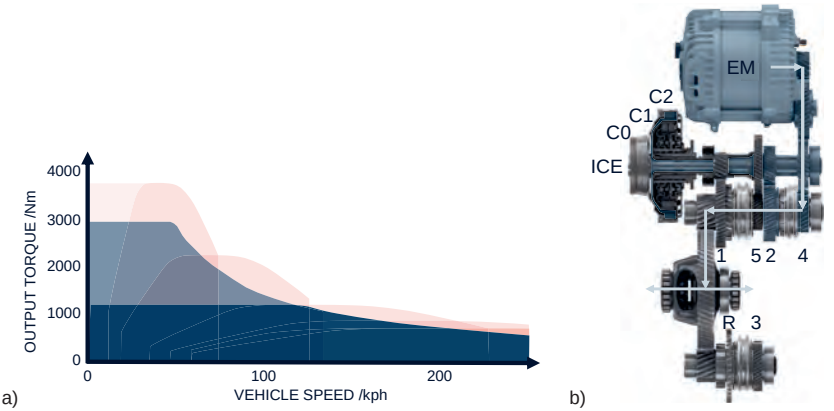

Figure 5: extended eDrive in 4th gear with a) axle torque over vehicle speed and b) DHD Plus torque flow path

With this principle, the DHD Plus can support ePowershifts as powered up as described, powered down, coast up and coast down.

2.3. eCrawler functionality

Another exclusive feature made possible by using the three clutches is the so-called eCrawler gear. It enables another short gear in electric driving with an overall ratio from the EM to the wheels of up to 25 delivering up to 3800 Nm output torque. This would typically be useful for situations, where very high tractive force during all-electric operation is required, for example for steep slopes. As shown in Figure 6, during eCrawler operation the Magna C0 clutch is open whereas the closed clutches C1 and C2 transmit the EM torque through a torque path using the 1st gear of the conventional sub-transmission.

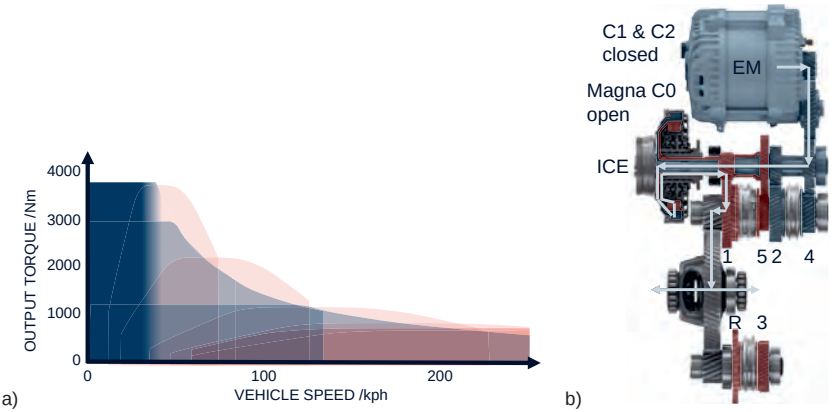

Figure 6: eCrawler functionality with a) axle torque over vehicle speed and b) DHD Plus torque flow path

2.4. DHD Plus bridged Crawler extension

For extreme off road capability requirements a bridged crawler extension is available. By adding an additional bridge gear that meshes with the loose gear of the 2nd gear to the second output shaft, both sub-transmissions can be bridged via a separate synchronizer connecting the bridge gear with the loose gear of the 3rd gear. The result is a forward crawler gear with a total ratio from the ICE to the wheels of up to 42, see Figure 7.

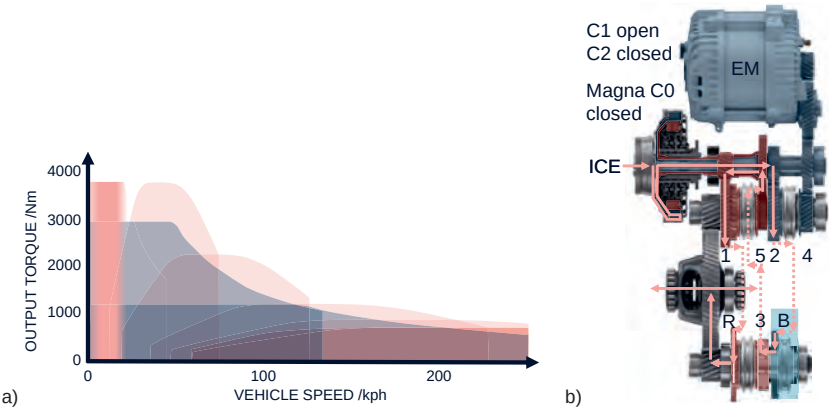

Figure 7: DHD Plus bridged Crawler extension with a) axle torque over vehicle speed and b) extended torque flow path

With this feature, under all SOC conditions any hill climbing operation can be supported. From approx. 3 kph onwards the clutch C2 is slip-free and electric energy can be generated in parallel to provide power for a potential electric rear axle.

2.5. Extended boosting capacity

Within the architecture of the DHD Plus the torque path of the electric machine to the wheels does not pass the primary clutches. Thereby the available boosted torque capability especially at higher driving speeds is extended. The two available torque paths for each EM and ICE enable a boosted hybrid operation not limited by the clutch torque capability. The result is an outstanding hybrid boosted drive performance with more than 250 kW temporary output power over the whole vehicle speed range, only limited by the maximum output torque capability, as shown in Figure 8.

The DHD Plus performance capability is underlined by the etelligent Launch functionality, enabled by the 120kW electric machine. Electric machines provide great controllability, much quicker response times and a higher accuracy compared to conventional combustion engines. Speed controlled eLaunch with improved traction limit will increase potential acceleration from standstill.

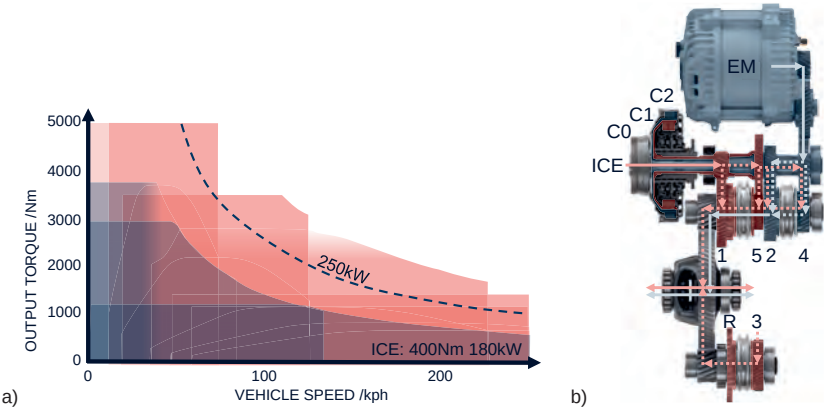

Figure 8: Boosted hybrid drive performance with a) axle torque over vehicle speed and b) DHD Plus torque flow paths

3. ICE start at anytime

A crucial feature for sophisticated plug-in solutions is the possibility to start the engine in all driving situations. The primary start of the DHD Plus in most situations is a clutch start, which means starting the engine via a clutch while compensating the cranking torque with the EM: By controlled actuation of C1 and C2, the EM torque can drag the engine up to the required ignition speed. To allow for this, a certain vehicle speed threshold around 15 kph is required. In case the driver or system request occurs below this threshold, the standard response is maintaining in electric mode until the threshold is exceeded, compare Figure 9.

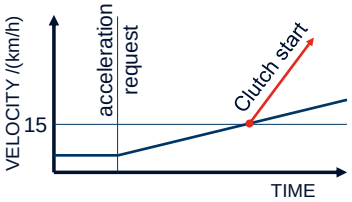

Figure 9: Schematic time-traces of an ICE start via clutch start as primary ICE start in eDrive

Other than P2 solutions, the arrangement of the DHD Plus features a torque split functionality, providing further benefit here: when driving in 2nd gear, the 5th gear can be preselected. So the torque reserve of the EM required to start the ICE without torque interference can be reduced

significantly [1]. As shown in Figure 10, this increases the available torque for electric driving in the DHD Plus by 17 %, maintaining a fully compensated ICE clutch start.

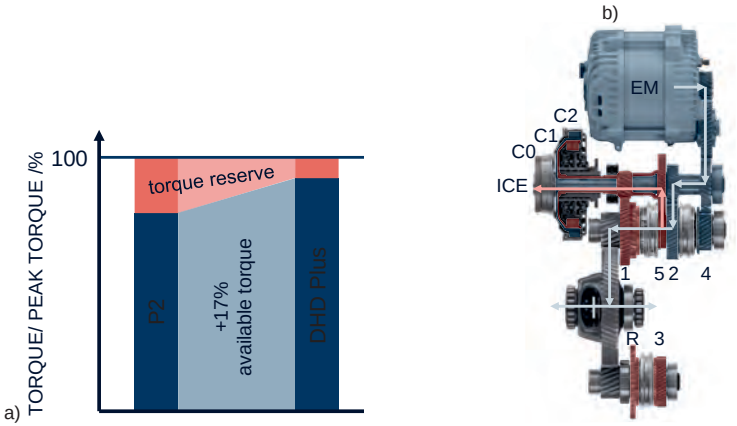

Figure 10: Increased ePerformance compared to P2 via torque split with a) +17 % available torque via shown b) DHD Plus torque-flow during ICE clutch start [1]

An alternative start procedure may be chosen in situations like an ICE start request during vehicle creeping, typically due to battery management requirements close to low state of charge (SOC). In this case, the transmission provides a smooth transition from electric creep in 2nd gear into electric creeping via a slipping clutch C1, thereby having C2 closed and C0 open. Comparable to a P2 solution, the EM can now increase its speed independent from the vehicle velocity. Closing the Magna C0, the ICE is now actively cranked, see Figure 11.

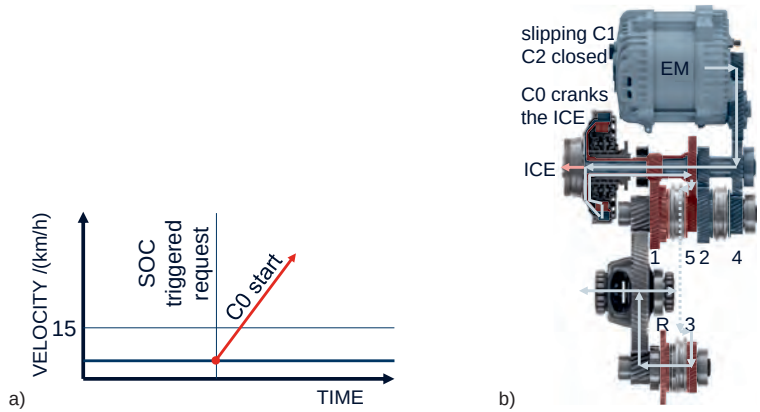

Figure 11: ICE start via C0 start for e.g. SOC triggered start in creep with Magna C0 with a) schematic time traces and b) DHD Plus torque-flow during C0 start

However, with a minor SOC margin the frequency of ICE start requests in an ongoing creep situation is expected to be significantly reduced.

4. Next generation efficiency

Another main development goal was best-in-class efficiency. The DHD Plus shares many components with other Magna products like the 7DCT300/400 and 7HDT300/400 based on a building block approach [5], [6]. These include optimized bearings, low friction gear meshes with reduced specific sliding speeds and common general design benefits like reduced splash losses [4].

While the ICE can be decoupled as described above during electric driving, the same applies vice versa: during conventional ICE driving in the highest gear, the EM can be disconnected, avoiding EM drag losses. At the same time, the 120 kW EM allows for a long ratio of the 5th gear, due to the high available boosting capacity.

Another best-in-class feature is the side-by-side design with no length increase. Compared to a co-axial design the efficient high-speed EM concept offers higher power density and a benefit of 2 % in WLTP charge depleting electric range, see Figure 12.

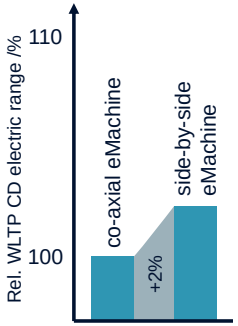

Figure 12: DHD Plus electric drive efficiency benefit of side-by-side vs. co-axial EM

Further benefit is given through a highly integrated inverter, the optimized insertion winding and efficient power modules.

Certainly, the two available and powershiftable gears for the EM greatly contribute to highest efficiency. The two well-chosen ratios of the electric sub-transmission of the DHD Plus enable high efficient operation conditions of the eDS system.

What further boosts the efficiency of the DHD Plus is that electric driving requires no actuation power: all the three clutches are open and the torque path in both available e-gears is positive locking, enabling lowest possible parasitic losses.

Finally, the ultra-low drag torques of the Magna C0 make the DHD Plus best in class for WLTP charge depleting electric driving range, as shown in Figure 13.

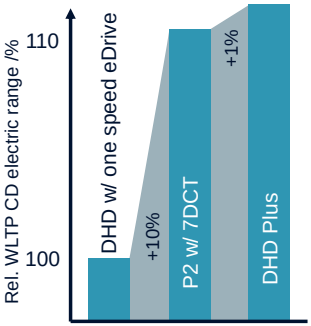

Figure 13: DHD Plus electric drive efficiency benefit of two speed eDrive with ultra-low Magna C0 drag torques and passive actuation in eDrive

5. Package and Production Flexibility

The shift to transverse vehicle platforms intended for multi-powertrain architectures requires a highly flexible transmission solution on the front axle. The compact Magna DHD Plus features no axial length increase by adding the EM and inverter compared to the 7HDT400 mild hybrid solution thanks to the side-by-side arrangement of the EM as shown in Figure 14.

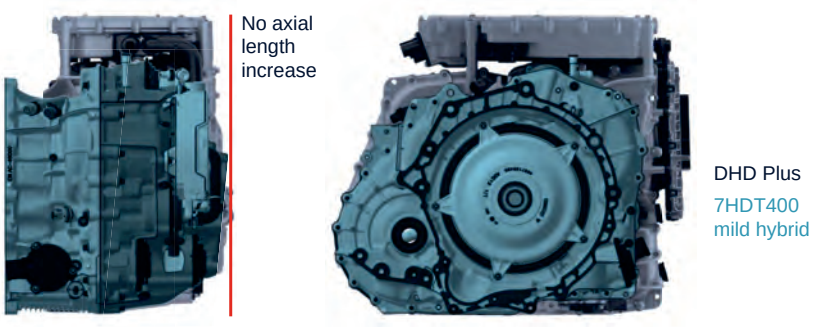

Figure 14: Optimized package for flexible DCT-, HDT- and DHD-architectures

Including a high-speed EM with a high power density into a decontented DCT, makes the DHD Plus best-in-class regarding torque-to-weight ratio. As shown in Figure 15, compared to several P2 products in the market, the DHD Pus offers the highest equivalent boosted input torque with a reasonable low weight.

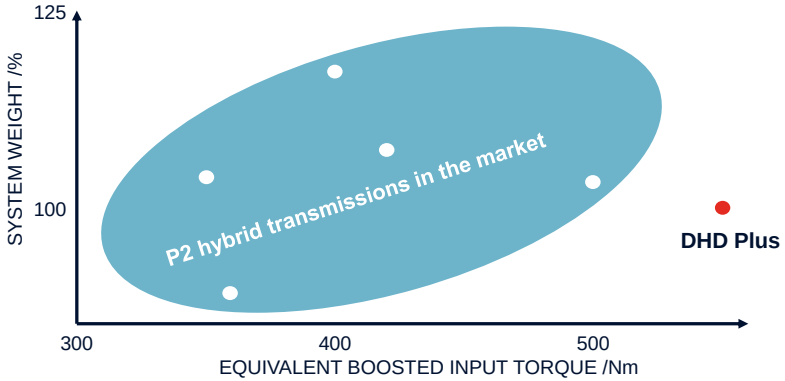

Figure 15: DHD Plus torque-over-weight ratio

One final huge benefit of the DHD Plus results out of the commonality with conventional dual-clutch transmissions as well as 48V and high-voltage variants: this family approach allows for a smart re-use of existing manufacturing equipment on flexible production lines that provides a technology mix that is able to cope with volatile future powertrain architecture demands, see Figure 16.

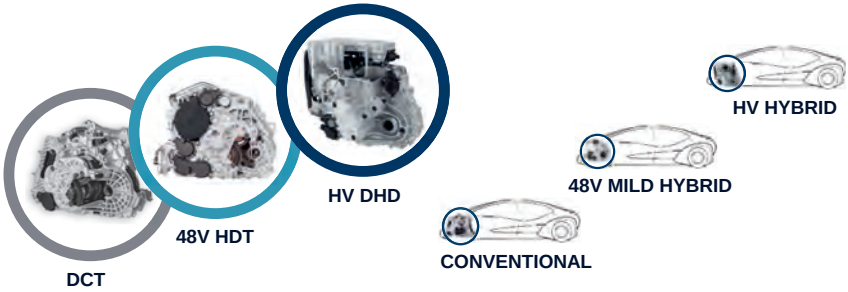

Figure 16: Flexible manufacturing set-up to cope with volatile technology mix

6. Summary

Given upcoming CO2 regulations and end-customer requirements, next-generation plug-in hybrid drives will have to be outstanding regarding efficiency and performance in any driving situation. This applies to all-electric driving as it does to hybrid mode and constant driving using the ICE.

The DHD Plus offers a value package with a multiple number of attribute claims, see Figure 17.

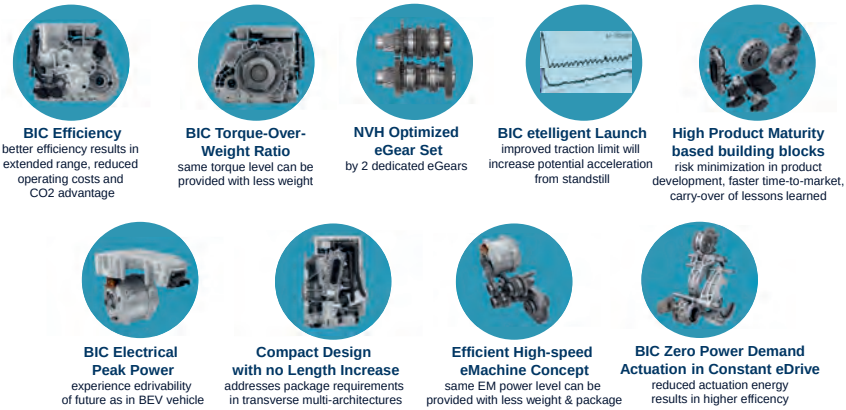

Figure 17: DHD Plus claims

The DHD Plus is based on proven layshaft transmission technology with lowest parasitic losses. Unlike common P2 hybrid solutions, it is able to decouple both ICE and EM in respective driving situations and features extended boosting capacity thanks to different torque paths of EM and ICE.

The Magna C0 boosts the electric drive efficiency by enabling an ePowershift in the electric sub-transmission and its ultra-low drag torques. Furthermore, it enables the eCrawler functionality to cover all use cases for upscale segment cars and SUVs. As a fourth major benefit, the Magna C0 empowers the DHD Plus to support ICE start at any time.

Finally, due to its compact design with no axial length increase and a high-speed EM with a high power density, the DHD Plus extends the DCT and HDT family, provides an interchangeable flexibility option and is thereby ready for next-generation vehicle platforms, which are intended for conventional, 48V and HV drives with DHD solutions meeting upcoming CO2 regulations.

References

[1] Blessing, U. C. und Strube, A.: 6HDT250 – The scalable solution from Mild- to Plug-In Hybrid. VDI Getriebe in Fahrzeugen 2011 (2011), Friedrichshafen

[2] Blessing, U. C., Meissner, J., Schweiher, M., Hoffmeister, T.: Skalierbares hybrides Doppelkupplungsgetriebe. ATZ - Automobiltechnische Zeitschrift. Ausgabe 12/2014, S. 12-16

[3] Bünder, C.: Scalability goes Live – Modular Hybrid Transmission Family for High-Volume Applications. CTI symposium 2019 (2019), Berlin

[4] Herdle, L.: 7DCT/HDT400 – New fuel-efficient FWD DCT and hybrid transmission for up to 400 Nm. Dritev – Getriebe in Fahrzeugen 2019 (2019) Bonn

[5] Mayer, A.: Powertrain of the future means scalable functions of a modular platform in a changing industry. CTI symposium 2018 (2018), Berlin

[6] Rucker, T.: Magna's view on the changing role of powertrains in PVs and LCVs. CTI symposium 2020 (2020), Berlin

Performances Validation of an electrically-commanded dog clutch system for multi-speed and disconnectable eDrives

Dipl.-Ing. **Gilles Herbillon**,
VCST Industrial Products, Sint-Truiden, Belgium

Company Introduction

VCST Industrial Products (automotive branch of BMT Drive Solutions) is a recognized gears supplier from the automotive field, and relies on a 40-year expertise in:

- gear sets design (Software programs for sub-systems durability, NVH, lubrication),
- gears & gearboxes testing (performances, durability, shifting, noise),
- fast-prototyping (wide range of processes incl. soft and hard machining, heat-treatment),
- mass production & control (fully automated factories).

Fig. 1: VCST strategy

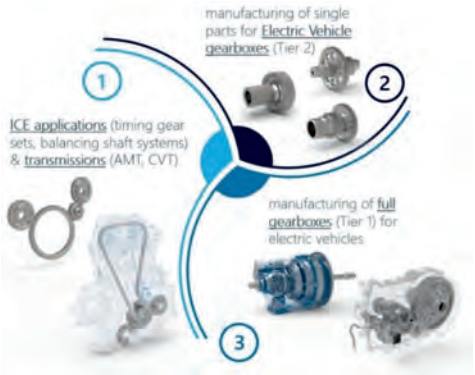

Fig. 2: VCST business scenario

VCST e-Drive department offers a smart portfolio of e-Drives concepts as perfect fits for the new EV categories. These are Offset or Coaxial / Layshaft or planetary / Single-speed or multi-speed / Wet or dry sump / incorporated differential unit or torque vectoring.

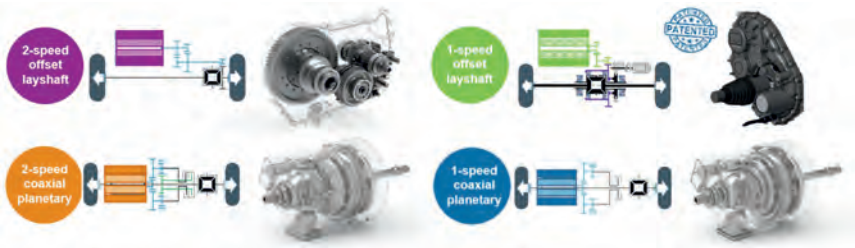

Fig. 3: VCST eDrives AMT-concepts including a dog clutch technology

ABSTRACT

The future transmissions for electric vehicles should be preferably

- Simple and inexpensive: low cost EDU's should balance battery packs' complexity.
- Efficiency: Low drag torque, traction motor operation within its best efficiency areas,
- Fast & smooth: low torque interruption, and low noise,
- Durable: no friction energy dissipation, seamless engagement or low impact

This paper summarizes the design validation of an electrically-commanded dog clutch that can be used for the "NextGen" eDrives either as SHIFTING system (for multi-speed gearboxes), either as DISCONNECTION system (for single-speed with disconnection clutch). Electrically-piloted dog clutches belong to AMT (Automated Manual Transmission) category. The drawbacks of the former technology of dog clutches, as the ones used in motorsport (backlash, spread in mechanical synchronization time, perceptible impact during the synchronization) are completely eliminated:

- Backlash eliminated and smooth engagement guaranteed with suitable clutch design,
- The spread of performances reduced by increasing the speed differential, and increasing the number of cavities, and shifting actuator speed.
- Efficient and durable since no friction energy dissipated during the speed synchronization as the kinetic energy of the decelerated parts is sent to the battery.
- High level of control (shifting fork electrically actuated in a double closed-loop system)
- Shifting performances optimized through a suitable control of the successive stages of the shifting process: torque build down and build up, reduced torque interruption,
- The shifting performances repeatability during UPSHIFTING & DOWNSHIFTING events was addressed (> 50 repetitions / setting). This test campaign was performed with a fixed difference of speed (10 values from 7 to 70 [1/min]) between the dog ring, and the free running gears to be synchronized

- Besides "constant speed synchronization", further level of controls are considered such as "variable speed synchronization" (a "smart speed differential control" would allow to reach simultaneously a smooth and fast mechanical synchronization).

The shifting performances of an electrically-actuated dog clutch were predicted, simulated and measured. The 3 main steps of the shifting process (such as disengagement, traction e-motor speed synchronization in neutral, mechanical synchronization) were analyzed in detail, under several test conditions. This paper highlights that a "simple" shifting technology combined with advanced control features is a good fit for the "NextGen" powertrains, and would allow to reach 0.1 sec DISCONNECTION time, or 0.3 sec OVERALL SHIFTING time.

1. eDrives - Background

Before 2020, this was already intended that electric powertrains would become the new trend for the road transport industry, chasing for carbon neutral technologies. The sanitary crisis has forced most of us to reconsider its own mobility, and has still reinforced this reality.

Statement #1: All vehicles categories (from micro-cars to heavy-trucks) are subjected to Battery electric or fuel-cell conversion, which means that the transport industry is in need of electric Drives capable of high torque.

Statement #2: As customers expect similar performances than ICE-propelled vehicles, the passenger vehicles top speed is also supposed to increase. Multi-speed eDrives seem to be a good alternative to high speed eDrives in order to reach vehicle performances (high wheels torque and high vehicle top speed) without compromise, also keeping the top speed to decent limit (< 8 000 – 11 000 RPM).

Looking back in mirrors, the first EV's released on the market in 2013 could achieve limited top speed (130 to 150 km/h) with a gear ratio selected between 8:1 and 10:1, and an e-motor top speed around 11 000 [1/min].

Today, the vehicles catalog top speed have raised to 160 km/h (VW ID.3, Q4 e-tron), 180 km/h (VW ID.4, Ford Mustang Mach-e, Audi Q4 e-tron), 190 km/h (Audi e-tron), 200km/h (NIO ES8, Ford Mustang Mach-e GT, Rivian R1T, Jaguar IPace EV400), 209 km/h (Tesla 3), 260 km/h (Porsche Taycan Turbo S).

If High Speed eDrives allow to keep relatively simple gearboxes layouts, they bring huge challenges on the input bearings (request for ceramic balls or shielded bearings) & gears durability (increased risk of scuffing would make necessary the use of oil spray. Ref [1])

Therefore, 2 trends will co-exist for premiums cars: High-speed & Multi-speed.

Multi-speed give OEM's the possibility to re-use existing e-motor in multiple applications.

Looking at commercial vehicles, the trend of multi-speed also offers further benefits compared to DIRECT drive layouts: as the downsizing/cost saving on the traction machine.

Statement #3: Dual-axle vehicles deliver high dynamic performances, but chase for efficiency improvement (to save the battery range). Future premium EV layouts would feature a secondary axle with disconnection clutch for efficiency optimization.

As all types of losses are tracked (such as e-motor drag torque, bearings drag torque, gears churning losses, sealing losses), the disconnection clutch should be inserted as close as possible to the wheels in order to eliminate most of these main contributors. VCST 1-speed-AMT e-Drives with disconnection clutch are already capable to disconnect the complete gear set from the wheels, and therefore get rid of gears churning losses, and e-motor drag torque.

2. Road Map of electrically commanded shifting systems applied to eDrives

Apart from electro-magnetic clutches, the main shifting systems that can be applied to eDrives are electrically-commanded derivatives from the ones used on ICE's: (A) synchromesh (ref. [3]) , (B) dog clutch, (C) dual-clutch, (D) electro-magnetic clutch (ref. [2]).

The working principle of all systems consists in the adjustment of the rotational speed of e-machine shaft with the rotation speed of the gearbox shaft directly connected to the wheels.

The potential of each type of shifting system can be defined considering the design (principle / robustness / cost), the performances (efficiency / shifting time / noise), and the control features (as all 4 systems can be electrically or electro-magnetically controlled).

DESIGN and ROBUSTNESS	Small radial teeth are weak and only engaged with a speed differential close to “zero”	Big axial teeth capable to absorb significant speed differential.	Lamellas tolerate higher speed differential (above 1000 [1/min])	Design with soft ferromagnetic materials. Quite hot conditions of work for solenoids
SHIFTING TIME	Long shifting time : only a low speed difference can be applied in order to preserve the small teeth.	Spread of shifting times performances, depending on the relative position of the teeth vs. cavity when engaging.	Torque interruption still present (ref. [4]) unless applying high slip strategy leading to low efficiency.	Low response time of the coils (ranging between 2 & 10 msec) depending on the level of force delivered.
EFFICIENCY	Kinetic energy converted into friction (within friction cones) – ref. [3]	Kinetic energy directly back to the battery (regen)	Kinetic Energy absorbed into friction in lamellas. Active oil cooling needed	Unless specific design, electro-magnet clutches are constantly supplied.

Fig. 4: Road map of Shifting system applied to eDrives

3. “Zero Backlash” DOG Clutch technology applied to “next gen” eDrives

HARDWARE: VCST’s dog clutch technology only includes 5 components:

- a dog ring supported by a fork translates between 2 gears with side protrusions/claws
- a shifting fork supported by a threaded bushing
- a threaded bushing moved by a threaded spindle
- a spindle driven by electrical rotary actuator

VCST’s dog clutch design gives specific benefits:

- Zero backlash (insertion of a protrusion into a cavity)
- Seamless or “Shock-free” (progressive engagement)
- Limited number of protrusions (on the gears side) and cavities (on the dog ring) as a compromise between shifting time, and teeth mechanical resistance and durability.
- “Self-locking”, as a gear is kept engaged without supplying the actuator.
-

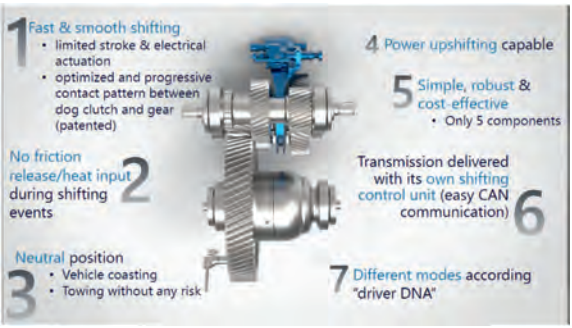

Fig 5: Dog clutch system benefits

Fig. 6: Layshaft / shifting fork

CONTROL: the main novelty compared to former DOG clutches relies on the ways of control:

- The former DOG clutches (previously used in motorsport with ICE's), were actuated manually or hydraulically, without any control of the speed differential. The kinetic energy (of the crankshaft) was dissipated into an uncontrolled shock.
- Combining with performant traction e-machines and electrical actuators, dog clutches can be monitored with a high level of accuracy (and redundancy):
    - the shifting fork is operated by an accurate actuator, part of a double closed-loop system (including a "contact-less" sensor on the fork, and resolver).
    - The torque interruption is minimized optimizing motors speed synchronization.
    - The spread of performances is reduced by increasing the speed differential,
    - the impact can be minimized applying a "smart" speed synchronization (according to variable speed pattern) without compromising the shifting time.

4. Breakdown of a shifting event into steps

A complete shifting sequence consists in following steps:

DISENGAGEMENT	Electrical & Software Communication Response Times
	Duration of Torque BUILD DOWN phase
	Extra Time to reach neutral
NEUTRAL	Time in neutral (input speed reached target)
	Time in neutral (lag before dog ring starts moving to next gear)
ENGAGEMENT	**MOTION from NEUTRAL to next gear** = duration for dog ring to touch next gear claws
	MECHANICAL SYNCHRONIZATION TIME = duration to find the cavity once the dog ring is in contact with gear's protrusions
	Duration from partial to full engagement

The linear motion of the dog ring along the layshaft can be visualized below:

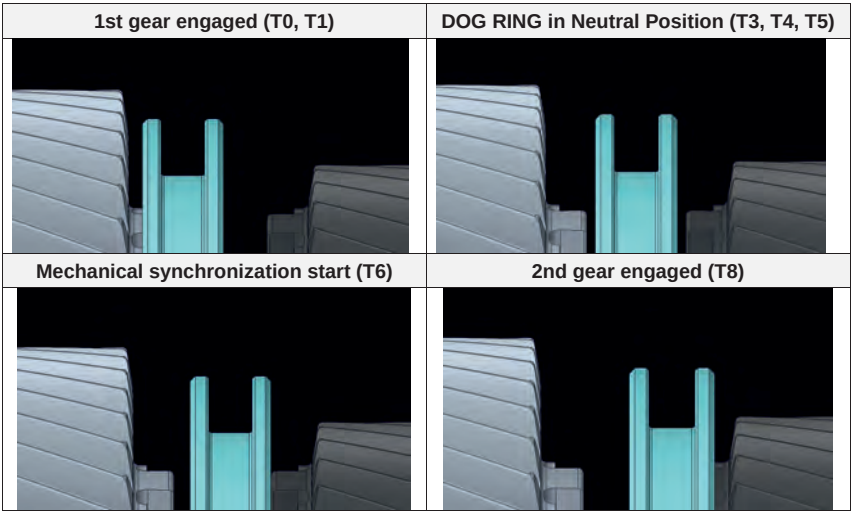

Fig. 7: Dog clutch side views during shifting event

Table 1: Reference timings for shifting

		Events Description		Lead time
DISENGAGEMENT	T0:	Order sent = change of the gear target	/	/
	T1:	The dog ring to start moving from the initial gear	ΔT1 = (T1 – T0)	Electrical & Software Communication Response Times = Delay time between change in gear target and start of torque build-down phase
	T2:	Torque build-down achieved	ΔT2 = (T2 – T1)	**Duration of Torque BUILD DOWN phase** = Time for the dog ring to get reduced to "zero" (e-motor related), including the **1st part of the MOVE to NEUTRAL**
	T3:	Dog ring reaches NEUTRAL position	ΔT3 = (T3 – T2)	Lag in NEUTRAL = Extra time required by the dog ring to reach the neutral position (once the torque is "zero") = **2nd part of the MOVE to NEUTRAL**
NEUTRAL	T4:	Dog ring in NEUTRAL + input shaft speed target reached	ΔT4 = (T4 – T3)	Duration of the SPEED synchronization phase
	T5:	Dog RING starts moving from neutral	ΔT5 = (T5 – T4)	LAG in neutral (lag before dog ring re-start moving from NEUTRAL)
ENGAGEMENT	T6:	Dog ring touches the next gear claws	ΔT6 = (T6 – T5)	**MOTION from NEUTRAL to next gear** = duration for dog ring to touch next gear claws
	T7:	Gear protrusion engaged in the cavity & Start of Torque build up	ΔT7 = (T7 – T6)	**MECHANICAL SYNCHRONIZATION TIME** = duration to find the cavity once the dog ring is in contact with gear's protrusions
	T8:	Dog RING completely engaged in	ΔT8 = (T8 – T7)	**LAG for FULL ENGAGEMENT** = time from partial to full engagement

The study focuses on DISENGAGEMENT / SPEED SYNCHRONIZATION / ENGAGEMENT:

		Events Description		Lead time
DISENGAGEMENT	T0:	Order sent = change of the gear target	/	/
	T3:	Dog ring reaches NEUTRAL position	ΔT3 = (T3 – T1)	DISENGAGEMENT TIME
NEUTRAL	T4:	Dog ring in NEUTRAL + input shaft speed target reached	ΔT4 = (T4 – T3)	Duration of the **SPEED synchronizatio**n phase
	T5:	Dog RING starts moving from neutral	/	/
ENGAGEMENT	T7:	Gear protrusion engaged in the cavity & Start of Torque build up	ΔT7 = (T7 – T5)	**MECHANICAL SYNCHRONIZATION TIME** = duration to find the cavity once the dog ring is in contact with gear's protrusions

5. SIMULATION & TEST PLAN

The purposes of this plan were:

- to tackle any discrepancy between SIMULATION & MEASUREMENTS
- to verify the reproducibility of the measurements
- to check the sensitivity of the speed differential on the UPSHIFTING & DOWNSHIFTING events
- to compare the shifting performances with 5-CAVITY & 10-CAVITY DOG RINGS
- to squeeze the SPREAD of performances due to the MECHANICAL synchronization
- to evaluate the impact of traction e-machine acceleration / deceleration settings.

Test conditions: 2 speed conditions were applied during the test campaign:

- Shifting from 6000 [1/min] (1st gear) to 2500 [1/min] (2nd gear) along vehicle road load,
- Shifting from 4000 [1/min] (1st gear) to 1675 [1/min] (2nd gear) along vehicle road load,

Test rig settings: The acceleration & deceleration performances were adjusted as follow

- Accel / Decel: 50 000 [1/min.s] (setting #1) / 80 000 [1/min.s] (setting #2)
- Torque Build-up/down: 100 000 [Nm/s] (setting #1) / 500 000 [Nm/s] (setting #2)

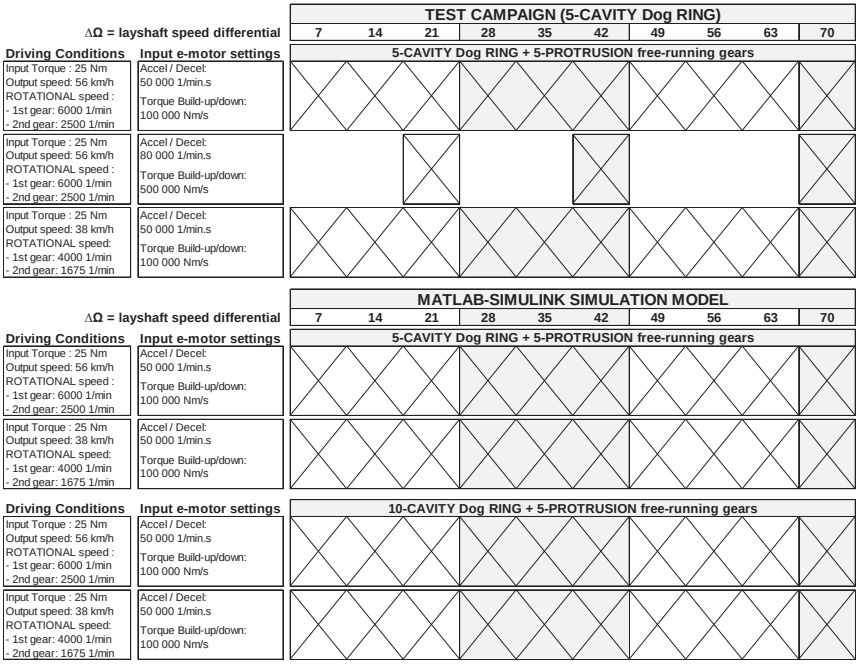

Fig. 8: Test & Simulation Plan

6. TEST SET-UP

The gearbox was mounted and tested on a test rig including 3 e-machines:

- M1: output Right wheel (up to 3600 Nm braking torque)
- M2: output Left wheel (up to 3600 Nm braking torque)
- M3: Input e-machine (up to 600 Nm propulsion torque / shaft inertia: 0.06 kg/m²)

Test bench overview

Fig. 9: Test Set-up

Test Layout

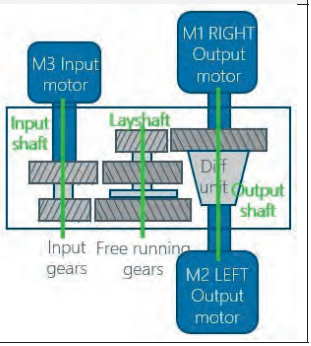

Fig. 10: 2-speed-AMT eDrive

Test bench configuration:

Input dyno	- Torque/speed mode (speed/torque limits/rates adjusted manually) - Input from VCU: Torque target, speed target, control mode target - Feedback: Actual speed, actual torque, actual control mode
Output dyno's	- Road load mode - Brake torque input from VCU

The electrical & communication response times also play a key role, and will be increased by an upgrade of the TCU performances, and the installation of a real-time environment:

	Former TCU 	Current TCU 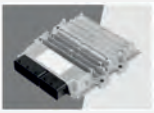
CPU	Infineon XC22xx 16/32bit @ 80MHz	TI ARM Cortex TMS570 32 bit @180MHz
Floating point operations	No support	64 bit FPU
Safety compliance	None	SIL 2; PL d; ASIL C
Programming	3S CoDeSys (PLC language)	C-code from Matlab-Simulink (model-based)
Max core task loop rate	100 Hz (10 ms)	1000 Hz (1 ms)
Actuator/motor communication	40 to 100 ms	10 ms, down to 1 ms
Control topology	Open loop (action-reaction based)	Closed loop (active control of components)

Fig. 11: – TCU performances

7. DISENGAGEMENT TIME

The disengagement takes [0.05 to 0.13] sec in upshifting, and [0.11 to 0.16] in downshifting.

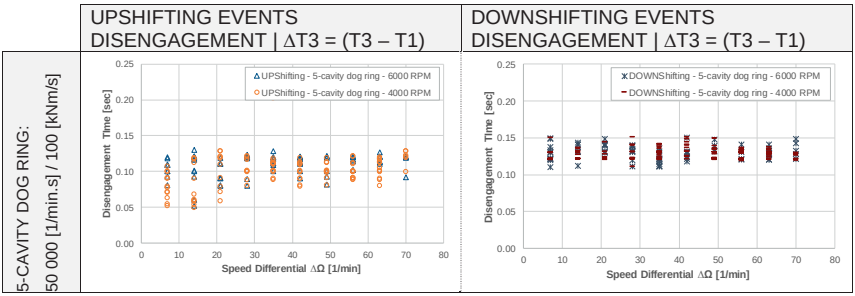

Fig. 12: Disengagement times

8. SPEED SYNCHRONIZATION TIME IN NEUTRAL

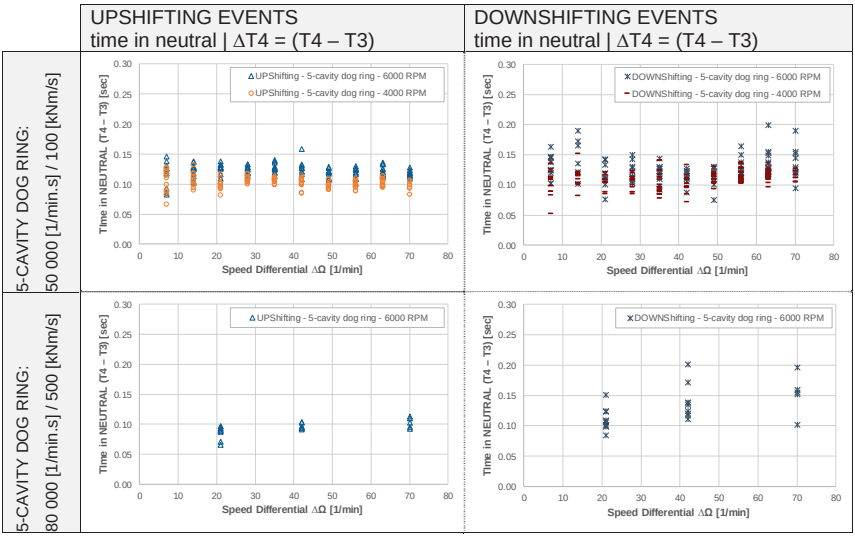

Fig. 13: Time spent in neutral for Speed synchronization

Table 1: Overall times spent in neutral for speed synchronization

	UPSHIFTING events :			DOWNSHIFTING events :		
	min	Ave.	Max	min	Ave.	Max
80 000 RPM/S settings 6000 to 2500 RPM	0.066	0.10	0.124	0.084	0.13	0.200
50 000 RPM/s settings 6000 to 2500 RPM	0.082	0.12	0.160	0.076	0.13	0.200
50 000 RPM/s settings 4000 to 1675 RPM	0.066	0.10	0.130	0.053	0.12	0.150

9. MECHANICAL SYNCHRONIZATION & SHIFTING TIMES / 1D-ANALYTICAL MODEL

By principle, the mechanical synchronization time of a gear with side protrusions with a dog ring's including cavities cannot be predicted with accuracy, since this is linked to the relative position between the face of the protrusion, and the face of the cavity when it needs to fit in.

Only the WORST synchronization time can be predicted, when the synchronization starts after the protrusion and the cavity overlap, and when the protrusion has to move the all sector until the next cavity. The mechanical synchro time depends on the speed differential, and the number of cavities. The higher number of cavities, the highest speed differential, the fastest shifting time.

Speed differential ΔΩ. [1/min]	Number of cavities in the dog ring [-]							
	3	4	5	6	7	8	9	10
7	2.31	1.73	**1.39**	1.15	0.99	0.87	0.77	0.69
14	1.15	0.87	**0.69**	0.58	0.50	0.43	0.39	0.35
21	0.77	0.58	**0.46**	0.38	0.33	0.29	0.26	0.23
28	0.58	0.43	**0.35**	0.29	0.25	0.22	0.19	0.17
35	0.46	0.35	**0.28**	0.23	0.20	0.17	0.15	0.14
42	0.38	0.29	**0.23**	0.19	0.17	0.14	0.13	0.12
49	0.33	0.25	**0.20**	0.16	0.14	0.12	0.11	0.10
56	0.29	0.22	**0.17**	0.14	0.12	0.11	0.10	0.09
63	0.26	0.19	**0.15**	0.13	0.11	0.10	0.09	0.08
70	0.23	0.17	**0.14**	0.12	0.10	0.09	0.08	0.07

Table 2: Mechanical synchronization times prediction

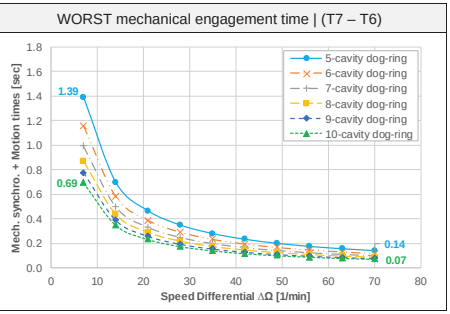

Fig. 14: Worst mechanical synchronization times prediction

Speed differential ΔΩ. [1/min]	Number of cavities in the dog ring [-]							
	3	4	5	6	7	8	9	10
7	2.77	2.19	**1.85**	1.61	1.45	1.33	1.23	1.15
14	1.61	1.33	**1.15**	1.04	0.96	0.89	0.85	0.81
21	1.23	1.04	**0.92**	0.84	0.79	0.75	0.72	0.69
28	1.04	0.89	**0.81**	0.75	0.71	0.68	0.65	0.63
35	0.92	0.81	**0.74**	0.69	0.66	0.63	0.61	0.60
42	0.84	0.75	**0.69**	0.65	0.63	0.60	0.59	0.58
49	0.79	0.71	**0.66**	0.62	0.60	0.58	0.57	0.56
56	0.75	0.68	**0.63**	0.60	0.58	0.57	0.56	0.55
63	0.72	0.65	**0.61**	0.59	0.57	0.56	0.55	0.54
70	0.69	0.63	**0.60**	0.58	0.56	0.55	0.54	0.53

Table 3: Full SHIFTING times prediction

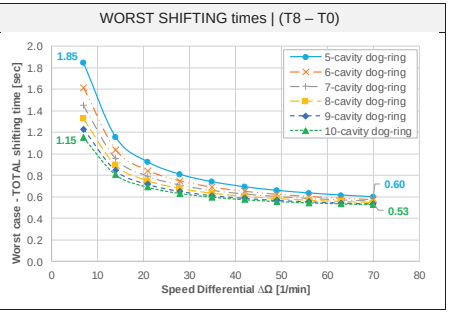

Fig 15: Full SHIFTING times prediction

The shifting times is predicted considering:

- Shifting Actuator speed : 200 [1/min]
- Electrical & Communication response time : 0.08 sec
- DISENGAGEMENT time: 0.15 sec
- Time in NEUTRAL (for speed synchronization): 0.13 sec

10. MECHANICAL SYNCHRONIZATION TIME / simulation & measurements

Simulation and measurement data are in-line with the trend for 5 & 10-cavity dog rings:

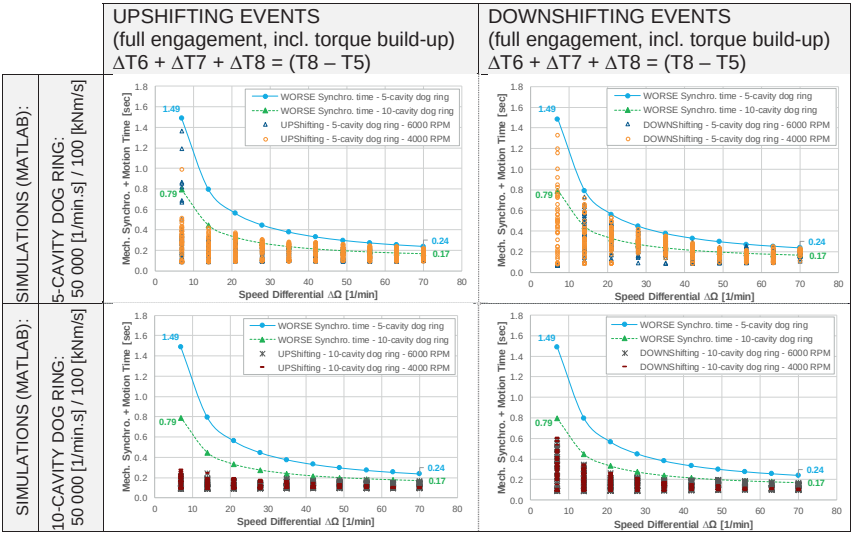

Fig. 16 : Mechanical synchro times (T8-T5) | Simulation results vs. 1D-trend

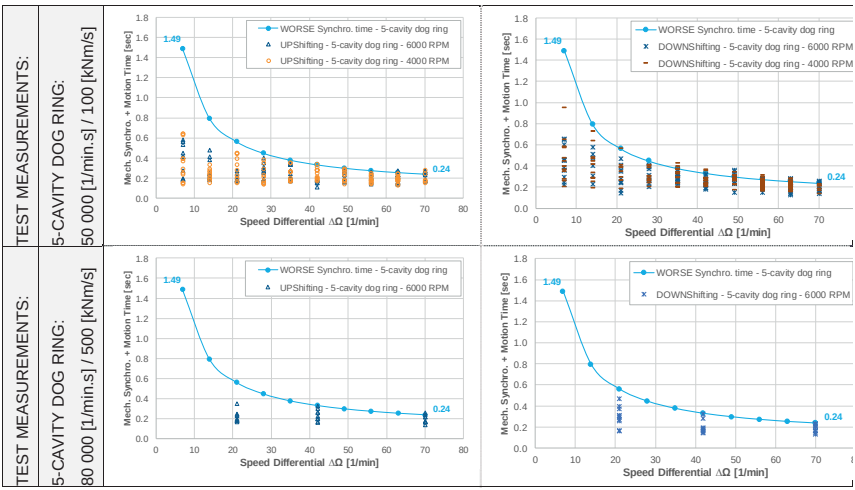

Fig. 17: Mechanical synchro times (T8-T5) | Measurements test data vs. 1D-trend

In the worst case of synchronization, the total engagement time can be restricted to 0.24 sec with a speed differential of $\Delta\Omega$ = 70 [1/min].

11. SHIFTING TIME / MEASUREMENTS

The FULL SHIFTING time (until FULL ENGAGEMENT) measured are reported below:

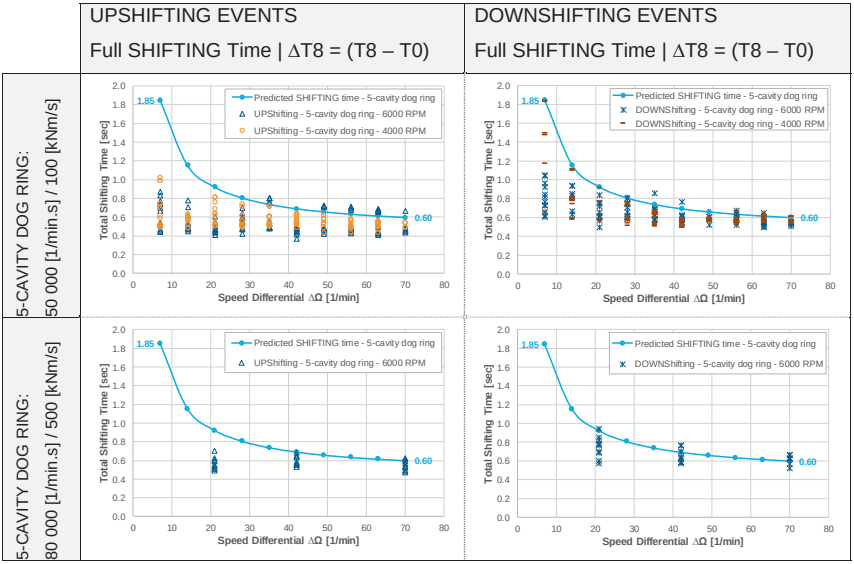

Fig. 18: Full Shifting times (T8-T0) | Measurements test data vs. 1D-trend

12. SHIFTING TIME BREAKDOWN

The best results achieved with a 5-cavity dog ring, a 200-RPM shifting actuator, and test rig e-motor (decel/accel 50 000[1/min.s] – Torque build-up/down 100 [kNm/s]) are plotted below:

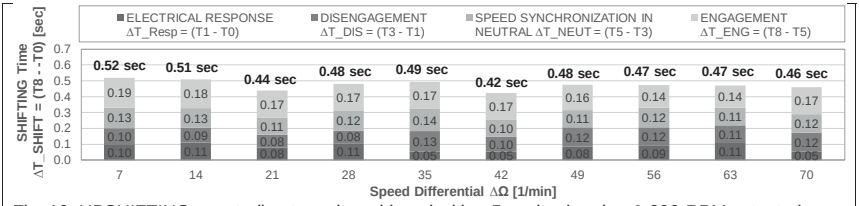

Fig. 19: UPSHIFTING events (best results achieved with a 5-cavity dog ring & 200-RPM actuator)

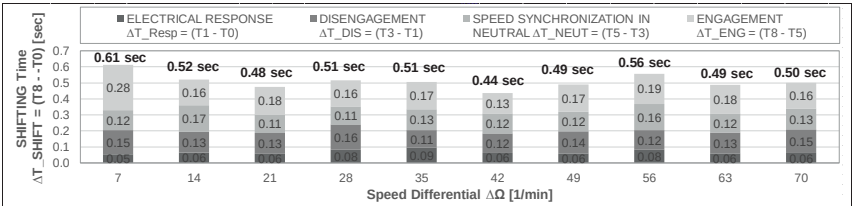

Fig. 20: DOWNSHIFTING events (best results achieved with a 5-cavity dog ring & 200-RPM actuator)

13. TRANSIENT MEASUREMENTS / 5-CAVITY DOG RING

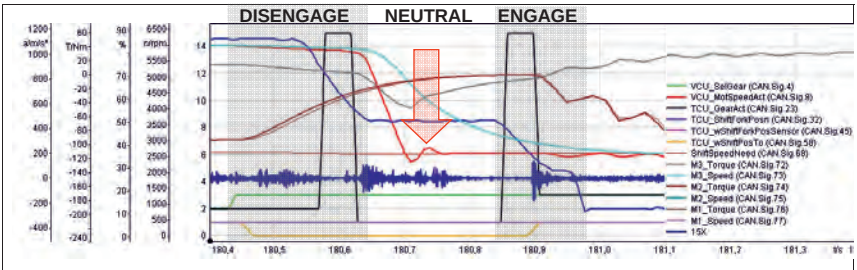

Fig. 21 : Upshifting event (1st→2nd gear) from 6000 to 2500 [1/min] input shaft speed - ΔΩ = 63 [1/min]

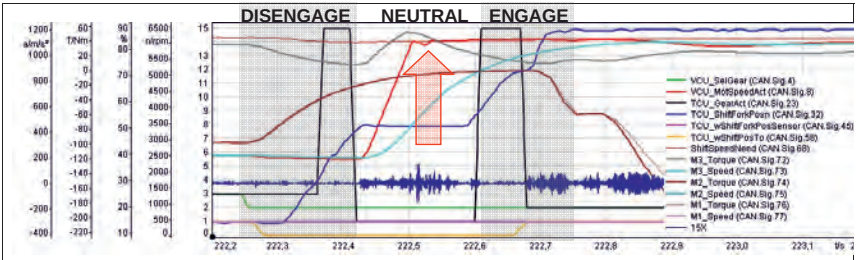

Fig.22: Downshifting event (2nd→1st gear) from 2500 to 6000[1/min] input shaft speed - ΔΩ= 63 [1/min]

14. SHIFTING TIME / SHIFTING ACTUATOR SPEED DEPENDENCY:

The next graphs predict the WORST-case engagement & shifting times, as a dependency of the actuator speed from 100 to 1000 [1/min].

FULL SHIFTING TIME: ΔT_SHIFT = (T8 – T0)	
5-cavity DOG RING:	**10-cavity DOG RING:**
- a full shifting time of 0.52 sec can be achieved for ΔΩ = 70 RPM, and for 300-RPM actuator speed. - a full-shifting time of 0.43 sec can be achieved for ΔΩ = 70 RPM, and for 600 RPM actuator speed.	- a full shifting time of 0.45 sec can be achieved for ΔΩ = 70 RPM, and for 300-RPM actuator speed. - a full-shifting time of 0.36 sec can be achieved for ΔΩ = 70 RPM, and for 600 RPM actuator speed.

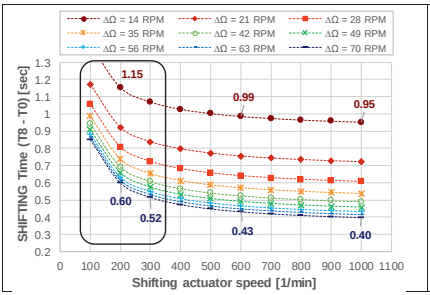

Fig.23: SHIFTING time prediction | 5-cavity dog ring

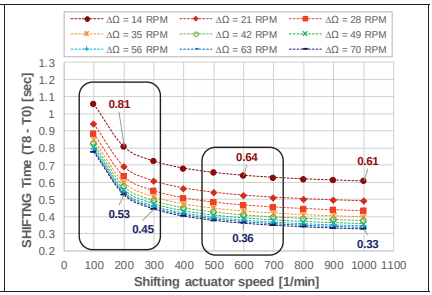

Fig.24 : SHIFTING time prediction | 10-cavity dog ring

15. OUTLOOK

Further actions are implemented on HARDWARE & CONTROL to reduce the shifting time:

15.1. HARDWARE

- **an increased number of dog-ring cavities**.
- **a faster shifting actuator** (600-1000 [1/min]).

15.2. CONTROL

The current control logic for the transmission is **action-reaction based**, which means that :

- once a setpoint for a certain variable is set, the TCU waits until the setpoint is reached with sufficient accuracy before the algorithm proceeds to the next steps.
- once an action is started, no change in target possible anymore until algorithm end.
- Furthermore, as the controllers for several actuators are not running on the TCU, but on external nodes, the TCU has no impact on the dynamics of the controller.
- in the current TCU software, no driveability filters (dynamic torque profiling for the traction motor) were used. Speed / torque targets were applied as steps, sometimes leading to undesired dynamic effects, such as torque oscillations or jerky shifts.

A more **centralized and integrated control approach** allows to overcome these limitations, where the TCU has full information of the transmission state and sufficient impact on the dynamics. This approach allows more optimal reactions of the transmission, and to schedule several phases of the shifting procedure partially in parallel.

- **Variable Speed synchronization**: changing the synchronization speed difference based on the axial location of the dog clutch can be implemented via a tracking of the angular difference between the two clutch parts, the remaining angle to travel to reach synchronization can be calculated, and a motion profile for the traction motor can be determined, including acceleration and deceleration phase. This approach allows to control the time duration of every shift and match the shifting times, so the

driver has a constant sensation of the shifts. As major drawback, this requires a control bandwidth (1 kHz) higher than typical automotive communication frequencies.

- **Position synchronization**: the most optimal shift performance can only be reached based on knowledge of the relative position of both dog clutch halves. This system knowledge would allow to fully skip the synchronization phase, as the input motor can be synchronised and aligned with the dog ring of the target gear already in neutral. This way, the overall shifting time can be reduced even further. The main difficulty of this approach is a fast and accurate position measurement: angle measurements on both shafts with an accuracy of 0.5 degree are required. The high speed of the traction motor and the limited sample frequency of the TCU increase the complexity.
-

16. CONCLUSIONS & NEXT STEPS:

Electrically-commanded dog clutches – belonging to AMT (Automated Manual Transmission) shifting category – are one of the most promising technology for the “NextGen” eDrives, as they can be used as SHIFTING system for MULTI-SPEED or as DISCONNECTON system.

- With a 5-cavity dog ring: shifting times of [0.42 to 0.60] sec are reached (with a speed differential of 70 [1/min], and a 200-RPM shifting actuator).
- An upgrade to a 10-cavity dog ring, and a 600-RPM shifting actuator would bring the shifting time down to 0.36 sec (constant speed control), and 0.31 sec (smart control),
- Overall Shifting performances reach the same orders of magnitude than hydraulically-actuated (C-segment) DCT such as reported in ref. [2] (Clutch: 0.250 sec aperture / 0.210 sec closure – Locking ring: 0.120 sec engage / 0.135 sec disengage).

Table. 4: Shifting time breakdown

	YESTERDAY	TODAY	TOMORROW	
HARDWARE:	- 5-cavity DOG RING	- 10-cavity DOG RING		
	- Actuator Speed: Ω = 200 [1/min]		- Actuator Speed: Ω = 600 [1/min]	
	- Speed differential : ΔΩ = 70 [1/min]			
ENVIRONMENT:	- Opened-Loop (action-reaction based)			- Real-Time Environment - Closed-Loop (active control)
CONTROL:	- CONSTANT SPEED Synchronization			- SMART SPEED control

	WORST CASE	BEST CASE	WORST CASE	WORST CASE	WORST CASE
ELECTRICAL RESPONSE Time [sec] ΔT_Resp = (T1 - T0)	0.08	0.05	0.08	0.08	0.03
DISENGAGEMENT Time [sec] ΔT_DIS = (T3 - T1)	0.15	0.10	0.15	0.05	0.05
SPEED SYNCHRONIZATION Time (NEUTRAL) [sec] ΔT_NEUT = (T5 - T3)	0.13	0.10	0.13	0.13	0.13
ENGAGEMENT Time [sec] (Actuator+mechanical synchro) ΔT_ENG = (T8 - T5)	0.24	0.17	0.17	0.10	0.10
TOTAL SHIFTING Time [sec] ΔT_SHIFT = (T8 - T0)	**0.60**	**0.42**	**0.53**	**0.36**	**0.31**

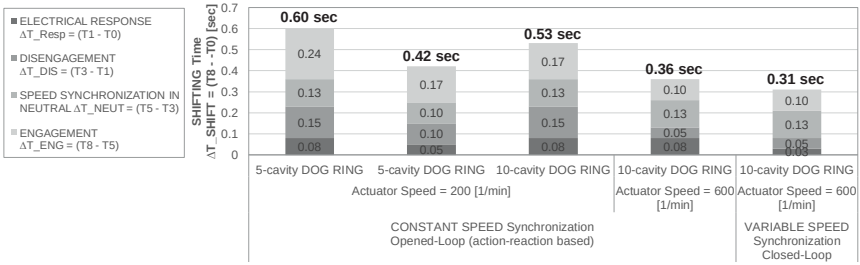

Fig. 25: VCST road map to 0.3 sec SHIFTING time target

17. REFERENCES

[1] "High Speed Electric Drive Unit for the Next Generation", Mathias Deiml, AVL, 15-19 May 2019, CTI USA 2019

[2] "Replacing hydraulic actuation in electrified drivelines", Alex Haldane, Vocis, Dana Incorparated, CTI Berlin 2019

[3] "Basics of synchronizers", Ottmar Back, Hoerbiger, Jan 2013

[4] "Shift dynamics and control of dual-clutch transmissions", Manish Kulkarni, Taehyun Shim, Yi Zhang, University of Michigan Dearborn (ScienceDirect 18 May 2006)

Flexible Electro-hydraulic Actuation System for Multi-speed Electrified Drivetrains

Requirements and Concept

Dipl.-Ing. **Alexander Nees**,
BorgWarner Drivetrain Engineering GmbH, Ketsch

Zusammenfassung

Mehrgängige Getriebe für elektrische Antriebe bieten verschiedene Vorteile, auch im PKW-Segment. Sie können unter anderem dazu beitragen, die Reichweite zu erhöhen und Geräusche und Vibrationen zu reduzieren. Noch wird dieses Potenzial zugunsten eines kostengünstigeren eingängigen Antriebsstrangs außerhalb von Nischenanwendungen nicht ausgeschöpft.

Die Vielzahl verschiedener Lösungen und Architekturen für den elektrifizierten Antriebsstrang ist dabei eine zusätzliche Herausforderung für die großflächige Einführung von Aktuierungssystemen. Flexible Betätigungslösungen und Schaltelemente können daher den Unterschied machen. Mit Blick auf den Kühlölbedarf der E-Maschine oder auch des Inverters bieten sich vor allem elektro-hydraulische Lösungen an, die einfach in den ohnehin benötigten Ölkreislauf integriert werden und an die individuellen Bedarfe und Bauräume angepasst werden können.

Dieser Beitrag zeigt die Variabilität der Anforderungen an das Betätigungs-System von mehrgängigen Getrieben in elektrifizierten Antrieben auf. Er stellt passende flexible elektro-hydraulische Betätigungskonzepte mit unterschiedlichen Systemdruckniveaus vor. Ein Schwerpunkt liegt in der möglichst effizienten Druckerzeugung und idealerweise verlustfreien dauerhaften Betätigung von Schaltelementen. Weitere Funktionen wie Kühlung, Schmierung und Systemdruckregelung sind Teil des Systems. Dabei werden die bisherige Entwicklung von elektro-hydraulischen Steuerungen und Ventilen wie auch Erfahrungen aus Serienanwendungen berücksichtigt und in maßgeschneiderte Module integriert.

Die flexible Nutzung vorhandener Serienkomponenten für die Getriebesteuerung kann dazu beitragen, mehrgängige Getriebe auch in der breiten Anwendung in elektrischen Antriebsträngen zu realisieren und so deren Potential auszuschöpfen.

Abstract

Multi-speed transmissions for electric drivetrains in passenger cars offer several advantages. Amongst other benefits they can contribute to increasing range and reducing noise and vibration,. This potential is not leveraged yet in favor of more cost-effective one-speed drivetrains beyond niche applications

The multitude of different solutions and architectures for electrified drivetrains thereby is an additional challenge for a broad introduction of actuation systems. Flexible actuation solutions and shift elements can therefore make all the difference. Looking at the cooling demand of e-machines and inverters, electro-hydraulic solutions lend themselves particularly well for this purpose as they can be easily integrated in the anyway required oil circuit. They can be designed according to individual requirements and installation space.

This paper shows the variability of requirements for the actuation system of multi-speed transmissions in electrified drivetrains. It presents suitable flexible electro-hydraulic actuation concepts with varying system pressure levels. One focus is on the most efficient pressure generation and on ideally lossless permanent actuation of shift elements. Other functions such as cooling, lubrication and system pressure control are part of the system. The previous development of electro-hydraulic controls and valves as well as experience from series applications are taken into account and integrated into customized modules.

The flexible use of existing series components for transmission controls can help to realize multi-speed transmissions in a wider range of applications and thus exploit their potential.

Introduction

Motivation

The transfer from conventional to electrified drivetrains is progressing quickly. Furthermore, pure electric vehicles are experiencing strong market growth. After the development of the first generations of pure electric and dedicated hybrid drivetrains there is a trend towards further optimization. Efficiency and range are being improved while retaining a good drivability, also for heavier vehicles like SUVs or transporters. Since the vehicle registration rate for SUV is as high as never before and overtaking the other segments, [1] there is a high probability of growing performance requirements for the electric drivetrain.

Although electric machines typically offer a wider range of efficient operation than combustion engines, there remains an area of conflict between high torque, high speed and efficiency. The implementation of an additional gear ratio can expand the range of efficient operation of the electric machine. Thereby it is not necessary to compromise between high peak torque for e.g. launch and towing operations and high velocities. With two speeds it can be possible to use a

smaller e-machine operated in the optimal efficiency range and/or reduce the battery size maintaining the same driving range to decrease the overall system cost.
To achieve a real value proposition for the OEM, a potential transmission system with two or more speeds must be efficient itself and fulfil challenging requirements at low cost level. A gear shift must not be noticed by the driver in most cases. The packaging space needs to be minimized and adjusted to the new electrified drivetrain architectures. Future multi-speed electric drive units (EDU) present a new set of requirements, especially for the actuation system. These requirements, as well as the given cost pressure, define the selection criteria for the actuation subsystem.

Target Setting
Overall goal of this paper and presentation is to identify possible requirements of multi-speed electrified drivetrain units (EDU) with regard to the actuation system and the discussion of potential flexible electro-hydraulic solutions. A solution fulfilling the identified requirements will be presented.

Market Outlook
Although most electric vehicles will have one speed only, there is a market growth of multi-speed EDUs forecasted (Fig. 1)

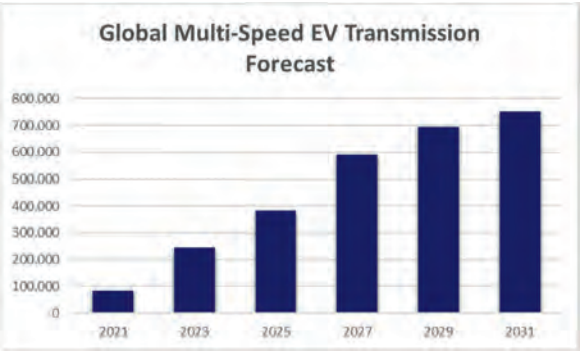

Fig. 1: Forecast on global multi-speed EV transmissions (source: IHS)

In parallel, there is a significant market growth expected for heavy electric passenger cars like SUVs and Pick-Ups as shown in Fig. 2. Since heavy vehicles require higher drive torque e.g.

for launching, towing or gradeability, these applications will probably require more speeds and therefore could lead to additional increase of the numbers of multi-speed EDUs.

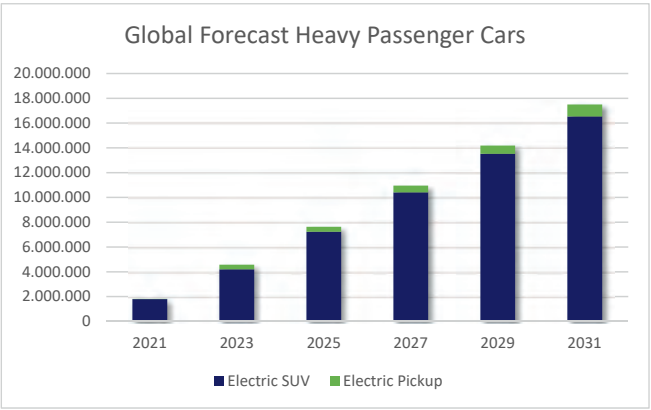

Fig. 2: Global market forecast for heavy battery electric passenger cars (source: IHS)

Despite some uncertainty of the market it is becoming obvious that OEMs and transmission manufacturers are working on concepts or even announced officially to go to serial production with multi-speed EDUs.

There are numerous reasons for a potential market growth of multi-speed EDUs. On the other hand, the introduction of multi-speed EDUs is facing some obstacles, which will be discussed in the next section.

Value Analysis of Multi-speed EDUs

Electric traction machines offer a higher range of torque over speed than combustion engines and a better fit for overcoming the driving resistances. They operate at a higher motor efficiency. However, there remains a conflict between launch torque and velocity as well as some room for efficiency improvement. Fig. 3 shows a typical torque-speed map including efficiency areas.

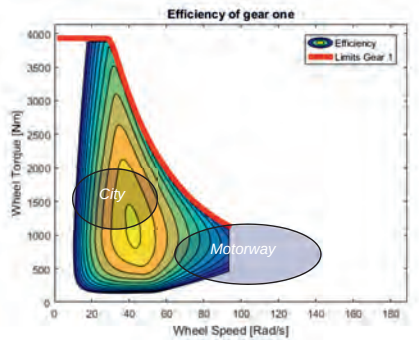

Fig. 3: Efficiency map of a one-speed drive

While a high torque level can be achieved, the speed range is limited due to motor and power electronics constraints. The area of best efficiency lies between a high torque city driving mode and a high-speed motorway mode as a compromise.

A second transmission ratio could help to increase the areas of best efficiency and thereby electric driving range while enabling a higher speed in this example case. Depending on the application it would be possible to achieve higher velocities and torque or to downsize the traction machine and battery to lower system cost. Fig. 4 illustrates the impact of a second speed.

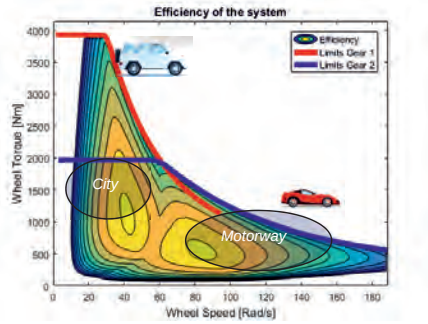

Fig. 4: Efficiency map of a two-speed drive

A multi-speed drive can provide an additional benefit by allowing a disconnect of traction machine and drivetrain. Additional efficiency can be gained by reducing drag and electrical losses. This can be interesting, especially for permanently excited synchronous motors that

generate electrical power in thrust mode, decelerating the vehicle instead of allowing a probably more efficient sailing mode.
Another benefit of multi-speed EDUs can be the differentiation between brands. This could be a saleable feature that is difficult to evaluate.
On the other hand, two-speed EDUs come with penalties in cost, weight and package. Furthermore, an actuation system is needed, which adds to the losses itself. The benefits shown above must clearly outweigh the drawbacks, which have to be minimized. The selection of a simple, flexible and efficient actuation systems can help to achieve this key target as shown later.

Topologies of multispeed EDUs

Before discussing the actuation system and its requirements, it is important to get an overview of how the future multi-speed electric drivetrain might look like. Since there are not many multi-speed EDUs on the market yet, a benchmark study of several publications was done to analyze the current development state. On drive unit level it can be found that using one traction machine and two speeds will be the mainstream. The second speed is realized by planetary gear sets or layshaft designs in most cases. The shift from first to second gear or back must not be felt by the driver, which seems understandable especially for electric driving with its high comfort. This requires a smooth power shift at all times. Transmission fluid will remain an important part of the drivetrain, used for cooling and lubrification of either traction machine (rotor) or gear sets.
Shift elements are needed to realize multi-speed drivetrains. The benchmark analysis shows that for layshaft designs the typical DCT-like architecture is used, including friction clutches and synchronizers. For planetary gear set control there is a variety of shift element combinations possible, which can be found in Fig. 5.

Fig. 5: Shift elements for planetary gear set control

As a common ground, the study concludes that most concepts use friction elements to ensure the required smooth powershift. The following section will discuss the requirements for the actuation system based on these different transmission architectures and types of shift elements that need to be actuated.

Identification of Requirements for the Actuation System

Specific requirements originate from all levels of the vehicle, including the EDU and its shift elements. In general a distinction can be made between three major fields as displayed in Fig. 6.

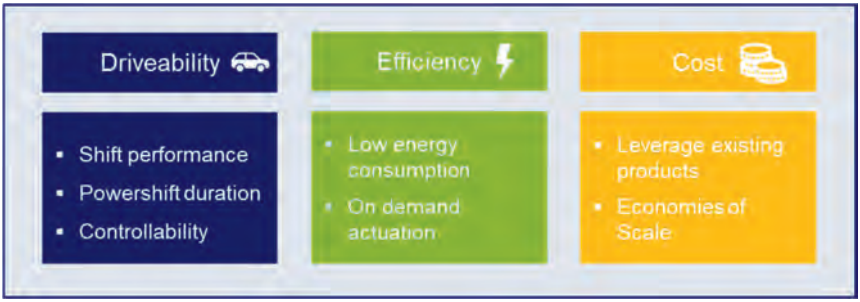

Fig. 6: Major requirement fields

The first field “driveability” concludes the requirements on the process of shifting itself. Does it have to be a spontaneous smooth powershift, also including a change of mind of the vehicle driver? Or can it be a planned shift event at a certain moment which could allow more time for the actuation? These questions can only be answered for each individual vehicle application.

This already indicates that there can be differences from application to application leading to a demand for flexible actuation systems that can be scaled accordingly.
The second field “efficiency” specifies the need for low energy consumption. The overall target of a multi-speed EDU with optimized efficiency and increased range can only be achieved if minimal power is consumed by the actuation system. Especially for BEVs it is expectable that shifts only occur from time to time and the EDU is operated in driving mode with neglectable actuation power. The system should work on demand, i.e. only consume energy when needed for the shift.
The field of “cost” is another significant driver for the value equation of EDUs. As mentioned before, the benefits of a multi-speed EDU must not be outweighed by the drawbacks. Considering this fact as well as the developing market, it would be disadvantageous to develop all new components for the actuation system. The target should be to leverage existing products and utilize economies of scale to limit development-, part- and manufacturing cost.
Given the multitude of different requirements on drivability, the various topologies of multi-speed EDUs and types of shift elements, it can be concluded that a preferred actuation system must be highly customizable, fitting to several environments and based on existing products.
The next step will be to find the adequate actuation system meeting these requirements.

Exemplary actuation system solution for multi-speed EDUs

Finding the right actuation concept has to be based on the topologies, given environment and constraints and the specific requirements defined before. On the top level it can be distinguished between electro-mechanic and electro-hydraulic solutions.
Electro-hydraulic systems offer the commonly known benefits and also some challenges as shown in Fig. 7.

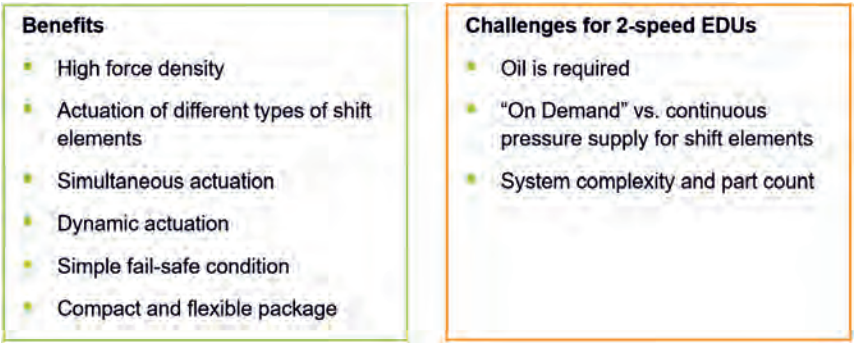

Fig. 7: Benefits and challenges of electro-hydraulic systems

High force density helps to provide high actuation forces, while the high dynamics enable a spontaneous shift. The possibility of simultaneous actuation of several shift elements is important to realize the required power shifts. Furthermore, hydraulic actuation offers the control of different types of shift elements serving the various EDU layouts discussed above. Pressure regulating solenoids and valves can be opened separately from the power supply (pump), which leads to a simple fail-safe condition in case no energy is available or other incidents. The package of electro-hydraulic systems is typically very compact. Only one central pump is needed while pressure and flow control for the shift elements is done by smaller size valves. The more shift elements are used, the more compact is the package when compared with separate electro-mechanic actuators.

On the other hand, there are some challenges coming with the electro-hydraulic actuation concept, especially for multi-speed EDUs. Hydraulic fluid, is obviously required. As shown before it can be assumed that oil or transmission fluid will remain present in future electric drivetrains. Either for cooling and lubrification of gear sets or for the traction machine. This fluid can be used by the electro-hydraulic system.

Hydraulic transmission control modules usually have to supply pressure at all times to retain the actuation forces in one or the other direction. This can contradict the requirement of minimal power consumption during driving mode, depending on the shift element. To address this requirement, electro-hydraulic on demand systems often use a pressure accumulator that is re-filled only from time to time while providing necessary clutch pressure. Using an hydraulic accumulator, would add components and complexity to the system and would compromise the overall target of a simple and lean system at minimized cost.

If the available transmission fluid can be used, and if a simple on demand system can be designed, the advantages of electro-hydraulic systems seem to make them the ideal actuation system for multi-speed EDUs. Especially if more than one shift element has to be controlled, the cost efficiency of an electro-hydraulic system increases because only single solenoid valves need to be added. No additional power supply is needed, which helps in creating a flexible package.
Hereinafter it will be discussed how to master the challenges above and why an electro-hydraulic system is preferable for this case. Of course, the specific EDU layout and performance requirements have a strong impact on the identification of the best solution. In order to identify and assess the target solution it is necessary to leave the abstract level of an arbitrary EDU and define a tangible case with specific boundary conditions, as presented in the next section.

Application Example and Electro-hydraulic Target Solution

An exemplary EDU application layout will be used to demonstrate the electro-hydraulic actuation system approach fulfilling the defined requirements. This planetary two-speed layout is very common in current developments as shown earlier. The planetary gear set is controlled by two friction clutches (or brakes) to realize two speeds. The friction clutches are actuated by the electro-hydraulic system as represented with its scheme in Fig. 8.
The actuation system itself consists of a central electric pump providing the oil flow, a high-pressure filter and four electro-hydraulic solenoid valves. A line pressure regulator controls the system pressure during clutch filling. The exhaust flow is used to deliver cooling and lubrication flow to the gear set and clutches. Optionally it could also be used to cool the traction machine. The clutch selector solenoid switches between the two clutches. One latching solenoid locks the pressure in each of the clutches. The latching solenoids are also used for draining the clutches when they need to be disengaged. Optionally pressure sensors are added to measure the clutch pressure.

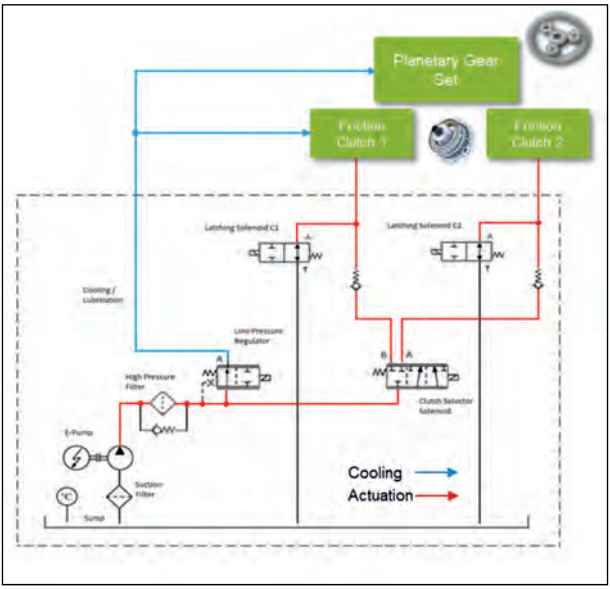

Fig. 8: Application example and electro-hydraulic actuation system

The components are embedded in a customizable housing which can be adjusted to the surrounding installation space of the EDU. For the demonstration purpose of the application example the system is designed as “power pack” that can be mounted onto the EDU having its own oil reservoir. EDU housing, clutches and actuation system (bright blue) are shown in Fig. 9.

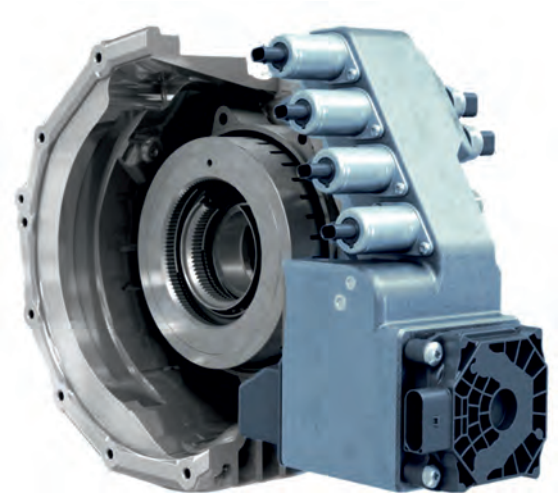

Fig. 9: Application example and electro-hydraulic actuation system

The electrical pump comes with on-board ECU that can be connected via CAN or FlexRay. The solenoids and pressure sensors can be controlled by the EDU- or inverter- ECU. The system itself is completely sealed and can be mounted externally.

Key functions and features of the target system

Table 1 provides an overview of the key functions and technology features responding to the requirements on drivability, efficiency and system cost as defined before, illustrated by the corresponding schematics. Thereby the lines highlighted in red provide flow at high pressure up to 18 bar. Black lines are pressure-less, empty or used for draining towards the tank. The yellow flash symbols show which of the components are supplied with electrical power.

Table 1: Overview on features fulfilling defined requirements

Drivability	The clutch is filled directly only through the selector solenoid without dedicated clutch pressure regulator. This allows a high flow which is necessary to ensure a fast fill and leads to a smooth powershift at the end fulfilling the requirements on drivability including "change-of-mind" shifts No accumulator is required	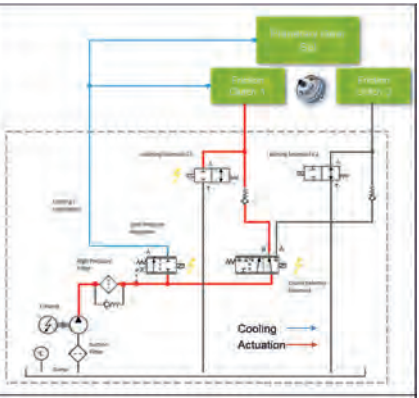
Efficiency	The shown driving mode is the major operation for BEVs since shifts occur only from time to time. To master the on-demand requirement while keeping the pressure on the normally open clutch, clutch pressure is locked using a latching solenoid with neglectable leakage. The e-pump can be switched off or operated at small speed to provide cooling flow, only a small current is needed for the latching solenoid, which consumes around 7W The latching solenoid is also used to drain the clutch during a gear shift event	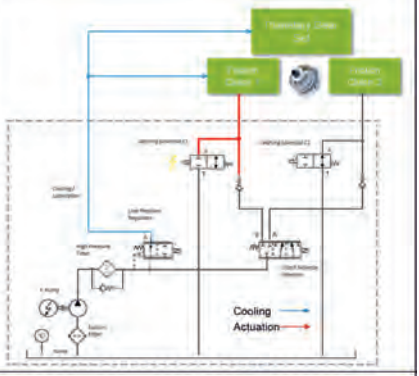
Cost	Due to the efficient hydraulic arrangement of the components, no accumulator is necessary to realize fast and repeatable shifts. The direct pump actuation and the clutch draining via latching solenoids made it possible to eliminate clutch pressure regulators and limit the number of components to a minimum. Furthermore the use of high-volume serial products reduces the component cost	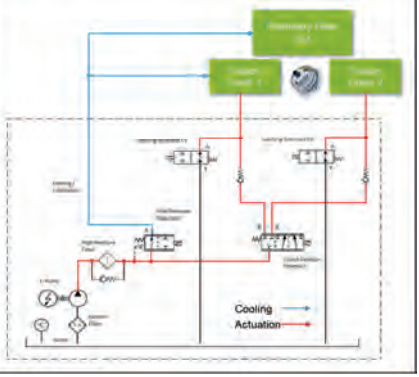

Looking back at the defined requirements and considering the topologies of future EDUs, the shown flexible electro-hydraulic actuation system addresses the challenges of efficiency and cost, while leveraging the known strengths on drivability. It utilizes proven serial components while preserving a high flexibility due to the customizable housing. Components like solenoids can easily be added to control further shift elements or enable further cooling.
A demonstrator part was already built and tested to verify the expected performance.
Hereinafter a short extract of the engineering validation is given as an example.

The desired shift performance can be achieved. The fast clutch filling, which is the main task for the actuation system, leads to a torque-handover time of less than 200 ms for a power shift. Fig. 10 shows an example of a recreated “kick-down” shift with a clutch filling time of 170 ms. Compared with a known solution with accumulator, no high pressure is needed to do the necessary pre-fill which leads to another energy saving. The e-pump delivers only the pressure, needed for the clutch filling.

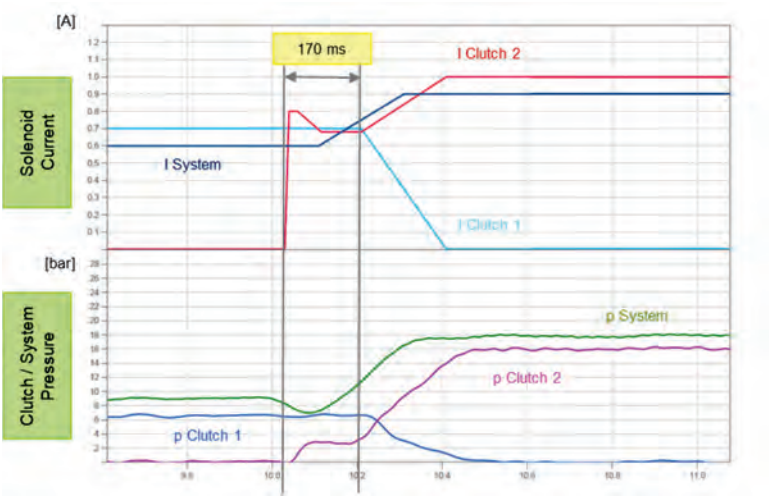

Fig. 10: Example measurement graph of clutch filling and torque- handover

Besides the shifting performance, the efficiency was evaluated by measuring the total power consumption of the components. In driving mode, the system consumes only 7 Watt. For a 100 km WLTP range cycle this would equal approximately 100 m (0,1%).

Flexibility of the Target Actuation System

As discussed before, the boundary conditions and topologies vary strongly between the different EDU concepts. The requirements on drivability depend strongly on each individual application. Therefore, the actuation system must be customizable to address these circumstances.

The exemplary system presented above can be adapted to various requirements as shown in Fig. 11. The solution presented in this paper is located in the center. It delivers high performance shifts and medium cooling flow of up to 5 L/min.

If gear shifts can take more time and cooling is provided by other subsystems, the choice would be a very basic system with only an e-pump and two solenoids in a very small package. If the application demands high performance shifts with a high cooling flow of more than 20L/min, the high-end system shown on the right with a 2-stage e-pump can be the right solution. The system itself is scalable while still using off-the-shelf components.

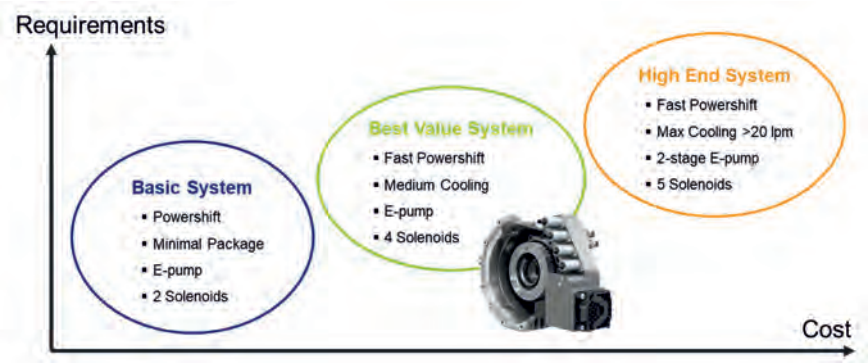

Fig. 11: Potential variants of the target solution

Summary

The market share of multi-speed EDUs will grow in the future in parallel with the increase of heavier electric vehicles. Multi-speed EDUs can improve the efficiency of the electric traction machine an improve gradeability and maximum velocity along with some other possible benefits. The total benefit must outweigh the drawbacks in cost, weight and drag losses. Actuation systems therefore play a major role in the value equation for transmission manufacturers and OEMs.

Most current multi-speed EDU concepts are based on a single traction machine with a two-speed transmission, realized by planetary gear set or layshaft design., Friction based shift elements remain an important part of the drivetrain. Furthermore, existing oil circuits in EDUs and the demand for smooth power shifts favor the use of electro-hydraulic actuation systems. The challenge of low power consumption, especially in driving mode, can be addressed by the presented pressure latching technology.

The presented flexible electro-hydraulic systems can meet the challenging performance and commercial requirements that come with multi-speed EDUs. “Off-the-shelf” production components help decrease system cost and development time while remaining scalable and customizable to every customer’s need.

[1] https://www.kba.de/DE/Statistik/Fahrzeuge/Neuzulassungen/Segmente/fz_n_segmente_archiv/2019/2019_n_segmente_kurzbericht_text.html?nn=2594996

Park by Wire System for current Electric Drive Units

Dr.-Ing. **Jan Nowack**, Dr.-Ing. **Gereon Hellenbroich**, **Arnab Ghosh**, **Valerij Shapovalov**, **Ralph Fleuren**, FEV Europe GmbH, Aachen

Abstract

Park lock systems are safety critical units. Due to intellectual property rights and different transmission configurations, a large variety of park lock design exists in the market. Furthermore, many park lock designs are still manually actuated. A new mechanical park lock system will be presented which is actuated by wire. The system has been optimized for rotary actuators and is extraordinarily compact. In addition, it minimizes the contact stresses due to optimized geometries. Furthermore, the functional safety and diagnostic concept for park-by-wire park lock systems, exemplarily for this system, will be presented. This will be done in accordance to current multi speed power-shift EDU concepts, including FMEA, legal, requirements summary, safety goal definition and error detection mechanism.

The following chapters are divided according to the park lock development steps shown in Fig. 1

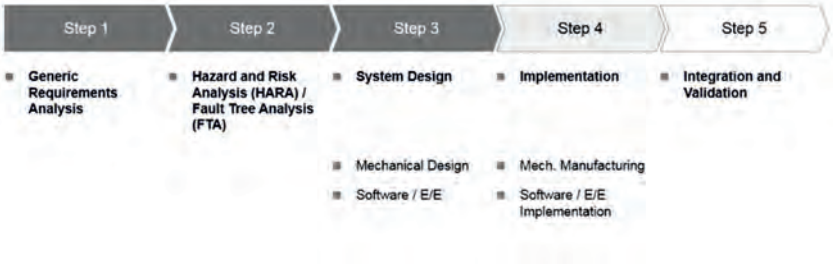

Fig. 1: Park Lock System development steps

Keywords: Functional safety and diagnostic concepts, Mechanical park lock concept, Park by wire concept

1 Generic Requirements Analysis

A requirement analysis has been performed to identify the major system requirements from a Park lock system for a passenger vehicle. An overview of the identified requirements is shown in **Fig. 2**. Some sample OEM requirements were assumed, based on prior experiences of FEV. These requirements helped in creating a baseline design of the system, hardware and software. The system design has been, however, kept flexible to meet customer and market specific requirements. Intellectual Property restrictions were also considered while creating the baseline requirements.

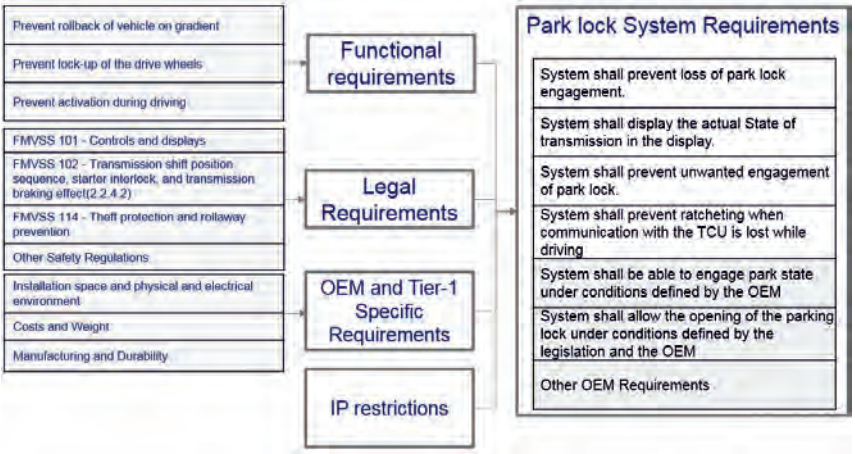

Fig. 2: Park Lock Requirements overview

2 Item Definition

A typical passenger vehicle has been considered for creating the item definition, see Fig. 3.

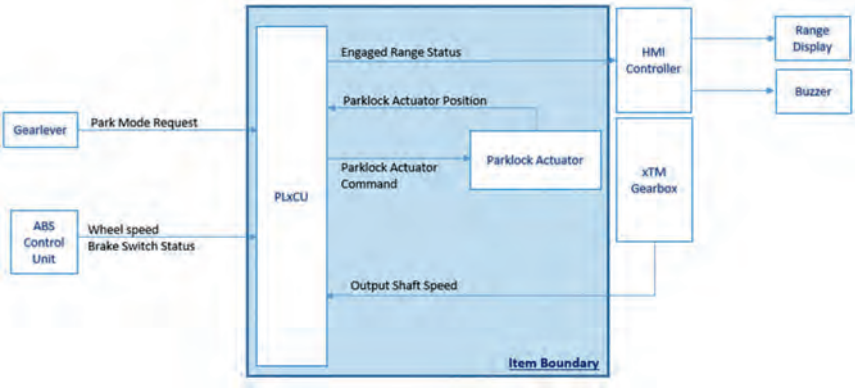

Fig. 3: Item Definition for FEV Park Lock System

This helps identifying the key elements of the vehicle and the Park lock system. The key elements are described below:

- Gear Lever: Element in vehicle through which driver request for Park state is communicated to PlxCU
- ABS Control Unit: Antilock braking system control unit
- HMI Controller: Human Machine Interface Controller responsible for controlling display to driver
- xTM Gearbox: Transmission (AMT, DCT, EDU etc.)
- Range Display: Display of Actual Engaged range to driver
- Buzzer: Audio warning to driver

The item definition has acted as a starting point for the control system and functional safety development.

3 Hazard and Risk Analysis (HARA)

Based on the item definition, a preliminary Hazard and Risk analysis (HARA) has been performed as described by ISO26262 Part 3. An overview of the process is shown exemplarily for a specific malfunction in the actuation control and resulting propulsion due to loss of Park range in Fig. 4.

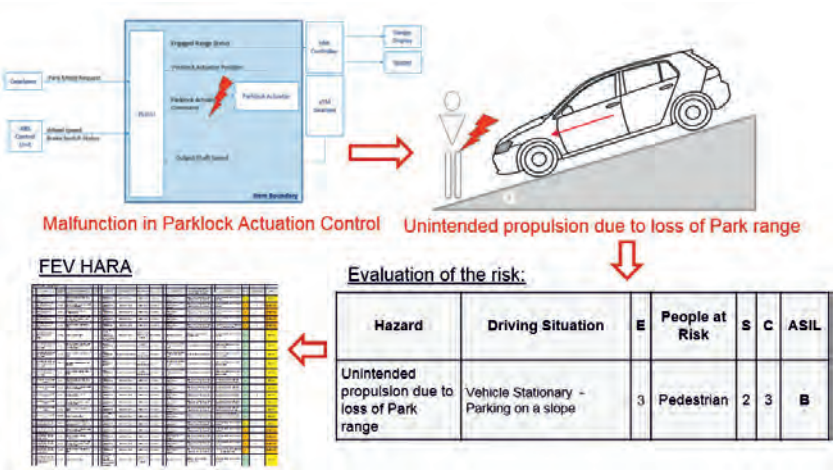

Fig. 4: Overview of FEV HARA Process

As step 1, the various hazards of the Park lock system has been identified.

As step 2, the hazards has been analyzed with various use scenario's to identify Severity (S), Exposure (E) and Controllability (C).

As step 3, the Safety goals and ASIL has been identified for the Park lock system.

ID	Safety goal	ASIL	Safe state / fallback level (if applicable)
1	Prevention of Unintended Display control for Park Function	B	1. Range to Show '-' (Or Blank) 2. 'Press Brake lamp' to turn on 3. Buzzer to turn on until driver presses brake pedal (All are CAN Signals)
2	Prevention of Unintended Park Mode disengagement	B	1. Range to Show Actual Range with Blinking 2. 'Press Brake lamp' to turn on 3. Buzzer to turn on until driver presses brake pedal (All are CAN Signals)
3	Prevention of Unavailability of Park Lock Control	QM	
4	Prevention of Unintended Park Mode engagement	QM	

Fig. 5: Overview of Safety Goals

Based on FEV preliminary HARA, the ASIL for the park lock system has been determined, as ASIL B. An overview of the safety goals including ASIL rating is given in Fig. 5. These were used for current system development and design of safety measures. However, for the final product development, Safety Goals / ASIL coming from OEM HARA shall also be considered. Based on final Safety goals, OEM safety Concept and ASIL, adequate safety measures shall be ensured by FEV.

4 Park Lock Development and Optimization

FEV has broad experience in the development of park lock systems. Within more than 15 projects, FEV has developed an unique in-house tool chain, which includes powerful lay outing tools for quick concept development as well as advanced CAE methods including Finite-Element-Analysis and Multi-Body Simulation, see **Fig. 6**.

The range of services does include:

- Benchmarking and target setting (function, durability, NVH)
- Concept development incl. full system specification
- Design & CAE incl. tolerance analysis
- DFMEA and definition of critical characteristics

- DVP definition based on vehicle duty cycle incl. limiting sample testing
- Hardware validation on bench and in vehicle according to FEV and/or customer standards
- By-wire S/W development incl. Functional Safety

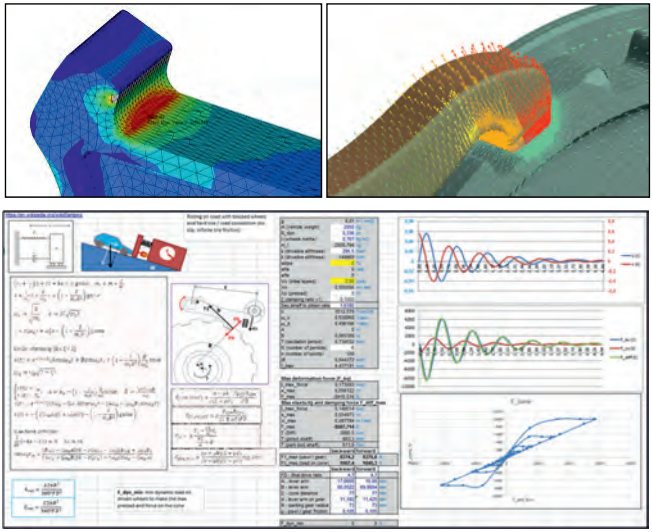

Fig. 6: Park Lock Development Tools

4.1 Universally applicable Park Lock Module for all global Markets

Based on generic requirements and targeting applications in all global markets, FEV has developed a compact park lock module. Due to its compact size and flexible orientation, it can easily be packaged in most transmissions. The module has been designed for rotary actuation and can be combined with a wide range of actuators and sensors. Paired with FEV's software and sensor concept, no smart actuator is needed. Manual cable actuation is also possible.
The current design has the following specification:

- Up to 2.400kg gross vehicle weight
- Up to 4.000 kg with small modifications
- Maximum parking slope: 30%
- Ratio park lock gear to wheels: >3

4.2 Compact, modular design

Fig. 7 gives an overview of the different components of the park lock module.

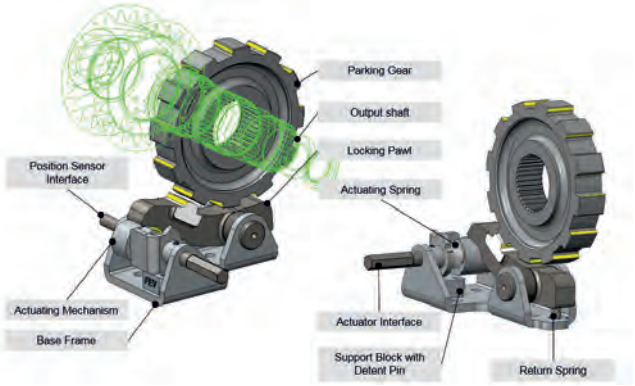

Fig. 7: Overview of Park Lock Actuation System

During the concept development, a lot of attention has been paid to the optimization of the contact area between the actuation mechanism and the pawl. Conventional pull-cone designs inherently have to deal with high contact stresses due to point or line contacts. High contact stresses can lead to friction instabilities and high wear, eventually resulting in lower lifetime, risk of functional failures and increased actuator power requirements.

The new design uses an eccentric actuation mechanism with a convex/concave contact zone, resulting in a much larger contact area and significantly reduced contact stresses. The advantages are higher reliability and less sensitivity to tolerances. In addition, the actuator torque and power requirements can be reduced.

Fig. 8 shows the contact stress between pawl and actuation mechanism as well as the required actuator disengagement torque for two different designs. Both designs have to deal with the same reaction force introduced by the pawl. The new design exhibits significantly lower contact stresses and more robust disengagement behavior.

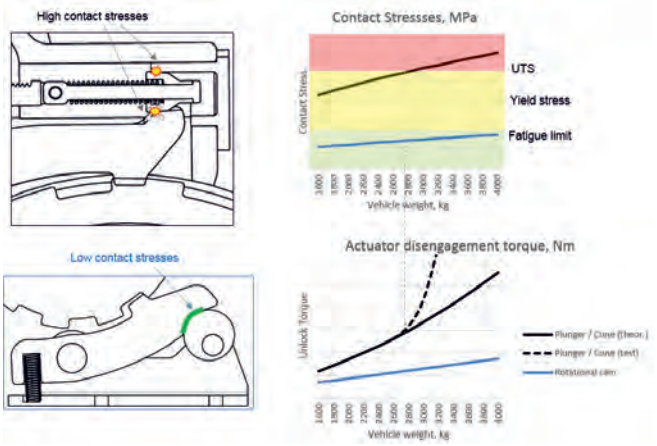

Fig. 8: Actuator disengagement torque over contact stress

5 FEV Transmission Software Architecture

For actuation of park lock system, a ‘PARK LOCK MANAGER’ control software has been developed. The Control Software has been developed using AUTOSAR architecture approach on application software level. An overview of the software architecture is exemplarily shown in Fig. 9 for a multi speed electric drive unit.

Thus, it can fit in the preexisting customer SW Architecture for the xTM transmission – thereby creating a predeveloped PARK LOCK MANAGER’ for the OEM. The primary characteristics of the FEV ‘PARK LOCK MANAGER’ are shown below.

- Physical components based on hardware components
- Logical components with encapsulated functionalities
- Standardized physical interfaces between all components
- Park Lock functionality is integrated in the Composition Vehicle and will run on TCU or combined VCU.

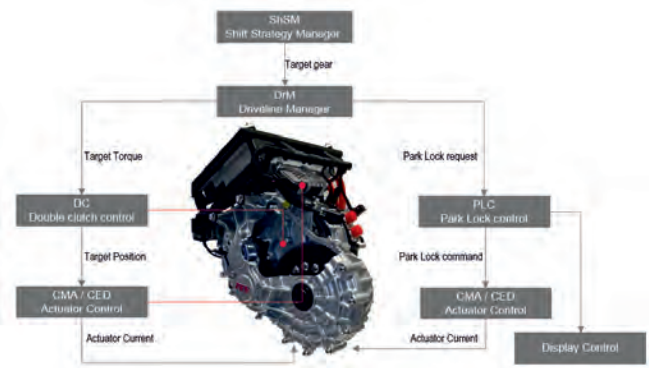

Fig. 9: Overview of FEV Control Software

6 Diagnosis Monitoring

Diagnostic coverage has been defined based on the ASIL and legal requirements. However, the coverage can be increased or decreased based on OEM requirements / Safety Concept. Currently the FEV Park lock Control System satisfies Medium Diagnostic Coverage as specified by ISO26262 Part 5 and satisfies sample OEM requirements from FEV experience. An overview of the included diagnostic is shown in Fig. 10.

Hardware Component	"Low" diagnostic coverage:	"Medium" diagnostic coverage:	"High" diagnostic coverage:	Required by OEM? (Sample)	Safety Mechanism / Measures required to cover
Harnesses including Splice and Connectors	Open circuit;	Open circuit;	Open circuit;	Y	Failure detection by on-line monit
	Short circuit (to ground);	Short circuit to ground (d.c coupled)	Short circuit to ground (d.c coupled)	Y	
		Short circuit to vbat	Short circuit to vbat	Y	
		Short circuit between neighboring pins	Short circuit between neighboring pins	Y	
			Resistive drift between neighboring pins;	N	NA
			Contact Resistance	N	NA
Actuator (detailed analysis may be necessary for technology specific failure modes*)	· Open circuit;	· Open circuit;	· Open circuit;	Y	H-Bridge internal diagnostic
	· Short circuit (to ground);	· Short circuit (to ground);	· Short circuit (to ground);	Y	
		· Short circuit (to ground, to power);	· Short circuit (to ground, to power);	Y	
			· Short circuit(to ground, to power, neighboring pins); Out-of-range;	Y	
	· Out-of-range;	· Out-of-range;	· Out-of-range;	Y	Failure detection by on-line monitoring/Functional diagnostic
	· Stuck (electrically, physically)	· Stuck (electrically, physically)	· Stuck (electrically, physically)	Y	
		· Frozen (physically or electrically stuck, locked);	· Frozen (physically or electrically stuck, locked);	Y	
			· Drift or oscillations or Offset in the valid range;	N	NA
Sensor/Switch (detailed analysis may be necessary for technology specific failure modes*)	Open circuit;	Open circuit	· Open circuit	Y	Failure detection by on-line monit
	Short circuit (to ground);	Short circuit to ground (d.c coupled)	Short circuit to ground (d.c coupled)	Y	
		· Short circuit (to ground, to power);	· Short circuit (to ground, to power);	Y	
			· Short circuit(to ground, to power, neighboring pins); Out-of-range;	N	
	Out-of-range	Out-of-range	Out-of-range	Y	
	Stuck in range	Stuck in range	Stuck in range	Y	
		Offsets	Offsets	Y	
			Oscillations	N	

Fig. 10: Overview of Diagnosis Coverage achieved for FEV Park lock System

7 Functional Safety Concept

The result of the development of the functional safety concept is shown in the following Fig. 11.

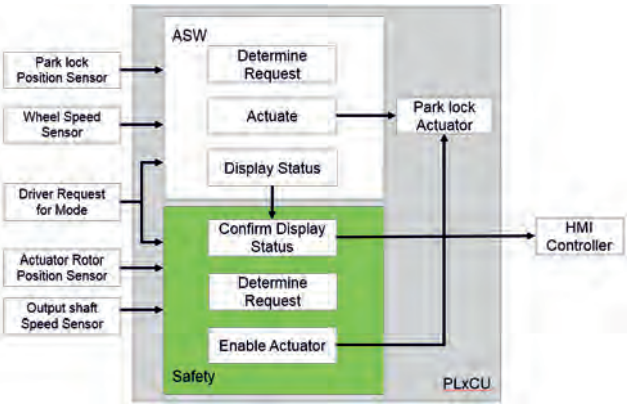

Fig. 11: Overview of Functional Safety Concept

The system was been decomposed into

- Normal Control : QM(B)
- Functional safety Monitoring: B(B)

The Functional safety monitoring checks for unintended disengagement and Wrong Display Control during park lock control. It actuates the safe states based on detected Safety violation

- Disable Display of range
- Disables actuator

The functional safety concept is also scalable for higher ASILs. Based on OEM HARA, the appropriate and adequate safety mechanisms can be applied to the system.

8 Conclusions and Outlook

FEV offers a one-stop solution for the complete park lock system including hardware, control software, diagnostics and functional safety, which was shown here exemplarily for a park by wire system, suitable for common EDUs. Such a synergistic approach reduces risk, cost and reworks as compared to distributed development. The predeveloped and pre-validated products help in accelerating projects. Further, the flexible software architecture allows plug and play of the product on an existing or a new control unit while managing implementation across multiple vehicle platforms. The architecture also allows flexibility to determine the failsafe operation dependent on vehicle or platform requirements. The functional safety software is scalable allowing the product to be compliant with ASIL B to D requirements.

The current development is in implementation phase and hence ready for series development project.

A demonstration model of this Park lock system has already been presented at the 18th CTI Symposium in Berlin; 9th to 12th of December 2019 at the FEV Booth.

References

1. Standardized E-Gas Monitoring Concept for Gasoline and Diesel Engine Control Units
2. ISO/FDIS 26262 parts 1-9: 2018.

Parking Lock Integration for Electric Axle Drives by Multi-Objective Design Optimization

Dipl.-Ing. **D. Lechleitner**, Dipl.-Ing. **M. Hofstetter**,
Associate Prof. Dr. **M. Hirz**, Graz University of Technology, Austria;
Dipl.-Ing. **C. Gsenger**, Dipl.-Ing. **K. Huber**,
Magna Powertrain GmbH & Co KG, Albersdorf-Prebuch

Kurzfassung

Aus Gründen der Fahrzeugsicherheit sind elektrisch angetriebene Achsen oftmals mit einer Parksperre ausgestattet, welche in Redundanz mit der Feststellbremse eine Bewegung des Fahrzeugs während des Parkens verhindert. Zur Integration der Parksperre in den Antrieb sind eine Vielzahl an Einbaupositionen denkbar, welche einen direkten Einfluss auf den notwendigen Bauraum des Antriebs haben. Darüber hinaus kann eine Betätigung der Parksperre bei kleiner Fahrzeuggeschwindigkeit und Talfahrt geschehen, was zu hohen Belastungen der Antriebsstrangkomponenten führen kann. Diese Belastungen hängen unter anderem von der Einbauposition der Parksperre ab und müssen bei der Auslegung des Antriebs berücksichtigt werden, um ein späteres Versagen zu verhindern. Dadurch ist die Gestaltung von Wellen, Zahnrädern und Lagern im Getriebe durch die Parksperrenintegration beeinflusst und eine suboptimal integrierte Parksperre kann zu unerwünscht hohen Kosten und verringerter Effizienz des Antriebs führen. Gemeinsam mit der Auswirkung auf den notwendigen Bauraum des Antriebs ergibt sich somit eine komplexe Problemstellung bei der Ermittlung der optimalen Parksperrenintegration. Um die Problemkomplexität zu reduzieren, wird eine um die Parksperrenintegration erweiterte Auslegungsmethode für elektrisch angetriebene Achsen vorgeschlagen, welche auf einer computergestützten, multikriteriellen Optimierung auf Systemebene des Antriebs basiert. Die vorgeschlagene Methodik wird anhand einer Fallstudie demonstriert und die Auswirkung der Parksperrenintegration auf die Optimalität eines exemplarischen Achsantriebs gezeigt.

Abstract

Due to safety considerations, electric axle drives (e-drives) are often equipped with a parking lock system, which prevents vehicle movement while parking in redundancy with the parking brake. In order to integrate the parking lock into the e-drive, various mounting positions inside the e-drive are eligible, which have a direct influence on the e-drive packaging. Furthermore, engaging the parking lock may happen at small vehicle velocities and while driving downhill,

leading to high loads on the e-drive components. These loads depend on the mounting position of the parking lock and have to be considered in the design phase to prevent failure of the system. That way, the designs of shafts, gear wheels and bearings of the gearbox are affected by the parking lock integration. A suboptimally integrated parking lock system can thus lead to undesirably high costs and reduced energy efficiency of the entire e-drive – all alongside the packaging aspect. Consequently, finding the best suitable parking lock integration for a certain e-drive is a complex task for the design engineers. To reduce the level of problem complexity, an established computer-based system design method for e-drives by means of a multi-objective optimization is extended to be capable of considering the parking lock integration. The proposed method is applied to a case study and the impact of the parking lock on the optimality of an exemplary e-drive system is shown.

1. Introduction

The market for passenger cars continues its shift from internal combustion engines (ICEs) towards electric drive systems. Although the long-term outlook for electric vehicles (EVs) still indicates an exponential growth of global sales by around 1700% in 2030 compared to 2020, the years until 2023 are expected to be challenging [1]. It is a key task for automotive original equipment manufacturers (OEMs) and suppliers to adopt their products and strategies quickly to the upcoming market changes and develop optimal EVs now for deployment after 2025 [2]. The optimal designing of the vehicle's powertrain plays a major role in this context.

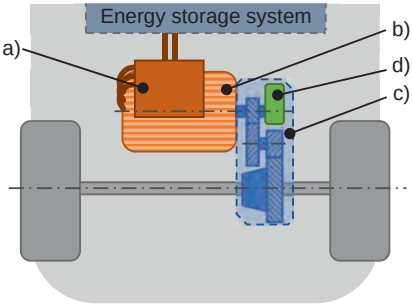

Fig. 1: Schematic illustration of an e-drive; a) power electronics unit, b) electric machine, c) gearbox, d) parking lock

Although many different electric powertrain architectures exist, the most common one is a purely electric axle drive (e-drive) that consists of the main components "power electronics unit", "electric machine" (EM) and "gearbox", which are schematically depicted in Figure 1. In

the design process, all of these components need to be designed to optimally fulfill the set requirements. Exemplary, minimum costs, maximum efficiency and favorable package integration of the e-drive system are typical concurrent design objectives. In order to find optimal designs regarding all set design objectives, a holistic multi-objective design optimization on system level ”e-drive” is required as presented e.g. in [3].

An additional subsystem in e-drives, which is not considered in comparable holistic design methods as described in [3], is a so-called parking lock (exemplary depicted in Figure 1 on the input shaft of the gearbox). A parking lock might be required due to considerations regarding the vehicle’s safety: in redundancy with the vehicle’s parking brake, the parking lock prevents vehicle movement while parking by mechanically locking the drivetrain. This function is typically achieved by mounting a parking lock wheel to a shaft inside the gearbox and a mechanically or electrically actuated pawl, which connects the parking lock wheel to the gearbox housing when the parking lock is engaged [4]. That way, an interlocking connection between housing and shaft is made and any rotation of the drivetrain is prevented. A simplified schematic of a parking lock is shown in Figure 2.

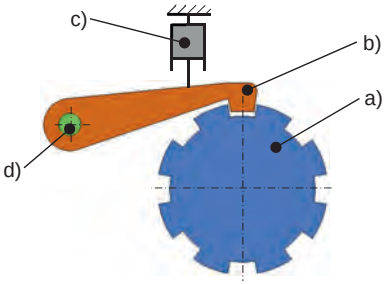

Fig. 2: Schematic illustration of a parking lock; a) parking lock wheel, b) pawl, c) actuator, d) pivot connecting the pawl to the gearbox housing

When integrating such a parking lock in the e-drive system, various mounting positions are eligible (e.g. on the input, intermediate or output shaft of a single-speed, two-stage gearbox as depicted in Figure 1). These mounting positions have a direct influence on the installation space demand of the gearbox. Furthermore, special load cases occur inside the drivetrain induced by an engagement of the parking lock at small vehicle speeds and at a certain slope of the road (e.g. speed < 5 km/h and a slope of 30%) or by towing the vehicle when the parking lock is engaged. In general, the former is critical for vehicles with separately driven axles (as common in EVs), the latter for vehicles with permanent all-wheel drives in conventional ICE-based transmissions [4]. The described load cases can result in high torques in the drivetrain

and thus impose high loads on the mechanical components (e.g. shafts, bearings and gear wheels). These loads need to be considered in the design phase to prevent a failure of the system [5]. Moreover, the loads on the mechanical components depend on the mounting position of the parking lock inside the gearbox, meaning a suboptimally integrated parking lock will result in higher loads and require larger shafts, bearings and gear wheels than the optimum. This in turn can lead to an undesirable increase of the e-drive costs and a decrease of the energy efficiency – all alongside the packaging aspect.

Due to this wide-ranging impact on the e-drive system, design engineers are confronted with a complex task when integrating a parking lock into the e-drive system. To reduce this complexity, an established computer-based design method for e-drives, described in [3], [6] and [7], is extended to be capable of integrating the parking lock by means of a multi-objective optimization on e-drive system level.

2. Methodology

For holistically designing the e-drive system, the already established design method described in [3], [6] and [7] is briefly outlined in the following. Additionally, extensions to this method for the parking lock integration are suggested. A schematic illustration of the design method based on multi-objective optimization on e-drive system level is shown in Figure 3. The method is applied in the early development stages with the aim to quickly find optimal design solutions for a given e-drive design problem. The resulting set of optima then serves as basis for decision-making in the subsequent development steps.

The input to the design method is represented by the defined requirements on the e-drive including the desired optimization objectives (e.g. minimal costs, maximal energy efficiency, favorable package integration of the e-drive in a given installation space). This information is then passed to a computer-based optimization phase, where certain design parameters of the e-drive are varied. Exemplary, in the case study presented in [7], 13 parameters of the electric machine (including dimensions of stator and rotor as well as magnet dimensions and the magnet arrangement of a permanent magnet synchronous machine), 23 parameters of the gearbox (including shaft dimensions, gear parameters, total center distance and gearbox topology) are directly formulated as optimization parameters and the power electronics unit is considered via optimization constraints.

Based on the requirements, the e-drive analysis involves electromagnetic simulations of the electric machine to verify that a sufficient torque-speed characteristic and a sufficiently low heat output for operation combined with the cooling system is present. Furthermore, the load capacity of the e-drive components to achieve the required service life based on a load

spectrum is investigated and aspects regarding noise, vibration, harshness (NVH) are considered. Additionally, it is verified that the maximum permissible junction temperatures of the semi-conductor elements in the power electronics unit are not exceeded and the voltage ripple at the DC side is sufficiently low. Besides verifying that the exemplary described requirements are fulfilled, the e-drive analysis involves the calculation of the e-drive properties (e.g. costs and energy efficiency) based on the provided values of the design parameters.

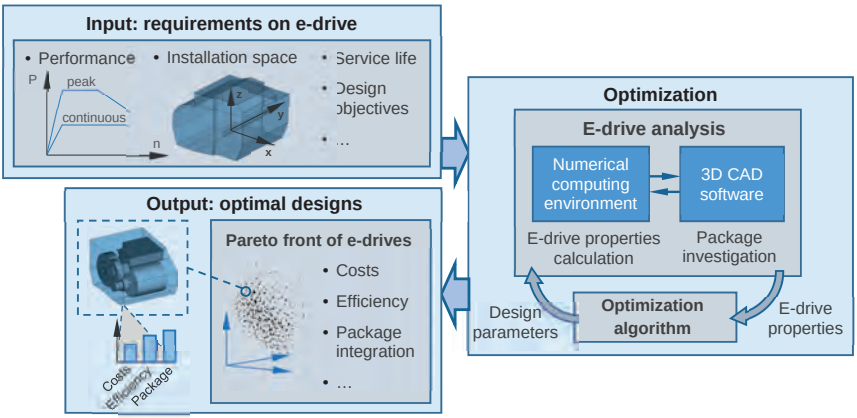

Fig. 3: Simplified e-drive optimization process

After calculating the system properties, the optimization algorithm – following the concept of differential evolution [8] – performs a rating of the design variants and decides about the next parameter sets to be evaluated. The described closed loop of system analysis and design synthesis is repeated until no more improvements in the optimization objectives are observable and converging behavior is present. The output of the method then consists of all found optimal e-drive design variants, which corresponds to the so-called Pareto front in the context of a multi-objective optimization. Promising design variants from this result set can then be further investigated and developed for production deployment.

In order to extend the described method with the capability to integrate the parking lock, two major aspects need to be discussed. The first aspect covers the geometrical integration of the parking lock into the e-drive package, the second aspect covers the calculation of the parking-lock-induced load cases and the consequences for sizing the mechanical components in the e-drive. The functional layout and design of the parking lock itself are described e.g. in [9] and [10] and not further discussed in the present work.

Geometrical Integration of the Parking Lock

As already mentioned in section 1, various mounting positions of the parking lock in the e-drive system are eligible. In the following, the focus is put on e-drives with a single-speed, two-stage helical gearbox with an offset between input shaft axis and output shaft axis, which is also schematically depicted in Figure 1. Furthermore, the rotor of the electric machine is directly mounted on the input shaft of the gearbox and this shaft is supported by three bearings. This architecture is common and will later be used in the case study presented in section 3. For such an e-drive architecture, a total of five different parking lock mounting positions on the input and intermediate shaft of the gearbox appear reasonable, considering aspects from series production as well as assembly. Positions on the output shaft are in general considered suboptimal due to the high torque level. The mentioned mounting positions are schematically depicted in Figure 4, where two positions on the input shaft (denoted as “INPA” and “INPB”) and three positions on the intermediate shaft (denoted as “INTA”, “INTB” and “INTC”) are visualized.

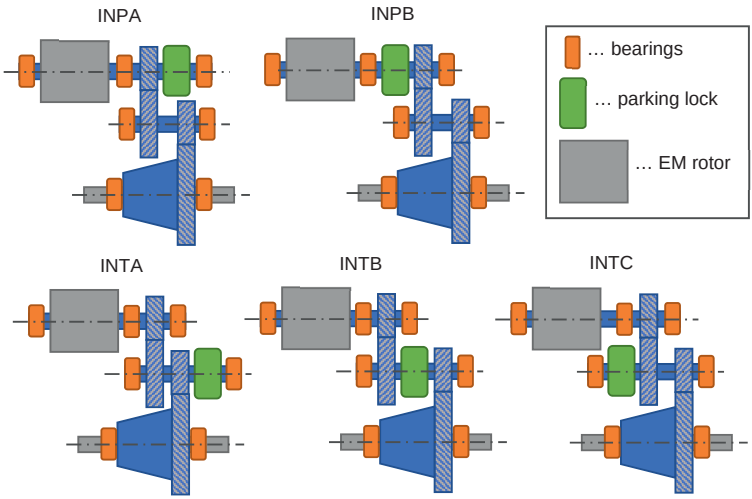

Fig. 4: Mounting positions of the parking lock inside an e-drive with a single-speed, two-stage helical gearbox with offset output shaft

When designing the e-drive system, a decision for one of the mounting positions needs to be made, which means the mounting position represents a design parameter c_{PLMount} that maps to an element in the set composed of the described positions:

$$c_{\mathrm{PLMount}} \in \{\mathrm{INPA}, \mathrm{INPB}, \mathrm{INTA}, \mathrm{INTB}, \mathrm{INTC}\}. \quad (1)$$

In the following, a given architecture of an electrically actuated parking lock is considered as shown in Figure 5, which will later be used in the case study presented in section 3. For such a parking lock – independent of the mounting position c_{PLMount} – further degrees of freedom exist when integrating the parking lock. These include the axial placement of the parking lock on the shaft y_{PL}, the mounting angle of the parking lock on the shaft Θ_{PL}, the mounting angle of the actuator Θ_{a} and two flipping parameters f_{PL} and f_{a}, which allow to rotate the parking lock and the actuator by 180 ° around the z-axis respectively. A visualization of all possible combinations of the parameters f_{PL} and f_{a} as well as the definition of the parameters y_{PL}, Θ_{PL} and Θ_{a} (measured from the closest possible position to the shaft) are depicted in Figure 5. The origin of the shown coordinate system (x, y, z) is defined by the position parameter c_{PLMount}.

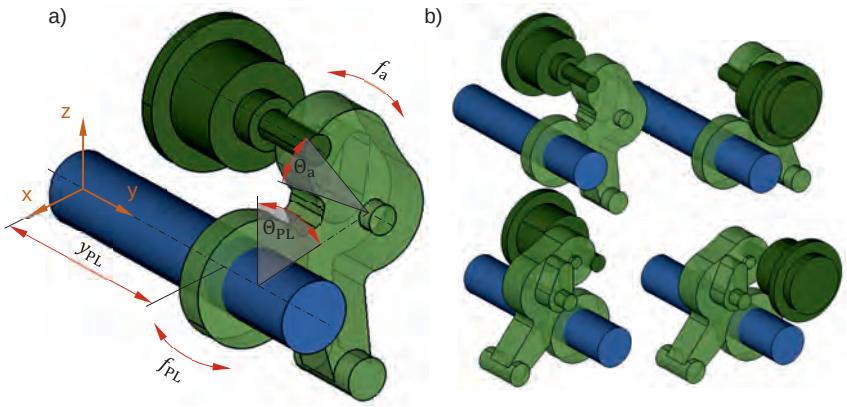

Fig. 5: Placement of an electrically actuated parking lock with given architecture; a) placement parameters, b) visualization of all possible combinations of the flipping parameters f_{PL} and f_{a}

That way, a total of six design parameters (c_{PLMount}, y_{PL}, Θ_{PL}, Θ_{a}, f_{PL}, f_{a}) are used to define the geometrical integration of the parking lock in the e-drive system. In order to extend the established design method depicted in Figure 3 and described in [3], [6] and [7] by the capability to integrate the parking lock, these six parameters are defined as additional optimization parameters for the optimization algorithm.

Moreover, certain restrictions apply when geometrically integrating the parking lock. In particular, the body of the parking lock must not clash with any other components in the e-drive

system (e.g. with shafts, bearings, gear wheels, rotor and stator of the electric machine). As the e-drive system and the parking lock itself in general show a 3D shape, a clash detection in 3D needs to be performed. This is done by the e-drive analysis, which uses 3D-CAD methods to automatically check for any clashes [13]. That way, it is determined if the integration suggested by the optimization algorithm is valid or not. In case clashes are identified, the design variant is considered invalid and removed from the optimization loop.

Consideration of Parking-Lock-Induced Load Cases

Aside from geometrically integrating the parking lock and checking for clashes, further constraints need to be satisfied. Specifically, the load cases induced by the parking lock, which are described in section 1, must not lead to a failure of the mechanical components inside the e-drive system. In order to determine if a sufficient load capacity of the mechanical components is present or not, a suitable model of the drivetrain and vehicle to approximately calculate the parking-lock induced loads on the components is required. Based on the loads determined by the model, further criteria need to be applied to determine the load capacity of the mechanical components. For that purpose, the minimal information required is the torque transmitted by both gear pairs and the acting torque on the parking lock.

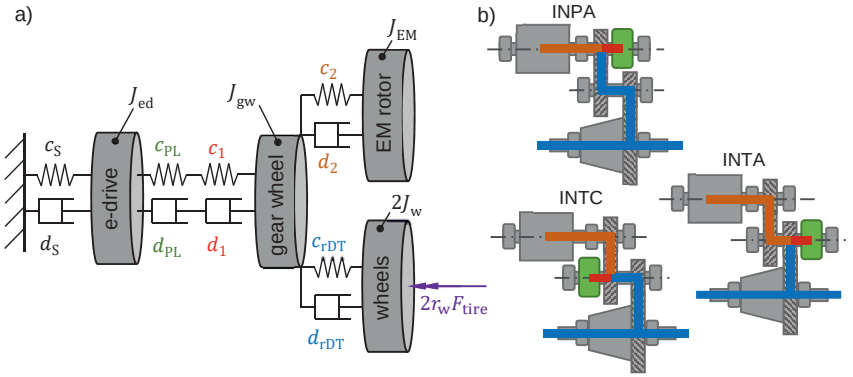

Fig. 6: Mechanical model of the drivetrain for mounting positions “INPA”, “INTA” and “INTC”: a) schematic of MBS model, b) visualization of the rotational spring-damper combinations in the respective torque paths

To calculate these torques, a simple multibody simulation (MBS) model is presented in the following, which requires low computational effort and is thus well suited for the application in the design optimization loop shown in Figure 3. The mechanical model for mounting positions

“INPA”, “INTA” and “INTC” is shown in Figure 6 and represents a rotational system composed of four masses, which are connected by rotational spring-damper combinations. For reasons of simplicity, all kinematic and kinetic quantities are referred to the level of the gearbox input shaft. The actual torques and velocities at the intermediate and output shaft can be calculated by applying the transmission ratios of the two gear pairs. The torques acting in the springs and dampers are given by

$$T_{\mathrm{c}} = c \cdot \Delta\varphi\,, \tag{2}$$

$$T_{\mathrm{d}} = d \cdot \Delta\dot{\varphi} \tag{3}$$

respectively, where c is the spring rate, d the damping coefficient, $\Delta\varphi$ the relative angle between the two end points of the spring and $\Delta\dot{\varphi}$ the relative angular velocity between the two end points of the damper. The e-drive with its moment of inertia J_{ed} around the pitch axis of the vehicle is mounted in a suspension with spring rate c_{S} and damping coefficient d_{S}. The parking lock is connected to J_{ed} by its spring rate c_{PL} and damping coefficient d_{PL}. Following the torque paths visualized in Figure 6, a certain spring rate c_1 and damping coefficient d_1 accounts for the elasticity and damping of the path between parking lock and the nearest gear wheel. The rotor of the electric machine with moment of inertia J_{EM} is connected to this gear wheel by c_2 and d_2. The elasticity and damping of the remaining drivetrain connecting the single wheels with moment of inertia J_{w} and the described gear wheel are considered by c_{rDT} and d_{rDT}. The gear wheel itself represents an intersection of the three spring-damper combinations and is modelled with moment of inertia J_{gw}.

Analogously, the model for mounting positions “INPB” and “INTB” is defined and shown in Figure 7. The model is slightly simpler due to the missing spring-damper combination defined by c_1 and d_1. The intersection of the three spring-damper combinations is now at the parking lock wheel, which is modelled with its moment of inertia J_{PL}.

The connection to the longitudinal dynamic of the vehicle is made by the torque $r_{\mathrm{w}}\,F_{\mathrm{tire}}$ acting on the wheels, where r_{w} is the effective rolling radius and F_{tire} is the longitudinal force at the tire-road contact modelled by the Magic Formula given in [11] (equation (4.49), page 173).

The mechanical model to describe the longitudinal vehicle dynamic is schematically shown in Figure 8 for a vehicle with a parking lock mounted on the front axle (for a parking lock mounted on the rear axle, the force F_{tire} would act on the wheels of the rear axle). The vehicle with body mass m_{b} is modelled on a slope with angle β. At the center of gravity (CoG) the gravitational force $m_{\mathrm{b}}g$ is acting. The single wheels with unsprung mass m_{w} are connected to the body by spring-damper combinations representing the longitudinal wheel suspension. The spring rates and damping coefficients for the front axle are given by c_{wsf} and d_{wsf}, the ones for the rear

axle by c_{wsr} and d_{wsr}. In analogy to equations (2) and (3), the spring and damper forces are determined by

$$F_{\mathrm{c}} = c \cdot \Delta x\,, \tag{4}$$

$$F_{\mathrm{d}} = d \cdot \Delta \dot{x}, \tag{5}$$

where Δx is the spring deflection and $\Delta \dot{x}$ the relative velocity between the two end points of the damper. That way, the force F_{tire} couples the longitudinal dynamic of the vehicle and wheels with the rotational dynamic of the drivetrain.

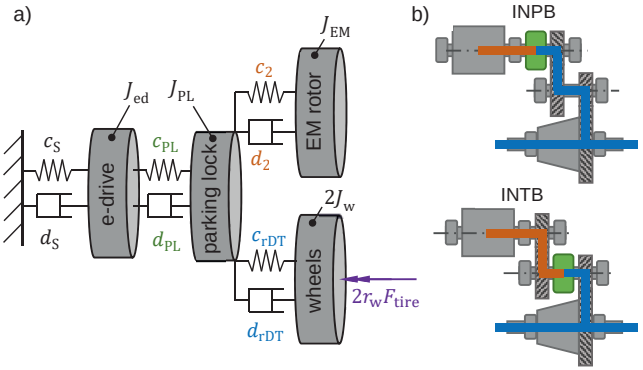

Fig. 7: Mechanical model of the drivetrain for mounting positions “INPB” and “INTB”: a) schematic of MBS model, b) visualization of the rotational spring-damper combinations in the respective torque paths

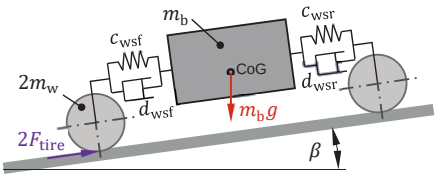

Fig. 8: Mechanical model to describe the longitudinal vehicle dynamic (drivetrain with parking lock mounted on the front axle)

Applying the conservation of momentum to the described models yields equations of motion for all masses, which are numerically solved to obtain the torques acting on the parking lock, gear pair 1 (connecting input and intermediate shaft) and gear pair 2 (connecting intermediate and output shaft). For an exemplary e-drive with parking lock mounting position “INTA”, the

described model is compared to a reference MBS model, which is implemented in Simcenter Amesim [14] and also considers the backlash between parking lock wheel and pawl. Figure 9 shows the obtained torque curves for an initial vehicle velocity of 3.5 km/h and slope $\beta = 0\,°$ from the suggested and the reference MBS model. Mainly due to the modelled backlash, the torques from the reference model tend to oscillate more and phase shifts compared to the curves from the suggested model are noticeable. However, the general torque levels are predicted well by the suggested model.

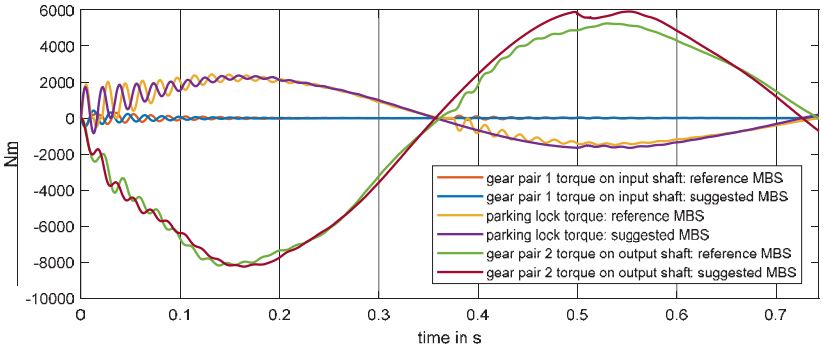

Fig. 9: Comparison of torque curves obtained from the suggested MBS model and a reference model for an exemplary e-drive with parking lock mounting position “INTA” (initial vehicle velocity of 3.5 km/h, $\beta = 0\,°$)

In order to calculate the load capacity of the mechanical components based on the obtained torque curves, the quasi-stationary forces acting on the gear wheels and the bearing reaction forces are determined from start of the simulation until the vehicle speed reaches zero for the first time. After that, the following criteria are applied to determine whether or not a sufficient load capacity for the parking-lock-induced load case is present:

- the maximal torque acting on the parking lock must not exceed T_{PLlim} (which is specified for a pre-defined architecture of the parking lock),
- the maximal nominal torsional stress in the shafts must not exceed a specified permissible stress τ_{lim},
- the minimal static safety factor of the bearings according to ISO 76 must not be less than a specified value $S_{0\mathrm{min}}$

- the minimal static safety factors for pitting and tooth bending of the gear wheels according to ISO 6336 must not be less than specified values S_{H0min} and S_{F0min} respectively.

These conditions are checked by the e-drive analysis and in case an insufficient load capacity is determined, the design variant is considered invalid and removed from the optimization loop. That way, the established design method described in [3], [6] and [7] for e-drives is extended to be capable of holistically integrating the parking lock by adding the parameters regarding the geometrical integration (c_{PLMount}, y_{PL}, Θ_{PL}, Θ_{a}, f_{PL}, f_{a}) as optimization parameters and checking the constraints regarding clashes and load capacity in the parking-lock-induced load cases.

3. Results & Discussion

The proposed method is applied to a case study that involves the optimization of an e-drive with a permanent magnet synchronous machine and an axially attached power electronics unit. The main requirements are given in Table 1, the available installation space is shown in Figure 11.

Table 1: Main requirements on e-drive

Peak power (30 s) in kW	160
Continuous power in kW	80
Maximal axle speed in rpm	1400
Maximal axle torque in Nm	4000
Required service life in h	8565
DC supply voltage in V	325
Maximal peak-to-peak DC voltage ripple in V	24
Coolant inlet temperature in °C	65

In order to investigate the impact of the parking lock integration on the e-drive, several optimization studies are conducted: First, the e-drive design is optimized without a parking lock; second, separate optimizations are performed for all e-drive mounting positions given by (1). That way, the optimal designs for all discussed parking lock mounting positions can be compared and the consequences of requiring a parking lock in the e-drive system by the vehicles safety concept is shown.

The power electronics unit, electric machine and gearbox are subject to optimization and the minimization objectives for all optimizations are defined as

- costs (considering the main cost drivers of power electronics unit, electric machine and gearbox),
- degree of losses of the e-drive based on the WLTC [12] and
- package metric.

The package metric is the protruding volume of the installation space by the e-drive in its most favorable position, meaning it takes a value of zero in case the e-drive completely fits inside the given installation space. Furthermore, the parking-lock-induced load case considered in the optimization is defined by a vehicle velocity of 3.5 km/h at the time of engagement and a slope of $\beta = 0\,°$.

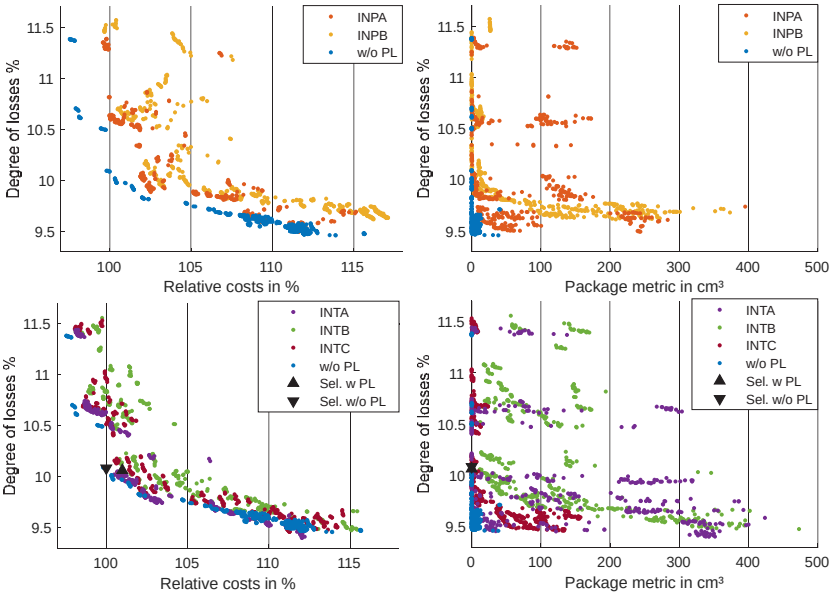

Fig. 10: Projections of the obtained Pareto front approximations

The result of the optimizations is shown in Figure 10. The relative costs are the e-drive costs as a ratio of those of a selected e-drive solution without a parking lock (denoted as “Sel. w/o PL” in Figure 10). This solution thus shows relative costs of 100%. Furthermore, the costs of the parking lock itself are excluded to allow a direct visualization of the cost increase caused by the necessity to adapt the e-drive system for a parking lock integration. The upper two charts in Figure 10 show the projections of the obtained Pareto front approximations for a parking lock mounted on the input shaft and for an e-drive without parking lock (denoted as

“w/o PL”). The increase in costs compared to a system without parking lock is significant, especially in the region of low costs and higher losses. However, mounting position “INPA” performs slightly better than mounting position “INPB” in dimensions costs and losses and performs significantly better when comparing the package metric. The mounting positions on the intermediate shaft are shown in the lower two charts of Figure 10. These positions in general are slightly more favorable than the ones on the input shaft, especially in the region of low costs and higher losses. Mounting positions “INTA” and “INTC” show particular strength when comparing them to the solutions without a parking lock. Similar good objective values are achievable for some regions of the Pareto fronts in the shown 2D-projections (but not simultaneously in all three dimensions).

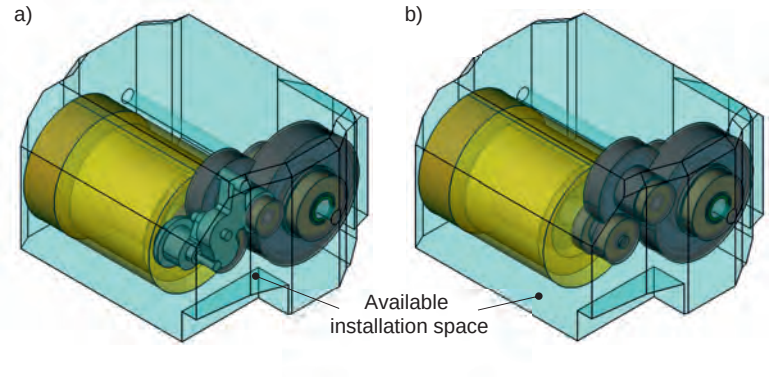

Fig. 11: CAD visualization of selected solutions depicted in Figure 10:
a) “Sel. w PL”, b) “Sel. w/o PL”

In the following, one design solution without a parking lock is selected from a region representing a balanced trade-off between costs and losses (denoted as “Sel. w/o PL” in Figure 10). This solution shows relative costs of 100%, a package metric of zero (meaning it completely fits inside the installation space) and losses of around 10.08%. Furthermore, a design solution with parking lock that approximately shows the same losses and also has a package metric of zero is selected (denoted as “Sel. w PL” in Figure 10). This e-drive uses mounting position “INTA” and shows relative costs of around 101%. In other words, an e-drive design with parking lock mounting position “INTA” was found that shows a marginal cost increase of 1% (excluding the costs of the parking lock itself) compared to a similar optimal e-drive without parking lock and otherwise equal objective values. That way, this design solution might be of high interest

for the detailed subsequent development phases. A CAD visualization of both selections is shown in Figure 11.

4. Summary & Conclusion

An extension to an established multi-objective design optimization method for e-drives is proposed, which enables to find the optimal integration of a parking lock in the e-drive system context. Various degrees of freedom in the geometrical integration of a given parking lock architecture are considered and additional optimization parameters are derived. Moreover, constraints regarding clashes between components and the load capacity of the mechanical system for parking-lock-induced load cases are discussed.

The method is applied to a case study and the various mounting positions of the parking lock inside the e-drive are investigated. The obtained Pareto front approximations show the impact on the system costs, energy efficiency and package integration compared to optimal e-drives without parking lock. Furthermore, in the region of a balanced trade-off between costs and losses, the results indicate that the integration of the parking lock can be achieved with only a marginal cost increase and otherwise same objective values compared to a system without parking lock. This information is of great value for the subsequent development steps and also enables to assess the consequences of requiring a parking lock by the vehicle's safety concept.

Acknowledgement

This work is supported by Magna Powertrain. To reduce development time and effort, Magna Powertrain is investigating a holistic optimal design approach for electric drive systems in cooperation with Graz University of Technology. The presented methodology is part of this project and aims to support early development stages by solving conflicts between efficiency, performance, package, weight and costs. Consequently, optimal e-drive solutions can be offered to customers in a fast-changing market.

References

[1] McKerracher, C., Izadi-Najafabadi, A., O'Donovan, A., et al.: Electric Vehicle Outlook 2020, Bloomberg New Energy Finance Limited. 2020. [Online]. Available: https://about.bnef.com/electric-vehicle-outlook/. [Accessed January 26, 2021].

[2] Hausler, S., Heineke, K., Hensley, R., et al.: The impact of COVID-19 on future mobility solutions, McKinsey Center for Future Mobility. 2020. [Online]. Available:

https://www.mckinsey.com/industries/automotive-and-assembly/our-insights/the-impact-of-covid-19-on-future-mobility-solutions/. [Accessed January 26, 2021].

[3] Hofstetter, M., Hirz, M., Gintzel, M., et al.: Multi-Objective System Design Synthesis for Electric Powertrain Development, 2018 IEEE Transportation Electrification Conference and Expo (ITEC), Long Beach, USA, 2018, pp. 286-292. doi: 10.1109/ITEC.2018.8450113

[4] Naunheimer, H., Bertsche, B., Ryborz, J., et al.: Automotive Transmissions. Friedrichshafen: Springer-Verlag Berlin Heidelberg 2011. doi: 10.1007/978-3-642-16214-5

[5] Zimmer, P., Krabatsch, T., Rühl, M.: Strength Testing of Parking Lock Mechanisms in Car Transmissions, ATZ worldwide, 120, 2018, pp. 56-61. doi: 10.1007/s38311-018-0136-2

[6] Hofstetter, M., Lechleitner, D., Hirz, M., et al.: Multi-objective gearbox design optimization for xEV-axle drives under consideration of package restrictions, Forschung im Ingenieurwesen, 82, 2018, pp. 361-370. doi: 10.1007/s10010-018-0278-9

[7] Lechleitner, D., Hofstetter, M., Hirz, M.: Cost Reduction of Electric Powertrains by Platform-Based Design Optimization, 2020 IEEE Transportation Electrification Conference and Expo (ITEC), Chicago, USA, 2020. doi: 10.1109/ITEC48692.2020.9161468

[8] Storn, R., Price, K.: Differential Evolution – A Simple and Efficient Heuristic for Global Optimization over Continuous Spaces, Journal of Global Optimization, 11(4), 1997, pp. 341-359. doi: 10.1023/A:1008202821328

[9] Dong, Y., Chen, Y., Yu, C., et al.: Performance of the Transmission Parking Mechanism of a Battery Electric Vehicle Simulated with Adams Software, Automotive Innovation, 1, 2018, pp. 114-121. doi: 10.1007/s42154-018-0023-y

[10] Förster, H.: Automatische Fahrzeuggetriebe. Berlin: Springer-Verlag Berlin Heidelberg 1991. doi: 10.1007/978-3-642-84118-7

[11] Pacejka, H.: Tire and Vehicle Dynamics. Rotterdam: Elsevier Science & Technology 2006. doi: 10.1016/B978-0-7506-6918-4.X5000-X

[12] Tutuianu, M., Bonnel, P., Ciuffo, B., et al: Development of the Worldwide harmonized Light duty Test Cycle (WLTC) and a possible pathway for its introduction in the European legislation", Transportation Research Part D: Transport and Environment, 40, 2015, pp. 64-75. doi: 10.1016/j.trd.2015.07.011

[13] Riegel, J., Mayer, W., van Havre, Y., et al.: FreeCAD (0.19.22522) [Software]. https://www.freecadweb.org/.

[14] Siemens PLM Software: Simcenter Amesim (2019.1) [Software]. https://www.plm.automation.siemens.com/global/en/products/simcenter/.

Energy-efficient Hydraulic Control for the Multi-speed Transmission of an Electric Vehicle

Thorsten Hillesheim, Freudenberg Sealing Technologies, Weinheim

Zusammenfassung

Elektromotoren müssen so ausgelegt werden, dass auch bei Autobahn-typischer Geschwindigkeit sichere Überholvorgänge möglich sind. Diese Auslegung geht einher mit einer geringeren Effizienz im urbanen Niedriglast-Bereich sowie einer insgesamt geringeren Reichweite bei gegebener Batteriegröße. Deshalb werden in der Automobilindustrie zunehmen Konzepte mit einem schaltbaren Getriebe – in der Regel mit zwei Übersetzungsstufen – entwickelt. Dabei ist es sinnvoll, eine besonders energieeffiziente Schaltaktuatorik zu wählen. Die von Freudenberg Sealing Technologies vorgeschlagene Lösung besteht in der Verwendung einer Speicherladeschaltung mit Hilfe eines Hydrospeichers zur Steuerölversorgung der Schaltaktuatorik.

Abstract

Electric motors need to be designed in such a way that safe passing maneuvers are possible even at the speeds that are often driven on the highway. This design is accompanied by lower efficiency in the urban low-load range and an overall shorter range for a certain battery size. The automotive industry is therefore increasingly developing concepts that feature a shiftable transmission – usually with two gear ratios. Here, it is wise to select a particularly energy-efficient shift actuator. Freudenberg Sealing Technologies is proposing a solution based on an accumulator storage system using a hydraulic accumulator for shift actuation.

1 Introduction

Whereas electric vehicles were designed primarily for short-haul urban use in the pioneering days, battery-powered electric drives are now being developed for virtually all passenger car segments. For vehicle manufacturers, this poses the challenge of also having to design the traction motor for long-distance highway driving. Electric drives are intended to achieve various target dimensions, some of which are in conflict with one another. The goal is to maximize their acceleration capability, starting phase, tractive torque, and top speed while at the same time

minimizing range and energy demand. Most importantly, however, electric drives need to remain affordable, even with increased performance.

Multi-speed transmissions have the potential to mitigate the conflict between efficiency and performance. Due to their higher efficiency in real operating cycles, they also have a cost-reducing effect, as the battery volume can be selected to be correspondingly smaller. An indirect cost effect also arises from the fact that, if a transmission is used, a larger number of vehicle variants can be equipped with identical motors. With this in mind, more and more vehicle manufacturers are looking into the use of shiftable two-speed transmissions in conjunction with battery-powered electric drives. At least one series-production application in a sporty vehicle is already known. If a vehicle is to cover a very wide range of velocity, even a design as a three-speed transmission could make sense. A fuel consumption simulation in WLTP also shows for an electrified SUV that the demand for electrical energy drops by 5.3 % if it has a shiftable three-speed transmission [2].

2 Higher efficiency thanks to a multi-speed transmission

In modern combustion engine drives with exhaust gas turbocharging, the torque curves remains constant over a broad range of speeds, while power increases up to the rated speed and then rapidly drops off again. The more gears the transmission has, the better the entire engine map can be utilized. In contrast, the power of an electric motor remains constant as it reaches the corner point up to high speeds. As a result, the torque that is initially constant at speeds great than 0/min drops steadily as the corner point is reached, a phenomenon that is often described as poor traction at higher velocities in vehicle tests. If a two-speed transmission is used, the torque available for starting in first gear can be significantly increased without making any modifications to the motor, while second gear allows for higher top speeds with identical motor output, **Fig. 1**.

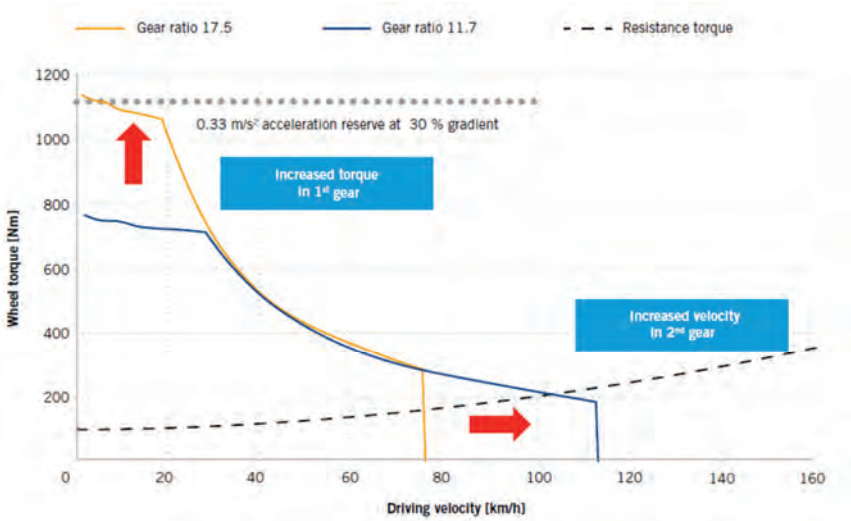

Fig. 1: Maximum wheel torque and driving velocity for a compact electric vehicle equipped with a two-speed transmission – advantages of shifting from first to second gear [1]

The map range with maximum efficiency is usually achieved by electric motors at speeds that are slightly higher than those of the corner point and at medium and high loads. Shifting the corner point towards higher speeds and lower wheel torques leads to a much wider map range with very good efficiency, as shown by example in **Fig. 2**.

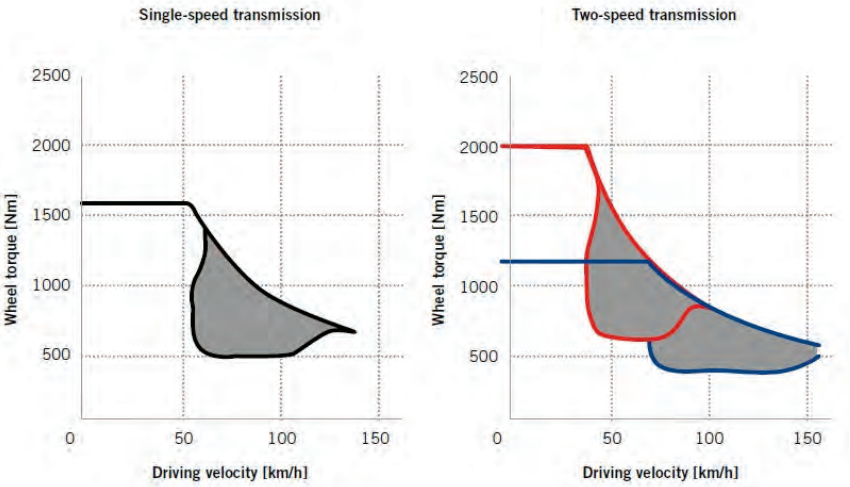

Fig. 2: Example of the influence of a two-speed transmission (red line: first gear; blue line: second gear) on the efficiency map of an electric motor in comparison to a single-speed transmission [5]

3 Comparism of two hydraulic shifting systems

3.1 Choosing a system

Once a shiftable transmission has been chosen, it is necessary to decide how the automatic transmission shifting is to be carried out. Here, it makes sense to place particularly high importance on the criterion of energy efficiency in order to maximize the battery range. Due to the fast shifting times and high forces needed, it is safe to assume that gear shifting will also take place hydraulically in an electric drive. Thus, the search for optimal shifting can be narrowed down to how hydraulic energy is introduced into the system. Theoretically a number of options are available for this [2]:

- oil pumps that operate at a constant flow rate
- switchable oil pumps with one high-pressure and one low-pressure stage
- high-pressure hydraulic accumulators
- direct electromechanical control of the individual actuators
- as well as hydrostatic actuator.

In the following, two solutions are compared in terms of their energy efficiency: on the one hand, the traditional solution, that is, a non-switchable oil pump with constant flow rate, and on the other hand, a hydraulic accumulator developed by Freudenberg Sealing Technologies. The latter has already been used millions of times for shifting automated manual transmissions or dual-clutch transmissions in conjunction with a combustion engine.

When using the oil pump with constant flow rate, the pump supplies the lubricating oil (which acts at the same time as a coolant) to both the transmission and the gear actuation via a corresponding valve block, **Fig. 3** (left). In contrast, with the hydraulic accumulator, an accumulator charging actuation operates with two oil circuits that have different pressure levels, **Fig. 3** (right). The High-pressure (HP) circuit is responsible for gear position and charging of the hydraulic accumulator, while the lubricating oil supply is provided via the Low-pressure (LP) circuit. Each of the two circuits has its own feed pump, which is optimized to the respective pressure level.

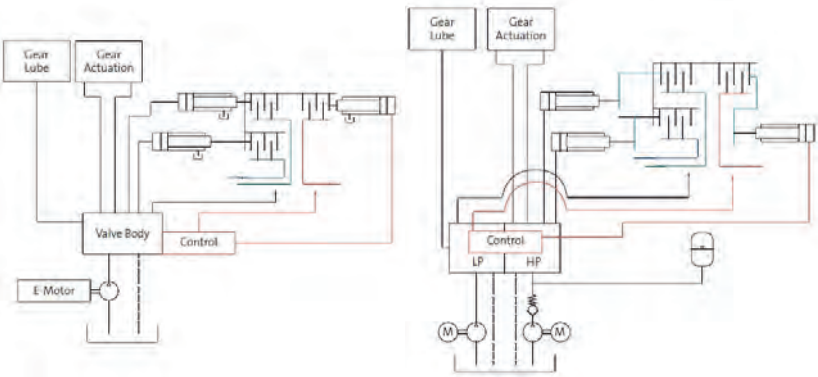

Fig. 3: Circuit diagram for a transmission oil supply with a gear actuator: solution based on a constant displacement pump and valve switching block (left); and accumulator charging actuation with two oil circuits (right) [2]

3.2 Boundary conditions and considerations of efficiency

In order to be able to compare the energy demand of shifting systems, the boundary conditions for the simulation must first be defined. Here it is important to select the driving cycle, since this significantly determines the number of gear shiftings via the vehicle dynamics. In addition, all of the main characteristics of the hydraulic system as well as the efficiencies of all individual components must be determined. Thus, for the investigations presented later on, a pressure level of between 40 and 60 bar was specified for the accumulator, which is maintained in this range via an electrically driven gear pump. The pump drive via a brushless DC motor operates with efficiency of at least 75%.

For the hydraulic accumulator, several designs are conceivable, although Freudenberg Sealing Technologies relies solely on piston accumulators that have a particularly high degree of volume utilization for transmission applications, since the movement area of the piston extends over nearly the entire accumulator working stroke. The efficiency of such a piston accumulator depends to a large extent on the frequency and the driving profile [3] and is 0.92 on average in this study. The accumulator volume is usually designed in such a way that three to four switching cycles are possible with a completely filled accumulator. Only then is the pump put back into operation. At the same time, the required volume flows on the “consumer side” have to be determined, in other words for the gear actuator and the clutch actuation. It must be taken into account that multiple gear changes must be possible if the respective driving maneuvers require this.

Using the data mentioned, it is then possible to carry out a multi-stage model calculation that shows the energy demand for feeding oil quite accurately. In [4], proof was provided in this way that the use of an accumulator charging system instead of a constant displacement pump designed for the maximum required flow rate reduces the energy demand by more than 80 %. The absolute amount of energy saved in the NEDC driving cycle in force at the time of the investigation was 33.4 Wh, **Fig. 4**. In the FTP75 driving cycle the absolute amount of energy saved was 46.1 Wh.

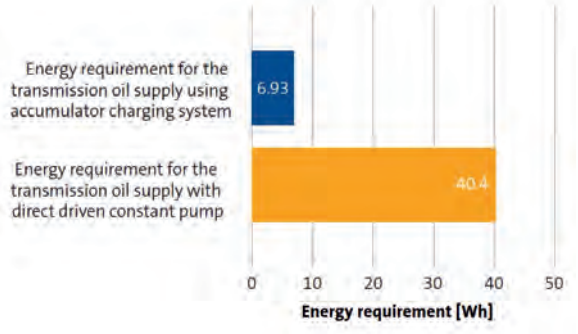

Fig. 4: Energy demand of transmission oil supply and shifting: comparison of conventional constant displacement pump (bottom) and accumulator charging actuation (hydraulic accumulator, top) [4]

It would be technically possible to transfer this principle from combustion engine drives to battery-powered electric drives without any limitations. However, one should bear in mind that the number of gear shiftings in an electric drive is lower than in an combustion engine; therefore, the absolute amount of energy in a given driving cycle is also lower. It can be assumed that the relative advantage remains. If the number of gear shiftings decreases as expected, then the storage volume could also be reduced. Nevertheless, it is known from bids for tender for hydraulic accumulators in battery-powered electric drives that the pressure level and the storage volume can vary considerably and, in some cases, even be lower than in combustion engine drives, which have an average accumulator volume of around 300 cm^3.

4 Further developments of accumulator technology

Hydraulic piston accumulators for vehicle transmissions are a mature product that has been installed millions of times. So far, series-production experience has been gained for automated manual transmissions, dual-clutch transmissions and torque-converter automatic transmissions. This experience can be put to good use for applications on multi-speed transmissions in electric powertrains.

At the same time, Freudenberg Sealing Technologies is constantly developing its accumulator technology further. The replacement of the steel piston separating the mediums by a plastic piston that is significantly lighter and easier to install represents a major innovation. The injection-molded piston requires only one mounted sealing ring instead of a complex sealing package, **Fig. 5**. At the same time, the weight of the patented piston has been reduced by around 50%. Because fewer components now need to be taken into consideration when assembling the hydraulic accumulators, the process can be simplified, which benefits process-reliable production. The biggest challenge was to find a plastic material for the piston that is roughly as gas-tight as the steel used in the past. The solution that was found is based on a thermoset composite material whose resistance to media such as transmission oil and hydraulic fluid has been proven in extensive tests.

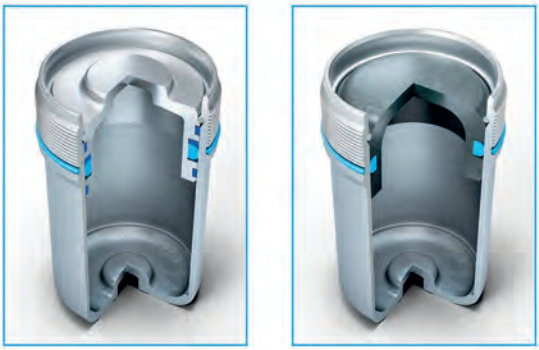

Fig. 5: Design of a showcase piston accumulator with a steel piston (left) and a plastic piston (right)

The next stage of further development is aimed at manufacturing the cylinder as a molded part without further machining (finishing), which would result in a substantial reduction in production costs. The major technical challenge here is that the gas tightness of the hydraulic accumulator needs to be ensured over the entire service life of the vehicle, as there is neither a provision for replacement nor nitrogen refillment. The demands placed on surface and manufacturing quality and are therefore quite high.

All in all, Freudenberg Sealing Technologies sees considerable potential for the use of hydraulic accumulators in particularly energy-efficient battery-powered electric drives and will present more detailed results on this in the future.

References

[1] Liebold, J., ed al.: 1, 2 or 3 - how much it would be? CTI Transmission Symposium, Berlin, 2018

[2] Ishihara, M.; Semenov, D.: Comparison of P2 Hybrid DCT Actuation Control System. 11th International CTI Symposium Automotive Transmissions, HEV and EV Drives, Novi/Michigan, 2017

[3] Hofmann, P.: Hybridfahrzeuge : Ein alternatives Antriebskonzept für die Zukunft. Wien: Springer, 2010

[4] Hillesheim, Th.: Hydrospeicher für die effiziente Getriebesteuerung. In: ATZ 116 (2014) 9, S. 70ff.

[5] Faid, S.: A highly efficient two speed transmission for electric vehicles. EVS28 Kintex, Korea, 2015

The Pendulum Rocker Damper

Providing flexible damper characteristics for hybrid powertrains

Dr.-Ing. **Martin Häßler**, Dr. rer. nat. **Olaf Werner**,
Schaeffler Automotive Buehl GmbH & Co. KG, Bühl

Zusammenfassung

Hybridisierte Antriebsstränge stellen aufgrund vielfältiger Konfigurationen und neuartiger Betriebspunkte besondere Herausforderungen bei der Erfüllung von Komfortzielen, was eine hochentwickelte Simulationstechnik zur zielführenden Entwicklung immer anspruchsvollerer Lösungen innerhalb der Systeme zur Torsionsschwingungsdämpfung erfordert. Heutige Torsionsdämpfer verwenden zur Darstellung der Torsionssteifigkeit in aller Regel mehrere Sätze von Federn, welche in Umfangsrichtung in Federfenstern von Ein- und Ausgangsteilen platziert sind und auf dem hierdurch gegebenen Abstand zur Drehachse eine nominal lineare Kennlinie erzeugen. Die bauliche Trennung von Leerlauf- und Volllastdämpfer und das Einrichten verschiedener Dämpferstufen mit Federn unterschiedlicher Anzahl oder unterschiedlichen Typs, welche stufenweise zum Eingriff kommen, bilden begrenzte Möglichkeiten, eine für jede Fahrsituation passende Torsionssteifigkeit zur Verfügung zu stellen.

Das innovative Betätigungskonzept für die Federn innerhalb des neu entwickelten Pendelwippendämpfers überwindet erstmals diese Einschränkung. Die Übersetzungen in rollenbestückten Kurvengetrieben ermöglichen es, eine Vielzahl nützlicher, kontinuierlich veränderlicher und sogar degressiver Torsionskennlinien aus ein und denselben Federn zu erzeugen, die gleichzeitig ein Maximum an Federenergie im gegebenen Bauraum bieten. Diese Kennlinien können in einfacher Weise an spezielle Anforderungen verschiedener Anwendungen angepasst werden, ohne das Gesamtkonzept ändern zu müssen. Der Pendelwippendämpfer eignet sich daher besonders für den Einsatz in hybridisierten Antriebssträngen, erlaubt eine Integration von Momentenbegrenzern und weist die von konventionellen Torsionsdämpfern bekannten Schnittstellen auf.

Abstract

Hybridized powertrains pose special challenges in the fulfillment of comfort targets due to a wide range of configurations and new types of operating points, which requires highly developed simulation technology for designing increasingly sophisticated solutions for

torsional vibration damping. In order to represent a torsional stiffness, today's torsion dampers generally use multiple sets of springs placed in circumferential direction in spring windows of torque input and output elements, thus creating a nominally linear characteristic at the given distance from the axis of rotation. Structurally separating idle and full load damper and settings with different damper stages using springs of different number or type, which are used in a stepwise manner, represent limited options to provide the appropriate torsional stiffness for every driving situation.

The innovative spring actuation mechanism of the well elaborated Pendulum Rocker Damper for the first time overcomes this limitation. The transmission ratios of roller equipped cam mechanisms give the option to create a wide variety of continuously variable and even degressive characteristics from one and the same set of springs offering the maximum energy in a given installation space. These characteristics can easily be adjusted to special requirements of different applications without changing the overall design. The Pendulum Rocker Damper is therefore particularly suitable for use in hybridized powertrains, allows the integration of torque limiters and offers the interfaces known from conventional torsion dampers.

1. Torsional vibration challenges within hybrid powertrains

Simulation technology, as well as the understanding of phenomena and requirements within the drivetrain, are indispensable in the development of new, targeted damper concepts for hybrids.

Simulation technology at Schaeffler

Simulation technology has been an integral part of the product development process at Schaeffler for decades. Particularly with regard to damper design, standardized and automated processes are exemplary in terms of the quality of the simulation results in the early design phase. The application of the processes is firmly anchored in the development process and is thus, for example, a necessary boundary condition for process steps such as the presentation of initial prototypes.

The current challenge is to extend the simulation platform concerning new issues associated with hybridization in the automotive sector. For this purpose, all drivetrain topologies with the respective operating points must be served (Fig. 1).

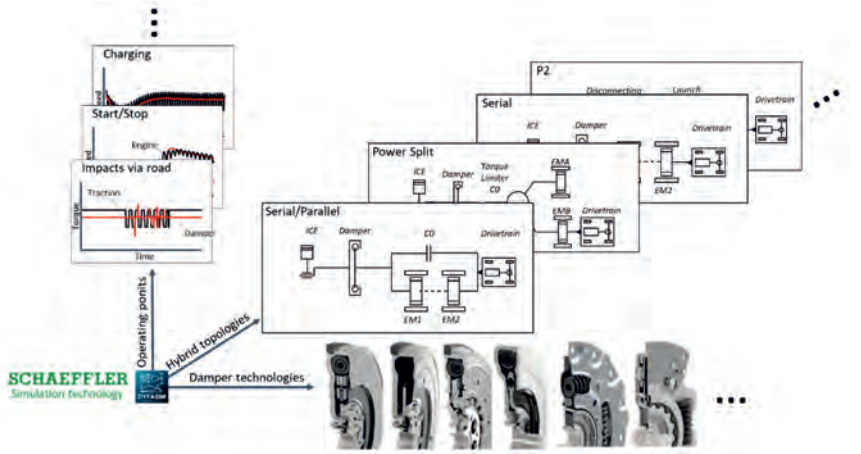

Fig. 1: Dimensions of potential simulation variants within hybrid technology

A further dimension is the selection and evaluation of the appropriate damper topology, starting with arc spring and coil spring dampers considering addons such as predamper stages, friction control units or centrifugal pendulum absorbers, each in their different design versions (Fig. 2). The range of variants of the spanned matrix goes far beyond that of a classic non hybridized powertrain.

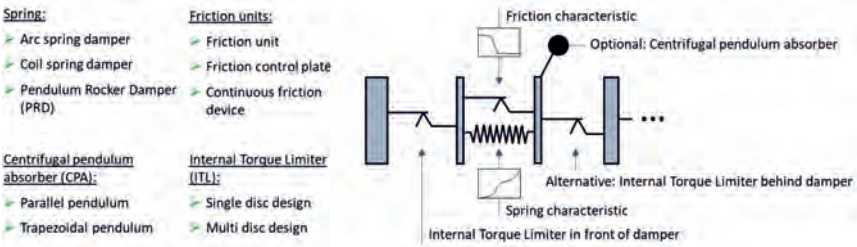

Fig. 2: Schematical damper concepts and technical coupling elements

Physical phenomena and options for optimization

The physical understanding of the dynamic phenomena within the damper system in the environment of the drivetrain is indispensable in defining the mechanical requirement during

damper development. The following figures show in very abstract form relatively simple physical phenomena that must be considered in the development of new damper systems.

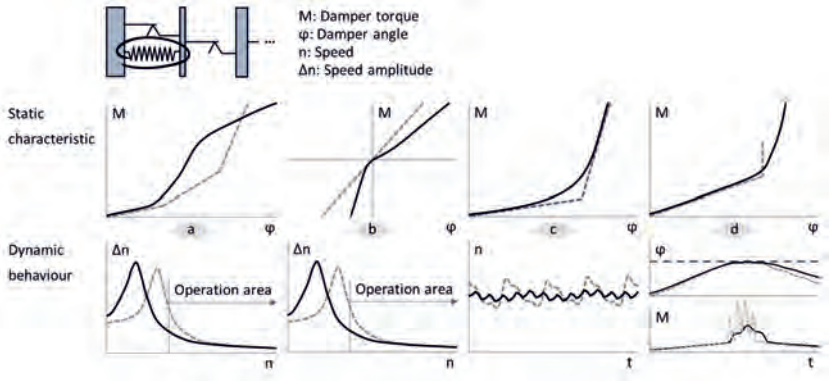

Fig. 3: Principle sketches conerning an optimized spring characteristic
(a: Improved Isolation with degressive characteristic, b: Improved isolation with asymmetrical characteristic; c: Reduced oscillations within soft transition;
d: Reduced impacts via a soft end stop)

For example, jumps in the gradient of the spring characteristic curve (Fig. 3c) should be avoided in order to prevent low frequency oscillations. A soft transition eleminates such problems, which could occur, for example, during charging mode at low loads.

The hybridized powertrain poses new challenges, but also shows potentials with respect to a targeted damper design. Usually, the combustion engine is no longer pulled up via a starter motor on the primary side of the damper. Instead, towing takes place via the secondary side forced by the electric motor or a clutch. In the new constellation, the damper is thus driven to the coast side during the starting process. This means that, for the purpose of isolation, a damper can be operated with the lowest possible friction on the drive side (Fig. 4a), while the coast side can be equipped with relatively high friction to improve the start process without any further disadvantages (Fig. 4b). In addition, it is conceivable to design the characteristic curve asymmetrically or even degressively for optimum utilization of the available spring energy with regard to improved drive isolation (Fig. 3a&b).

Another aspect are possible impacts caused by misfiring or wheel excitation (e.g. uneven road in conjunction with ABS braking). If hybrid drivetrains do not contain any separating elements in the form of a friction clutch (e.g. power splitters) or if dog clutches are preferred instead of friction clutches, additional measures are usually required to protect the damper and the transmission elements from high torque peaks. Here, a bumper stage integrated into the damper characteristic curve (Fig. 3d) and/or an integrated torque limiter (Fig. 5) can be an indispensable measure.

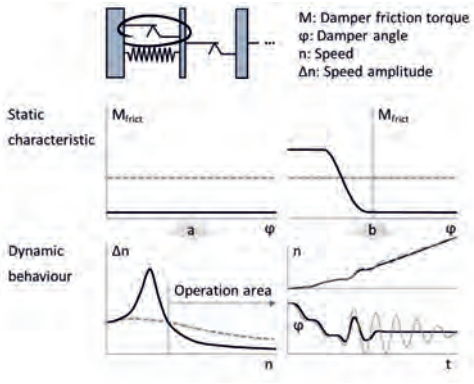

Fig. 4: Principle sketches concerning an optimized friction characteristic (a: Improved isolation with low friction; b: Improved start behaviour with asymmetrical friction)

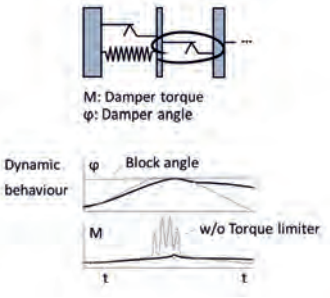

Fig. 5: Principle sketches concerning the potential of an additional torque limiter

Irrespective of the principles presented, a simulation based design including the verification of all relevant operating conditions is essential in all future application. The correct mapping of inertia distributions and elasticities in the powertrain plays an important role here. In particular new hybrid concepts entail risks and must be appropriately validated by simulation. The avoidance of these risks and the supply of optimum solutions for all hybrid topologies is the aspiration of Schaeffler.

2. A new torsion damper concept: The Pendulum Rocker Damper (PRD)

In order to avoid damage and disturbing noise, the main task of torsion dampers within drivetrains is to keep irregularities of the combustion engine away from the driven components. The best decoupling usually is given by a supercritical behaviour by means of a soft connection between the exciting system and the system, which has to be protected. This

means that always the torsional stiffness of the damper connecting the masses of inertia of the system has to be designed as low as possible. However, the need to cover the maximum torque requires an accordingly high torsional angle at the same time. Therefore, the spring elements have to offer a sufficiently high energy capacity to provide the desired torsional characteristic. So, in general, the performance and the flexibility in the application are strongly linked to the torsional angle and the energy capacity of the springs that can be implemented. In the following sections a new torsional damper concept based on an innovative coil spring actuation is presented, that pushes existing limits in terms of torsional angle, spring energy, realizable torsional characteristics and unwanted external friction, thus generating new options in the design of efficient torsion dampers for hybrid powertrains.

Principle

On the left of Fig. 6 the basic design of a torsion damper with the essential parts needed to represent the new concept for coil spring actuation is shown. In order to explain the kinematics of the mechanism a corresponding translatory model is illustrated on the right. The torque appears like a force and the torsional angle like a displacement. Furthermore, some equations are given which explain the basic system properties also mathematically.

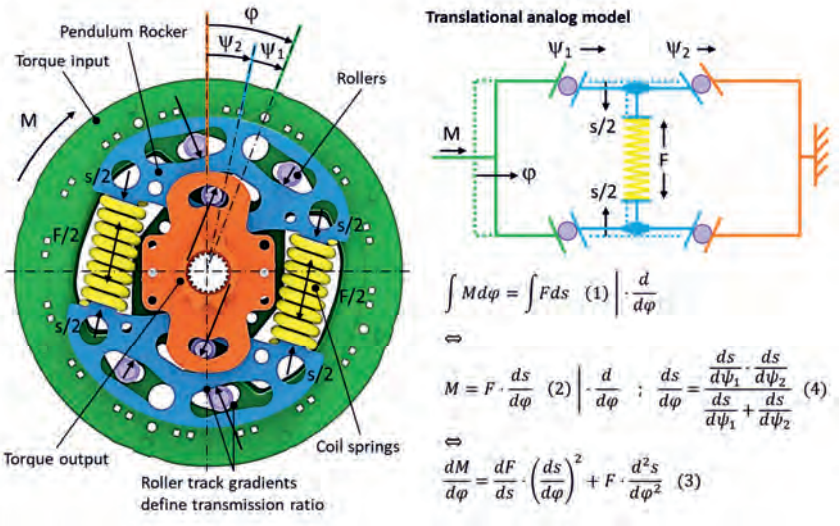

Fig. 6: Principle of a new concept for representing the torsional stiffness of a torsion damper

The general operation principle is as follows: When the side plates (torque input elements) are rotated a torsional angle ψ_1 is generated. Simultaneously a 1st cam mechanism equipped with 2 x 2 rollers controls the motion of two opposing intermediate elements called pendulum rockers in such a way, that the coil springs placed in between, are actuated increasingly and always in parallel. This requires a certain torque which is introduced from the side plates via the 1st cam mechanism into the unit consisting of pendulum rockers and coil springs. This torque is subsequently transmitted into the flange towards the hub (torque output element) via a 2nd cam mechanism equipped with 2 x 1 roller. In order to ensure a kinematically compatible motion process, the 2nd cam mechanism is designed in such a way, that the unit of rockers and springs rotates with respect to the hub. Thereby a torsional angle ψ_2 is generated and the pendulum rockers perform the very same motion towards the springs already caused by the 1st cam mechanism. Overall, with the cam mechanisms a transmission ratio from torsional into translatory direction and a corresponding force actuation of the coil springs is realized, which generates a targeted torsional characteristic.

Transmission Ratio

The changes in coil spring travel s with the corresponding torsional angle ψ_1, ψ_2 can be considered as the transmission ratios of the cam mechanisms. The resulting total transmission ratio is given in equation (4) and represents the fact that the two cam mechanisms act in a series connection (Fig. 6). Equation (1) states the basic fact that the energy required to apply a torque M along a torsional angle φ has to be found in the stored energy of the coil springs as a result of applying the force F along the actuation s. The derivative of equation (1) with respect to the torsional angle gives a direct correlation between coil spring force and torque depending on the total transmission ratio, which is shown in equation (2). The derivative of equation (2) again with respect to the torsional angle finally leads to equation (3), in which the instantaneous torsional stiffness turns out to be a function of spring rate, transmission ratio, spring force already achieved and change in transmission ratio. It is not a surprise that the torsional stiffness depends on the spring rate, but unlike conventional torsion dampers, where the spring installation radius means a fix correlation, the effect of the spring rate on the torsional stiffness can be varied almost arbitrarily within the Pendulum Rocker Damper by means of the transmission ratio embodied by the roller track gradients. The following sections will show how this leads to completely new options for defining useful torsional characteristics.

Torsional angle

The total torsional angle φ between the side plates and the hub turns out to be always the sum of the torsional angles ψ_1, ψ_2 occuring within the two cam mechanisms respectively, which is a result of the series connection. Choosing a low transmission ratio the available spring travel can be transformed in significantly higher torsional angle than known from conventional coil spring dampers. The limiting factor for the torsional angle is no longer the spring travel on a certain installation radius but rather the representable length of the roller tracks in side plates, flanges and rockers. Asymmetrical roller tracks with respect to the neutral position at zero torque easily allow to provide different characteristics for drive and coast in terms of covered torque, torsional angle and torsional stiffness. Roller track length, i.e. torsional angle, that is not necessarily required on coast side, can be added to the drive side. Still both sides can profit from the whole energy of the coil springs. The latter is not possible with conventional coil spring dampers.

Spring energy

When the torque is transmitted from the side plates to the unit consisting of pendulum rockers and coil springs and further to the flange and hub, the coil springs are not in the direct torque flow. They only supply the energy required to rotate the torque input with respect to the torque output. So, for the effect of the spring rate on the torsional stiffness the installation radius of the coil springs doesn't matter. Accordingly, the coil springs can be placed wherever the most installation space is available for maximizing their energy content. Coil springs for conventional dampers usually are designed to provide a certain force together with a minimized spring rate according to the torque to be covered and the intended lowest torsional stiffness possible by exhausting the tolerable material stresses. However, given a feasible length and outer diameter and keeping the producibility in mind coil springs do have their maximum energy, when the tolerable material stresses are exhausted and the spring travel is only about 20% of the initial length. The consequence is, that energy-maximized coil springs have comparatively high wire thicknesses and short spring travels. The resulting spring rates in combination with a corresponding installation radius would be by far too high being able to serve as torsional stiffness in a conventional coil spring damper for passenger car applications. Reducing the effects of the spring rate on the torsional stiffness by means of the transmission ratio within the PRD, energy maximized coil springs become applicable here. In addition, the coil springs are actuated exclusively in parallel. No stresses from transversal and angular deflection have to be taken into account, when the tolerable material stresses in spring design are exhausted.

Torsional characteristics

Fig. 7 shows an example of several torsional characteristics for the drive side all designed for an engine torque of 180 Nm, an end stop torque of 300 Nm, a torsional angle of 30° and an energy content of 37 J. The upper two characteristics represent what can be achieved at high expense with today's standard torsion dampers by means of adapted torsional stiffnesses here in e.g. 3 stages. The constant torsional stiffnesses within a stage increase abruptly and disturbingly at the stage transitions due to the addition of further springs with generally different spring rates, which at the same time means a restriction to progressive characteristics in all conceivable variants. Whereas the lower two characteristics show what is possible with the Pendulum Rocker Damper, where the torsional stiffness is given by the coil spring characteristic and the series connection of the transmission ratios in the cam mechanisms. Since the transmission ratios can be designed variably via the torsional angle, non linear torsional characteristics with continuously variable gradients are feasible with linear coil spring characteristics. In this way, continuously progressive as well as progressive-degressive torsional characteristics can be represented.

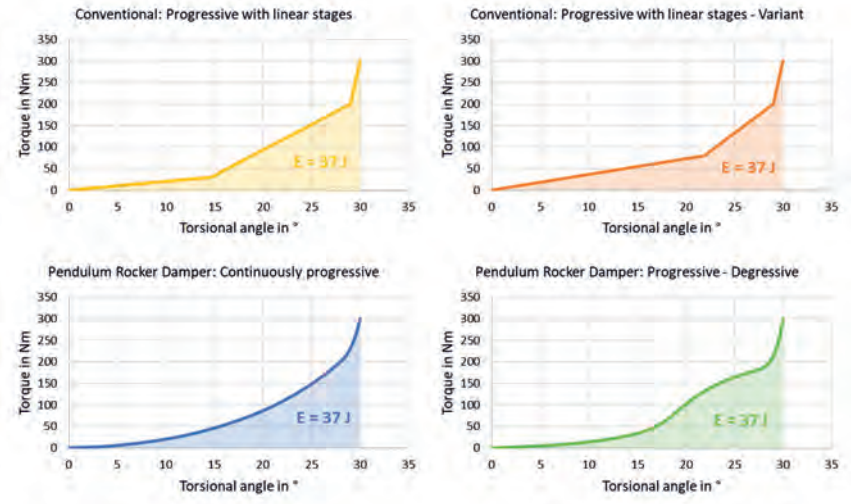

Fig. 7: Options for variation of the torsional characteristics with conventional dampers and with Pendulum Rocker Damper for a given torque, torsional angle and spring energy

Thanks to the Pendulum Rocker Damper mechanism one and the same coil springs can provide for example an area with a very low gradient for stationary charging of the battery at low torque, a continuous transition towards a degressive section with adapted gradients corresponding to the engine non uniformities via torque for drive operation and, subsequent to the lowest gradient at full torque, a continuous transition to an end stop area for reducing peak torques during impacts. In other words, a torsional characteristic can be represented that has been simply impossible until now. A characteristic with variable gradient, and in particular a degressive section, allows the available spring energy to be distributed to the torque levels where it is needed to provide a required torsional stiffness without wasting it where it is not needed and as a result unnecessary torsional angle is created.

Roller Track Derivation

The method to derivate appropriate roller tracks to achieve a desired torsional characteristic is strictly based on the conservation of energy and the application of roller kinematics. At each point in the torsional characteristic given by a torsional angle, the corresponding torque and the shape of the characteristic up to there, the energy applied so far is stored in the coil springs. In this manner, the spring actuation which has occurred to that point can be calculated. So, given a spring rate and following the torsional characteristic step by step the complete necessary motion of the pendulum rockers actuating the coil springs can be derived. Starting with an initial roller position and specifying the motion of the pendulum rocker relative to the side plates and flanges respectively the roller tracks in all parts involved can be computed by integrating the corresponding contact point velocity conditions that must be fulfilled to guarantee pure rolling.

Roller contact pressure

Each pendulum rocker is in contact with 3 rollers that clearly define its position and rotational orientation. The rollers establish contact forces in response to the spring forces according to the force and torque balance of the pendulum rocker. These roller contact forces act in normal direction of the roller track surface. Their circumferential components represent the transferred torque, their components in direction of the coil spring axes equal the spring forces. Depending on the roller diameter, the roller profile and the sheet thickness of the counterparts these forces imply certain contact pressures and Hertzian stresses that could lead to wear and damage of the parts during their service life. Extensive investigations on test rigs under real operating conditions and accompanying calculations on damage accumulation based on real driving cycles led to clear specifications for allowable contact

pressures as well as corresponding roller profiles, materials and heat treatments which enable a life time resistant design of the parts building the roller contact.

External Friction

The spring actuation within the Pendulum Rocker Damper exclusively is based on the motion of bodies rolling freely on each other by means of roller equipped cam mechanisms. The external friction is correspondingly low even at high speeds. This ensures an excellent decoupling effect in the supercritical speed range that usually is significantly reduced by increasing external friction at higher speeds with conventional torsion dampers. Also, the parts in contact with the coil spring ends do not alternate, when the load direction changes from drive to coast or vice versa. This means significantly less wear than otherwise occurs on spring guiding elements of most conventional torsion dampers.

Innovative Friction Device

It is obvious that the Pendulum Rocker Damper with its continuously adjustable torsional stiffness would perfectly work together with a similar type of friction device, where the hysteresis continuously is adapted to the operating points and the prevailing gradients. For the following reason, this challenge arises anyway. Since the very same components rotate relative to each other over the entire torsional angle of the PRD, it is no longer possible to create different hysteresis levels having the components of several friction devices consecutively perform relative rotation in separated stages with the corresponding friction surfaces each being subjected to the axial force of an own diaphragm spring or wave washer. Here, Schaeffler has developed an innovative solution, where the axial force of a single diaphragm spring is modulated depending on the torsional angle in such a way that, for example, a low hysteresis on the drive side for perfect drive isolation as well as a significantly higher hysteresis on the coast side to manage start impacts are generated within one single friction device.

3. Application Examples

This chapter gives two examples of the PRD being applied within an established and forward looking dedicated hybrid transmission (DHT) concept respectively each including an integrated torque limiter (ITL) at different locations in order to protect the drivetrain from torque peaks during impacts.

Fig. 8 shows a PRD designed to be placed between the internal combustion engine (ICE) and the planetary gearset of the well known power split transmission which also is connected to two electric machines that serve either as motors or generators and control the speed of the internal combustion engine so that it can operate in an efficient range. In this application the ITL is located in front of and radially outside the actual PRD. It consists of a single friction disc clamped between two friction facings that are placed in between the side plates together with a support plate and a diaphragm spring that generates the clamp load. The connection of the friction disc to the crank shaft is done via an inertia ring which is not shown here.

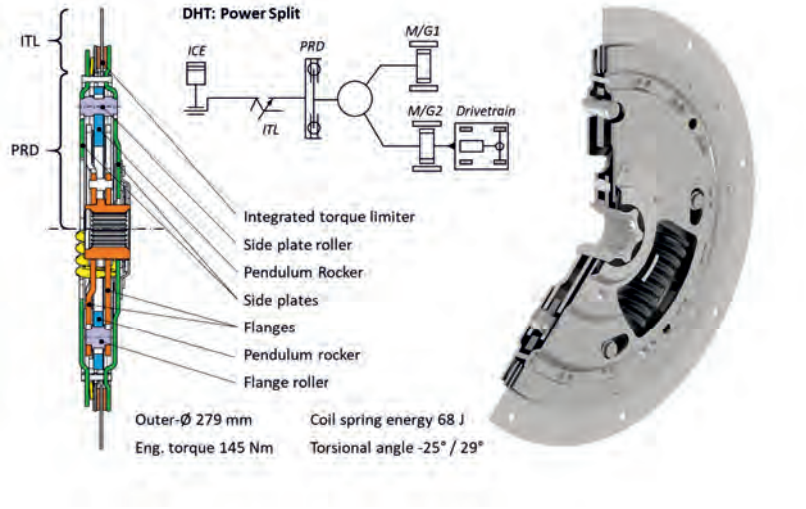

Fig. 8: PRD combined with a single disc torque limiter in front of the damper

Since the side plates in their outer diameter area have to support the friction facing and the diaphragm spring respectively along the whole circumference, they are designed as two full discs held at a certain distance by a plurality of spacer sheets to exactly define the gap for installation of the torque limiter parts. Therefore, the side plates do not only contain the roller tracks of the 1st cam mechanism but also two cut outs for the two springs are necessary. These cut outs do not touch or introduce forces to the springs. They just give the space for their length and diameter under consideration of the relative rotation between the side plates and the unit of rockers and springs. The torque flow within the PRD is from the side plates via the side plate rollers to the rockers and from the rockers via the flange rollers to the

flanges which are connected to the hub each by means of a spline. The two springs are outside the torque flow but supply the forces and the full energy for creating the torsional characteristic.

An even more compact design is given in Fig. 9 for an application where the PRD is placed between the ICE and a DHT that allows operation in both serial and parallel mode. Here, the ITL is located behind and radially inside the actual PRD. It consists of multiple friction facings connected via outer splines to a housing and alternating with friction discs connected to the transmission input shaft via inner splines, all clamped by a diaphragm spring between housing and the flange to which the housing is riveted.

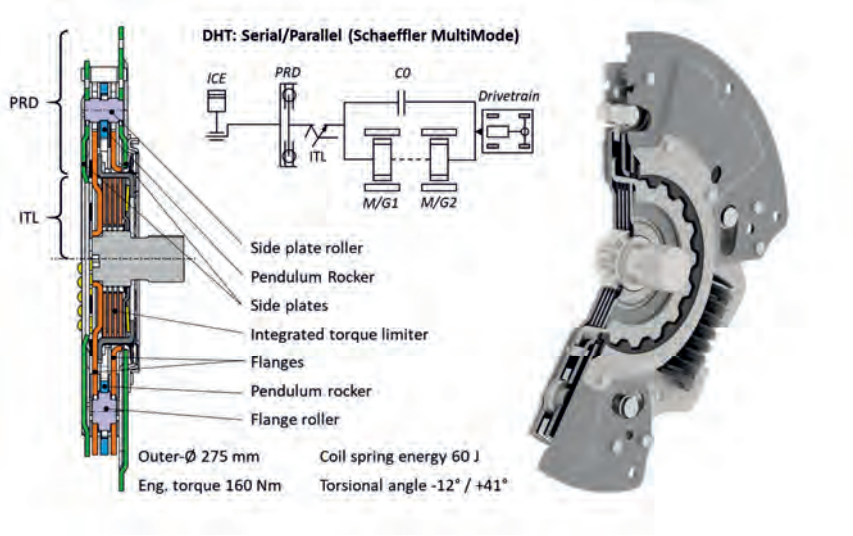

Fig. 9: PRD combined with a multiple disc torquer limiter behind the damper

The torque flow within the PRD is unchanged compared to the previous example and again only two springs outside the torque flow supply the full energy for the torsional characteristic. Since here the side plates of the PRD don't serve as a component of the ITL, they can be designed optimized in terms of material usage and weight. Several corrugations increase the stiffness of the side plate in the area where they still offer the roller tracks for the 1st cam mechanism. In the recessed area, they now allow an unrestricted view of the spring

actuation. In addition to centering areas for the spring inner diameters, the pendulum rockers have fingers that secure the springs against radial displacement under centrifugal force.

In both designs shown in Fig. 8 and Fig. 9 all rollers present 3 running surfaces with two differing diameters. The one in the center is in contact with the pendulum rocker and the two outer ones are in contact with the two mating side plates and flanges respectively. In addition to the diameter step, the running surfaces are separated by little shoulders that ensure a proper axial guidance of the parts. In both designs a friction device is riveted to the side plate on transmission side that is driven according to the damper's torsional angle by an outer spline of the hub and the housing respectively.

4. Simulation Examples

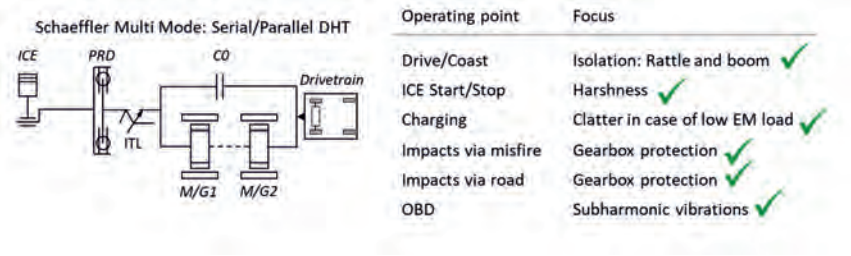

Fig. 10: Structure of a serial parallel hybrid topology (Schaeffler Multi Mode) including an overview of all relevant operating points and potential issues

The example of a serial parallel hybrid topology shows the result of an optimization calculation. The system is delivering very good efficiency in pure EV mode which makes it advantageous especially for plug-in hybridization (Fig. 10). It has one internal combustion engine and two electric machines, which are optionally connected via a C0 clutch. When the clutch is closed, the combustion engine and electric machines can be operated in parallel mode. In serial mode, the clutch is open and the E-machine 1 is operated as a generator while the E-machine 2 drives the vehicle. In this case, the internal combustion engine can basically be brought to the optimum operating point in terms of speed and torque. All relevant operating points (Fig. 10) were evaluated by simulation with regard to defined target values.

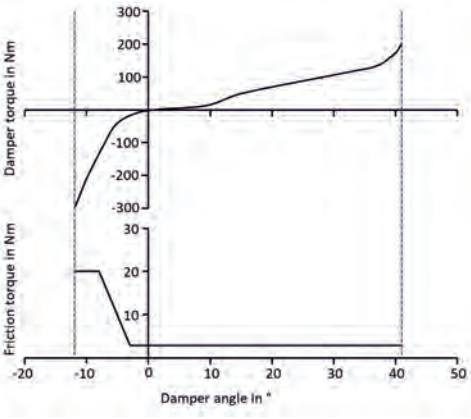

Fig. 11: Spring and friction torque characteristic

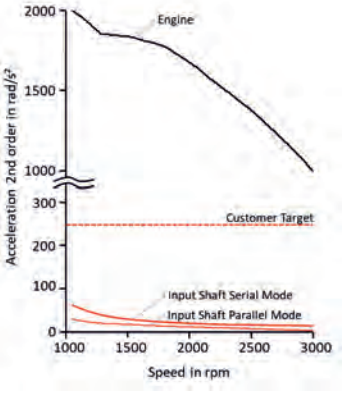

Fig. 12: Simulated full throttle isolation of a specific design

Fig. 11 shows how the drivetrain isolation is optimized by an asymmetrical and at the same time degressive characteristic curve on the drive side of the damper characteristic with respect to boom noise. Simultaneously the hysteresis is closely tolerated to low values. A friction device acting on the coast side of the damper characteristic can be used to bring the start process to the target independently of the train isolation with respect to e.g. longitudinal vehicle vibrations and clatter noise.

Figures 12, 13 and 14 show the corresponding basic simulations. The results concerning isolation and start are in good agreement with the customer and Schaeffler expectations.

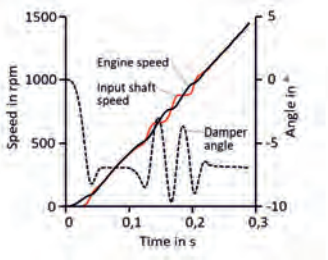

Fig. 13: Simulated ICE start performance

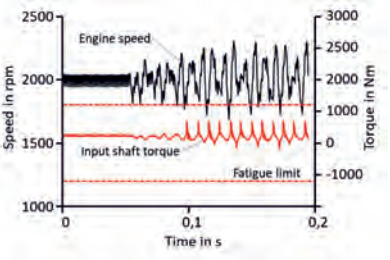

Fig. 14: Simulated ICE misfiring

Particular attention must be paid to the meshing between the internal combustion engine and the electric motor 1. Periodic lift off as a result of the internal combustion engine excitation

must not occur here. This would result in a clatter noise. In principle, it is necessary to ensure a certain preload of the drivetrain and thus of the backlashes. For this purpose, the E-machine 1 and/or E-machine 2 must be operated as an electric motor or generator with a minimum load via the operating strategy.

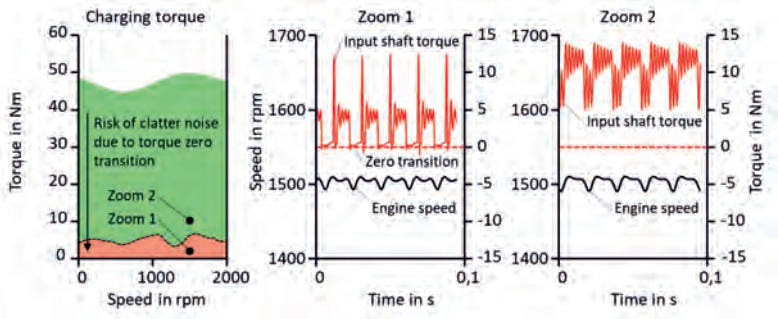

Fig. 15: Simulation result concerning charging (Zoom 1: Critical operating point; Zoom 2: Uncritical operating point)

Fig. 15 shows the necessary preload of the E-machine 1 at this operating point using the example of stationary charging. Due to the flat entry into the characteristic curve of the PWD and the smoothed transition into its steeper branch, the PWD ensures good isolation of the combustion engine excitation and avoids low frequency oscillations. As a result, the torque oscillation in the transmission and thus also the necessary preload torque can be reduced to a minimum.

5. Conclusion

Simulation technology has been an integral part of the product development process at Schaeffler for decades. The physical understanding of the dynamic phenomena within the damper system in the environment of the drivetrain is indispensable for defining the mechanical requirements during damper development. In particular new hybrid concepts entail risks and must be appropriately validated by simulation. The avoidance of these risks and the supply of optimum solutions for all hybrid topologies is the dedication of Schaeffler.

The PRD is a technical solution that can basically match all requirements in a new manner without the compromises of the past technologies. Due to its modularity and flexibility in design, the PRD can be optimally configurated to all customer targets. Furthermore, a

chosen basis PRD topology can be easily tuned to the specifics of different applications. Therefore, mainly the spring capacities and the roller tracks are adapted.

New challenges in the context of powertrain electrification require new solutions. One solution has been found impressively with the development of the PRD in close exchange between simulation and design.

References

[1] Rusch, A., Häßler, M., Kessler, M.: Torsionsschwingungsdämpfer, Deutsches Marken- und Patentamt, DE 10 2015 211 899 A1, Offenlegungsschrift, 2016

[2] Kooy, A., Seebacher, R.: Minimize Torsional Vibrations – Full Isolation if Necessary, VDI-Berichte 2354, pp. 313 - 328, VDI-Congress Dritev, July 10 and 11, Bonn, 2019

[3] Kooy, A., Eireiner, D., Krause, T., Herbers C., Vögtle, B.: Torsional Damping for all relevant Powertrains – Extending current Damping Technologies, VDI-Congress Drivetrain for Vehicles, June 21 and 22, Friedrichshafen, 2016

[4] Faust, H.: Forming the Transformation – How Electrification Changes the Portfolio of Transmissions, VDI-Congress Dritev, June 24 and 25, virtual Event, 2020

Modular Starting and Damping System integrated in 48V Hybrid Architectures

Efficient Starting System for Hybrid Vehicle Architectures

Dr.-Ing. **Tobias Kaufhold**, M.Sc. **Florian Schneider**,
B.Sc. **Oliver Groneberg**, Dipl.-Ing. **Alexander Moser**,
BorgWarner Drivetrain Engineering GmbH, Ketsch

Zusammenfassung

BorgWarner hat eine Permanent Eingespurte Startkupplung (PES) entwickelt. In Verbindung mit einem vereinfachten Ritzelstarter weist dieses effiziente Verbrennerstartsystem keine Verluste bei und über Leerlaufdrehzahl auf. Der PES befindet sich zwischen Motor und Getriebe und ermöglicht riemenlose sowie axial-bauraumoptimierte Verbrenner-konfigurationen. Die Integration eines Zweimassenschwungrads (ZMS) mit dem PES bietet zusätzliche axiale Bauraumvorteile. Weiterhin sind serielle Anordnungen des PES mit ZMS oder Drehmomentwandlern möglich, sodass das Startsystem in CVT-, DCT- und AT-Anwendungen verwendet werden kann.

Abstract

BorgWarner has developed a Permanently Engaged Starter clutch (PES). In conjunction with a simplified pinion starter, this efficient ICE starting system has no losses at and above idle and a good cold start performance. The system is located between the ICE and the transmission, enabling beltless and axial space optimized ICE configurations. The integration of a Dual Mass Flywheel (DMF) with the PES offers additional axial design space saving advantages. Furthermore, serial arrangements of the PES with DMFs or torque converters are feasible, so the starting system can be used in CVT, DCT and AT applications.

1. Introduction

Hybrid vehicle architectures based on 48V technology are emerging globally. While these systems have their benefits, they must face challenges like limited power in comparison to High-Voltage (HV) applications, [1]. In addition, the pure electric driving range is limited by the smaller battery size, for which reason system efficiency and reduced losses grow on importance, [2]. HV P2 hybrid systems can be quick and powerful enough to start the Internal

Combustion Engine (ICE) without significant torque drop and negative feedback to the driver. In comparison, 48V P2 systems need either an additional ICE starting device or a power reserve for the P2 to deliver comparable comfort at ICE start. The latter has a direct negative impact on the e-driving performance and is therefore not recommended. Today, Belt-driven Starter Generators (BSG) are widely used to start the ICE. Due to the direct connection to the crankshaft, there are system-related losses depending on engine speed, which ends up in a lowered overall system efficiency.

This paper highlights the advantages of the PES-DMF module in combination with a 48V P2 mild-hybrid architecture, which is limited in electric power and battery capacity. For this purpose, a simulation-based comparison is carried out between widespread 48V BSGs and the PES, in terms of functions and efficiency. In addition, the simulation-based PES design process is described, dependent on important design criteria. Also, various DMF integration options are presented and compared. Finally, the differences between 48V and high-voltage hybrid systems, in combination with a PES are discussed.

1.1. ICE Starting Systems

There are various possibilities on the market to start an ICE. The traditional pinion starter, which was state of the art for a long time, is nowadays mostly replaced by the belt-driven starter generator. Also, Integrated Starter Generators (ISG) as well as architectures using P2 e-machines without additional starting device are in the field. Despite the cost benefit, the traditional pinion starter is more and more repressed due to its limited Change Of Mind (COM) performance, durability, and lack of hybrid functionality.

The following functions need to be addressed by an ICE starting system today:

- Cold start, warm start
- Increased amount of starts (> 400k)
- Change of mind start above 100rpm residual ICE speed
- Boost- and generator-functionality (depending on hybrid architecture)
- Fast and comfortable start
- High efficiency and low mechanical losses

1.2. PES Introduction

The permanently engaged starter clutch is a dry roller freewheel clutch system in combination with a simplified pinion starter, located between the internal combustion engine and the transmission. The main functions are the ICE start and the physical starter disconnect. The biggest value added through the PES is its drag free operation at and above idle, while keeping

a beneficial change of mind performance, [3]. The main PES components are: ring gear, dry freewheel clutch system - which consists of preloaded rollers, inner and outer race - and a dry bushing, Figure 1.

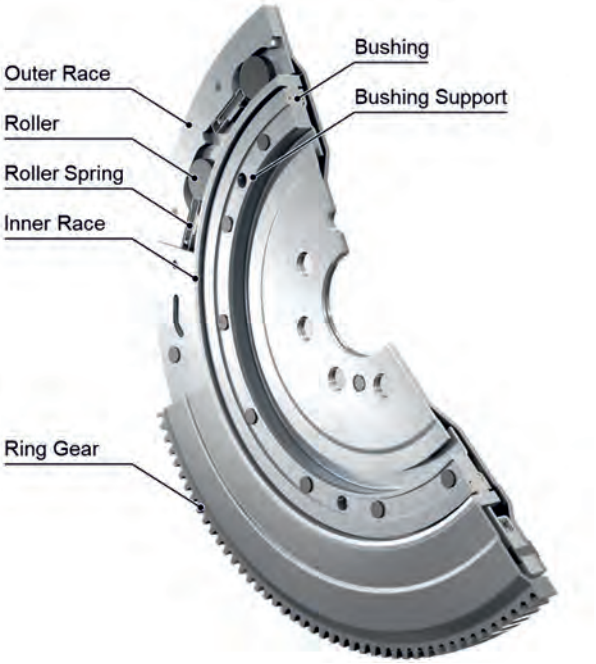

Fig. 1: Cut CAD model showing the main components of the PES

2. PES Design Process

The development of a PES system is divided into six main steps, utilizing state of the art technologies, Figure 2. In the first step, the customer input data like design space and engine torque is used to determine the Hertzian stress and the elastic tilt angle, which results in roller dimensions and quantity as well as inner- and outer-race dimensions. The developed calculation toolbox uses an iterative process which alters the calculation parameters until the desired stress limit and therefore the lifetime requirement is met.

The second step targets the dynamics of the PES in combination with the addressed engine. This step is most important for the NVH behavior of the system and requires the engine start- and idle-oscillations as input for the multi body simulations. Of course, the output of the calculation toolbox like roller and general clutch dimension as well as spring stiffness is used

as input for this simulation. Besides the NVH, there are several other objectives in this step: Verification of the desired lift-off and re-engagement speed to ensure the drag free operation at idle and the best possible change of mind performance, as well as the investigation of the roller dynamics to avoid unwanted roller movements due to resonances. If the multi-body-simulations show unwanted roller behavior, the input for the calculation toolbox (e.g. roller dimensions, spring characteristics, outer race slope) is altered and the simulation is run again. This process is repeated until satisfying results are achieved.

Building on the calculation and simulation steps, the CAD is started. Besides the available installation space, the tolerances and required clearance are important for this task. If there is a conflict with the dimensions of the calculated clutch, the design process is restarted with adjusted input data and verified by MBS.

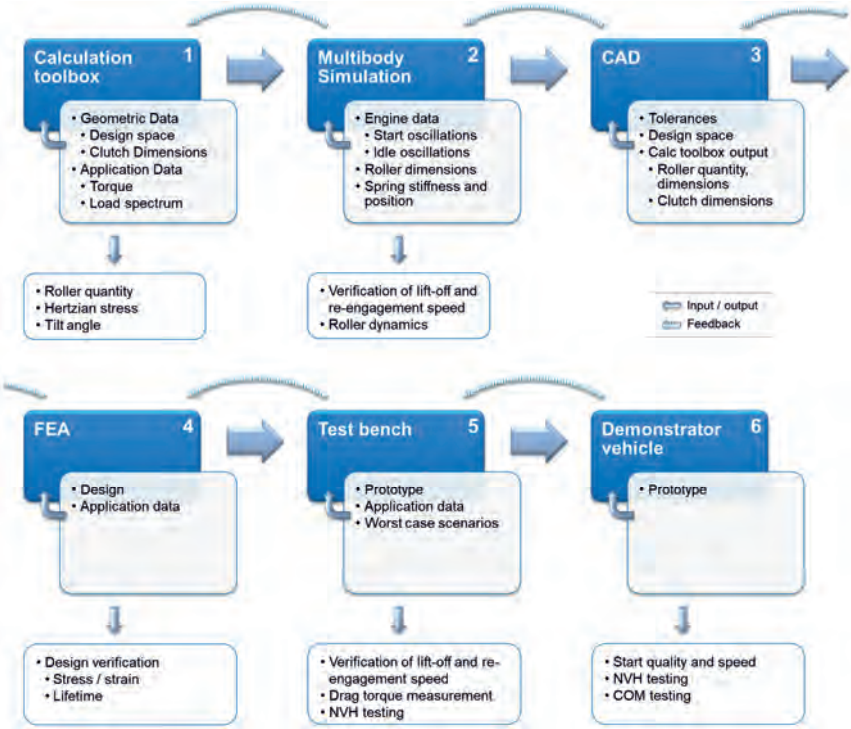

Fig. 2: Six steps of the PES design process with input, output, and feedback of the respective steps

The fourth step targets the verification of the developed 3D model under application specific data. Focus is to investigate the stress on the freewheel components by application of maximum torque and speed. This step is in close collaboration with the CAD step to optimize the design to its full potential.

The analyzed design is built up in first prototypes and undergoes extensive test bench testing for verification. The tests include (excerpt):

- stroker tests: to ensure the main functionality of the system,
- drag torque tests: to ensure the beneficial drag torque behavior,
- speed tests: to verify the design and to measure the lift-off and re-engagement speed of the rollers, and finally
- dynamic testing to check for NVH.

The design process is completed with the verification of the developed product in a demonstrator car under real driving conditions. Therefore, start quality and speed is checked as well as general NVH and COM performance.

2.1. Main Clutch Design Parameters

The main design parameters of the PES related to the efficiency and functionality are roller mass, spring stiffness, spring pre-tension, outer race slope and roller pocket design, Figure 3, [4]. Since the outer race has a direct and permanent crank shaft connection, all these parameters influence the behavior of the roller under increasing or decreasing crank shaft speed and can be adjusted to the target application to deliver best performance.

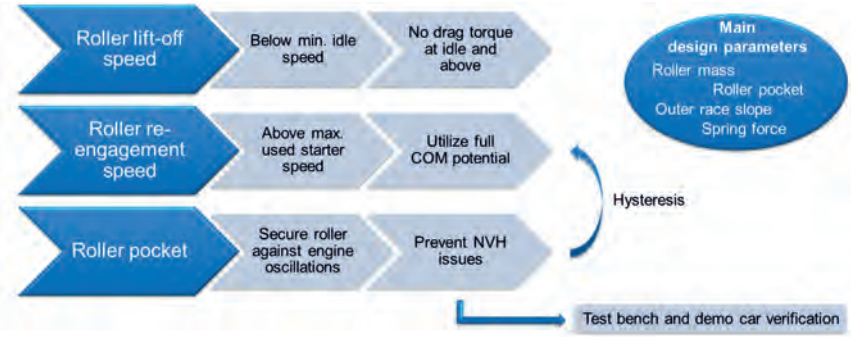

Fig. 3: Main PES design parameters and their influence

To ensure the drag free operation at idle, the roller lift-off speed needs to be below the target idle speed. In this case, the force sum acting on the roller must be dominated by the centrifugal force, thus the roller will move against the spring and roll upwards the slope, Figure 4 middle.

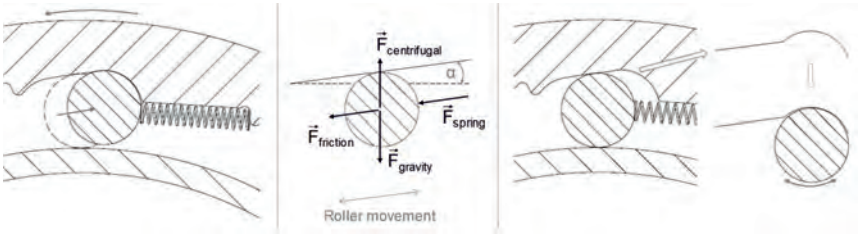

Fig. 4: Left: roller movement under increasing crank shaft speed; middle: forces acting on roller; right: simplified and exaggerated schematic of roller pocket

To ensure the best change of mind performance, the roller re-engagement speed needs to be above the maximum used starter speed and below idle. By increasing the spring pre-tension or reducing the roller mass, the roller will be able to engage at higher speeds, which results in a wider range for COM starts. Lowering the roller mass below a certain level is not recommended, since the impact of friction and contamination rises, which results in a bigger hysteresis between lift-off and reengagement and poor repeatability.

The roller pocket holds the roller in place to prevent NVH issues under certain engine oscillations at low speeds or speed drops in idle. Since the roller pocket layout directly influences the re-engagement speed, it needs to be adjusted simultaneously with the roller mass and spring characteristic.

Figure 5 shows simulation results for an exemplary selected set of input parameters for the PES. The engine in this simulation is a 4-cylinder gasoline engine with 750rpm idle. The blue graph shows the crank shaft speed over time. The engine is fired up with a 48V starter through the PES. After ignition the engine speed is lowered in steps to defined speed levels to verify the robustness of the roller spring system against the engine oscillations. The grey curve shows the movement of the roller over time. During the first ignitions, the roller reacts to the crank shaft accelerations and decelerations. After reaching a certain speed level, it moves into the pocket. It can be observed that the movement after ignition is neglectable. Also, for the oscillations after a speed drop to around 650rpm, the roller is still stable and moves less than 0.5mm between the single oscillations (peak to peak). Low movement in the pocket is necessary to guarantee high durability and low wear over lifetime. After switching the engine

off, the spring pushes the roller back into the engagement position and the PES can perform an COM start at any time below 400rpm crank shaft speed for the selected set of parameters.

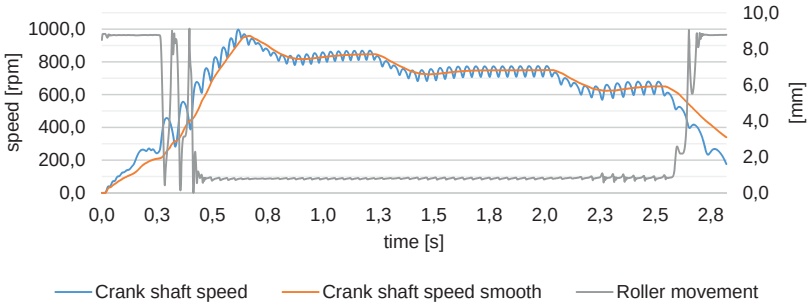

Fig. 5: Results from engine start simulation; speed and movement over time

To verify the drag torque free operation, the contact force between the roller and the inner race is analyzed, Figure 6. The roller is in contact with the inner race due the the pretension of the spring before the engine start. During cranking, the contact force rises since the torque is transmitted from the inner race to the outer race through the rollers. It can be observed, that there is no contact between the roller and the inner race after the engine is started. Re-engagement of the roller can be detected around 2.7s resulting in a force spike.

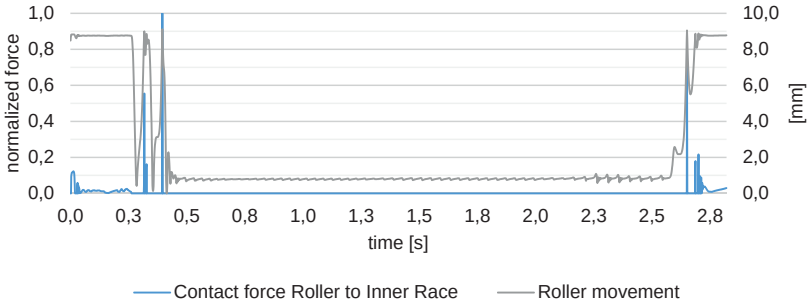

Fig. 6: Results from engine start simulation; force and movement over time

Since there are engine oscillations in the down ramp too, there will be roller movement and therefore a contact force change regarding to the engine oscillations, Figure 7. The highest torque spike between the roller and the inner race occurs around 0.4s during the cranking phase. Since the cranking is a dynamic event were an interaction between the starter, gas

pressure, and mass/inertia forces is present, there can be events where the crankshaft speed will outrun the ring gear speed for a short time. Since the engine is not able to run up by itself at that time, the crank shaft will slow down, and the ring gear speed will match the crank shaft speed again. The PES components are designed to withstand this torque spikes over lifetime. Figure 7 also shows no contact force between the roller and the inner race above 400rpm.

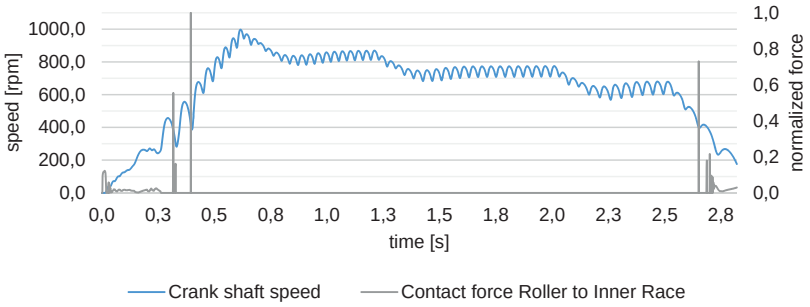

Fig. 7: Results from engine start simulation; speed and force over time

3. BSG vs. ISG vs. PES

The belt-driven starter generator is located in front of the engine and is basically an enhanced alternator with additional functionality. It has a direct and permanent connection to the crank shaft through a belt drive. To transmit high torques, the belt needs high pretension to avoid slipping. The BSG can speed up the ICE to high speeds for late ignition and has good start quality. It also has good COM capability and can be used for load shifting or boosting as well as recuperation. All these benefits, which arise from the permanent crankshaft connection, are faced with speed and torque dependent belt losses. Especially more powerful 48V or HV BSG systems have increased losses since they need higher belt tension to transmit their full torque. To increase the efficiency of an ICE, one option is to remove the Front-End Accessory Drive (FEAD) and therefore eliminate the inherent belt and bearing losses. Doing so, the BSG is no longer available as ICE starting system. As the start system position switches from the ICE front end to the back end, two options are present: the internal starter generator and the permanently engaged starter clutch. Both systems utilize the same position between the engine and the transmission. The ISG features a permanent crank shaft connection like the BSG. However, it has no belt and consequently no belt related mechanical losses. The ISG is capable of all BSG functionalities and delivers the same performance. Since the integration of

the ISG in an existing architecture needs high effort, it is more suitable for new engine designs and not revisions.

The PES is located between the engine and torque converter or dual mass flywheel. The starter which is required for the PES utilizes the traditional pinion starter position, Figure 8. On consideration of an DMF, the ring gear is moved to the PES and the remaining DMF stays unchanged. The PES is easy to integrate in existing architectures but also an option for new designs. Since the PES is a passive system, the start performance is directly determined by the starter power and overall specification. For example, a 48V starter can be capable of starting crank shaft speeds over 400rpm to ensure good start quality and low emissions during start.

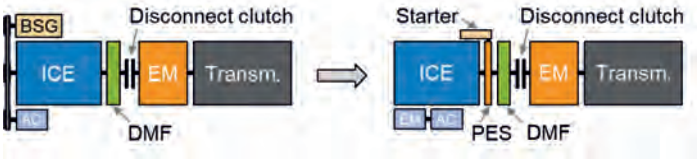

Fig. 8: Visualization of PES Position in comparison to a BSG and removal of the FEAD

The starter, which is essential for a PES system, is a simplified version of a traditional pinion starter. Since the pinion does stay engaged in the ring gear, the pinion engagement magnet and lever mechanism aren't needed anymore, which results in a cost reduction for the starter besides the simplification. Also, the PES starter gets a more cylindrical shape and is even easier to integrate into existing architectures.

3.1. Fuel Economy Simulation

To compare the BSG and PES in terms of fuel economy, several detailed WLTC simulations were carried out. The considered architectures are based on a 48V P2 in combination with a 1.5l and a 2.0l gasoline four-cylinder engine with an eight-speed transmission and vehicle data from a mid-sized SUV, [5]. The 48V BSG has 10kW and is combined with a seven ribs belt with about 300N pre-tension. For better comparison of the losses between the systems, the BSG is not used for boosting or recuperation in the simulations. All hybrid functions are realized by the P2. Figure 9 shows the mechanical losses of the BSG and PES in dependency of the engine speed. Due to the direct and permanent crank shaft connection of the BSG, the mechanical losses rise with engine speed. In contrast, the PES has only small losses during start phase which are induced by the radial forces of the pinion and ring-gear connection which results in minor drag torque of the dry friction bushing. After engine start, the ring-gear and the

starter are disconnected by the clutch and therefore the bushing speed is zero. In the cycle, the engine is restarted about 57 times and has a total running time of about 940s.

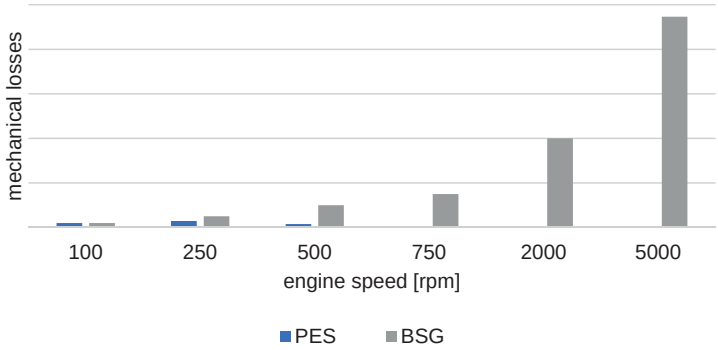

Fig. 9: Mechanical losses of PES vs. BSG

The outcome of the WLTC simulations shows that for both engines more than one percent of fuel can be saved by using the PES instead of the considered BSG system. Keeping in mind, that the WLTC is not very dynamic and that the engine speed is mainly below 2000rpm during the cycle, the fuel saving potential is even bigger under real driving conditions, meaning that this result can be interpreted as a minimum saving.

4. PES in 48V and HV P2 Hybrids

Depending on the desired e-driving range and performance as well as cost target for the considered car or segment, different voltage levels are used to integrate hybrid functionalities. 12V hybrid systems are very limited in power and therefore in their e-driving capabilities but have lowest cost. Due to the rising CO2 regulations, 12V systems are not powerful enough to reach a certain level of electrification as well as e-driving performance. Therefore, such systems are not further considered. Current 48V P2 systems have power ratings up to 25kW and are capable of local emission free driving, [2].

HV systems deliver the highest power and thus best e-driving performance but this performance is paid with high system cost. Also, there are HV hybrids on the market, which feature no starting system in addition to the P2 EM, since the used P2 in these plug-in hybrids is powerful enough to reliably start the ICE under any condition. This means, the PES targets only such HV hybrid applications which benefit from an additional starting device, like lower power HV hybrids. Because the power level of 48V architectures is limited, an additional

starting system is beneficial for this voltage level. Main reason is the ICE restart from electrical driving. If no additional starting device is present, the P2 cannot be used to its full potential since it must be able to start the ICE anytime. Thus, a certain power reserve is kept, to realize a fast and comfortable restart. This power reserve will strongly limit the e-driving capabilities of the vehicle.

4.1. PES-DMF Integration

Through removal of the FEAD and usage of the PES, the overall axial system length can be reduced. Due to the positioning of the PES between the engine and the transmission, the PES needs additional axial space in this area, but no space in front of the engine. The required design space depends on the specific application and the chosen integration option:

- Standalone PES with flex plate connection: bolted on crank shaft and torque converter
- Standalone PES with flex plate connection: bolted on crank shaft and DMF
- PES-DMF module with parallel integration
- PES-DMF module with concentric integration

An overall optimized axial space usage can be achieved by integration of the PES with a DMF. Doing so, no clearance between PES and DMF parts is needed and it is even possible to reduce part count since functionality and parts can be shared between both systems. Consequently, a PES-DMF module will always require less axial space than standalone side by side versions.

The selection and implementation of a parallel or concentric layout depends not only on the given design space but also on the peak ICE torque. Small engines with low torque have no need for big dampers. In that case, the PES utilizes the radial space around the damper and only needs minor additional axial space, Figure 10.

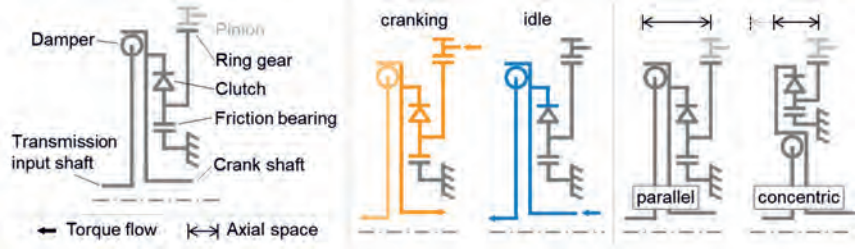

Fig. 10: Left: schematic of PES-DMF module; middle: torque flow during cranking – orange, and in idle – blue, grey parts are stationary; right: axial length difference for parallel and concentric layout

Depending on the damper design, the integration of the PES can also be possible with almost no additional axial space in the concentric configuration. For high torque applications this layout may be not feasible due to the bigger working diameter of the damper. In this case, a concentric layout would cover up more radial space.

In both layouts the PES-DMF-Module shares the damper shell as common part between PES and DMF. The shell features a rivet connection to the outer race and the cover plates and connects these parts with the crank shaft. Therefore, the flex plate of the standalone PES can be omitted. Figure 11 shows a cut CAD model of the parallel layout. This module was built and tested in several demonstrator vehicles.

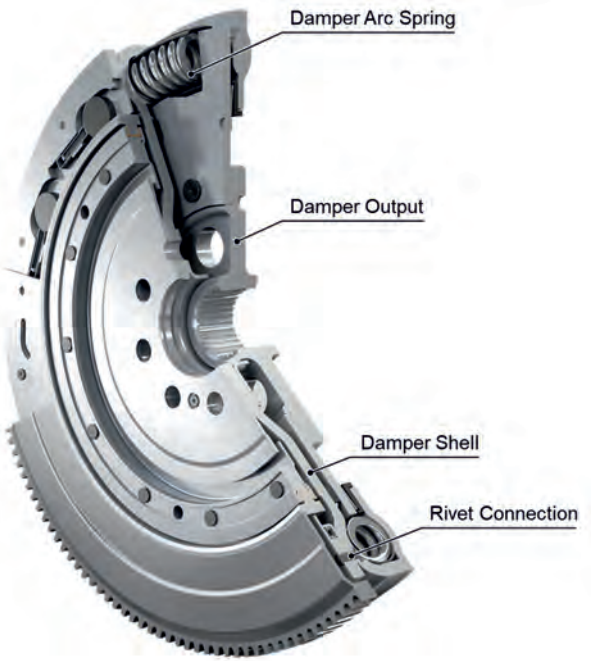

Fig. 11: PES-DMF-Module, parallel layout

5. Conclusion

The permanently engaged starter clutch is an efficient ICE starting system in combination with a simplified starter. Due to its positioning between the engine and the transmission, it offers the opportunity to realize beltless engines. The biggest value added through the PES is its

drag free operation at and above idle, while keeping a beneficial change of mind performance. In comparison to a BSG, it reveals a fuel saving potential of about one percent in the WLTC. The PES should not be seen as a replacement for all BSG applications, it is more of an additional option to choose from. The different integration options with DMFs help to realize axial space optimized hybrid configurations. 48V and low power HV hybrid architectures benefit from an additional starting system to maximize the electrical driving performance.

References

[1] Dilzer, M.: BorgWarner P2 Modules – from HV to 48V. VDI dritev, Bonn, 2021

[2] Spangler, C.A.: Borg Warner's P1 and P2 Hybrid Drive Modules Modular Kit for P1 and P2 Hybrids. VDI dritev, Bonn, 2020

[3] Bäumler, R.; Moser, A.; Schäfer, M.: Dry running, Permanently Engaged Starter System (PES) for a comfortable start of combustion engines providing further potential to reduce fuel consumption, Motortechnische Zeitschrift, 12/2014

[4] DE-P 10 2015 011 415 A1, US-P 10 385 933 B2, CN-P 106481690 A

[5] Bongards, A.: Comparing 48V Mild Hybrid Concepts using a Hybrid-Simulation-Toolkit. Stuttgart International Symposium, Stuttgart, 2019

Driveability optimization of electrified powertrains utilizing machine learning based control and the interaction with ADAS/AD systems

M. Sc. **Xianfeng Zhang**, Prof. Dr.-Ing. **Ferit Küçükay**,
Institute of Automotive Engineering,
Technische Universität Braunschweig

Zusammenfassung

In den letzten Jahren wurden elektrifizierte Antriebsstränge aufgrund ihrer hervorragenden Kraftstoffeffizienz und Emissionsreduzierung zunehmend eingesetzt. Es gibt viele verschiedene Architekturen und Merkmale elektrifizierter Antriebsstränge, wie z. B. Add-on, DHT (Dedicated Hybrid Transmission) und andere Hybridlösungen. Im Vergleich zu konventionellen Antriebssträngen nutzen elektrifizierte Antriebsstränge die inhärenten Eigenschaften der EM, um die mechanischen Komponenten in Bezug auf Start, Rückwärtsgang und Synchronisierung zu eliminieren. Der Wegfall dieser mechanischen Komponenten hat jedoch große Auswirkungen auf das Fahrverhalten, wie z.B. die Schaltqualität und die Drehmomentübertragung, und führt zu Schwingungsproblemen, die wiederum Probleme beim Fahrverhalten verursachen und gleichzeitig hohe Anforderungen an die Steuerungs- und Kalibriertechnik stellen.

In diesem Paper werden wir zunächst die verschiedenen elektrifizierten Antriebsstrangkonfigurationen vorstellen und dann das Fahrverhalten von konventionellem Antriebsstrang, P2 und DHT unter Verwendung eines objektiven Bewertungssystems mit aktuellen Testdaten analysieren und vergleichen.

Ein Modell der Antriebsstrangdynamik einschließlich eines detaillierten EM-Modells und eines EM FOC (Field Oriented Control)-Steuermodells wird entwickelt, um Simulationen der Antriebsstrangschwingungen und des Fahrverhaltens durchzuführen. Anschließend wird eine auf maschinellem Lernen basierende aktive Dämpfungssteuerung entwickelt, um die Antriebsstrangschwingungen und Fahrbarkeitsprobleme durch Überwachung des Antriebsstrangzustands zu erkennen und die Antriebsstrangschwingungen durch hochdynamische EM-Drehmomentsteuerung zu kompensieren.

Um die Effektivität der aktiven Fahrbarkeitsoptimierung weiter zu verbessern, wird versucht, die Antriebsstrangsteuerung mit ADAS/AD System zu verknüpfen. Wobei die vom ADAS/AD System bereitgestellten Informationen, wie Fahrzeugabstand, Soll-Beschleunigung etc., als

Referenzgröße für die aktive Dämpfungsregelung verwendet werden, um eine proaktive Fahrbarkeitsoptimierung zu ermöglichen.

Abstract

In recent years, electrified powertrains have been increasingly used due to their excellent fuel economy and emission reduction. There are many different architectures and features of electrified powertrains, such as Add on, DHT (Dedicated Hybrid Transmission) and other hybrid solutions. Compared to conventional powertrains, electrified powertrains use the inherent properties of the EM to cancel out the mechanical components in terms of start, reverse and synchronization. However, the elimination of these mechanical components has a large impact on driveability such as shifting quality and torque transmission capability, thus causing oscillation problems, which in turn cause driveability issues, and at the same time places high demands on control engineering and calibration technology.

In this paper, we will first introduce the different electrified powertrain configurations, and then analyze and compare the driveability of conventional powertrain, P2 and DHT using objective assessment system with actual test data.

A powertrain dynamics model including detailed EM model, and EM FOC (Field Oriented Control) control model is developed to perform powertrain oscillation and driveability simulations. Based on the simulation model, a machine learning based active damping control is developed to identify the powertrain oscillation and driveability problems by monitoring the powertrain state, and to compensate the powertrain oscillation by high dynamic EM torque control.

To further improve the effectiveness of active driveability optimization, efforts are being made to link powertrain control with ADAS/AD system. Whereby the information provided by the ADAS/AD system, such as vehicle distance, target acceleration, etc., is used as a reference variable for the active damping control to enable proactive driveability optimization.

1 Introduction

Nowadays, hybrid vehicles and electric vehicles play an important role due to increasing environmental burdens. Compared to internal combustion engine vehicles, hybrid and electric vehicles are more environmentally friendly. At the same time, with increasing number of hybrid and electric vehicles, there are some problems that cannot be neglected. One of them is the optimization of the driveability of hybrid and electric vehicles.

The speed oscillation of the electrified powertrains occurs due to the dynamic of the powertrains. The large change of torque is the main reason that causes the oscillation of the

powertrains. Typically, a large change in torque occurs during tip-in and tip-out. Electrified powertrains are more prone to oscillation problems than conventional powertrains, because in the conventional vehicle, the internal combustion engine has matched passive dampers and the hydrodynamic torque converter can also reduce the torsional oscillation. Due to the smooth torque of the electric motor, the control of the torque is sufficiently precise. Furthermore, an additional passive damper for the electric motor is unnecessary. In addition, the direction of rotation of the electric motor can be easily changed. With the electric powertrain, the maximum torque is available immediately and constantly over a wide speed range. Therefore, the use of a multispeed transmission in the electrified powertrain is not essential to achieve the desired speed. A simplified transmission without additional passive dampers or clutches will cause torsional oscillation in the electrified powertrain when large torque changes occur. Such torsional oscillation is perceived as judder in the passenger compartment, reducing ride comfort and driveability. Active Damping Control (ADC) is therefore used in the electrified powertrain to damp the speed oscillation.

2 Dedicated Hybrid Transmission

A DHT describes a transmission that operates alongside the internal combustion engine (ICE) only in conjunction with one or more E-machines [9]. An electrified powertrain consists of several mechanical elements, e.g. electric motor, transmission, differential, final drive, etc. Fig. 1 shows the classification of powertrains according to the degree of electrification, where hybrids can be classified as Add-on and DHT.

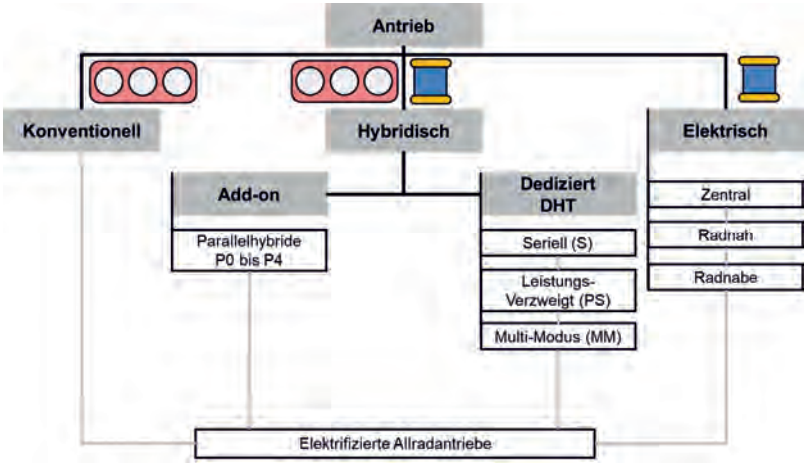

Fig. 1: Classification of powertrains according to the degree of electrification [5]

All DHT currently in series production are shown in Fig. 2. X axis is vehicle weight, Y axis is total EM power. The VKM power is classified by color and circle size, the larger the circle, the higher the VKM power. Interesting would be, all new developed DHT always uses simple concept, DHT with planet wheelset use only GM, Geely and Toyota, and those were actually developed long time ago. The all-other vehicles shown here have a Serial-Parallel DHT, so they drive the most time in EV or serial mode. Most DHT was used for compact, mid-size and small SUV. A few OEMs (BYD, Great Wall and Mitsubishi) have also used DHT for large SUVs.

Fig. 2: DHT currently in series production

Fig. 3 shows one Serial-Parallel DHT. Vehicles equipped with this DHT are pure electric drive most of the time. In addition, the electrified powertrain expands by integrating a combustion engine (ICE) with a generator, so that the electrical energy can now be generated in this compound and sent directly to the electric motor. After which the ICE is kept at a single operating point to achieve the best efficiency. The generator converts the mechanical energy generated from ICE to electrical energy. The battery is then kept at high State of Charge (SoC) so that the electric motor always has the electrical power available to provide continuous power here as well. When the power demand is high, the wheel is directly connected to the ICE via a clutch so that the vehicle can continue to maintain high continuous power. In this paper we will focus on the driving evaluation and optimization of this DHT.

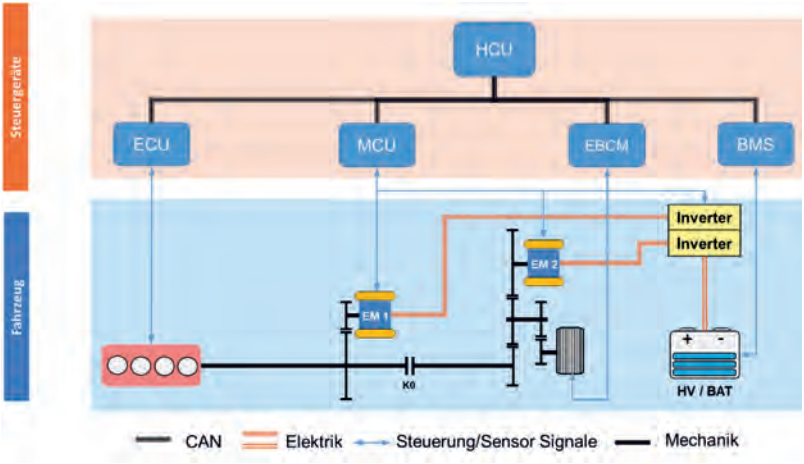

Fig. 3: Serial-Parallel DHT

3 Objective driveability evaluation

The vehicle driveability directly reflects the driver's subjective driving experience and is an important indicator for evaluating the quality of vehicles. With the continuous development of automotive technology, objective driveability evaluation is increasingly used to improve the limited reproducibility and comparability of subjective driveability evaluation. The application of objective driveability evaluation system enables the quantification of driver's subjective driving experience, which can provide engineers with more quantitative information during the development process to reduce the development time and improve the calibration efficiency [11]. Regarding the continuous application of virtual development [10], automated optimization and calibration, the objective driveability evaluation system has become indispensable to realize the virtual driveability evaluation without a test vehicle in the pre-development stage.

In recent years, we have conducted various vehicle benchmarks for objective driveability evaluation, including conventional, P2 hybrid and electric vehicles. It is useful to develop a unified evaluation tool to compare vehicles with different powertrain concepts. At this point we have used existing data and machine learning method to develop a unified objective rating model for tip-in driving manoeuvre. In total we have selected 6 vehicles, Fig. 4 shows torque weight and power to weight ratio. Vehicles 1 and 2 are conventional vehicle, vehicles 3 and 4 are P2 hybrid, vehicles 5 and 6 are electric vehicle. In the middle is accelerator pedal position and normalized max. acceleration, thus we can very well identify the differences

between conventional, P2 hybrid and electric vehicle. With this we have created a good basis that the new rating model works for conventional as well as for hybrid and electric vehicle, so that we can also evaluate DHT.

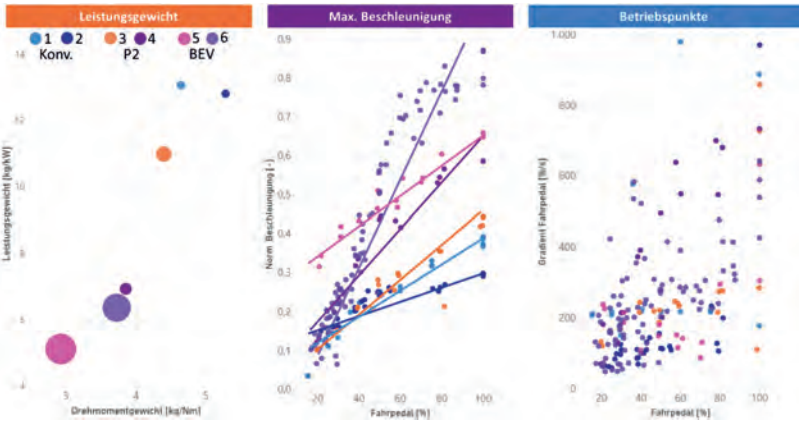

Fig. 4: Vehicle testing data

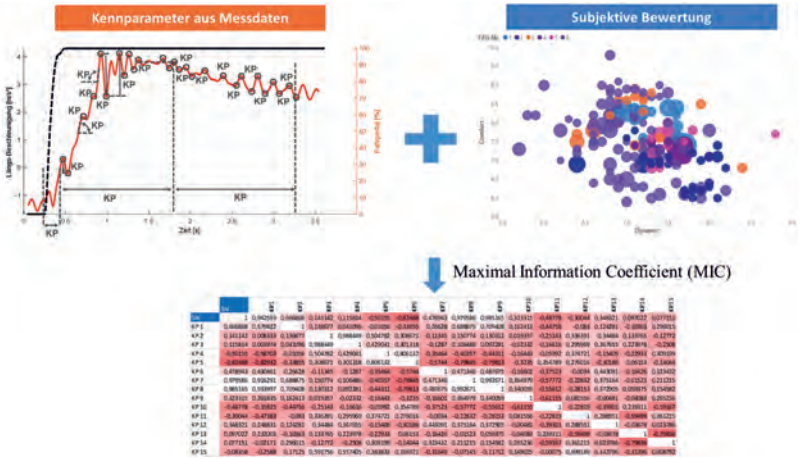

Fig. 5: Correlational study using MIC

The method for objectification is first calculated characteristic parameters and performed correlation study with subjective evaluation (Fig. 5), with aspects comfort and dynamic Instead of correlation coefficient here we used Maximal Information Coefficient (MIC), so that not only linear relationship but also non-linear relationship between characteristic parameters and subjective evaluation can be identified. Through the heat map we can then select relevant characteristic parameters

For the rating model building, we used machine learning method instead of linear and polynomial model to take into account the complicated relationship between characteristic parameters and many boundary conditions such as pedal position, pedal gradient and power weight. In the past, we normally considered pedal position and gradient with linear or polynomial weighting factor, but the human feeling is not always so proportional, but more complicated. Therefore, we have tried whether machine learning method is more suitable at this point (Fig. 6).

As the first stage, objective ratings are calculated for individual characteristic parameters, with pedal position and pedal gradient info. As a second stage, the comfort and dynamics ratings are calculated from individual ratings of parameters with consideration of vehicle power-to-weight ratio. Both ratings have shown very good coefficient of determination.

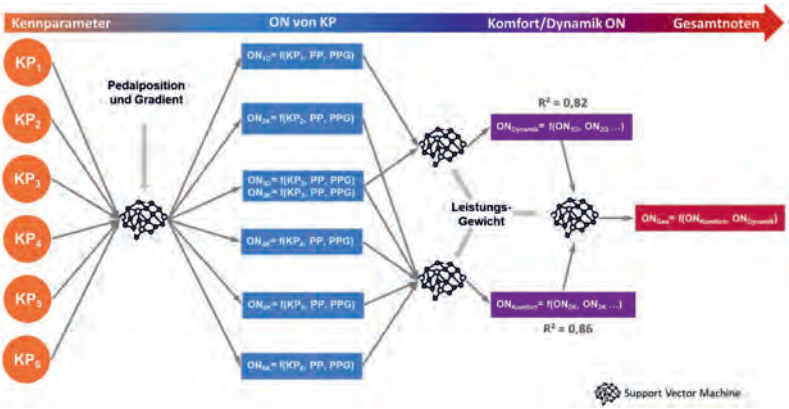

Fig. 6: Rating model using SVM

With the new rating model for tip-in driving manoeuvre, we can then compare different vehicles (Fig. 7). The acceleration of P2 Hybrid has reached maximum acceleration faster than conventional, the acceleration interruption at the top is due to engagement of the C0

clutch. Then BEV1, the acceleration curve is clean and harmonic, but a bit slow, however, when reaching max acceleration has a few oscillations, which often happens in BEV, because the powertrain is also relatively poorly damped. The acceleration of BEV2 can almost not complain, this is a very good progression, and with very good ratings, both comfort and dynamic. To the end is DHT, strange is that the DHT has particularly large backlash during load changes and jerk after reaching the max. acceleration has. And therefore, has in comparison with dynamics ratings a worse comfort rating. However here are only individual vehicles, with this comparison we cannot overall say BEV is better than P2 or P2 is better than DHT etc.

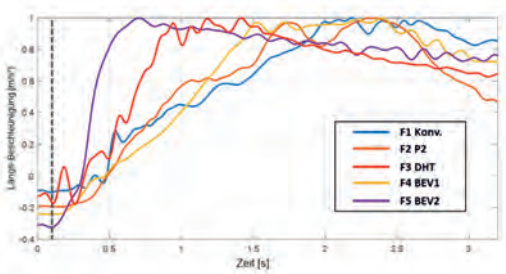

	Komfort	Dynamik
F1 Konv.	7,08	7,52
F2 P2	7,83	8,55
F3 DHT	7,35	9,02
F4 BEV1	8,24	8,35
F5 BEV2	8,62	9,59

Fig. 7: Comparison of vehicles

4 Model building

For the control system design, a four-mass powertrain simulation model was developed, and the nonlinear backlash was also considered. In many studies, the most commonly used model is the linear two-mass system. The model can also be found in [3], [8] and [7]. Since the model is only a simplification of the real system, the elements of the simplified model do not have a one-to-one corresponding component in the real system. The torsion spring with a spring constant c represents all elastic elements in the drive train and the damper with a damping constant k represents all damping elements in the powertrain. The moment of inertia J_1 includes the rotor of the electric motor. Moment of inertia J_2 includes everything from the gearbox to the wheels.

In this paper, to better study the dynamic characteristics of the powertrain, we use a non-linear four-mass model (Fig. 8). In this model the moment of inertia J_1 nevertheless includes the rotor of the electric motor, J_2 represents the first half of the gear and J_3 the second half of the gear, J_4 represents the residual moment of inertia up to the wheels. A torsion spring c_1 and a damper k_1 stand for the axle between the rotor and the gear unit. The axle connecting the gearbox to the wheel is also replaced by a torsion spring c_2 and a damper k_2. All elastic

components between each mass are also replaced by a torsion spring and damper. A backlash is added between the output of the gearbox and axle to represent the nonlinear dynamic property.

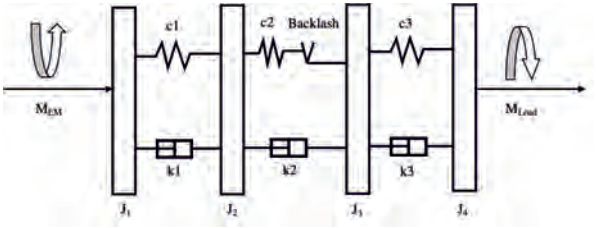

Fig. 8: Non-linear four-mass model with backlash

According to Fig. 8, the total moment equilibrium for the four-mass model is obtained:

$$J_1 \cdot \ddot{\varphi}_1 = M_{EM} - k_1 \cdot (\dot{\varphi}_1 - \dot{\varphi}_2) - c_1 \cdot (\varphi_1 - \varphi_2) \quad (8)$$

$$J_2 \cdot \ddot{\varphi}_2 = k_1 \cdot (\dot{\varphi}_1 - \dot{\varphi}_2) + c_1 \cdot (\varphi_1 - \varphi_2) - M_G(\Delta\varphi, \Delta\dot{\varphi}) \quad (9)$$

$$J_3 \cdot \ddot{\varphi}_3 = -k_3 \cdot (\dot{\varphi}_3 - \dot{\varphi}_4) - c_3 \cdot (\varphi_3 - \varphi_4) + M_G(\Delta\varphi, \Delta\dot{\varphi}) \quad (10)$$

$$J_4 \cdot \ddot{\varphi}_4 = k_3 \cdot (\dot{\varphi}_3 - \dot{\varphi}_4) + c_3 \cdot (\varphi_3 - \varphi_4) - M_{Load} \quad (11)$$

In Fig. 9 we have put measured and simulated acceleration together, the simulation shows reasonable results. Quite crucial to the simulation is the angle speed difference between electric motor and wheel, which is the cause of powertrain oscillation. After The comparison, we can find that this simulation model is good for further investigation. When we compare the comfort and dynamics ratings, the rating of simulation is a bit worse than measurement but is still in green area.

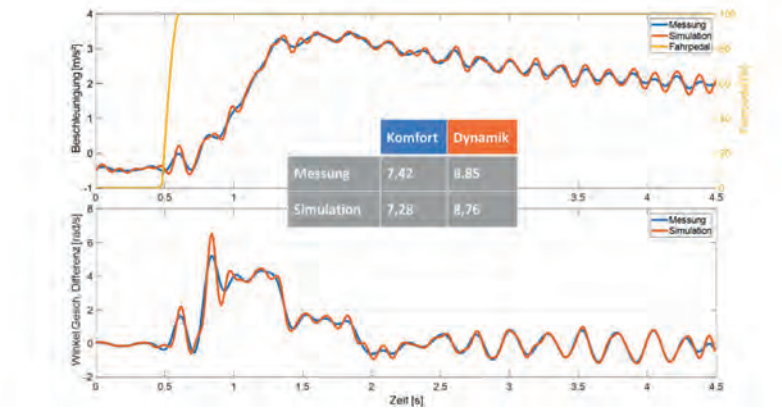

Fig. 9: Measurement and simulation results

4 Active Damping Control

The basic idea of Active Damping Control is to detect and measure the unwanted torsional oscillation by some procedures. Then with this detecting unwanted torsional oscillation, a torque feedback is determined to compensate the unwanted torsional oscillation. At present, there are two methods to detect and measure the unwanted torsional oscillation. One is to use observer, another is to use Fast Fourier Transform (FFT). A good explanation of the observer method can be found in [1] and [3]. The application of the FFT method can be seen in [4]. Based on the possibility of real-time use in real vehicles, the observer method is selected and used as the traditional method in this paper.

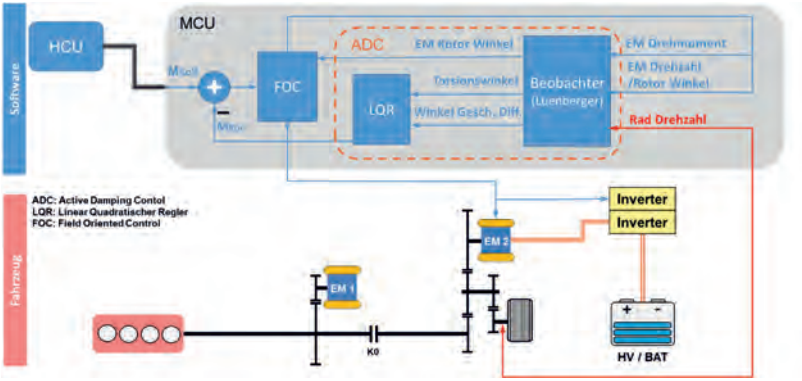

Fig. 10: Control strategy using Luenberger observer and LQR

An observer consists of a group of equations of state, which is used to represent a model of state. The unmeasurable quantities, the angles of the wheel $\varphi_{\_wheel}$ and the rotor $\varphi_{\_R}$, are then offered by the observer. After that, the damping torque is calculated. In addition, the torque control of the electric motor can be improved by the measurable quantities from the observer, which is found in [2] and [3].

With the observer we can determine torsion angle and angle velocity difference, then we give the two signals to linear quadratic controller (LQR) to calculate the damping moment. P or PI controller can also use, but the LQR has shown best results. The observer can also calculate a corrected EM rotor angle, and then send to FOC controller for EM, so the control quality of EM torque can be further improved (Fig. 10). The problem with this active damping control is that the Luenberger observer can only observe linear behaviour with the system state equation, non-linear behaviour such as backlash cannot be observed. Therefore, we have tried to develop a new control strategy: reinforcement learning (RL) based model predictive control so-called LMPC to enable a predictive or proactive optimization.

The LMPC consists of two parts (Fig. 11), like conventional MPC, the first part is powertrain model, at this part the model is trained with neural network to monitor the system behaviour like an observer and predict the future system behaviour. The second part is the controller, here is replaced by RL. Very important are the Reward function and Actor Network. The Reward function is like a reward that judges how well the system performs and how much effort it takes to maintain that performance, and the Actor Network calculates the damping torque needed to compensate for the oscillation. After each episode, the learning algorithm

would optimize the neural network to increase the gains in the direction that increases the reward (i.e., performance is improved, and effort is decreased).

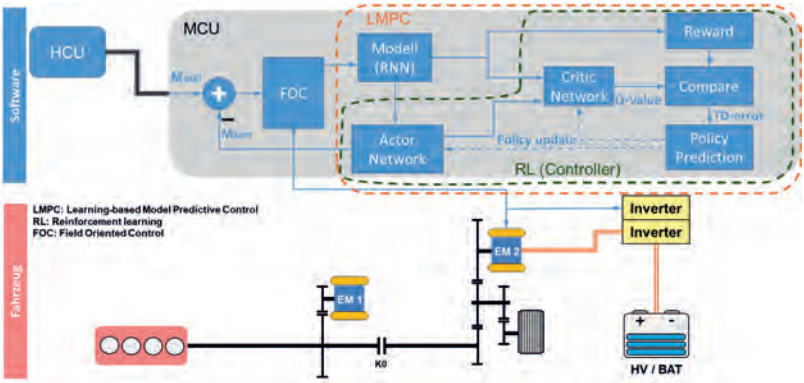

Fig. 11: Control strategy using LMPC

Fig. 12 shows the simulation results with LQR and LMPC. The top of Fig. 12 are the accelerations, and the bottom are the determine angle velocity difference and the damping torques. The acceleration response with LQR is noticeably better as the base, but there is still a lot of oscillations left, since Luenberger observer can only calculate linear behavior. If we then look at the acceleration with LMPC, the acceleration is smoother. The corresponding damping torque is also higher than with LQR.

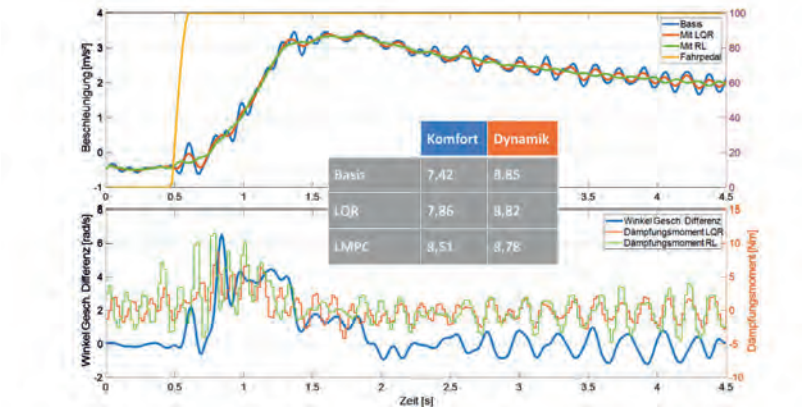

Fig. 12: Comparison of LRQ and LMPC control effects

If we look at the objective ratings, the dynamic rating is almost unchanged and the comfort rating has improved by about 0.5 with LQR and about 0.9 with LMPC. Of course, the high dynamic damping torque has a negative impact on EM, in terms of lifetime and temperature increase. For this reason, torque limitation is also used here, the maximum remains in the range of 10 Nm.

6 Interaction with ADAS/AD systems

As a further investigation, we have analysed the interaction between powertrain control and ADAS/AD systems and checked the linkage possibility. It would be ideal, for example, by linking between powertrain control and ADAS/AD systems, to optimize the target acceleration early in terms of powertrain dynamics, so that less oscillation occurs during acceleration, and to reduce the high damping dynamic torque, as explained before, which has negative influence on EM.

As just introduced, we have developed a LMPC for driveability optimization, but the advantage of RL is not exploited, because RL is a powerful method, can simultaneously calculate multiple outputs as control parameters to strive for optimal control results from the entire system. However, in the previous section only the damping torque was calculated.

As an example, Fig. 13 lower side is a typical ACC system, consists of ACC controller and powertrain coordinator, the ACC controller has several function modules, such as speed control, distance control, curve control etc. [6] The speed control is P controller or characteristic curve, distance control is usually more complicated than speed control, often uses fuzzy, sliding mode control etc. With signals from radar or other sensors, vehicle acceleration is calculated, through a mixer a target acceleration is determined, normally the minimum target acceleration is used. In the powertrain coordinator, target torque is calculated by acceleration control and then sent to HCU.

Our goal is to link RL with ACC controller and validate ACC controller parameters during vehicle acceleration. For this, we have extended the reward function to consider the demand of ACC, and the Actor network additionally calculates 2 control parameters for ACC controller selected by us. Of course, we have also considered the delay of CAN communication.

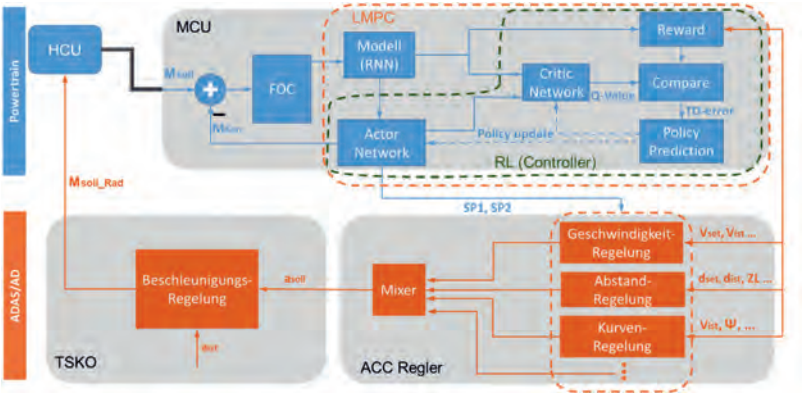

Fig. 13: Combination of powertrain and ADAS/AD control strategies

As results in Fig. 14 we have the target acceleration from original ACC controller, this signal is a replicated signal in simulation model and was validated and verified with measurement signals. The yellow curve is Simulated vehicle acceleration in response of target acceleration signals, here we can observe some unwanted oscillations which causes poor driveability. The lower graph is then angle velocity difference between EM and wheel, the larger the difference the larger the damping torque, we then want to reduce this with validation of ACC controller.

Then here we have optimized target acceleration with RL and the vehicle acceleration, the oscillation is noticeably less. The target acceleration was optimized by the validation of ACC controller during acceleration and caused few oscillations of powertrain, and at the same time without much influence on driving dynamics. And the angular velocity difference has also become correspondingly small. therefore, smaller damping torque is also needed, thus reducing the highly dynamic behaviour of the EM some masses. In this example the acceleration is only less than 2 m/s², if here a sporty designed ADAS system is considered then the improvement will probably be even bigger.

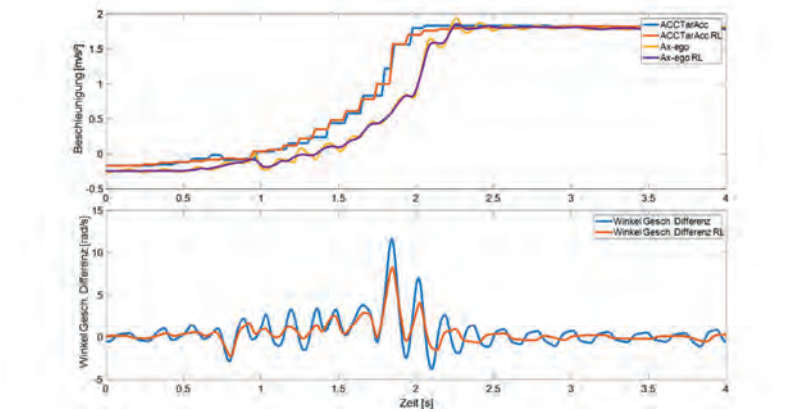

Fig. 14: Comparison of control effects

7 Summary

This paper first introduces the classification of powertrains, especially DHTs which have received much attention in recent years and their current mass production worldwide. An objective evaluation system for driveability is then presented, and a new driveability evaluation system of tip-in for all powertrain types is built using machine learning based on existing subjective evaluation data. A detailed dynamics model is then developed for the oscillation problem analysis of electrified powertrain and the driveability is improved using LQR and LMPC control. Finally, the possibility of joint control of powertrain and ADAS/AD systems is explored, and a study based on ACC controller is also presented.

8 References

[1] Amann, N., Böcker, J., Prenner, F.: Active Damping of Drive Train Oscillations for an Electrically Driven Vehicle. IEEE/ASME TRANSACTIONS ON MECHATRONICS, Bd. 9, Nr. 4, pp. 697-700, 2004

[2] Götting, G.: Ermittlung der Rotorlage zur Regelung einer PSM in Hybird- und Elektrofahrzeugen. AUTOREG, 2011

[3] Götting G., Kretschmer, M.: Development and Series Application of a Vehicle Powertrain Observer Used in Hybrid and Electric Vehicles. EVS27 International Battery, Hybrid and Fuel Cell Electric Vehicle Symposium, 2013

[4] Kim, J.S., Eo, J. S.: Apparatus and method for active oscillation control of hybrid electric vehicle. US Patent US10266171B2, 2019

[5] Lange, A.: Optimierung modularer Elektro- und Hybridantriebe, Technische Universität Braunschweig Diss. 2018

[6] Liesner, L.: Automatisierte Funktionsoptimierung von Adaptive Cruise Control, Technische Universität Braunschweig Diss. 2017

[7] Obando, H.S.: Reinforcement Learning Framework for the self- learning Suppression of Clutch Judder in automotive Drive Trains, Karlsruher Institut für Technologie Diss. 2016

[8] ÖTKÜR, M., ATABAY, O., EREKE, İ. M.: Model Based Predictive Engine Torque Control for Improved Driveability. Journal of Polytechnic, Nr. 20, pp. 71-82, 2017

[9] Sieg, C.; Küçükay, F. Benchmarking of Dedicated Hybrid Transmissions. Vehicles, 2, 100-125, 2020

[10] Zehetner, J., Schöggl, P., Dank, M., Meitz, K.: Simulation of Driveability in Real-time, SAE Technical Paper. 2009-01-1372. 2009

[11] Zhang X., Ebner T., Arntz M., Ramsauer A., Küçükay F.: New Solution Supporting Efficient Vehicle Calibration Using Objective Driveability Evaluation and AI. 21. Internationales Stuttgarter Symposium. Springer Vieweg, Wiesbaden. 2021

Holistic Design of All-Wheel Drive Electric Powertrains Using a Multi-Objective Optimization Algorithm

A Simultaneous Optimization of Technical and Economic Objectives

M.Sc. **Bastian Krüger**, M.Sc. **Giovanni Filomeno**,
Dr.-Ing. **Dirk Dennin**, BMW Group, Munich;
Prof. Dr.-Ing. **Peter Tenberge**, Ruhr-University, Bochum

Zusammenfassung

Der vorliegende Beitrag behandelt die ganzheitliche Antriebsauslegung für batterieelektrischen Allradfahrzeuge mithilfe von Algorithmen zur Mehrzieloptimierung. Hierzu werden gleichzeitig Parameter der elektrischen Maschine und des Getriebes hinsichtlich der Zielgrößen elektrischer Verbrauch, Performance und Kosten optimiert. Seitens der elektrischen Maschine werden Leistung, Spannungslage, Eckdrehzahl und relative Länge variiert. Hierzu wird ein Open-Source Auslegungswerkzeug herangezogen. Dieses ermöglicht die Auslegung von sowohl Asynchronmaschinen als auch permanent erregte Synchronmaschinen, womit der Einfluss unterschiedlicher Maschinentypen bewertet werden kann. Im Subsystem Getriebe werden die Übersetzungen optimiert und die Auswirkung einer Abkopplungseinheit untersucht. Die Lösungsgüte setzt sich aus elektrischem Verbrauch und Beschleunigungszeit von 0-100 km/h zusammen. Zur Berechnung des elektrischen Verbrauchs kommt eine quasi-statische Rückwärtssimulation in Kombination mit einer verlustminimierenden Betriebsstrategie zum Einsatz. Die Beschleunigungszeit wird mithilfe einer Längsdynamiksimulation ermittelt. Um die Fahrleistungsreproduzierbarkeit zu berücksichtigen, erfolgt die Bewertung der Beschleunigungszeit sowohl mit Peak- als auch mit Dauerleistung. Neben der Bewertung technischer Eigenschaften, ermöglicht ein Kostenmodell die Bestimmung der Antriebskosten. Aufgrund der sich ergebenden Lösungsvielfalt ist eine reine Brute-Force Optimierung aller Lösungsvariationen zu rechenaufwändig. Um optimale Lösungen in der Lösungsmenge identifizieren zu können, wird ein Mehrziel-Optimierungsalgorithmus angewandt. So können Pareto optimale Lösungen gefunden werden, ohne den gesamten Lösungsraum betrachten zu müssen. Durch eine Analyse der Pareto optimalen Lösungen, werden Zusammenhänge zwischen den Opti-

mierungsparametern und den Zielwerten aufgezeigt. Diese Erkenntnisse dienen dazu zielführende Antriebsstrangkonfigurationen abzuleiten und wichtige Zusammenhänge im Antriebsstrang aufzuzeigen.

Abstract

In this paper, all-wheel drive (AWD) systems in battery electric vehicles (BEVs) are fully examined within a multi-objective optimization. Therefore, both EM parameters and the transmission ratios are optimized simultaneously aiming at maximum range, maximum performance and minimal cost. Applying an open-source EM design tool, both induction machines (IMs) and permanent magnet synchronous machines (PMSMs) are designed allowing to investigate the machine type influence. The optimization parameters related to the EM are the nominal power, the voltage level, the nominal speed and the relative length. In case of the transmission, the speed ratio is optimized and the application of a disconnect unit is investigated. To assess the fitness of a solution, the electrical energy consumption and the acceleration time from 0-100 km/h is calculated within a simulation environment. The electrical consumption is calculated using a quasi-static backwards simulation in combination with an operation strategy, which minimizes the electrical consumption. The acceleration time from 0-100 km/h is determined in a longitudinal dynamic simulation. To unveil the reproducibility of these performance values, the acceleration time is both calculated with peak power and with continuous power. Additionally, the powertrain costs are calculated. To identify optimal solutions among the huge number of possible design candidates, a multi-objective optimization algorithm is applied. This allows the identification of Pareto optimal solutions without calculating all possible solutions. After the set of Pareto optimal solutions has been identified, an analysis of these solutions offers a holistic insight in the correlation between the optimization parameter and the fitness of the system. Based on that, target-orientated powertrain designs can be derived.

1 Introduction

To meet the legislative requirements concerning carbon-dioxide emissions, car manufacturers increase the supply of BEVs within their vehicle portfolio. Many of those demand AWD systems to fulfill customer requirements. While conventional drivetrains usually employ mechanical AWD systems driven by a central engine, electric all-wheel drive systems are realized as axle split systems. Both geometrical constraints imposed by the battery and the geometrical compactness of electric axle systems make an axle-split arrangement favorable. Apart from geometrical aspects, these arrangements offer significant functional degrees of freedom. As an example, the total power can be distributed freely between both axles allowing to reach an

optimal utilization of both machines. Additionally, different electrical machine (EM) types can be applied at front and rear axle offering the possibility to combine the advantages of two machine types in one powertrain. Furthermore, integrating a disconnect unit at one axle, enables to decouple this axle when driving at part-load conditions, which further leverages the overall efficiency. These three design aspects only represent an extract of all degrees of freedom within the system, pointing out the complexity of the underlying design process. Consequently, identifying the optimal combination of design parameter among all possible design candidates requires automatized optimization frameworks.

Within the state of the art, the electrical powertrain design problem has been addressed in many studies. Vaillant focuses on the optimization of powertrains for battery electric sports vehicles and applies a multi-objective genetic algorithm [1]. Within his framework, he employs a pre-defined library of EM efficiency maps. The optimization algorithm identifies the transmission ratios and EMs, which in combination optimize the technical objectives. In contrast, Eghtesaad conducts a design of experiments and derives a meta model of the powertrain fitness depending on all design parameters first. Subsequently, she applies a multi-objective optimization algorithm to examine the optimal powertrain configuration within this meta model with respect to technical and economic objectives [2]. The EMs are varied using a torque scaling approach. Using a similar modelling approach, Othaganont et al. [3] directly apply a multi-objective genetic algorithm to optimize different electric powertrain topologies with respect to technical and economic objectives. Danzer chooses a brute force optimization to optimize technical objectives [4]. To investigate the effect of different EMs, he empirically variates the efficiency characteristics.

In this paper, a design framework is proposed to identify optimal physical design parameters both for EM and transmission, which minimize technical and economic objectives. Therefore, an analytical EM design tool, a powertrain model and a simulation environment are merged with a multi-objective optimization algorithm. This allows to optimize all-wheel drive BEVs towards maximum performance, performance reproducibility, high energy efficiency and low powertrain cost. The remaining paper is structured as follows. Initially, the powertrain configuration considered in this paper is explained. Then, the overall design framework is introduced with all its subsystems. Subsequently, each subsystem is specified in detail. In conclusion, a case study is conducted applying the presented design framework to a relevant design problem.

2 All-wheel drive electric powertrain

The principal layout of the investigated powertrains including all components is shown in Fig. 1. Both front and rear axle are driven by a separate electric drive unit, comprising one EM and a transmission connecting the EM to the wheels. The latter is realized as a two-staged spur transmission, which is mainly characterized by the input stage ratio and the differential stage ratio.

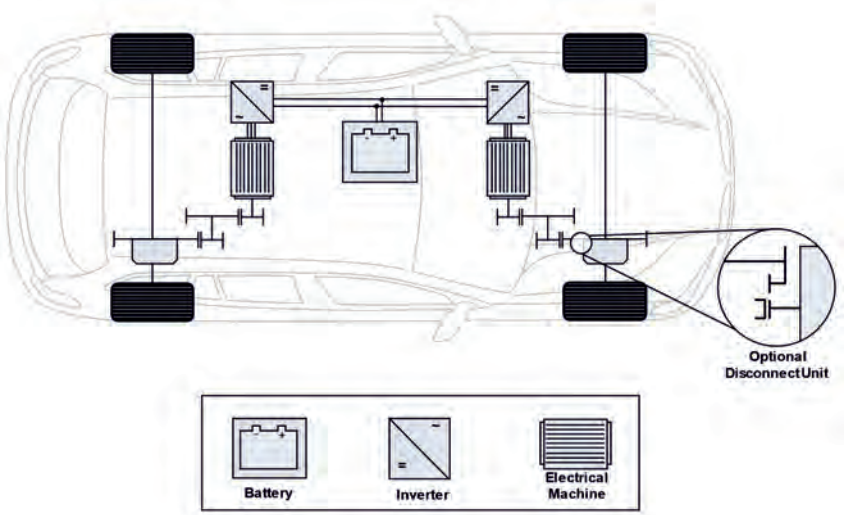

Fig. 1: Powertrain layout of an all-wheel drive electric powertrain.

At the front axle transmission, a disconnect clutch can be integrated optionally. Its position is indicated in Fig. 1, allowing to disconnect the differential gear from the differential cage. The disconnect unit is realized as an electro-mechanically actuated dog clutch. This position is chosen, as it offers a significant energy saving potential. Further decreasing the front axle drag torque would require decoupling both drive shafts, which is not considered in this paper. While the considered transmission is mainly characterized by its ratio, the EM is characterized by multiple parameters such as voltage level, maximum torque, peak and continuous power. Each electrical machine is supplied by its separate inverter, converting the direct magnitudes supplied by the battery into the required rotating magnitudes. The battery is the only energy storage and provides the power required to propel the vehicle. Being composed of multiple single cells, the fundamental cell characteristics as well as their connection influence the overall battery characteristics.

3 Design Framework

Multiple design parameters define the behavior of the presented powertrain architecture. To find the optimal parameter configuration, a design framework is presented in Fig. 2. The framework is composed of an input interface, a model library, a simulation environment and the optimization algorithm. Initially, within the input interface the powertrain configuration, the EM designs, the characteristics of the battery cell and the vehicle characteristics must be defined.

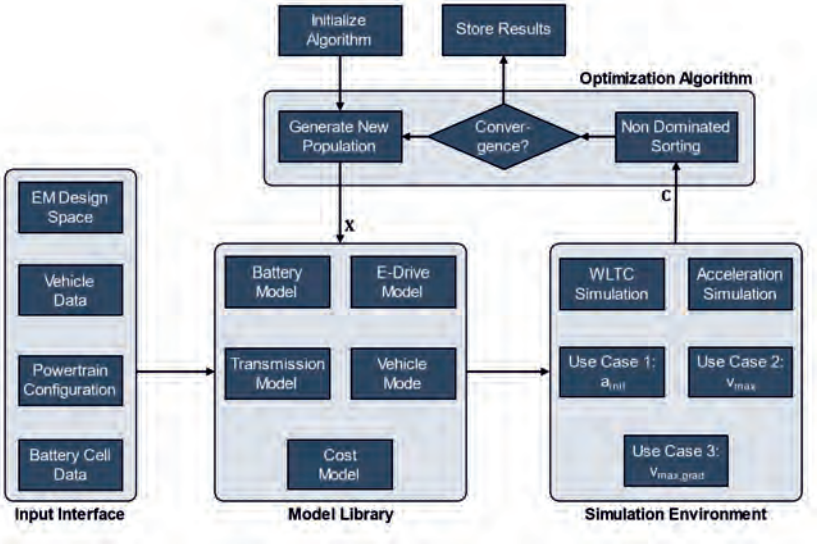

Fig. 2: Holistic design approach, showing the four major subsystems as well as their relations.

To identify optimal design candidates, the algorithm generates a set of design candidates, which is referred to as population. A single design within the population is defined by the design vector $\boldsymbol{x}$, which is also referred to as optimization vector in the following. Combining all optimization vectors with the input data, a simulation model can be created from the model library for each specific design candidate. Incorporating this simulation model into the simulation environment, all evaluation criteria can be calculated. Subsequently, all evaluation criteria are stored in the multi-dimensional cost vector $\boldsymbol{c}$. Again, for each design candidate an individual cost vector exists representing its fitness with respect to the objectives. All cost vectors within the population are combined to the set $\mathbf{C}$ and the procedure can be repeated. As the problem

is characterized by multiple objectives, an optimization algorithm is required, capable of identifying Pareto optimal solutions. The optimization algorithm iteratively analyzes the cost vectors $\boldsymbol{c}$ in the current populations set of cost vectors $\mathbf{C}$ and subsequently creates a new population of design candidates $\mathbf{X}$ based on that. In addition to the objectives, which are minimized during the optimization process, minimum requirements exist. In case one of these requirements is not fulfilled, all cost vector entries are set to a number so large, so that the solution can be considered non-valid. In this paper, all entries are set to 10,000.

3.1 Input Interface

Within the input interface, all data must be provided, which are necessary to define the design problem. This includes the configuration of the powertrain, both constant and variable EM design parameters as well as vehicle and the battery characteristics. The powertrain configuration is defined by the EM type applied to front and rear axle and the presence of the front axle disconnect unit. To create the multi-variable EM design space, the analytic tool presented in [5] is used. Principally, the tool is composed of two major blocks. In a first step, the motor geometry is designed based on the input parameters. This includes winding scheme, geometrical dimensions of stator and rotor as well as all the resistances and inductances. Within the second step, the operating characteristics of the designed machine are determined. Therefore, in each operation point the voltage and the current along both d- and q- axis are optimized aiming at maximum torque or minimal loss, resulting in a full load torque curve and a respective efficiency map. For IMs the tool is adapted, so that iron losses are neglected at zero output torque [6]. Further input parameters are the rated power P_{em}, the rated voltage U, the nominal ω_N as well as the maximum speed ω_{max}, the number of pole pairs p_{em} and the relative length λ_{em}. Moreover, materials must be chosen, such as winding material or magnetic steel sheet material for rotor and stator. Using this tool, multiple machine variants are designed, which are stored within a multi-dimensional matrix. For each EM design variant, the corresponding inverter losses are calculated and merged with the EM losses. In Fig. 3 different EM designs are shown, with varying nominal speed, voltage level and power. To calculate battery loss map, the cell characteristic as well as the target energy content must be defined. Furthermore, the respective vehicle data must be provided.

3.2 Model Library

The model library contains all mathematical models of the components contained in the system boundaries. Within the model library, the battery is modelled as voltage source with an inner

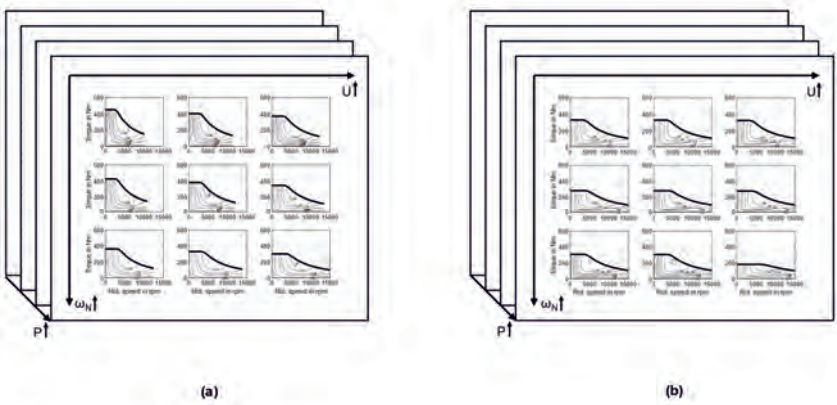

Fig. 3: Three-dimensional EM design space for a) IMs and b) PMSMs.

resistance. The open circuit voltage depends on the state of charge (SOC), while the resistance is assumed to be constant. Based on the required battery power and the SOC, the losses can be calculated and stored in a two-dimensional consumption map. EM and inverter are modelled using steady-state electric consumption maps. As both consumption maps for electrical machine and inverters can be expressed depending on the torque and the rotational speed, they can be combined in a single consumption map. Using bilinear interpolation, the required electrical power is then being calculated based upon the torque and speed required. In this investigation, the voltage level and the component temperature are assumed to be constant. Furthermore, dynamic effects within inverter and EM are neglected.

The transmission enables a speed-reduction from in- to output shaft, which is subject to load-dependent and load-independent losses and is modelled as a fixed speed ratio. Both loss types are modelled as friction torques imprinted on the input shaft. The transmission losses are stored in a torque loss map depending on output speed and torque. Again, for each state of operation, the torque loss can be calculated using bilinear interpolation. As an optional decoupling device is assumed to allow a disconnection of differential cage and ring gear, in disconnect state only the differential cage produces a drag torque. This drag torque must be compensated by the rear axle machine in disconnect mode and is therefore added to the rear axle torque loss map.

To keep the simulation model lean, the vehicle is modelled as a point mass. The required traction force F_{wheel} to overcome the driving resistance is composed of the rolling resistance F_{roll} the gradient resistance F_{grad}, the air resistance F_{air} and the acceleration resistance F_{acc}.

$$F_{wheel} = F_{roll} + F_{grad} + F_{air} + F_{acc} \tag{5.1}$$

To transform the available torque into a vehicle acceleration, the tires must transmit the delivered torque to the road. Within the tire road contact, the slip limit defines the maximum transmittable torque. Assuming the friction coefficient to be constant, the maximum traction force $F_{wheel,max}$ is calculated using the friction law.

$$F_{wheel,max} = \mu_0 G_{dyn} \tag{5.2}$$

Here, G_{dyn} represents the dynamic axle load and μ_0 the tire friction coefficient. While μ_0 can be assumed constant, G_{dyn} depends on the vehicle state and geometry.

3.3 Cost Model

The overall powertrain model also includes a cost model in addition to the technical models. All cost values are taken from [7, 8] representing potential values for the year 2030. The cost for the EM and the corresponding one-speed transmission are expressed in a single value, which depends on the continuous power. For PMSMs the costs amount to 10 €/kW. In this case, the ratio between peak and continuous power is 2. IMs, on the contrary, cost 8 €/kW, assuming a peak to continuous power ratio of 3. The overload capacity of PMSMs is lower, as permanent magnets tend to demagnetize in overload situations. If a disconnect unit is applied, the respective costs must be added to the previous values. Neither the dog clutch itself, nor the actuation system significantly scale with the transmittable power and torque, allowing to assume a constant cost value for the disconnect unit. In analogy to the EM and transmission unit, the inverter costs scale with the continuous power. Compared to EMs, the peak to continuous power ratio is close to 1. The potential costs for the entire battery pack amount to 95 €/kWh.

Table 1: Cost values for all considered powertrain components according to [7, 8].

Component	Value	Unit
IM & Transmission	8	€/kW
PMSM & Transmission	10	€/kW
Inverter	3	€/kW
Battery (60 Ah Cell)	95	€/kWh

3.4 Simulation Environment

Within the simulation environment, all technical powertrains characteristics are determined. The electrical consumption E_{bat} is calculated using a quasi-static backward simulation with a time step Δt of 1 s. At each cycle point, the required battery power P_{bat} is evaluated depending on the control vector $\boldsymbol{u}$. The optimal control vector $\boldsymbol{u}$ contains the torque split factor u_{ts} defining the torque distribution between front and rear axle and the state of the disconnect unit u_{dc}. While the torque split factor is a continuous value within the range of 0 to 1, the state of the disconnect clutch is a binary variable.

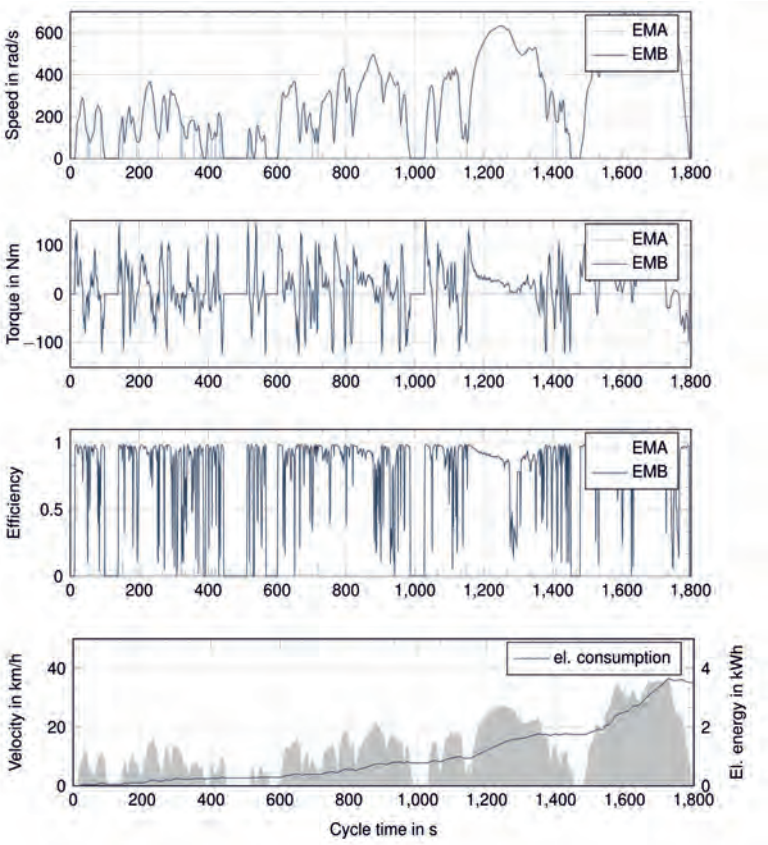

Fig. 4: Exemplary results of a WLTC energy consumption simulation (EMA: front axle machine; EMB: rear axle machine).

The energy management strategy chooses u_{ts} and u_{dc} aiming at minimizing/maximizing (drive/coast) the absolute battery power. At this point, drivability aspects are not considered as well as losses which occur in the decoupling actuation when (de-)coupling the front axle machine. The resulting consumption, therefore, represents an upper limit potential. Exemplary results for a consumption simulation in the worldwide harmonized light vehicles test cycle (WLTC) are shown in Fig. 4. In this Figure, EMA corresponds with the front axle and EMB with the rear axle machine. Within the first subfigure, the rotational speed of both EMs is shown. The second shows the torque curves, while the third contains the resulting efficiencies. In the last subfigure, the cumulated electrical consumption is illustrated. This specific powertrain is almost exclusively operated in rear-wheel drive operation with a disconnected front axle machine EMA. Only in very few driving situations, EMA is coupled to the front wheels, indicating that for the respective powertrain it is beneficial to shift the driving load to one EM instead of distributing it among both machines.

To assess the longitudinal dynamic performance values, the theoretically available wheel torque is calculated for both front and rear axle. Subsequently, the initial acceleration and the maximum vehicle speed can be determined. For the initial acceleration the dynamic load shift and the wheel slip limits at both axles must be considered. In the next step, a longitudinal dynamics simulation is conducted evaluating the acceleration time from 0-100 km/h. Again, the vehicle dynamics and the resulting slip limits at front and rear axle limit the vehicle acceleration and define a physical limit for the minimal acceleration time.

3.5 Optimization Algorithm

All previously described subsystems are required to evaluate the fitness of each design candidate, based upon the respective design parameters. The optimization algorithm closes the loop by iteratively adapting the set of optimization vectors $\mathbf{X}$ and observing the effects on the cost vectors $\mathbf{C}$. Therefore, many different algorithms exist in the state of the art all having strengths and weaknesses. Depending on the characteristic of the optimization problem, a suitable algorithm must be identified. The present optimization is derivative-free, multi-objective and multi-variable. Within the state of the art, natural analog algorithms have been proven to be suitable to solve such optimization problems. In particular, various studies successfully applied genetic algorithms to optimize both purely electric and hybrid powertrain architectures [1, 3, 9, 10, 11].

Consequently, a multi-objective genetic algorithm is chosen in this study. Specifically, the multi-objective genetic algorithm available at the global optimization toolbox from MATLAB® is

applied. The underlying algorithm is a variant of the well-proven NSGA-II [12]. A detailed analysis of the optimization algorithm goes beyond this paper's scope; however, the main idea and steps are briefly outlined. Genetic algorithms are inspired by Darwin's theory of evolution. All design candidates are described as genes with a corresponding fitness. Using reproduction and selection schemes, like in biological evolution, the solutions are continuously improved. In particular, the NSGA-II works as follows. Initially, a random set of design candidates is generated and evaluated. Based on the set $\mathbf{C}$ of cost vectors, the NSGA-II sorts all solutions depending on their ascending level of non-domination and selects a subset of the current population. The selection has an elitist character, which means the best solution is always kept within the population. Based on this subset, the convergence criteria are checked. If fulfilled, the optimization terminates, if not a new population is created applying genetic operators. To generate a new population, a subset of design candidates is chosen from the current population using a tournament selection. These remaining candidates are called parents. Then, crossover and mutation are applied to the parents to generate new optimization vectors, which in combination with the parents represent the new population $\mathbf{X}$. Subsequently, for each design candidate within the new population, the fitness can be calculated leading in an updated set of cost vectors $\mathbf{C}$. This procedure is repeated iteratively until the convergence criteria is fulfilled. The main parameters describing the explained optimization algorithm are population size, mutation and crossover probability and the convergence criteria.

4 Case Study

The presented design framework is now applied within a case study to demonstrate how it can be used to design AWD electric powertrains.

4.1 Case Study Setup

This case study is conducted with an upper medium class sports agility vehicle. The combination of vehicle and power class arises customer expectations towards specific use-cases. In this paper, three use-cases are assumed representative for the underlying vehicle. For a powertrain to be valid, all three must be fulfilled. First, a permanent maximum speed of 200 km/h is required. Furthermore, a minimum speed of 50 km/h must be maintained permanently at a road slope of 15%. Third, a temporal minimum initial acceleration of 5 m/s^2 is demanded. The permanent use-cases address the continuous power, while the temporary use-cases are a peak power requirement.

Table 2: Morphological box with all powertrain configurations.

Component	Options	
Front axle EM type	IM	PMSM
Rear axle EM type	IM	PMSM
Front axle disconnect clutch	applied	not applied

In this design study, eight different configurations, which can be derived using the morphological box in Table 2, are optimized individually. Both the front axle and the rear axle EM can be chosen to be either an IM or a PMSM. Additionally, the front axle can be optionally equipped with a decoupling device. At both axles a one-speed two-staged spur gear transmission is applied, with a fixed differential stage ratio of 3.5. Within the design algorithm, the overall ratios at the front axle i_f and at the rear axle i_r are optimized. The electrical machine design space is generated with the following input parameters. Both for IM and PMSM a double layer distributed three phase copper winding is chosen. The power factor is assumed to be 0.9. For both machines types the voltage level, the rated power, the nominal speed and the relative length are variable. The magnets within the PMSM rotor are integrated in a v-shape three pole pair arrangement, while the IM rotor has two pole pairs with aluminum as cage material.

All variable parameters are stored in the optimization vector $\boldsymbol{x}$, containing the voltage level U, the ratio of front i_f and rear axle i_r, the nominal speed of the front $\omega_{N,f}$ and rear axle $\omega_{N,r}$ machine and the maximum peak power of front $P_{em,f}$ and rear axle $P_{em,r}$.

$$\boldsymbol{x} = \begin{bmatrix} U \\ P_{em,f} \\ P_{em,r} \\ i_f \\ i_r \\ \omega_{N,f} \\ \omega_{N,r} \end{bmatrix} \tag{8.1}$$

Within the optimization, four objectives are minimized. The first objective is the electrical energy consumption E_{bat} within the WLTC. To ensure high and reproducible performance, the acceleration time is optimized both with peak power $t_{acc,p}$ and with continuous power $t_{acc,c}$. Lastly, the powertrain cost is minimized as well.

$$\boldsymbol{c} = \begin{bmatrix} E_{bat} \\ t_{acc,p} \\ t_{acc,c} \\ cost \end{bmatrix} \tag{8.2}$$

The cost term in $\boldsymbol{c}$ only contains EM, inverter and transmission costs (excluding the disconnect unit). Both the costs for the battery and for the disconnect are considered in the subsequent

analysis. Based on the evaluated energy saving potential, the battery reduction potential is calculated, assuming the same range target to be met. Combined with the battery costs, this results in a cost saving potential, which at the same time represents the trade-off costs for the disconnect unit.

$$\mathrm{cost}_{\mathrm{dc}} = \Delta E_{bat} * range * cost_{bat} \tag{8.3}$$

4.2 Results

All Pareto optimal results of the design study are shown in Fig. 5 and 6. Each subfigure represents one specific configuration. While the x-axis is denoting the electrical energy consumption in the WLTC in Wh/km, the y-axis shows the acceleration time from 0-100 km/h in seconds, which can be achieved with the systems peak power. Each configuration is shown four times to highlight four parameters. Both left-hand plots indicate the two remaining entries of $\boldsymbol{c}$ (cost and $t_{acc,c}$), while the two right-handed plot show highlight the peak power rear axle share and the front axle ratio for each respective solution.

In Fig. 5, all configurations with an IM rear axle are shown. Both configurations in 5a and 5b additionally have a front axle IM. These charts indicate, that the approximate disconnect potential is below 5 Wh/km. Among all Pareto optimal solutions, the rear axle share pre-dominantly varies between 40 and 60 %. Close to the slip limit, the rear axle tends to be higher, due to the dynamic axle load shift. While solutions without a disconnect unit have low front axle ratios, applying a disconnect allows for a shorter front axle ratio, without decreasing the maximum speed. These shorter ratios are beneficial for a higher acceleration time with continuous power. At high speeds, the front axle machine can be decoupled, so that the short ratio does not affect the maximum vehicle speed.

In 5c and 5d all Pareto optimal configurations with a front axle PMSM are shown. Although PMSM have higher zero load losses than IMs, the disconnect potential is neglectable low. For solutions with no front axle decoupling device, within the WLTC the load is pre-dominantly shifted to the small front axle PMSM, as the rear axle IM only causes mechanical losses. In combination with high rear axle shares (pre-dominantly between 40 and 70 %), this leads to an efficient operation of the front axle PMSM. If a disconnect unit is applied, the rear axle share generally drops for solutions not limited by the slip limit. While not increasing the efficiency, this leads in a better performance reproducibility, as the PMSM has a higher ratio between peak and continuous power. In combination with a disconnect unit, optimal solutions have slightly higher front axle ratios, having a positive impact on performance reproducibility.

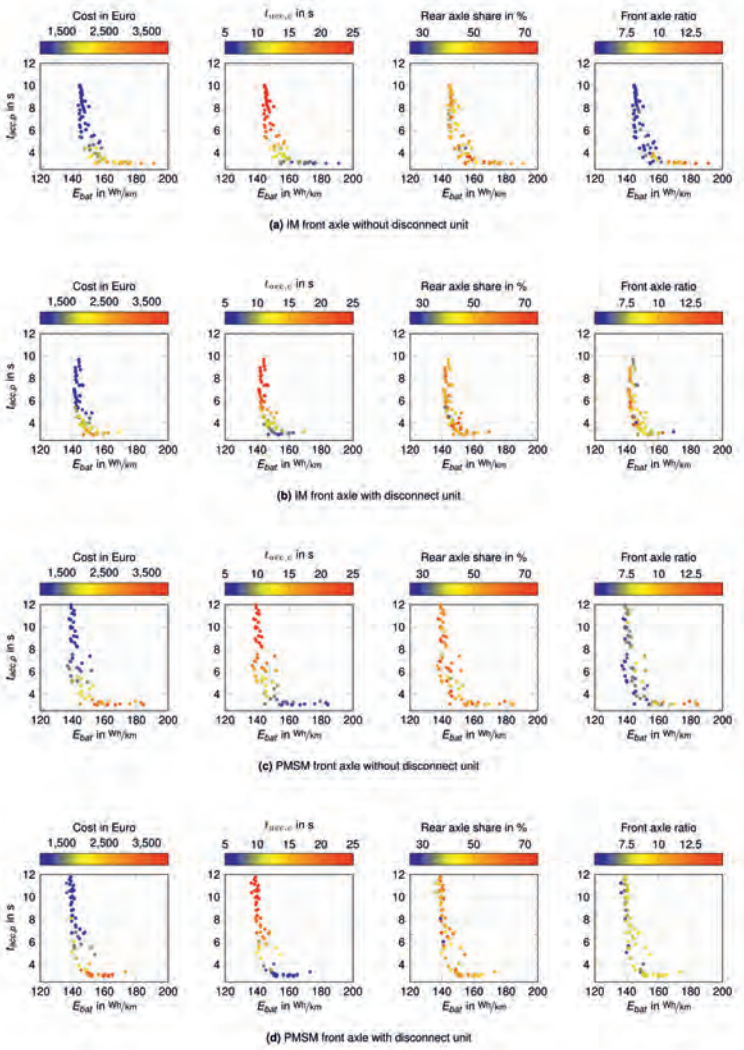

Fig. 5: Pareto optimal results for the configurations with an IM rear axle.

In Fig. 6 the PMSM rear axle variants are shown. For the IM front axle configurations in 6a and 6b the disconnect unit increases the efficiency. Avoiding the mechanical losses caused by the IM and the transmission results in an approximate disconnect potential of up to 5 Wh/km. Also, the performance of the system in thermal derating slightly improves with a disconnect unit. The rear axle share ranges between 30 and 60 %. Without a disconnect unit, lower rear axle power shares are optimal. Like the PMSM front axle IM rear axle configuration, this means a relatively small PMSM combined with a large IM. However high-performance solutions have an increased rear axle share, which is caused by the dynamic slip limit at front and rear axle. In combination with a front axle disconnect unit, the rear axle share increases. Again, optimal front axle ratios get shorter in combination with a disconnect unit.

In contrast to that, in PMSM only configurations, a disconnect clutch heavily increases the efficiency, as the zero torque losses of PMSM are significant (see 6c and 6d). For instance, high performance solutions benefit by an electrical consumption decrease of up to 10 Wh/km. The rear axle share is mostly in between 40 and 60 %, both with and without a disconnect unit. Again, applying a disconnect makes shorter front axle ratios favorable.

To identify the profitability of a disconnect unit, the energy saving potential must be quantified in an additional cost value. Assuming a range target of 800 km, this results in a trade-off cost value of 76 Euro per Wh/km according to eq. 8.3. In case of two PMSMs and a required acceleration close to the slip limit, the respective maximum costs can amount up to 760 Euro. For configurations with a front axle IM, the benefit is below 5 Wh/km, depending on the achieved acceleration time. Consequently, the trade-off cost range for the disconnect unit amounts to 380 Euro at most. If the front axle is a PMSM and the rear axle is an IM, a disconnect clutch does not increase efficiency, but performance in thermal derating.

Overall, solutions with an IM front and rear axle have the lowest cost level, but also the highest energy consumption and acceleration times in derated operation. On the contrary, powertrains with two PMSMs are most expensive, especially as low energy consumption requires a decoupling unit. With a decoupling unit, a PMSM only powertrain offers high efficiency combined with the highest performance reproducibility among all powertrain layouts considered in this study. In between, there are both mixed topologies. The IM rear axle mixed topology is highly efficient even without a disconnect unit and being less expensive compared to the PMSM rear axle mixed topology. The latter, however, is beneficial with respect to the performance reproducibility.

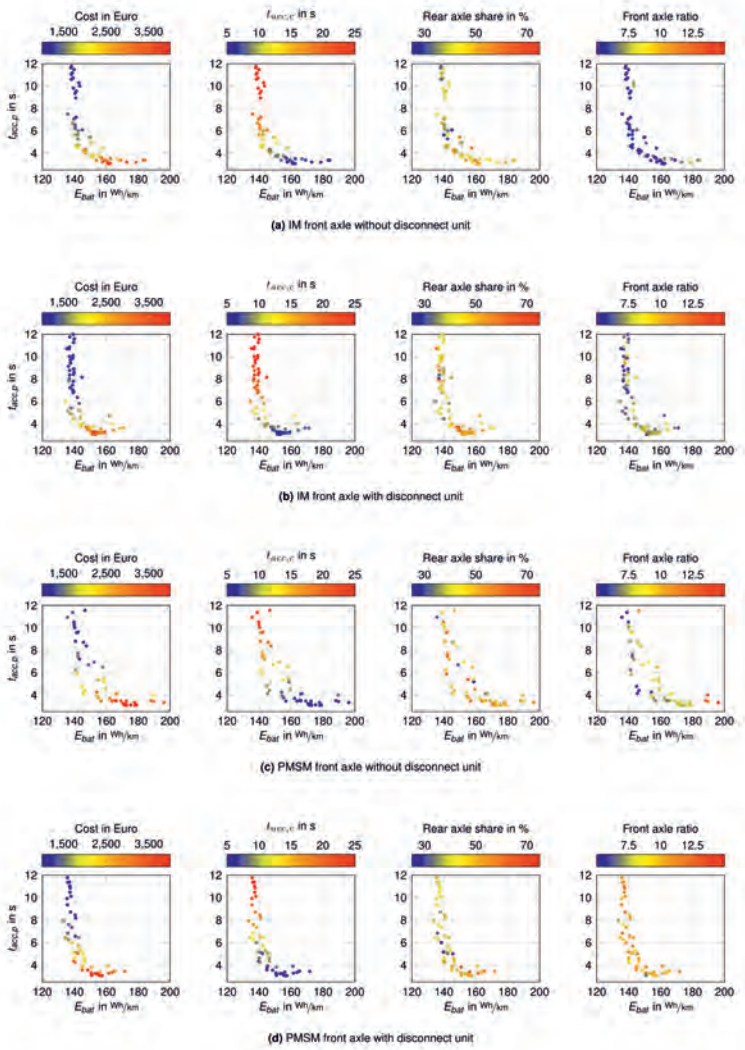

Fig. 6: Pareto optimal results for the configurations with a PMSM rear axle.

5 Conclusion

In this paper, a holistic design framework is being proposed to optimize all-wheel drive electric powertrains. Within a case study, the proposed framework was applied to a relevant design problem. Considering the premises in this paper, the following conclusions can be made:

- Configurations with a front axle IM only comprise a low disconnect potential at the front axle.
- In case of a rear axle IM and a front axle PMSM, decoupling the front axle PMSM leverages the derated performance, but not efficiency.
- If both front and rear axle are equipped with a PMSM, a front axle disconnect unit considerably improves energy efficiency for high performance configurations.
- In combination with a front axle disconnect clutch, higher front axle ratios are optimal, which increases the continuous wheel torque and the performance reproducibility.
- For mixed configurations with one IM and one PMSM, a front axle disconnect unit influences the optimal power share between front and rear axle.

The results generated by the design approach revealed important relations, proving that the proposed framework is suitable to get a holistic insight into the design problem and the cross-correlations of electrical all-wheel powertrains. A further investigation requires more detailed simulation data, such as numerically designed EMs, and additional factors to be considered, such as transverse dynamics, aspects of drivability, geometrical integration, and the thermal behavior of IMs and PMSMs.

Literature

[1] M. Vaillant, Design Space Exploration zur multikriteriellen Optimierung elektrischer Sportwagenantriebsstränge, Dissertation Karlsruher Institut für Technologie, 2015.

[2] M. Eghtesaad, Optimale Antriebsstrangkonfigurationen für Elektrofahrzeuge, Dissertation Technische Universität Braunschweig, 2014.

[3] P. Othaganont, F. Assadian und D. J. Auger, „Multi-objective optimisation for battery electric vehicle powertrain topologies," *Proceedings of the Institution of Mechanical Engineers, Part D: Journal of Automobile Engineering,* pp. 1046--1065, 2017.

[4] C. Danzer, Systematische Synthese, Variation, Simulation und Bewertung von Mehrgang- und Mehrantrieb-Systemen rein elektrischer und hybrider Fahrzeugantriebsstränge, Dissertation Technische Universität Chemnitz, 2016.

[5] S. Kalt, J. Erhard und M. Lienkamp, „Electric machine design tool for permanent magnet synchronous machines and induction machines," *Machines,* 2020.

[6] M. Zeraoulia, Benbouzid, E. H. Mohamed und D. Diallo, „Electric Motor Drive Selection Issues for HEV Propulsion Systems: A Comparative Study," *IEEE Transactions on Vehicular Technology,,* p. 1756–1764, 2006.

[7] M. Fries, M. Kerler, S. Rohr, S. Schickram, M. Sinning und M. Lienkamp, „An Overview of Costs for Vehicle Components, Fuels, Greenhouse Gas Emissions and Total Cost of Ownership Update 2017," ResearchGate, 2017.

[8] B. Propfe, Marktpotentiale elektrifizierter Fahrzeugkonzepte unter Berücksichtigung von technischen, politischen und ökonomischen Randbedingungen, Dissertation Universität Stuttgart, 2016.

[9] T. Reuschlé, Multizieloptimierung von Plug-in-Hybidantriebssträngen, Dissertation Karlsruher Institut für Technologie, 2019.

[10] C. Schulte-Cörne, Multikriterielle integrierte Systemoptimierung von hybriden Plug-In-Antriebssystemen, Dissertation RWTH Aachen, 2015.

[11] F. Weiß, Optimale Konzeptauslegung elektrifizierter Fahrzeugantriebsstränge, Dissertation Technische Universität Chemnitz, 2017.

[12] K. Deb, A. Pratap, S. Agarwal und T. Meyarivan, „A fast and elitist multiobjective genetic algorithm: NSGA-II," *IEEE transactions on evolutionary computation,* pp. 182-197, 2002.

High-voltage composite test bench for component testing of battery-electric vehicles

High-voltage component test of battery electric vehicles? Only in a system context!

Sven Hönicke, **Konrad-Fabian Wittwer**, **Jens Liebold**,
IAV GmbH, Stollberg

Zusammenfassung

Im Zuge der Elektrifizierung von Fahrzeugen müssen nicht nur Traktionsantriebe und immer leistungsfähigere Energiespeicher, sondern auch Peripheriegeräte und Nebenverbraucher im Hochspannungsnetz betrieben werden. Im Rahmen eines Projekts mit Audi hat IAV einen Hochvolt-Verbundprüfstand in Betrieb genommen, auf dem alle relevanten Komponenten getestet werden können, bevor sie in das Fahrzeug integriert werden. Dadurch lassen sich Entwicklungszeit und -kosten reduzieren.

Der von IAV entwickelte Hochvolt-Verbundprüfstand ermöglicht es, das Verhalten von Hochvolt-Komponenten – von der Batterie bis zum Fahrmotor mit allen notwendigen Steuergeräten und Nebenaggregaten – in einem Gesamtverbund zu untersuchen. Dadurch ist es möglich, die Funktion von Soft- und Hardware, insbesondere im Zusammenspiel miteinander, bereits in einem frühen Entwicklungsstadium zu validieren. Dabei werden die Eigenschaften von noch nicht im Hochspannungsnetz vorhandenen Komponenten durch Simulationen ersetzt. Alle Komponenten werden bei Bedarf individuell klimatisiert. Mittels einer selbst entwickelten Software werden die Testfälle direkt aus dem Anforderungsmanagement erstellt und getestet. Das spart Entwicklungszeit und Kosten. Damit stellt der Hochvolt-Verbundprüfstand in seiner Komplexität einen Benchmark im Bereich der Entwicklungsprüfstände dar.

Es hat sich gezeigt, wie wichtig es ist, Hochvoltkomponenten im Systemnetz zu untersuchen. Einen großen Einfluss auf die Testergebnisse hat die sogenannte Impedanz des Hochspannungsnetzes. Daher ist es erforderlich, anstelle einer Dummy-Last den „echten“ Nachbau eines Hochspannungsnetzes zu verwenden.

Für erste Untersuchungen zur Hochvoltsicherheit werden keine Testfahrzeuge eingesetzt. Dies gilt insbesondere in sehr frühen Phasen der Fahrzeugentwicklung. Die Strategie, solche frühfreigaberelevanten Untersuchungen auf dem Prüfstand und nicht auf der Straße durchzuführen, wird in Fachkreisen als „Road-to-Rig-Strategie“ bezeichnet.

Sicher haben Sie Ihre eigene Meinung, ob der eine oder andere Test wirklich relevant für den Fahrbetrieb Ihrer Kunden ist. Dennoch müssen wir die Standards erfüllen, die an unsere Produkte gestellt werden. Der Hochvolt-Systemprüfstand hilft uns, das gesamte Hochvolt-Komponentennetz zu untersuchen, ohne auf die Verfügbarkeit von Fahrzeugen angewiesen zu sein.

Abstract

In the course of vehicle electrification, not only traction drives and increasingly powerful energy storage systems, but also peripherals and auxiliary consumers must be operated in the high-voltage grid. As part of a project with Audi, IAV has commissioned a high-voltage compound test bench that allows all relevant components to be tested before they are integrated into the vehicle. This allows development time and costs to be reduced.

The high-voltage composite test bench developed by IAV makes it possible to investigate the behavior of high-voltage components - from the battery to the traction motor with all the necessary control units and auxiliary units - in an overall network. This makes it possible to validate the function of software and hardware, particularly in terms of their interaction with one another, at an early stage of development. In the process, the properties of components not yet available in the high-voltage network are replaced by simulations. All components are individually air-conditioned if required. By means of a self-developed software the test cases are created and tested directly from the requirements management. This saves development time and costs. In its complexity, the high-voltage composite test bench thus represents a benchmark in the field of development test benches.

It has become clear how important it is to examine high-voltage components in the system network. The so-called impedance of the high-voltage network has a great influence on the test results. It is therefore necessary to use the "real" replica of a high-voltage network instead of a dummy load.

No test vehicles are used for initial investigations regarding high-voltage safety. This is particularly true in very early phases of vehicle development. The strategy of carrying out such early release-relevant investigations on the test bench and not on the road is known in specialist circles as the "road to rig strategy".

Sure, you have your own opinion as to whether one test or another is really relevant for your customers' driving operations. Nevertheless, we have to meet the standards that are demanded of our products. The high voltage system test bench helps us to examine the entire high voltage component network without having to rely on the availability of vehicles.

Road to rig – Versuche von der Straße auf den Prüfstand holen

- „Road to Rig“ bedeutet, notwendige Untersuchungen nicht mehr im Fahrzeug auf einer Straße oder Teststrecke durchzuführen
- Ziel vieler Hersteller: Halbierung der Fahrzeugversuche um 50 % bis 2023
- Nochmalige Halbierung der Zeit im Fahrzeug bis 2030
- Um diese zu validieren müssen jedoch auch Komponenten abgebildet werden, die noch nicht existieren. In Fahrzeugen ist das so nicht möglich.

Das Herzstück: Der Multiplexer

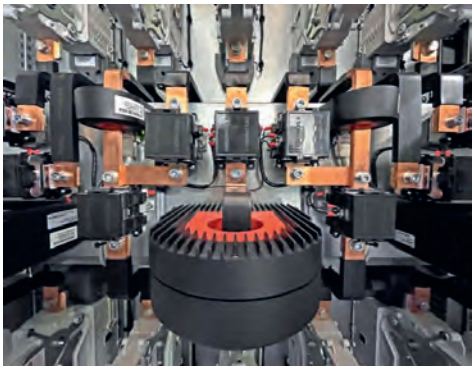

- Verschaltung der einzelnen Hochvolt-Komponenten zu einem Prüfsystem
- Anbindung einer realen Fahrzeugbatterie auch im Wechsel von Laden und Entladen
- Ableitung der Konfiguration vom Anforderungsmanagementsystem zur Prüfstandssteuerung und Durchführung von Prüfläufen voll automatisiert
- Elektrische Energie aktuell bis zu einem Megawatt Leistung möglich

→ **Vollständige Automatisierung von komplexesten Prüfabläufen**

13 IAV 05/2021 TS-T7 JLd Status: released, public

Zusammenfassung

- Das Prüfen von Komponenten für elektrifizierter und rein elektrische Fahrzeuge kann sehr komplex sein.
- Viele Freigaben bedingen das korrekte Verhalten zwischen den einzelnen Komponenten. Auch im Fehlerfall.
- Früher wurden einzelne Komponenten auf Basis von synthetischen Lastprofilen und Fehlerfallanalysen qualifiziert
- Aufgrund der immer komplexer werdenden Struktur aus immer mehr Hauptrechnern und immer weniger Steuergeräten, werden auch die Freigaben immer aufwendiger.

→ **Hochvolt-Komponenten sind im Systemverbund zu untersuchen**

→ **„road to rig strategy“**

16 IAV 05/2021 TS-T7 JLd Status: released, public

Development of a method for the automated validation of the shift quality of modern dual clutch transmissions on full-vehicle test benches

Univ.-Prof. Dr.-Ing. Dr. h. c. **A. Albers**, Dr.-Ing. **M. Behrendt**,
Karlsruher Institut für Technologie KIT, Karlsruhe;
Dipl.-Ing. **J. Köber**, Dipl.-Ing. (FH) **T. Breitinger**,
Dr. Ing. h.c. F. Porsche AG, Stuttgart

Zusammenfassung

Die Komplexität in der Fahrzeugentwicklung hat in den letzten Jahren deutlich zugenommen. Dies hat zur Folge, dass eine vollständige Validierung mittels physischer Fahrversuche auf der Straße oder Teststrecke nur mit sehr hohem Kosten- und Zeitaufwand realisierbar ist. Besonders deutlich wird dies am Beispiel der Validierung der Schaltqualität moderner Doppelkupplungsgetriebe, bei der bis zu 8500 Schaltungen pro Derivat und Motor-Getriebe-Variante auf separaten Testgeländen geprüft und für die Freigabe subjektiv bewertet werden müssen. Um dem Anspruch einer vollständigen Produktvalidierung mit reduziertem Kosten- und Zeitaufwand gerecht zu werden, wird eine Methode vorgestellt, um komplexe Manöver der Schaltqualität frühzeitig auf Gesamtfahrzeugprüfstände zu übertragen und automatisiert zu validieren. Dabei soll infolge der Reproduzierbarkeit die statistische Aussagekraft der Validierung erhöht werden.

Abstract

The complexity of vehicle development has increased significantly in recent years. As a result, complete validation by means of physical driving tests on the road or test track can only be realized at very high cost and time. This is particularly evident in the example of validating the shift quality of modern dual-clutch transmissions, where up to 8500 gearshifts per derivative and engine-transmission variant have to be tested on separate test tracks and subjectively evaluated for approval. In order to meet the demand for complete product validation at reduced cost and time, a method is presented for transferring complex shift quality maneuvers to full vehicle test benches at an early stage and validating them automatically. As a result of the reproducibility, the statistical significance of the validation is to be increased.

State of Research

Albers formulates as a fundamental hypothesis of his research on product development processes that validation is the central activity in the development process [2]. The basic idea is that, as a result of continuous validation in the development process, a constant comparison is made between the objectives and purposes of the product and the stage of development reached in each case [3]. With this understanding, validation shapes the entire product development process and makes a significant contribution to finding creative solutions [4]. Due to the time and cost constraints to which every product development process is subjected, a fully comprehensive validation is hardly possible or only possible with very great effort. Consequently, the goal must be to derive efficient reference processes based on the experience and competencies of the developers by means of methodical principles [2]. Based on this basic understanding, Albers and Matros present the Pull-Principle of validation [5]. This takes up the disadvantages of the sequential process models (e.g. V-model according to VDI 2206) with regard to the integration of validation activities and transfers them from a post-process validation (Push-Principle) to a process-accompanying, activity-initiating validation (Pull-Principle). In the sense of the Pull-Principle, the validation activities should not take place as a concluding phase, but should be continuously integrated into the Product Development Process (PDP) [6].

To meet this continuous validation, Albers transfers and extends the "in-the-loop" validation approach to powertrain and complete vehicle level. He describes the IPEK-X-in-the-loop (IPEK-XiL) approach for any (sub)system under investigation that is integrated into a validation environment (VE) either physically, virtually or combined physically-virtually [7, 2]. The aim of the approach is to connect VEs based on models, methods and tools used across VEs and to make their use more flexible along the PDP. Compared to conventional approaches, the IPEK-XiL approach offers the advantage that the system (X) to be validated is not exclusively integrated into virtual environments. Depending on the validation objective, the connected systems can therefore also be physical, virtual or physical-virtual.[2].

Since this paper presents a method for automated validation of shift quality on full vehicle test benches, the following chapter will provide basic knowledge about the shift sequence of dual-clutch transmissions and the resulting shift quality. Dual-clutch transmissions and transmissions in general are an integral part of the powertrain [8]. In addition to the technical design, the control and regulation of the gearboxes have a decisive influence on the characteristics of the product [8]. In addition to selecting the most suitable gear depending on the current driving situation, one of the essential functions of the transmission control unit (TCU) is to control and regulate gear changes and the engine interface. Gear changes are

consciously perceived by the driver, which is why ensuring optimum shift quality at all operating points is one of the primary task of the TCU [8]. Depending on the orientation of the torque on the wheel or drive train, gearshifts are subdivided into drive or coast gearshifts. If the torque is positive, these gearshifts are referred to as drive gearshifts. In the case of a negative torque, they are referred to as coast gearshifts [1]. In addition, a distinction is made between upshifting and downshifting, i.e. whether the target gear is increased or decreased. Depending on the resulting four main shift modes, individual gearshift sequences are executed by the TCU. In addition, there are gearshifts in which the driver's request changes during the gearshift sequence in the form of increasing or decreasing the accelerator pedal or the brake pedal (so-called change-of-mind gearshifts or abort gearshifts) [1]. The transmission control system must react adequately to this change and adapt the gearshift sequence if necessary. The gearshift sequence of a dual clutch transmission is illustrated by means of a drive upshift. The TCU must react adequately to this change and adapt the gearshift sequence if necessary. The gearshift sequence of a dual clutch transmission is illustrated by means of a drive upshift (see Fig. 1). Basically, the gearshift sequence is divided into four phases, which is shown by the four time markers. In phase 1, the clutch K_1 is closed. The clutch K_2 is initially open, whereby at the start of the gearshift the hydraulic cylinder for actuating K_2 is filled with a rapid pressure increase and then kept approximately constant in order to find the touch point [9]. At this point, the clutch plates just touch, the clutch torque is about 0 Nm and the clutch turns from open to slipping state [9]. Nevertheless, the entire torque is still transmitted completely via K_1. The clutch torque M_{K1} is lower than the engine torque by $J_{ENG} \cdot \dot{\omega}_1$. In phase 2, K_2 closes continuously and,

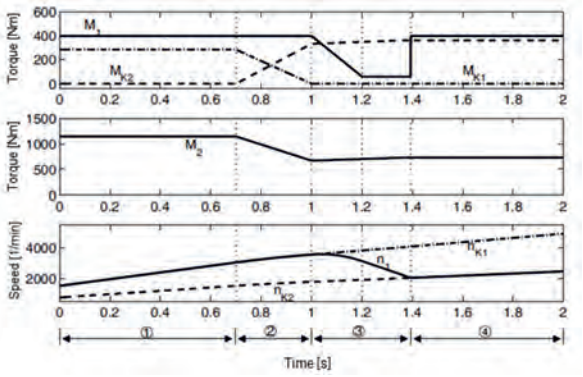

Fig. 1: Drive upshift with engine intervention [M_1 – Engine torque; M_2 – Transmission output torque; $M_{K1/K2}$ – Torque at clutches K_1/K_2; $n_{k1/K2}$ – Speed at clutches K_1/K_2; n_1 – Engine speed] [1]

consequently, torque is transmitted. Meanwhile, K_1 opens, which is why the torque M_{K1} on K_1 decreases. At the end of the phase 3, the torque is completely transferred to K_2. Due to the new gear ratio, the gearbox output torque M_2 is reduced. In the subsequent speed synchronization phase (phase 3), the engine torque is reduced to match the speed to the target speed. This is primarily done for comfort reasons, since an increase in acceleration torque during gearshifts without intervention of the engine is perceived as inharmonious [1]. After the speed has adapted to the target speed n_{K2}, the motor torque is increased as quickly as possible to the original level in the last phase. Again, the transmitted clutch torque M_{K2} is lower than the engine torque by $J_{ENG} \cdot \dot{\omega}_1$. The gearshift sequence described corresponds to an ideal process. Any deviations in the system reactions of the transmission and engine can significantly affect the shift comfort. For example, inharmonious sequences when opening or closing the clutches can lead to disturbances in the torque characteristics, which are perceived as very uncomfortable (e.g. flares or tensions) [1]. As already described, the control of the gearshift sequence including engine intervention is intended to ensure the best possible gearshift. The optimum is always defined as a function of the current driving style and the selected mode (e.g. Normal, Sport, etc.). Comfortable gearshifts are therefore aimed for in Basic or Normal mode with balanced driving, whereas performance-optimized and thus more dynamic or noticeable gearshifts are required in Sport mode with sporty driving. Validation of the resulting shift quality is currently primarily carried out as a function of subjective perception within the framework of driving tests on the road or test track. However, subjective assessments are always subject to non-measurable variations and influences such as the experience or daily form of the test persons. To counter these disadvantages, there are already some approaches to objectifying shift quality [9–11]. A very widespread and frequently used tool for objectification by automotive manufacturers is the AVL-Drive tool. Chandrasekaran et al. were able to demonstrate a very high correlation (R^2=0.8) between subjective perception and objective AVL-Drive scores [12]. Schöggl et al. state an accuracy of 95% of the AVL-Drive scores compared to the subjective assessment [13]. Due to the described performance and distribution of the tool in the automotive environment, AVL-Drive will serve as the basis for the further consideration of the present work. AVL-Drive processes physical variables such as engine speed, vehicle velocity and longitudinal acceleration. By means of fuzzy logic, a driving state detection (e.g. drive upshift or start-up) is performed, which can be evaluated on the basis of multiple criteria [13]. Depending on the weighting and evaluation of the individual criteria, an overall score is formed for each driving condition, which is based on the ATZ scale [14]. In 15 of 21 criteria for evaluating shift quality, longitudinal acceleration is a relevant and in 11 of 21 it is the sole basis for evaluation [15]. Consequently, it can be hypothesized, that longitudinal

acceleration on a plane road is the most relevant measured parameter for evaluating shift quality in AVL-Drive. For the evaluation of measurements from real driving tests, sensor signals of the longitudinal acceleration can be used, which are either already installed in the vehicles or additionally attached. It is evident that these sensors cannot be used in full vehicle test benches, since the vehicle does not encounter real acceleration. In particular for full Vehicle-in-the-Loop (ViL) or Powertrain-in-the-Loop (PiL) test benches, the longitudinal acceleration must be calculated using suitable models, since a measurement - such as with roller dynamometers using a force gauge - is not possible. For this purpose, a longitudinal force is calculated based on the measured output torques of each wheel and the correlating tire models. Taking the vehicle mass into account, the resulting longitudinal acceleration can be determined from this (see Fig. 2) [16]. This trivial model of a single-mass oscillator can represent longitudinal acceleration well in steady-state situations. However, as Bauer et. al. already observe, in transient conditions these models are not able to represent the real road behavior with sufficient accuracy. He describes the curves of the calculated longitudinal acceleration as too "smooth" [16]. To address this problem, Bauer et. al. present an approach in which linear actuators on the shafts between the wheel flange and the dyno are used to reproduce a more accurate behavior of the longitudinal acceleration. For this purpose, the axles are physically excited with the longitudinal force, which is calculated from the measured wheel torques and the associated tire model. An acceleration sensor in the vehicle is used to

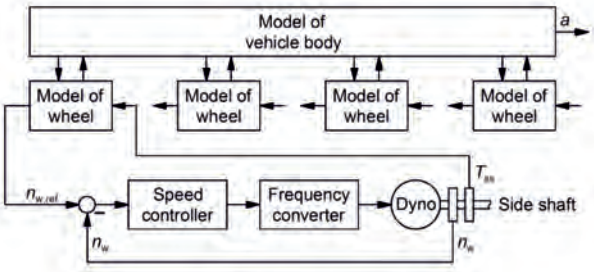

Fig. 2: Calculation of longitudinal acceleration on full vehicle test benches using single-mass oscillator [16]

record the real transmission behavior of the physical actuator excitation from the axles to the body. The measured oscillation is subsequently imposed on the calculated longitudinal acceleration of the initial single-mass model using a special data fusion. It could be shown that with this approach significantly more realistic curves of the longitudinal acceleration in transient

conditions can be obtained. Nevertheless, this approach has two major drawbacks. On the one hand, setup and calibration of the actuators are very time-consuming. On the other hand, this approach is only applicable on ViL test benches. Transfer in the context of the IPEK-XiL approach to PiL test benches without a physical body is not possible. In contrast, a method presented by Albers et. al can be used to parameterize physical models using experimental data, independent of the selected validation environment [17]. The parameters are selected in such a way that the model delivers sufficiently accurate results with respect to initially selected criteria. This procedure is exemplified by the calculation of the longitudinal acceleration. Here, as well, it is shown that the calculated longitudinal acceleration of the model does not represent the real driving test with sufficient accuracy. In particular, the higher-frequency components are not represented, which Albers et. al explain with the missing elasticities in the model. [17] In order to reduce the time required for measurement to generate the test data for model parameterization and optimization, Albers et. al present a suitable method [18]. The maneuvers of the individual parameter variations are arranged in such a way that the total time required between the maneuvers is minimized. They explain this approach using the example of the evaluation of shift quality on roller test benches. It was shown that this optimization approach can reduce the required validation time by 80% [18]. However, it is not investigated whether the shift quality on roller test benches can be validated in principle and whether the time optimization has an influence on the shift quality.

Situation Analysis, Motivation and Objective

At present, despite the existence of alternative validation environments (e.g. ViL or PiL), powertrain development and especially the application are still heavily dependent on driving tests with physical prototypes. This is primarily due to the fact that the application requires subjective perception as a relevant evaluation parameter as part of its development and validation activities. This connection has already been vividly illustrated using the application of the gearshift sequence in the state of the research. Furthermore, there is a lack of directly usable methods for transferring validation activities from the road to alternative validation environments. This is primarily due to the fact that method development in the automotive environment often runs concurrently with the series development process rather than in support of it. For example, a very extensive maneuver catalog for validating shift quality continues to be driven on separate test tracks and subjectively evaluated in the context of transmission application. This maneuver catalog is made up of all shift types already described in the state of research, which in turn cover all driving modes (normal, sport, race), loads and operating states. Depending on the derivatives to be validated (e.g. conventional or PHEV),

this results in approx. 7500-8500 gearshifts to be evaluated. In total, the applicators need about one week per derivative to run and evaluate the entire maneuver catalog. This approach has a number of disadvantages, some of which are described below. First of all, the dependence on prototype vehicles means that validation of the shift quality is only possible at a very late stage in the PDP, and potential problems can only be identified at a correspondingly late stage. In addition, real driving tests are always very time-consuming and costly, while at the same time lacking reproducibility. Furthermore, evaluations by means of subjective perceptions are always subject to variations, which has also already been discussed in the state of research. Thus, both the maneuver and the evaluation are not reproducible, which ultimately significantly increases the scatter of the results. On the basis of this situation analysis it can be stated that on the one hand a transfer of the validation activities to early in the development process in the sense of the pull principle makes a significant efficiency increase possible. On the other hand, an automation and objectification make a substantial increase of the statement quality possible due to the better reproducibility. From this, the objective of the present work is derived. A method for fully automated, test bench-based validation of shift quality is to be developed. In the sense of the IPEK-XiL approach and the associated consistency and flexibility throughout the entire PDP, the method is to be implemented in such a way that it can be used not only on ViL test benches, but also on PiL test benches at an early stage. This ensures that, in accordance with Albers' pull principle, the most suitable validation environment is available and usable at any point in the PDP [5]. The disadvantage of very late problem identification can thus be countered. In addition to transferability, complete automation is another essential requirement for the method. This is particularly relevant, in addition to easier handling by the application engineers, to ensure the reproducibility mentioned. This offers the possibility of making well-founded statements about the scatter of the gearshift sequences under constant conditions. In addition, automation offers the possibility of running test runs overnight on the test bench, for example, which in turn enables a reduction in prototype operating time.

Maneuver plan as a requirement for automated validation

In order to meet the requirements of automation, it is essential to establish a suitable logic for controlling the vehicle on the test bench. For this purpose, the maneuvers of the existing maneuver catalog must first be analyzed with regard to their input parameters and then transferred to a suitable maneuver plan. It is evident that all gearshifts with a positive transmission input torque (drive gearshifts) require an accelerator pedal as input parameter. However, in addition to the accelerator pedal, other information is required. For example, the shift strategy determines the shift points for drive upshifts in D depending on velocity and

accelerator pedal value. In addition to the specification of an accelerator pedal, a velocity for the gearshift to be driven is thus also required. In contrast, upshifts in M do not require a velocity, but an engine speed at which the gearshift is to be actuated, since the request for a gearshift is initiated by the driver and not by the shift strategy (see Fig. 3). Drive downshifts also require this speed specification, since an accelerator pedal jump (so-called Tip In) is to be made to a defined value at a given speed. In all gearshifts with negative transmission input torque, the decisive input parameter is therefore not the accelerator pedal but the brake pedal or the resulting negative acceleration. In addition to this, the speed for actuating the gearshift is also specified in M in the case of coast downshift and coast upshifts, whereby the latter are usually actuated without braking. Regardless of the gearshift type, the gearshift sequences are applied differently depending on the current mode (Normal, Sport, etc.), which is why this is also a relevant input parameter for all maneuvers.

Drive Upshift | Normal | D					
	1 - 2	2 - 3	3 - 4	4 - 5	5 - 6
20%	7,5	8,0	8,5	8,5	9,0
40%	7,0	7,5	8,0	8,5	8,5
60%	7,5	7,5	8,0	8,0	9,0
80%	7,0	7,0	7,5	8,5	8,5
100%	6,5	7,0	8,0	8,0	7,5

Drive Upshift | Normal | M						
		1000 1/min	2000 1/min	3000 1/min	4000 1/min	5000 1/min
80% Pedal	1-2	7,5	7,5	8,5	8,0	8,5
	2-3	7,0	7,5	8,0	8,5	9,0
	3-4	7,0	8,0	7,5	8,0	8,5
	4-5	6,5	6,5	7,5	7,5	9,0
	5-6	6,5	7,0	8,0	8,5	8,0

Fig. 3: Excerpt from an example filled maneuver catalog with ratings according to the ATZ scale for drive upshifts in D and M

Based on the identified input parameters, the following section illustrates how the existing maneuver catalog can be transferred into a suitable maneuver plan using the example of the drive upshift in D. In the context of this work, a maneuver plan is a sequence of individual maneuvers that can be run chronologically by the test bench. Thus, the maneuver catalog represents the collection of all maneuvers to be validated, which are transferred into a chronologically drivable maneuver plan for an automated validation [19]. Each maneuver of the maneuver plan contains the relevant input parameters (e.g. accelerator pedal value, mode, etc.) and a target value (so-called progression criterion), which must be reached so that the next maneuver is executed. As already described, the gearshift strategy determines the velocity at which the desired gearshift is executed at the current accelerator pedal value. Accordingly, it is theoretically sufficient to set the required accelerator pedal value just below this velocity, wait for the gearshift and then reduce the pedal again directly afterwards. However, it is necessary to set the required accelerator pedal value already at a lower velocity in order to take into account the delayed torque rise of the combustion engine. This offset is also relevant for the evaluation of the shift quality, as it ensures that the load change has no unwanted influence on the evaluation. e.g. as a result of acceleration disturbances. The same applies to all activities after the end of the gearshift. It must be ensured that the accelerator

pedal is held constant for a defined time afterwards. To prevent subsequent gearshifts within this time, a change from D to M must be made directly after the identified end of the gearshift. To do so, the exact end of the gearshift must be identified. This information is usually provided by the TCU via the BUS architecture and can consequently be measured. The resulting process of the described drive upshift is shown in Fig. 4. Maneuver 1 shows how the brakes are applied to a defined target speed. When the speed is reached, the brake is reduced (longitudinal acceleration increases) and then the required accelerator pedal value is set (maneuver 2). This maneuver is active until the test bench control detects a change of the gear. This moment indicates the start of the gearshift and is followed by maneuver 3. In this maneuver, the end of the gearshift is waited for. This point in time is reached when the engine speed has adapted to the speed of the 2nd gear shaft (t≈3.2 sec). Subsequently, the maneuver and thus also the accelerator pedal are kept active for a defined dead time (Δt=0.5sec). This is followed by maneuver 4, in which the accelerator pedal is reduced and the test sequence for this drive upshift is thus completed. Consequently, the maneuver plan for each gearshift consists of several individual maneuvers. Once the required target value of the respective maneuver has been reached (e.g. braking to speed, accelerating to gearshift), the next maneuver follows seamlessly.

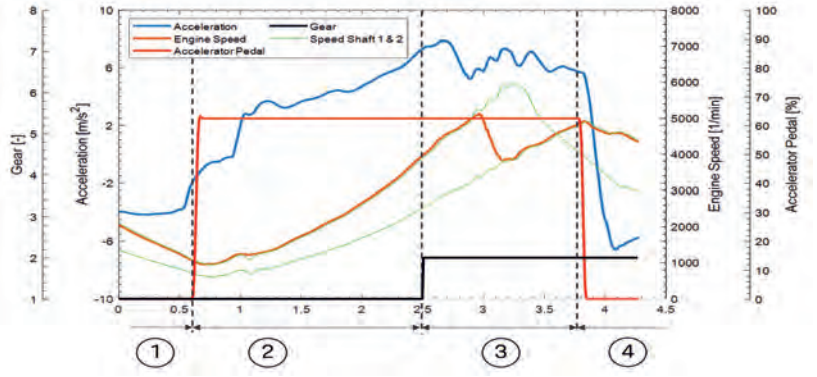

Fig. 4: Sequence of a fully automated drive upshift at the ViL *[1 – Braking until start velocity; 2 – Accelerate until gearshift; 3 – Wait until end of gearshift + time; 4 – Accelerator pedal reduction + Start next maneuver]*

In accordance with the initial requirement for automation, the transfer of the maneuver catalog to the maneuver plan is algorithm-based. Each maneuver is assigned a unique number (so-called load step ID). This enables a subsequent, fully automated assignment of the evaluations in the original maneuver catalog of the test bench measurements. In addition, the loadstep ID

simplifies a detailed analysis of the gearshifts by the application engineers, since the gearshift being searched for can be located directly in the potentially very large measurements. In order to ensure complete automation not only in the generating of the maneuver plan, but also in the test sequence, it is essential to implement an algorithm that intervenes in a regulating manner in the event of discrepancies between the target and actual states. In the present context, this discrepancy is primarily caused by different gears. For example, the target gear of multi drive downshifts cannot always be accurately predicted as a result of minimal deviations in the speed at the time of the accelerator pedal increase. In order to not disturb the further test sequence, the algorithm has to detect this discrepancy and shift automatically to the required target gear by means of manual gearshifts. With this approach, it is possible to run the entire maneuver catalog for validating shift quality completely automatically on the test bench. The order of the maneuvers in the maneuver plan does not have to be chronological but can also be optimized according to the approach of Albers et. al with regard to the time required [18].

Development of a suitable model for the calculation of the longitudinal acceleration

As already discussed in the state of research, AVL-Drive is used for the evaluation of the shift quality in the context of the present work. Furthermore, it has already been shown that the longitudinal acceleration in AVL-Drive is the most relevant parameter for evaluating shift quality and that this is not described with sufficient accuracy using existing approaches, especially in transient states. Although negative gearshift sequences are powertrain-induced, transient phenomena, the author is not aware of any publications in which their influence on the calculated longitudinal acceleration at ViL has been investigated. Therefore, in an initial proof-of-concept study, it was first investigated whether bad gearshifts could in principle be identified on ViL. For this purpose, a special gearshift was applied in such a way that the clutches are tensioned during torque transfer, which leads to a noticeable shock in the powertrain. Subsequently, this gearshift was driven in a road test and on the ViL and the measured and calculated longitudinal acceleration were compared. The calculation on the ViL is based on the conventional model, which was already presented in the state of research. Considering the curves, it can be seen that both the amplitudes and the damping behavior of the ViL deviate significantly from the road measurement. The resulting curves of the longitudinal acceleration are shown in the upper section of Fig. 5. If we transfer the time-dependent curves into the frequency domain (Fig. 5, bottom), it can be seen that especially the frequencies in the range of 10-13Hz are not represented at the ViL. The characteristic frequency of the body of the vehicle, which was used for the proof-of-concept study, lies in this range. Considering that the integrated acceleration sensors of modern vehicles are typically attached to the body in the

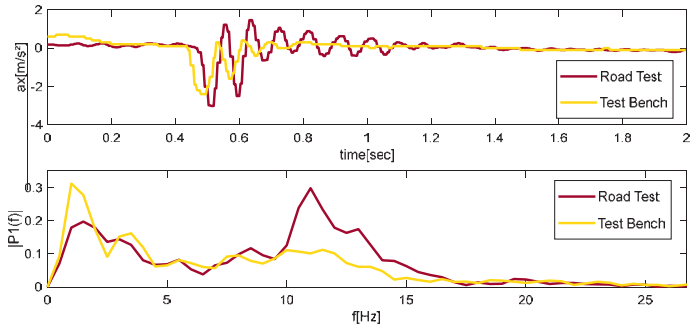

Fig. 5: Curves of longitudinal acceleration in the time domain (top) and frequency domain (bottom) based on a negatively calibrated drive upshift in D

area of the Center of Gravity (CoG), it becomes apparent that the measured longitudinal acceleration of the road test represents the resulting vibration of the body. Since these vibrations are ultimately also those perceived by the driver, they are decisive for the evaluation of shift quality. As a trivial single-mass oscillator, the existing model cannot represent the transmission behavior of the powertrain-induced oscillations from the aggregates via the subframe to the body. Consequently, the model must be extended so that a more realistic longitudinal acceleration can be calculated. Essential masses of the oscillating system are the body, the aggregates (engine and transmission) and the axles. If the aggregates are considered as one mass, three relevant oscillating masses are obtained. The axles are connected to the body via the subframe mountings and the aggregates in turn are connected to the body via the aggregate mountings. Since the individual wheel torques on the ViL can be measured directly via the dynos and converted into resulting longitudinal forces by a suitable tire model (e.g. Pacejka model), this force can be used as an input variable for the resulting three-mass oscillator. The final setup of the three-mass oscillator is shown schematically in Fig. 6. It should be noted that the parameterization of the model with regard to masses and spring and damper characteristics requires explicit knowledge of the vehicle. A striking

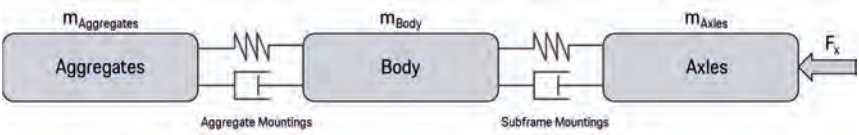

Fig. 6: Schematic set-up of the three-mass oscillator for the calculation of a longitudinal vehicle acceleration in transient states

advantage of the model approach compared to physical solutions is that it can also be used on the powertrain test bench (PiL). Furthermore, with appropriate preparation of the model, no additional setup time is required at the test bench for any actuators, etc.

Analysis and classification of the results

When analyzing the results, it is first necessary to investigate how the three-mass oscillator approach affects the resulting longitudinal acceleration. Based on this, the next step is to analyze the impact of this modified longitudinal acceleration on the evaluation of the shift quality using AVL-Drive. Fig. 7 shows that the longitudinal acceleration, which was calculated on the basis of the three-mass oscillator, achieves a much better accuracy in relation to the driving test. Both the amplitudes and the post-oscillation behavior are significantly better reproductions of the real driving test. Since the model is still a simplified representation of the real oscillation system, absolute comparability cannot be achieved, but this is also not the claim of the present investigations. Nevertheless, the model of the three-mass oscillator is able to represent the time-dependent graph of the longitudinal acceleration in stationary as well as in transient states sufficiently accurately.

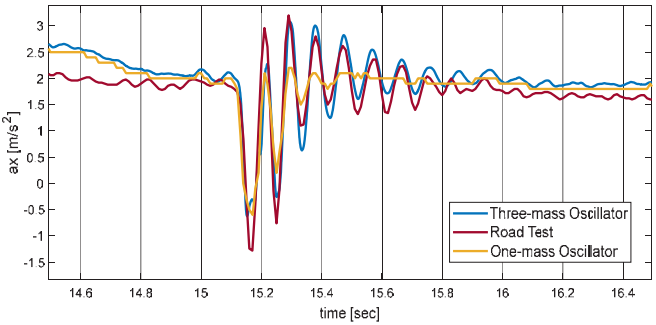

Fig. 7: Influence of the three-mass oscillator on the calculated longitudinal acceleration

Based on these findings, the next step is to investigate the influence on the evaluation of shift quality using AVL-Drive. For this purpose, all four main shift modes are approached with different accelerator pedal and speed inputs. To account for the natural scatter of the gearshifts, all gearshifts are driven five times each, both on the ViL and during the drive test. The results of each of the five measurements are combined into a mean value and corresponding standard deviation. In order to create a direct comparability between road and test bench, it is necessary to reduce all interfering factors of the road measurement during the evaluation. In the present context, the primary disturbance variable is road excitation due to

bumps. In order to neglect these unevennesses in the evaluation, AVL-Drive offers a so-called Road Interference Compensation, which acts as a bandpass filter from a freely selectable limit value onwards [15]. Road excitation is recorded via additionally attached acceleration sensors in the vertical direction on the wheels. Fig. 8 shows an example of the mean values and standard deviation of the resulting AVL-Drive ratings of the shift quality of drive upshifts with different gearshifts and accelerator pedal values. As already presented in the state of the research, the grades are based on the well-known ATZ scale. First of all, it is evident that the three-mass oscillator approach, and the longitudinal acceleration obtained with it, have a significant influence on the AVL-Drive rating. The acceleration curves obtained with this approach allow much more accurate results compared to the conventional single-mass oscillator approach. This confirms the initial hypothesis that longitudinal acceleration has the

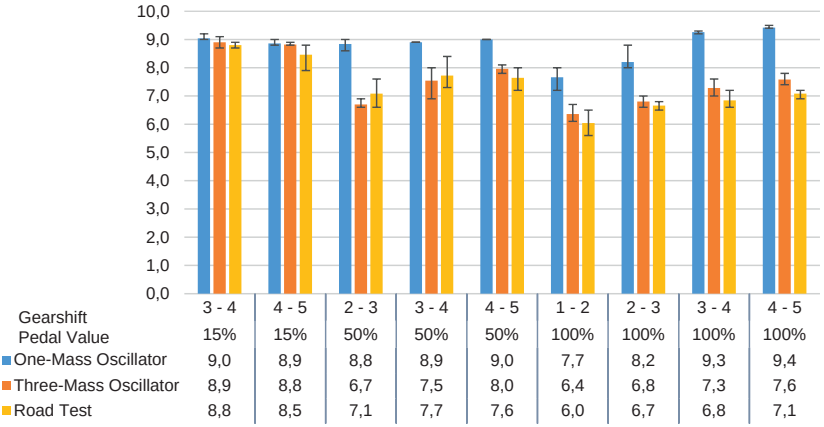

Gearshift	3 - 4	4 - 5	2 - 3	3 - 4	4 - 5	1 - 2	2 - 3	3 - 4	4 - 5
Pedal Value	15%	15%	50%	50%	50%	100%	100%	100%	100%
One-Mass Oscillator	9,0	8,9	8,8	8,9	9,0	7,7	8,2	9,3	9,4
Three-Mass Oscillator	8,9	8,8	6,7	7,5	8,0	6,4	6,8	7,3	7,6
Road Test	8,8	8,5	7,1	7,7	7,6	6,0	6,7	6,8	7,1

Fig. 8: Comparison of the shift quality evaluation of the conventional single-mass oscillator (blue), the three-mass oscillator (orange) and the real driving test (yellow)

most relevant influence on the evaluation when using AVL-Drive for analysis. If this can be mapped more accurately, the results are also more comparable to real driving tests on test tracks. In addition, it can be seen that the three-mass oscillator model has a much greater influence for lower grades than for very good grades. For example, the rating of the three-mass transducer for the 3-4 drive upshift with 15% accelerator pedal is only 0.1 grade points worse than with the conventional single-mass transducer. This is due to the fact that with very good gearshift sequences, no oscillation or discontinuity can be detected on the longitudinal acceleration. Consequently, even with the three-mass oscillator, no relevant oscillation on the longitudinal acceleration will be seen with a very good gearshift. With more negative gearshift

sequences, the influence is much more pronounced due to the transient state, which is also evident in Fig. 8 (e.g. 3-4 with 100% accelerator pedal). Taking into account the standard deviation shown, it becomes apparent that repeated driving of the gearshifts is necessary in order to generate a valid statement regarding the shift quality. Even under fully reproducible conditions on the test bench, the gearshift sequence has a standard deviation of up to ±0.5 grade points.

Summary and Outlook

In this contribution a method could be presented, which makes a completely automated validation of the shift quality on the test bench possible. The implementation of a maneuver plan was explained, which acts as the basis for automation. Based on this, it was shown how existing approaches for calculating the longitudinal acceleration on ViL test benches were further developed in order to generate a more comparable result to the road measurement, especially in transient conditions. The resulting model for calculating longitudinal acceleration, based on a three-mass oscillator, offers the fundamental advantage that no additional setup and calibration time is required at the test bench. In addition, the model offers the possibility, in the sense of the pull principle of validation and the consistency of the IPEK-XiL approach, to be used on PiL test bench as well. The only prerequisite for this is the ability to measure the wheel torques accurately. In this way, precise validation of the shift quality can be carried out at a very early stage of development, even if, for example, prototype vehicles are not yet available. Even with the reduced model quality due to the lack of support reactions of the body on the PiL, poor gearshifts can be identified and corrected at an early stage with the three-mass oscillator. This allows a significant reduction in the amount of time the application engineer needs to be in the vehicle, since with much more sophisticated transmission data sets, the first prototype vehicles can already be put into service.

The full automation of the method offers a significant increase in efficiency for the company and the application engineer. Thus, using a time-optimized maneuver plan, the time required for the gearshift quality validation for 8500 gearshifts can be reduced from previously five days on restricted test sites to eight hours on the ViL with comparable results. Due to the significant reduction of the required time and the fully reproducible framework conditions, it is possible for the first time to investigate the scatter of the gearshift sequences of all gearshifts of the maneuver catalog. Whereas up to now all gearshifts were driven only once, in the future all gearshifts will be driven at least three times. In addition, the time during which the continuously reduced prototype vehicles are not used can be minimized, since validation is possible overnight due to automation.

The existing approach to validating shift quality can be extended in future studies. For example, start-up processes can also be investigated, or load changes can be introduced into the gearshifts in order to force change-of-mind gearshifts or gearshift aborts. In particular, load changes in gearshifts pose special challenges for the application engineers, since the resulting, very individual gearshift sequences can hardly be reproduced and thus validated. Furthermore, it is possible to combine the validation of the gearshift sequence with additional emission measurement technology in order to meet the requirements of the future exhaust gas standards at an early stage. For example, emissions resulting from engine interventions during gearshifts at different loads can be investigated and optimized at an early stage.

References

[1] Fischer, R.; Kücükay, F.; Jürgens, G. *et al.:* Das Getriebebuch. Springer Vieweg, Wiesbaden, 2016.

[2] Albers, A.; Behrendt, M.; Klingler, S. *et al.:* Verifikation und Validierung im Produktentstehungsprozess. *In: Lindemann, U.* (Hrsg.): Handbuch Produktentwicklung. Carl Hanser Verlag, München, 2016, S. 541-568.

[3] Albers, A.; Behrendt, M.; Ott, S.: Validation - Central Activity to Ensure Individual Mobility. *In:* Automobiles and sustainable mobility – Proceedings of the FISITA 2010 World Automotive Congress, Budapest, Hungary, May 30 - June 4, 2010, S.l., 2010.

[4] Albers, A.: Five Hypotheses about Engineering Processes and their Consequences. *In:* Proceedings of the TMCE 2010, Ancona, Italien, 2010.

[5] Albers, A.; Matros, K.; Behrendt, M. *et al.:* Das Pull-Prinzip der Validierung – Ein Referenzmodell zur effizienten Integration von Validierungsaktivitäten in den Produktentstehungsprozess. *In:* Verein Deutscher Ingenieure (Hrsg.): Konstruktion – Zeitschrift für Produktentwicklung und Ingenieur-Werkstoffe, Heft 6. VDI Fachmedien GmbH & Co. KG, Düsseldorf, 2015, S. 74-81.

[6] Matros, K.: Entwicklung von Hybridantriebssystemen auf Basis des Pull-Prinzips der Validierung und des IPEK-X-in-the-Loop-Ansatzes. Dissertation. Institut für Produktentwicklung, Forschungsberichte IPEK Heft 95, Karlsruher Institut für Technologie (KIT), 2016.

[7] Albers, A.; Düser, T.; Sander, O. *et al.:* X-in-the-Loop-Framework für Fahrzeuge, Steuergeräte und Kommunikationssysteme. *In:* ATZelektronik 13 (2010), Heft 05, S. 60-65.

[8] Gruhle, W.-D.: Steuerung und Regelung von Automatikgetrieben. *In: Isermann, R.* (Hrsg.): Elektronisches Management motorischer Fahrzeugantriebe – Elektronik,

Modellbildung, Regelung und Diagnose für Verbrennungsmotoren, Getriebe und Elektroantriebe, ATZ / MTZ-Fachbuch. Vieweg+Teubner Verlag / GWV Fachverlage GmbH Wiesbaden, Wiesbaden, 2010, S. 288-305.

[9] Kahlbau, S.: Mehrkriterielle Optimierung des Schaltablaufs von Automatikgetrieben. Dissertation. Brandenburgischen Technischen Universität, 2013.

[10] Hagerodt, A.: Automatisierte Optimierung des Schaltkomforts von Automatikgetrieben. Zugl.: Braunschweig, Techn. Univ., Diss., 2003, Schriftenreihe des Instituts für Fahrzeugtechnik TU Braunschweig Heft 4, Shaker, Aachen, 2003.

[11] Wurm, A.: Ein Beitrag zur robusten mehrkriteriellen Optimierung des Schaltablaufs von Automatikgetrieben. Dissertation, Berichte aus der Fahrzeugtechnik, 2015.

[12] Chandrasekaran, K.; Rao, N.; Palraj, S. *et al.:* Objective Drivability Evaluation on Compact SUV and Comparison with Subjective Drivability. *In:* SAE Technical Paper Series, SAE Technical Paper Series. SAE International400 Commonwealth Drive, Warrendale, PA, United States, 2017.

[13] Schöggl, P.; Ramschak, E.; Bogner, E. *et al.:* Driveability Design. *In:* ATZ - Automobiltechnische Zeitschrift 103 (2001), Heft 3, S. 186-195.

[14] Aigner, J.: Zur zuverlässigen Beurteilung von Fahrzeugen – The Reliable Evaluation of Motor Vehicles. *In:* Automobiltechnische Zeitschrift (ATZ), 9/1982. Vieweg+Teubner Verlag / GWV Fachverlage GmbH Wiesbaden, Wiesbaden, 1982, S. 447-450.

[15] AVL List GmbH: AVL-DRIVE 4.4 – The Objective Assessment of Vehicle Attributes. Function Description - DCT, 36 Ausgabe November 2020.

[16] Bauer, R.; Rossegger, W.; Uphaus, F. *et al.:* Agility Simulation for Driveability Calibration on Powertrain Test Beds. *In:* 7th International Symposium on Development Methodology, Wiesbaden, 2017.

[17] Albers, A.; Schwarz, A.; Behrendt, M. *et al.:* Time-Efficient Method for Test-Based Optimization of Technical Systems Using Physical Models. *In:* Volume 11: Transportation Systems. American Society of Mechanical Engineers, Houston, Texas, USA, 2012, S. 113-118.

[18] Albert, A.; Schwarz, A.; Behrendt, M. *et al.:* Method for time-saving capturing of characteristic gear-shifting diagrams of vehicles on the rollertest bench carried out with dual clutch transmissions. *In:* Innovative Automotive Transmissions, Hybrid & Electric Drives. CTI, Rochester, MI, USA, 2012.

[19] Matros, K.; Schille, F.; Behrendt, M. *et al.:* Manöverbasierte Validierung von Hybridantrieben. *In:* ATZ - Automobiltechnische Zeitschrift 117 (2015), Heft 2, S. 64-71.

Development of an innovative and modular test bench to analyse gear shifts in electrified powertrains

Design approach, realization and use cases of the component test bench

Guanlin Gao, M.Sc., **Daniel Schöneberger**, M.Sc.,
Prof. Dr.-Ing. **Stephan Rinderknecht**,
Institute for Mechatronic Systems in Mechanical Engineering (IMS),
Technical University of Darmstadt

Gefördert durch:
Bundesministerium für Wirtschaft und Energie
aufgrund eines Beschlusses des Deutschen Bundestages

Zusammenfassung

Im Forschungsbereich Fahrzeug-Systeme am Institut für Mechatronische Systeme im Maschinenbau (IMS) der Technischen Universität Darmstadt wird der komplette Entwicklungsprozess der Antriebssysteme in Fahrzeugen von der Konzeption bis zur realen Erprobung abgedeckt. Hierbei werden neben der modellbasierten Entwicklung und Optimierung von Antrieben oder Antriebskomponenten insbesondere auch eigens entwickelte Prüfstände genutzt. Im Bereich der elektrifizierten Fahrzeugantriebe ergeben sich beispielsweise. neue Anforderungen und Herausforderungen an die Schaltelemente, Schaltaktoren und die Antriebs- bzw. Getriebesteuerung. Für die Untersuchung von elektrisch synchronisierten Schaltvorgängen mit formschlüssigen Klauenkupplungen und neuartigen, dedizierten Schaltaktoren für elektrifizierte Antriebe [1], wurde im Rahmen des Speed4E-Projektes ein neuartiger, modularer Prüfstand entwickelt und aufgebaut.

In diesem Beitrag werden zunächst die Konzeptionierung und der Aufbau des Prüfstands vorgestellt. Der Prüfstand besteht im Wesentlichen aus drei Antriebsmodulen, wobei zwei Losräder und der Abtrieb individuell angetrieben werden können. Mit diesem Aufbau ist es somit möglich die Differenzdrehzahl bei Schaltvorgängen der Klauenkupplung für die beiden Gänge variabel zu wählen. Die modulare Bauweise ermöglicht die Untersuchung von

verschiedenen Schaltaktoren, sowohl für 12 V als auch für 48 V Bordnetzsysteme. Ebenso können unterschiedliche Ausführungen von Klauenkupplungen in Verbindung mit diesen Aktoren und deren Zusammenwirken detailliert untersucht werden. Ein Echtzeitsystem ermöglicht die zentrale Ansteuerung und Auswertung aller Prüfstandskomponenten und Sensoren, sowie die Ansteuerung der Prüflinge. Zusätzlich kann dieses für eine Restbussimulation genutzt werden, um beispielsweise HiL (Hardware-in-the Loop) Simulationen durchzuführen.

Im Anschluss wird die Anwendung des Prüfstands zum Testen des in [2] vorgestellten smarten Aktors in unterschiedlichen Szenarien vorgestellt und auf Basis von Messdaten diskutiert. Einlegevorgänge mit dem dedizierten Aktor erfolgen dabei mit kurzen Schaltzeiten von unter 50 ms. Es wird an Beispielen von Schaltvorgängen mit einer Klauenkupplung gezeigt, dass mit diesem Prüfstand nicht nur Schaltvorgänge im Stillstand bei Momentenfreiheit untersucht werden können, sondern auch gesamte Schaltvorgänge mit winkelgenauer Drehzahlsynchronisation, Auslegevorgänge mit Schleppmomentensimulation und Einlegevorgängen unter Differenzdrehzahl.

Abstract

In the research area of Vehicle Systems at the Institute for Mechatronic Systems in Mechanical Engineering (IMS) at the Technical University of Darmstadt, the entire vehicle development process from conception to real testing is covered. In addition to the model-based development and optimization of powertrains or its components, self-developed test benches are used. In the field of electrified vehicle powertrains, there are new requirements and challenges for dog clutches, shift actuators, and powertrain- or transmission control. For the investigation of electrically synchronized shifting processes with dog clutches and new, dedicated shift actuators for electrified powertrains [1], a new and modular test bench is developed and utilized as part of the Speed4E project.

In the first part of this contribution, the conception and realization of the test bench is presented. The test bench essentially consists of three modules, whereby both idler gears and the output shaft can be driven individually. With this structure, it is possible to select the speed difference during gear shifts for the two gears of the dog clutch freely. The modular design enables also the investigation of various shifting actuators, for both 12 V and 48 V on-board power supplies. Different dog clutches combined with these actuators and their interaction can also be examined in detail. A real-time system enables the central control and evaluation of all test bench components and sensors, as well as the control of the unit under test. In addition, the test bench can be used for a rest bus simulation to carry out hardware in-the-loop simulations.

In the second part, the application of the test bench for testing a shift system with a smart actuator [2] and dog clutch is presented in different scenarios and discussed on the basis of measurement data. Gear shifting processes with the dedicated actuator are designed for short shifting time of less than 50 ms. Using examples of shifting processes with dog clutches, it is shown that this test bench can be used to examine not only shifting processes at standstill with no torque, but also the entire engagement processes with precise angle synchronization, disengagement processes with drag torque and engagement processes at differential speeds.

1. Introduction

Given the same system power, multiple-motor and multiple-speed electrified powertrains can increase the launch torque and maximum vehicle speed. Furthermore, it leads to increased efficiency and thus, higher range for a given battery capacity compared to a fixed-speed transmission. [3]

In the scope of the publicly funded research project “Speed4E”, such an innovative powertrain for battery electric vehicles is developed with a dedicated mechatronic shifting system, which will be assembled in a demonstration vehicle.

In a conventional vehicle transmission, frictional synchronizers are used to synchronize the speed difference between two gears while shifting. In some electrified powertrain however, the friction elements are not necessary, since the differential speed between the gears can be controlled with the electric motors.

During the development process of such innovative shifting systems, various tests should be performed in different development phases to assure the functionality and robustness of the system. Before the shifting system is assembled in the powertrain and thereafter in the demonstration vehicle, extensive system tests should be performed in a component test bench, which is the subject of this contribution.

This paper is organized as follows. In chapter 2, the requirements of the test bench regarding the shifting system, especially in an electrified powertrain, will be analysed. The concepts based on the requirements will then be proposed and evaluated. The modularity and flexibility of the test bench is considered from the very beginning. The realized test bench is presented in chapter 3, where the modularity and flexibility of the test bench is showed. Finally, in chapter 4, some representative experimental results of the shifting system on the test bench are discussed.

2. Requirements and conception

In this chapter, firstly the requirements of the test bench are discussed and summarized. Test bench layouts are then extracted and evaluated.

2.1 Unit under test

The central elements of the test bench are the units under test (UUT), which in this case are the shift components and shift actuator. The kind of UUTs under consideration and the test scenarios related to them determine the layout of the test bench, the selection of sensors and test bench drive units.

Shift components

The test bench should be capable to test conventional units with frictional synchronization, for which the lubrication of the synchronizer is necessary. On the other hand, dog clutches for gear shifts gain increased attention in an electrified powertrain. A typical axial dog clutch compared with the conventional shift components is depicted in Fig. 1. One key element is the shift sleeve, in which the shift fork of the actuator engages. By moving the shift sleeve in the direction of the clutch body, the engagement of the claws creates a form fit, thereby connecting the input gear shaft to the output shaft. The different representative geometries of the shift components are to be considered when designing the test bench. An interface of the unit to the test bench should be designed as simple as possible, so that other shift components can be installed in the future.

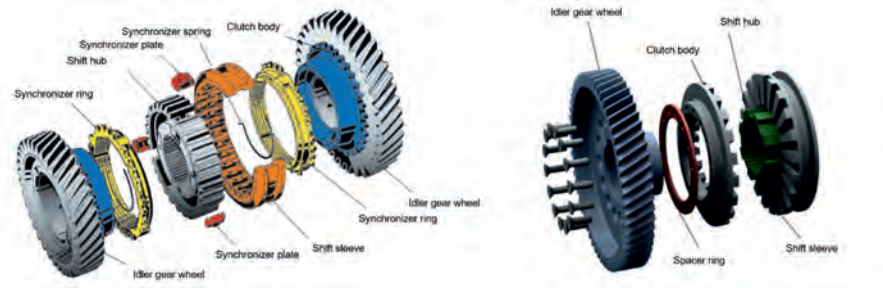

Fig. 1: Exemplary shift components (left: conventional unit [4], right: dog clutch [5])

Shift actuators

Four different shift actuators with different topologies as listed in Table 1 are considered in the design phase. It is intended to provide an exemplary overview of possible shift actuators. Shift drum actuator on the left is commonly used, it transforms the rotation of the motor into axial

movement of the shift fork via a drum with predefined geometry. And the magnetic shift actuator acts directly on the shift sleeve and moves it in an axial direction. The housing of the shift sleeve is firmly connected to the transmission housing. With this system, the actuator is not sitting next to but on the shaft, sufficient installation space must be provided in this area. The linear actuator in the middle is an actuator that generates a pure stroke movement. It uses a principle similar to that of a plunger coil, whereby a magnetic shaft performs stroke movements within two coils. The linear actuator is connected to the shift rod and thereby moves the shift fork axially. Accordingly, installation space must also be kept free for this actuator and a connection to the shift fork must be constructed. Another shift actuator to be integrated into the test bench is a dedicated hybrid transmission assembly (DHT) for hybrid transmissions, as can be seen on the right of the table. With this shift actuator, the movement of the shift fork is initiated with the aid of a servomotor. A dedicated mechanism converts the rotary movement of the motor into an axial movement.

Table 1: Exemplary shift actuators

Shift Drum actuator	Magnetic shifting sleeve	Linear actuator	DHT Assembly [6]
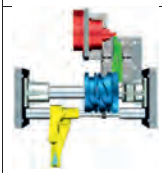		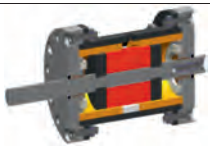	

The shift components and shift actuators can be regarded as two modules that have different requirements regarding installation space due to the variety of geometries. For specific use cases e.g. with conventional shift components, lubrication is needed, which should also be considered as a separate module. It is important that sufficient space should be provided for the modules. Thus, it is obvious that they should be modularized with easily separable interfaces for a flexible switch between different combinations of shift actuator and shift components. To achieve more generality, no gear wheels of specific transmission should be assembled on the test bench. In addition, the shaft inertia should be adaptable since it has an essential influence on the behaviour of shifting under differential speed.

2.2 Test Scenarios

The test scenarios to be performed affect the selection of the actuators and sensors for the test bench. In Table 2, an overview of the main test cases with respect to the shift actuators,

shift components and the shift process are given. It can be clearly concluded that angle sensor with sufficient accuracy is needed, especially for the shift process with precise angle synchronization. For the testing of the shift process, there exist requirement conflicts between different shifting principles. For shift process with precise angle synchronization, the two input shafts and the output shaft should be driven individually. In contrary, for the shifting under differential speed, a fixed output shaft with ability to absorb torque would be preferred, whereby the shaft torque is to be measured. The conflict will be resolved by providing different modules for the output shaft for different test cases.

Table 2: Summary of test scenarios

Testing of shift actuators	• Shift time • Shift force • Controllability • Communication • Control strategy
Testing of shift components	• Full engagement probability (for dog clutch)
Testing of shift process	• Torque-free shifting at standstill • Engagement under differential speed • Disengagement with load • Precise angle synchronization • HiL with other control units • Driving cycle

2.3 Requirement Summary

With the discussion above, the requirements for the test bench are summarized in Table 3. Electric motors are used to drive the input shafts and output shaft, because they are easy to control and suitable for laboratory use. In order to simulate the disengagement process with load, another requirement is to provide the shaft at standstill with 20 Nm torque. The third point on the list of requirements is the environmental conditions. An oil encapsulation must be provided in order to limit the spread of the spray oil. All parts in contact with the oil must be oil-resistant. A housing is intended to protect the operator in the event that rotating parts become detached. Yet it is also to be ensured that the test bench can be viewed during the test. Regarding the installation space, the listed assemblies must be functionally integrated in the test bench. Due to the complex geometry of the individual modules, the requirement is not quantified, but sufficient installation space should be assured. The modularity of the test bench is characterized by a switchover time for shift actuators, inertias and shift components of maximum two hours.

Table 3: Summary of requirement

Number		Type*	Requirement	Target	Unit
1			**Drive Units**		
	1.1	C	Rotational speed at clutch element	0 - 1000	min^{-1}
	1.2	C	Shaft torque at stand still	20	Nm
	1.3	D	Decoupling from drive shaft (to achieve maximum drag torque)		Nm
	1.4	D	Motor variety	1	
	1.5	C	Voltage supply	12 - max. 60	V
2			**Sensors**		
	2.1	C	Rotational speed	0 - 1000	min^{-1}
	2.2	C	Resolution of rotating angle near clutch element	0.2	°
	2.3	D	Resolution rotational speed	min. 720	1/RPM
	2.4	D	Recognition of drive shaft standstill		
3			**Environment**		
	3.1	C	Temperature	15 - 100	°C
	3.2	C	Oil enclosure		
	3.3	C	Enclosure of drive motor against oil		
	3.4	C	Oil resistance of test bench component		
	3.5	C	Visibility of unit under test during test		
	3.6	D	Simple open and close of the enclosure		
	3.7	C	Housing		
	3.8	C	Protection against flying object		
	3.9	D	Low noise operation		
4			**Installation space**		
	4.1	C	Assembly table		
	4.2	C	Linear actuator (length and width)	at least 200	mm
	4.3	C	DHT shift components inclusive Inertia, damper		
	4.4	C	Shift drum		
	4.5	C	Magnetic position sensor for shift fork		
	4.6	C	Magnetic shift component		
5			**Modularity**		
	5.1	C	Changeability of the shift actuators	max. 2	h
	5.2	C	Changeability of the shift components	max. 2	h
	5.3	C	Alignability of the shifting element		
	5.4	C	Adaptiveness of shaft inertia	max. 2	h
	5.5	D	Central I/O terminal block with reserved clamp		
	5.6	C	Hardware-in-the-Loop with other Control Units	min. 1	

Table 3: Summary of requirement continued

6		**Dynamic**		
6.1		Inertia internal combustion engine J_{ICE}	0 - 0.15	$\mathrm{kg/m^2}$
6.2		Inertia transmission J_{Transm}	0.01 - 0.04	$\mathrm{kg/m^2}$
6.3		Stiffness of torsional element	500 - 1500	$\mathrm{Nm/rad}$
6.4		Damping factor of torsional element	0.1 - 3	$\mathrm{Nms/rad}$

* C: Compulsory, D: Desirable

2.4 Mechanical Layout

In a first step, the basic concept for the test bench is developed. For this purpose, the overall problem is analysed using a process structure model, which subdivide a process into sub-processes. This reduces the complexity of the task [7]. One possible version for a process structure model is shown in Fig. 2.

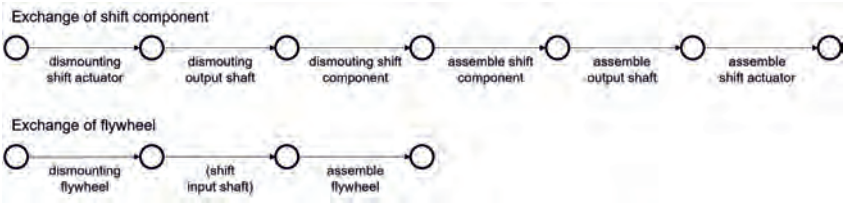

Fig. 2: Exchange process structure model

The test bench can be divided into three high-level sections:

- Drive units: input and output shafts with the associated bearings, drive motors, flywheels and shift components
- Actuators: shift forks and their drives
- Sensors: All elements for measuring the relevant variables such as torque, speed and position

The arrangement of the drive units is essential, as it influences the exchange of the shift components. The drive units consist of the output shaft, two input drive shafts, the substitute inertia and the bearing of the shafts. The shift components and the substitute inertia must be easily accessible in order to guarantee the required modularity. The analysis results in three versions, which are illustrated in Fig. 3. It should be noted that in all three versions, the output shaft can also be firmly clamped to a torsional element: in which case the tests of shifting under differential speed can be performed. In contrary, the output shaft driven by an electric motor is

suitable for the tests of shifting with precise angle synchronization. The realization of this form will be described further in chapter 3.

The choice of installation space for the shift actuators is similar for all versions and reduces the installation space restriction for the actuators to a minimum. The drive unit 2 is connected to the shift components via either a gear wheel or belt. All drive units in itself contain a gear transmission that can be varied by changing the gearbox.

The main difference between the versions is the layout for drive unit 1. In version 1, the motor is connected coaxially to the shaft. In order to be able to integrate the flywheel into the system, a shaft coupling must be integrated. The second and third versions rely on a parallel drive shaft with a gear stage. Version 2 relies on a gear wheel, whereby version 3 works with a belt drive.

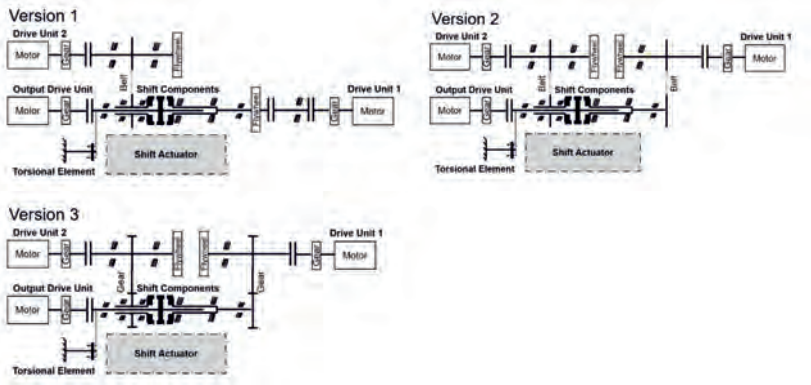

Fig. 3: Mechanical layout concepts

For the evaluation of the versions, evaluation criteria are defined:

- Measurement accuracy: number of interfaces between the flywheel and the shift components
- Ease of flywheel replacement: number of steps to replace the flywheel
- Ease of shift components replacement: number of steps to replace the shift components
- Complexity of bearing: number of dismountable bearings
- Complexity of the version: number of different assemblies

The criteria have a strong focus on the modularity. They will be weighted via a pair comparison. The versions are then evaluated with awarded points that describe the fulfillment of the criteria.

The version that best fulfills the criterion receives 2 points, the second best 1 point and the worst 0 point. The points are multiplied by the weights and added up. This results in a total value for each version.

With this method, version 1 has the highest number of points and thus represents the most promising version. It is therefore be selected as the layout for the test bench. The realization will be discussed in the following chapter.

2.5 Electric/Electronic Layout

Besides the mechanical layout design with a focus on modularity, another often underestimated yet important aspect is the electronics of the test bench. The corresponding requirements are number 5.5 and 5.6 in Table 3. The requirements are mainly fulfilled with a modularized wiring concept as illustrated in Fig. 4. The intention of this concept is to make subsequent changes or extensions as easy as possible. Therefore, all devices, plugs etc. are always connected to a terminal block and from there to the destination pin. Although this leads to a significantly higher number of terminals, it is much easier to expand because only cables have to be wired to terminals. ECU 1 and ECU 2 are displayed with dashed lines to hint that they are optional. It provides the possibility to extend the hardware-in-the-Loop environment with maximal two further ECUs.

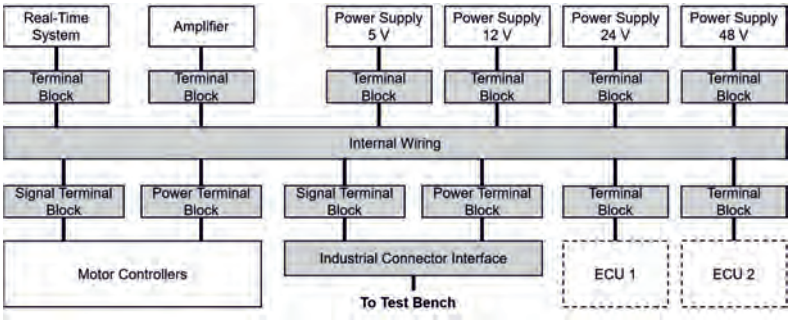

Fig. 4: Modularized wiring concept

3. Test Bench InnoShift

With the discussed concept above with a focus on extendable functionality and modularity, the test bench is successfully built and commissioned. The key technical data of the test bench are listed in Appendix Table 4.

Fig. 5 shows the real test bench in laboratory with the simplified layout above for better understanding. It is a setup for tests of shift systems with precise angle synchronization. The test bench is named “Innovative, modular test bench to analyse gear shifts in electrified powertrains” with the acronym “InnoShift”. In the following, the test bench will simply be called InnoShift.

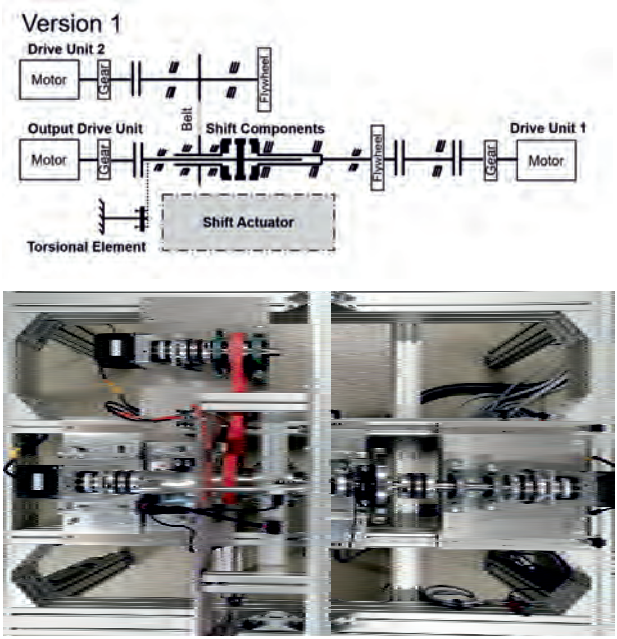

Fig. 5: InnoShift test bench (bottom) and its simplified structure (top)

Fig. 6 shows the gear shift system mounted on the InnoShift. Instead of using a complete gear stage, the clutch bodies on the two gears and the shift hub are driven individually so that the differential speed can be specified independently of the absolute speed. Substitute inertia can be applied for investigations of shift processes under differential speed in order to achieve realistic shifting behavior, especially with regard to the engagement probabilities. All drives have incremental encoders to investigate the angle- precise synchronization. All drives consist of gear motors with their own motor controller. These communicate via CAN with a central real-time system, via which the actuator can also be controlled directly. In this way, any shifting maneuvers can be carried out.

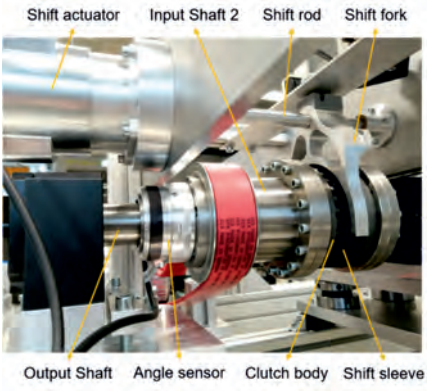

Fig. 6: Gear shift system on InnoShift

As discussed in the previous chapter, one of the main requirements of the test bench is the modularity. This can be generally divided in mechanical and electric/electronic modularity. The realization of these two aspects will be presented in the following.

3.1 Mechanical Modularity

As discussed in chapter 2, the shift components that need to be exchanged should be easily accessible and the various shift actuators should also be exchangeable in a few simple steps. For this reason, the test bench is divided into a main module, a secondary module and an actuator module. As shown in Fig. 7, the entire structure is built on a table made of construction profiles. The secondary module is built on a separate plate. Thus, it can be positioned at the desired location along the grooved construction profile. The actuator module on the other hand is mounted vertically above the main module, which can be completely dismounted without modifying other modules.

The main module is the core of the test bench. It consists of several submodules. Submodules A and B in Fig. 8 can slide axially via guide rails. It enables the quick replacement of the inertia and clutch body. Submodule A contains the drive unit for input shaft 1 and provides a bearing for the flywheel. In area B, the rotating angle of the input shaft 1 next to the clutch body is measured. Furthermore, a mounting option for an additional flywheel is available. On the left end of this area, the clutch body is attached. On the output side of area C, the interface to area E of the output drive unit is formed, which can be replaced by a torsional element. In addition,

the shift hub and shift sleeve sit on the output shaft. Submodule D connects the secondary module with the main module where the rotational angle of the input shaft 2 is also measured. On the right end, the clutch element is attached.

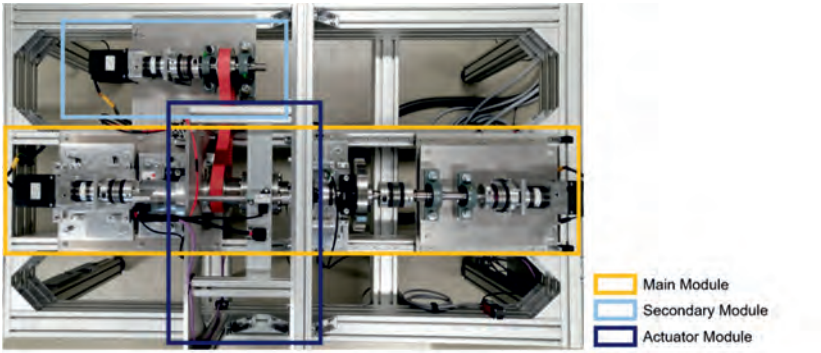

Fig. 7: Modules of the test bench

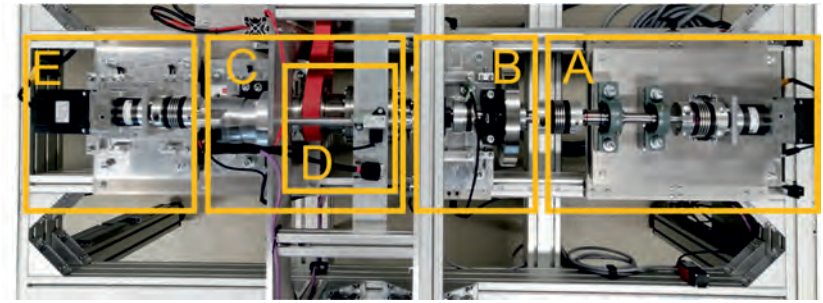

Fig. 8: Main modules of the test bench

Dedicated shaft alignment mechanism

The alignment of the modules for first commissioning or after component exchange is made possible due to the dedicated alignment mechanism as illustrated in Fig. 9. At first, the vertical alignment will be adjusted by raising or lowering the adjusting chocks. Then the horizontal alignment will be tuned by rotating the horizontal adjusting screws, which effectively rotates the module mounting plate. Finally, after the tuning procedure, the module mounting plate is firmly pressed against the press beam by tightening the screw to the module lower plate.

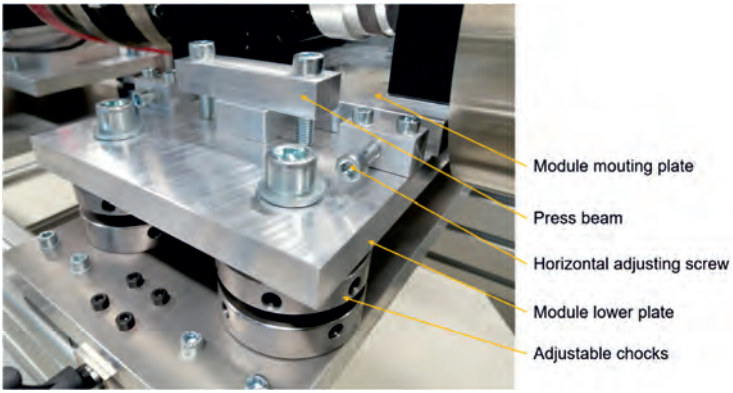

Fig. 9: Dedicated shaft alignment mechanism

3.2 Electric/Electronic Modularity

As described in chapter 2, the modularity of electric/electronic parts are also thoroughly considered. The benefit of such a modularity will be showcased with the simple switch between two different types of applications. This will be explained in the following.

As shown in Fig. 10, the InnoShift control runs in a central real-time system, where the sensor signals are evaluated and controller commands for InnoShift drive units are set.

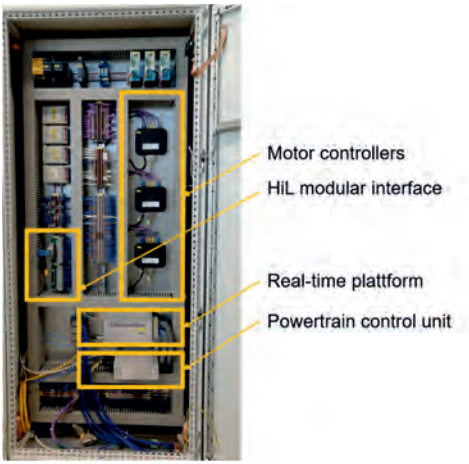

Fig. 10: Modular Interface for general Hardware-in-the-Loop Simulation

Furthermore, as shown in Fig. 11, models for the shift actuators and control strategy for gear shifting can also be run in the same real-time system, thus the calibration and basic function test of the UUT is made simpler.

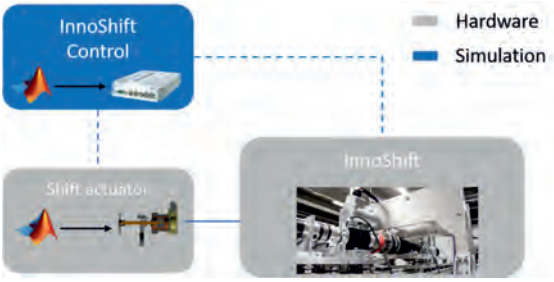

Fig. 11: InnoShift structure for commissioning and application of shifting actuators and shifting sequence control

The gear shift control is ultimately implemented on the powertrain control unit (PCU). To test the interaction of the real shift actuator with the PCU, the shift actuator should be connected directly to the PCU (see Fig. 12), where other required signals will be provided by a restbus simulation. To switch to this more complex Hardware-in-the-Loop application, only the corresponding HiL modular interfaces as shown in Fig. 10 must be plugged in. It is the layout concept with modularized terminal blocks, as shown in Fig. 4, that makes the simple switch possible.

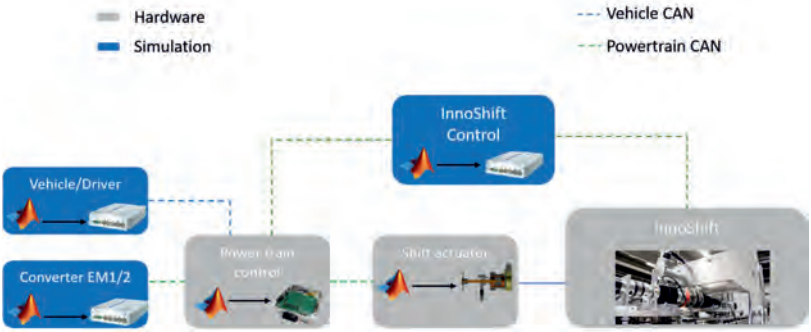

Fig. 12: InnoShift setup for more extensive applications (e.g. driving cycle simulation)

4. *InnoShift Application*

The program for InnoShift control was developed in Matlab-Simulink. It includes the evaluation of the sensor signals, the different controllers for the InnoShift motors and also safety measures. The Simulink model is then compiled and runs on the real-time platform. The InnoShift motors have two operating modes: speed control with an integrated PI controller and torque control with direct current command. Operating modes will be switched depending on the application cases.

In the scope of Speed4E project, an innovative gear shift system, which consists of a dog clutch dedicated for shifting with precise angle synchronization and a smart shift actuator, is developed and in [8] presented. In this chapter, some typical test cases of this system using the InnoShift will be discussed.

4.1 Test of shifting actuator at standstill

Tests of the shift actuator at standstill are among the most basic applications performed with the InnoShift. In this case, the shift actuator is put into operation with the dog clutch at standstill in a manually aligned tooth-to-gap position of the clutch body and shift sleeve. An example of the shifting results – a measurement of a shift into first gear – is illustrated in Fig. 13. The engagement process begins at 0.01 s and reaches the end position at about 0.03 s, such that the engage process takes approximately 20 ms. The actuator force is formulated in duty cycle of the H-bridge, where 100% represents the maximal force. It can be seen that at the beginning of the engagement process, the force almost reaches its maximum. The step form is due to the transmit of the position signal via CAN with a cycle time of 1 ms to the real-time platform.

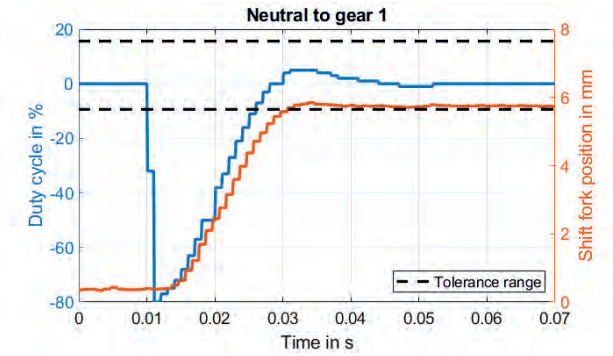

Fig. 13: Shift fork position and duty cycle during gear shifting from neutral to gear 1 at standstill [8]

4.2 Algorithm for precise angle synchronization

In the Speed4E case, not only the speed is synchronized with the active synchronization, the dog clutch is also specifically regulated to a tooth-to-gap position such that gear can be engaged without contact between the tooth flanks or the tooth tops. Before implementing on the powertrain, the control method of this precise angle synchronization can be initially investigated at lower absolute speeds at the InnoShift. As shown in Fig. 14, a constant speed of the output shaft – where the shift sleeve is mounted – is specified for the investigation of the synchronization, which corresponds to a constant drive of the vehicle. The speed of the clutch body of gear 1 is initially zero, which corresponds to a standstill of the electric motor in the Speed4E drive. Active synchronization starts at around 0.25 s. The target speed of the control corresponds to the current speed of the output shaft.

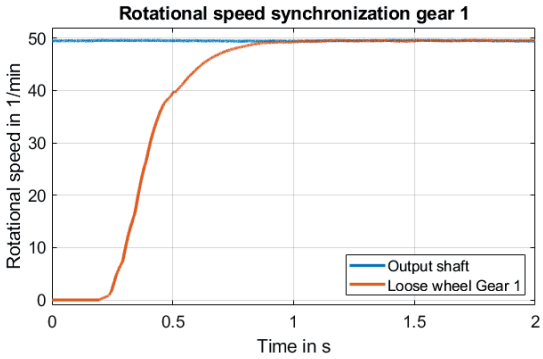

Fig. 14: Rotational speed of the active synchronization of output shaft and clutch body of gear 1 [8]

With the high-resolution angle sensor, the angle difference between the shift sleeve and the clutch body can be investigated in detail, as showed in Fig. 15. The tolerance band marked in the figure corresponds to the backlash of the dog clutch. It is important that the angle difference in particular must not leave the tolerance band for a certain time. Only then the power electronics report back "synchronized" to the powertrain control, which requests the shift actuator to engage the gear. If there is a lack of synchronicity, there will be a resulting flank contact and thus a higher power requirement or, in the worst case, a roof-on-roof position. InnoShift provides a system environment to analyze and further develop this particular shifting control algorithm at an earlier development phase.

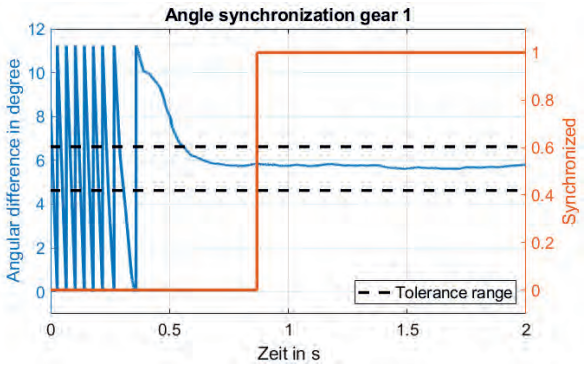

Fig. 15: Angle difference from tooth to tooth of clutch body in gear 1 and output shaft during synchronization [8]

4.3 Gear disengagement with drag torque

The aim of active synchronization is that the dog clutch is completely relieved from load torque before each disengagement process. In this case, just like at a standstill, only the locking force acts on the dog clutch. Nevertheless, the shift actuator is dimensioned in such a way that the gear can still be disengaged with a certain drag torque. In this situation, it is to be avoided that the positional overshoot during the disengagement process becomes so significant that a tooth contact occurs between the sleeve and the clutch body of the other gear that is not synchronized. This aspect needs also be investigated in detail.

Two tests of gear disengagement are performed on InnoShift with medium and high drag torque. The measurement results regarding duty cycle and the position of the shift fork are depicted in Fig. 16. Measurement 1 shows that the disengage process was just successful. In measurement 2, the drag torque is too high and the gear is not fully disengaged since the disengagement attempt is canceled after a certain time to protect the electronics. With this example, it showcases that the InnoShift provides a system environment to investigate the robustness of the gear shift controller.

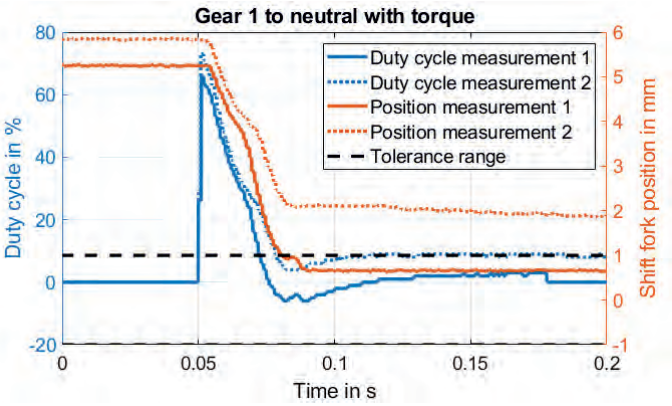

Fig. 16: Gear disengagement with various drag torques [8]

5. Summary and Outlook

In this contribution, an innovative and modularized test bench for the analysis of gear shift systems is introduced. Based on the diversity of the units under test and the various test scenarios, the requirements for the test bench are extracted with a special focus on the modularity and flexibility. The developed test bench InnoShift is thus capable to investigate various gear shift systems especially for electrified powertrains, where precise angle synchronization or gear shifting under differential speed are possible. The modular design enables the investigation of various shifting actuators, for both 12 V and 48 V on-board power supplies. For a better generality the gear stage is dispensed at the InnoShift, which means that the clutch bodies of the two gears can be driven individually. The output shaft can be connected to a drive unit for testing of precise angle synchronization, or to a torsional element for tests of gear shifting under differential speed. Finally, exemplary application cases using the InnoShift are described. It shows that besides the tests of basic gear shifting functionality, the investigation of gear shift control algorithms and their robustness are also possible using the InnoShift.

Currently the testing of precise angle synchronization can be performed at relatively low speed. In further works, measures will be taken to facilitate testing of gear shifting system with higher speeds. The test bench is also equipped with brake choppers to dissipate the braking energy from a driving cycle simulation. This functionality will also be further investigated.

6. References

[1] A. Reul, R. König, S. Rinderknecht: Overall optimization of electrodynamic shifting systems. In: Forsch. Ingenieurwes. 81, 437–446 (2017) https://doi.org/10.1007/s10010-017-0252-y

[2] D. Schöneberger, M. Mileti, K. Stahl, S. Rinderknecht: Development of an Innovative Shift Actuator for Electrified Multispeed Transmissions. In: 2019 International Conference on Advanced Vehicle Powertrains

[3] Viehmann, A.; Schleiffer, J.-E.; Rinderknecht, S.: Evaluation of the Dedicated Range-Extender Transmission Powertrain Concept DE-REX regarding Efficiency, Costs and Complexity. 19th International VDI Congress, “Drivetrain for Vehicles 2019“. Bonn 2019

[4] INA (2005): Informationsbroschüren der INA Schaeffler KG, D-91072 Herzogenaurach

[5] Institut für Maschinenkonstruktion und Tribologie, Leibniz Universität Hannover: CAD Modell von Speed2E Klauenkupplung, 2017

[6] O. Sarmiento; A. Riedel; D. Runkel; J. Auweiler; D. Schöneberger; S. Rinderknecht: Dedicated Hybrid Transmission: How a systemic approach accelerates engineering process from concept development to real applications. In: 18th International VDI Congress, “Drivetrain for Vehicles 2018“. Bonn 2018

[7] Birkhofer: Produktinnovation. Sommersemester. Darmstadt 2017

[8] D. Schöneberger, G. Gao, S. Rinderknecht: Entwurf, Applikation und Test eines innovativen, dedizierten, smarten Schaltaktors für elektrische Mehrgangantriebe. In: VDI Mechatronik Tagung 2021

7. Appendix

Table 4: Technical data of the InnoShift test bench

Component	**Technical Data**
Drive Unit 1	Rated speed 3000 1/min, Rated torque 1,4 Nm Gear ratio: 3 or 16
Drive Unit 2	Rated speed 3000 1/min, Rated torque 1,4 Nm Gear ratio: 3 or 16
Output Unit	Rated speed 3000 1/min, Rated torque 1,4 Nm Gear ratio: 3 or 16
Power Supply Shift Actuator	Voltage: 12 - 48 V Current: up to 90 A
Speed Sensor	SIKO magnetic sensor
	resolution 0.18°
System Plattform	dSPACE real-time system

Test method A/16,6/90 with injection lubrication for discriminating different lubricants for dual-clutch transmissions

Dr.-Ing. **Michael Hein**,
HOERBIGER Antriebstechnik Holding GmbH, Schongau;
Josef Pellkofer, M.Sc., Dr.-Ing. **Klaus Michaelis**,
Dr.-Ing. **Thomas Tobie**, Prof. Dr.-Ing. **Karsten Stahl**,
Gear Research Centre (FZG), Technical University of Munich, Garching;
Dr.-Ing. **Daniel Kadach**, AGCO GmbH, Marktoberdorf

1. Kurzfassung

An Schmierstoffe für Doppelkupplungsgetriebeanwendungen werden aufgrund eines oft gegensätzlich geforderten Reibungsverhaltens in den Komponenten besondere Anforderungen gestellt. Fressen als klassischer Spontanschaden kann zum Totalausfall eines Getriebes führen und muss daher zuverlässig verhindert werden.

Erfahrungen zeigen, dass etablierte Schmierstofftests zur Ermittlung der Fresstragfähigkeit nur bedingt geeignet sind, derartige Schmierstoffe für Doppelkupplungsgetriebeanwendungen zu differenzieren. Daher wurde in Anlehnung an den Stufentest A/16,6/90 ein geeignetes Testverfahren zur Bestimmung der Fresstragfähigkeit niedrigviskoser Schmierstoffe für Doppelkupplungsgetriebeanwendungen entwickelt. Im Gegenzug zu den etablierten Testmethoden wird das neu entwickelte Testverfahren bei Einspritzschmierung und konstanter Einspritztemperatur und nicht bei Tauchschmierung durchgeführt. Diese Art der Durchführung führt zwar zu Testergebnissen, welche eine aussagekräftige Differenzierung von verschiedenen Schmierstoffen für Doppelkupplungsgetriebeanwendungen zulassen, stellt jedoch auch sehr hohe Anforderungen an die Qualität der Versuchsdurchführung. Diese soll im Rahmen dieses Beitrags detailliert beschrieben werden.

Die FZG war und ist nach wie vor an der Entwicklung von standardisierten Prüfmethoden zur Ermittlung der Fresstragfähigkeit beteiligt und auch in den entsprechenden Normungsgremien aktiv. Die neuesten Erkenntnisse hinsichtlich Doppelkupplungsgetriebeanwendungen sollen im Rahmen dieses Beitrags vorgestellt werden.

2. Abstract

Lubricants for dual clutch transmissions must meet different requirements regarding the frictional behavior for different components of the gearbox. Scuffing as typical spontaneously appearing damage on gears can lead to a total break-down of the gearbox and has to be prevented on a reliable basis. Experiences show that established lubricant tests for evaluating the scuffing load capacity (for example according to ISO 14635) are suitable to only a limited extent for differentiating typical lubricants for dual clutch transmissions. Gear Research Centre (FZG) is very active in the development of standardized test methods for evaluating the scuffing load capacity of lubricants and is also active in the corresponding standardization committees. The latest findings regarding DCT applications will be presented in the scope of this publication.

A suitable test method for evaluating the scuffing load capacity of low-viscosity lubricants for DCT applications was developed in accordance to the FZG stage test A/16,6/90. In contrast to the established test methods which are carried out with dip lubrication and specified oil volume, the newly developed test method is carried out with injection lubrication and constant lubricant temperature.

This test set-up leads to meaningful test results regarding the scuffing load capacity of lubricants for dual clutch transmissions and establishes a possibility for differentiating them on the one hand. On the other hand, the requirements regarding the test set-up and the practical realisation are very high, if reliable and reproducible test results should be achieved. This will be described in the scope of this publication.

3. Introduction and objective

Due to increasing power density in gears as well as the trend of decreasing oil quantity and viscosity to reduce no-load power losses, the scuffing load-carrying capacity has to be considered within the design of a gear set and the whole gearbox. Therefore special lubricants for different applications, which help to avoid the failure mode scuffing, have been developed. Furthermore, these lubricants should not have a negative effect on other failure modes and components of the gear box. Lubricants for dual clutch transmission (DCT) for example must meet different requirements regarding the frictional behavior for different components of the gearbox. High coefficients of friction are required for synchronizers and clutches, low coefficients of friction are favorable for bearings and gears in order to increase the total gearbox efficiency.

Scuffing as a typical spontaneously appearing damage on gears can damage the surface of the tooth substantially, which can lead to consequential failures and partially even to a total break-down of the gearbox. The safe design of the tribological system consisting of gears and lubrication is therefore an essential component of gear development and design. As experiences show that established lubricant tests for evaluating the scuffing load capacity (for example according to ISO 14635) are suitable to only a limited extent for differentiating typical lubricants for dual clutch transmissions, the scope of the presented project is the development of a scuffing test method which allows the evaluation and differentiation of the scuffing load capacity of low-viscosity lubricants for DCT applications under conditions near to the real gearbox application.

4. Failure mode scuffing

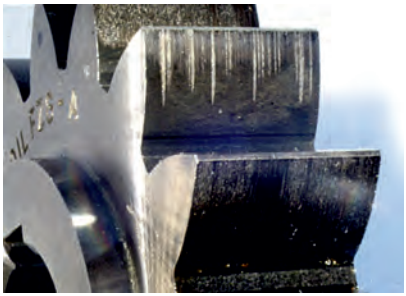

Fig. 1: Typical scuffing marks on type A gearing (source: FZG)

Scuffing is a spontaneously appearing damage mechanism on gears that occurs if the lubricant film thickness is insufficient to prevent significant metal-to-metal contact and chemical protection of the surfaces from gear oil additives is not sufficient. Scuffing usually occurs at high circumferential speeds and high loads. Scuffing is characterized by a welding of the contacting tooth flanks and a following tearing of the welded junctions due to the occurring sliding. Scuffing marks are always orientated in the direction of the relative speed of the rolling partners and usually start in the addendum and dedendum area of the tooth flank where high sliding velocities occur. Damaged areas show a melted structure that is orientated in direction of the relative speed of the rolling partners and “smears up” at the end. Scuffing marks always appear in the corresponding flank areas on pinion and wheel and are also transferred to other tooth flanks mating with a damaged flank.

A calculation of the scuffing load carrying capacity can be performed for example acc. to ISO/TS 6336-20 and 21 [11, 12] for cylindrical gears. This calculation is based on the

comparison of an occurring temperature on the investigated gear contact and a permissible scuffing temperature which is mainly lubricant dependent. This permissible scuffing temperature can be determined by different lubricant test methods. The most commonly used test methods are the FZG stage tests according to ISO 14635 and their modifications.

This permissible scuffing temperature can e.g. also be used as a basis of a relative comparison of different oils. It is also possible to relatively compare results of different scuffing test methods. Fig. 2 shows the scuffing temperatures $\vartheta_{S\,int}$ for the integral temperature method acc. to DIN 3990-4 [4].

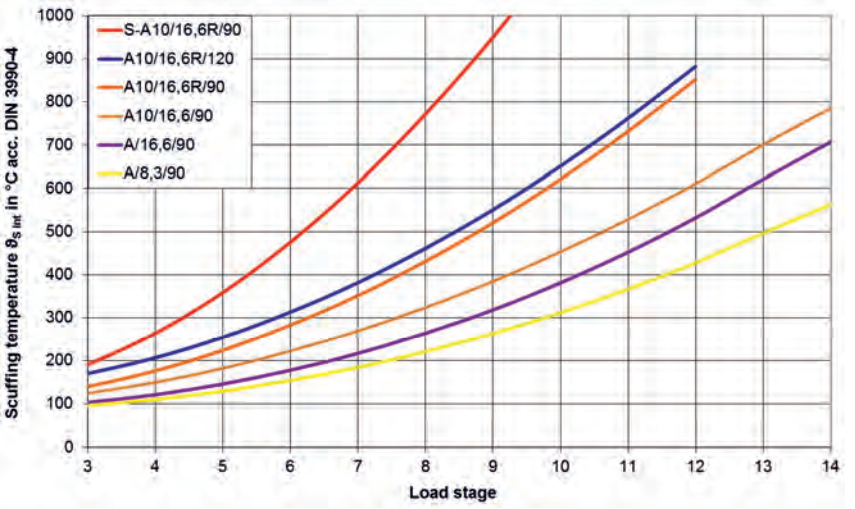

Fig. 2: Scuffing temperature $\vartheta_{S\,int}$ according to the Integral Temperature Method acc. DIN 3990-4 [4] for different test methods (all with oil splash lubrication)

The commonly used test methods for evaluating the scuffing performance of different lubricants are shortly presented in the following.

5. Test methods for evaluating the scuffing performance of lubricants

For the determination of the scuffing performance of lubricants, several test methods are available. The most common methods and their modifications are described in the following.

5.1. Standard Stage Test A/8,3/90 and Modifications

The standard stage test A/8,3/90 according ISO 14635-1 [8] is used for the differentiation of the scuffing capacity of low to medium EP oils. These are typical engine oils which are also used in gears, lubricants for automatic transmissions (ATF), turbine gear oils as well as hydraulic (HL) and industrial gear oils (CL) with oxidation and corrosion inhibitors. ISO 14635-1 [8] is equivalent to CEC-L-07-095 [1].

The test is run on the standard FZG back-to-back gear test rig with center distance a = 91,5 mm. Test gears type A are used. The pitch line velocity in the test is v = 8,3 m/s corresponding to a pinion speed of n_1 = 2170 rpm. The sense of rotation is “outward” with the long distance of some 270° of the oil into the gear mesh. For standard load application with load lever and weights the pinion is the driver (speed reducer). The gears are sump lubricated with an oil volume of 1,25 l in the test gear box. The starting oil temperature in each load stage is ϑ_{oil} = 90 °C without external cooling. Load is stepwise increased until scuffing is visually observed. The running time in each load stage is approximately 15 min. If no scuffing occurs up to load stage 12 (T_1 = 534,5 Nm) the test is terminated. As a modification of the standard test the load range can be extended to load stages 13 and 14.

For a valid result of scuffing load stage over 12 the total weight loss of the gear must not exceed 20 mg. A higher weight loss indicates a wear scar in the gear dedendum which leads, similar to pinion tip relief, to reduced local load in the region of maximum sliding and thus prevents scuffing damage.

A detailed description of the test method A/8,3/90 can be found in [8].

Modifications of the standard test are tests at higher speed (double speed v = 16,6 m/s (A/16,6/90), triple speed v = 24,9 m/s (A/24,9/90) or quadruple speed v = 33,2 m/s (A/33,2/90)) or at different oil temperatures as e.g. ϑ_{oil} = 60 °C or 120 °C (A/8,3/60 or A/8,3/120) for practical applications at lower or higher oil temperatures. The test at double speed is more severe by approximately 1 – 2 load stages. For EP oils higher oil temperatures often lead to higher scuffing capacity where the expected reduced scuffing capacity due to lower viscosity is overcompensated by higher additive activity [6]. In the opposite situation a lower oil temperature can lead to lower scuffing capacity. This may lead especially for large gears to an unexpected scuffing risk which cannot be derived from the result of a standard test A/8,3/90.

The special tests A/24,9/90 and A/33,2/90 with increased speed v = 24,9 m/s respectively v = 33,2 m/s is designed for the investigation of the influence of pitch line velocity on scuffing load capacity. The test is carried out in the FZG back-to-back gear test rig with an additional speed

increaser between motor and slave gear box. The speed is adjusted to v = 24,9 m/s (A/24,9/90) / v = 33,2 m/s (A/33,2/90), corresponding to a pinion speed of n_1 = 6510 min^{-1} (A/24,9/90) / n_1 = 8680 min^{-1} (A/33,2/90). Direction of rotation and torque application is chosen according to ISO 14635-1 [8] so that the pinion drives the gear in the test gear box. The test procedure is similar as specified in ISO 14635-1 [8], however, the running time in each load stage is 7,5 min. The results of the test can be introduced into the scuffing load capacity rating according to Collenberg [2].

From the test result the scuffing temperature limit $\vartheta_{S\,int}$ can be derived for introduction into the scuffing load capacity calculation of gears in practice. For cylindrical gears DIN 3990-4 [4] or ISO/TS 6336-20/21 [11, 12] applies, for bevel gears DIN 3991-4 [5] or ISO/TS 6336-20/21 [11, 12].

5.2. Stage Test A10/16,6R/90

In the stage test FZG A10/16,6R/90 the scuffing characteristics of lubricants can be tested where the standard FZG scuffing test A/8,3/90 acc. ISO 14635-1 [8] is not able to differentiate between lubricants. A differentiation in the test is expected for lubricants up to an EP treat level of API GL4. From the test result, additionally the scuffing temperature limit $\vartheta_{S\,int}$ can be derived for introduction into the scuffing load capacity calculation of gears in practice according to DIN 3990-4 [4], DIN 3991-4 [5] or ISO/TS 6336-20/21 [11, 12]. The test is run on the standard FZG back-to-back gear test rig with center distance a = 91,5 mm. Type A test gear geometry is used, except for a reduced face width of the pinion to b_1 = 10 mm. The pitch line velocity in the test is adjusted to v = 16,6 m/s, corresponding to a pinion speed of n_1 = 4340 min^{-1}. The direction of rotation is inverted, compared with the standard test A/8,3/90, so that for same torque loading the wheel drives the pinion (speed increaser). The starting oil temperature in every load stage is ϑ_{oil} = 90 °C. The load is increased in stages until scuffing is visually detected. In case of no scuffing damage occurs up to load stage 10 (T_1 = 372,6 Nm) the test is normally terminated. The lubricant can then be rated as API GL 4 concerning scuffing characteristics. A detailed description of the test method A10/16,6R/90 is given in [15].

The test method A10/16,6R/120 with increased starting oil temperature in each load stage $\vartheta_{lubricant}$ = 120 °C is standardized in ISO 14635-2 [9].

For a valid result of scuffing load stage over 10 the total weight loss of the gear must not exceed 20 mg. A higher weight loss indicates a wear scar in the gear dedendum which leads, similar to pinion tip relief, to reduced local load in the region of maximum sliding and thus prevents scuffing damage.

5.3. Shock Test S-A10/16,6R/90

The shock test S-A10/16,6R/90 can be used for discrimination of scuffing characteristics of lubricants which cannot be discriminated in the stage test A10/16,6R/90 as described in 5.2. Differentiation is expected up to an EP treat level of API GL-5 or above. From the test result, additionally the scuffing temperature limit $\vartheta_{S\,int}$ can be derived for introduction into the scuffing load capacity calculation of gears in practice according to DIN 3990-4 [4], DIN 3991-4 [5] and ISO/TS 6336-20/21 [11, 12].

In contrary to the stage test the shock test is started directly in the expected load stage and PASS or FAIL is reported. All other operating conditions remain unchanged. Due to the omission of the run-in the test method is considerably more severe and EP oils up to a treat level of API GL-4 and GL-5 or above can be differentiated. More than one test run is necessary in the shock test if the limiting scuffing load has to be evaluated.

A detailed description of the test method S-A10/16,6R/90 is given in [15].

5.4. Review of commonly used scuffing test methods and their applicability to lubricants for dual clutch transmissions

Fig. 3 summarizes the test methods described above under splash lubrication and shows their typical areas of application briefly. Fig. 4 gives a detailed overview of the gears used in the tests described, the velocities investigated and the driving directions, and illustrates the significant differences in the individual test methods. The test methods shown in Fig. 4 are the most widely used test methods to determine the scuffing load performance of lubricants for gearbox applications.

	Method	Standard	Application	Test rig
Standard test	A/8,3/90	ISO 14635-1 CEC L-07-A-95 ASTM D 5182-97	industrial gear oils	standard FZG rig
Modifications of the standard test	A/16,6/90 A/16,6/140	-	industrial gear oils	standard FZG rig
Grease test	A/2,76/50	ISO 14635-3	flow greases	variable speed
EP step test	A10/16,6R/90 A10/16,6R/120	FVA 243 ISO 14635-2 CEC L-84-02	automotive gear oils API GL 4	reversed rotation
EP shock test	S-A10/16,6R/90 S-A10/16,6R/120	FVA 243	automotive gear oils API GL 4 and GL 5	reversed rotation

Fig. 3: Overview of the available scuffing test methods for different lubricants using the FZG back-to-back gear test rig (all with oil splash lubrication)

	A/8,3/90 DIN ISO 14635-1 CEC L-07-A-95	A10/16,6R/90 Stage test	S-A10/16,6R/90 Shock test
Gear geometry	Type A	Type A	Type A
Pinion face width	20 mm	10 mm	10 mm
Wheel face width	20 mm	20 mm	20 mm
Pitch line velocity	8,3 m/s	16,6 m/s	16,6 m/s
Driving gear	Pinion	Wheel	Wheel
Direction of rotation			
Torque	Standard	Standard	Standard
Hertzian stress	Standard	√2 * Standard	√2 * Standard
Load application	Stage	Stage	Shock
Oil temperature	90° C	90° C	90° C
Failure criterion	≥ 20 mm	≥ 10 mm	≥ 10 mm
Test result	Failure load stage	Failure load stage	PASS - FAIL

Fig. 4: Comparison of different scuffing test methods (all with oil splash lubrication)

All described test methods are carried out on a FZG back-to-back gear test rig with centre distance a = 91,5 mm and the type A test gears. This means that all of these test methods are based on a test design of the real component that is investigated and give a realistic assessment of the lubricant scuffing load capacity in real gearbox application.

For a long time, the stage test A10/16,6R/90 was the preferred test method for automotive gearbox applications. Due to the recent trend towards lower viscosity oils and different additive packages, the test results of common automotive gearbox lubricants in the test A10/16,6R/90 became more and more unreliable. The scattering of the test results for the same oil at different laboratories or test rigs increased. In a recent round robin test, failure load stages between 5 and 10 have been evaluated for the same lubricant [13]. One possible reason might be an insufficient running-in of the test gears.

Usually, the running-in process in the described stage tests is completed after load stage 4 or 5. For low-viscosity lubricants with a complex additive package, running-in effects might be possible until load stage 5 to 7. If the running-in process is not completed, the scuffing risk is significantly increased [14]. As a consequence, it might be possible, that the same oil shows an early FAIL in load stage 5 in the one test A10/16,6R/90 if the running-in process is not

finished and on the other hand a late FAIL in load stage 8-10 in the other test A10/16,6R/90, if the running-in process is finished early enough.

Based on these findings, a test method A10/16,6/90 was established for automotive gear transmission fluids. The underlying investigations are described in [13]. By using the standard direction of rotation, the test gets less severe. Test results can be expected approx. 2 load stages higher [7].

Common to all the test methods discussed so far is that they are carried out under oil splash lubrication. This means that a lubricant volume of approx. 1,25 l is placed in the test gearbox. At the start of each load stage from load stage 4 on, the oil temperature is set to 90 °C (or another temperature depending on the test method) by heating or cooling. By starting the test run, the heating or cooling unit is completely switched off. Consequently, the lubricant temperature increases during the 7,5 or 15 minutes test run due to the heat input of the gear mesh and the other system losses. Especially for the more severe test methods like A10/16,6R/90 very high lubricant temperature of ϑ_{oil} > 130 °C can be reached at the end of higher load stages.

Such high oil temperatures may lead to an additive reaction that cannot be seen in real application if such high temperatures do not appear. Thus, the test results might not be helpful for a detailed gearbox design. This is the case for many DCT applications when oil coolers are installed and higher oil volumes are needed. Consequently, a new scuffing test method was developed to differentiate lubricants for DCT applications which is described in detail in the following.

6. New Test method “A/16,6/90 spray lubrication”

A suitable test method for evaluating the scuffing load capacity of low-viscosity lubricants for DCT applications was developed in accordance to the FZG stage test A/16,6/90. The newly developed test method is described in detail below. For discriminating different lubricants for dual-clutch transmissions, a modified FZG stage test A/16,6/90 under spray lubrication was developed. This modified test runs with the standard type A gear set at speed condition v = 16,6 m/s. Furthermore, the gears are lubricated by spray lubrication with a flow rate of 1,0 l/min and controlled oil inlet temperature of 90 ± 2 °C. The running time per load stage is 7,5 min. The changed type of lubrication is the main change compared to the modified FZG stage test A/16,6/90.

The test method is described in detail in the following subsections. Wherever information is missing, refer to ISO 14635-1 [8] as the herein described test method is just another modification of the standard FZG stage test according to ISO 14635-1 [8] or CEC L-07-95 [1].

6.1. Failure criteria

In the newly developed test method, the failure is assessed visually. The failure criteria is fulfilled if a tooth width of 20 mm summed up over all teeth shows scuffing. The result of the test method is the load stage after which the damage was detected. Exemplary pictures of scuffing failures on test gears can be taken from ISO 14635-1 [8].

Fig. 5 shows an exemplary scuffing damage in the herein described test method. Due to the borderline lubrication conditions with a flow rate of 1,0 l/min, a beginning scuffing failure on one tooth flank usually develops very fast to severe scuffing with increased material removal (up to more than 1000 mg per test gear) and burr formation at the flank ends.

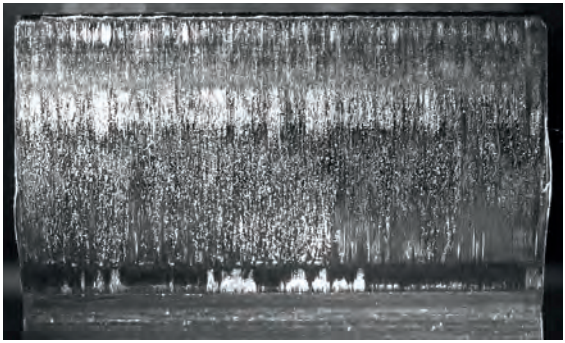

Fig. 5: Exemplary scuffing damage in the test “A/16,6/90 spray lubrication”

For a valid PASS result after load stage ≥ 12 the total weight loss of the gear must not exceed 20 mg. A higher weight loss indicates a wear scar in the dedendum flank area which leads, similar to a pinion tip relief, to reduced local load in the area of maximum sliding and thus prevents scuffing damage. If the gears don’t show any scuffing damage after load stage 12 but the total weight loss of the gear exceeds 20 mg, the test is INVALID.

6.2. Test gears

For investigating the scuffing load carrying capacity of lubricants for DCT according the presented test method test gears type A with an effective face width of b = 20 mm are used. The basic geometry data of the gear set is shown in Fig. 6.

Dimension	Symbol	Numerical Value and Unit
shaft centre distance	a	91,5 mm
effective face width	b	20 mm
number of teeth	z_1 z_2	16 24
addendum engagement	e_{a1} e_{a2}	14,7 mm 3,30 mm
flank modification	none	

Fig. 6: Test gears type A

6.3. FZG back-to-back spur gear test rig

The test is run on the standard FZG back-to-back gear test rig with center distance a = 91,5 mm which works according to the principle of a closed power circuit (see Fig. 7). Two spur gear sets, the test gear and the slave gear, are connected over two parallel shafts by use of a mechanical load clutch. The load is applied when the clutch is open by applying load lever and weights corresponding to the respective load stage and then fixing the clutch with several screws. The load level is measured by the torque measuring clutch. In this arrangement, the electrical drive unit solely compensates the power losses induced by the components of the FZG back-to-back spur gear test rig. Further information on the FZG back-to-back spur gear test rig can be found in DIN ISO 14635-1 [8].

To enable tests with injection lubrication, the standard FZG back-to-back spur gear test rig is supplemented by an additional oil unit. In the following, the implementation and the requirements for injection lubrication when carrying out the newly developed test are described in detail.

The herein presented test method for evaluating the scuffing performance of lubricants for DCT applications is based on injection lubrication and therefore differs significantly from other scuffing test methods used. Using injection lubrication makes the test much more sensitive to external influences and requires a careful test execution in order to achieve reliable results.

The used oil supply system should consist of an oil tank with a volume of approx. 5 liters, an oil pump, a heating and cooling system for the oil, an oil injector at the test gear box (see Fig. 8) and an oil return pipe from the test gear box to the oil tank.

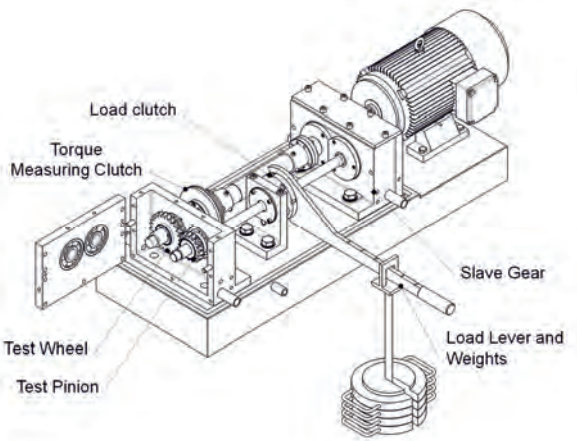

Fig. 7: FZG back-to-back spur gear test rig

6.4. Injection lubrication and lubricant temperature

By now, this test method is – according to the authors knowledge – only systematically carried out by the Gear Research Centre (FZG). The detailed test procedure is not published or standardized until now. Regarding the used injection lubrication, the following points should be carefully considered.

The oil temperature is regulated to 90 ± 2 °C (other temperatures possible as modification) at the oil inlet during the whole test. The oil temperature is constantly measured by a temperature sensor in the oil inlet of the test gearbox. The constant control and regulation of the oil temperature at the oil inlet is done by a heating and cooling device.

The injection nozzle is placed directly above the gear mesh (see Fig. 8). The ways between oil supply unit and oil inlet should be very short in order to reduce heat losses. An additional insulation of the pipe system and the tubes from the oil supply unit to the oil inlet and also for the oil return pipe is needed to reduce heat losses and to achieve the lowest possible temperature in the oil tank. The maximum temperature difference to the desired temperature at the oil inlet (90 ± 2 °C) in the oil supply system should be 10 K in order to prevent damage to the oil and additives.

The oil flow rate through the injection nozzle has to be set to 1,0 l/min ± 0,1 l/min and is measured directly by a flow meter at the oil inlet in the test gearbox and is controlled manually just before the test run at the test oil temperature.

The lubrication system of the slave gear unit has to be separated from the test gear unit.

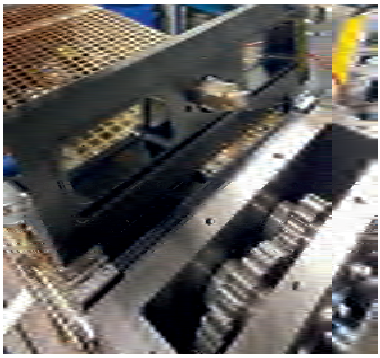

Fig. 8: Injector with nozzle and test gear

6.5. Preparation and test procedure

The preparation and test procedure is briefly described in the following. All relevant steps should be carried out in accordance to ISO 14635-1 [8] if not stated differently herein.

- Clean the test rig including bearings and oil supply unit, ensuring that all components are free of the previous oil sample, flush the test gearbox twice with test oil.
- Clean and weigh the test gears to the nearest 0,001 g
- Assemble the test gearbox with the pinion on the right-hand side shaft.
- Start heating up the oil in the oil circuit with running oil pump in order to avoid local hot spots in the oil sump. Regulate the oil temperature to 90 ± 2 °C at the oil inlet and the oil flow to 1,0 l/min ± 0,1 l/min at the oil inlet.
- Apply the first load stage using the specifications given in ISO 14635-1 [8].
- Start the test after reaching the target temperature and oil flow.
- The duration of a test run in one load stage is 7.5 min or 21 700 motor revolutions.
- Visually inspect the test gears after each load stage.
- Continue the tests with step wise increasing load.
- Continue the procedure until the failure criterion according 6.1 or load stage 12 is reached.
- Weigh the test gears if load stage 12 is reached without failure.

The test procedure and summarized in Fig. 9.

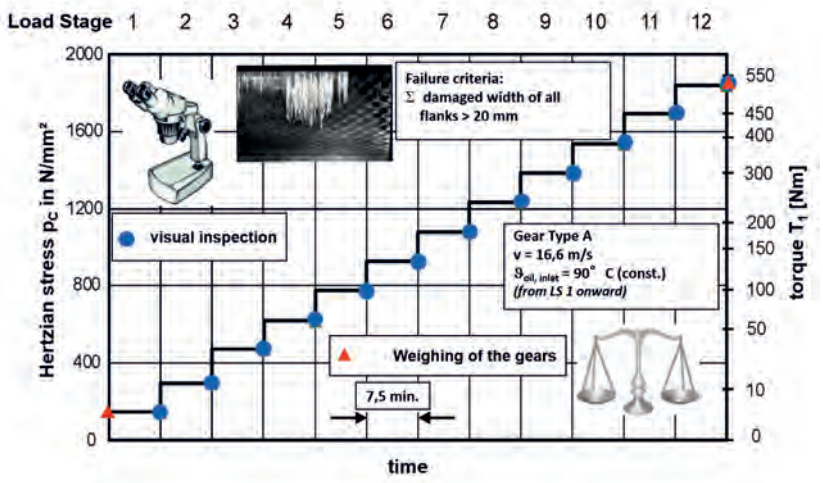

Fig. 9: Test procedure “A/16,6/90 spray lubrication” (source: FZG)

6.6. Reporting of results

As a result of the newly developed test procedure, the load stage achieved and the corresponding pinion torque at which the failure criterion occurred are indicated. In addition, the designation of the test “A/16,6/90 spray lubrication” must be noted on the result protocol. If the test was completed without reaching the failure criterion and the loss of mass of the wheel after passing load stage 12 is less than 20 mg, the result “load stage greater than 12” shall be documented.

6.7. Precision of the test method

Based on several test runs carried out at the Gear Research Centre (FZG) and experiences with other scuffing test methods, the repeatability (r) of the presented test method is assumed to be “r = 1 load stage”. As this test method is – according to the author’s knowledge – not yet carried out by other institutes, data regarding the reproducibility are not yet available. It is assumed by the authors, that the reproducibility (R) will be comparable to the already known test methods and therefore “R = 2 load stages”.

6.8. Possible modifications

As possible modifications of the herein presented test method “A/16,6/90 spray lubrication”, the following points may be applicable:

- Extension of the load range to load stages 13 and 14. The validity of the test (mass loss of the wheel < 20 mg) has to be checked after load stage 12, 13 and 14.
- Higher or lower oil temperatures may also be possible. The oil temperature should be carefully chosen in accordance to the oil temperature in real application. A test “A/16,6/60 spray lubrication” may be conceivable for lubricants for BEV-gearboxes as it is known that lower oil temperatures are possible in this application. If higher oil temperatures than 90°C are required special care has to be applied in the heating system to safely avoid additive deterioration.

7. Conclusion

In the scope of this contribution, a suitable test method for evaluating the scuffing load capacity of low-viscosity lubricants for DCT applications was developed in accordance to the FZG stage test A/16,6/90. This test method “A/16,6/90 spray lubrication” and the test procedure were presented in detail.

With this test method, it is possible to evaluate and differentiate the scuffing performance of lubricants for dual-clutch transmissions under realistic conditions. Contrary to the widely used scuffing test procedures specified in ISO 14635 or according CEC, this test method requires a test rig with an external oil supply unit. Flow rate as well as a constant inlet oil temperature are specified in the test procedure. The repeatability of the test procedure is one load stage. As this test procedure is currently only carried out by the Gear Research Centre (FZG), da regarding the reproducibility is not yet available.

8. References

[1] CEC L-07-95:2014-09: FZG Gear Machine - Load Carrying Capacity Test for Transmission Lubricants (2014).

[2] Collenberg, H.: Untersuchungen zur Freßtragfähigkeit schnelllaufender Strinradgetriebe. Dissertation, Technische Universität München (1991).

[3] DIN ISO 14635-1:2006-05: Zahnräder – FZG-Prüfverfahren – Teil 1: FZG-Prüfverfahren A/8,3/90 zur Bestimmung der relativen Fresstragfähigkeit von Schmierölen (2006).

[4] DIN 3990-4:1987-12: Tragfähigkeitsberechnung von Stirnrädern Berechnung der Freßtragfähigkeit (1987).

[5] DIN 3991-4:1988-09: Tragfähigkeitsberechnung von Kegelrädern ohne Achsversetzung Berechnung der Freßtragfähigkeit (1988).

[6] Höhn, B.-R.; Michaelis, K.; Collenberg, H.; Schlenk, L.: Temperature Effects on the Scuffing Load Capacity of Gear EP-Lubricants. Technische Akademie Esslingen 12th International Colloquium "Tribology 2000 - Plus" , January 11-13, 2000 2000, S. 601–08 (2000).

[7] Höhn, B.-R.; Michaelis, K.: Ermittlung der Fresstragfähigkeit von Schmierstoffen für Zahnräder. GETLUB Tribologie- und Schmierstoffkongress, Würzburg (2010).

[8] ISO 14635-1:2000-06: Gears - FZG test procedures - Part 1: FZG test method A/8,3/90 for relative scuffing load-carrying capacity of oils (2000).

[9] ISO 14635-2:2004-04: Gears - FZG test procedures - Part 2: FZG step load test A10/16,6R/120 for relative scuffing load-carrying capacity of high EP oils (2004).

[10] ISO 14635-3:2005-09: Gears — FZG test procedures — Part 3: FZG test method A/2,8/50 for relative scuffing load-carrying capacity and wear characteristics of semifluid gear greases (2005).

[11] ISO/TS 6336-20:2017-11: Calculation of load capacity of spur and helical gears — Part 20: Calculation of scuffing load capacity (also applicable to bevel and hypoid gears) — Flash temperature method (2017).

[12] ISO/TS 6336-21:2017-11: Calculation of load capacity of spur and helical gears — Part 21: Calculation of scuffing load capacity (also applicable to bevel and hypoid gears) — Integral temperature method (2017).

[13] Kadach, D.; Michaelis, K.; Hein, M.; Tobie, T.; Stahl, K.: Fresstragfähigkeit von Schmierstoffen für Doppelkupplungsgetriebe. antriebstechnik 2021. Heft: 04, S. 52–59 (2021).

[14] Michaelis, K.: Die Integraltemperatur zur Beurteilung der Fresstragfähigkeit von Stirnradgetrieben. Dissertation, Technische Hochschule München (1987).

[15] Schlenk, L.; Eberspächer, C.; Graswald, C.: Method to Assess the Scuffing Load Capacity of Lubricants with High EP Performance Using an FZG Gear Test Rig - Information Sheet No. 243/2. Forschungsvereinigung Antriebstechnik, Frankfurt/Main (2000).

Development of a new test method to investigate the wear behaviour of hypoid gear oils

M.Sc. **Alexander Drechsel**, M.Sc. **Josef Pellkofer**,
Prof. Dr.-Ing. **Karsten Stahl**,
FZG – Forschungsstelle für Zahnräder und Getriebebau,
Technical University of Munich;
Josef Sandor, Technical University of Munich;
Dr.-Ing. **Michael Hein**, HOERBIGER Antriebstechnik Holding GmbH

Zusammenfassung

Verschleiß kann im Antriebsstrang eine lebensdauerbegrenzende Schadensart darstellen. Insbesondere hochbelastete Hypoidgetriebe, die bevorzugt in Achsgetrieben von Fahrzeugen eingesetzt werden, weisen auf Grund des Achsversatzes, ihrer Flankengeometrie sowie deren Anwendungsgebieten eine bezüglich Verschleiß ungünstige Kombination aus hohem Quer- und Längsgleiten sowie hohen Flankenpressungen bei niedrigen Schmierfilmdicken auf. Die Verschleißtragfähigkeit von Hypoidgetrieben wird maßgeblich durch den verwendeten Schmierstoff und dessen Additivierung beeinflusst. Da es im Allgemeinen nicht möglich ist, den Einfluss des Schmierstoffes auf die Tragfähigkeit von Zahnrädern allein anhand der physikalischen oder chemischen Öldaten zu bestimmen, sind experimentelle Prüfverfahren notwendig.

Um die Verschleißtragfähigkeit von Hypoidölen untersuchen und klassifizieren zu können, wurde in Anlehnung an Erkenntnisse aus Verschleißuntersuchungen an Stirnrädern und Scheiben eine experimentelle Prüfmethodik entwickelt. Hierbei wird das Prüföl entsprechend des Anwendungsgebietes unter Verwendung einer Hypoidtestverzahnung hinsichtlich der Verschleißtragfähigkeit untersucht. Insgesamt besteht das Prüfverfahren aus drei Testphasen, wobei die ersten zwei Phasen einen vollständigen Verzahnungseinlauf gewährleisten.

Im Rahmen dieses Beitrages soll die Entwicklung der neuen Prüfmethode zur Klassifizierung und Untersuchung der Verschleißtragfähigkeit von hochbelasteten Hypoidölen sowie erste experimentelle Ergebnisse vorgestellt werden.

Abstract

Wear can be a life-limiting type of damage in the driveline. In particular, highly loaded hypoid gears, which are preferably used in vehicle axle drives, exhibit an unfavorable combination of high transverse and longitudinal sliding and high flank pressures with low lubricant film thicknesses in terms of wear due to the axle offset, their flank geometry and their areas of application. The wear resistance of hypoid gears is significantly influenced by the lubricant used and its additives. Since it is generally not possible to determine the influence of the lubricant on the load carrying capacity of gears on the basis of physical or chemical oil data alone, experimental test methods are necessary.

In order to be able to investigate and classify the wear resistance of hypoid oils, an experimental test methodology was developed based on findings from wear investigations on spur gears and discs. Here, the test oil is examined for its wear resistance in accordance with the area of application using a hypoid test gear. In total, the test procedure consists of three test sections, with the first two sections ensuring a complete running-in.

This paper presents the development of a new test method for classifying and investigating the wear resistance of highly loaded hypoid oils as well as initial experimental results.

1 Introduction and objective

Hypoid gears are bevel gears with a hypoid offset. Due to their preferred application in vehicle axle drives, they are subject to highest demands in regard to load carrying capacity and efficiency. The hypoid offset leads to sliding in tooth lengthwise direction additional to the sliding in tooth profile direction. This results in higher sliding velocities in the tooth contact compared to spur gears or bevel gears without a hypoid offset. In combination with high contact stresses and low lubricant film thicknesses, wear-critical conditions occur. Since the wear resistance of hypoid gears is significantly influenced by the lubricant used and its additives, knowledge of the suitability of the lubricant for the respective application is necessary.

Fig. 1: Running and wear marks on a pinion flank of a hypoid gear

The gear oil classification of the American Petroleum Institute (API) provides support in the selection of a suitable gear oil for the respective application. The API classifies gear lubricants into six categories based on the common areas of application of these lubricants additionally supplemented by the MT-1 category. The API MT-1 category is for gear lubricants used for unsynchronized manual transmissions in buses and heavy trucks. The higher the class, the higher the chemical and physical demands on the gear lubricant, e.g. increasing contact stresses, sliding speeds and oil temperatures. However, at the moment only the classes API GL-4, API GL-5 and API MT-1 are active [API13]. A market analysis by Tuszynski [Tus11] from 2011 regarding the percentage share of gear oils of particular API GL categories (including universal - multi grade oils) in the total market offer of automotive gear oils has shown that oils of API GL-4 and GL-5 category have the largest share. API GL-4 category oils are suitable for spiral bevel gears “operating under moderate to severe conditions speed and load, as well as for hypoid gears under moderate conditions speed and load” [API13]. API GL-5 category oils are suitable for particularly hypoid gears “operating under various combinations of high-speed/shock load and low-speed/high-torque conditions” [API13]. At the moment test equipment for performance verification of the API GL-4 class is not available according API [API13]. The classification procedure of API GL-5 category oils is standardized in ASTM D7450 – 19 [AST19]. This contains several chemical and physical tests to determine the suitability of the lubricant, such as the hypoid test L37 [AST17a] and the more recent L37-1 [AST17b] to verify sufficient wear, pitting, ridging and rippling load carrying capcity of the lubricant. Both tests are standardized and recognised worldwide by lubricant manufacturers as well as gear manufacturers and operators as test methods for gear lubricants for use in highly loaded hypoid gears. In addition to high costs, the tests are associated with low global availability and high testing effort. Therefore, the scope of the presented project was to develop a new testing method which allows the determination of the wear load carrying capacity of hypoid oils and at the same establishes a reference to the API classification. A key objective is to identify gear oils with sufficient wear load carrying capacity so that they can be used in highly loaded hypoid gearboxes with regard to wear and thus also can pass the L37 / L37-1 test. To investigate the wear load carrying capacity of gear lubricants for spur

gear applications the FZG slow speed wear test [Bay97] exists. Since the focus here is on gear lubricants for use in highly loaded hypoid gears, the L37 / L37-1 test forms the basis for the development of the new test method.

2 The L37 / L37-1 test (brief description)

To meet the requirements of anAPI GL-5 classification, a lubricant must pass the L37-1 test in addition to chemical and physical tests. The L37-1 test is a standardized and globally accepted gear oil test for “evaluating the load carrying capacity, wear performance, and extreme pressure properties of a gear lubricant in a hypoid axle under conditions of low-speed and high-torque operating” [AST17b]. The previous L37 test is no longer feasible due to the lack of hypoid test gear sets [Kle13]. The L37 test is documented in the ASTM standard D6121 [AST17a] and the L37-1 test in the ASTM standard D8165 [AST17b]. In the L37-1 test, a Dana Model 60 axle with a grinded hypoid gear set (manufacturer: Gleason) is used for the experimental investigations. The axle assembly is driven by an AC electric motor and the output is realized by two axle dynamometers. In total, the test consists of a gear conditioning phase and a gear testing phase. Both phases take place at constant wheel load and wheel speed. There are two versions of the L37 / L37-1 test: The standard test and the Canadian test. Compared to the Canadian test, the standard test takes place at elevated oil temperatures. In order for the gear oil to obtain API GL-5 classification, the standard test is sufficient. The Canadian test is for example used for evaluation of SAE 70W and 75W viscosity-grade lubricants according to SAE J2360 [SAE12] for automotive gear lubricants for commercial and military use. After the test run, an ASTM-trained inspector visually inspects the hypoid gear set in accordance with TMC Distress Rating Manual 21 (CRC manual 21) [Ame12] for ridging, rippling, pitting, scuffing and also wear.

3 Development of the new test method

In the following, the development of an experimental test method for investigating the wear behavior of gear lubricants for use in highly loaded hypoid gears is presented. For this purpose, suitable operating conditions are determined by means of local recalculations based on a selected hypoid test gear and in orientation to the L37-1 test. Furthermore, a gear running-in is defined on the basis of local recalculations and experimental investigations to enable the testing of API GL-4 and GL-5 categorized oils in the same test procedure and achieve comparable and reproducible test results. Finally, first experimental results of the newly developed test method will be presented.

3.1 Test equipment

The experimental investigations were carried out on a hypoid-back-to-back test rig, which works according to the principle of a closed power circuit (see Fig. 2). Two hypoid gear sets, the test gear set and the slave gear set, are connected to a spur gear set over to parallel shafts by use of a mechanical load clutch which allows the application of a defined torque. The torque applied to the test pinion is measured using strain gauges that are mounted on the torsional shaft. The electric motor only injects the power losses induced by the components of the the hypoid-back-to-back test rig. The test rig offers the possibility of injection or dip lubrication as well as a combination of both types of lubrication. The oil temperature in the gearboxes can be regulated by use of oil supply units.

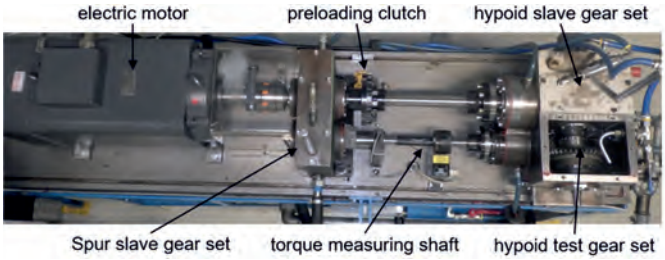

Fig. 2: Setup of a Hypoid-back-to-back test rig

Within the experimental investigations one gear geometry, the G44 hypoid test gear, was examined. The basic geometry data are given in Table 1. The test gears are made of the steel 18CrNiMo7-6. The load carrying capacity of the G44 hypoid test gear has already been investigated in the research project FVA 411 [Wir09]. Therefore, findings on the pitting load carrying capacity of the test gear are already available. The test gear geometry is designed with the aim of preferentially causing failures on the gear flank. Failures such as tooth root breakage should be reliably avoided due to the design.

Table 1: Basic geometry data of the hypoid test gear

Test gear name			**G44**
Hypoid offset	a	mm	44
Shaft angle	Σ	°	90
Teeth ratio	z_1/z_2	-	9 / 34
Mean normal module	m_{mn}	mm	4.19
Face width	$b_{1,2}$	mm	36.9 / 26
Normal pressure angel ratio drive/coast side	α_{nD}/α_{nC}	°	13.2 / 26.8
Mean spiral angle	$\beta_{m1,2}$	°	49.5 / 16.5
Profile shift coefficient	$x_{hm1,2}$	-	0.45 / -0.45

Five different gear oils based on mineral oil were used as test oils. Table 2 gives an overview of the oils examined. The oils 1 to 3 are based on the standard oil FVA 3 with different concentrations of the EP-additive “Anglamol 99”. For Oil 4 and 5 the composition as well as the type of the additive is unknown. Oil 1 and 2 have passed the L37-1 test. Oil 4 was confirmed in 2011 to have passed the L37 test. Test results for the oils 3 and 5 are not available. According to the manufacturer, oil 5 is to be assigned to the classes API GL-3/4.

Table 2: Gear test oils

Designation	Content	Result in L37-1
Oil 1	FVA 3 + 6,5 % A99	passed
Oil 2	FVA 3 + 4 % A99	passed
Oil 3	FVA 3 + 2 % A99	unknown
Oil 4	unknown	passed L37
Oil 5	unknown	unknown

3.2 Procedure of the new test method

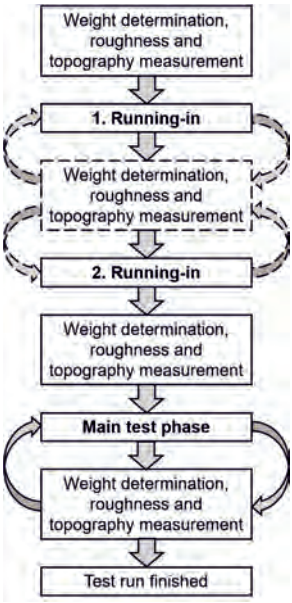

Fig. 3: Test procedure

In total, the test procedure includes three test sections. The first two sections ensuring complete gear running-in. The wear occurring is determined by means of weighing of the wheel at regular intervals. Weighing is performed using a precision balance with a measuring accuracy of +/- 1 mg. Due to the design of the test rig, only the wheel is removed for weighing. This ensures that the dismounting and mounting of the wheel in one test run has no influence on the contact pattern position. A change in the mounting position would result in an invalid test, as there would be no comparability and reproducible between other test runs.

Fig. 3 illustrates the procedure of the newly developed test method. In the first step, the weight of the wheel is determined and its roughness and topography measured using a P40 Klingelnberg Precision Measuring Center. The topography measurement is performed on three teeth distributed around the circumference. The roughness measurement is performed on three teeth in the middle of the contact pattern. Should the running-in behavior of the gear oil also be considered, the running-in can be interrupted at regular intervals. Afterwards, the main test

phase takes place, in which the wear load carrying capacity of the gear oil is documented. Within the main test stage regular interruptions take place for weighing the wheel as well as for measurement of the topography and flank roughness. The aim is to determine the continuous wear. If flank damage such as scuffing or pitting occurs, the test has to be ratet invalid because it is no longer possible to determine wear by weighing.

3.3 Operating conditions of the main test phase

The operating parameters of the main test phase, speed and torque, are derived from the parameters of the L37-1 test. For this purpose, the parameters contact stress and sliding velocity are used as the relevant comparison parameters. Applying a loaded tooth contact analysis to the G44 hypoid test gear, a pinion torque of 590 Nm and speed of 900 rpm allow good comparability with the test L 37-1. In the investigation according the L37-1 test, the drive side is used with the pinion as driving member. The oil temperature is regulated to 79 °C, which is equal to the oil start temperature of the gear test phase of the L37-1 test.

In the following, the suitability of the selected operating parameters for a wear test using the G44 hypoid test gear is verified by local recalculation. Therefore, the contact temperatures, the minimum film thicknesses and the scuffing as well as pitting safeties were examined in detail. The local values are calculated based on a loaded tooth contact analysis using the program BECAL [Wag20], considering the load-induced deflections of the test rig.

Fig. 4 shows the local contact temperatures plotted on the pinion flank calculated by use of the calculation method according to the research project FVA 516/I [Hom13]. The erratic changes in the calculated contact temperatures at the contact area near the tooth root can be attributed to numerical boundary effects and are not to be regarded as representative. The majority of the contact pattern shows contact temperatures between 300 °C and 600 °C. This is a temperature range in which phosphorus additives, used in particular as AW additives, are activated [Bar10]. Since the wear load carrying capacity of the gear oil is to be tested, the occurring contact temperatures, which are

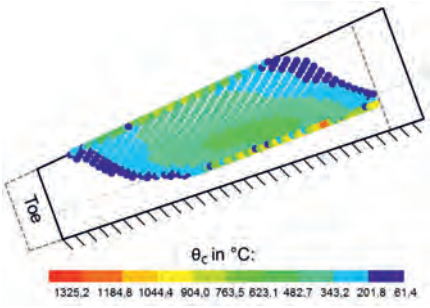

Fig. 4: Calculated local contact temperatures (pinion flank)

favorable activation temperatures for phosphorus additives, are considered suitable for the new test method. In view of the scuffing resistance of the G44 hypoid test gear and the possibility of also testing API GL-4 categorized oils, higher contact temperatures should not occur.

Based on experimental investigations on spur gears, Plewe [Ple80] showed that material pairings of the same surface hardness are at risk of wear at lubricant film thicknesses below approximate 0.05 µm. Fig. 5 presents the local occurring minimum lubricant film thicknesses plotted on the pinion flank calculated according to the research project FVA 516/I [Hom13, Pel19b]. With the exception of small peripheral contact areas, minimum lubricant film thicknesses of less than 0.05 µm are present throughout the tooth contact. Thus, the selected operating parameters are suitable for wear investigations.

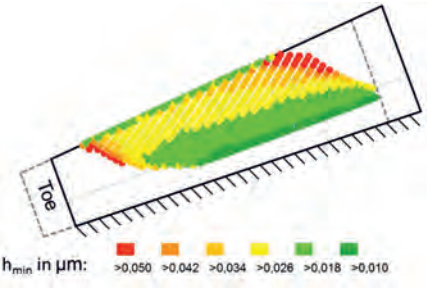

Fig. 5: Calculated local lubricant film thicknesses (pinion flank)

To be able to determine the occurring wear by means of weighing, no other types of damage may occur. Since the G44 hypoid test gear was designed to investigate flank failures only [Wir09], the pitting and scuffing load carrying capacity was investigated in detail within a previous reseach project. Fig. 6 shows the experimental results and the derived S-N curve for pitting for 50 % failure probability determined in the research project FVA 411 [Wir09]. In green, the S-N curve for 1% failure

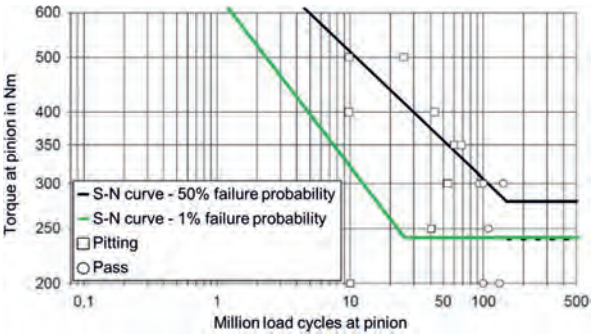

Fig. 6: S-N curves for pitting of hypoid test gear G44 for different failure probability according to [Wir09] (S-N curve for 1 % failure probabilitiy is added)

probability was added, determined according to Stahl [Sta99]. Even in the high torque range of 600 Nm, a possible number of load cycles at pinion of over 1 million without pitting can be expected with a very high degree of probability. Following the experimental tests on hypoid gears by Langenbeck [Lan65] and on spur gears by Plewe [Ple80], it is assumed that 1 million load cycles at pinion are sufficient to be able to characterize the continuous wear behaviour of the test gear respectively the investigated oil.

Fig. 7 shows the local scuffing safety factors, plotted on the pinion flank, calculated using the local calulation method according to the research project FVA 519 [Kle13, Pel19a]. The use of a API GL-4 categorized oil is assumed for determining the permissible scuffing temperature. Within experimental investigations at spur gears of the research project FVA 243 [Sch96], API GL-4 and API GL-5 categorized gear oils were examined for their scuffing load carrying capacity using the scuffing shock test S-A10/16.6R/90 [Kad16]. It was found that oils of the API GL-5 category pass at least load stage 9 without damage. This recommendation is also given in ISO 10300-20 [ISO21]. Since the new test method should also allow the use of API GL-4 categorized oils, the permissible scuffing temperature was determined with the assumption of a gear oil that achieves load stage 8 in the scuffing shock test A10/16.6R/90. Neglecting the numerical boundary effects in the local calculation results shown in Fig. 7, the entire tooth flank shows a scuffing resistance above 1.0. Considering that sufficient knowledge of the G44 hypoid test gear is available, it can be assumed that no scuffing occurs [Pel19a].

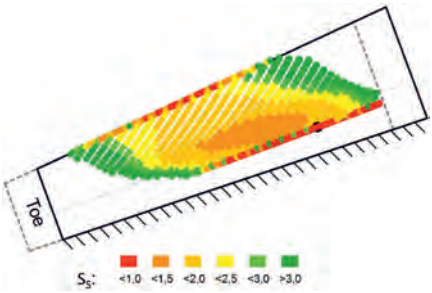

Fig. 7: Calculated local scuffing safety factors after running-in (pinion flank)

Based on the comprehensive local recalculations, it can be statet that the defined operating parameters are suitable for testing the wear load carrying capacity of gear oils of classification API GL-4 and GL-5 using the G44 hypoid test gear set.

3.4 Gear running-in

Adequate gear running-in is considered important for the following three reasons:

- Increasing the scuffing load carrying capacity of the test gear
- Minimizing the influence of manufacturing-related scatter in flank roughness
- Isolated consideration of the continuous wear independent of the running-in wear

Fig. 8 shows the local scuffing safety factors of the G44 hypoid test gear in new condition (without running-in) under operating conditions of the main test phase and assuming the use of an API-GL4 categorized oil. In the flank area of highest contact stresses, local scuffing safety factors below 1.0 occur. Consequently, scuffing is to be expected in comparison to the G44 hypoid test gear with running-in (see Fig. 7). Since API GL-4 categorized oils generally have a lower scuffing load capacity compared to API GL-5 oils, and the new test method uses a hypoid test gear where there is a high risk of scuffing, the scuffing resistance of the test gear must be increased. This can be achieved by a complete gear running-in [Höh10, Kle13, Lec66]. Therefore, a running-in is necessary. The running-in should be carried out at least at test load to ensure a smoothing of the whole load-carrying flank area. Using a high load carrying capacity gear oil for running-in would be one possibility. Experimental investigations on discs and spur gears have shown that the damage and friction behaviour, in addition to the surface roughness, is largely dependent on tribo-induced layers that can already appear on the flanks during the running-in process. [Loh15, Sch18]. Depending on the additivation different gear oils lead to different tribo-induced layers. Thus, the use of a separate high load carrying inlet oil is not expedient. Therefore, a two-stage running-in is necessary. Aiming to increase the local scuffing load carrying capacity, the following operating conditions were determined by varying the drive speed, torque and oil temperature in local recalculations:

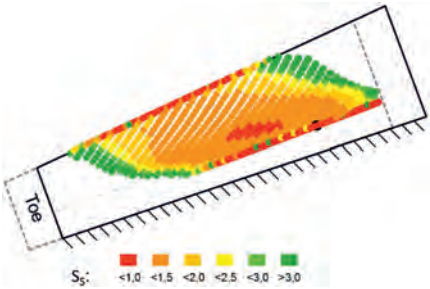

Fig. 8: Calculated local scuffing safety factors without running-in (pinion flank)

Section 1: T_1 = 210 Nm, n_1 = 1600 rpm, T_{oil} = 90 °C

Section 2: T_1 = 590 Nm, n_1 = 200 rpm, T_{oil} = 79 °C

Section 1 is used to increase the scuffing load capacity of the G44 hypoid test gear due to smoothing the most scuffing-critical flank area under low load. Thus, at beginning of

section 2, the scuffing load carrying capacity of the hypoid test gear is already higher than in new condition. In Section 2, the smoothing of the whole contact pattern at test load is performed. This allows test oils to be classified on the basis of their continuous wear behavior irrespective of their running-in behavior.

The required duration of the individual running-in sections was determined experimentally. For this purpose, the running-in was regularly interrupted, to carry out a roughness measurement in the center of the contact pattern. If almost identical roughness values were determined between two measurement times, the test section was stopped and the next test section was started. Fig. 9 presents the arithmetic mean flank roughness over the load cycles at pinion using the five test oils. Each test section is indicated by a different line type. Oil 1, oil 2 and oil 5 were used to define the duration of the test sections of the running-in.

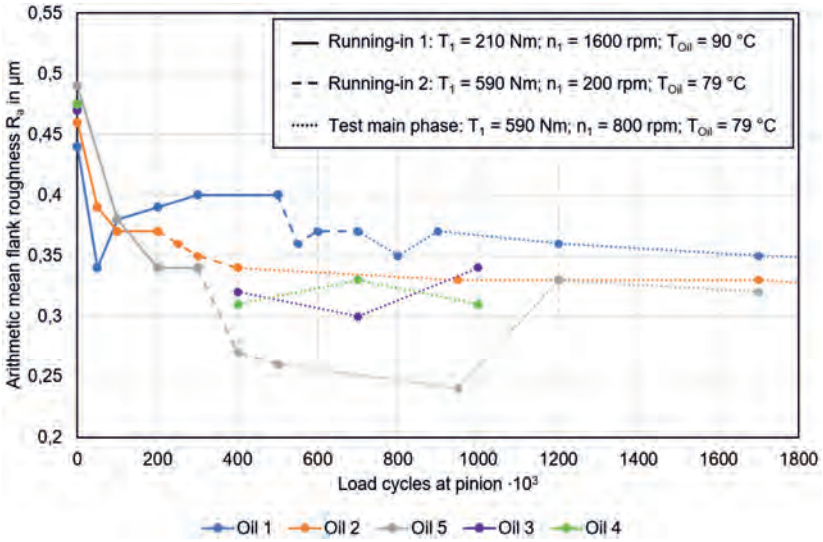

Fig. 9: Roughness measurements during the test run

A significant smoothing of the contact flank area occurs in the first 50,000 load cycles at pinion of running-in section 1. The increase in load and reduction in speed in running-in section 2 further reduces the roughness level. For all three oils, oil1, oil 2 and oil 5, an almost constant flank roughness level is detected in both running-in sections after 200,000 load cycles at pinion at the latest. The flank roughness level after running-in corresponds for oils 1 and 2 to the flank roughness level in the main test phase. Oil 5 has the same flank

roughness level after running-in compared to the first measurement point in the main test phase. Afterwards, however, an increase in flank roughness can be seen. Since the three measurement points at the low flank roughness level do not fit in with the rest of the results, it is assumed that there is probably a measurement error here. In the further test run using oil 5, the roughness level is at a similar level compared to the main test phase of the other test runs. Overall it can be stated that 200,000 load cycles at pinion per running-in section is sufficient to smoothing the tooth flank. Consequently, it should be possible to record the continuous wear independently of the wear occurring by smoothing the tooth flanks. The test runs using oil 1 and oil 2 are continued over 2 million load cycles on the pinion. Again, no significant change in roughness level can be detected compared to the roughness level at the end of the running-in. The duration of the running-in is also verified in the tests using oils 3 and 4. Roughness measurements were carried out at the end of the complete running-in with 200,000 load cycles per running-in phase and at regular intervals during the main test phase. The roughness level at the end of the running-in corresponds to that of the main test phase.

Furthermore, the G44 hypoid test gears usually show manufacturing-related scatter in the flank roughness. In one production batch a scatter range of up to 0.6 µm is present when considering 15 hypoid test gears. These fluctuations can be minimized by means of sufficient smoothing through a defined running-in in order to ensure the best possible comparability of the test runs among each other [Sch10].

4 Experimental results of the main test phase

Fig. 10 shows the experimental results of the main test phase. The progress of wear loss of the wheel is plotted. The test runs investigating oils 1, 2 and 5 were run up to 1 million load cycles at pinion. No identifiable mass loss was generated with oil 1. Comparable wear loss was identified in the test runs with oil 2 und oil 5, whereby oil 2 generated slightly higher mass losses. Since only small mass losses can be identified in these first three test runs, the running time of the test runs using oils 3 and 4 were extended. The first section was run at the operation conditions presented above up to 600,000 load cycles at pinion. Both oils show increased mass loss compared to oils 1, 2 and 5. In the second section, the pinion speed was reduced to 100 rpm with the assumption that this would make it more difficult to build up a lubricant film and make the test more wear-critical. In both tests, however, a decrease in continuous wear can be observed. Reasons may be the activation of the wear additives. Further investigations are necessary for a precise explanation of the behavior observed here.

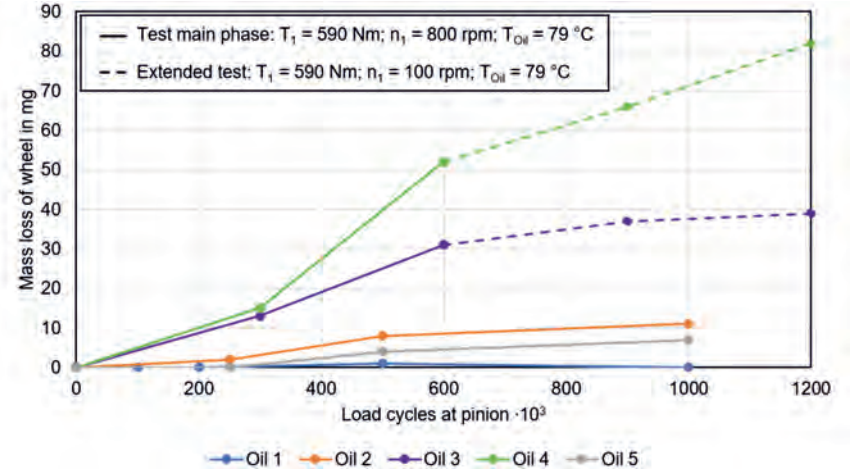

Fig. 10: Experimental results of the new test method

Overall it can be stated that the newly developed test method makes it possible to differentiate between the gear oils in terms of their wear resistance. This can be seen clearly in a comparison of oils 1, 2 and 3. These three oils differ only in the amount of additive. The base oil and additive type are identical. As the amount of additive decreases, an increase in mass loss and thus in continuous wear can be identified. Thus, a tightening of the test to increase the wear rates is also not considered necessary. Therefore, it is not deemed necessary to intensify the test conditions in order to increase the wear rates.

5 Summary and outlook

In this paper, the development of a new hypoid test for investigating the wear resistance of high-performance gear lubricants were presented. Also, first experimental results were shown. On basis of theoretical recalculations and experimental investigations, a running-in was defined. This enables the continuous wear to be determined in the main test phase, unaffected by the smoothing of the tooth flank and as unaffected as possible by manufacturing-related scatter in flank roughness. Furthermore, the running-in allows testing of API GL-5 and API GL-4 classified oils. The operating conditions for the main test phase were determined by means of local calculations using a tooth contact analysis in orientation to standardized and globally accepted L37-1 gear oil test. Initial experimental investigations show that the test allows the differentiation of gear oils on basis of their wear resistance.

Due to the difficult accessibility of pass and fail reference oils in the L37 test, a pass limit should be determined using a large number of test oils. Should the limit be reached by a test oil, it can be assumed that it has the wear resistance of an API GL-5 categorized oil. However, this is part of future research.

6 Acknowledgement

The authors would like to thank for the sponsorship and support received from the Bundeswehr Research Institute for Materials, Fuels and Lubricants (WIWeB).

7 References

[AST17a] ASTM D6121-17: Standard Test Method for Evaluation of Load-Carrying Capacity of Lubricants Under Conditions of Low Speed and High Torque Used for Final Hypoid Drive Axles. ASTM International, West Conshohocken, PA (2017). DOI: 10.1520/D6121-17

[AST17b] ASTM D8165-17: Standard Test Method for Evaluation of Load-Carrying Capacity of Lubricants Used in Hypoid Final-Drive Axles Operated under Low-Speed and High-Torque Conditions. ASTM International, West Conshohocken, PA (2017). DOI: 10.1520/D8165-17

[AST19] ASTM D7450-19: Standard Specification for Performance of Rear Axle Gear Lubricants Intended for API Category GL-5 Service. ASTM International, West Conshohocken, PA (2019). DOI: 10.1520/D7450-19

[Ame12] American Society for Testing and Materials (ASTM): TMC Distress Rating Manual 21 (Formerly CRC Manual 21), No. 21 (2012).

[API13] API Publication 1560: Lubricant Service Designations for Automotive Manual Transmissions, Manual Transaxles, and Axles. American Petroleum Institute, Washington, D.C., 18. Edition (2013).

[Bar10] Bartz, W. J.: Einführung in die Tribologie und Schmierungstechnik - Tribologie - Schmierstoffe - Anwendungen. expert verlag, Renningen, 1. Auflage (2010).

[Bay97] Bayerdörfer, I.; Michaelis, K.; Höhn, B.-R.: Method to Assess the Wear Characteristics for Lubricants FZG Test Method C/0,05/90:120/12 - Infoblatt. Deutsche Wissenschaftliche Gesellschaft für Erdöl, Erdgas und Kohle e.V., DGMK 377-1, Hamburg (1997).

[SAE12] SAE J2360: Automotive Gear Lubricants for Commercial and Military Use. SAE Inernational (2012). 10.4271/J2360_201204

[Höh10] Höhn, B.-R.; Michaelis, K.; Klein, M.: Ermittlung der Fresstragfähigkeit von Schmierstoffen für Zahnräder. FVA - GETLUB Tribologie- und Schmierstoffkongress, Würzburg, S. 157–168 (2010).

[Hom13] Hombauer, M.; Hutschenreiter, B.; Michaelis, K.; Schlecht, B.; Höhn, B.-R.: Hypoidgraufleckigkeit - Bestimmung der Graufleckentragfähigkeit von Kegelrad- und Hypoidverzahnungen. Forschungsvereinigung Antriebstechnik e.V., IGF-Nr. 14870 BG, FVA-Nr. 516/I, Heft 1055, Frankfurt/Main (2013).

[ISO21] ISO/TS 10300-20: Calculation of load capacity of bevel gears - Part 20: Calculation of scuffing load capacity - Flash temperature method (2021).

[Kad16] Kadach, D.; Tobie, T.; Michaelis, K.; Stahl, K.: Testverfahren zur Ermittlung der Fresstragfähigkeit von Schmierstoffen für Zahnräder. FVA - GETLUB International Tribology and Lubrication Congress, Würzburg, S. 112–125 (2016).

[Kle13] Klein, M.; Michaelis, K.; Stahl, K.: Hypoidfressen - Bestimmung der Fresstragfähigkeit von kegelrad- und Hypoidverzahnungen. Forschungsvereinigung Antriebstechnik e.V., IGF-Nr. 14863N, FVA-Nr. 519/I, Heft 1071, Frankfurt/Main (2013).

[Lan65] Langenbeck, K.: Die Verschleiß- und Freßgrenzlast der Hypoidgetriebe, Dissertation, Technical University of Munich, Institute of Machine Elements (1965).

[Lec66] Lechner, G.: Die Freß-Grenzlast bei Stinrrädern aus Stahl, Dissertation, Technical University of Munich, Institute of Machine Elements (1966).

[Loh15] Lohner, T.; Mayer, J.; Michaelis, K.; Höhn, B.-R.; Stahl, K.: On the running-in behavior of lubricated line contacts. Proceedings of the Institution of Mechanical Engineers, Part J: Journal of Engineering Tribology, Volume 231, S. 441–452 (2015). DOI: 10.1177/1350650115574869

[Pel19a] Pellkofer, J.; Boiadjiev, I.; Kadach, D.; Klein, M.; Stahl, K.: New calculation method of the scuffing load-carrying capacity of bevel and hypoid gears. Journal of Mechanical Engineering Science, Volume 233, S. 7328–7337 (2019). DOI: 10.1177/0954406219843954

[Pel19b] Pellkofer, J.; Hein, M.; Reimann, T.; Hombauer, M.; Stahl, K.: New calculation method of the micropitting load carrying capacity of bevel and hypoid gears.

Forschung im Ingenierwesen/Engineering Research, 83(3), S. 603–609 (2019). DOI: 10.1007/s10010-019-00344-7

[Ple80] Plewe, H.-J.: Untersuchungen über den Abriebverschleiß von geschmierten, langsam laufenden Zahnrädern, Dissertation, Technical University of Munich, Institute of Machine Elements (1980).

[Sch10] Schedl, U.; Oster, P.; Tobie, T.; Höhn, B.-R.: Pittingtest – Einfluss des Schmierstoffes auf die Grübchenlebensdauer einsatzgehärteter Zahnräder im Einstufen- und im Lastkollektivversuch. Forschungsvereinigung Antriebstechnik e.V., FVA-Informationsblatt 2/IV, Frankfurt/Main (2010).

[Sch96] Schlenk, L.; Eberspächer, C.; Michaelis, K.; Höhn, B.-R.; Winter, H.: Fressen EP-Öle - Festigkeitswerte hochlegierter Schmierstoffe zur Berechnung der Fresstragfähigkeit. Forschungsvereinigung Antriebstechnik e.V., FVA-Nr. 243/I, Heft 489, Frankfurt/Main (1996).

[Sch18] Schwarz, A.; Emrich, S.; Lohner, T.; Michaelis, K.; Brodyanski, A.; Merz, R.; Kopnarski, M.; Höhn, B.-R.; Stahl, K.: Einfluss triboinduzierter Schichten auf Schäden und Reibungsverhalten von Zahnrädern unter besonderer Berücksichtigung des Einlaufvorgangs – experimentelle und analytische Untersuchungen, Heft 3, S. 12–26 (2018).

[Sta99] Stahl, K.; Michaelis, K.; Höhn, B.-R.: Lebensdauerstatistik - Statistische Methoden zur Beurteilung von Bauteillebensdauer und Zuverlässigkeit und ihre beispielhafte Anwendung auf Zahnräder. Forschungsvereinigung Antriebstechnik e.V., AiF-Nr. 11154N, FVA-Nr. 304, Heft 580, Frankfurt/Main (1999).

[Tus11] Tuszynski, W.; Michalczewski, R.; Piekoszewski W.; Szczerek M.: Modern Automotive Gear Oils - Classification, Characteristics, Market Analysis and Some Aspects of Lubrication. New Trends and Developments in Automotive Industry, S. 297–322 (2011). DOI: 10.5772/13014

[Wag20] Wagner, W.; Schumann S.; Schlecht, B.: BECAL 6 - Durchgängigkeit lokale Berechnungsverfahren - Durchgängie Berechnung lokaler Kenngrößen zur Beanspruchung und Tragfähigkeit an kegelrad- und Beveloid-Verzahnungen in der FVA-Workbench NG. Forschungsvereinigung Antriebstechnik e.V., FVA-Nr. 777 III, Heft 1383 (2020).

[Wir09] Wirth, C.; Michaelis, K.; Höhn, B.-R.: Berechnung der Grübchen- und Zahnfußtragfähigkeit von Kegelrädern. Forschungsvereinigung Antriebstechnik e.V., IGF-Nr. 13124, FVA-Nr. 411, Heft 887, Frankfurt/Main (2009).

Simulation of induced axial forces on planet gear bearings at example of ZF's 8-speed automatic transmission

S. Dussinger, **T. Wiedemann**,
Engineering System International GmbH, Neu-Isenburg;
Dr. B. Harter, **B. Wiedenmann,** ZF Friedrichshafen AG

Zusammenfassung

Mit dem Ziel der Verbesserung der Energieeffizienz und Reduktion der CO2-Emissionen gilt es Reibungsverluste innerhalb von Komponenten des Antriebsstrangs stetig zu minimieren. Mit Fokus auf ein ZF 8-Gang-Automatikgetriebe werden Axialkräfte an planetaren Anlaufscheiben untersucht, die in Kombination mit Relativrotationen zu ebensolchen Reibungsverlusten führen. Die Untersuchung wird mit Hilfe von Finite-Elemente-Simulationen durchgeführt. Dabei werden wichtige Einflussparameter wie z.B. die Profilierung der Nadeln der Planetenlagerung, sowie Fertigungstoleranzen identifiziert. Aufbauend auf den gewonnenen Erkenntnissen wird das vorhandene Optimierungspotential bewertet. Im Rahmen der Verifikation der Simulationsmethode wird eine detaillierte Prüfung der Plausibilität durchgeführt. Abschließend wird eine noch laufende Initiative zur Reduktion der Berechnungslaufzeit mittels Anbindung an die Systemsimulation erläutert sowie Untersuchungen zum Thema Öl-Management mittels voller Kopplung zwischen Strömungs- und Finite-Elemente-Löser vorgestellt.

Abstract

With the aim of improving energy efficiency and reducing CO2 emissions, friction losses within driveline components must be continuously minimized. Focusing on a ZF 8-speed automatic transmission, axial forces on planetary disc washers are investigated which, in combination with relative rotations, lead to such friction losses. The investigation is carried out using finite element simulations. Important influencing parameters such as the crowning of the planetary needles and manufacturing tolerances are identified. Building on the knowledge gained, the existing optimization potential is further evaluated. As part of the verification of the simulation method, a detailed plausibility check is carried out. Finally, a still ongoing initiative to reduce the computation time by connecting the FE solver to system simulation is explained and investigations on the topic of oil management by coupling computational fluid dynamic and finite element solver are presented.

1. Introduction

In the scope of resource efficiency and reduction of CO2 emissions the pressure to reduce energy loss inside drivetrain components such as gear assemblies increases steadily. Friction effects in planetary gear sets from ZF's 8-speed-automatic transmission 8HP75 [1] are investigated with the focus on induced axial forces at the planetary discs.

Despite the gearing design of compensating axial forces, the gearset planets show signs of wear on the thrust washers. In the context of lean validation and based on existing data from test stand experiments the investigation was started to reproduce friction effects and identify parameters of influence.

2. Automatic 8-speed transmission 8HP75

The investigated gear sets 1 and 2 belong to ZF's 8-speed transmission 8HP75 as highlighted in Fig. 1. The study initially began with gear set 1 due to available experiment data and has been later extended to gear set 2. The reason for this was that in the hardware the axial discs from gear set 2 showed more signs of wear.

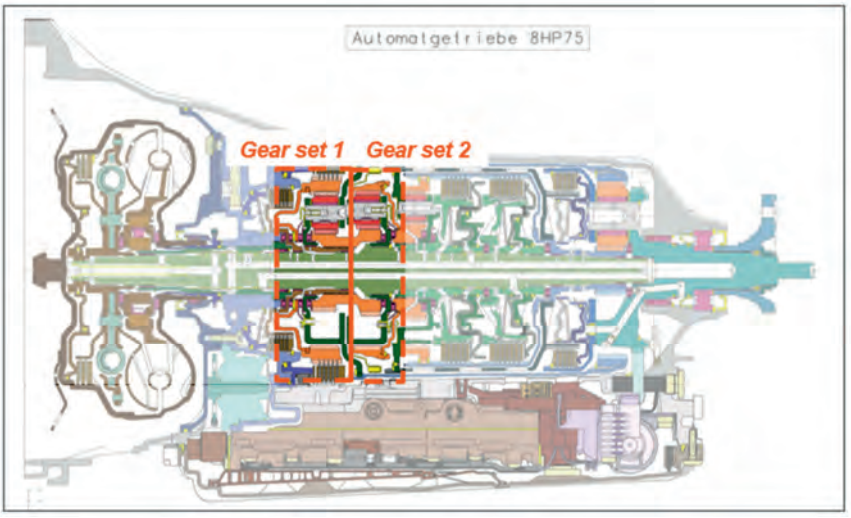

Fig. 1: Cross section drawing 8-speed 8HP75 gear assembly, gear sets 1 and 2 highlighted

3. Simulation solver and special options used

For the analysis the VPS [2] simulation software is utilized, which supports both implicit and explicit analysis and features a single-core-model technology to serve a wide variety of applications. Two options from the PAM-Medysa solver as part of the VPS solver were critical for the feasibility of the investigation:

- Total Lagrangian material formulations and
- Contacts with smoothed analytical master surface

The Total Lagrangian material formulations avoid precision issues due to rounding effects over time when the structure is subjected to large rotations and velocities.

The contact with smoothed analytical master surface helps to eliminate the error from geometric discretisation. Its functioning principle is illustrated in Fig. 2. The smooth analytical surface is fitted through all nodes of the segments from the master selection.

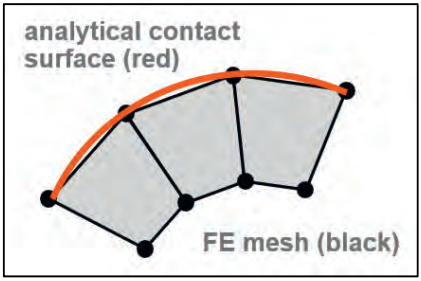

Fig. 2: Schematic sketch of analytical contact surface based on finite element nodes

4. Simulation model

In addition to the usage of special solver contact options a specific modelling strategy on the slave side of such contact interfaces is applied. The slave surface is modelled with relatively fine shell elements with so-called null material (no stresses or strains are computed). For a consistent contact behaviour these shell elements are then kinematically constrained to the deformable structure. The maximum allowed mesh size of the fine null shells can be determined based on geometric considerations with respect to the maximum allowed error.

An example for a fine mesh on the slave side is shown in Fig. 3: the dark blue elements with null material are constrained to the deformable bolt and are in the slave selection of the contact between planetary bolt and needles. The needles themselves are in the master selection, whose surface is analytically smoothed.

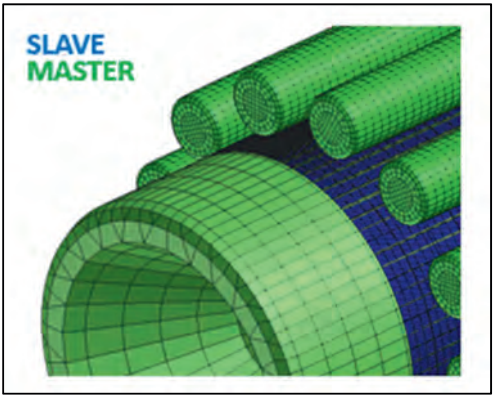

Fig. 3: Example of a contact definition with the analytical master surface assigned to the small needle parts

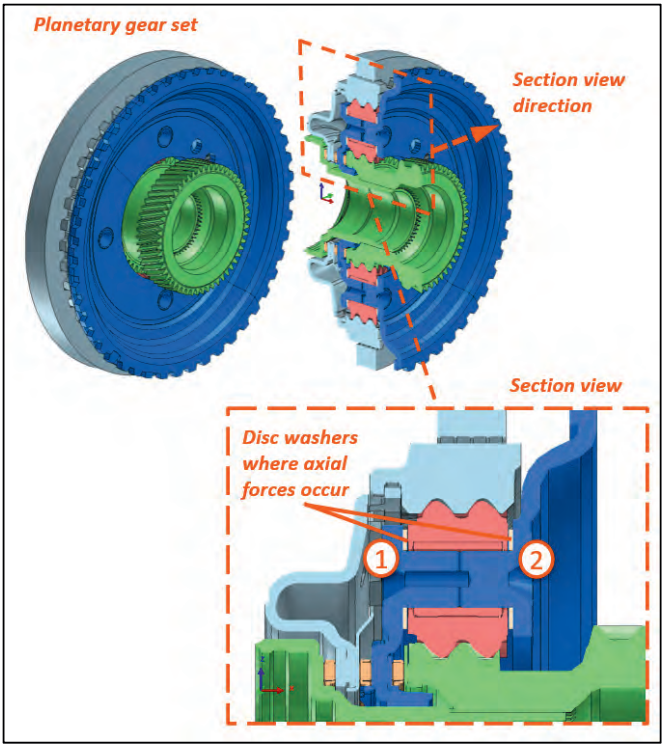

Fig. 4: Finite element model for gear set 1 with detailed section cut view for region of interest

Fig. 4 shows the simulation model for gear set 1. It consists of the inner sun shaft and wheel, four planets with carrier, a ring gear and the outer clutch disks. The region of interest is visible in the section cut detail with the locations 1 and 2 marking the two carrier sides for which the axial contact forces are evaluated. The analysis is done for all four planets which results in a total number of 8 locations, where axial forces from contact with planetary discs may occur. The planets themselves consist of the actual gear, the planetary needles and a needle cage. The model for gear set 2 has been derived from the gear set 1 model by applying changes on topology, loading and boundary conditions. It is not presented in detail in this section.

5. Boundary and loading conditions

The boundary and loading conditions for the gear set models 1 and 2 differ with respect to the location of the kinematic rotation load, the output moment and rotational constraints, Fig. 5

gives an overview. Furthermore, the magnitude of the kinematic rotation and load moment differ between the two models.

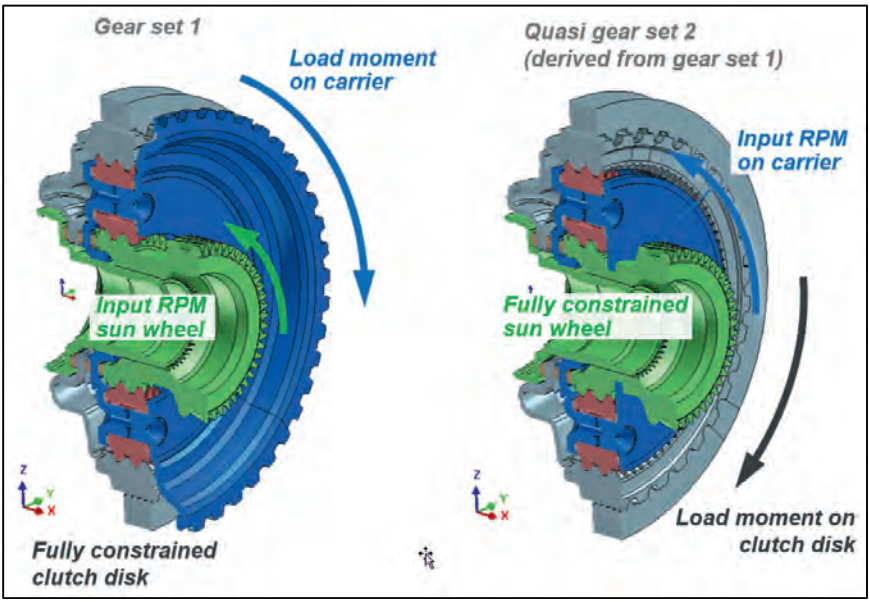

Fig. 5: Models gear set 1 and 2 with boundary and loading conditions

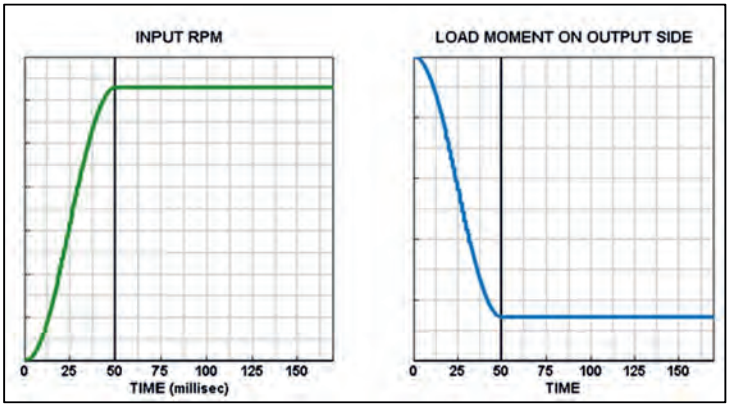

Fig. 6: Curve history for ramping up the rotation load on the drive side and the moment on the output side

The load is not applied fully from the beginning of the simulation since the exact state of motion and loading is not known for all components in stationary operation mode. Instead the kinematic rotation and moment loading at drive and output side are smoothly ramped up in the first 50 milliseconds and then kept constant as shown in Fig. 6. The simulation duration corresponds to a full turn of the planetary gear after the load has been ramped up.

6. Plausibility of results

To confirm plausibility of the simulation results they are compared with targets from experiments. The resulting rotational velocities and moments for gear set 1, in a specific load case, are shown in Fig. 7 together with their targets.

The check marks within the diagrams indicate that all targets are met. Additionally, one diagram is marked with an arrow icon, which means that for this physical entity the target value is also used as input for the load definition. Consequently, this diagram only indicates that the load magnitude is defined correctly in the input. For the axial moments the additional check sum diagram is showing that a stationary operation mode is reached after 50 milliseconds. Global axial forces and their targets are not shown here for simplicity. They correlate just as well as the other entities shown.

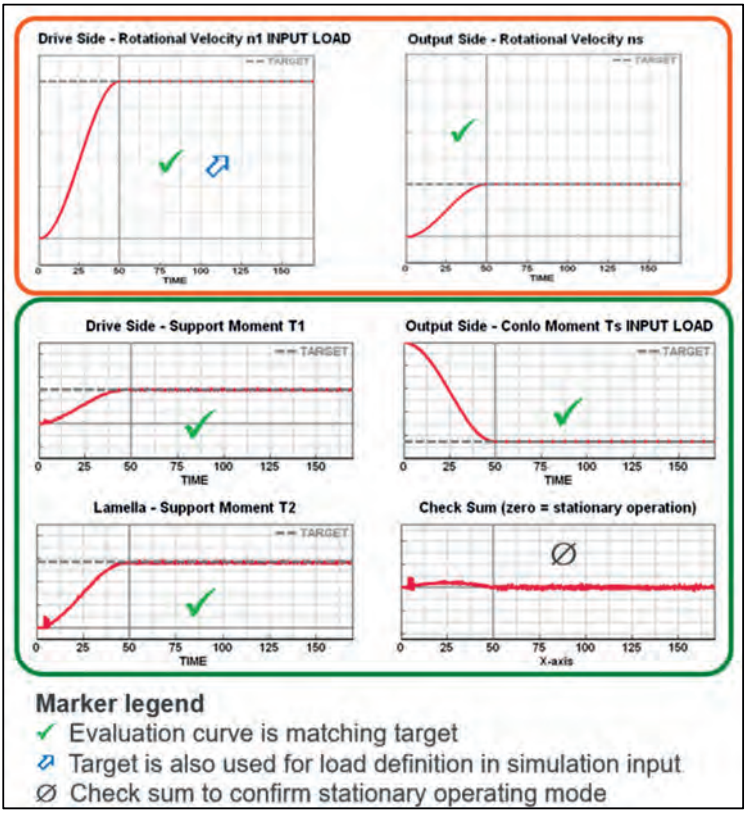

Fig. 7: Verification of global model rotations, forces and moments compared to targets

7. Investigation parameters

Various parameters are investigated and their influence on simulation results assessed. The most interesting ones with respect results are briefly listed:

- Temporary numerical damping on planetary needles to mimic oil viscosity effects
- Positioning tolerance bolt hole drilling in planetary carrier
- Crowning of the needles
- Load moment and rotational velocity for gear set 1 and 2

The variation is described in detail below, the corresponding key results are presented in the subsequent section 8.

Temporary mass proportional numerical damping on planetary needles

In this study the oil inside the gear assembly is generally not modelled as a fluid with the assumption that its influence on the kinematics of the mechanical structure is negligible. Instead a very low friction coefficient of 0.05 is set for most contact interfaces (except for the carrier press-fit contact) to achieve a realistic global friction loss over time (global = on assembly level). In one parameter variation however an additional mass proportional damping factor of 0.5 for the planetary needles is defined to possibly mimic effects from the oil fluid inside the planet. The needles with additional damping are shown in Fig. 8 and highlighted in solid red colour.

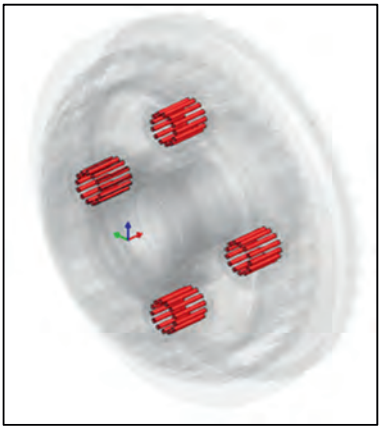

Fig. 8: Parameter variation mass proportional nodal damping for planetary needles (highlighted in solid red)

Planetary bolt and bore hole out of position (tolerance)

Another parameter variation aims towards the manufacturing tolerances of the planetary bolt and bore hole position in the carrier. Here the position of one planetary bolt/bore hole together with the planet, needles, cage and discs are moved radially or tangentially in either one of the four directions as shown in Fig. 9. Then the influence of the modified position is assessed. In section 8 only the key results for moving the bolt radially in direction 02 are shown, since for

this direction the most significant change in results compared to the nominal model can be observed.

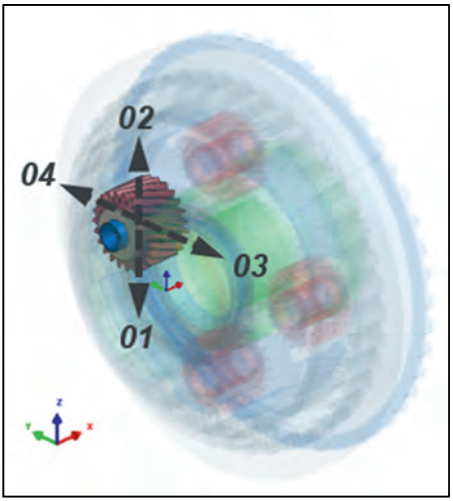

Fig. 9: Parameter variation one planetary bolt and drilling out of position

Modified crowning of the needles of the planetary bearings

Based on a preliminary load path analysis, which is explained at the beginning of section 8, the needles of the bearing have a strong influence in the generation of the axial disc forces. Therefore, the crowning shape of the planetary needles is modified as illustrated in the principle sketch in Fig. 10. The different crownings at the end of the needle rollers shown in Fig. 10 are: nominal, removed and doubled crowning (from left to right). Again in the subsequent key results section 8 only a subset of the results from the variation is shown, in this case the variation where the crowning of the needles is removed.

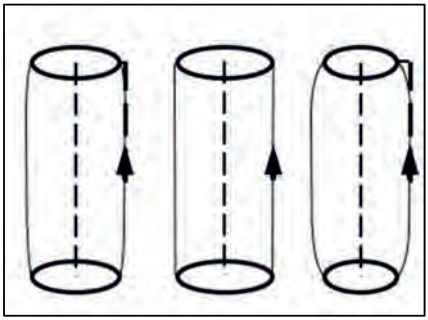

Fig. 10: Parameter variation crowning of planetary needles - off-scale principle sketch

8. Key results

From analysis of results it is confirmed that none of the variation parameters have an influence on the global forces and moments. Only the local axial disc forces are influenced.

Preliminary load path analysis

After plausibility confirmation of the global results a detailed load path analysis is conducted for one planet to gain early insight on the local axial forces.

In Fig. 11 axial forces for different contact interfaces are shown together with their check sum:

- Top left: the contact forces between planetary gear teeth and ring- and sun gear are close to zero. The small resulting force results from the helical gear in combination with a minimal incline during operation under load.
- Top middle: the contact force between needles and planet has a noticeably higher magnitude than the interface between planetary gear teeth and ring- and sun gear.
- Bottom left: the contact force magnitude between planet and disc washer at location 1 is similarly high as the contact force between planet and needles. It correlates with the contact interface to the needles, which leads to the interim finding that the planetary needles contribute to the effect of axial forces at the disc washers and the load path is as follows: bolt to needles => needles to planet => planet to disc at location 1.
- Bottom middle: the contact force between planet and disc washer at location 2 is zero, which is plausible since the planet is already applying force at location 1.
- Bottom right: the check sum of all four previously described contact forces is zero, which means that all relevant interfaces are considered

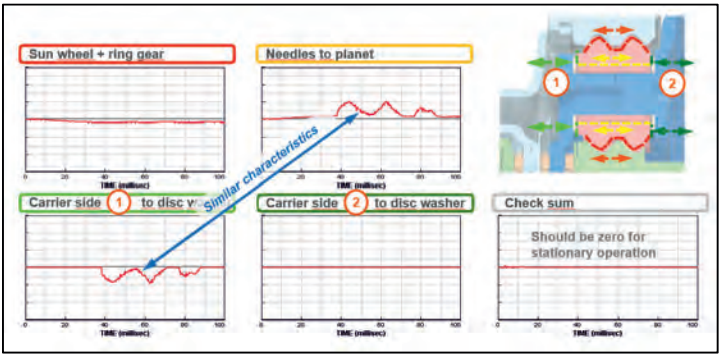

Fig. 11: Exemplary load path analysis with subdivided contact interfaces to planet

To avoid misinterpretation of the results it is noted one more time that the loading condition at drive and output side are stationary only after 50 milliseconds in the simulation, so the focus should be on the time interval from 50 until 170 milliseconds.

Results from temporary damping for the planetary needles

The axial forces on the planetary discs for the configuration without and with a mass proportional nodal damping factor 0.5 on the planetary needles are shown in Fig. 12. With the temporary additional damping the axial disc forces at the location 1 for each of the four planets become more stationary. So, there is a chance that the oil inside the planet may really influence the axial forces. Since these findings are hard to confirm in experiments the respective modification is not used in other simulations. Instead it is checked if other modification parameters are generating stationary axial disc forces even without additional loading to mimic oil effects.

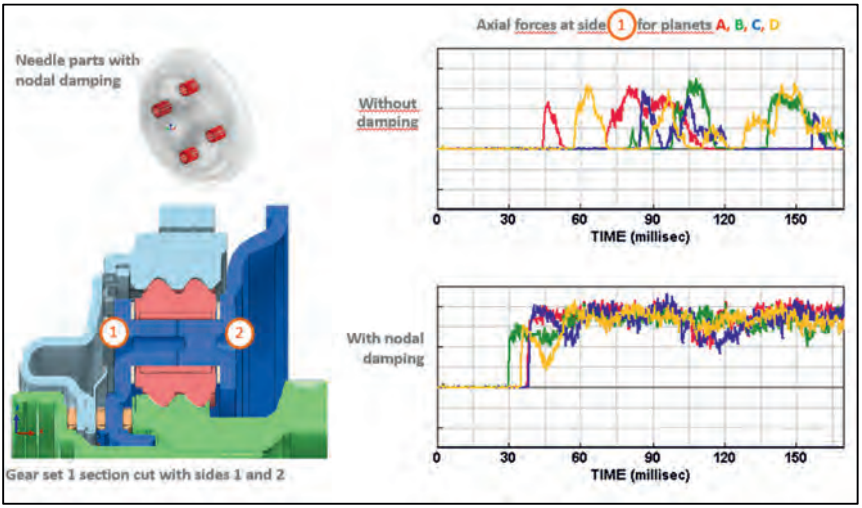

Fig. 12: Axial disc forces for gear set 1 with and without additional damping on the needles

Result comparison between gear sets 1 and 2 under specific load conditions

When comparing the axial disc forces between the gear assemblies 1 and 2 with their specific load conditions it can be observed that gear set 2 shows a more pronounced trend for stationary axial disc forces even without additional modifications, see also Fig. 13.

With this an important part of the initial scope is achieved. The remaining parameter variations are performed for gear set 2 since an extended goal is to not just reproduce the axial disc forces via simulation but to identify parameters to reduce them.

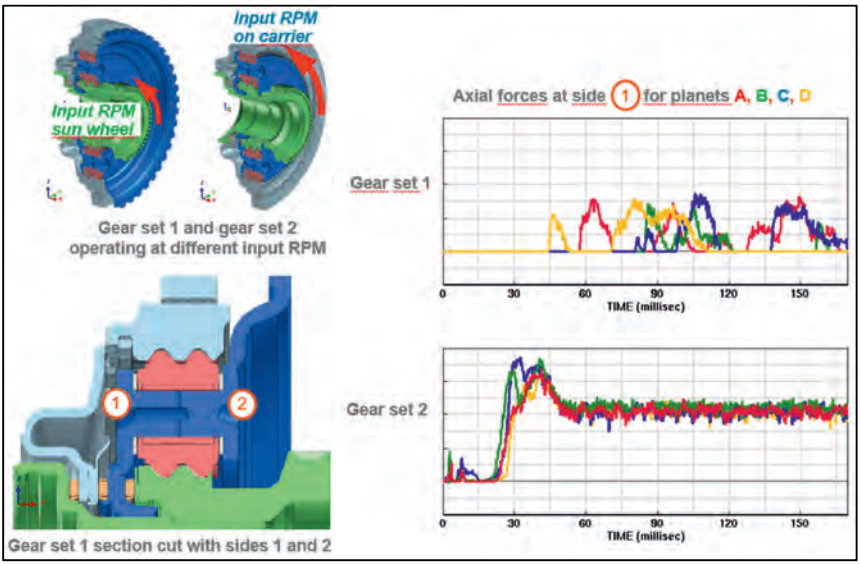

Fig. 13: Axial disc forces at the location 1 for gear sets 1 and 2 with different load condition

Results from a removed crowning of the planetary needles

With the previous findings from the preliminary load path analysis and the comparison of results for gear sets 1 and 2 the needle crowning is removed in one parameter variation for gear set 2. The results for nominal and removed needle crowning are presented in Fig. 14. From the comparison it can be observed that removing the needle crowning can substantially reduce the axial forces at the planetary discs. With these findings the extended goal to identify parameter(s) with which the axial forces can be reduced is reached.

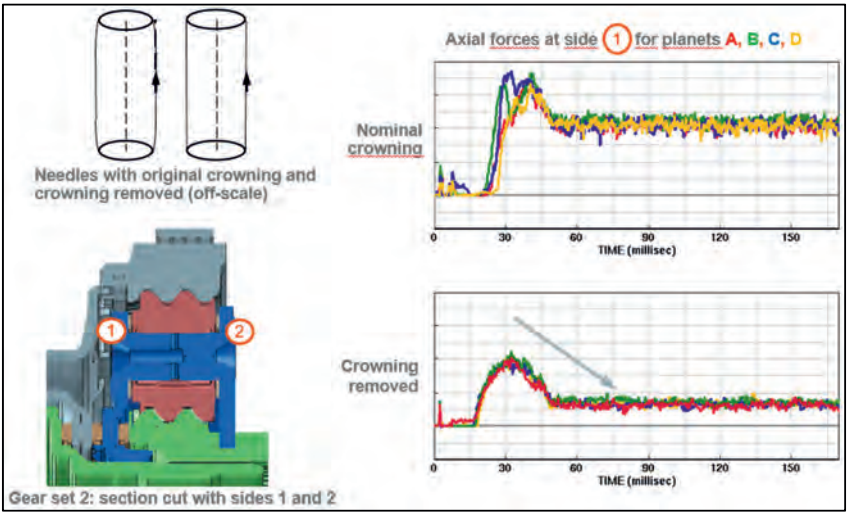

Fig. 14: Axial disc forces for gear set 2 with nominal needle crowning and crowning removed

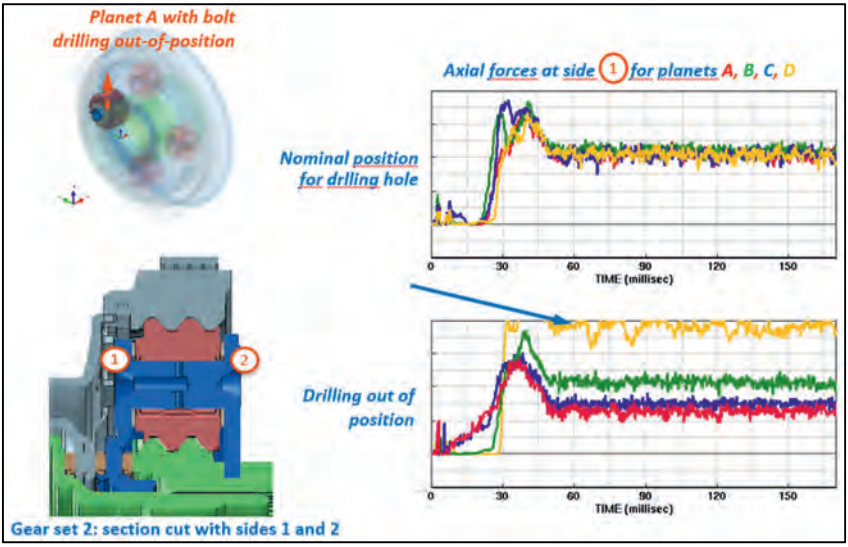

Fig. 15: Axial disc forces for gear set 2 for planet A out-of-position and with nominal position

Results for planet A with bolt out-of-position (tolerance)

The results of planet A moved out-of-position compared to the nominal position are presented in Fig. 15. It becomes clear that this modification introduces a noticeable unbalance in axial forces over the planet. The axial force magnitude for planet A drops whereas the force magnitude for planet D shows a substantial increase. This means that manufacturing tolerances for the position of the bolt and bolt drilling have an important influence and need to be closely monitored.

9. Summary

In this study VPS simulation models for two gear sets from the ZF transmission 8HP75 have been build and status simulations for specific loading and boundary conditions performed.
The results have been thoroughly checked for plausibility. Furthermore, in-depth analyses such as local load-path analysis have been made.

Several modelling parameters have been modified and their influence on the effects of local axial forces at the planetary discs have been evaluated.

The effect of axial disc forces has been reproduced for both gear sets whereas for gear set 2 they have proven to be more stationary. Several variation parameters with noticeable influence have been identified.

The most important findings are that

- the disc forces can be reduced by reducing the crowning of the planetary bearing needles
- the manufacturing tolerance for the position of the planetary bolt/bore hole needs to be closely monitored to avoid a further increase in local disc forces for individual planets

10. Outlook

Currently an additional study is ongoing at ESI to assess the potential of oil management simulations. They are performed with so called strong coupling with the VPS solver with the scope to identify regions with insufficient oil flow, see also Fig. 16. In the wet map contour all segments coloured in bright magenta have been reached by oil during up to that moment. It must be noted that here an early simulation state is shown and that more segments would be covered by oil with an increased simulation time

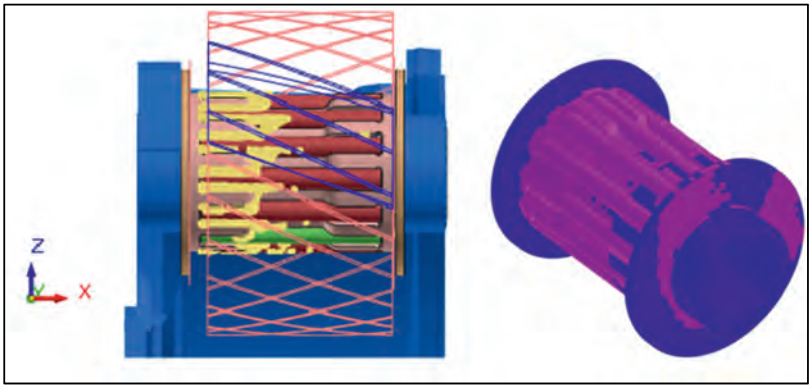

Fig. 16 left: carrier and inner planet with oil, right: oil wet map contour

Another activity at ESI aims to reduce the simulation time by outsourcing parts of the structure to system modelling. In Fig. 17 a principle scheme is shown, the VPS model has been reduced. The gear teeth contacts are modelled in the system model.

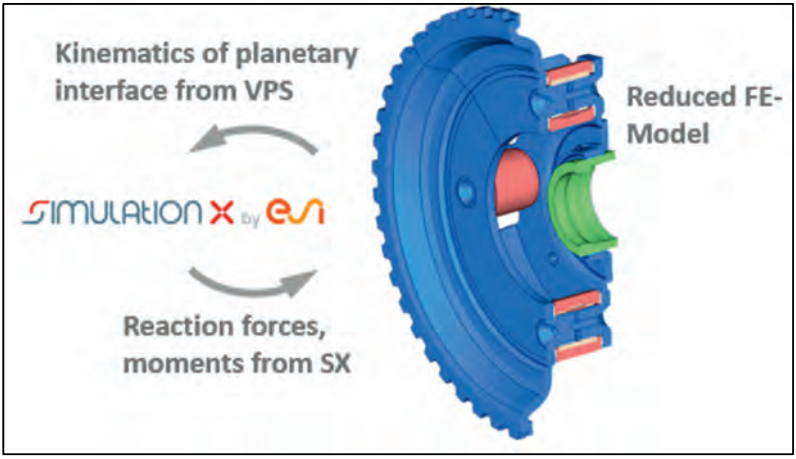

Fig. 17: Coupling scheme between Simulation X and a reduced VPS model

[1] ZF 8HP transmission, Wikipedia, *https://en.wikipedia.org/wiki/ZF_8HP_transmission#List_of_ZF_8HP_variants* (2021-08)

[2] *Virtual Performance Solution, simulation software, ESI Group,* https://www.esi-group.com/products/virtual-performance-solution *(2021-08)*

Shift Elements for Electric and Hybrid Drivetrains

Shift elements with low drag losses, high actuation energy efficiency and integrated overload protection

Dr.-Ing. **T. Skubacz**, M.Sc. **Ch. Burkhardt**, Dipl.-Ing. **S. Krischke**,
Diehl Metall Stiftung & Co. KG, Röthenbach

Zusammenfassung

Es werden zwei neue Lösungen für Kupplungs- und Schaltfunktionen in elektrischen und hybriden Antriebssträngen vorgestellt. In Abgrenzung zu existierenden Lösungen wird neben einer hohen Energieeffizienz für das Halten und Wechseln des Zustands und niedrigen Schlepp- und Reibungsverlusten in beiden Zuständen (offen/geschlossen) auch die spezielle Anforderung eines Überlastschutzes (Drehmomentbegrenzung) erfüllt. Beide Lösungen basieren auf einem bistabilen Verhalten („stable state“) und benötigen sowohl im geschlossenen als auch im offenen Zustand keine Aktuierungskraft. Bei Überlast nimmt das System einen Schlupfzustand mit begrenztem Moment ein und kehrt selbsttätig in den geschlossenen Zustand zurück. Dadurch wird ein Beitrag zu Fahrzeug-Sicherheitsanforderungen geleistet und die Überdimensionierung von Umgebungskomponenten kann reduziert werden. Durch den Einsatz von Reibelementen statt formschlüssiger Verbindungen wird auch das Schalten unter Differenzdrehzahl ermöglicht. Der Einsatz von Konuskupplungen erhöht die Drehmomentkapazität.

Beide Lösungen basieren auf innovativen systeminternen Mechanismen zur Kraftaufbringung: Die erste Lösung basiert auf einer speziellen bistabilen Tellerfeder, die zweite Lösung nutzt Federvorspannung mit Änderung der Federausrichtung.

Abstract

Two new solutions for clutch and shift functions in electric and hybrid powertrains are presented. In contrast to existing solutions, the special requirement of overload protection (torque limitation) is also satisfied in addition to high energy efficiency for holding and changing the state and low drag and friction losses in both states (open/closed). Both solutions are based on a bistable behavior ("stable state") and require no actuation force in both closed and open state. In the event of an overload, the system automatically enters a slip state with limited torque and then automatically returns to the closed state. This contributes to vehicle safety requirements and allows the oversizing of surrounding components to be reduced. The use of friction elements instead of positive engagement connections also enables shifting under differential speed. The use of cone clutches increases torque capacity.

Both solutions are based on innovative system internal force application mechanisms: The first solution is based on a special bistable diaphragm spring, while the second solution uses spring preload with a change in spring alignment.

1. Motivation

Hybridization and electromobility are current trends in the powertrain development of modern automobiles. The target is usually the energy-efficient design of the powertrain. There are a variety of hybridization concepts (serial, parallel, mixed forms). In parallel hybrids, the electric engine can be positioned anywhere from the belt starter generator (P0), on the combustion engine (P1), between the combustion engine and transmission (P2), on the transmission (P3), close to the axle (P4) up to wheel-integrated (P5). Depending on their position, this provides boosting, sailing, recuperation, charging while driving, purely combustion-engine or pure electric driving modes. Serial hybrid configurations enable pure electric driving, recuperation, but also charging while stationary, as well as range extender operation. Hybrid configurations, such as a combined serial-parallel hybrid (see Fig. 1), combine the above-mentioned operating modes with the smallest possible battery and potential use of renewable fuels (bio/e-fuels).

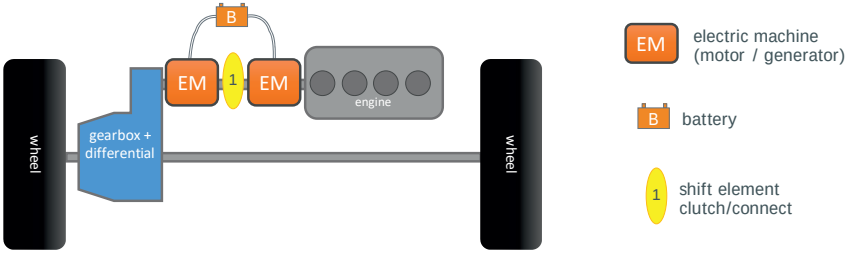

Fig. 1: Configuration of a combined serial-parallel hybrid powertrain with position of the switching element

Depending on the topology of the powertrain, it may be necessary or useful to utilize switching elements to separate or connect powertrain components. Switching elements either implement different load paths, e.g. transmission pathways, or serve to increase energy efficiency by disconnecting drive train sections that are not required. In the example shown (Fig. 1), the switching element has an essential function of switching between serial and parallel operating modes. An obvious solution would be to use a conventional switching element, e.g. a multi-disc clutch, with the use of existing components. The disadvantage here is the monostable design (NC = normally closed or NO = normally open), which means that force must be applied to the rotating component in one of the two switching states in order to maintain the state. Since both states take up a considerable proportion of the operating time in the concept shown, the resulting frictional losses of the actuation force are relevant. In addition, power is permanently required to generate the actuation force (hydraulics, electric drive, ...).

Furthermore, with regard to the design and dimensioning of adjacent powertrain components, overload protection or damping elements are useful to limit load peaks in special driving situations (dynamic change in wheel force distribution, e.g. curb launch, railroad crossings, one-sided wheel slip) or to prevent the powertrain from oscillating. In addition, an emergency disconnect function is required for functional safety reasons.

These and other modular product profile requirements for switching elements in future powertrains were worked out as part of systematic, scenario-based product development with the support of IPEK (Karlsruhe Institute of Technology):

We need a system that …
… can limit or cut off the power flow within the drivetrain.
… realizes high energy efficiency and low drag torque in each state.
… enables imperceptible switching regarding NVH, energy and torque interruption.
… reduces torque vibrations and overloads by and into engines.

It is to be expected that further requirements for corresponding switching elements will arise in the next vehicle generations. Other possible applications are switching functions for rotating components or aggregates, also in the industrial environment, which have similar requirements.

In the following, two innovative solutions for switching elements Diehl ecoClutch DS ("disc spring") and Diehl ecoClutch FM ("force modulation") are presented (Fig. 2).

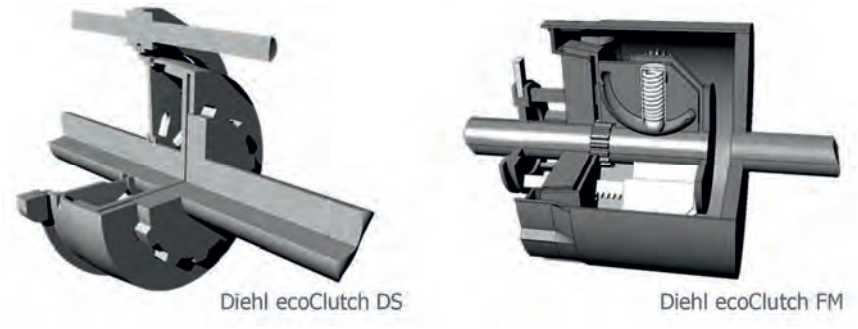

Fig. 2: Diehl switching elements of the ecoClutch series

Both solutions use the functional principle of bistability, which is also known in other applications (e.g. ballpoint pens, light switches, detents, ropeway clamps). Bistability allows the actuation energy to be optimized, since energy is only required for the change, but not for keeping the state.

2. Diehl ecoClutch DS

Structure

In the closed state, a friction clutch transmits the torque between the two shafts, for example for coupling an electrical machine (cf. Fig. 3). A cone-shaped friction clutch, e.g. known from synchronizers, achieves a higher capacity (quotient of transmittable torque / contact force) due to the cone amplification. Nevertheless, the principle would also be applicable with a (multi-) plate clutch. If required, the transmittable friction torque can be adjusted by the number of friction surfaces and the friction diameter or cone angle. The dogs of the outer cone engage in an axially displaceable coupling on the second shaft.

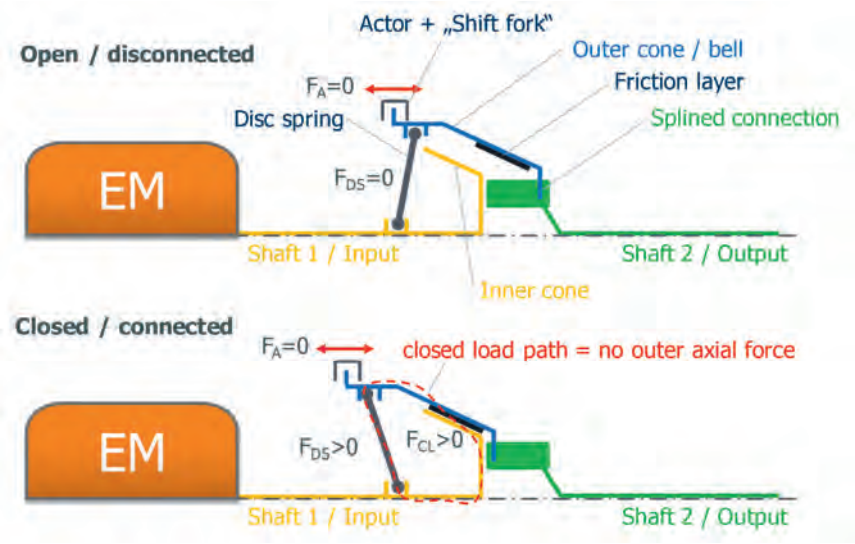

Fig. 3: Schematic diagram Diehl ecoClutch DS

The second key component of the Diehl ecoClutch DS switching element is a bistable disc spring with a characteristic curve as shown in Fig. 4. The bistability ("stable state") is achieved by adequate geometrical design, cf. [1].

In the closed state, the friction clutch is pressed by the compressed disc spring in the area of its first force maximum. In the process, the disc spring is supported on the shaft and a closed, internal force flow is created on the rotating shaft, i.e. no external force is required to maintain the closed state.

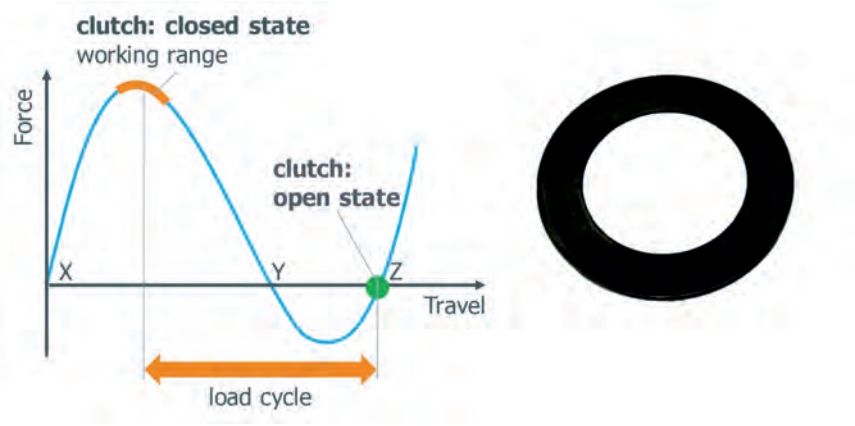

Fig. 4: Characteristic curve of bistable disc spring and operating points

If the outer cone (clutch bell) is moved under force, the diaphragm spring finally reaches the second stable point Z of the characteristic curve. This is also the open resp. released state of the clutch. In this position, too, no external force is necessary to maintain the state. Leaving this state by itself is reliably prevented by the force barrier of the disc spring. In both states, a small amount of play in the actuation engagement ensures low drag losses and freedom from axial forces.

The friction clutch in combination with the diaphragm spring enables the realisation of a self-reversible overload protection with regard to load peaks: If the torque applied to the clutch is greater than the maximum torque that can be transmitted with the static coefficient of friction, the friction surfaces slip and limit the torque to the torque that can be transmitted with the dynamic coefficient of friction. As soon as the applied torque falls below the transmittable torque again, the slip ends and the clutch remains closed. In the event of long-lasting overloads or critical conditions, the clutch can, of course, be additionally opened by actuators independently of this.

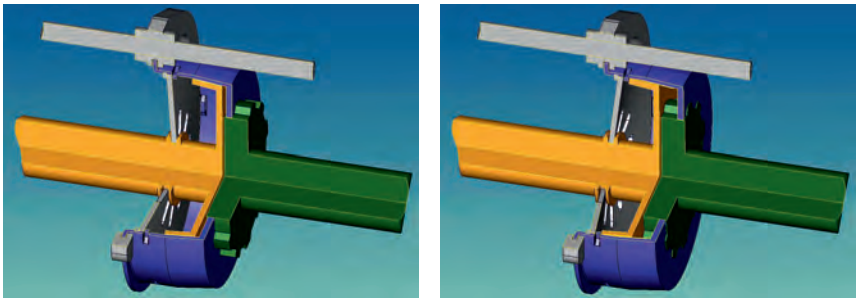

Fig. 5: Diehl ecoClutch DS shift element in closed (left) and open state (right)

A feature and at the same time an advantage of the friction clutch is the possibility to close at differential speed. In this case, the friction clutch takes over or supports the synchronization of the two shafts. Usually, an external electrical/motor synchronization will significantly shorten the synchronization time and relieve the friction system, so that the friction process only starts at a lower differential speed or at synchronous speed. Load switching is therefore not initially envisaged, but may be possible with suitable dimensioning. The friction system is dimensioned according to the known calculation formulas for synchronizers and (cone) clutches; accordingly, the friction surfaces are coated with friction linings that are also suitable for torque transmission. Even with normal wear of the friction clutch, the system remains fully functional, as the disc spring is operated in the flat range of the maximum force.
Moreover, the friction clutch allows opening under applied torque - in contrast to positive-locking elements with undercut, e.g. dog clutches.

Core element disc spring: tests on function and service life

The main challenge of the development was the design of the disc spring as the core component of the solution. Therefore, this topic was tested as a central stop/go criterion before all other activities. Using sample parts in the real size, the characteristic curve and the service life requirement or hypothesis were confirmed and an initial geometry optimisation was carried out. In addition, functionally relevant changes in the characteristic curve of the disc spring over the service life could be excluded.
For the tests, an adaptation for an electrodynamic testing machine was set up. The test parts were fixed in the same way as in the final system. The device can also be used to measure the spring characteristics in the complete deflection range. Subcritical test frequencies of up

to approx. 18 Hz in displacement-controlled operation allow an enormous time reduction of the tests. The travel positions around the maximum force of the disc spring characteristic were chosen as horizons for determining the service life curves; the reversal point was the second stable position Z of the disc spring.

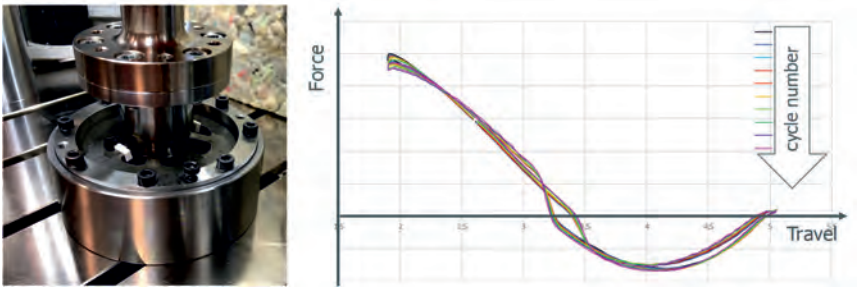

Fig. 6: Testing device for disc spring and characteristic curve over service life (exemplary)

3. Diehl ecoClutch FM

Structure and Function

This solution is also based on a (cone) friction clutch that transmits the torque between the two shafts when closed. Here, too, the principle of cone amplification and torque adjustment through the number and diameter of the friction surfaces applies. The dogs of the outermost cone engage in an axially displaceable toothing on the housing connected to the second shaft, comparable to the clutch basket in the known multi-plate clutches.

The contact pressure for the clutch is applied by a preloaded spring arrangement (coil spring or disc spring arrangement) via a thrust piece and a race.

Fig. 7: Diehl ecoClutch FM shifting element in closed state

In the closed state, the thrust piece presses against the clutch via the race of the thrust element. In case of overload, the clutch can slip against the spring force and, as with the first solution, reversibly changes to the closed state after the overload has decreased.

Fig. 8: Diehl ecoClutch FM switching element in intermediate state

To open the clutch, the spring is tilted together with its guide and the thrust piece. This shifts the pressure angle and the pressure point on the race so that the axial force on the clutch decreases and finally changes direction (Fig. 8 left). This causes the thrust element to move axially and the clutch to open (Fig 8 right). Due to the friction and the shape of the race, bistability is achieved in both end positions.

Fig. 9: Diehl ecoClutch FM shifting element in open state

This switching element also results in a closed load path within the first shaft, so that the system is free of axial forces to the outside in the open and closed state (Fig. 7 and 9).
The energy required for opening and closing is comparatively low, as only the friction of the pressed-on thrust piece has to be overcome and only minimal compression work is performed on the spring. The switching force can be about one range of magnitude smaller than the clutch force, which means that the actuator can be dimensioned smaller.
In principle, it would even be possible to dynamically adjust the maximum transmittable clutch torque for special situations if the bistable position is temporarily omitted.

4. Assessment, outlook, further procedure

Both solutions presented enable the coupling and uncoupling of drive train components. They achieve a high actuation energy efficiency as well as low drag and friction losses due to the bistability and the absence of forces in both switching states. In contrast to positive-locking shift elements, they enable shifting under significant differential speed with support in synchronizing the shafts. In addition, they offer self-reversible, sensor-free overload protection for adjacent components in the drive train in the form of torque limitation and as a contribution to functional safety. Fig. 10 shows a tabular overview of the two solutions and existing switching and overload protection elements with a qualitative evaluation of the degree of fulfilment of the requirements (traffic light system: green = complete; yellow = with restrictions; red = not fulfilled). It can be seen that the two solutions Diehl ecoClutch DS and Diehl ecoClutch FM offer advantages for the application in the overall combination of properties.

Currently, prototypes are under construction with subsequent testing on component and system test benches. In the further course of the project, it is planned that functional samples will be provided to interested customers from the beginning of 2022.

next page:

Fig. 10: Degree of fulfilment of requirements for switching elements: Diehl ecoClutch in qualitative comparison to established systems

	Clutch (manual, NC)	Clutch (DCT, NO)	Dog clutch	Synchronizer	Safety clutch	Shear element (predetermined breaking point)	Diehl ecoClutch DS	Diehl ecoClutch FM
Reversible switching	yes	yes	yes	yes	yes/no	no	yes	yes
Outer force/power to keep state	monostable (closed)	monostable (open)	by notch / undercut	by notch / undercut	mono-/ bistable depending on design	no force	bistable	bistable
State after energy loss	closed	open	stable	stable	closed	closed	stable	stable
Shift under relevant speed difference								
Load shift								
Low drag torque								
Switching/actuation force						—		
Nominal Torque depending on design space	middle-high	middle-high	low-high	low-middle	low-high	low-high	low-middle	low-middle
Torque density								
Overload protection	yes	yes	NO	NO	yes	irreversible	yes	yes
State after overload	previous	previous	---	---	open or previous	open	previous	previous

[1] Almen, J. O., László, A.: The Uniform-Section Disk Spring, Transactions ASME 58 (1936) S. 305-314

Gear Design Challenges of 2-speed-AMT High Torque E-Drives

Pranav Barve, VCST Industrial Products (part of BMT Drive Solutions), Sint-Truiden, Belgium

Company Introduction

VCST Industrial Products (automotive branch of BMT Drive Solutions) is a recognized gears supplier from the automotive field and relies on 40-year expertise in:

- gear sets design (Software programs for sub-systems durability, NVH, lubrication),
- gears & gearboxes testing (performances, durability, shifting, noise),
- fast-prototyping (wide range of processes incl. soft and hard machining, heat-treatment),
- mass production & control (fully automated factories).

Fig. 1: VCST strategy

VCST e-Drive department offers a smart portfolio of e-Drives concepts as perfect fits for the new EV categories. These are Offset, or Coaxial / Layshaft or planetary / Single-speed or multi-speed / Wet or dry sump / designed to incorporate differential units or torque vectoring.

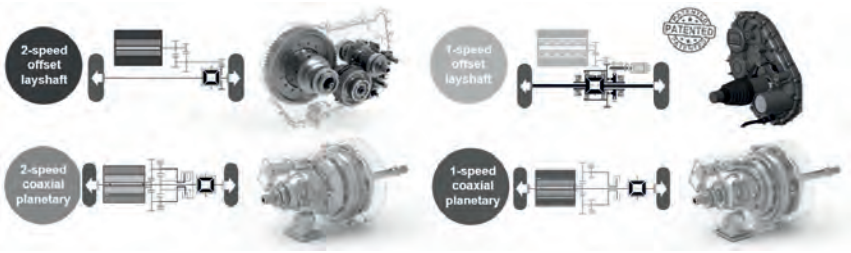

Fig. 2: VCST eDrives Portfolio

Abstract

2-speed gearboxes offer a promising solution to achieve high efficiency and performance for electric vehicles. The trade-offs between city and highway driving can still be met while ensuring that operating points are within the best efficiency zones of the electric motor. The resulting efficiency improvements can increase the driving range or downsize the batteries or the powertrain. One of the main challenges for the 2-speed gearbox is to develop a shifting system that gives minimum torque interruption and is inexpensive. VCST Industrial Solutions has developed an innovative 2-Speed AMT gearbox that uses e-synchronization and its patented dog clutch system to achieve short shift times and is inexpensive compared with friction clutches. The 2-Speed AMT gearbox is suitable for SUVs, sports cars, supercars and, N1 and N2 LCV applications.

Developing a 2-Speed AMT gearbox for various applications also posed challenges to gear design due to the packaging constraints, durability requirements, and NVH targets. The driveline noise can contribute to a large proportion of the overall noise in an electric vehicle. Thus, more stringent NVH design targets were set.

This paper presents a system-level approach to consider the influence of gears, shafts, bearings, and housing on durability and NVH performance. The author presents a method to set up design requirements for these components to control their influence. Several iterations between gear macrogeometry, shaft design, bearing selection, and housing design were done to ensure that the design requirements were achieved—subsequently, a gear microgeometry was defined to achieve PPTE, contact stress, and contact pattern targets. The influence of manufacturing variation in lead, profile and bias error was considered to ensure robustness. A final step gear whine analysis was carried out in the software MASTA,

and the resulting responses were compared with company targets to confirm the design process.

1. Introduction

The 2-speed AMT gearbox consists of a 2-stage gear reduction include 3 shafts. The intermediate shaft supports 2 free-running gears and the patented dog clutch system. The gearbox has a top sump and uses forced lubrication to minimize drag losses.

Fig. 4 shows the design process that is followed for the transmissions. The process is iterative, and prior design experience and understanding of the hierarchy of the design parameters is essential to expedite the process. The centre distance and widths of the gears are chosen so that the gearbox can be used for different applications with minor modifications.

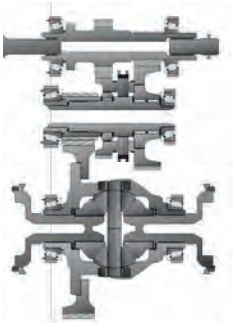

Fig. 3: 2-Speed AMT gearbox Layout

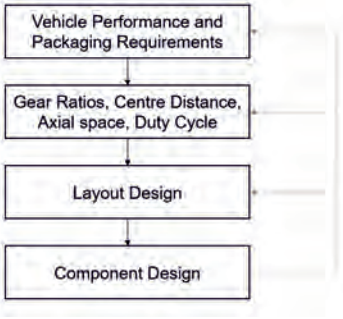

Fig. 4: Design Process

A multi-load case duty cycle is created from measured road load data and drive cycle simulation. The duty cycle is used to calculate the safety factor against different failure modes. Under various operating conditions, the components are subjected to a variety of probable failure modes. The shafts, bearings, and housing are sized to achieve the target safety factor against the failure modes and so that their influence on gear stresses and excitation is under control.

The E-machine and gears are the two primary excitation sources for whine noise from an Electric Drive Unit. This paper focuses on whine noise caused by gear excitation from

Transmission Error. Transmission Error is the difference between the angular position that the output shaft of a drive would occupy if the drive were perfect and the actual position of the output [1]. The relative displacement between the teeth generates a vibrating force between the teeth and the subsequent vibrations through the system [1]. Peak-to-peak Transmission Error (PPTE) must be minimum across the operating torque range to avoid NVH issues. Gear macrogeometry, gear microgeometry optimization, shaft, bearing, and housing design are considered to achieve the PPTE target.

Apart from gear design, the NVH issues can arise from the dynamic interaction between the gears, shafts, bearings, housing, and mounting. These interactions are evaluated using a system model, and alternate solutions are explored. The steps involved are outlined in table 1.

Table 1: Gear Design process

Step	Details	Remarks/Targets
1	Gear Macrogeometry Design	Transmission ratio, Contact ratio, mesh order separation, Gear contact and bending fatigue safety for duty cycle
2	Component Sizing	Sizing shaft, bearings and housing to achieve target safeties against failure modes and gear mesh misalignment
	MicrogeometryOptimization	
3	Defining load cases	Based on various vehicle operating scenarios, critical load cases and weightages are selected
4	Define Targets	Design targets for contact stresses and Peak to Peak Transmission Error (PPTE) are selected based on experience
5	Full Factorial DOE	Two parameter DOE is performed to study the behaviour of various microgeometry modifications, e.g. Lead crown vs Profile Crown, Lead crown vs Lead error on contact stress and PPTE. Optimum microgeometry design is then selected
6	Contact pattern Evaluation	Contact patterns using Masta's Advanced LTCA are evaluated, and microgeometry is modified to prevent edge loading and ensure contact stresses are within acceptable limits
7	Monte Carlo Simulation	The robustness of the designed microgeometry is evaluated using Montecarlo Simulation leveraging VCST's know-how on series production manufacturing capability
8	Multi-Level Statistical Optimization	Target to reduce the spread of PPTE and also minimize the maximum contact stress. Involves Statistical evaluation, i.e. main effects and interactions, multi-level design for manufacturing variables
	NVH	
9	Gear whine Analysis	Simulate housing response to excitation from Transmission error, shuttling force
10	Testing	Bench level and vehicle level tesing as part of DVP

2. Design requirements for system components

Each component in the gearbox has distinct failure modes, pitting for bearings and bending fatigue for shafts. Table 2 shows the usual failure modes observed in gears, shafts, bearings, and housings. The components were designed with a margin of safety to reduce the risk of these failures.

Table 2: Common Failure modes of gearbox components

Gear	Shaft	Bearing	Housing
Pitting	Bending Fatigue	Pitting	Plastic Deformation
Bending Fatigue	Torsional Shear	Scuffing	Rupture
Scuffing		Fretting Corrosion	
		False Brinelling	

The stiffness of these components is also a primary design criterion as the deflection of the gear, shafts, bearings, and housing under load results in misalignment. A high misalignment causes reduced load-carrying capacity of the gears due to uneven load distribution and edge loading, and higher excitation from TE. Fig. 5 shows the contact pattern in gear with and without misalignment. Lead and profile corrections can be applied to avoid edge loading, improve load distribution, and mesh stiffness variation. However, the microgeometry correction needed for good contact pressure distribution for durability can increase TE. It becomes challenging to maintain a balance. The gear misalignment also varies with load, and the microgeometry must be insensitive to these variations.

Therefore, minimization of the gear mesh misalignment and its variation is essential. In the design process, iterations that arise from not meeting TE targets and contact pressure targets can be reduced by setting up targets for Gear Mesh Misalignment for each gear pair. These targets can be based on legacy transmission designs and benchmarking. The gear mesh misalignment can be treated as the additional requirement in the concept stage for sizing the gear blank, shafts, bearings, and housing. The gear mesh misalignment targets must be met before taking up gear microgeometry design.

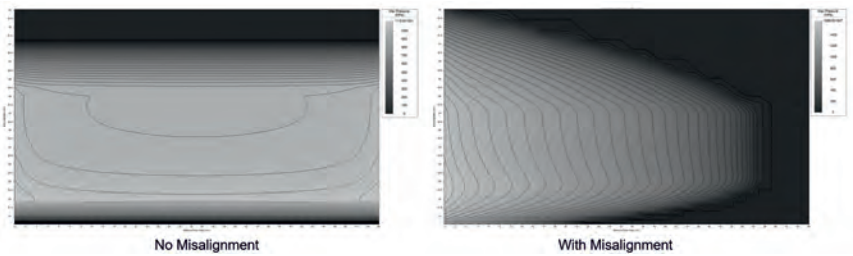

Fig. 5: Contact Pressure Distribution

Gear Mesh Misalignment (GMM), defined as the total displacement along the line of action of the gear in the transverse plane, is calculated for the 2-speed AMT gearbox using Masta, a CAE software (Fig. 6) that can analyze system deflection, including contributions from gear blanks, shafts, bearings, and housing. Design iterations were made to achieve the GMM targets for each of the three gear mesh after evaluating the contribution of each component.

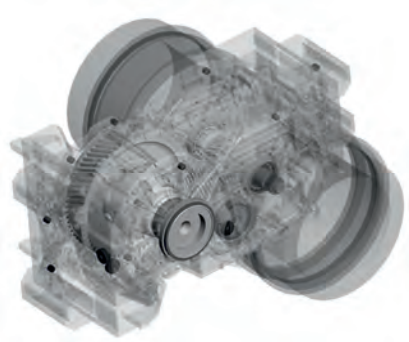

Fig. 6: Model of the 2-Speed AMT Gearbox made in SMT Masta

The GMM of the final gear mesh (Fig. 7) was above the target by 28%. The influence of the stiffness of each component was calculated by modifying their stiffness (Fig. 8). It was observed that the housing (32%), the layshaft, differential housing and the final drive wheel are the main contributors of the gear mesh misalignment of the final gear mesh.

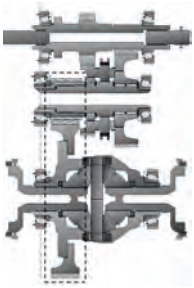

Fig. 7: Cross-sectional view of the 2-Speed AMT Gearbox with differential. Highlighted gear pair is the final reduction

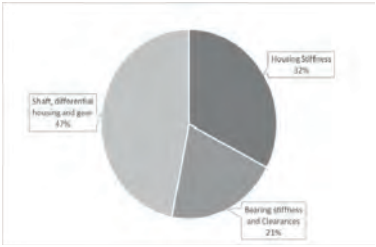

Fig. 8: Breakdown of the influence of various components of the gearbox on Gear Mesh Misalignment of the final gear pair

Design iterations to improve the housing stiffness were carried out to reduce the gear mesh misalignment. Fig. 9 shows the design modifications that were made that reduced the gear mesh misalignment by 15%.

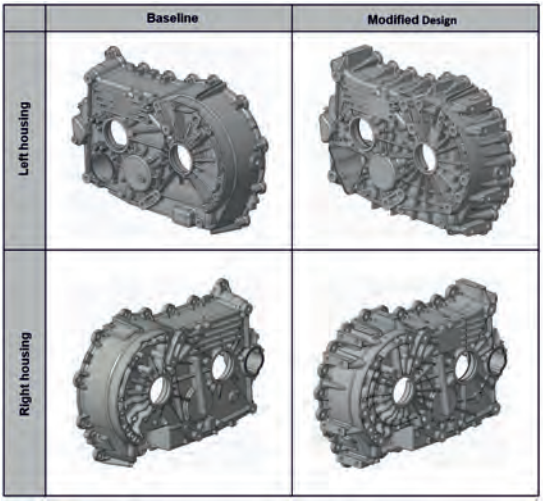

Fig. 9: Modifications to housing Design. a) Baseline Design, b) Modified stiffening ribs to increase housing stiffness

The final gear pair wheel had a high contribution to the gear mesh misalignment. Fig. 10 and Fig. 11 show the impact of modifying the web thickness and rim thickness. The increase in the rim thickness reduces the gear mesh misalignment by 13.6% without a considerable increase in the weight of the gear.

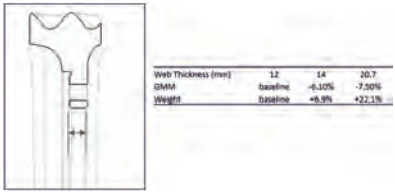

Web Thickness (mm)	12	14	20.7
GMM	baseline	-6.10%	-7.50%
Weight	baseline	+6.9%	+22.1%

Fig. 10: Modification of web thickness of final gear pair wheel

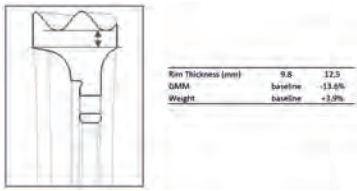

Rim Thickness (mm)	9.8	12.3
GMM	baseline	-13.6%
Weight	baseline	+3.9%

Fig. 11: Modification of rim thickness of final gear pair wheel

The 2-speed AMT is also available without differential suitable for LCV and pickup truck applications, wherein it can be used to replace the engine transmission in an existing ICE driveline. Fig. 12 shows the cross-sectional view of the gearbox.

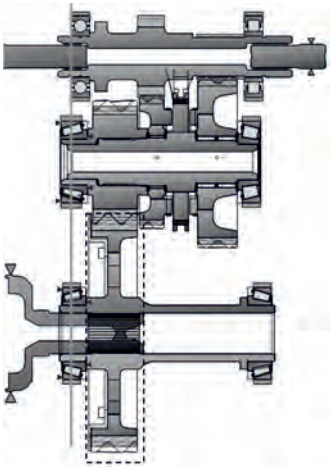

Fig. 12: Cross-sectional view of the 2-Speed AMT Gearbox without differential. Highlighted gear pair is the final reduction

The final drive gear pair did not meet the target GMM at the maximum regeneration load (Fig. 13). An increase in web thickness resulted in a higher reduction in the GMM than an increase in rim thickness (Fig. 14). The web thickness was increased to meet the GMM target.

Load	Regeneration
GMM/target GMM	1.54
Weight	baseline

Fig. 13: Final Drive Wheel

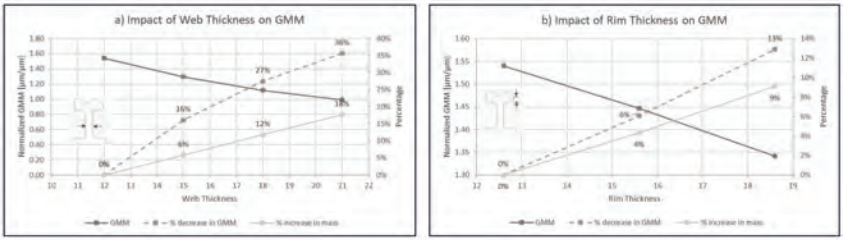

Fig. 14: Design modifications to the Final Drive Wheel

3. Gear macrogeometry design

Once the gearbox's gear ratios are selected, centre distance and face widths are determined based on the application, packaging space and layout. Then the gear macrogeometry parameters like the number of teeth, module, pressure angle, helix angle, profile shift coefficient are selected. The gear macrogeometry design process begins with establishing targets for durability (bending safety, contact safety, and scuffing risk), NVH and efficiency. At this design stage, the NVH performance can be evaluated by the total contact ratio. Design studies are performed by varying the gear macrogeometry parameters to achieve the design targets. Due to insufficient tip thickness, bottom clearance, form diameter, and SAP clearances, the infeasible candidates are eliminated. The design parameters affect the

targets in different ways. These trade-offs need to be assessed, and optimum gear design must be allocated to achieve all targets.

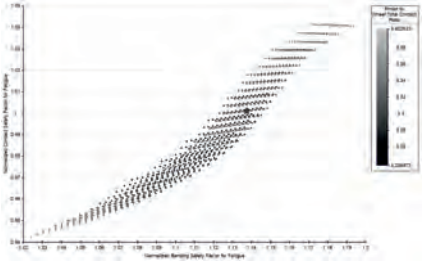

Fig. 15: Example of design study

Parameter	Bending & Contact Stresses	NVH	Scuffing	Efficiency
Pressure angle ↑	↑	↓	↑	↑
Helix angle ↑	↑	↑	↑↓	↑↓
Profile shift Coefficient ↑	↑	↑	↓	↓
Module ↑	↑	↓	↑↓	↑↓
Transverse Contact Ratio ↑	↑	↑	↓	↓
Tooth Depth ↓	↓	↓	↑	↑
Equal profile shift coefficient	↑↓	↑↓	↑	↑

Fig. 16: Trade-offs between gear macrogeometry parameters and design targets

Further iterations can be expected when the influence of system deflections and gear contact is considered. Initially, a high helix final drive gear pair was designed, which achieved design targets for durability and total contact ratio. But the high helix angle resulted in high gear mesh misalignment that had to be compensated with high amounts of microgeometry modifications. As a result, the contact length variation at low load increased, causing high TE. With the next iteration, a gear pair with a lower helix angle was designed to reduce gear mesh misalignment and shot peening was added to compensate for the reduced gear safety factors.

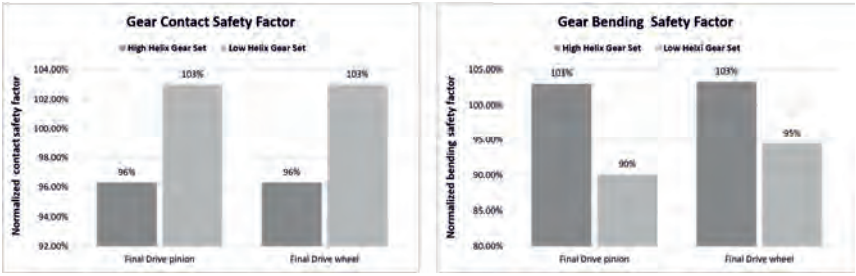

Fig. 17: Final Drive gear safety factor

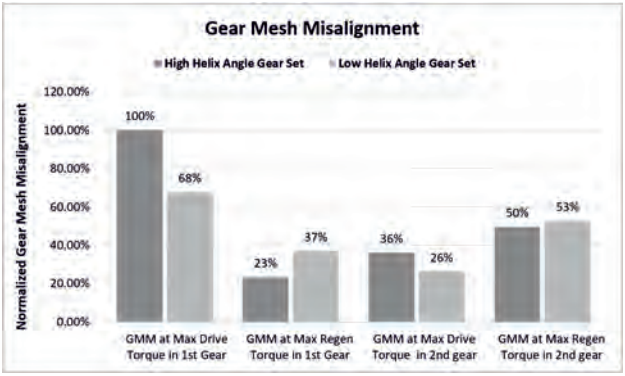

Fig. 18: Final Drive gear mesh misalignment

4. Gear Microgeometry Design

The next step in gear design is the definition of gear microgeometry modifications. The microgeometry modifications are designed to ensure that:

- Peak contact stresses do not occur on tooth edges, and the gear mesh misalignment is compensated
- Transmission Error is minimized
- Scuffing risk is minimized

Specific targets for maximum contact stress, face load factor ($K_{H\beta}$), PPTE and contact temperature (scuffing risk) are defined. Depending on the motor characteristics and Vehicle specification, maximum and minimum operating loads were determined. The effect of operating temperature is also considered. Tooth contact analysis is performed using Masta's Advanced LTCA- a hybrid FE and Hertzian based loaded tooth contact model [2]. Profile and Lead modifications are defined using manual and automated optimization. The modifications needed to ensure that contact stresses are minimum and centred are not always conducive to good NVH performance. The trade-offs need to be analyzed, and a balance needs to be maintained. Maintaining this balance becomes difficult primarily when the gear mesh misalignment and the contact ratio targets are not achieved in the previous steps in the design process.

Load Case	Max Load	50% of Max Load	Low load
Design v00 nominal pinion/wheel Crowning=16/16 Lead Slope=-35/0 barrelling=5/5 profile slope=0/0 tip relief=8/30	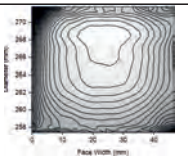	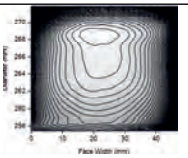	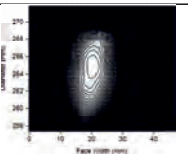
Normalized PPTE (% of target)	72%	162%	68%

Fig. 19: LTCA results of final drive gear pair

Fig. 19 shows the nominal microgeometry, resulting contact pattern, and PPTE for the final drive gear pair for different load cases. The extent of corrections applied to ensure the contact stress target at the maximum load is achieved results in a high PPTE at 50% load. Improving the PPTE at 50% load was possible by applying a design twist (Fig. 20). When grinding helical gears with crowning, a non-uniform profile and lead geometry are created due to the process kinematics (Fig. 21) [3]. Depending on the module and helix angle of the gear, considerably high amounts of twist error can be generated, which can increase excitation and contact stresses. Gear grinding machines now have provisions to compensate for this twist with the ability to apply different profile modifications at different sections along the gear face width. Thus, in effect, topological modifications are possible. In this design, along with compensation of the natural twist, the gear is produced with the specified design twist.

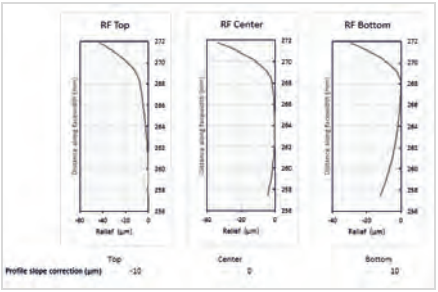

Fig. 20: Design Twist applied to the final drive gear pair

Iteration	Max Load	50% of Max Load	Low load
Design v00 nominal pinion/wheel Crowning=16/16 Lead Slope=-35/0 barrelling=5/5 profile slope=0/0 tip relief=8/30 Twist= 0/20	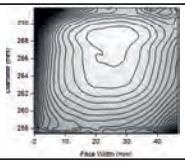	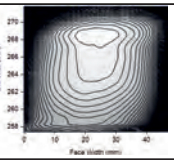	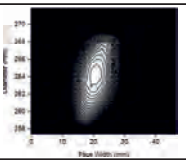
Normalized PPTE (% of target)	63%	132%	97%

Fig. 21: LTCA results of final drive gear pair with a Design twist

The next step involves the effect of manufacturing variations that would affect the contact stresses and TE. A process based on references [4, 5] is used to define optimum microgeometry and tolerances profile and lead deviations. The impact of interaction like the lead crown and lead slope, profile crown and profile slope, profile crown and lead crown on Contact stresses, and TE are studied using full factorial DOE. They analyzed using plots shown in Fig. 22. These interactions at different operating torque values are analyzed, and design cases are identified. For example, from Fig. 22, it can be observed that a design with profile crowning of 6 µm would be less sensitive to variation in profile slope. This would be considered a possible design case and then would be checked for different operating torque points.

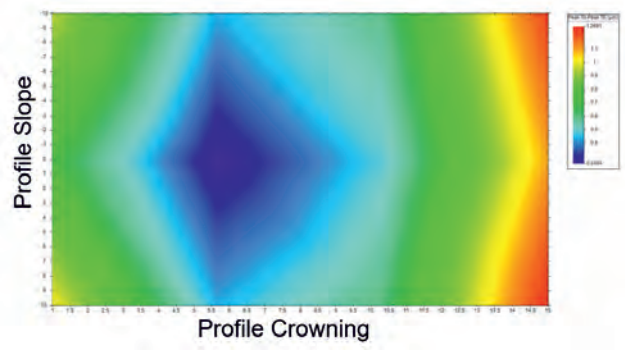

Fig. 22: Impact of Profile crowning and Profile slope variation on PPTE at one operating torque

Optimum profile and lead modifications are then identified. Fig. 23 shows the contact stress and PPTE values achieved for the final drive gear pair using this procedure. Note that the values of contact stress and PPTE are normalized using the maximum values.

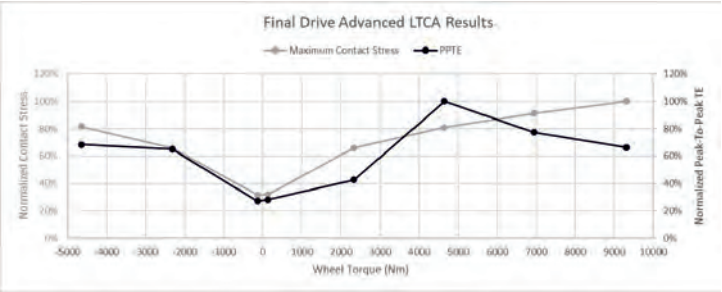

Fig. 23: Normalized PPTE and Contact Stress results at various Operating Torque

The final step in the gear microgeometry design process involves the robustness analysis. A Monte Carlo Simulation with 100 statistical studies is carried out; randomly selected errors in profile slope, profile crowning, lead slope, lead crowning, tip relief, and twist are applied. The standard deviation for each variable is defined based on the expected manufacturing quality. Then loaded tooth contact analysis is carried out on the 100 designs at different operating torque values.

The results of the robustness analysis for the 2nd gear pair are shown in Fig. 24 and Fig. 25. The average value and the average plus three standard deviations (A+3σ) indicates that the worst case is within the acceptable range.

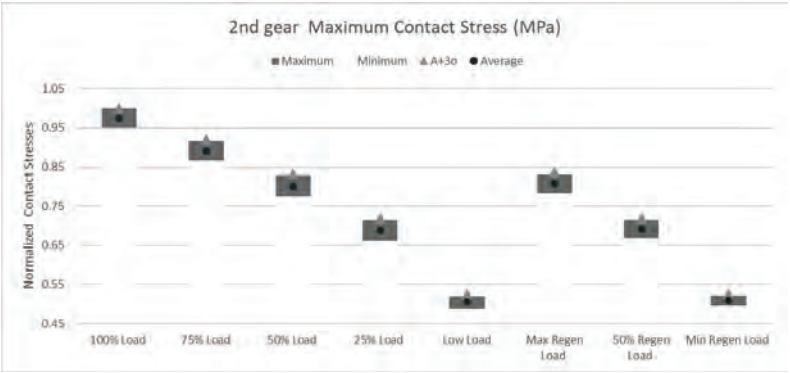

Fig. 24: Normalized Contact Stresses from Robustness analysis for 2nd gear pair

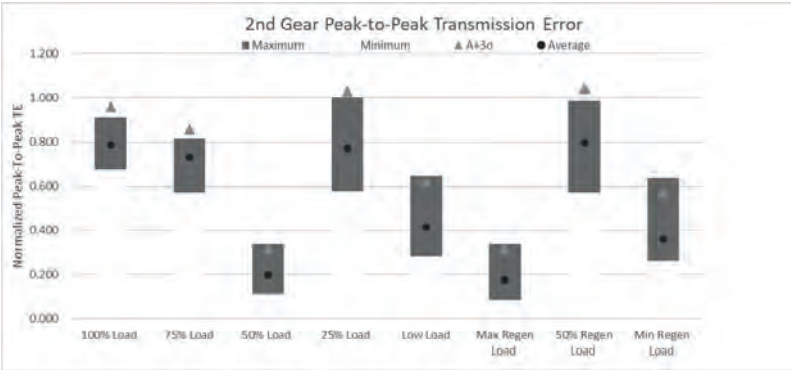

Fig. 25: Normalized PPTE from Robustness analysis for 2nd gear pair

5. Gear Whine Analysis

The previous steps focused on static analysis and ensuring that NVH issues don't arise by ensuring that the TE is minimum and meets the company targets. However, even when the TE targets are met, NVH issues can still arise due to the system's dynamics. Significant increases in the response magnitude can be observed when the gear mesh frequencies or

their harmonics cross the system's natural frequencies. Ideally, the natural frequencies in the operating range are minimized, and their overlapping is avoided.

The dynamics of the system are analyzed using a Masta model similar to the model described in references [6, 7] via modal and harmonic analysis. Virtual accelerometers are placed at different positions on the housing. The response on these accelerometers to the excitation from TE at different torque values and speed sweep from zero to maximum rpm on the motor torque-speed curve is analyzed. The acceleration responses are compared with the company targets, and alternative design changes are considered if required.

Fig. 26 shows the impact of the design changes made during the previous steps on acceleration response at an accelerometer position on housing from the simulation. Interventions needed to meet the gear mesh misalignment target, let to a gear pair design with a lower helix angle. The PPTE requirements led to the inclusion of a design twist.

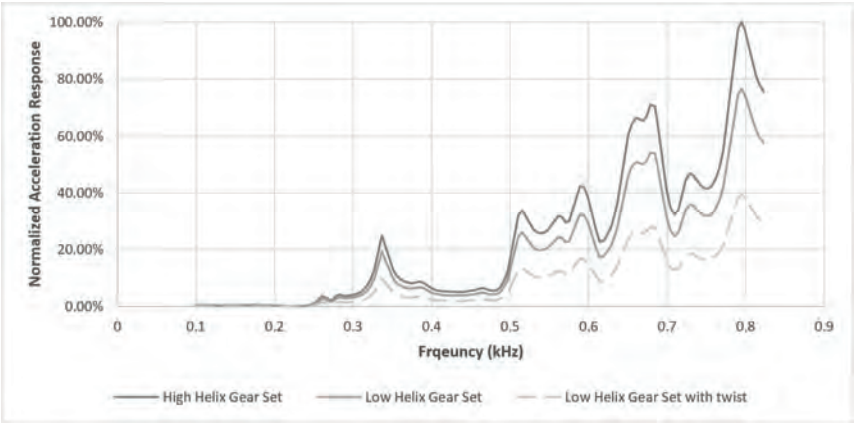

Fig. 26: Effect of gear design of final drive gear pair on acceleration response

6. Conclusion

The development of gearboxes for electric drives is a complex and iterative process. The design requirements were established at different steps in the design process by cascading the system level NVH and durability requirements. The system-level approach to consider the impact of design decisions on the NVH and durability with the same model led to the iterations and the time required to be significantly reduced.

7. References

[1] Smith, J. D.: Gear Noise and Vibration,2nd Edition. New York: Marcel Dekker 2003

[2] Langlois, P.; Baydu, A.; Harris, O.: Hybrid Hertzian and FE-Based Helical Gear-Loaded Tooth Contact Analysis and Comparison with FE. Gear Technology, July 2016, 54 – 63

[3] Türich, A.: Producing Profile and Lead Modifications in Threaded Wheel and Profile Grinding. 09FTM03, Technical Paper, AGMA, September 2009

[4] Houser, D.: The Effect of Manufacturing Microgeometry Variations on the Load Distribution Factor and on Gear Contact and Root Stresses. Gear Technology, July 2009, 51 – 60

[5] Harianto, J.; Houser, D: A Methodology for Obtaining Gear Tooth Microtopographies for Noise and Stress Minimization over a Broad Operating Torque Range. Gear Technology, July 2008, 42 – 55

[6] Langlois, P.: The Importance of Integrated Software Solutions in Trouble Shooting Gear Whine. Gear Technology, May 2015, 2 – 6

[6] Harris, O.J.; Langlois, P.P; Cooper, G.A.: Noise Reduction in an EV Hub Drive Using a Full Test and Simulation Methodology. Gear Technology, May 2016, 44 – 53

9GH-TRONIC Plug in Hybrid Transmission Gen4

J. Kiesel, Mercedes Benz AG, Stuttgart

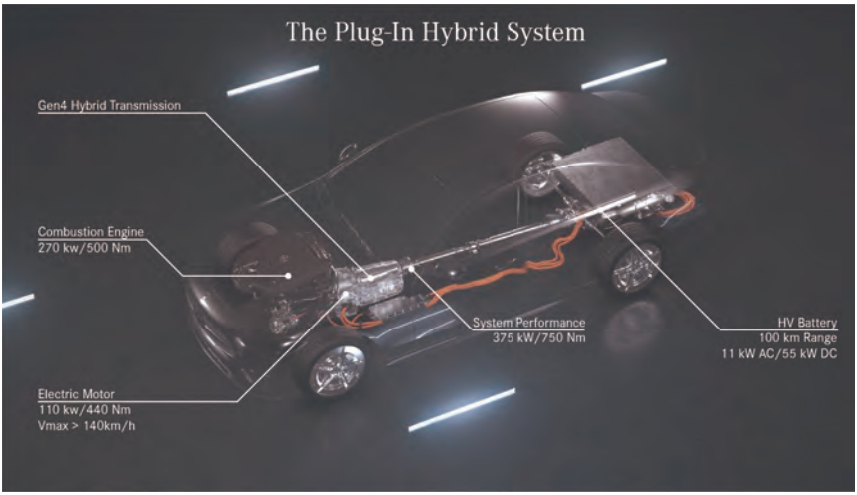

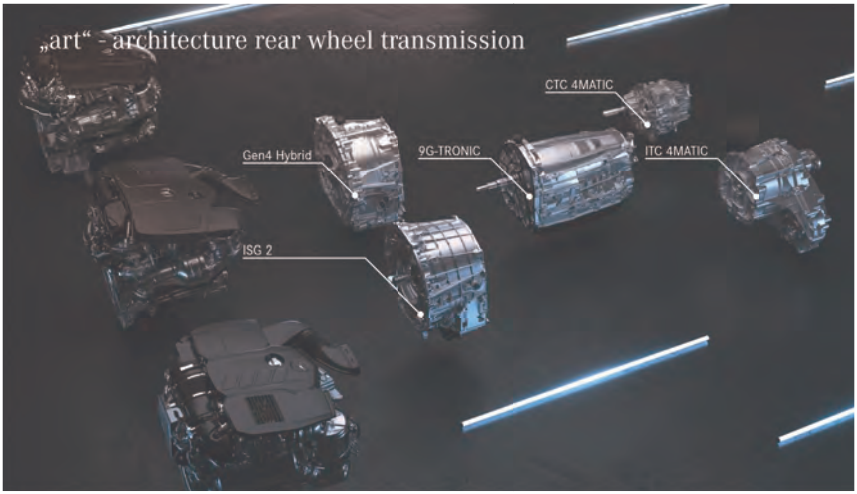

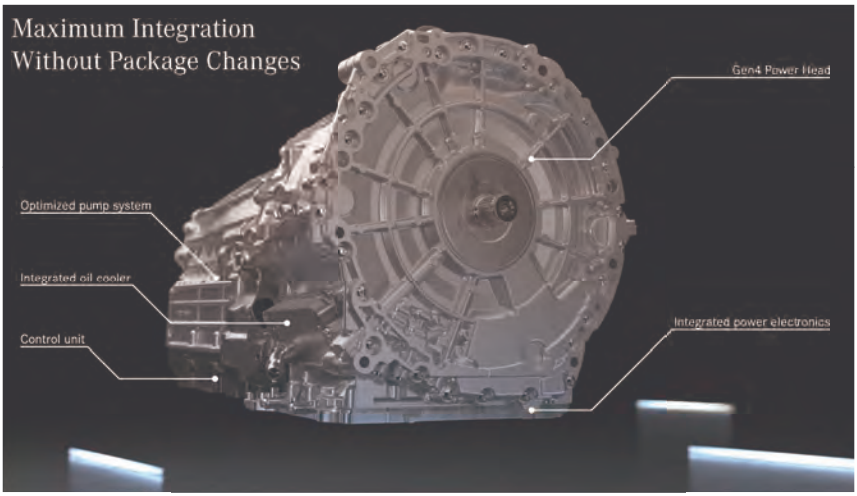

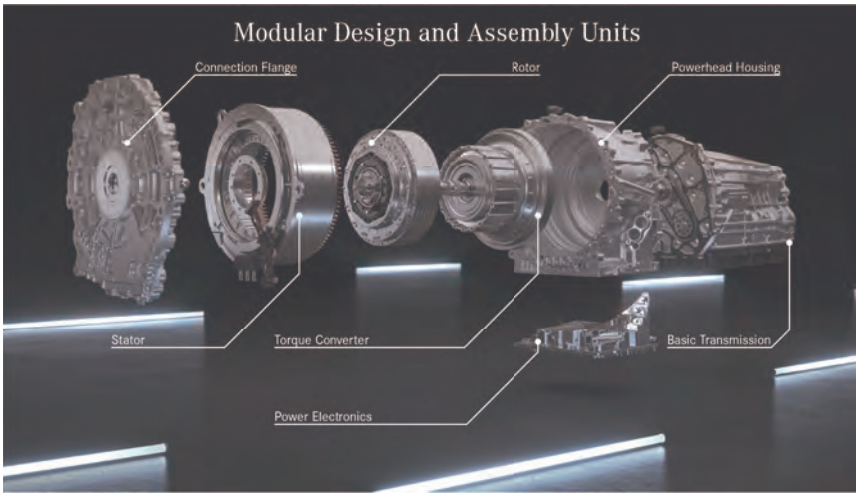

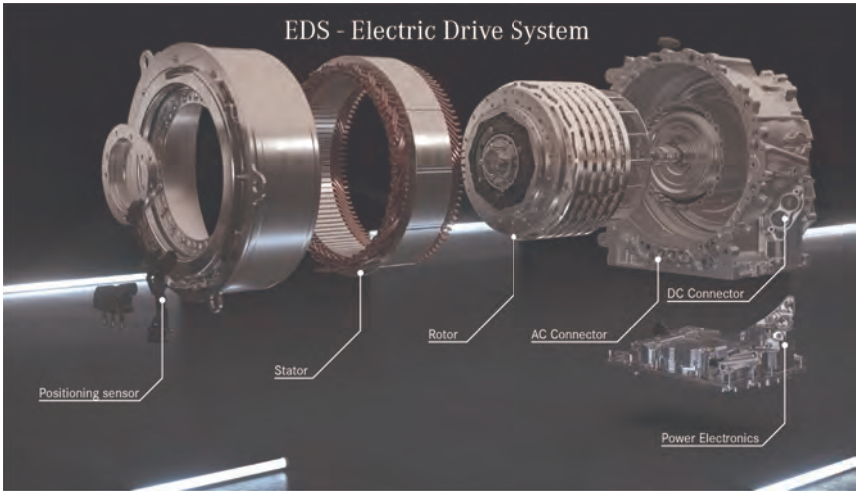

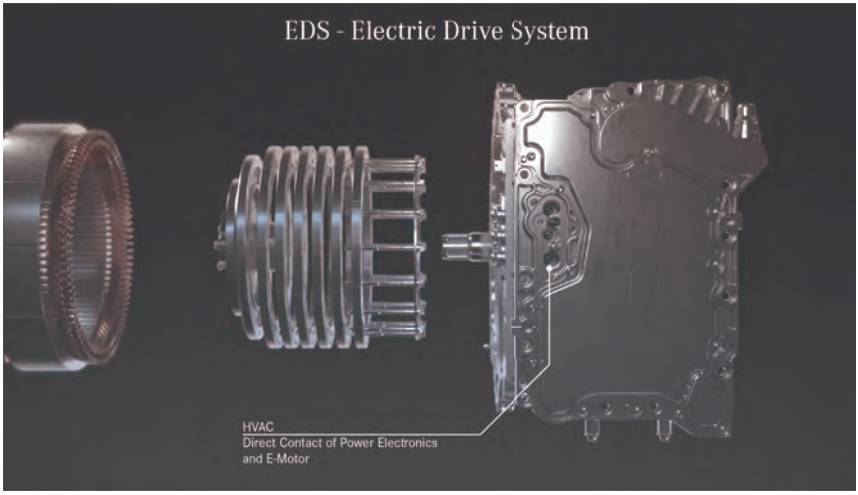

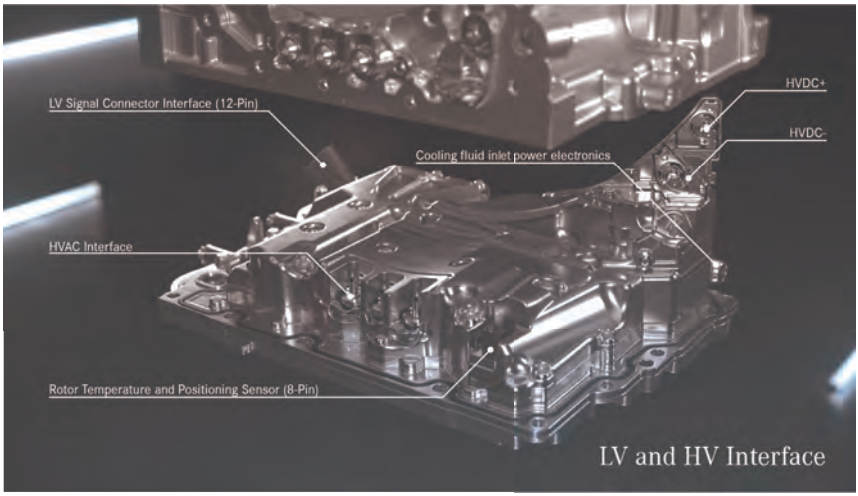

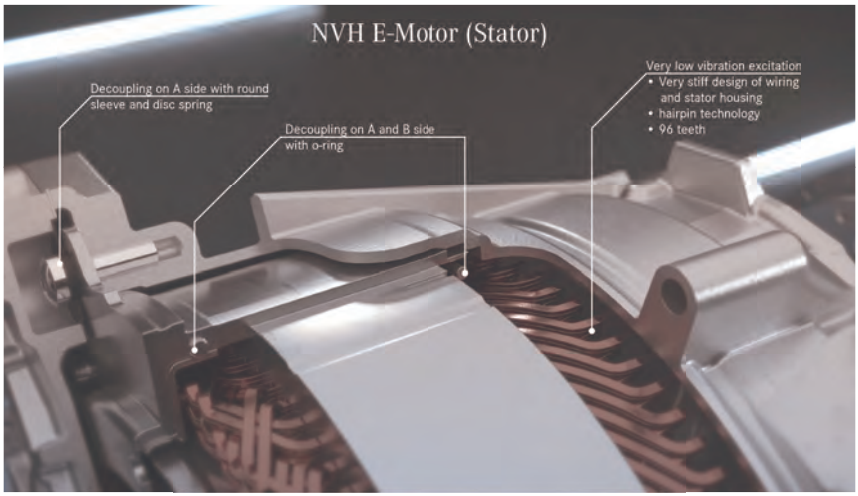

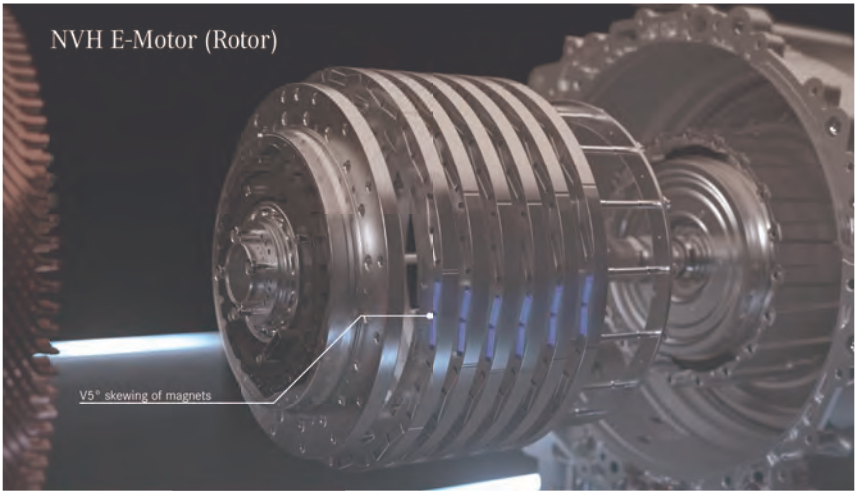

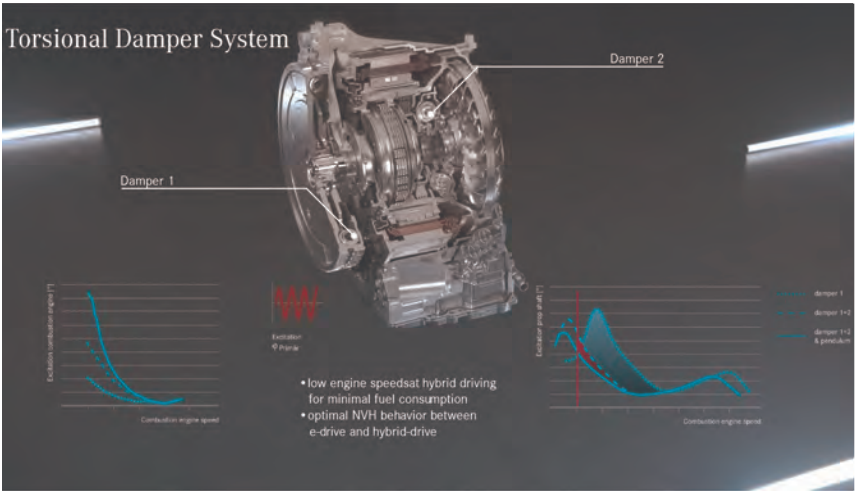

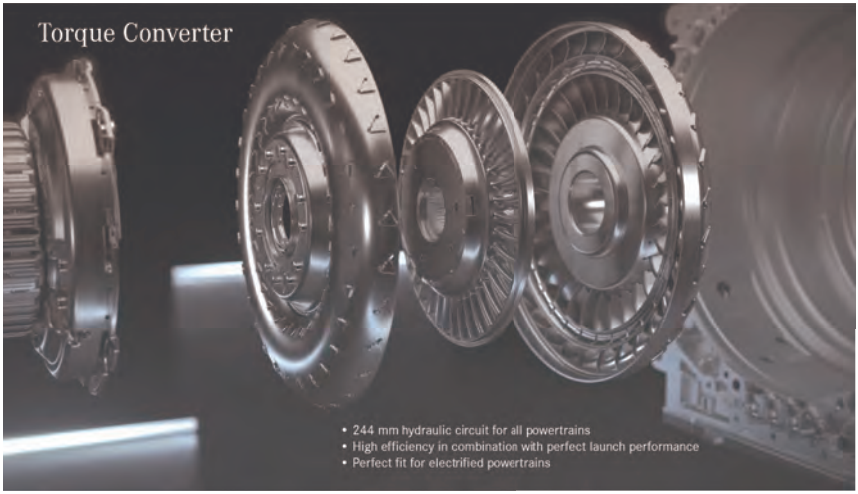

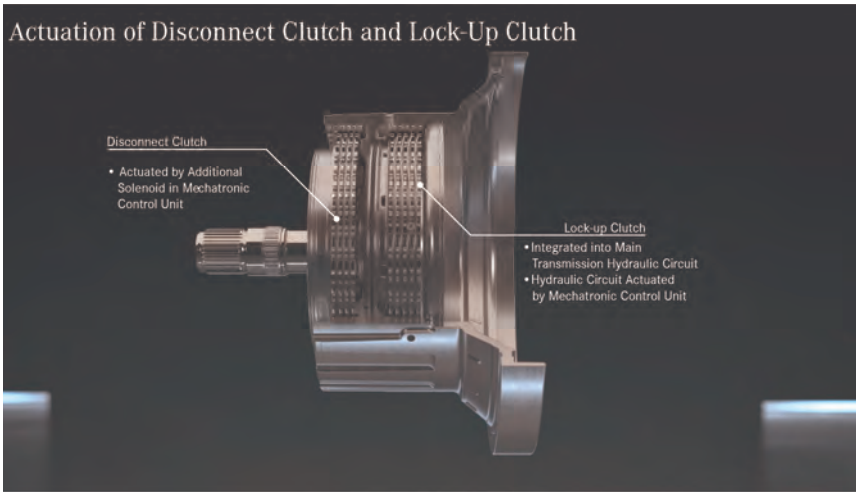

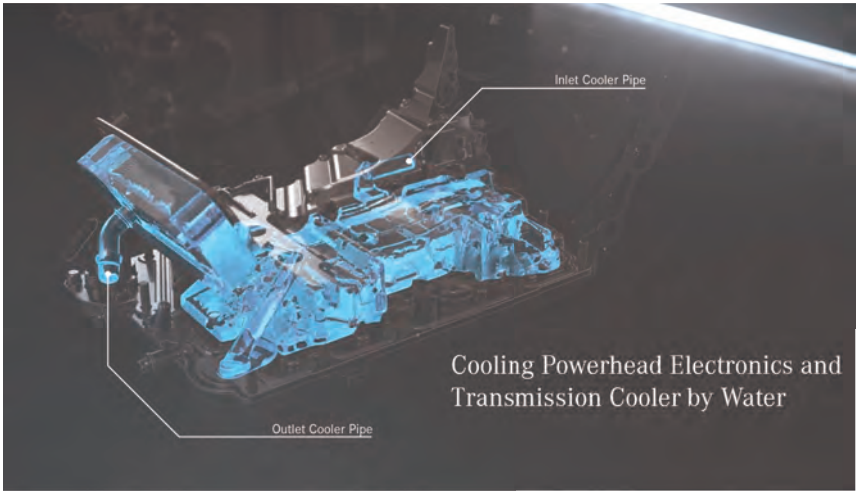

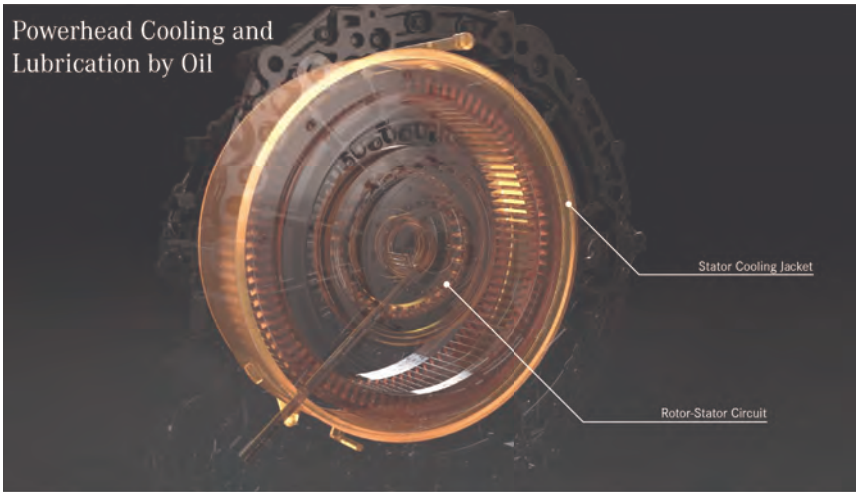

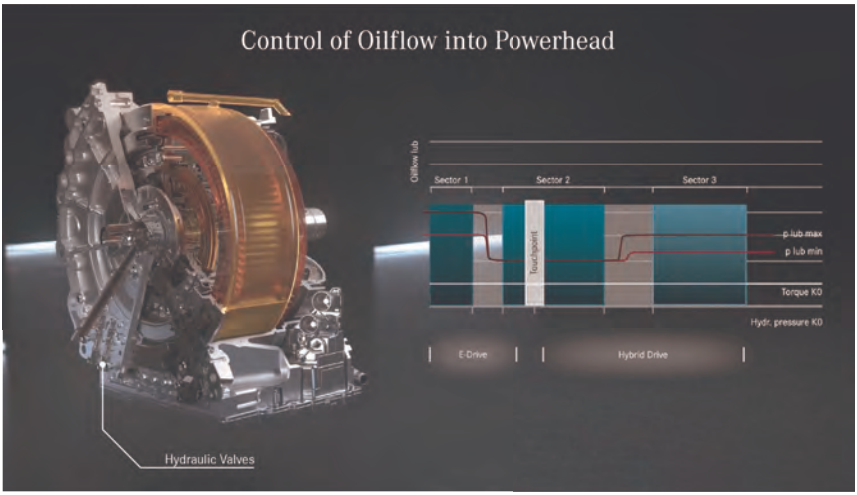

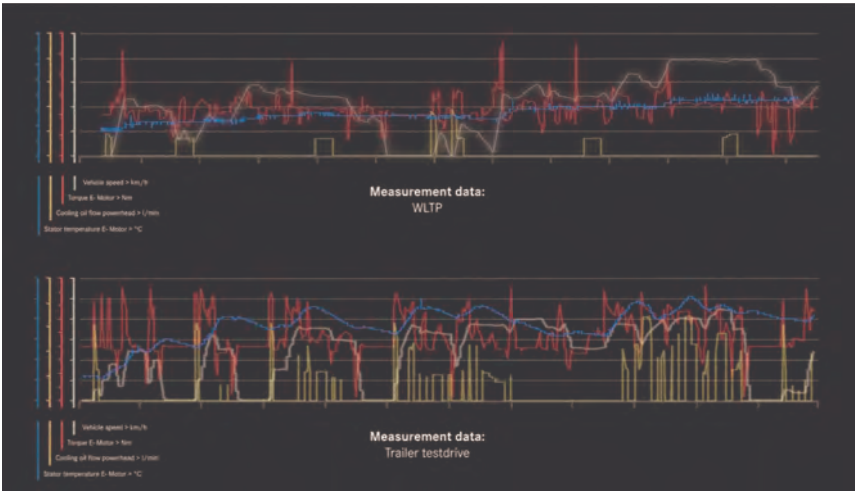

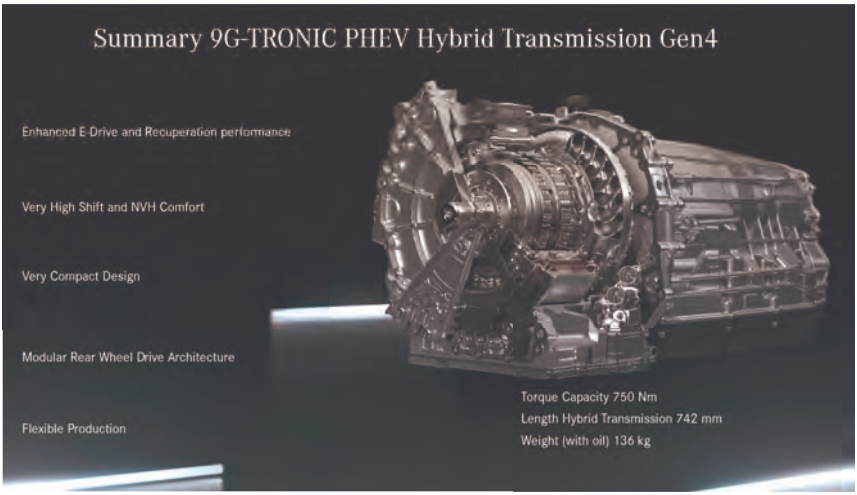

VDI Wissensforum

VDI-Berichte 2381

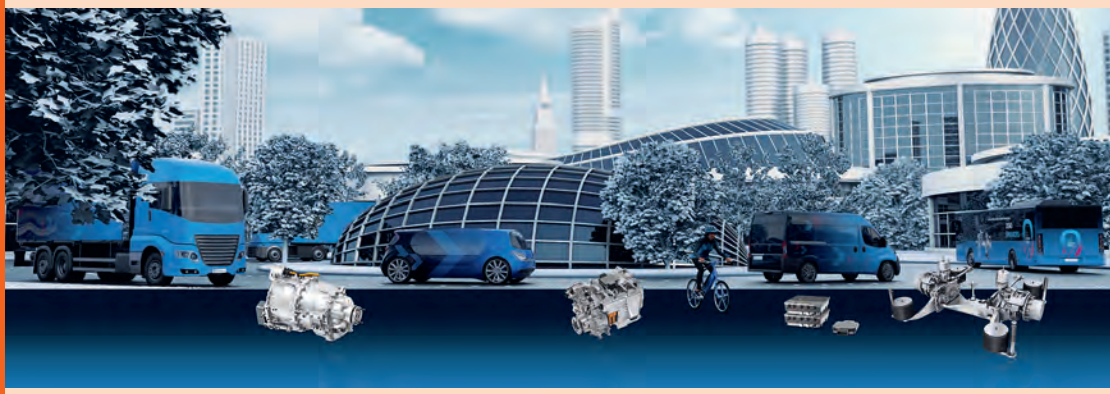

7th International VDI Conference

Drivetrain Solutions for Commercial Vehicles

October 13-14, 2021, World Conference Center Bonn (WCCB)

Image credits: ©ZF Friedrichshafen AG

Development trends towards CO2-neutral powertrains for HD applications

M. Muether, **B. Heuser**, **L. Virnich**, FEV Europe GmbH, Aachen;
A. Guedden, RWTH Aachen University, Aachen;
T. Luediger, FEV Consulting, Aachen;
D. van der Put, FEV Group GmbH, Aachen

Abstract

As the EU has set regulations to reduce the CO2-emissions by 15% in 2025 and by 30% in 2030 with 2019 as baseline, solutions must be developed to de-fossilize for the heavy-duty sector. In the long term, it is the target to find solutions for Zero-CO2- or CO2-neutral-powertrains, as aimed for by global greenhouse gas (GHG) regulations. With their specific needs and requirements, such as reliability, versatility and, above all, total cost of ownership (TCO), these CO2 targets are especially challenging for heavy-duty vehicles. This goes hand in hand with increasing freight traffic and growing vehicles sizes as well and weight restrictions as additional constraints.

Based on the specific requirements of heavy-duty applications, this presentation will provide a comprehensive overview of available and future propulsion systems, their specific development targets, and possible contributions to reducing CO2-emissions. This includes combustion engines and fuel cell systems, but will be extended also to battery electric vehicles, with the focus on this technology currently coming from the passenger car sector. It will be discussed how many possible powertrain solutions are viable depending on the specific application. This will be accompanied by a brief outlook on how vehicle measures need to support the future reduction of CO2-emissions from heavy-duty vehicles.

While the EU legislation targets at newly sold vehicles, a powertrain de-fossilization of the existing vehicle fleet can only be achieved with de-fossilized / de-carbonized fuels for combustion engines. A special focus will be on the use of such fuels (E-Fuels) and especially hydrogen. With a lot of different fuel options currently under discussion as energy carriers (e.g., hydrogen, methanol, Fischer-Tropsch fuels), it will be shown how a specific fuel defines the fuel storage, the combustion concept as well as the exhaust gas aftertreatment system and possible additional technologies such as waste heat recovery systems.

Introduction

Alongside the energy sector and industry, transport is one of the major contributors to CO2 emissions worldwide. To limit the extend of climate change, which is dominantly caused by the increasing CO2 emissions, the European Commission has set strict reduction targets for the CO2 emissions of many sectors, including transport. The long-term vision until 2050 is to realize a CO2-neutral economy. To achieve this, the transport sector must cut its emissions by 90-95% within the next 30 years. To meet these ambitious targets, it is necessary to make use of the available technologies and to optimize every aspect of propulsion and vehicle technology.

FEV has explored different low carbon pathways to achieve the goal of reducing the greenhouse gas emissions in heavy-duty transportation by 80 to 95% until 2050. These scenarios are based on four measures: first, optimization of usage; second, electrification of the powertrain; third, an increase in vehicle efficiency; and finally, adaptation of energy carriers. Depending on the scenario, the measures have different degrees of impact, see Figure 1.

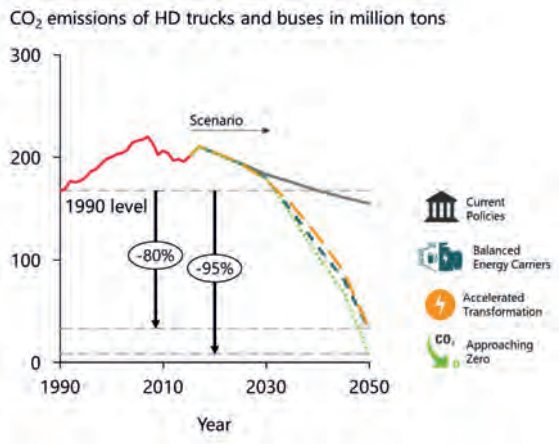

Fig. 1: Pathways towards the CO2 reduction target by 2050, source: historical data EEA, Low Carbon Pathways Until 2050 – Deep Dive on Heavy Duty Transportation [1]

In all scenarios, the adaptation of energy carriers contributes the most to the CO2 emission reduction, followed by the electrification of powertrains. In any case, the HD truck original equipment manufacturers (OEMs) have only little influence on the development of CO2-neutral energy carriers needed to meet the long-term targets. But when it comes to the interim targets

set for 2025 and 2030, -15% and -30% of CO2 emissions compared to 2019, respectively - OEMs must employ a combination of measures. For the first time in Europe, the CO2 legislation is linked to a penalty system in case of non-compliance, with fines of 4,250 euro per gCO2/tkm in 2025 and 6,800 euro per gCO2/tkm in 2030. Hence, there is an urgent need for the truck manufactures to employ cost-efficient CO2 reduction measures. [2]

In the short term, technology options include vehicle and powertrain efficiency improvements, electrification of the powertrain and optimization of vehicle usage through smart mobility functionalities. Additional CO2 reduction technologies, mainly related to longer term implementation scenarios like fully automated driving and an even stronger electrification of powertrains, are likely to be employed by 2030 and onwards. Furthermore, the adaptation of energy carriers will make a significant contribution to reduced CO2 emissions. Significant shares of CO2-neutral energy carriers are expected to enter the market after 2030. However, this requires significant changes in legislation to not only credit for CO2-free, but also for CO2-neutral fuels. Figure 2 shows the technology roadmap to 2050.

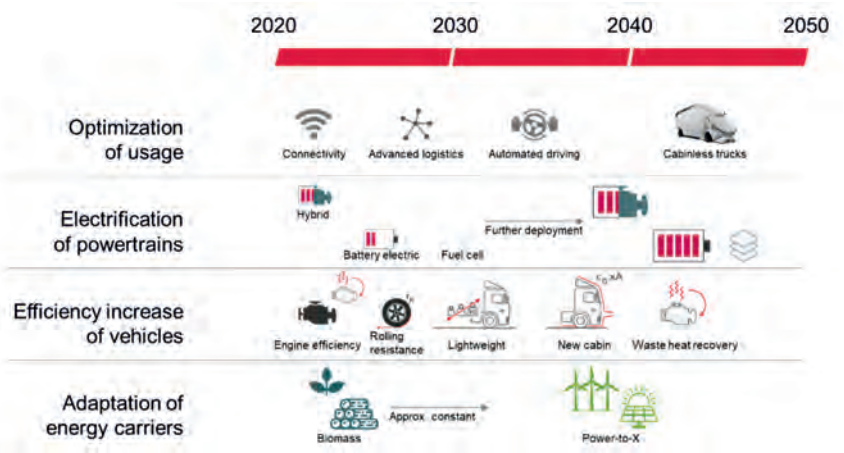

Fig. 2: A roadmap for measures to reduce CO2 emissions by 2050, source: FEV

CO2 emission reduction by optimization of existing technologies

In parallel to technologies that will be completely carbon-neutral, an initial focus lies on optimizing existing technologies. Figure 2 shows an overview of measures, where further improvements will significantly contribute to a reduction of CO2 in the upcoming years.

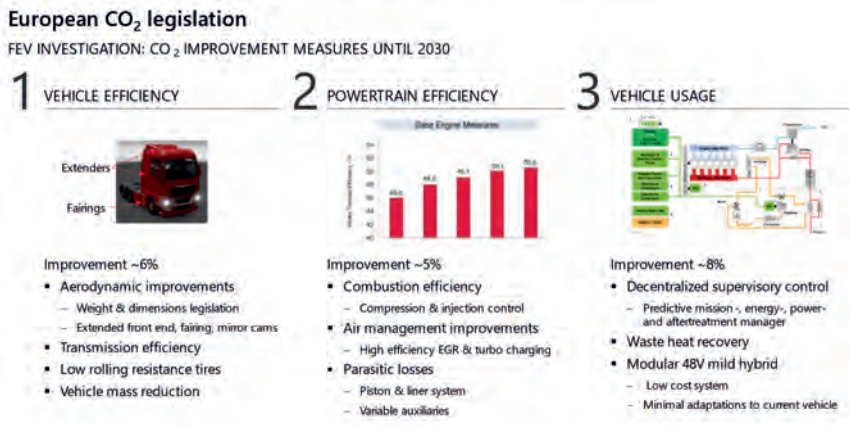

Fig. 3: CO2 improvement measures until 2030

Based on the weights and dimensions directive that came into effect on 1st of September 2020, an increase in overall vehicle length is allowed, if the turning radius is not compromised. Although every OEM can decide where to add this additional length, it is believed that the aerodynamic gain of this increase will be in the order of 4 % fuel economy improvement. In addition, low rolling resistance tires are assumed to bring a further 2,5 % improvement [3]. As a third, but very cost-intensive point, vehicle mass is a factor that contributes to reduce overall fuel consumption. Hence in total, the fuel consumption reductions that can be achieved by measures on the vehicles with limited effort and cost will amount to about 6 %.

Engine advancements can be achieved through a combination of various measures. Figure 4 presents an efficiency walk towards a brake thermal efficiency (BTE) of >55 %, a concrete target for the next decade. These engine advancements will be introduced in engine development by three evolution phases in the next years.

The first phase deals with engine improvements based on next generation peripherals without re-designing the base engine. An optimization of the combustion system by increasing the compression ratio, and thus increasing maximum cylinder pressure, higher injection pressure combined with advanced combustion control can lead to an efficiency increase of about 2 %-

points. Sophisticated air management leading to gas exchange improvements, consists of optimized turbo charging and Miller timings. With this, another 1.1 %-points could be gained. Reducing the parasitic losses and reducing engine friction improves efficiency by ~1.0 %-points.

In the second phase an updated engine architecture provides additional improvements through 48 V mild-hybrid electrification together with advanced engine extensions that open new degrees of freedom. High efficiency electric-assisted fixed-geometry turbochargers in combination with low-pressure EGR enable further optimization of cylinder filling and reduced gas exchange leading to 1.0 %-points engine efficiency improvement. Thereby, component electrification supports turbocharger response during transient maneuvers and allows exhaust energy recuperation at engine braking events in parallel. Another 0.3°%-point efficiency can be achieved with electrified auxiliaries thanks to decoupling from the engine and fully flexible control. Unconventional piston design by additive manufacturing enables improved combustion i.e. through increased free spray length and enhanced air utilization. Reducing heat transfer during combustion and the exhaust stroke can be achieved by coating the piston crown, exhaust valves and exhaust ports. New coating composite materials applied by plasma spray allow thin surface layers and smooth roughness's with an optimized thermal conductivity and diffusivity to enable thermal swing insulation. Altogether, this leads to an additional increase of 1.2 %-point engine efficiency.

The third phase of the introduction of advanced technologies provides by far the highest leap in fuel efficiency gain. It can be achieved by Waste Heat Recovery with a Rankine Cycle and by introducing alternative fuels into the market.

The further optimization of conventional technologies shows sigificant potential and is shown as an overall efficiency walk in Figure 5. Starting with the 2019 industry average, a reduction of CO2 emissions of 12% is expected until 2025, another 4 %-points can be achieved by 2030. These improvements can only be realized by optimizing all aspects of the vehicle as described before: mainly powertrain, aerodynamics and rolling resistance. With the target in 2025 to reduce CO2 emissions by 15%, it seems obvious that besides conventional HD vehicles, already some alternative trucks with zero CO2 emissions need to be sold. While in 2030, with a required CO2-reduction of 30% (or even 40%), a significant share of zero emission trucks needs to be achieved.

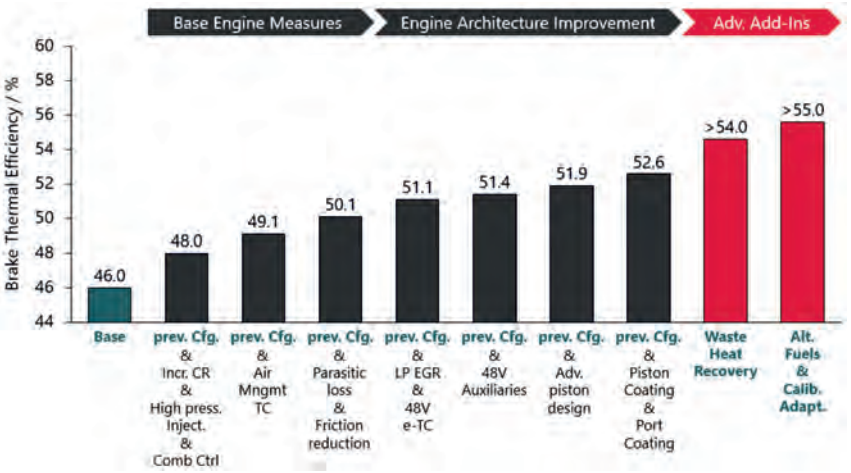

Fig. 4: Highly efficient powertrains for commercial vehicles, a possible engine technology roadmap for CO2 reduction

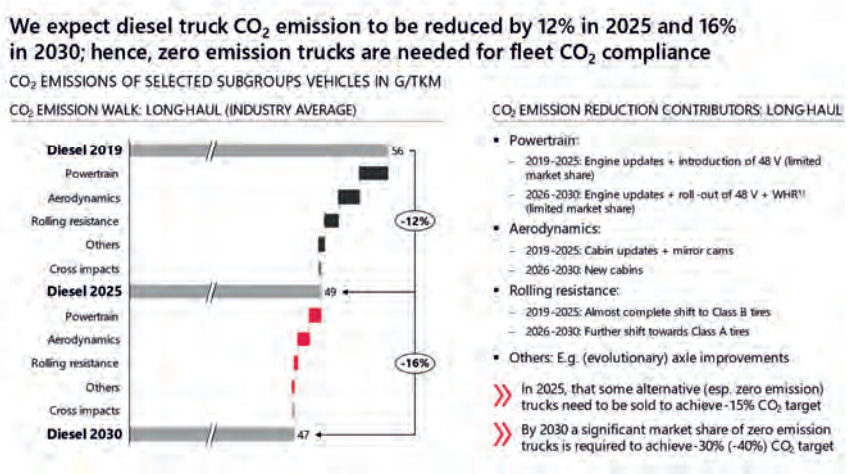

Fig. 5: Diesel truck CO2 emission reduction by 2025 and 2030 – efficiency walk

Technologies for Zero CO2 emission trucks

While it is believed that the targets set for 2025 can mainly be achieved by significant optimization of the existing technologies, to achieve the targets for 2030 will require the introduction of a significant share of Zero CO2 Emission vehicles. Figure 6 gives an overview of the propulsion technologies that enable “Tank-to-Wheel” zero CO2 emissions, as well as their main challenges.

- Battery electric propulsion: Because of the required energy density, main application could possibly be urban and regional delivery with one main challenge being the required charging infrastructure to reduce downtimes for charging
- Fuel Cell propulsion: With higher energy density a possible solution for long haul operation, main challenges today are the fuel cell durability, which might require an exchange of the fuel cell stack over lifetime, as well as the general availability and the costs of hydrogen
- H2-ICE propulsion: Like fuel cell propulsion suitable for long-haul operation with the efficiency of the combustion engine remaining a main development target. At the same time, also here, the general availability and the costs of hydrogen are challenges

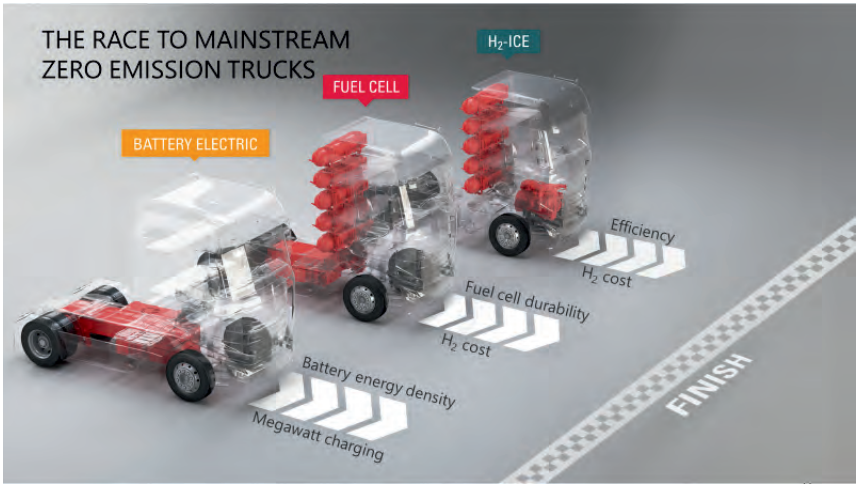

Fig. 6: Zero CO2 Emission Trucks: Overview of possible propulsion systems

Also, for the upcoming new technologies for zero CO2 emission trucks, the attractiveness of a HD vehicle for a possible customer is mainly determined by the total cost of ownership (TCO) and the reliability. Figure 7 gives an overview of the customer requirements and expectations that must be considered.

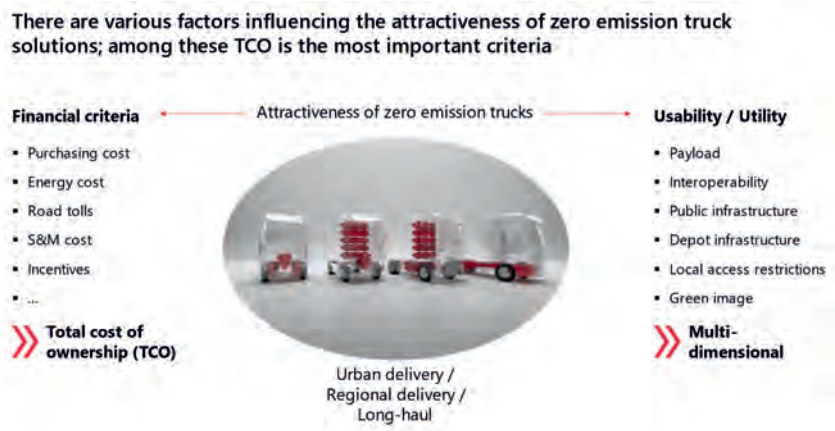

Fig. 7: Customer requirements and expectations

It is obvious that there is no “one fits all” solution for the future. Depending on the use case and the boundary conditions, different solutions are benefitial for the customer. FEV has developed competetive technology strategies and solutions to assess the feasibility of these technologies under changing boundary conditions and considering further technology advancements. Figure 8 gives an overview of these strategies and solutions, that lead to a technology definition for commercial vehicle CO2 compliance.

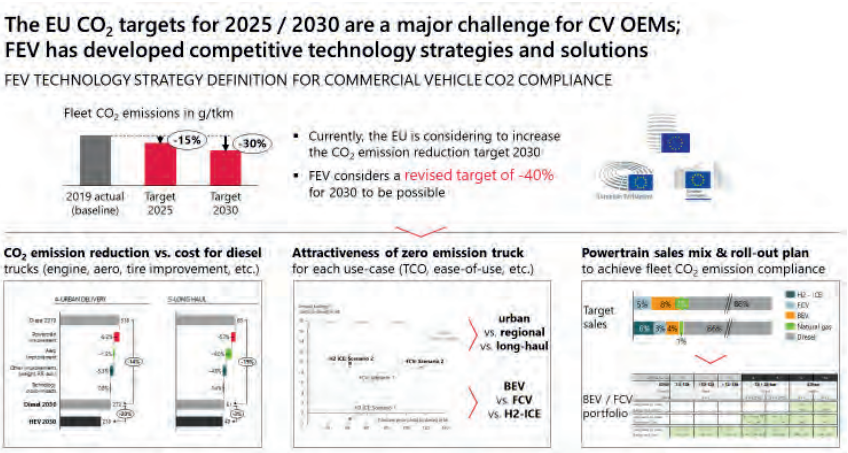

Fig. 8: FEV technology strategy definition for commercial vehicle CO2 compliance

To define competitive product strategies for battery electric vehicles (BEVs), fuel cell vehicles (FCVs), and hydrogen internal combustion engines (H2-ICE), it is necessary to analyze which propulsion system offers the greatest benefits. Due to their different advantages and disadvantages, the most suitable powertrain strongly depends on a truck's use case. Figure 9 gives an overview of three different use cases (urban delivery, regional delivery, and long-haul) and their boundary conditions.

To calculate total cost of ownership for several truck use-cases, most relevant cost drivers are varied reflecting different scenarios for 2030

2030 SCENARIOS: TRUCK USE-CASES AND BOUNDARY CONDITIONS

	1 Use-case 1	2 Use-case 2	3 Use-case 3
Vehicle	18 t, Rigid	26 t, Rigid	40 t, Tractor
Driving cycle	Urban delivery	Regional delivery	Long-haul
Annual mileage	45,000 km	75,000 km	120,000 km
Range (with one H_2 tank / battery fill)	250 km	400 km	600 km
Toll road share[1]	15%	40%	75%
Battery electric truck: Charging	Depot: 95% Public: 5%	Depot: 80% Public: 20%	Depot: 30% Public: 70%

Fig. 9: Overview of truck use-cases for TCO assessment

Figure 10 shows FEV's forecast for the total cost of ownership of zero emission trucks for these representative use-cases. In this assessment, in urban delivery, the BEV is the most attractive zero-emission solution; in regional delivery, the BEV still is better than the FCV; in long-haul transport, the FCV is best, followed by the H_2-ICE. These TCO analyses are regularly updated as technology advances.

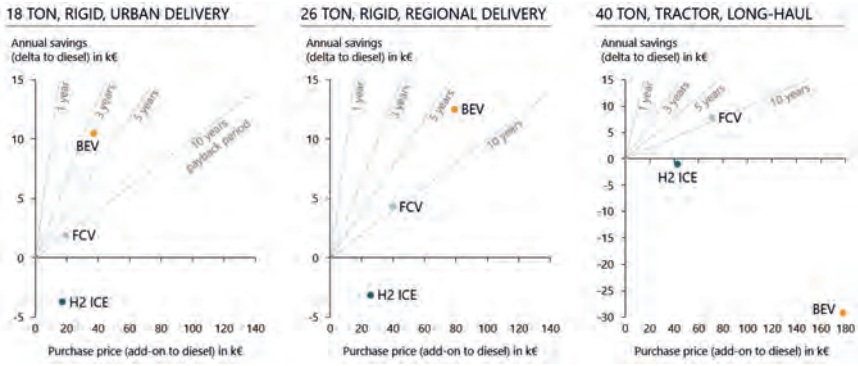

Fig. 10: Total cost of ownership for different technologies and applications in 2030

When elaborating scenarios, it must be clear what boundary conditions are assumed, and a lot of these boundaries are still unclear as well as the technology progress. For a long-haul truck, when comparing an FCV with an H_2-ICE, the outcome of the analysis can easily change due to the assumed H_2 price, battery costs, FC system costs and possibly required FC replacements. Figure 11 shows, that under changing boundary conditions (H2-ICE favored scenario), for the 40-ton long-haul use-case, the H2-ICE could be a competitive solution.

The EU regulations mainly push Zero Emission Vehicles (ZEVs) including battery electric, fuel cell and H_2 ICE vehicles. Natural gas and renewable fuels have less support so far. Specifically, a variety of regulations will come into force in the coming years, which CV market players will have to consider in their product/technology strategies (Figure 12). These regulations, which are prescribed by various legislators, include e.g., the "CO_2 fleet emission targets for 2025 and 2030", the "Clean Vehicle Directive" or the expected EURO VII pollutant emissions regulations. Some of the regulations are not clearly defined yet and/or have major uncertainties (e.g., local access restrictions). Commercial vehicle OEMs need to take all possible regulations into account for product portfolio and technology strategy definition. Due to the typically long

product life cycles, R&D periods and the short-term introduction of regulations, OEMs need to prepare for various scenarios.

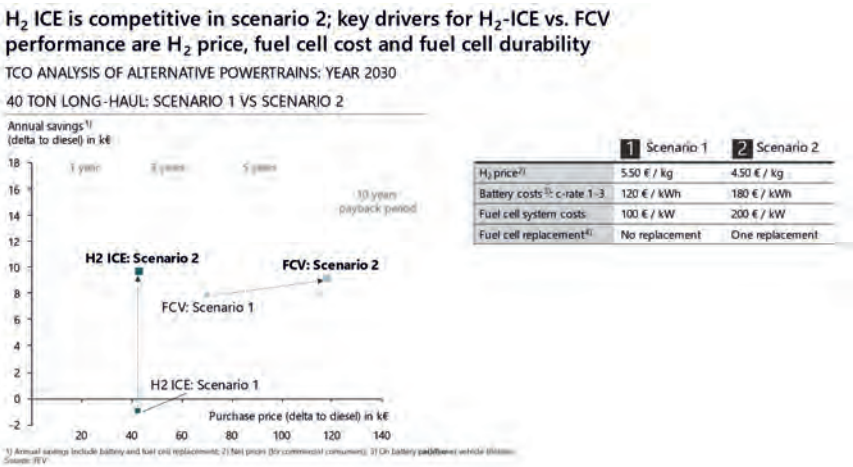

Fig. 11: Impact of changing boundary conditions on the TCO for CV powertrains

Fig. 12: Key regulatory challenges for the European commercial vehicle market

CO2 emission reduction by non-fossil energy carriers

Optimizing powertrain efficiency, aerodynamic drag improvements and electrification of the propulsion system will massively reduce the energy consumption. But, of course, there are some limitations that restrict the total CO2 emission savings potential of these measures. First, all measures can only be applied to new vehicles entering the market. The existing fleet remains unaffected. With an average fleet age for HD trucks of ~11 years in Europe and with up to 21 years in some European countries – the real-world CO2 reduction will be small and slow. Secondly, powertrain optimization and other efficiency improvements only reduce the need for fuels. Moreover, the use of battery electric drivetrains for long-distance and heavy goods transport is still not reasonable from an ecological and economic perspective. Thus, given the long-term goal of a CO2-neutral transport, obviously “green” chemical energy carriers – synthetic fuels – will be urgently required. [4]

Synthetic fuels circumscribe various fuels based on biomass, CO2 and H2. These include hydrogen itself, methanol, other long-chain alcohols, oxymethylene ethers (OME) and alkanes, as well as gaseous fuels such as methane (Synthetic Natural Gas, SNG) and dimethyl ether (DME), see Figure 13. Many of these fuels can be produced from different raw materials and along specific production pathways. Due to their different molecular structures, these fuel candidates have significantly different chemical and physical properties. What they all have in common, however, is that both the engine efficiency and the pollutant emissions can be significantly improved compared to fossil liquid fuels. But production pathways and thus costs, as well as energy density and handling safety, differ substantially. In addition, the combustion systems and the fuel injection systems also require substantial adjustments. The same applies to the storage of the fuels. Currently, focus of both research and industry is mainly on hydrogen, methanol, and diesel-like so-called drop-in fuels.

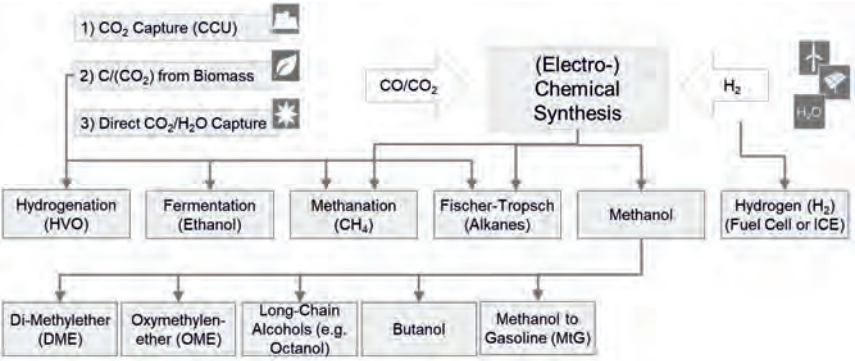

Fig. 13: Different synthetic fuels from non-fossil carbon sources

In Figure 14 the most promising renewable fuel candidates are assessed, with every fuel having its individual benefits and drawbacks. While hydrogen and methanol are renewable energy carriers that are rather cheap to produce, fuel storage (especially for hydrogen) is considered to be more difficult. FT-Fuels are more energy and cost intensive to produce, but have the benefit, that they can be used directly in the existing vehicle fleet.

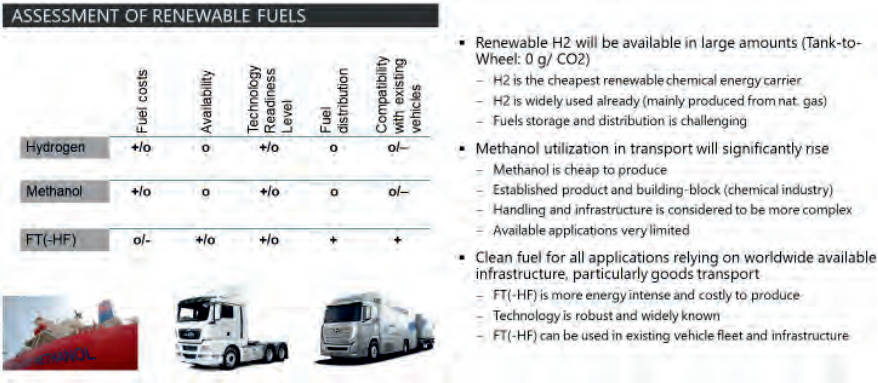

Fig. 14: Assessment of renewable fuels

Hydrogen

For hydrogen (H2) synthesis, only water and (renewable) electricity are required. H2 is a reactant for all other synthetic fuels, and it is not only the simplest, but also cheapest fuel to produce. However today, green H2 from renewables is more expensive than any other fossil fuel. But new electrolysis technologies, such as High-temperature PEM and Solid Oxide Fuel Cells, jointly with an increasing market size, will continuously reduce costs. Current estimations foresee a H2 sales price at the pump of 2.5-6 EUR/kgH2 in 2030 as realistic.

The major driver for the near-term use of H2 as a fuel is the EU's increasingly stringent CO2-regulations, which require a reorientation of powertrain concepts in on-road transportation. With the given Tank-to-Wheel legislation carbon-free or low-carbon fuels produced from renewable sources are coming into focus. Hydrogen as a zero-carbon fuel offers enormous potential but poses major challenges in terms of storage and short-term availability.

Possible powertrains for zero CO2 emission trucks are BEV, FC and H2-ICE. Figure 15 compares hydrogen to BEV, and H2-ICE to FC to show the possible benefits that can be taken from the H2-ICE in short term.

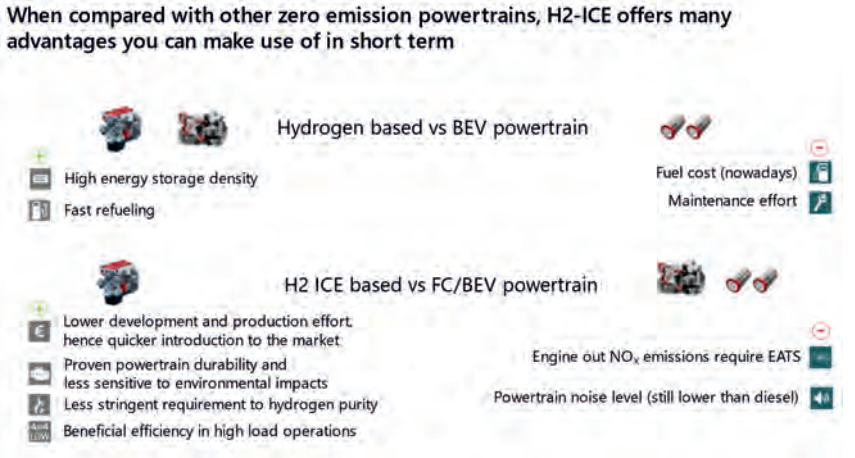

Fig. 15: Short-term advantages of the H2-ICE in comparison to BEV and FC

As a gaseous fuel, hydrogen is not well suited for high pressure direct injection, unless liquefied hydrogen is used. This is due to the power requirements for pressurization. Hydrogen´s key feature unquestionably is its very fast combustion leading to superior lean burn and EGR tolerance. [5] There is significant room for further optimization of the H2-ICE technology with

the target to further increase efficiency. The specific challenges and solution approaches for hydrogen combustion engines are shown in Figure 16.

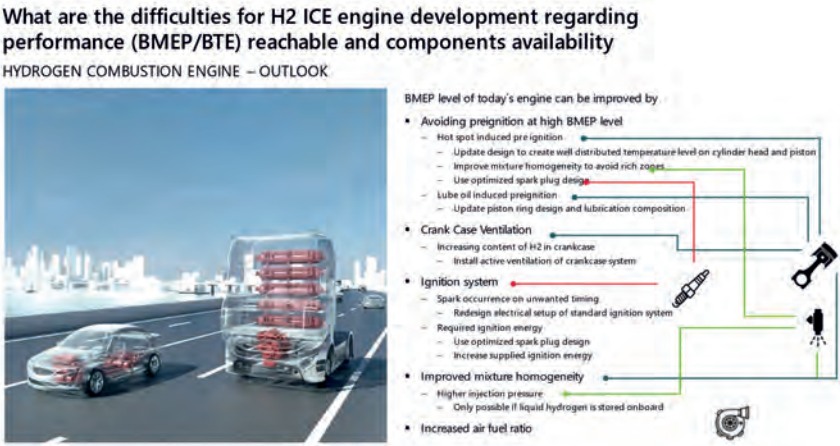

Fig. 16: H2-ICE development targets: challenges and solution approaches

Whereas engine out CO2- and soot emissions are nearly completely diminished with hydrogen combustion, NOx emissions are a significant challenge. The fast and hot burn of hydrogen combined with sufficient oxygen availability in lean conditions results in a shift of the NOx peak to a leaner relative air/fuel ratio (AFR = ~1.4) with very high concentrations. While NOx raw emissions in some parts of the operating map will require little work from a SCR system, especially transient operation and deviations in the rel. AFR at increasing load are a major challenge.

FEV is carrying out hydrogen combustion investigations on different engine sizes. Figure 17 shows results obtained on a heavy-duty single cylinder engine (2.13 l) and on a medium-duty 6-cylinder engine (7.7 l).

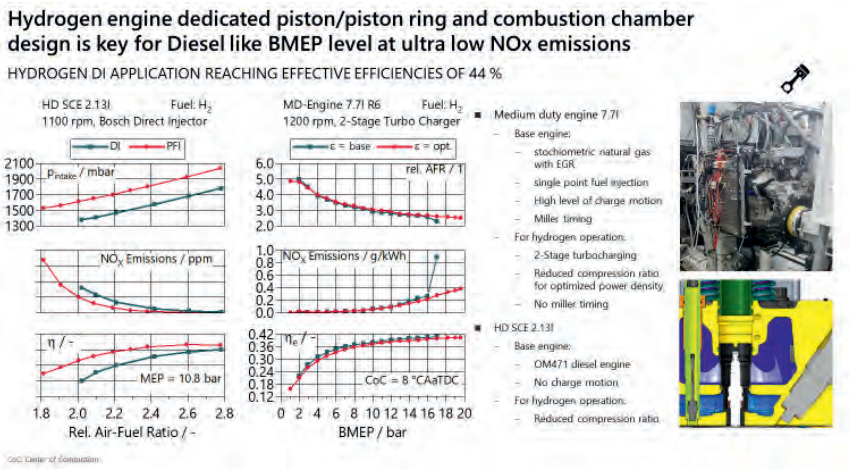

Fig. 17: Hydrogen combustion: Lambda and load variations on HD and MD engines

On the HD SCE, the difference between Port Fuel Injection (PFI) and Direct Injection (DI) was investigated (left column of diagrams). To achieve the results for DI hydrogen combustion, the DI combustion system was comprehensively optimized (e.g., combustion chamber design) to achieve an improved mixture homogeneity. At a constant air/fuel ratio, the efficiency is lower, and the NOx-emissions are higher compared to the PFI-combustion, which achieves a better hydrogen/air mixing. At constant boost pressures though, the NOx emissions improve for DI with the efficiency remaining on a similar level. The target for further optimization is clearly to achieve a PFI-like mixing for high efficiencies, with the benefits of a DI regarding transient response and power density.

Investigations with hydrogen on the MD engine show, that with a CNG-derived compression ratio (CR), the maximum load is limited because of preignition events and knocking combustion. The maximum achievable load using the piston from CNG engine is around 16 bar BMEP (Diesel and CNG engine 19.6 bar max. BMEP). An optimization of the CR though reduces knock tendency and Diesel- and CNG-like BMEP levels can be demonstrated.

In summary, a hydrogen engine for heavy duty applications will most likely feature a lean burn spark-ignited (SI) combustion system combined with an SCR NOx aftertreatment system. While the first generation of hydrogen engines might be PFI engines to reduce the time to market, DI is the way to go to improve the load range, rel. AFR capabilities and the transient response. Injectors are in development and testing is ongoing.

One of the major challenges and the most important prerequisite for the use of hydrogen in the transport sector is still the development of an infrastructure for refueling since the volumetric energy density of hydrogen is very low and the effort for liquefication is high. The transport costs for hydrogen are also significantly higher than for liquid energy carriers.

Methanol

Methanol is the simplest and easiest to produce liquid synthetic fuel that can be synthesized from CO2 and renewable H2. It is expected that renewable methanol can be imported to Europe at costs below 1 €/lDieselequivalent by 2030, e.g., from the Middle East and North Africa as well as from Chile and Australia.

Today, in Europe, the use of methanol as an additive to conventional gasoline is limited to 3% v/v in accordance with EN228. For heavy duty applications, methanol plays a larger role already especially in China and India. In China, methanol-operated trucks are in series production now.

Figure 18 shows results from methanol engine testing at FEV. Here, a so-called Dual Direct Injection Compression Ignition (DDI CI) was realized, with a central methanol main injector and a lateral Diesel pilot injector. The exhaust gas aftertreatment system layout comprises a Coated Diesel Particulate Filter (CDPF) for PN, HC and CO reduction especially at low loads. The SCR system can be adopted from the diesel engine and, depending on the calibration, can be operated with less reducing agent.

Due to the strongly reduced NOx level in lean-burn operation, the use of EGR in methanol DDI CI is only useful for achieving NOx values below the level of current on road EU VI engines. Especially for stationary and high-speed applications in general, lean operation with a larger SCR catalyst might be the better option. The higher reducing agent consumption is compensated by a severe increase in efficiency due to the faster combustion, the improved gas properties and – at least for higher load operation – the positive scavenging pressures.

In Figure 18, a constant scavenging pressure of 500 mbar was applied for the boost pressure variation. In general, smoke is absent from the exhaust. For rel. air/fuel ratios (AFRs) of 2 (calibration value in EGR case) or leaner, both CO and HC emissions are near zero. Brake Specific NOx Emissions (BSNOx) are mostly constant at 9 g/kWh and only rising slightly with the increasing oxygen concentration due to the faster burn. The exhaust gas temperature is significantly reduced by at least 100 K compared to the diesel application with EGR partially due to the lower backpressure. The turbocharger must be adapted for such an application. The benefit of this calibration of course shows in the gain of efficiency of up to 3 %-points, elevating

the effective efficiency to 49 % compared to 46 % of current state-of-the-art diesel engines of similar size.

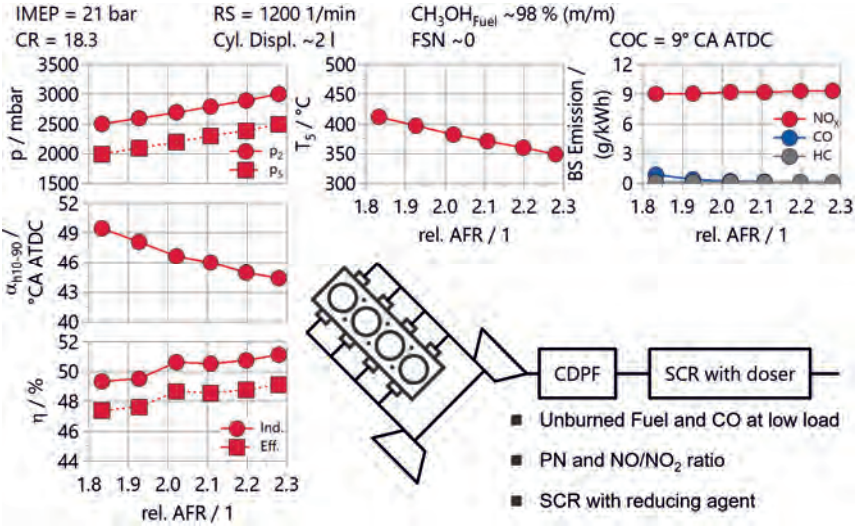

Fig. 18: Boost pressure variation for methanol DDI CI [6]

Drop-In Diesel Fuels

Because the climate goals must be implemented quickly also with the existing vehicle fleet and infrastructure, there is no alternative to fuels that are very similar to conventional fossil diesel fuel in terms of their chemical and physical properties. A good indication for a backwards compatibility is the fulfilment of current fuel standards, such as EN 590 and EN 15940.

Fuels that best meet these standards are typically paraffinic fuels such as Hydrogenated Vegetable Oils (HVO) and, e.g., Fischer-Tropsch Gas-to-Liquid (GtL) fuels. However, due to absence of aromatic components these fuels typically do not have a sufficient density to fully comply with the EN590 diesel standard. A countermeasure is the blending with high-density components like long-chain alcohols. These components typically also reduce soot emissions and raise the density of the blend towards the required 800 kg/m³. [7]

FEV Europe is investigating the medium-chain alcohol 1-octanol as a possible energy source for commercial vehicle applications within the joint research project “Closed Carbon Cycle Mobility – Climate-neutral Fuels for the Traffic of the Future”. Due to its properties, high blending rates are possible without violating the fuel standard EN 590. A diesel/1-octanol blend

with 30 vol% of 1-octanol was selected for experimental investigations. This blend largely complies with the EN 590 standard, with a slightly reduced cetane number of 48.3.

Figure 19 shows the results of Real Driving Emission (RDE) measurements with a Portable Emission Measurement System (PEMS). The test vehicle was a Mercedes-Benz Actros 1843 heavy-duty truck. For the same payload, the diesel/1-octanol fuel blend enables a soot emission reduction of 33% and a NOx emission reduction of 13% at constant HC and CO emissions without adjustment of the vehicle hard- or software.

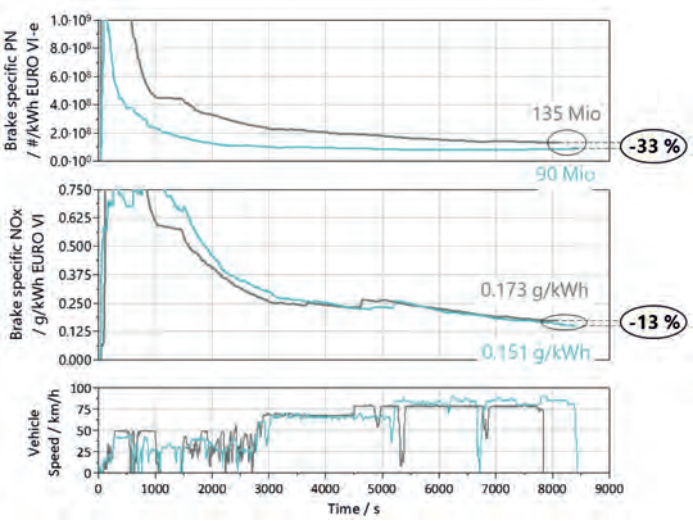

Fig. 19: PEMS results of RDE tests with an EU VI Mercedes-Benz Actros 1843 comparing operation with diesel and a diesel/1-Octanol blend [8]

Summary

To achieve a rapid reduction of the CO2 emissions from the transport sector, the application of all suitable technology options is needed. In the short-term, these are primarily powertrain and vehicle optimizations, including electrification.

The challenging targets set by legislation to reduce CO2 emissions require zero CO2 emission trucks (“tank-to-wheel”) to be brought into the market as well, since significant penalties will be applied to OEMs in case of non-compliance with these targets. The technologies in discussion are battery-electric propulsion (BEV), fuel cells (FC) and hydrogen combustion engines (H2-ICE), with each technology having its specific benefits and drawbacks. Based on the specific

use case and the assumed boundary conditions, with a special focus on the total cost of ownership (TCO), different powertrains can be advantageous.

Promising engine testing results with hydrogen-specific hardware optimizations show that hydrogen engine operation allows achieving similar loads as the Diesel base engine while being able to manage the critical NOx-emissions. Further potential for optimization is given by combining the benefits of PFI- and DI-combustion, with the target to continuously improving efficiency as well as the transient behavior. For methanol as a possible liquid renewable fuel, even lower pollutant emission and higher efficiencies compared to conventional Diesel operation are possible.

Today, the realization of electric mobility and the use of hydrogen, which will certainly make a major contribution to reducing CO2 fleet emissions, are strongly favored over alternative technologies by the current “tank-to-wheel” accounting, where the use of de-fossilized e-fuels and biofuels has been left out of the current CO2 legislation. Still, to achieve the long-term goal of CO2-neutral transport, a contribution of non-fossil energy carriers (e.g., methanol or FT-fuels) is required as well. A revised legislation that credits all CO2 mitigation technologies, including synthetic fuels, should have a high priority to accelerate CO2 emission reduction most efficiently.

[1] FEV Consulting: Low Carbon Pathways until 2030 – Deep Dive on Heavy-Duty Transportation, https://www.concawe.eu/wp-content/uploads/Low-Carbon-Pathways-Until-2050-Deep-Dive-on-Heavy-Duty-Transportation-Final-Report.pdf

[2] Van der Put, D., et al.: Efficient Commercial Powertrains – How to Achieve a 30% GHG Reduction in 2030, In: Proceedings of the FISITA 2020 World Congress, Prague, 14 – 18 September 2020

[3] Gbologah, F. E., Li, H., & Rodgers, M. O.: Demonstrating an Empirical Tool to Predict FleetWide Heavy-Duty Vehicle Fuel-Saving Benefits from Low Rolling Resistance Tires. Transportation Research Record, 0361198119838269(2019)

[4] Alt, N: It's not the combustion engine that's the problem, but the fossil fuel, In: MTZ Worldw 81, 22–25 (2020). https://doi.org/10.1007/s38313-020-0196-8

[5] Güdden, A., et. al.: Methanol and Hydrogen – CO2 Neutral Synthetic Fuels for Heavy Duty and Large Bore Applications, In: 29th Aachen Colloquium Sustainable Mobility 2020, Aachen, 5-7 October 2020

[6] Güdden, A., et. al.: Green Methanol – A CO2 Neutral Energy Carrier Enabling 50+% Engine Efficiency with Ultra-Low Pollutant Emissions, In: 42nd International Vienna Motor Symposium 2021, Vienne, 29-30 April 2021

[7] Heuser, B., Schernus, C., Alt, N. et al: Kohlenstoffneutraler Transport - die Rolle synthetischer Kraftstoffe, In: ATZ Extra 24, 34–37 (2019). https://doi.org/10.1007/s35778-019-0067-6

[8] Pischinger, S. et al.: Future Perspectives of the Internal Combustion Engine, SAE International Powertrains, Fuels and Lubricants, 22 September 2020, Krakow

ENTWICKLUNGSTRENDS HIN ZU CO2-NEUTRALEN ANTRIEBSSTRÄNGEN FÜR HD-ANWENDUNGEN

- Kurzfristig wird die CO2-Reduktion durch Optimierungen von Antriebsstrang und Fahrzeug, einschließlich Elektrifizierungsmaßnahmen, vorangetrieben.
- Die Ziele der Gesetzgebung zur weiteren CO2-Reduktion erfordern CO2-freie Fahrzeuge ("tank-to-wheel") wie batterieelektrische Antriebe (BEV), Brennstoffzellen (FC) und Wasserstoff-Motoren (H2-ICE). Je nach spezifischem Anwendungsfall und angenommenen Randbedingungen sind unterschiedliche Antriebsoptionen vorteilhaft.
- Um langfristig eine CO2-Neutralität zu erreichen, ist ein Beitrag von nicht-fossilen Energieträgern erforderlich, was eine überarbeitete Gesetzgebung erfordert. Motorentestergebnisse mit möglichen E-Fuels (z.B. Wasserstoff und Methanol) zeigen erhebliches Potenzial für höhere Wirkungsgrade und eine weitere Schadstoffreduzierung.

DEVELOPMENT TRENDS TOWARDS CO2-NEUTRAL POWERTRAINS FOR HD APPLICATIONS

- In the short-term, a reduction of the CO2 emissions is driven by powertrain and vehicle optimizations, including electrification.
- The challenging targets set by legislation for CO2-reduction require zero CO2 emission trucks (“tank-to-wheel”) such as battery-electric propulsion (BEV), fuel cells (FC) and hydrogen combustion engines (H2-ICE). Based on the specific use case and the assumed boundary conditions, different powertrain options are advantageous.
- To achieve the long-term goal of CO2-neutral transport, a contribution of non-fossil energy carriers is needed and requires a revised legislation. Engine testing results with renewable e-fuel candidates (e.g. hydrogen or methanol) show significant potential for increased efficiencies and pollutant reduction

The outlook for E-Trucks

Adam Panayi, RhoMotion, London, United Kingdom

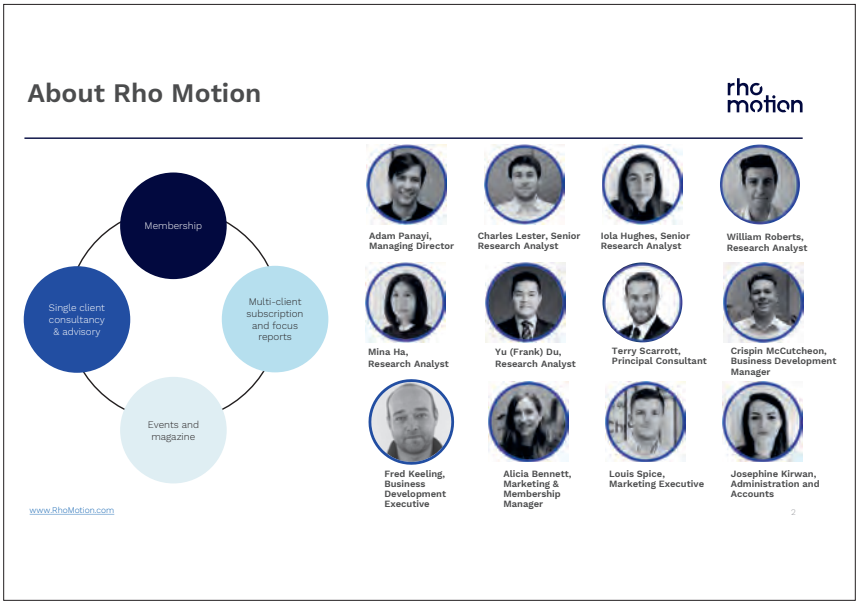

Our suite of regular reports and data provide detail and context with long-term outlooks

rho motion

Monthly Assessments & Databases

Quarterly Outlooks

Focus Reports

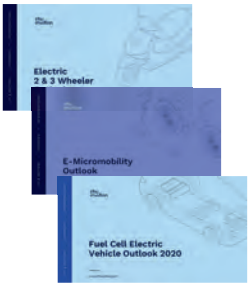

www.RhoMotion.com

OEM strategy analysis: Truck Developments

rho motion

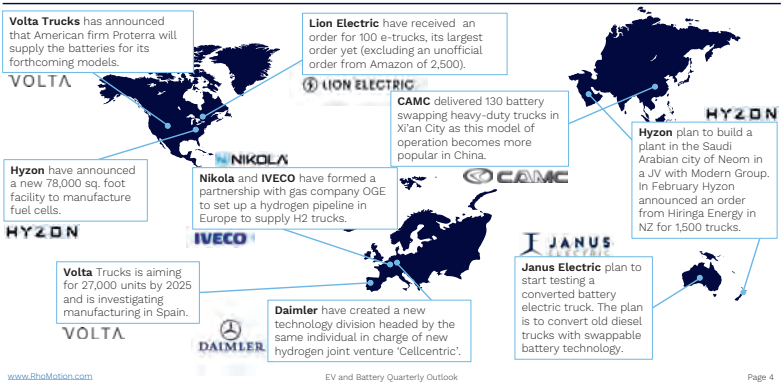

www.RhoMotion.com EV and Battery Quarterly Outlook Page 4

OEM strategy analysis: Heavy-duty EVs

Roadmap to commercialisation of electric heavy-duty trucks

- Many majors OEMs are looking at alternative fuel sources for its fleet of heavy-duty vehicles. We use these charts to illustration the position many of these OEMs are at, and the road to commercialisation as well as technology direction.

OEM strategy analysis: Heavy-duty EVs

Major heavy-duty OEMs and electrification targets

Heavy-duty sales
2019:-
2020: 66,899

2025
10% of total vehicles sold to be electric in Europe

2030
50% of total vehicles to be electric in Europe by 2030

Heavy-duty sales
2019:-
2020:-

Heavy-duty sales
2019:-
2020: 140,652

2030
>35% electric sales

Heavy-duty sales
2019: 275,239
2020: 376,389

Heavy-duty sales
2019: 240,618
2020: 310,916

2025
1 million EV sales – PV and HD combined sales

Key developments

- Investment into battery assembly plant, with construction beginning in 2021, and the plant running in 2023. The cells will be delivered from Northvolt's battery facility.
- Operates Daimler eActros. Also, Freighliner models.
- Under Volvo Trucks, UD, Mack, Renault Trucks. Owns 45% of Dongfeng trucks.
- So far, FAW does not have a clear electrification plan. Their first passenger EV factory will be completed in 2022. There is no news from HD branch.
- Dongfeng Group has announced its three "million" plans – 1 million PV sales, 1 million commercial vehicle sales, and 1 million EV sales (PV + commercial)
- On the following slide, we outline the major heavy-duty vehicles that have been released, or expected to be released in the next few years.

OEM strategy analysis: Heavy-duty EVs

Heavy-duty BEV models, current and planned releases, pack size and range

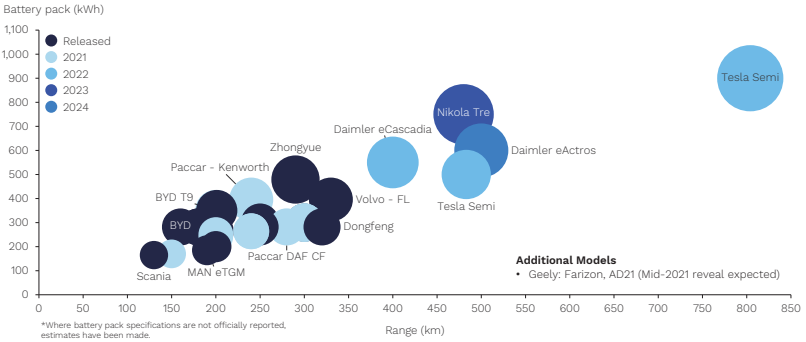

*Where battery pack specifications are not officially reported, estimates have been made.

OEM strategy analysis: Electric heavy-duty vehicles

- Over the past 6 months, there have been over 100 MIIT applications for electric heavy-duty vehicles in China

Chinese MIIT application for heavy-duty (>16t) electric vehicles, last 6 months

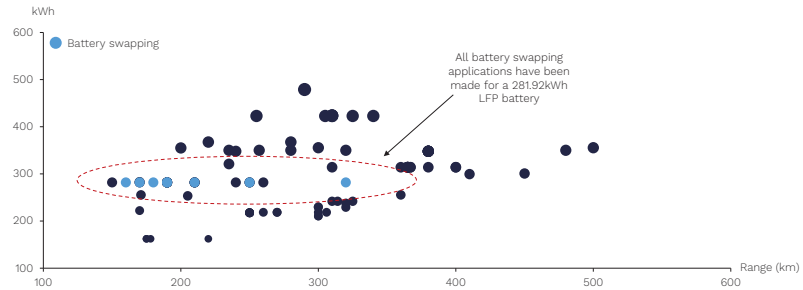

Electrification of heavy commercial vehicles from the perspective of a bodybuilder

B.Sc. **Nico Mueller**,
Liebherr-Mischtechnik GmbH, Bad Schussenried

Abstract:
A truck mixer is stationary for about 1/3 of its working day. During this time, however, the drum must rotate and therefore the truck's engine must be running. A truck diesel engine with power take-off needs about 4-6 liters per hour when idling and hence not exactly less.
With an electric motor and a battery as energy source, the drum can rotate self-sufficiently. Likewise, the diesel engine of the truck can remain switched off and a fuel saving of up to 30% can be achieved. The saving of up to 30% also applies analogously to the CO2 pollution and a significant noise reduction is achieved by the electric drive.
What exactly can this system look like and where are the advantages in detail.

New interface of the "e-PTO" instead of the previous mechanical power take-off: standardization and performance specification

A PTO (power take-off) or the so-called mechanical power take-off is a switchable mechanical drive source. It is usually available as a secondary output of a transmission. The PTO is mainly found in the commercial vehicle segment, especially in trucks. Power is usually transmitted via a cardan shaft, but a distinction must be made between direct and indirect drive.
Direct drive in the case of PTO is used when equipment is to be driven while the vehicle is stationary; this is possible by actuating it with the accelerator pedal or a hand throttle. The speed of the engine, and the PTO speed, controls the PTO in this case. In the case of indirect drives, which is now the standard for trucks and commercial vehicles, this is usually achieved by means of a hydraulic pump. The hydraulic pump supplies smaller oil motors or lifting cylinders with energy via hose lines. This technology is also used in our hydraulic truck mixers.
The type of PTO can also be differentiated - engine PTO, transmission PTO or directional PTO are the most common forms.
The engine PTO is connected directly to the engine via a separate clutch or double clutch. It runs at a standard speed only as a function of the engine speed.

The geared PTO is connected to the engine via the traction clutch and a gearbox. The nominal speeds here are standardized and, via the appropriate gear ratio, the standard speeds can be achieved in the range of the nominal engine speed.
The directional power take-off is also common, here the torque is taken off via the travel gear. The speed and often also the direction of rotation is dependent on the selected gear and the speed.
In the case of truck mixers in particular, the clutch-independent power take-off plays a major role: Here, too, there are different variants that can be installed regardless of the type of vehicle driveline. Each variant can be used when the vehicle is at a standstill, but also while driving, which is also the advantage of this type of power take-off - the power take-off can be controlled or switched on and off from the outside. For this reason, a clutch-independent system is also the only variant that can be considered for a truck mixer, since the power take-off must be permanently available.
There are also differences between manual and automatic transmissions. In manual transmissions, the drive takes place via the flywheel of the engine. Speed and power are controlled exclusively by the engine. The power take-offs are equipped with an electropneumatic or hydraulic engagement system consisting of a multi-plate clutch.
In automatic transmissions, the system is driven by the engine flywheel via the torque converter housing. With the help of a sturdy gear wheel, the driving force is transmitted to the power take-off. The power take-off can be engaged via an electric or hydraulic system, even while the vehicle is moving.
In general, it can be stated that the power take-off of a truck mixer is always independent of the clutch and works differently for automatic and manual transmissions. Likewise, the system depends on the power requirement as well as on the different power stages: One stage for turning the drum while driving and the other for filling or emptying the drum. Typical power requirements for rotating the drum while driving is 15 - 20 kW. Much higher power is required for drum emptying, between 40 and 70 kW are needed here. However, the power is only required over a short period of time.
In summary, it can be said that clutch-independent power take-offs are generally used in a truck mixer, as the hydraulic system must also operate while the truck is in motion.

An ePTO (electric power take-off), or electric power take-off, consists of an inverter and an electric motor powered by a DC source such as a battery.
This setup of the aforementioned components creates a self-sufficient system, which means that the truck's engine does not have to operate at idle, but the auxiliary units can still work.

In practice, two alternatives are available for recharging the battery:

Alternative 1: Rechargeable battery.
With the help of a rechargeable battery and a certain battery capacity, a full working day can be managed. Recharging is done during the night.

Alternative 2: Generator-powered battery
In this variant, the battery is charged by a generator directly while the vehicle is in motion and can therefore be sufficient for the entire day, depending on the capacity and power requirements that are tapped.

In conventional drives, PTO systems or the PTO drive shaft belong to the combustion engine or the transmission. Therefore, the engine must be idling for the mixing drum to start up. This results in exhaust emissions that are approximately two times higher than those from an engine that is in motion. The exhaust emissions release pollutants such as carbon monoxide, nitrogen oxide and particulate matter into the atmosphere.
The ePTO system, on the other hand, makes the vehicle more environmentally friendly and is the first step toward hybrid and/or all-electric drives, ensuring that work can be done in the best yield zone with higher efficiency and lower fuel consumption. In order to have the truck mixer's auxiliary systems powered, the vehicle must be equipped with an additional power supply. Often this is connected directly to the hydraulic pump, this creates a transmission of mechanical power to any part of the vehicle where a hydraulic motor or cylinder converts the power into rotary or linear motion.

How does the ePTO work on truck mixers and what other benefits does the system provide?
The ePTO system is put under enormous strain in truck mixers because it requires a continuous and relatively high torque demand on the entire ePTO duty cycle in order to mix the cement or concrete mix even while driving. Duty cycle is an expression of the percentage of maximum power at which pulse width modulation (PWM) drives a load. The pulse frequency is the frequency that can be calculated from the edges of the PMW. A PWM is used, for example, in vehicles with electric drives.

The truck mixer passes through a total of three phases:

1) Mixing and drawing the concrete into the drum.
2) Traveling to the construction site and the drum rotating in the process.
3) The spreading of the concrete on the construction site.

In order to rotate the drum of the truck mixer, a direct connection between the transmission and the ePTO system is provided, so that the hydraulic circuit is completely eliminated. The truck mixer can also be operated here, even if the engine is switched off. This is now done by the battery-powered ePTO systems, by charging the battery with a mains connection or with the help of a generator.

The aim of this system, as already mentioned, is a significant reduction in fuel consumption, but there is also a significant reduction in noise, which has enormous advantages. Construction site noise is reduced and the so-called noise emission, which is becoming more and more important, decreases. The reduction in noise emission increases the safety of the operating personnel, as clearer communication is possible on the construction sites. Construction sites in urban areas could be completed more quickly, as noise limits may not be exceeded and therefore residents are not affected or are not affected as much.

Standardization and performance specification ePTO

Standardization or a general performance specification is not yet the case, but this should be a goal in any case. Standardization enables body manufacturers to offer more cost-effective systems and keeps development costs within limits. Also, the performance of the systems is still divergent, depending on the manufacturer and the components used.

Analysis of continuous and peak power at the power take-off

The continuous and peak powers at the power take-off are very divergent, depending on the size of the truck mixer, payload and the class of concrete transported.

Continuous powers at a standard load spectrum are also very divergent from each other depending on the working step of the truck mixer.

However, the following power ranges can be approximated for the drum:

- Loading operation 20 - 55 kW
- Travel to construction site 3 - 10 kW
- Mixing at the construction site 20 - 55 kW
- Unloading 15 - 30 kW

Different ways to access the traction battery: application of a dc-dc converter in terms of costs and performance

Access to the traction battery of the vehicle is basically possible if the vehicle has a battery, i.e. as soon as the vehicle itself has also been electrified. If the battery is then suitably powerful,

access to the traction battery can eliminate the need for a further battery for the superstructure. The DC/DC converter is needed when the available system voltage does not match the supply of the existing electrical or electronic components. A DC/DC converter is in fact a so-called voltage converter or electrical converter, which are capable of converting DC voltages. For this reason, they are also called DC voltage converters or DC/DC converters or DC/DC converters. There are many suppliers in the field of voltage converters, but many are not suitable or too expensive for use in the construction segment. One of the reasons for this is that the technology is not yet fully developed and is still in the development phase. In the course of this development phase, however, the costs for the aforementioned voltage converters will certainly drop and the components will become even more powerful.

Prediction for the service lives of drive-train units by model-based development with the measured operational conditions

M.Eng., **Kenji Seno**, Hino Motors Limited, Tokyo, Japan

Abstract

In the development of drive-train units in commercial vehicles, it is of significant importance to accurately predict the service lives of the mechanical components in order to determine the design in the early stage of the development. The aim of this study is to accurately predict the service lives of the mechanical components by elaborating an evaluation method called model-based development in which operational conditions measured in real vehicles and simulation. Through this study the validity of the model-based development was confirmed and the service lives of the mechanical components were accurately predicted under several operational conditions.

Reliability evaluation of transmission gears

Calculation of a reliability target in the early stage of the development allows to accurately design transmission gears depending on requirements for each country. Fig.1 shows a procedure of the reliability evaluation for the transmission gears. Firstly, the operational torque data are measured with actual vehicles on the site where actually used at. Next, the service lives are calculated with the torque data and S-N curve applying Miner's rule. It is difficult to evaluate for worldwide vehicles due to the necessity of measuring actual torque data.

Fig. 2 shows a procedure of the model-based development examined in this study. Firstly, the operational conditions of the vehicles, such as road condition from a satellite navigation system or vehicle speed, are measured on the real vehicles. Next, the simulations with the selected driver, mechanical components, power-train units and vehicle models are run with the measured operational conditions. Then, by running the simulation, the corresponding torque data are obtained and analysed. Finally, the service lives of the mechanical components are calculated with the simulated torque data to determine the design.

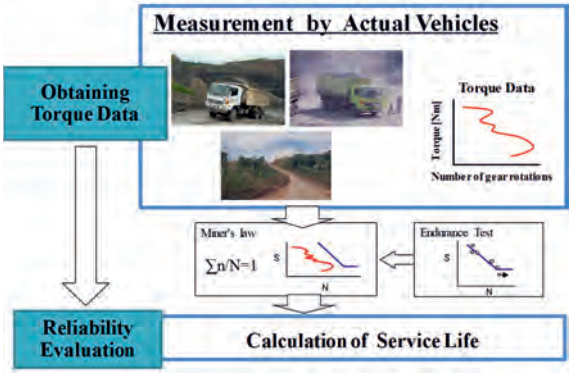

Fig. 1: Conventional development process

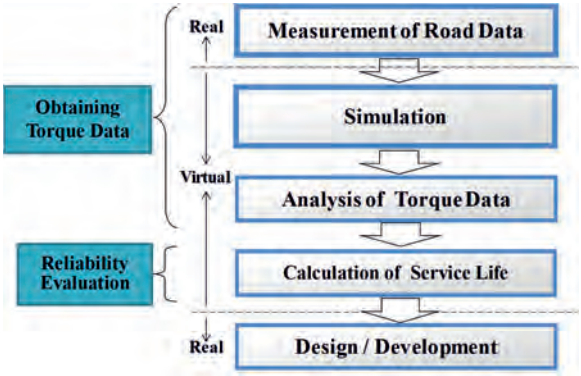

Fig. 2: Process with model-based development

Correcting of the operational condition data

A data recording system called TDAS was used to obtain the operational condition data efficiently in each of the vehicle destinations. Fig. 3 shows the data logging terminal and Fig. 4 shows the automatically recording system. The operational condition data were measured by using a data logging terminal which was installed on the vehicles and connected with the Controller Area Network (CAN) and a satellite navigation unit of the vehicles. The terminal has a communication module to send the measured data to a data server automatically.

Fig. 3: Online data recording terminal

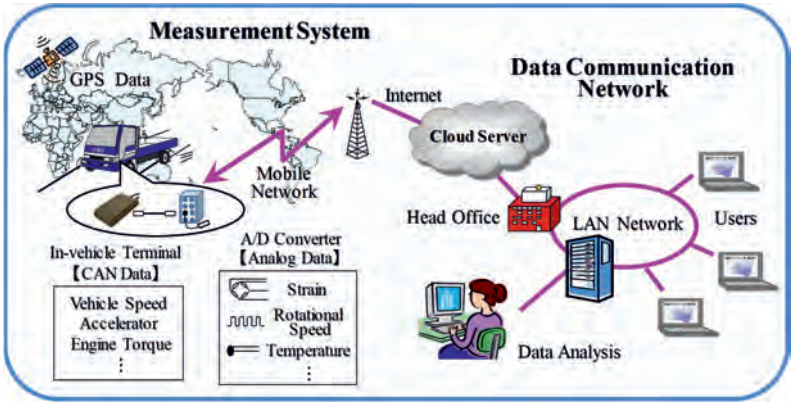

Fig. 4: Online data recording system

Simulation system

Fig. 5 shows a schematic of the simulation system. it consists of test scenario model, controller model, network model, plant model. the test scenario model contains a driver and a road model, and the plant model has a vehicle and an engine model. Fig. 6 shows a flowchart of the simulation. Firstly, the road model was built by using the collected operational data in each destination. Then, the built driver model was run so that the vehicle speed corresponded with a target vehicle speed that was provided by a set road model. The driver model selected appropriate operations such as, controlling the engine throttle, shifting the transmission gears

or braking, depending on the given road situations. The corresponding torques generated by the engine model were inputted into the drive-train unit models (e.g. transmission or final gear), and accordingly the vehicle model was run. Automated Manual Transmission (AMT) can be evaluated by connecting an actual software of AMT as controller model. It is possible to evaluate the software as well as the reliability of the components with this simulation system.

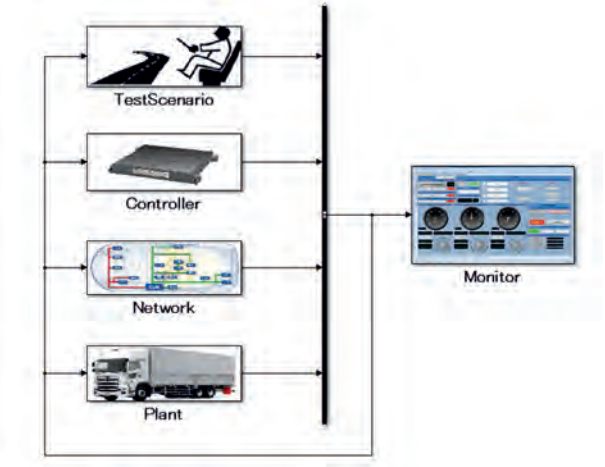

Fig. 5: Simulation system

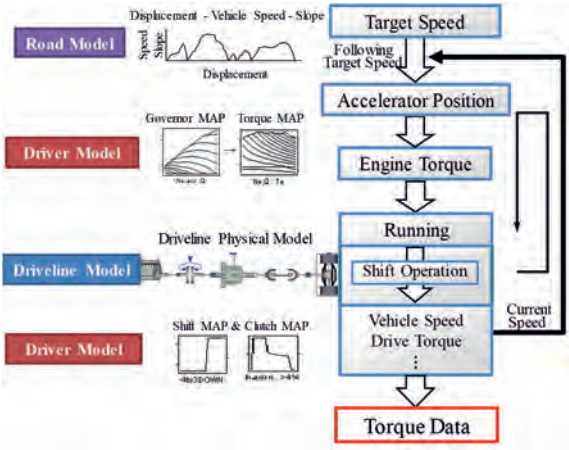

Fig. 6: Simulation process

Prediction for the service lives of transmission gears

A result of the conducted simulations is presented in Fig.7. It can be seen that the vehicle model was driven following the measured vehicle speed, and the simulated torques on the propeller shaft corresponded well with the measured data. The agreement between the simulated vibration and the measured vibration was not great, which could have been caused by the difference of the operations by the driver model and the actual driver. The driver's operations were similar to each other as shown in Fig 8, but these were not in good agreement. It is possible to regulate parameters in driver model for the good agreement, but it is just an adjustment for the specific data measured with the specific driver. The driver model has been adjusted to work as an average driver on the site.

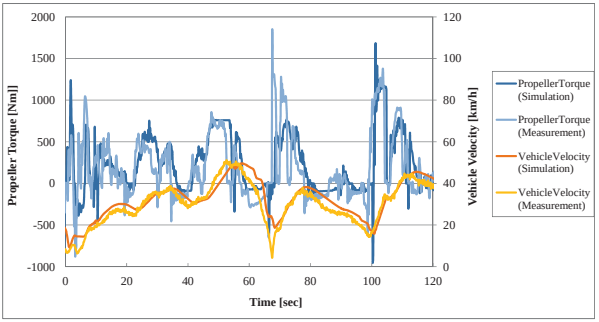

Fig. 7: Result of simulation

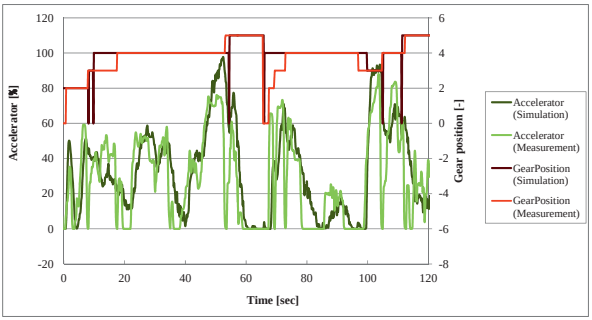

Fig. 8: Comparison of driver's operation

Fig.9 shows torque data of the gear simulated with operational data which measured in Japan, Thai, Ecuador, Australia on the simulation conditions in Table 1. It shows torque at a gear in the transmission when vehicles in which a new transmission under development was installed run in the four countries. Each torque data was different due to differences in operational data, and these shows the feature of usage in each country. These torque data allow to predict for the service lives and calculate reliability targets considering usage of vehicles in each country.

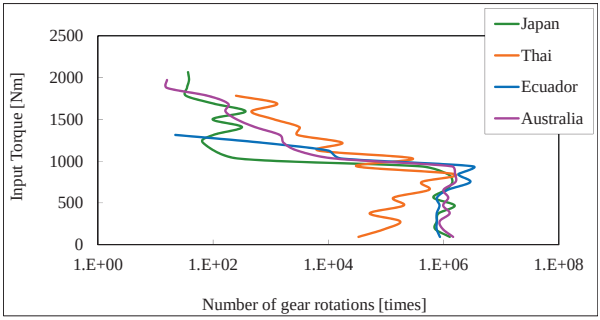

Fig. 9: Torque data of the gear

Table 1: Conditions for Simulation

	Japan	Thai	Ecuador	Australia
Vehicle Type	Cargo	Dump	Bus	Cargo
Gross Vehicle Weight [kg]	20,000	26,000	15,000	15,000
Engine Torque [Nm]	794	794	745	794
Differential Gear Ratio [-]	4.333	6.428	4.625	4.875
Transmission Series	New 6-Speed Transmisssion			

Conclusion

The evaluation method using the model-based development for drive-train units was established, and it allows reliability evaluation of the mechanical components efficiently with simulated torque data. The service lives of the mechanical components were accurately predicted under several operational conditions collected by using TDAS for each of the worldwide vehicle destinations. The prediction for the service lives of the transmission gears were described as an example in this paper. The reliability for the components of drive-train units (e.g. clutch, differential gear and shafts) and also the software of AMT can be evaluated with the model-based development.

Sustainable drivetrain architecture for hybrid and electric trucks

Modular drivetrain architecture for hybrid and electric medium- and heavy-duty trucks, bridging the gap between AMT, torque converter automatics and EVs

M.Sc. **Geir Brudeli**, Dr **Bård Vestgård**, **Sven Bjørkgård**, **Lasse Bjørkhaug**, Brudeli Green Mobility AS, Hokksund, Norway

Abstract

Brudeli Green Mobility (BGM) is disclosing a novel concept for a hybrid drivetrain in which increased fuel saving and reduced Total Cost of Ownership (TCO) is combined through a modular and scalable approach, maximising the hybrid functionalities including powershift. The technology is targeting Heavy Duty (HD) truck Automated Manual Transmissions (AMT) through an add-on module. The technology supports a roadmap – as presented herein – which is modularized and scalable toward the majority of plug-in electric driving. By following the roadmap and using the BGM hybrid layout, a TCO lower than for conventional diesel is estimated. Furthermore, in Generation 3 of the BGM roadmap, a hybrid vehicle which is cost-neutral versus a diesel engine and AMT drivetrain is within reach – while supporting the emission regulations like (EU) 2019/1242 and similar CO2 regulations in other markets.

1 Introduction

Looking at drivelines of truck fleets globally, present and announced, there are various solutions attempting to cover the range of user needs: AMTs for long distance driving, torque converter automatics with more comfortable gear shifting for city buses and refuse collection vehicles, and BEV (Battery Electric Vehicle) or FCEV (Fuel Cell Electric Vehicle) – although still at high cost. The BGM modular hybrid aims at making a scalable, affordable, and fuel-efficient driveline that can bridge the gap between the mentioned drivelines, while offering a path to zero emission with manageable investment cost.

As the comparative cost and use scenarios for various energy carriers – diesel, biogas, hydrogen or electricity – differs between markets, some markets will be quicker to adopt fully electric trucks, while others will take longer to reach full electrification. The first is obviously valid for electric city buses, but even for some regional operations fully electric trucks will

become commercially competitive and reach a significant share of the market. However, the aim of this paper is to discuss solutions that can provide a scalable degree of electrification to suit the wider global transportation needs while meeting both TCO and environmental targets.

2 The BGM hybrid system

The BGM system can be used with most stepped transmission technologies, both planetary gear and standard AMT. Figure 1 shows an example of the system interfacing an AMT.

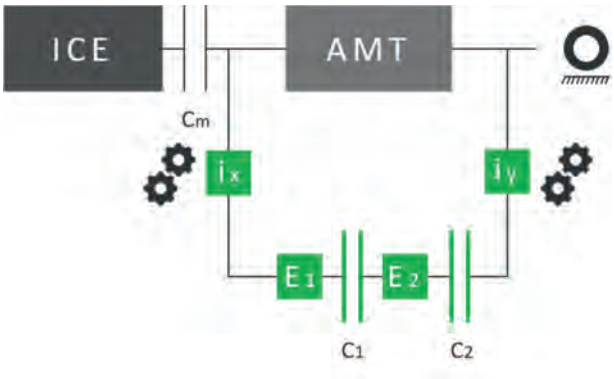

Fig. 1: The BGM parallel-serial hybrid system. Main components in green.

The electric motor E_1 is connected to the input shaft of the AMT via a gear ratio i_X to increase the speed and reduce the size of the motor and clutch C_1. The electric motor E_2 is either connected to the input shaft via C_1 and i_X or to the output shaft via C_2 and i_Y. Thus, the system is capable of parallel hybrid operation using one or both e-machines in generator or motor modes, or serial hybrid operation keeping C_1 open and using E_1 in generator mode and E_2 in generator or motor mode.

The benchmark for hybrid systems in the HD truck market today is the P2, with the electric rotor fixed coaxially to the input shaft of the AMT transmission. Although present in the market for many years, it has not reached a high market penetration; we will here point to some reasons why, and we will offer an alternative solution to improve the overall business case for hybrids. Firstly, due to the low rpm of such motors, size and cost become significant. Secondly, although many features can be realized with such a system (Figure 2) certain functionalities

cannot be fully utilized, such as powershift, continuous brake assist and ICE efficiency improvement through serial hybrid operation.

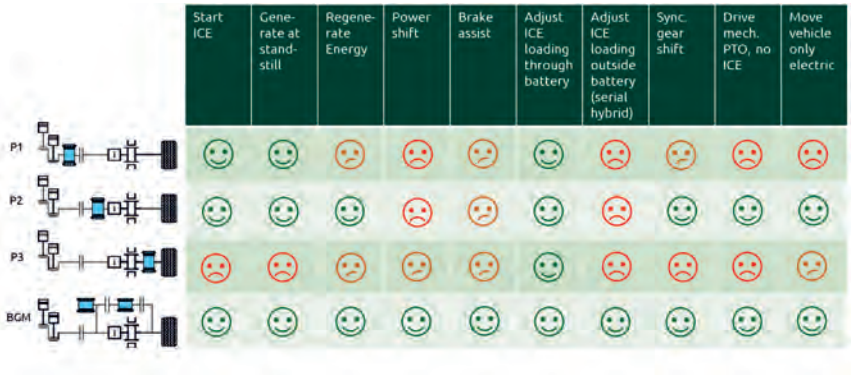

Fig. 2: Functionalities of existing hybrid solutions and BGM proposal.

The BGM system aims to fulfil all functional requirements for a hybrid system while optimizing the total cost of the driveline.

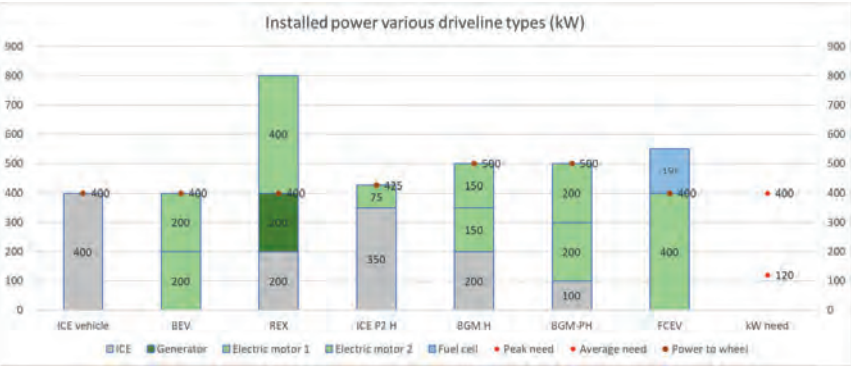

Fig. 3: Installed power of various driveline configurations, including BGM proposal

Figure 3 shows the total installed kW power in various drivelines. It is customary to think of a serial hybrid as a range extender (REX) but as Figure 3 indicates, the installed power and cost is high. The BGM parallel-serial hybrid, on the on the other hand, utilizes all installed power for traction.

3 Characteristics of the BGM hybrid system

Compared to the P2 hybrid, the BGM hybrid system offers several advantages, of which the most important are:

- Fuel saving through serial hybrid operation
- Powershift for both fuel optimization and driver comfort
- Geared motors and clutches for reduced weight and packaging flexibility

3.1 Serial hybrid operation

Serial hybrid operation provides increased flexibility toward maintaining efficiency high in situations where the required positive torque from the ICE is low. Figure 4 shows a typical efficiency map where the efficiency of the ICE can be improved significantly in the low torque region by reducing ICE rpm.

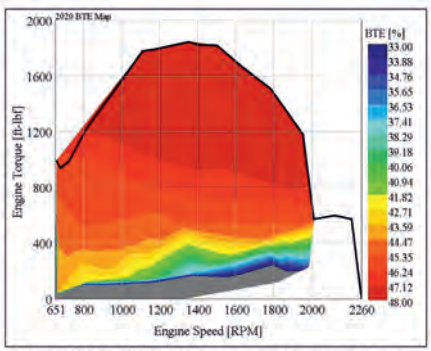

Fig. 4: ICE efficiency map from “Heavy-Duty Vehicle Diesel Engine Efficiency Evaluation and Energy Audit“ [1]

This can be exploited by the serial hybrid in several ways. One example is driving almost flat downhill (false flat) in a 1-2% slope. This is a driving situation that occurs quite commonly and is illustrated in Figure 5 with virtual overdrive gears 13 and 14, where ICE rpm is pulled down into a higher efficiency range and where generator E_1 is powering motor E_2 directly.

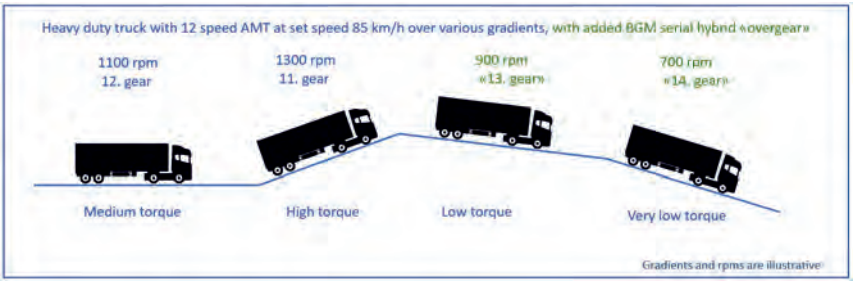

Fig. 5: Illustration of serial hybrid “overdrive” gears.

Another example is driving scenarios incorporating frequent cycling between fairly low positive and negative torque, and where frequent stop-start of the ICE is disruptive toward both efficiency and comfort. In such a case the serial operation provides a better alternative by maintaining the ICE rotating at low rpm with E_1 either charging the battery or feeding E_2 directly. Another positive effect that follows is fewer charging and discharging cycles of the battery, impacting battery specifications and cost, especially for batteries of 150 kWh capacity or less.

Figure 6 summarizes typical contributions to a P2 hybrid wheel torque from various sources as function of road gradient. The two brown lines “ICE eff. torque band upper” and “ICE eff. torque band lower” represent upper and lower limit for the high-efficiency area of the ICE.

The contribution by the ICE is typically not optimal on the flatter sections, depending on speed. The BGM system in contrast allows the ICE rpm to be modulated freely from vehicle speed.

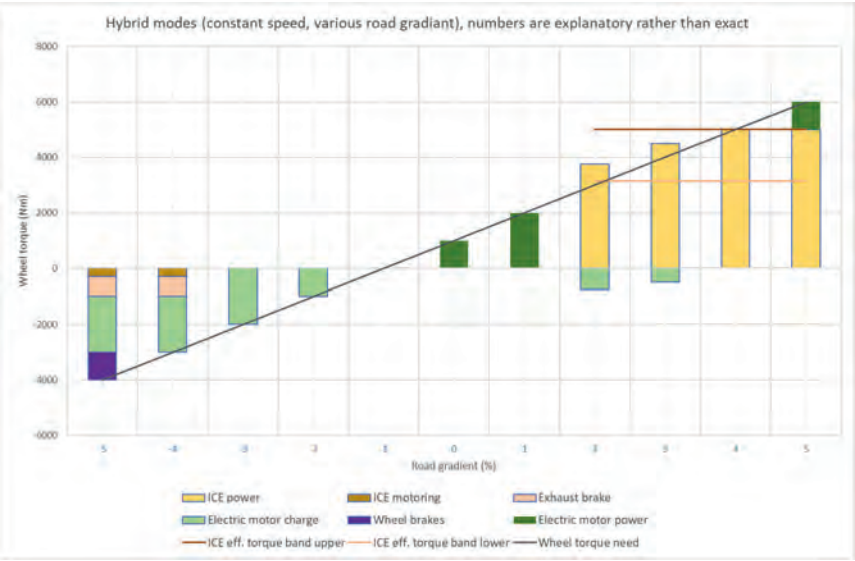

Fig. 6: P2 estimated contribution to torque by various sources versus road gradient.

3.2 Efficient powershift strategy

Avoiding full torque interruption during gear shifting gives increased acceleration, which in turn allows further downsizing of the ICE and motors. By fuel optimizing the important 11-12-11 shift strategy it is possible to have a lower rear axle gear ratio and thereby a lower rpm in the highest gear, and driveability is maintained through powershifting. The negative impact on creep manoeuvre at low speed is effectively compensated by electric tractive power. Eindhoven University estimates this effect could be typically 5% fuel saving [2].

The serial hybrid functionality is especially useful as parallel torque transfer path to providing powershift. More efficient powershift gives more opportunities to shift to the ideal gear (BGM estimates 1% fuel saving from this effect alone). Additionally, certain gearshifts can be avoided or delayed by utilizing both motors for maximum output torque. This is attractive in for example passing over a hill facing a significant loss of acceleration in case of a conventional AMT shift.

Below is a demonstration of three different powershift modes: Economy torque transfer, Comfort torque transfer, and maximum acceleration torque transfer.

Economy, Figure 7:

The normal situation would be that the ICE and both motors are driving the input shaft of the AMT. In electric mode, the main clutch would be open and ICE shut down. Strategy is

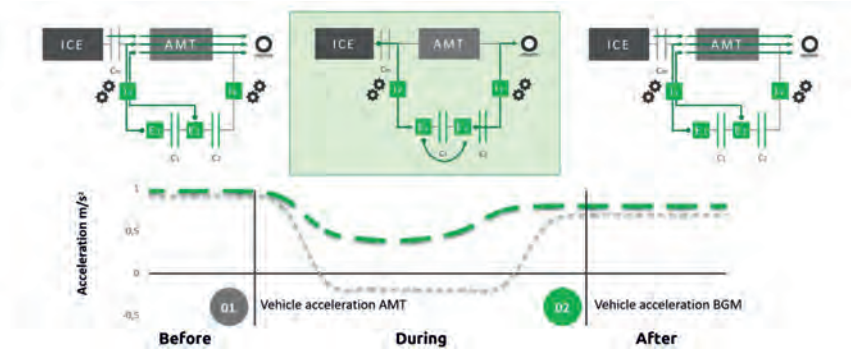

Fig. 7: Economy torque powershift mode.

- E_2 connect to output shaft, C_1 open.
- Establish zero torque at the input shaft by E_1 braking with same torque as main clutch. E_1 generates electricity transferred to E_2 and driven wheels. Serial hybrid.
- When zero torque is established, shift AMT gear.

Efficiency is improved by maintaining constant torque at ICE and minimized shift time. Serial hybrid is better than slipping clutches. This mode will be used for all low torque gearshift and nearly all higher gears; a significant contributor to efficiency.

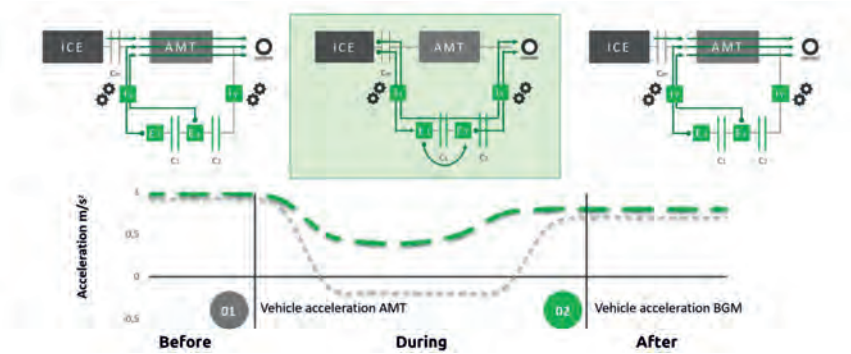

Fig. 8: Comfort torque powershift mode.

Comfort, Figure 8:

Low torque transfer identical to Economy. Medium torque transfer:

- E_2 connect to output shaft, C_1 slipping
- Establish zero torque at the input shaft. (E_1+C_1) divided by i_x is braking with same torque as the main clutch. E_1 generates electricity transferred to E_2 and C_1 transfers torque to the wheels. Serial hybrid + powershift clutch.
- When zero torque is established, shift AMT gear.
- Efficiency is improved by maintaining constant torque at the ICE and minimized shift time. Serial hybrid does a significant part of the powershift, better than slipping clutches.

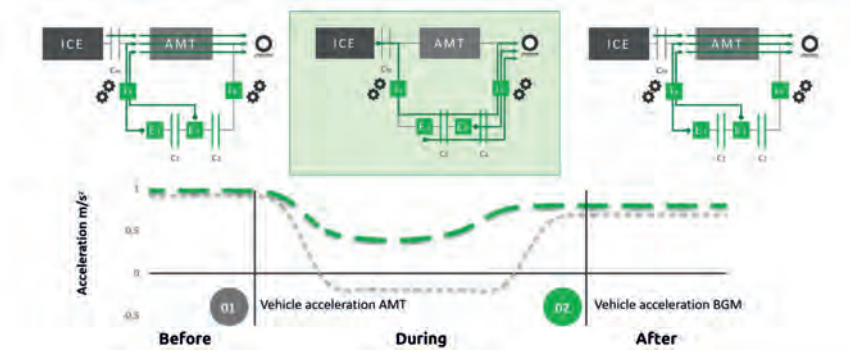

Fig. 9: Maximum acceleration torque powershift mode.

Maximum acceleration, Figure 9:

- E_2 connect to output shaft, C_1 slipping
- Establish zero torque at the input shaft by C_1 transfers all torque from ICE and E_1. (E_1+C_1) divided by i_x is braking with same torque as the main clutch. No serial hybrid.
- When zero torque is established, shift AMT gear.
- Efficiency is improved by maintaining constant torque at ICE and minimized shift time.

3.3 Packaging and interfacing

The following is an example applied to a generic 12-speed AMT HD truck transmission with two split gears, three main gears and two range gears. Our target is to:

- utilize existing interfaces and minimize modifications to the transmission,
- maximize functionality with less parts and complexity,
- replace engine and transmission auxiliaries where possible (ICE starter, lay shaft brake)
- Interface to the retarder gear and layshaft PTO (in this particular example)
- Modular design with similar packaging as retarder (e-machines ideally replace retarder function)

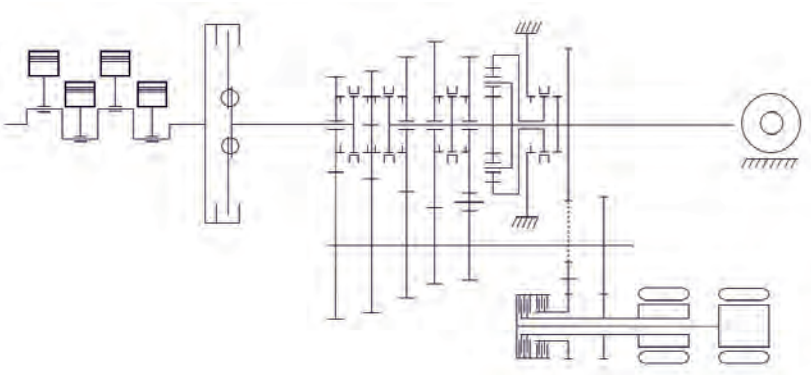

Fig. 10: Generic 12-speed AMT with BGM module schematic.

Fig.11: Generic 12-speed AMT with BGM module.

4 Roadmap for hybrid and electric truck transmissions modular architecture

As the price of batteries continues to drop, the share of electric driving on a given route should accordingly increase, reflecting the economy (payback on battery investment) and regulatory requirements. BGM believes the following roadmap fills an important gap, exemplifying a scalable pathway between diesel and all-electric trucks.

Key points for further development of hybrid drivetrains:

- Electric motors to increase in power [kW] output to cover more driving situations – leading to further downsizing of ICE power [kW] requirement.
- With a lower share of the driving being provided by the ICE, the need for gears will be reduced, i.e. the cost-optimal number of gears will be lower (for all-electric drivetrains typically 3-4 gears)
- ICE technology and various electrified drivetrains will exist in parallel, driving modularization to avoid market segments cannibalizing each other.

BGM believes Table 1 is a representative roadmap for hybridization of HD trucks.

Table 1: BGM roadmap for hybrid drivetrain development

BGM ROADMAP	GENERATION 1	GENERATION 2	GENERATION 3
Strategic position with product offer	Giving best fuelsaving	In markets where electricity is significantly cheap enough to balance battery investment within 3 years	DHP - Dedicated Hybrid Powertrain
% share of electric driving/operation	10-30%	30-70%	50-90%
			
ICE Engine	**15L/12L**	**6.7L**	**3.8L or 2.5L**
Std weight	1343kg/930kg	522kg	280kg/214kg
Weight saving on engine	413Kg (compared to 15L)	821kg (compared to 15L) 408kg (compared to 12L)	1063kg/1129kg (compared to 15L) 650kg/716kg (compared to 12L)
ICE Engine main function in the drivetrain	Primary source of propulsion		Adding range and giving fast payback on battery investment
Transmission	AMT	AMT cost optimized	Very cost optimized AMT layout or other DHT (Dedicated Hybrid Transmission)
Numbers of gears in transmission	12-speed	9-7 speed	7-3 speed
Component saving in transmission	Countershaft brake	1-2 gearsets, 1 shiftactuator	2-3 gearsets, 1-3 shiftactuators
Electric power	40-80kW, 48V	120-240kW	200-350kW
Added customer values			
Powershift (torquefill)	0%	Assumed 100%	Assumed 100%
Retarder functionality	0%	Assumed 100%	Assumed 100%
Electric PTO	Yes	Yes	Yes

Knowing that the e-motor has a lower cost per kW than typical ICEs and that the cost of a basic AMT transmission will reduce with reduced number of gears, a total drivetrain cost of Generation 3 on pair with a standard diesel AMT drivetrain should be within reach.

5 Total cost of ownership

We compared the cost of 3 variants of drivelines for a 400kW 4x2 tractor used for HD long haul truck in a European context.[1] Our study is trying to estimate TCO in 2025 by using the scenario for a medium level market penetration of the new technologies, including reduced cost level of batteries and related technology.

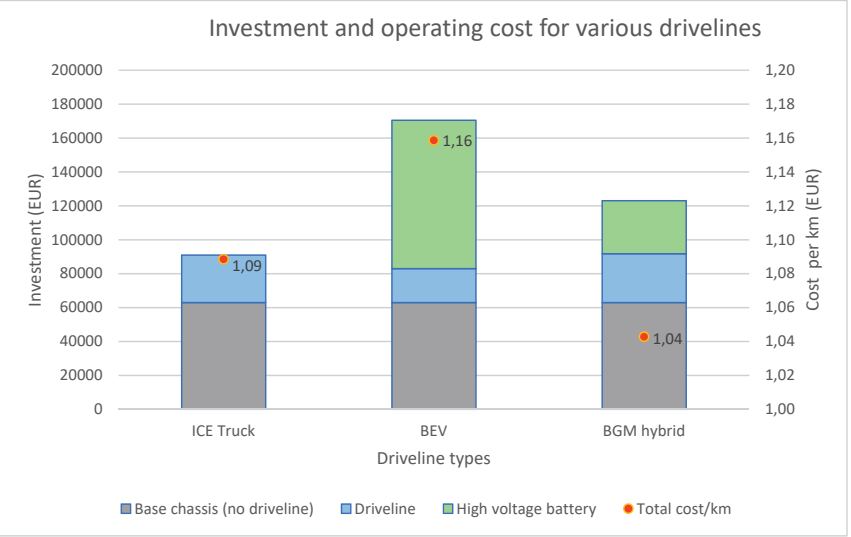

Fig. 12: Total cost of ownership. Vehicle investment on the left y-axis is made up from: base chassis which is same for all 3 variants, the driveline and the high voltage battery. On the right y-axis is the total cost to operate the vehicle, including depreciation, fuel, driver and other variable cost.

[1] Numbers partly taken from [3] “Fuel Cells Hydrogen Trucks” from Roland Berger, dated December 2020, and supplemented by additional cost figures generally valid in Europe and aligned for the given power level at 400kW combining the scenarios from “rather niche” and “rather mass”

As can be seen the upfront investment for a BEV is still rather high in 2025. With respect to operating cost difference is not so much higher than diesel anyway, due to lower fuel cost and maintenance.

However, to be able to realize such an efficient payback for BEV high investment many high-power charging stations and predictable routes are needed. Even so the study is showing 138 hours of “lost driving time” due to charging per annum; the vehicle is not running and earning money.

For the third variant, the BGM hybrid, the upfront investment is somewhat higher than a for a standard ICE diesel truck, but significantly lower than a BEV. The total operating cost is the lowest of all 3, while benefitting from a high degree of full electric driving.

6 Summary/conclusions

The proposed BGM concept and strategy offers a performance improvement and cost reduction compared to normally used P2 parallel hybrid in HD-trucks. The BGM integration allows an easy way of making a parallel-serial hybrid from existing AMT, obtaining key features like powershift functionality and improved fuel efficiency.

The BGM powershift hybrid can be packaged as a module that offers:

- Modular design with similar packaging as a retarder
- Minimal initial investment for the AMT manufacturer
- Replacement of the retarder

References

[1] P. Arvind Thiruvengadam, „Heavy-Duty Vehicle Diesel Engine Efficiency Evaluation and Energy Audit," West Virginia University, Morgantown, WV, 2014.

[2] M. M. J. Nievelstein, „Design of a Powershift Module," Eindhoven University of Technology, 2005.

[3] Roland Berger, „Fuel Cells Hydrogen Trucks, Heavy-Duty's High Performance Green Solution," 2020.

MAHLE 48V Battery for Truck applications

Dr. **Peter Geskes**, **Joachim Treier**, **Michael Moser**,
MAHLE Filtersysteme GmbH, Stuttgart

Summary

Mild hybrid drive systems for medium heavy-duty segments on a 48-volt basis are expected to achieve significant growth in the near future. The 48-volt architecture has a number of technical benefits e.g., electrification of auxiliaries, hoteling, boosting and recuperation power up to 40kW with an advantage of possible fuel consumption reduction up to 4.5% (MAHLE Motorway) depending on vehicle type and usage. For the battery itself a 48-volt architecture has cost- and package wise advantages in comparison to high-voltage applications. Their lower voltage, however, means that the expected currents are extremely high. MAHLE provides a modular 48-volt mild hybrid drive system including a 48V electric motor and a 48-volt battery pack. This pack ensures charging and discharging power of up to 40kW for 10 sec. MAHLE explains the concepts how to meet the increased requirements on battery pack and electric motor.

1 Introduction

The 48-volt system can bring considerable contribution to fuel savings and CO_2 reduction if energy can be stored in and retrieved from the battery in very short time. This is particularly necessary for vehicles used for freight, commercial, and specialized applications.

MAHLE is developing a modular 48-volt battery system that can significantly contribute to sustainable mobility. Hybridization makes it possible to recover energy that can support the electrical system or can be fed back to the powertrain under high loads. Braking energy can be stored temporarily in the battery during downhill driving conditions and is then available for the next acceleration phase.

Because of transient driving conditions high cycle rates are expected over lifetime which has to be considered in the development of the complete mild hybrid system including battery and electrical motor.

The requirements for the battery system in MHD applications are significantly higher in terms of service life, power output, range of application, availability, and cycle durability in

comparison with current 48-volt MHEV batteries for passenger cars. In addition, very compact and weight-optimized systems are necessary.

The 48-volt mild hybrid battery family developed by MAHLE meets these requirements with a compact, universally deployable, modular system structure:

On one hand a system with high charging and discharging capability over a broad range of charge states maximizes battery performance with reduced installation space and weight in comparison to conventional systems.

On the other hand, a battery system with higher capacity and high charging and discharging capability for extended usage is in development.

Therefore, MAHLE offers a modular 48-volt battery system:

1.) High performance: 48-volt MHEV battery with an energy content of 1kWh and 2kWh for high power and therefore high energy turnover in a small packaging with low weight, combined with high expected service life and cycle durability, making battery replacement typically unnecessary and with an availability over a broad temperature range.

2.) Extended capacity with best performance: 48-volt MHEV Battery with up to 6kWh energy content for electrification of auxiliaries, recuperation and boosting and hoteling with high service life.

2 48-volt MHEV high performance system

The scope of application of the 48-volt MHEV battery pack is tailor-made for the usage in commercial vehicles and public transport. Main advantages are in the P2 architecture: a mild hybrid application with an electric motor for boosting and recuperation and additionally for electrical system support.

An increase in powertrain efficiency can be achieved by significantly improved cold-start capability and low-temperature availability. The 48-volt mild hybrid battery supports the combustion engine even at low ambient temperatures, helping to reduce the vehicle's consumption and emissions.

Due to its high durability and the associated extended service life the battery has substantial potential for economic and environmental benefits.

2.1 Key requirements

For the basic requirement of storing recuperation energy, the battery must have high power input and output capacity over a long service life. The cyclic ageing respectively the number of lifetime cycles is essential for the development of this battery.

MAHLE is working on two applications to cover customer needs for different applications. On one hand a 1kWh system with peak power of 23 kW over 10 seconds and continuous power of 5 kW was developed and guarantees full cycle durability of more than 15,000 full cycles. On other hand a 2kWh system with up to 40kW peak power and 12 kW continuous power is in the development. The batteries are designed for an operation temperature between –30°C and 60°C. Table 1 shows an overview over all specification parameters.

Table 1: Specifications

Specifications		
Capacity	20Ah	40Ah
Energy Content (BOL)	920Wh	1840 Wh
Voltage	30 – 54V	30 – 54V
Cell	20s1p	20s2p
Peak power (time)	23kW (10s)	40kW (10s)
Operating temperature pack	-30°C to 60°C	-30°C to 60°C
Weight	15kg	30kg
Cooling	Liquid cooling	Liquid cooling

To achieve these requirements, the battery cells are based on LTO/NMC chemistry. The lithium-ion cell with LTO anode provides increased safety, high cyclic stability and long service life, high charge and discharge currents, a wide state-of-charge range (SOC), and a temperature range in which charging, and discharging are also possible at negative temperatures.

2.2 Basic concept

MAHLE has developed a modular concept for the 48-volt MHEV battery with integrated optimized cooling and integrated BMS. The modular system offers a high system compatibility at low costs for different applications and can be used and validated for multiple use-cases.

Fig. 1: MAHLE 48-volt MHEV Battery 1 kWh

The 1kWh battery system, shown in Fig. 1 and 2, consist of a lower housing and top cover. For the standard housing MAHLE is using plastic materials. Optional metal housing is possible. The housing is scalable for different customer requirements. For the high-power applications MAHLE provides a battery cooling underneath of the cell stack. The Battery Management system with the mechatronic components is located above the cell stack. The cell stack consists of 20x 20Ah LTO prismatic cells in a 20s1p connection. Several interfaces are located in the upper housing: LV connection for communication (J-1939) with the vehicle control unit, 48-volt connection, venting valve and fluid connection for the cooling.

The efficient, active cooling system uses a water/glycol mixture. Active cooling further increases cycle and calendric service life. With the ability to run the battery at higher temperatures compared to other battery systems the optimization and simplification of the complex system is possible.

Operation at higher temperatures reduces the cooling capacity on the system side and saves energy. Under the defined boundary conditions currently being investigated, it is possible to operate thermal management only via the vehicle’s low-temperature circuit. The need for a secondary circuit with refrigerant, shown in Fig. 3, is therefore eliminated and reduces complexity and costs (see. Fig. 4).

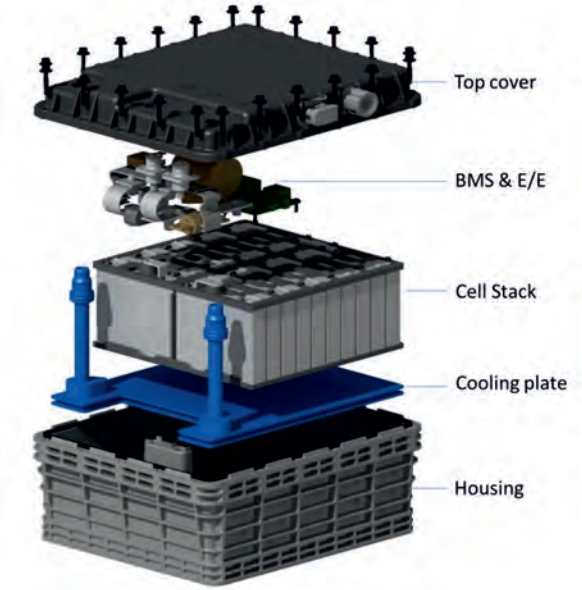

Fig. 2: MAHLE 48-volt MHEV Battery 1 kWh – exploded view

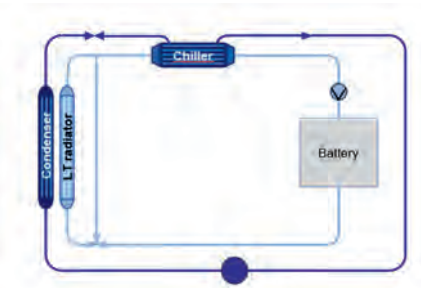

Fig. 3: Cooling circuit with low temp and secondary circuit

Fig. 4: Cooling circuit with low temp circuit

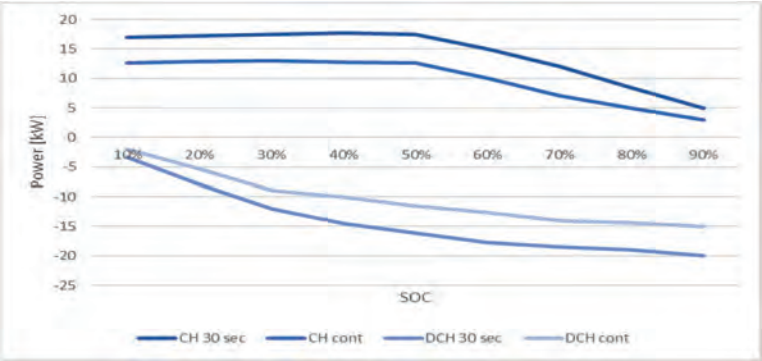

Fig. 5: 48V MHEV Battery 1 kWh; Power vs SOC @ 25°C

In case of reduced cooling demands from customer with reduced power and number of driving cycles, the MAHLE 48-volt modular battery can be operated without active cooling and the battery cooling plate can be removed from the battery system. In order to offer a compact concept, all electronics and the BMS are integrated in the batter housing under the top cover. The system is designed to meet the standard safety goals and availability. The CAN communication protocol refers to J1939.

Fig. 5 shows the charging and discharging of the 1 kWh battery between SOC 10% and 90% for continuous conditions and 30sec operation conditions. It is obvious that the battery can be charged until SOC of 50% with relatively constant power. The performance objective of the battery is high power output for recuperation and boosting over a wide state-of-charge range. For this the battery was designed and developed to ensure high C-rates (C-rate > 20) without over-dimensioning.

System simulations have shown that the combination of a 40kW electrical motor and a 2kWh battery is perfect for best fuel consumption benefits in respect to costs. Batteries with higher energy content than 2 kW would worsen the ratio of installation costs/cost benefits (fuel consumption). Therefore, MAHLE has decided to develop a 2kWh battery pack beside the 1kWh battery system. Fig. 6 shows the 2kWh battery based on the same modular concept as the 1 kWh battery. All single components are comparable but the number of cells is increase from 20 cells (20 Ah) to 40 cells. That means the cell stack has a 20s2p connection.

In Fig. 7 the charging and discharging curves are shown for the 2kWh battery. The behavior is comparable to the 1 kWh battery: nearly constant charging power until 50% SOC and then continuous power reduction with further increased SOC level. For discharging the power starts at high power values from 90% SOC and shows increasing drop of power with reduced SOC for 25°C temperature. The lifetime of the battery can be increased by running it between 20% and 80% SOC. Nevertheless, an operation between 10% and 90% SOC is possible.

Fig. 6: MAHLE 48-volt MHEV Battery 2 kWh

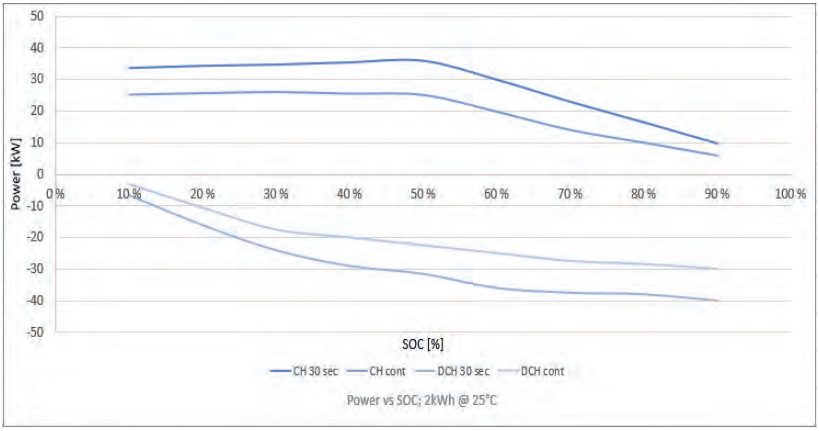

Fig. 7: MAHLE 48-volt MHEV Battery 2 kWh; Power vs SOC @ 25°C

The 48V battery pack, developed by MAHLE guarantees a high cycle life until EoL capacity of 80%. Capacity fade from begin of life to end of life is much lower than in other systems, which is significantly reflected in the capacity required for end of life and the design of beginning-of-life capacity. This leads in nearly constant availability of capacity over the entire operational life.

Operating temperatures for charging and discharging is between –30°C and 60°C while storage at ambient temperatures is between –40°C and 70°C and cold cranking of the combustion engine is possible down to –30°C.

With the modular concept of the MAHLE battery pack an optimal recyclability can be secured. The concept allows the battery to be disassembled down to the cell level with minimal effort so the components can be sorted for disposal.

3 48-volt extended capacity with best performance

Beyond boosting and recuperation there is another use case for 48V applications. The modular concept enables MAHLE to extend its 48-volt battery family with a higher capacity system with a primary focus on recuperation, support of the 48V electrical system and the reduction of combustion engine idling during driving and parking.

With a nominal capacity of up to 6 kWh the system offers more capacity for not only boosting and recuperation mode but also for long time combustion engine-off support of the 48-volt electrical consumers. This system is based on a 14s2p connection of the cells.

With a continuous power of 6kW and a peak power of 15kW (30s) recuperation and boosting is possible. Therefore, a high recuperation potential in combination with enlarged capacity for fuel and CO_2 reduction is possible.

Due to changed priority from high performance and high peak power to extended capacity this larger 48-volt battery system is based on LFP cell chemistry. The challenge for the battery and the cell is to achieve still higher performance requirements in combination with a much higher capacity requirement compared to a battery where the focus is set only on a higher performance. The optional integrable active cooling is depending on cycle and performance requirements.

4 48-volt traction drive system

The potential for hybridization is largely determined by the power performance of the drive system: the electric motor and its power electronics. While the recuperation potential for P2 applications in passenger cars is often reasonably exhausted at 20–25 kW, commercial vehicle applications still have significant recuperation potential at substantially higher power levels. The potential depends greatly on the driving cycle. The frequency and incidence of decelerations depend on the height profile as well as the driving strategy. A predictive driving strategy does reduce the fuel consumption of the combustion engine, but also influences the recuperation cycles of the electric motor. The required battery size depends on the electrical output and the driving cycle, especially on the maximum C-rate.

Fig. 8: MAHLE 48-volt 40kW drive system

Internal testing at MAHLE has shown that for a Class 5 truck (VECTO) weighing 40 tons, for example, a power class of 40 kW is an appropriate size for long-distance routes. In a less dynamic cycle such as the VECTO cycle, higher power classes have little further potential to offer. At the same time, however, 40 kW and a reasonable battery size can still cover the majority of the theoretical recuperation potential for more dynamic driving.

In order to set up the best possible cost-benefit ratio, MAHLE is now pairing its 40 kW motor–inverter system (Fig. 8) with a 2kWh battery. The mutually tuned systems enable optimal peak

performance for recuperation and boosting. The most important parameters of the motor are shown on Table 2.

Table 2: Specifications

Specifications	
Topology	IPM, 2x3phase, integrated inverter
Voltage	48V
Power (motor mode at 48V)	40kW (peak) 25kW (continuous)
Power (generator mode at 52V)	48kW (peak) 30kW (continuous)
Torque at 48V	110Nm (peak) 50Nm (continuous)
Max. speed	12.000rpm
Motor efficiency	95%
Dimensions	230mm x 290mm
Weight	33kg

To avoid a dual-motor solution which is difficult to integrate MAHLE is developing a two times three-phase solution comprising motor and inverter. With this solution high-power output at 48 volts in smallest possible package with minimal weight can be achieved. The axial integration of the inverter enables efficient routing of electrical power and cooling lines. The form factor is also easy to integrate. In order to avoid an additional oil cooling system, MAHLE is using a pure coolant cooling system that is easier to integrate in vehicle systems. With an IPM design, the motor reaches a torque of 110 Nm with an outside housing diameter of 230 mm. Paired with speeds of up to 12,000 rpm, the MHEV requirements for a mild hybrid system specific to commercial vehicles are covered. Peak power in generator mode at 52 volts is greatly increased again, rising up to 48 kW.

5 Summary and outlook

With the 48-volt mild hybrid system for heavy duty applications, MAHLE provides an optimized drive system that meets the future requirements for MHD mild hybrid applications. With a view toward further VECTO legislation, MAHLE combines a modular, scalable battery system with

high availability, high power output or high capacity and long service life in a drive system with high power density, in order to maximize energy savings potential at low weight, in a small package, at low cost.

6 References

[1] Sources: VECTO – Vehicle Energy Consumption Tool – European Commission

[2] ATZ worldwide issue 9/2020: 48-volt Mild Hybrid System for Medium- and Heavy-Duty Trucks; P. Geskes, M. Moser, M. Rinderle

7 Abbreviations

LTO	Lithium Titanium Oxide
LFP	Lithium Iron Phosphate

AEROFLEX – Distributed Hybrid Drivetrain for Long Haul Freight Vehicles

A contribution to improve efficiency of road freight transport

Henning Wittig, Fraunhofer Institute for Transportation and Infrastructure Systems, Dresden;
Julius Engasser, MAN Truck & Bus SE, München;
Andelko Glavinic, WABCO Vehicle Control Systems, Hannover

1 Abstract

To serve the growing demands on the road transport system, it is paramount to increase the efficiency of freight transport. The AEROFLEX project develops and demonstrates new technologies, concepts and architectures for complete vehicles that are energy efficient, safe, configurable and cost-effective. Improvement of the overall efficiency is mainly based on the integration of more flexible and advanced powertrains, the reduction of energy consumption through improved vehicle aerodynamics and the effective usage of loading space. The paper concentrates on the concept and development of the distributed hybrid powertrain. In long-haul vehicles a distributed powertrain can be realized by installing additional power units in the towed vehicles like dollies and/or trailers. Thus, fuel consumption of the whole vehicle combination is reduced by the usage of electric powertrains. Furthermore, the driveability of longer and heavier long-haul vehicles is improved by adding additional drive axles, which e.g. improve gradeability. This concept might allow installing a downsized combustion engine, which is supported by electric drives in the trailer units, if coupled to the truck. Consequently, such AEROFLEX vehicles will allow a flexible combination of intrinsically efficient vehicle units, which bring their own driveline into the combination when required.

AEROFLEX aims to reduce fuel consumption up to 12 % for European Modular System (EMS) vehicles by hybrid powertrain technology. To optimize efficiency, all available powertrains – especially electric ones – are integrated in an advanced energy and torque management. In the following, this system is referred to as Advanced Energy Management Powertrain (AEMPT).

For the assessment of fuel-saving potential and vehicle dynamics, a small number of suitable vehicle combinations had to be chosen, which are most likely to play a major role in the future European transport market. The EMS1 combination is the major development focus of

the AEMPT in AEROFLEX. It complies with the 25.25m length restriction for long and heavy vehicles currently valid for Sweden, The Netherlands, Belgium, Denmark and Germany. In the most advanced configuration it consists of a 6x2 rigid truck with the Global Energy and Torque Management System (GETMS), the Smart Power Dolly (SPD), which has a steerable front axle and an electrically driven rear axle, and a semitrailer, which is also equipped with an electrically driven axle.

Fig. 1: AEROFLEX AEMPT EMS1 vehicle

The benefit of the integrated drivetrain technologies will be assessed in terms of two Key Performance Indicators (KPIs). KPI 1 is the fuel efficiency in [l/(ton-km)], KPI 2 is the fuel consumption in [l/km], while each KPI is specified as percentage fuel consumption reduction compared to a reference vehicle (4x2 Tractor – Semitrailer). The paper will present this assessment in the form of simulation results and measurement results of a sophisticated vehicle test campaign.

The AEROFLEX – AEROdynamic and FLEXible Trucks for Next Generation of Long Distance Road Transport – project receives funding form the European Union's Horizon 2020 research and innovation programme under grant agreement No. 769658.

1 Introduction

Today the transport sector produces to about 25% of total CO_2 emissions in the EU, while its contribution is still increasing [1]. Moreover, the demand of road transport will grow about 20% by 2030 [1]. On the other hand, the Green Deal target for transport sector states a CO_2 reduction of 90% by 2050 [1].

Taking into account these framework conditions it is paramount to improve efficiency of road freight transport including reduction of CO2 emissions and impact on climate, total cost of ownership (TCO) and vehicle kilometres per ton freight [2] and the cost of pre and post related processes.

Thus, the AEROFLEX project develops and demonstrates new technologies, new concepts and architectures for complete vehicles with optimized aerodynamics, powertrains and safety systems as well as flexible and adaptable loading units.
In the following the concept and system architecture of an EMS1 vehicle combination with a hybrid powertrain distributed among the vehicle units is presented. Furthermore, the vehicle and powertrain configuration, its core functions and the results of the extensive test campaign are shown.

2 Concept

The basic idea of the distributed hybrid powertrain is to combine a conventional or hybrid powertrain of the pulling vehicle with electric drives in other vehicle units. This concept might allow to install a downsized combustion engine which is supported by the electric drives in the trailer units, if coupled to the truck. In turn AEROFLEX vehicles would allow a flexible combination of vehicle units which bring their own driveline into the combination.
In the TRANSFORMERS project the concept of a distributed hybrid powertrain was investigated by combining a conventional tractor unit with an electrified semitrailer. The communication between tractor and trailer was limited to a minimum in order to make the system retrofit capable. To maximize the impact of the electric powertrains on the overall fuel consumption the AEROFLEX concept aims at integrating the powertrain control into a global energy and torque management system. This also requires a dedicated communication system including communication technology and protocol.
When looking at a representative fleet of future EMS vehicles in Europe, for example defined in the FALCON project, it becomes obvious that only a small subset of vehicle configurations can be assessed in terms of fuel saving potential and vehicle dynamics, which are also influenced by additional powertrains in trailer units. Therefore, the project focuses on the following vehicle combinations:

- 4x2 Tractor – Semitrailer
- 6x2 Truck – Dolly – Semitrailer (25.25 m, EMS1)
- 4x2 Tractor – Semitrailer – Dolly – Semitrailer (32 m, EMS2)

The integration of an electric powertrain in a dolly enables the additional use case of automated shunting of a Dolly – Semitrailer combination in terminals and hubs. Thus, it is necessary to integrate a steering axle and an external control into the dolly.

3 System Architecture

In this chapter the system components of the AEMPT will be explained alongside the scheme of Fig. 2. Only one trailer unit is depicted, but up to five units are possible. Fig. 2 highlights the newly developed functions (AEMPT Functions) that are necessary to control the distributed powertrain. Further functionalities, which are part of the control system of the distributed powertrain but not in the scope of the Aeroflex project, are depicted as Series Functions. These include components and functionalities that are already existing in a conventional vehicle, e.g. cruise control, as well as those delivered by external suppliers, e.g. the electric motor/generator (EMG) and the energy storage unit (ESU).

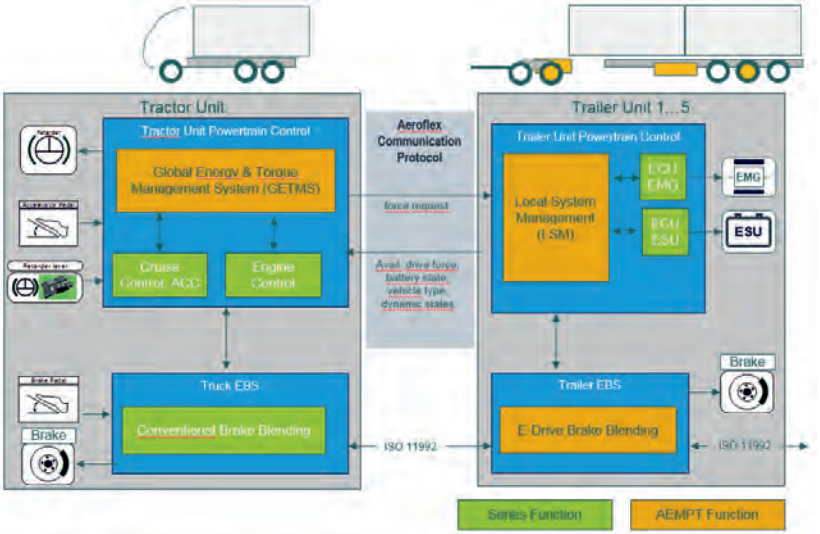

Fig. 2: AEMPT system architecture

An AEMPT truck is equipped with a Global Energy and Torque Management System (GETMS), which receives torque requests from different sources, processes all information about the current powertrain states and controls the engine, the electric drives and the retarders in a consistent and efficient way. Sources of positive torque request are the accelerator pedal and assistance functions such as cruise control. Sources of negative torque requests are the retarder lever, an endurance brake request of the EBS (conventional brake blending) or assistance functions. All requests are consolidated and distributed to the

different actuators, which are: the combustion engine, the electric drives in the trailers and the conventional endurance brakes in the truck. The system communicates with the engine control, e.g. to lower engine torque if the energy management requests positive force from the electric drives. As powerful electric drives can affect vehicle dynamics in a non-favourable way, a driving stability guard function restricts the room for torque distribution.

In each trailer unit a Local System Management (LSM) controls the electric drives and communicates with the GETMS and the trailer EBS. The LSM receives state information from the EMG and the ESU, consolidates this information and reports the current e-drive potential to the GETMS and the trailer EBS. Vice versa, the LSM receives force requests to the electric drives from the GETMS and the trailer EBS, which must be consolidated. Furthermore, the LSM comprises a drive controller which translates force requests to signals understandable by the electric motors ECU.

The dolly EBS includes a brake blending function, which can distribute a service brake request between the friction brakes and the electric drive. The service brake request is distributed with the aim of maximizing recuperation of brake energy. Thus, regenerative braking with the electric powertrain is preferred.

The Aeroflex communication protocol defines the communication between the GETMS and the LSM of the trailer units. The protocol defines how traction or brake force can be requested by the GETMS and, in turn, how the LSM must provide information about the state of the electric powertrain and the dolly. The Aeroflex communication protocol is established in addition to the existing ISO 11992 truck trailer interface. The Automotive Ethernet Router (AE Router) combines both protocols by transferring the communication into the Automotive Ethernet standard.

To demonstrate manual operation mode a remote control for industrial applications were installed. It sends force requests as well as steering commends to the LSM. The latter are translated to digital signals understandable by the steering axles ECU. During manual operation the LSM can distribute brake requests between the electric drive and the friction brakes. Therefore, it communicates with the dolly EBS via an additional ISO 11992 CAN connection (see Fig. 3). During manual operation the AE Router only forwards the ISO 11992 communication from the LSM to the dolly EBS and the towed vehicle. As there is no GETMS available, the Aeroflex communication protocol is not used.

All interfaces, mechanical, electrical and pneumatic, between truck and the SPD as well as the SPD and the semitrailer remain unchanged. The electrical interface consists of a 15-pin connector according to standard ISO 12098 and a 7-pin connector according to standard ISO 7638-1. The physical connection between truck and dolly is realized via a fixed cable. The

physical connection between dolly and semitrailer must be established via conventional coiled cables. An additional plug at the dolly according to standard ISO 7638-1 provides an electrical interface to realize the communication between LSM and dolly EBS based on standard ISO 11992 CAN during manual operation mode.

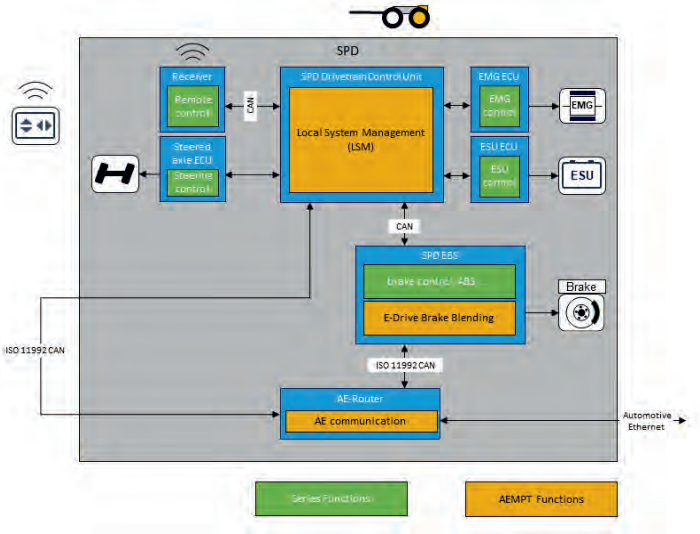

Fig. 3: System architecture of the Smart Power Dolly for manual operation

4 Functions

In the AEMPT concept, fuel saving is achieved by two measures: recuperation of brake energy and optimization of the operating point of the trucks internal combustion engine (ICE). In addition, the GETMS comprises a stability guard function, which avoids negative impact of the electric drives on the overall vehicle stability.

For recuperation the underlying idea is obvious: In braking events the GETMS shifts as much braking force as possible to the electric drives. Thereby the GETMS can only consider endurance brake requests for recuperation, as service brake requests are managed by the truck EBS. However, in state-of-the-art trucks the EBS can automatically distribute a service brake request between friction brakes and endurance brakes. Thus, also a brake request from the brake pedal can be considered from the GETMS via that way. In addition, a service brake request distributed by the truck EBS to the friction brake is not fully lost for recuperation, as brake blending functions in the dolly/trailer EBS can shift the service brake request to the electric drives.

In the following, the main functions of the AEMPT are summarized. The definition is based on the operation request generated by the driver and/or assistance systems. Furthermore, it contains operating conditions of the powertrain components, e.g. gear shift strategy or current powertrain performance/capability parameters.

4.1 Acceleration Request

The AEMPT allows driving with the ICE of the truck or a combined driving with ICE and the electric drives of the trailer units. For combined driving the GETMS requests a positive force from the LSM. The intention of combined driving can be

- To maintain the optimal operating point of the ICE by supporting the ICE with the EMG,
- To provide maximum possible acceleration by using maximum traction force of all available engines, or
- To maintain direct/higher gear by supporting the ICE with the EMG.

If the LSM reports no available force, the GETMS must not request any positive force.

4.2 Service Brake Request

The AEMPT allows braking with friction brakes and/or the electric drives via a brake blending function realized by the dolly/semitrailer EBS. The GETMS of the towing truck is not involved in this function. If the LSM reports an available negative force to the EBS, the EBS can shift brake power from the friction brakes to the EMG, thereby recuperating energy. In an emergency brake situation, no brake power is shifted to the EMG for safety reasons. An emergency brake situation is detected by the EBS typically if the braking pressure is higher than 80% of the maximum braking pressure.

4.3 Endurance Brake Request

The AEMPT allows braking with common retarder and/or the electric drives while any traction command is prohibited. In state of the art systems, the protocol for truck-trailer EBS communication according to standard ISO 11992 supports endurance brake control for trailers, but truck and brake manufacturers do not implement them yet. In order to support an implementation in near future, the AEMPT considers this scenario. If the LSM reports an available negative force to the GETMS, an endurance brake request issued by the retarder lever or cruise control can be realized by the EMG, thereby recuperating energy. If no negative force is available, e.g. because of a high state of charge of the battery, the endurance brake request is directed to the conventional retarders.

4.4 Combined Braking

The AEMPT allows combined braking with friction brakes and/or common retarder and/or the electric drives. Any traction demand is prohibited. A combined braking situation appears when an endurance brake request and a service brake request are issued at the same time, e.g. by activation of retarder and brake pedal or due to conventional brake blending in the truck to reduce brake wear. In such situation the LSM can receive force requests from the GETMS (endurance brake request) and the dolly/trailer EBS (service brake request) simultaneously. Up to the maximum possible force, the LSM can add up the requests. If the added requests exceed the available force, the LSM must prioritize the requests and accordingly lowers the reported available force to the GETMS.

5 EMS1 Demonstrator Vehicle

The Aeroflex EMS1 (European Modular System) vehicle comprises three units: A conventionally driven 6x2 truck, an electrically driven dolly and an electrically driven trailer:

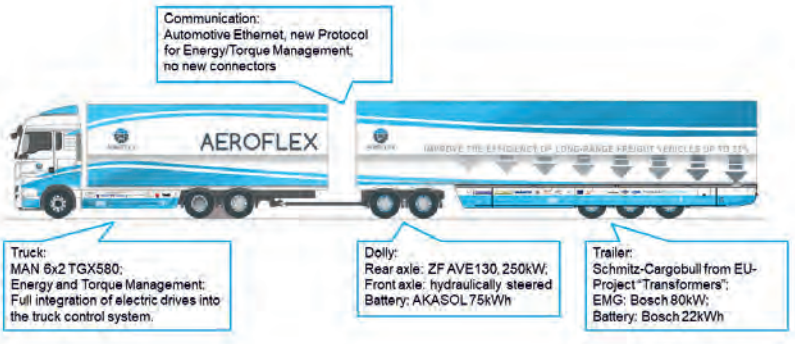

Fig. 4: AEMPT demonstrator vehicle scheme

The towing unit is a conventionally (diesel) driven truck with a power rating of 560hps. Its powertrain management is extended by the GETMS as described in chapter 3 in order to deal with the electric drives of the dolly and trailer. To visualize the status of the electric powertrains a display was installed in the driver cabin that shows the current state of charge of the energy storage units and forces of the electric engines (see Fig. 6).

For the demonstrator a double axle dolly with a drawbar at low level was developed, to couple under a rigid truck. It is equipped with a complete electric powertrain including an

energy storage unit, an electrically driven axle, which require a liquid cooling system, and a Local System Management according to chapter 3.

The battery system by Akasol was developed for automotive applications according to several safety standards, e.g. ECE R10, UN 38.3, ECE R100. To provide the power capability required by the EMG, three battery trays of type AKASYSTEM 15 OEM 37 PRC were installed. Each tray consists of 16 battery modules, while each module contains 12 lithium ion nickel-manganese-cobalt cells (Li-Ion NMC).

Fig. 5: AEMPT demonstrator vehicle

Fig. 6: electric drive display

The electric portal axle AVE130-400VAC by ZF is an integrated system including the EMGs, traction converters and an electronic control unit. Each wheel of the axle is driven by a liquid cooled asynchronous motor that is connected to the wheel with an additional gear stage. Although separate traction converters power the EMGs, torque requests to the driven axle are distributed equally between the left and right wheel whereby a torque vectoring capability is not provided.

The electric powertrain contains two cooling circuits, which are separated due to their different temperature levels: one for the driven axle, the traction converters and the 24V inverter and one for the battery system.

The dolly can be maneuvered with an electro-hydraulic steering system by V.S.E. Vehicle Engineering B.V installed with a steered axle by BPW Bergische Achsen Kommanditgesellschaft. The steered provides a digital interface to receive steering commands by an external control system to support maneuvering at speeds below 12 km/h. The steering angle is measured by a sensor integrated in the steering knuckle of the BPW axle. The signal is provided on the CAN bus, that connects the steered axle ECU and dolly EBS. The steered axle ECU also receives the vehicle speed via this connection.

While driving in trailer operation the steering angle is fixed in centered position. Using this configuration, the EMS1 combination fulfils the requirements of the Dutch and Scandinavian turning circle with an outer radius of 14,5 m. Although it cannot cope with the German turning

circle of 12,5 m, installation of a steered front axle enables maneuvering of the dolly on yards.

The semitrailer used in the AEMPT EMS1 vehicle was developed in the EU project TRANSFORMERS. Some details about the concept can be found in [3] and [4]. It is equipped with an additional control unit in order to adapt the TRANSFORMERS specific communication protocol between truck and trailer to the newly developed Aeroflex communication protocol.

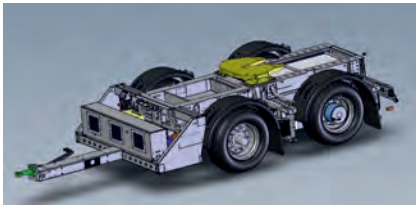

Fig. 7: CAD model of the Smart Power Dolly as designed

Fig. 8: Smart Power Dolly

6 Testing and Results

The EMS1 demonstrator vehicle was part of an extensive test campaign conducted by IDIADA. To accurately determine the improvement in fuel economy for the distributed powertrain technological innovations and other developments of the Aeroflex project in a structured manner for different vehicle configurations and types of tests, a test matrix and a test protocol were defined. It included various reference and demonstrator vehicle units as well as test use-cases like steady-state speed tests at proving ground, a real world route, airdrag and dynamic tests on test track ([5]). This chapter focuses on the results in terms of fuel consumption reduction obtained with the AEMPT EMS1 vehicle.

6.1 Test Vehicles

The vehicles used in the test campaign are classified as shown in Table 6-1. The zero-case classification represents the current state-of-the-art with high market sales volume in the EU of the tractor-semitrailer configuration. The EMS1 reference vehicle is the 25.25m combination treated as reference for the AEMPT demonstrator vehicle. The advanced reference vehicle comprises a standard truck and an electrically driven semitrailer (indicated as TF-SCB curtain in Table 6-1) with a so-called Hybrid on Demand system that was developed in the TRANSFORMERS project. It is the same semitrailer that is indicated as

AEROFLEX-SCB in the EMS1 AEMPT Demonstrator vehicle, while in this configuration the semitrailers electric drivetrain is controlled by the GETMS.

During the fuel consumption tests a control vehicle was driving in front of the test vehicles. The fuel consumption results obtained on the control vehicle were used to eliminate the influence of different external conditions found in a long testing season. Fuel consumption evaluation was done according to SAE J1526 protocol to compare different test vehicles using a control vehicle. Control vehicle characteristics were not modified during the entire project and the test load was fixed at 30.297 kg.

Due to delays in the development and construction of the AEMPT demonstrator vehicle and time constraints on the test planning only tests at 50% of payload were performed.

Table 6-1: Overview of the tested vehicle configurations

Zero-case vehicle 	- 16,5 m vehicle combination - GVW: 40 ton - EU directive 96/53 compliant
EMS1 Reference vehicle 	- 25,25 m vehicle combination - GVW: 60 ton - EU directive 96/53 compliant with exception for length and weight, allowed in several EU countries under specific conditions
Advanced reference vehicle 	- 16,5 m vehicle combination - GVW: 40 ton - EU directive 96/53 compliant
EMS1 AEMPT Demonstrator vehicle 	- 25,25 m vehicle combination - GVW: 60 ton

6.2 Test Use-Cases

The purpose of the test use-case performed for investigating the AEMPT demonstrator innovations was the quantification of fuel consumption under real world conditions. Each vehicle configuration was tested at least three times on the public road from IDIADA to Fraga and back which is 242,5 km in total. The route characteristics are summarized in Fig. 9 and Table 6-2. Over 95 % is highway, mainly two-lane with an additional lane at steeper slopes, and takes about 3,5 hours. Traffic conditions are very light, so there was very little influence

of other road users during the tests. The hilliest part of the route is a toll road with maximum gradients of 6 – 7 %.

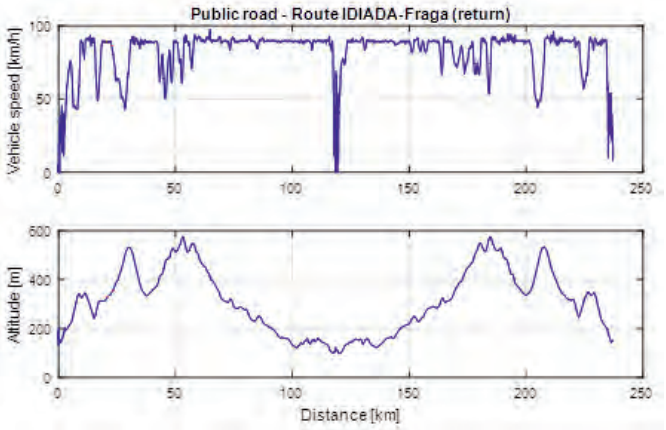

Fig. 9: Example vehicle speed and slope profile of the IDIADA-Fraga route (GPS data) [5]

Table 6-2: IDIADA-Fraga route characteristics

Concept	Unit	Value
Trip duration	s	11.600
Trip distance	m	242,5
Average speed	km/h	73,5 (>95% highway-distance based)
Min/max altitude	m	87 / 573 m
Max up- and downhill slope	%	6.6 / -6.8
Traffic conditions	-	Light (6 exits in between origin and destination)

6.3 Key Performance Indicators

The performance of the AEMPT demonstrator vehicle was rated by two Key Performance Indicators (KPIs) which are fuel consumption in l/100km and fuel efficiency in l/ton-km. The first one evaluates the average vehicle fuel consumption in liters fuel (diesel) consumed per driven kilometer over a particular trip. Furthermore, it contains relative fuel consumption using the same absolute values compared to a specific reference vehicle configuration. The second one evaluates the vehicles fuel efficiency in liters fuel (diesel) consumed per driven

kilometer and ton payload over a particular trip. It also contains relative fuel efficiency using the same absolute values compared to a specific reference vehicle configuration.
All absolute values of fuel consumption measured at the AEMPT demonstrator vehicle were corrected according to the total battery energy of the electric powertrains consumed and provided during the test.

6.4 Test Results

This section describes the results in terms of KPIs obtained for the different vehicles listed in Table 6-1. All results are based on the fuel consumption and fuel efficiency of the zero-case vehicle. Positive values indicate a higher, negative values indicate a lower fuel consumption result.
For security reasons the electric powertrains of the AEMPT demonstrator vehicle was switched off in the urban part of the route, which is about 15 km of the total distance.
The first tests of the EMS1 AEMPT demonstrator vehicle with deactivated electric powertrains showed a higher fuel consumption compared to the EMS1 Reference vehicle, even when testing with a similar GCW. This is mainly caused by the demonstrator characteristics of the implemented technologies that can significantly improved in a series product. Thus, it was decided to use an EMS1 vehicle combination consisting of the MAN 6x2 truck, a standard dolly and the TRANSFORMERS semitrailer. This eliminated the influence of the Smart Power Dolly while keeping the vehicle characteristics of the remaining vehicle units.

Table 6-3: Test results in terms of fuel consumption (l/km) and fuel efficiency (l/ton-km) of the EMS1 AEMPT demonstrator vehicle compared to the Zero-case vehicle

Test vehicle	relative fuel consumption		relative fuel efficiency	
	Result	Confidence interval	Result	Confidence interval
Zero-case	0	0,8 %	0	0,8 %
Advanced Reference vs. Zero-case	-5,0 %	2,5 %	-4,8 %	2,5 %
EMS1 New Reference vs. Zero-case	44,5 %	2,1 %	-5,6 %	2,1 %
EMS1 AEMPT Demonstrator vs. Zero-case	38 %	1,7 %	-9,8 %	1,7 %

Due to the benefits of the electric powertrain in the Hybrid on Demand configuration of the semitrailer, fuel consumption results of the Advanced Reference have been lower compared to the Zero-case vehicle. The results in terms of fuel efficiency could be further improved by

using an EMS1 vehicle configuration, while the improvement is partly influenced by the higher load capacity.

Table 6-4: Test results in terms of fuel consumption (l/km) and fuel efficiency (l/ton-km) of the EMS1 AEMPT demonstrator vehicle compared to the EMS1 new reference vehicle

Test vehicle	relative fuel consumption		relative fuel efficiency	
	Result	Confidence interval	Result	Confidence interval
EMS1 New Reference	0	1,9 %	0	1,9 %
EMS1 AEMPT Demonstrator vs. EMS1 New Reference	-4,5 %	1,2 %	-4,5 %	1,2 %

The benefit of the EMS1 AEMPT Demonstrator in comparison to a conventional EMS1 vehicle can be seen in Table 6-4. The results of fuel consumption as well as fuel efficiency show a reduction of 4,5 %. To analyse the potential of the electric powertrains further tests with fully charged traction batteries were conducted. Assuming an electric powertrain with plug-in capability, the fuel consumption could be reduced by up to 13,5 % with the current battery configuration.

7 Summary

The paper presented the concept and development of a distributed hybrid powertrain in an EMS1 vehicle combination. It shows the fuel saving potential of electric powertrains in trailer units under the assumption of a global energy and torque management system. This potential can be further increased by optimizing the vehicle configuration according to certain use cases.

8 References

[1] Commission, European. (2011). WHITE PAPER – Roadmap to a Single European Transport Area – Towards a competitive and resource efficient transport system.

[2] AEROFLEX Deliverable D1.1. (2018). Transport market and its drivers with respect to new vehicle concepts

[3] G. Nitzsche, S. Wagner und M. Engel, „Electric Drivelines in Semi-Trailers - TRANSFORMERS: An additional Way to Hybridisation," in VDI Commercial Vehicles, Friedrichshafen, 2017.

[4] S. Wagner und G. Nitzsche, „Demonstrator of a Mission Adaptable Hybrid-on-Demand Driveline installed in a Tractor Semi-Trailer Vehicle," Public Deliverable D3.4, TRANSFORMERS, 2017.

[5] AEROFLEX Deliverable D6.5. (2021). Demonstration testing results

Multi-speed e-axle for electrified heavy commercial vehicles

Dr. **Ziya Caba**, **Melih Zafer**, **Caner Harman**,
Ford Otosan, Istanbul, Turkey;
Dr. **Gereon Hellenbroich**, FEV Europe GmbH, Aachen;
Özgür Eyigöz, FEV Turkey

Abstract

Within the Longrun project funded by the “EU Horizon 2020” program, Ford Otosan and FEV are developing an electric axle for heavy duty commercial vehicles. The unit is intended to be put on a 40-ton long haul tractor in a P4 configuration, but can also be used for pure electric trucks up to 27 tons. In an extensive concept definition phase, a 3-speed AMT layout with two integrated, coaxial electric machines has been selected based on the vehicle-level requirements, including a challenging package envelope, and based on detailed energy consumption simulations. The final design includes an electro-mechanical, shift-drum-based actuation system and an active lubrication system with an electric oil pump. The first prototype unit has been assembled, with the next steps being the start up testing including lubrication and contact pattern tests. After the completion of the dyno testing, the unit will be integrated into the target vehicle and used to demonstrate the H2020 project targets.

This project has received funding from the European Union’s Horizon 2020 research and innovation programme under Grant Agreement no. 874972

“Longrun” project introduction within EU Horizon 2020 program

Longrun is the acronym for the project «Development of efficient and environmentally friendly LONG distance poweRtrain for heavy dUty trucks aNd coaches», which is funded by the “EU Horizon 2020” program. The Longrun project intends to address the topic LC-GV04 “Low emission propulsion for long-distance trucks and coaches” [1]. Ford Otosan and FEV are partners for Ford Trucks use case, which intends to demonstrate a P4 hybrid concept for a 40-ton heavy-duty long haul tractor application.

Target application and project objectives

Fig. 1 shows the target application.

Fig. 1: Target application

The project objectives are:

- 10% energy saving by hybridisation of the truck with smart control algorithms
- Using HVO fuel instead of diesel fuel to achieve reduction of well-to-wheel CO_2 by 50% to 90% depending on HVO feedstock
- Zero emission and low noise capability provided by pure electric drive with at least 10 km range

To meet project objectives, Ford Otosan has identified roadmap items which consist of both hardware and software actions. Hybridisation of the tractor is the most significant action on the vehicle side with impacts on almost all vehicle sub-systems. To meet project timing, targets and to enable reusability, a P4 layout is chosen, for which a newly developed e-axle is fitted to a conventional tractor as a third axle. This e-axle can then also be installed into pure electric truck applications.

Fig. 2 shows the architecture of many current electric trucks, which are basically conversions from existing conventional trucks. With the increasing volume of Electric truck production, more integrated, purpose-built e-drive solutions will be preferred of which an example is shown on Fig. 3.

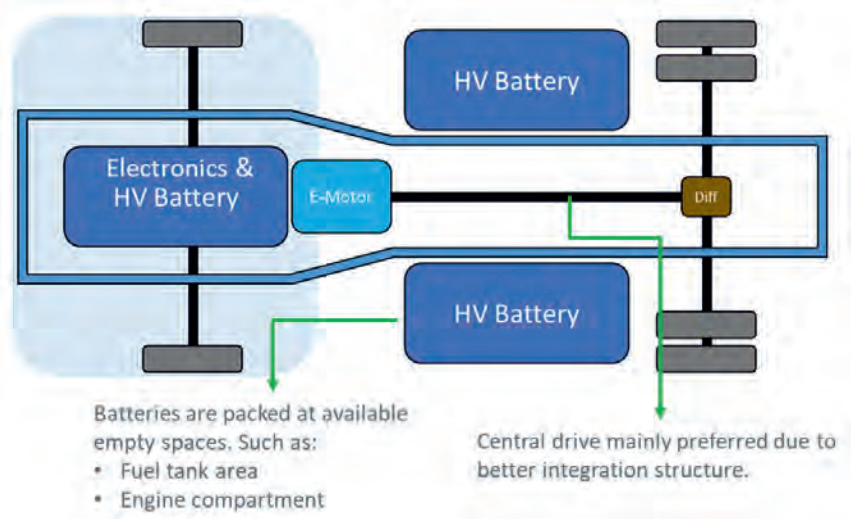

Fig. 2: Current electric trucks

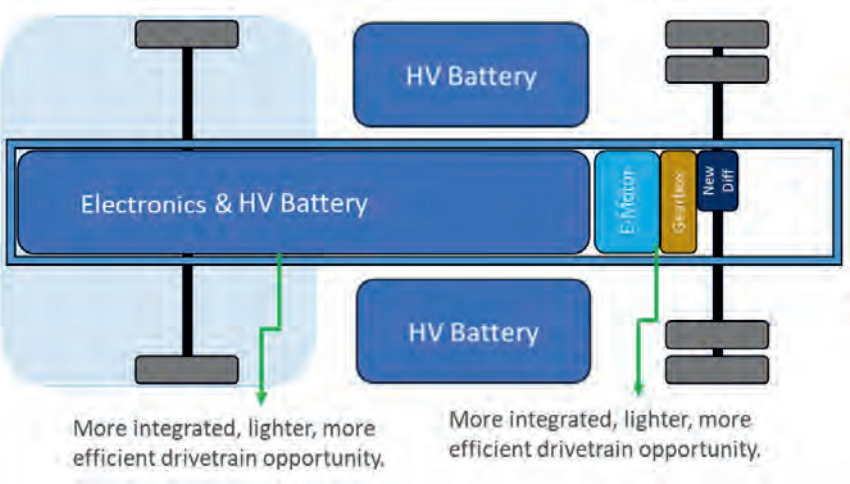

Fig. 3: Next generation electric trucks

The following targets have been set for the development of the new e-axle:

- Efficiency: Decrease battery capacity need while meeting milage targets
- Performance: Meet gradeability and top speed targets
- Flexibility:
  - Ability to use alternative e-motors including other power ratings
  - Total gear ratio flexibility
- Simplicity:
  - No synchornizers – dog-clutch usage
  - Shifting system driven by e-motor instead of pneumatics
  - Commonality with existing mechanical axle
- Packaging:
  - Dimension to fit to existing product line-up
  - Compatibility to different suspension types

Table 1 shows the requirements that have been defined for the 40-ton tractor application:

Table 1: Vehicle-level requirements for 40-ton tractor

Condition	Metric
Standing Start	>20%
Grad. @ 9 kph	>20%
Grad. @ 30 kph	>10%
Grad. @ 55 kph	>5%
Grad. @ 80 kph	2,2%
Grad. @ 90 kph	0%

Grade	Power
>20% @ 9 kph	> 200 kW
>10% @ 30 kph	> 330 kW
> 5% @ 55 kph	> 330 kW
2,2% @ 80 kph	> 275 kW
0% @ 90 kph	> 100 kW

Based on these requirements, a screening for available electric machines has been performed, and the following criteria have been used in the evaluation of the identified candidates:

- Continuous power
- Maximum speed
- Volume and mass
- Continuous power density
- Cooling type
- Efficiency
- Scalability

As a result of the evaluation, it has been decided to use two motors with 160 kW of continuous power each, very close to the required 330 kW from the table above. This amount of power is also sufficient for a pure electric 27-ton application.

Concept selection based on energy consumption simulation

More than 20 different gearset layouts (stick diagrams) have been analyzed to identify the optimum transmission architecture. The list of potential candidates has been reduced to two, for which an in-depth energy consumption analysis was performed.

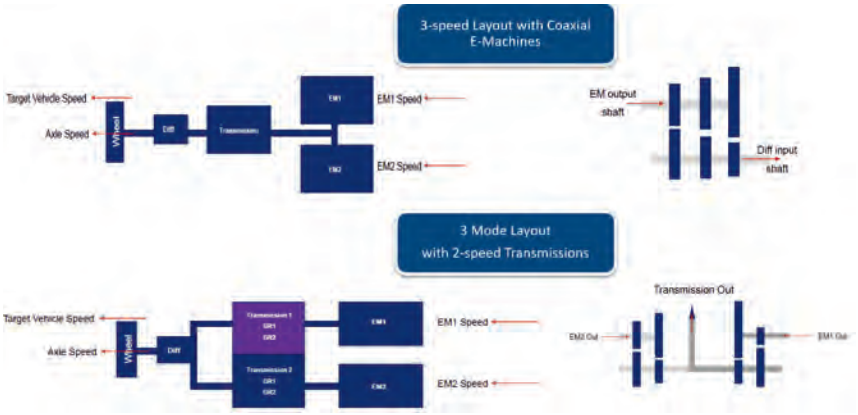

Fig. 4: Final architecture candidates

Multiple drive cycles were evaluated such as Vecto Regional, Urban, and Ford Otosan's own Municipal Utility Cycles. Load distribution between electric motors was considered during the optimization, including fully variable torque split between electric motors even when coupled with different gear ratios. Thousands of different gear ratio combinations where analyzed to optimize the gearing for best efficiency, performance, and driveability. Table 2 shows the energy consumption simulation results.

Table 2: Energy consumption simulation results

Vecto Cycle	3-speed E-axle Energy Consumption	3-mode E-axle Energy Consumption
Regional	100%	106.4%
Urban	100%	107.2%
Municipal	100%	106.7%

The following conclusions were derived from the simulation results:

- A 3-speed transmission is significantly more efficient compared to a 3-mode transmission in the evaluated drive cycles
- Adding up a 4th speed does not provide attractive efficiency improvement
- Torque interruption is evaluated not to be a major concern because of:
    - low number of the shifts in the drive cycles and
    - the advantage of e-motors being quick and precise enough for dog-clutch control

Stick diagram and package

Based on the conclusions mentioned above, a 3-speed AMT layout was selected for further development. Fig. 5 shows the corresponding stick diagram.

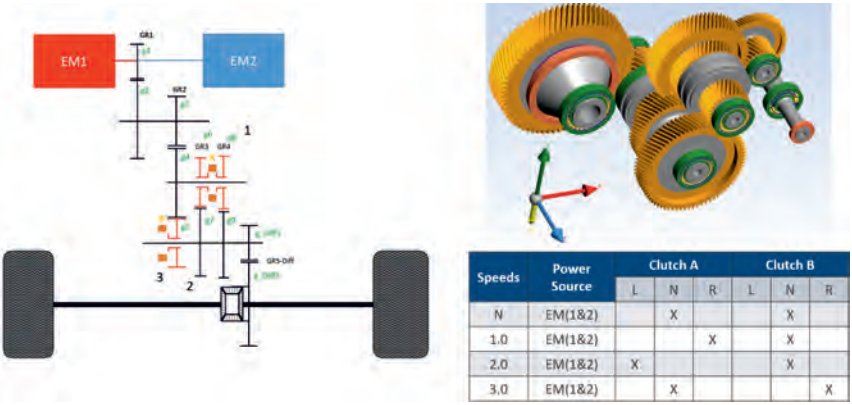

Speeds	Power Source	Clutch A			Clutch B		
		L	N	R	L	N	R
N	EM(1&2)		X			X	
1.0	EM(1&2)			X		X	
2.0	EM(1&2)	X				X	
3.0	EM(1&2)		X				X

Fig. 5: Stick diagram

To realize the required total gear ratios, a 4-stage design has been selected. A three- gear-chain, although being disadvantageous for NVH, has been implemented for 3rd speed because of more compact package and reduced weight.

A challenging package envelope was defined based on the existing truck chassis, and with the target to be compatible with different suspension types. Fig. 6 shows the Package envelope and how the final design was fitted into it. It is visible how the narrow area in between air bellows is not occupied by the e-axle.

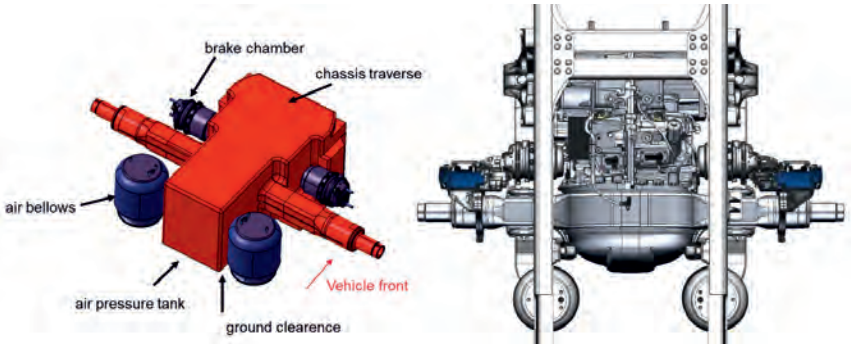

Fig. 6: Package envelope and final design fitted into it

Design features

The E-axle transfers the power from the twin e-motors to the vehicle wheels and consists of four main sub-systems:

- Twin E-motors
- 3-Speed Transmission
- Electrical shifting system
- Active lubrication system

Fig. 7 shows an outside view of the final design. It is visible to the right of the picture how the two electric machines are coaxially arranged and integrated into the axle housing. The final casing design was completed after several iterations based on package constraints and CAE analysis results.

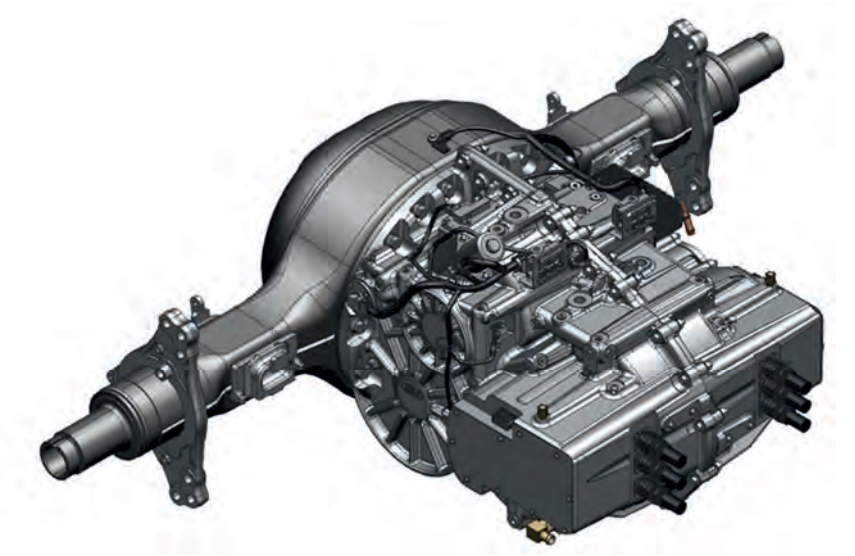

Fig. 7: Final design, outside view

The shifting system is dog-clutch based and actuated by a shift drum driven by an electric actuator motor. Fig. 8 shows more details of the components of the actuation system.

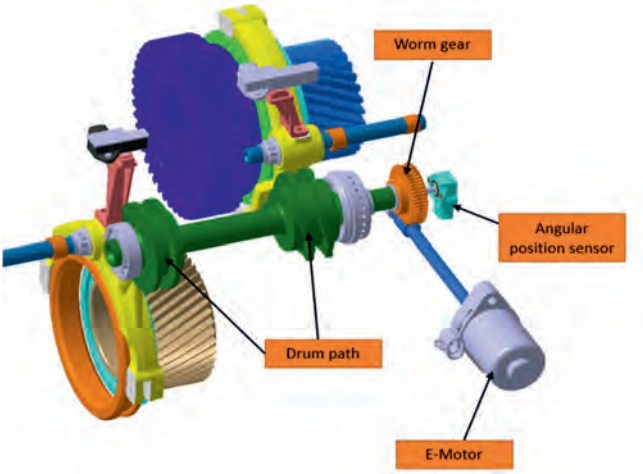

Fig. 8: Actuation system

An active lubrication system was designed to provide sufficient oil volume flow to all relevant lubrication points. A 1D CFD study was performed to determine circuit and orifice diameters. Oil Cooler, oil filter, strainer and an electric oil pump have been selected based on the requirements and simulation results. Fig. 9 shows how the lubrication channels are arranged and how they have been integrated into the housing design.

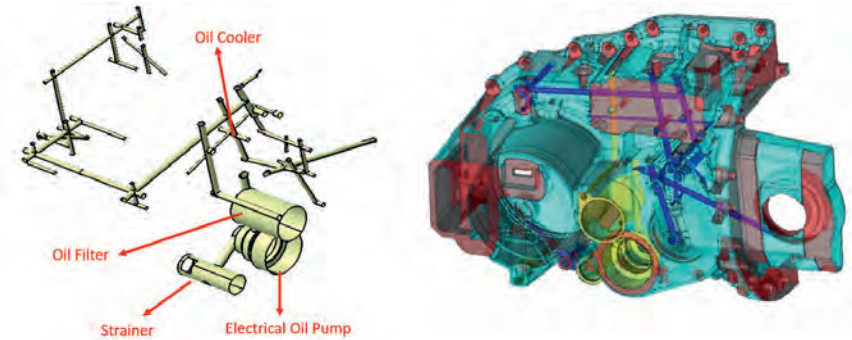

Fig. 9: Active lubrication circuit

.

Status and outlook

The first prototype unit has been assembled, with the next steps being the start up testing including lubrication and contact pattern tests. Fig. 10 shows the assembly of the 1st prototype unit.

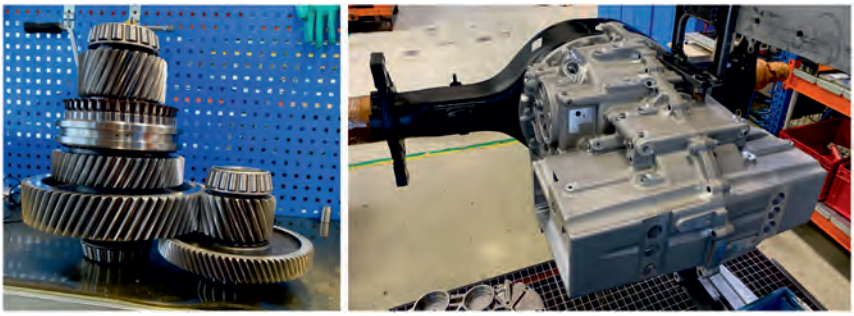

Fig. 10: Assembly of 1st prototype unit

After the completion of the dyno testing, the unit will be integrated into the target vehicle and used to demonstrate the H2020 project targets.

[1] https://ec.europa.eu/info/funding-tenders/opportunities/portal/screen/opportunities/topic-details/lc-gv-04-2019

Development of a Heavy-Duty E-Axle

Felix Bayer, M.Sc., **Jürgen Tochtermann**, Dipl.-Ing.,
AVL Commercial Driveline & Tractor Engineering GmbH, Steyr, Austria

Abstract

In recent years, AVL has been developing an e-axle solution for heavy-duty trucks in an internal research program. The target application for this development was an HD long-haul truck. The main focus of this development was a highly-integrated, compact e-axle, which also features a high power density and can be integrated into todays' standard HD truck architectures, in order to support BEV as well as FCEV powertrains in the future [1]. The AVL e-axle solution offers 400 kW of continuous power and 540 kW peak power, which will be sufficient to handle all typical requirements for a long-haul tractor-trailer application. The paper contains two major parts. The first describes how the design solutions are derived from a "stick diagram" to an A-sample hardware, considering the integration of such an e-axle into a donor vehicle with an existing and given vehicle architecture. The second part of the paper focuses on all the non-mechanical design topics, such as e-motor development, E/E, cooling and controls concept.

E-Axle for Heavy-Duty Trucks

AVL's target for this specific research program was to develop an A-sample prototype for an HD long-haul truck. Nevertheless, the target setting was already oriented towards the requirements of trucks in series production. The basic concept of the stick diagram and the resulting advantages was presented in 2019. [2] From there, the concept was further developed. While the initial design was based on requirements derived from analysis of certain European use cases, such as crossing the Alps on different highway routes, the requirements were refined over time to incorporate feedback from our customers.

This led to the specification of the e-axle as follows:

Peak Power: 540 kW

Continuous Power: 400 kW

Max Output Torque 40,000 Nm

The e-axle is intended for use in 40-42 ton long-haul trucks with 4-bellow air suspension and offers the ability to shift without torque interruption. The transmission is a traditional layshaft arrangement using a conventional differential.

The two e-motors use internal Permanent Magnet Synchronous technology and offer a peak power of 270 kW each, with a continuous power output of 200 kW each. Maximum e-motor speed is 9,000 rpm. The overall design can be seen in Fig. 1

Fig. 1: AVL e-axle with and without suspension system

Mechanical Integration of E-Axles in Conventional Vehicles

The new e-axle should fit into the very limited space available in the donor truck, with minimal adaptation of the chassis. This, in general, is a big challenge for the design of an e-axle, where additional components like e-motor(s), transmission and even an inverter need to be packaged. The components of the suspension system of a conventional truck are arranged close to the axle, in order to achieve a compact overall packaging. *Fig. 2* shows the top view of two typical arrangements of conventional rear axles and the suspension systems. Especially in the area in front of the axle, the space is usually well utilized. Air bellows, brake cylinders, stabilizer and dampers can be positioned at various positions.

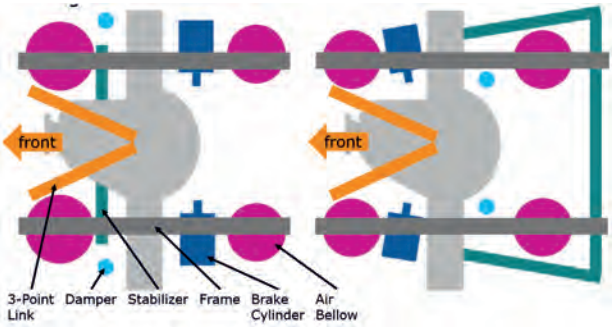

Fig. 2: Top view of two different configurations of conventional axles and suspension systems to demonstrate the limited installation space for an e-axle in a conventional HD truck

It is obvious that an e-axle that is to be integrated into a conventional vehicle needs to be tailored to the selected target vehicle. Nevertheless, it is quite likely that some modifications of the suspension system are necessary to create the required space for the new e-axle. This is particularly applicable to heavy-duty trucks, where high e-motor power and multi-speed transmissions must be installed in the e-axle.

If different trucks with different suspension systems are to be equipped with an e-axle, it needs to be evaluated carefully to determine whether more effort should be put into modifying the suspension systems or if it would be more beneficial to install different e-axles. In the second case, it is a huge advantage if the e-axle architecture provides a high degree of flexibility and modularity. This makes it possible to develop modular e-axle families for different power ranges, numbers of speeds, and ratio adaptions, as well as different packaging options with a high re-use of components and similar production technologies.

In the long term, with increasing production volumes of electrically-driven trucks, it will become increasingly beneficial to develop suspension systems and e-axles together as functional units. That would provide even more options for modular systems.

Mechanical Integration of the AVL HD E-Axle into the Fuel Cell Demo Truck

When it was decided that a fuel cell demonstrator truck was to be built, it was consistent to continue the development of the heavy-duty e-axle for the selected donor truck. At that time, an initial concept design was already available for the e-axle. As such, the required packaging space for the e-axle was already known. An alignment with the boundaries of the donor truck showed that adaptations of the e-axle and also of the truck's suspension system were required.

Modifications of the Truck Suspension System

The general arrangement of the e-axle can be derived from the e-axle topology. Fig. 3 shows the stick diagram of the e-axle.

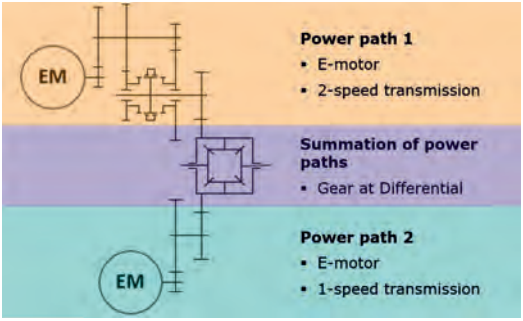

Fig. 3: Topology of the AVL HD e-axle

The e-axle consists of two power paths: path 1 includes e-motor 1 combined with a two-speed transmission with three shafts, while path 2 includes e-motor 2 combined with a single-speed transmission with 2 shafts. Both e-motors are identical and both paths are connected to the gear wheel at the differential. With this topology, it is pre-defined that one of the paths is located in front and one at the rear of the axle. It is also obvious that path 1 requires significantly more installation space compared to path 2. A look at the general arrangement of the suspension system of the donor truck in *Fig. 4* clearly shows that the space at the front of the axle is much more limited compared to the rear area. Therefore, the smaller part of the e-axle with path 2 is located at the front side and the larger part with path 1 at the rear.

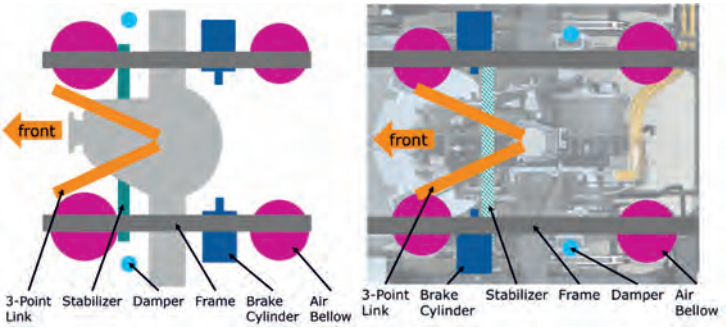

Fig. 4: Schematic visualization of the general arrangement of the original suspension system of the donor truck and the updated suspension for integration of the e-axle

One development target was to keep the effort involved in adapting the suspension system to a minimum. Therefore, the kinematics of the suspension system were not changed. All pivot points stayed in the original positions. To increase the installation space to the rear of the axle, the brake cylinders were turned towards the front of the axle. Consequently, the front air bellows had to be moved further to the front and, to increase the space in the center, they were moved laterally as far as possible. Due to the longer distance and the longer lever, the forces applied to the air bellows are reduced so that smaller air bellows could be used at the front, as already used in the original truck at the rear. *Fig. 4* also shows the modified suspension system. Based on these changes, dynamic 3D motion models were created, showing the movement of the suspension. This was also used to create the 3D installation model of the space finally available for the e-axle. Motion models and the final installation space are shown in *Fig. 5*.

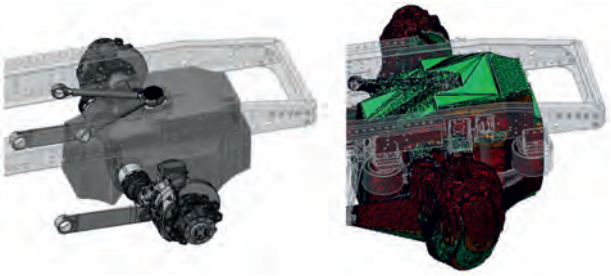

Fig. 5: 3D installation space for e-axle in static (left side) and dynamic (right side) conditions

Optimized Packaging of E-Axle

Even with the increased packaging space in the vehicle, a compact e-axle design is necessary. Beside the packaging in the donor vehicle, a compact design reduces the axle weight and increases possibilities to integrate this axle configuration into other vehicles with minor changes to the chassis.

To avoid the losses of a bevel gear set, an e-axle topology with laterally-arranged e-motors and layshaft transmission was chosen. The main challenge with such a lateral arrangement is to minimize the overall length of e-motors and transmission to fit into the given space. *Fig. 6* shows the 2-dimensional sketch of the length-optimized gear arrangement. It shows that the shaft with the shifting element primarily defines the transmission length. One fixed gear, the two loose gears with the shifting element in between, and the bearings need to be packaged side by side at this shaft. To avoid a further increase in the length of the transmission, it was necessary to use the same axial space for all other gears without any additional axial offsets. This could be achieved by optimized gear ratios for each gear mesh and by optimized center distances of all shafts. One important advantage of layshaft transmissions is that ratios and center distances can be adjusted flexibly. The final arrangement of the shafts avoids collisions between gears and bearings at the related countershafts. *Fig. 6* shows that all gears are aligned with the gears and the shifting element of the length-defining layshaft. The layshaft arrangement also provides great flexibility in choosing the positions of the shafts. This flexibility and the short length of the transmission were used to avoid collisions with air bellows, brake cylinders and the stabilizer. Additionally, the overall length of the e-axle was kept to a minimum. Therefore, the shafts are arranged in a way that makes full use of the height of the given installation space.

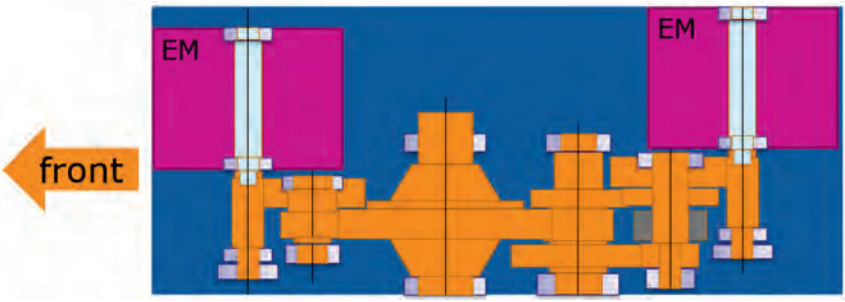

Fig. 6: 2-dimensional sketch of the gear layout to demonstrate the length-optimized gear arrangement

Packaging of Shifting and Hydraulic Cooling and Lubrication System

In the next step, the pneumatic shift actuator and the hydraulic components had to be positioned. The hydraulic system of the e-axle is described later in this paper. As the e-axle was to be designed as a prototype, it was decided to attach these components outside to the e-axle housing. This solution provides more flexibility to change to other components and to react to the availability of components. The lateral and 3-dimensional views in *Fig. 7* show that there is some space available in the front area and some space in the rear of the axle, which could be utilized without increasing the length of the e-axle. The shifting element is located in power path 1 at the rear of the e-axle, so the pneumatic shift actuator had to be placed in that area. The hydraulic components had to be distributed to the front and rear. At the front, two oil pumps were placed face to face. The advantage is the shortest possible distance to the oil-water heat exchanger, which is located further to the front of the vehicle. The pressure filter, the valve block and the distribution of the oil to the e-motors and the transmission components are located at the rear. This split requires some piping to connect the components. However, it was not necessary to modify the vehicle layout. For the prototype e-axle, the optimal arrangement is to use add-on components to utilize the available space. For e-axles in series production, it might be beneficial to provide sufficient space at one side of the e-axle and to head for more integrated solutions.

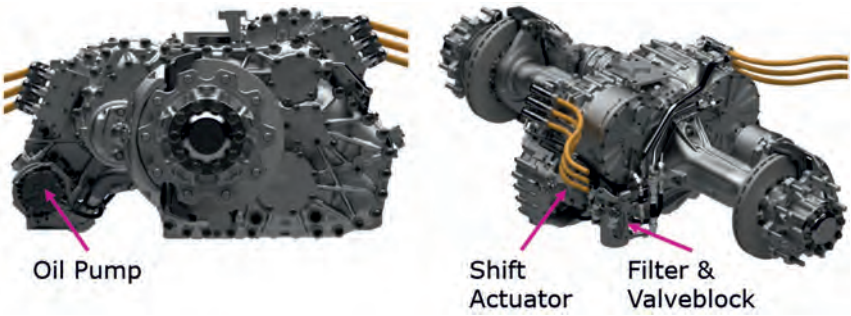

Fig. 7: Position of shift actuator and hydraulic components

Design of E-Axle Housing

In order to meet packaging, strength and durability requirements, the axle tubes are integrated into the housing parts. As such, the basic shape of a conventional housing could be implemented and the bolt connections between the individual housing parts are located in areas with large cross-sections. This made it possible to meet strength requirements for housings and bolt connections. With this design, the interfaces to the suspension system can also stay unchanged. This final housing structure is shown in *Fig. 8.*

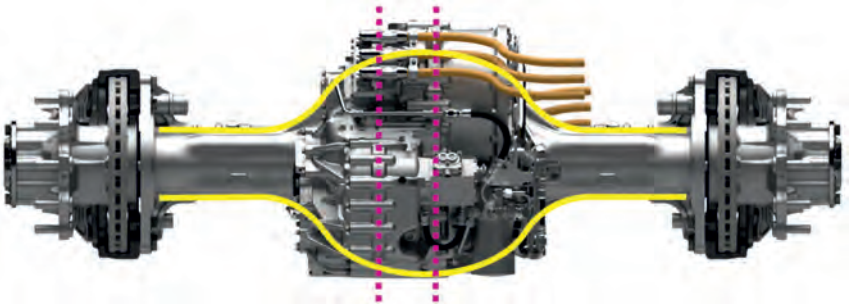

Fig. 8: Main shape of the e-axle housing follows the line of a conventional axle (yellow lines). Bolt connections of e-axle housings are located in areas with large cross-sections (purple dotted lines)

Bearing System of Rotor and Transmission Input Shaft

When designing an e-axle, one focus has to be on the bearing system for the rotor and transmission input shaft. On the one hand, a high rotation speed of the e-motor should be reached to enable compact e-motors. On the other hand, especially in heavy-duty applications,

high power is required. Combined with high lifetime requirements, e.g. for long-haul application, it becomes difficult to find suitable bearings that are available on the market. Bearing suppliers are already working on optimized bearings, which are suitable for higher speeds but still high capacity [3]. For series production, such optimized bearings could reduce the number of bearings and enable more compact design solutions compared with the prototype design, which is described below.

Nevertheless, the design target for the e-axle prototype was to find a suitable bearing system by using available standard bearings. The support of the transmission input shaft is critical. The shaft runs with the same high speed as the rotor, but radial and axial forces from the gear mesh must also be supported. This means the capacity of the bearings needs to be significantly higher compared with the rotor shaft bearings. With conventional bearing arrangements, it was not possible to find feasible solutions. As such, the bearing loads were separated and distributed to different bearings. *Fig. 9* shows the chosen bearing arrangement. The radial loads are supported by cylinder roller bearings. They provide a high capacity for radial loads combined with high speed limits. The axial loads are supported by a separate deep groove ball bearing. As it is de-coupled from the radial loads by lower radial clearance to the housing, a bearing size with suitable capacity and sufficient speed capacity was available.

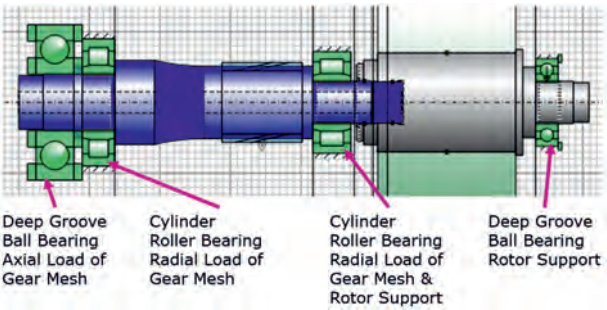

Fig. 9: Bearing system for rotor shaft and transmission input shaft

Efficiency

As the e-axle is planned as a demonstrator for long-haul applications, the efficiency of the e-axle is of upmost importance. A high efficiency saves initial costs, due to the dimensioning of energy storages as well as running costs.

The e-axle efficiency is driven by three main contributors.

1. E-drive (e-motor and inverter) efficiency
2. Mechanical transmission efficiency
3. Control strategy

This project used off-the shelf inverters, which limited the opportunity for efficiency improvements in this area. On the e-motor side, however, efforts were made to increase the overall efficiency. The main area of improvement was the number of pole pairs vs. the resulting length and the efficiency. A compromise was found at six pole pairs, providing sufficient torque density to achieve the requirements while giving a good efficiency in the e-motor speed ranges, corresponding to 80-90 kph and below.

The transmission ratios chosen were longer than initially required. Most European countries have speed limits for trucks in the range of 80-90 kph. Gearing the e-axle to achieve a maximum speed of 100 kph would have been sufficient to achieve this. However, to achieve a compromise between the required torque and the efficiency, gearing was chosen to have a good e-motor efficiency at highway speeds. This gives a theoretical top speed of 120 kph.

To achieve a high mechanical efficiency, only spur gears were used, as these have higher efficiency compared to planetary gearsets or bevel gears. Additionally, a target of just two gear stages was set in the fixed ratio path to further increase efficiency, especially when only one e-motor is engaged.

E-Motor Concept

In trucks, the required continuous power and the peak power of the e-motor should be as close as possible, as the e-motor size and costs are mainly driven by the peak torque and peak power. To achieve the highest possible continuous power density at best size and costs, it was decided to use an e-motor utilizing AVLs patented direct oil cooling. As the cooling fluid directly touches the main heat source, namely the end and stator windings, the heat is efficiently taken out of the motor. This makes it possible to achieve a continuous power level that is almost 75 % of the peak power.

As a basis for the design, the proven AVL-designed HM-132 e-motor was selected. As the original design neither fulfilled the power nor the packaging requirements, the e-motor was scaled to the appropriate outer diameter. After the simulations regarding the ideal number of

pole pairs were finished, it was seen that the e-motor resulting from this scaling, with the ideal six pole pairs, exceeds the power and torque requirements by some margin. This margin was taken to achieve a further length reduction, by increasing the number of windings while drastically reducing the length. However, this cost some efficiency towards higher e-motor speeds.

All of the electromagnetic simulations were directly followed by thermal simulations, to ensure that the required continuous working points, as well as those required for limited time amounts, can be reached.

The result is an extremely compact e-motor providing a continuous output power of 200 kW, a peak power of 270 kW and a peak torque of 835 Nm. Further optimization steps in later phases then focused on improving the NVH behavior.

Cooling Concept

Cooling of the e-axle is crucial to achieving a high power density. Even with the high efficiency of e-motors and spur gear transmissions, there is still the need for a considerable amount of cooling power. The cooling power from gear losses, as well as e-motor losses, was taken for a rough dimensioning using static load points and input values. From there, a first draft calculation of the required amount of cooling fluid was made.

As mentioned before, the decision was made to use direct oil cooled e-motors. This decision then drove further decisions regarding the cooling design. To avoid having different tanks and a high number of different fluids, the decision was made to have only one common oil sump for e-motor cooling, transmission cooling and lubrication. The risk here is that metal contamination from transmission parts gets into the e-motor and increases the electrical conductivity. Additionally, the overall oil flow required can be relatively big.

To address the issue of high flow, two electric oil pumps were planned to achieve the required cooling flow. Additionally, as oil flow is also power, measures were taken to reduce the oil flow. The main point was that when e-motor 1 is disconnected and shut off, the oil flow to the e-motor and the corresponding gears is also reduced. To avoid corrosion due to micro movements, 10% of the maximum oil flow is provided at all times. This corresponds to a power saving of 150 W.

The contamination problem is addressed by using an intake strainer before the pumps, as well as a pressure filter after the pump. The remaining contamination of the oil is accepted. The level of contamination from transmission wear and the resulting oil changing intervals will be monitored during testing.

The oil circuit itself is cooled via an oil/water heat exchanger, from where the heat is dissipated via radiators on the vehicle. For packaging reasons, the heat exchanger is mounted on the vehicle chassis. The water circuit is also used to cool the inverters. The required cooling flow of two inverters is in the same range as the required cooling flow for the oil cooler. Also, the temperature requirements allow for a serial arrangement, where the waterflow is first split into the two inverters and afterwards joined again to flow through the oil cooler. The full cooling system schematic can be seen in Fig. 10.

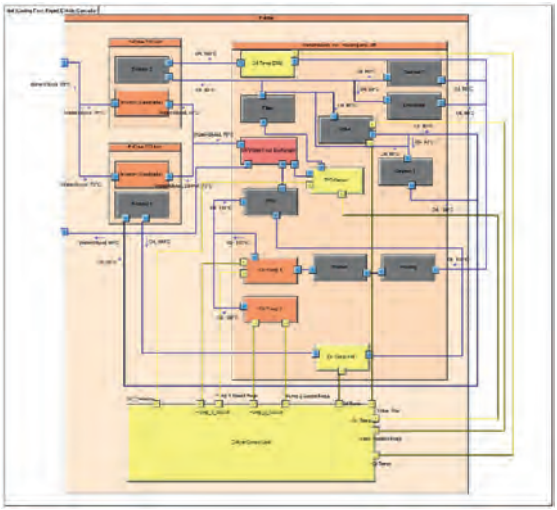

Fig. 10: Cooling flow and control flow for thermal functions

To verify the function of the cooling system, CFD simulations were undertaken. Two types of simulation were performed. First to ensure that the oil pumps can deliver sufficient pressure to reach all points of the cooling system and ensure the correct oil amount at each point. In a second simulation, it was verified that the oil amounts were sufficient to keep the temperatures within the limits used for the initial calculations. Generally speaking, this showed a good correlation, with only minor adjustments necessary.

E/E Architecture

The E/E architecture for the e-axle was based around the decision to have a central control unit (e-axle Control Unit, EACU) responsible for all e-axle functions. This eases the implementation in different vehicles. The software for the e-axle is in one centralized unit and

only adjustments to the interface, as well as the adaptation of parameters and calibration, are necessary to modify it for new vehicles.

The EACU is fully responsible for selecting the appropriate torque split between the e-motors, as well as the gear selection, based on vehicle speed and the requested drive torque from the VCU or directly from the accelerator pedal. Power limitations due to the derating of the inverters or e-motors will also be taken into account. In addition, the EACU also controls the oil flow via the pumps and performs the full diagnosis of the e-axle. To do so, it is connected to several sensors and actuators via CAN and via direct wiring.

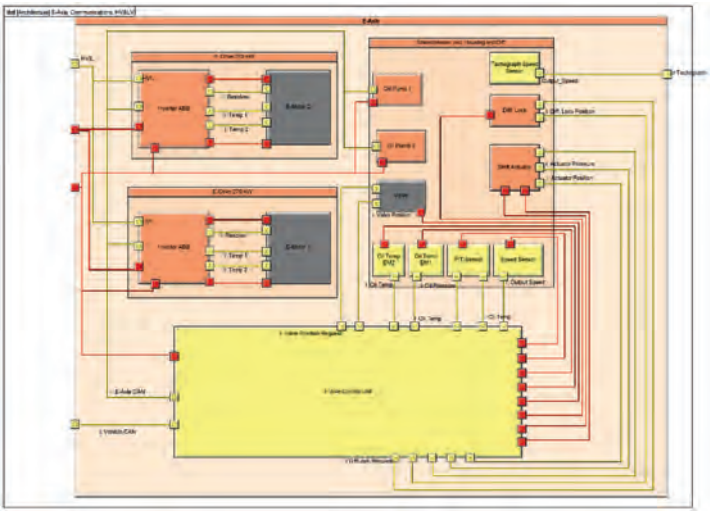

Fig. 11: E/E architecture overview showing HV connections (thick, red), LV connections (thin, red), and communication connections (yellow)

The diagnosis of the e-motors is included in the inverters, but important values are relayed to the EACU. This offers the best possible protection, while giving the EACU some degree of freedom to enforce additional limits not covered by the inverter software, such as time-based limitations.

For the LV and HV supplies to different consumers, the target was to have the connections as simple as possible. The two inverters are directly connected to the vehicle PDUs, and from there the AC lines run to the e-motors. For the LV consumes, the aim was to have the sensors and low-power actuators, such as the valves for the pneumatic actuation of the gear shifter,

supplied from the EACU to minimize the number of power cables from the LV PDU. The only exception are the two oil pumps, as their power demand is too high to route through a control unit. The overall E/E architecture for the axle can be seen in Fig. 11.

Operation Strategy

The operation strategy of the e-axle utilizes two degrees of freedom

- Gear selection
- Torque split

Both degrees of freedom can be used to achieve different targets.

Baseline strategy is an operation strategy, which is mainly focused on driveline efficiency. To achieve maximum driveline efficiency, the main driver is the use of the neutral gear on e-motor 1. This means that the vehicle is fully driven by e-motor 2, which also has higher transmission efficiency. With 200 kW of continuous power, this works at highway speeds, even with some inclination.

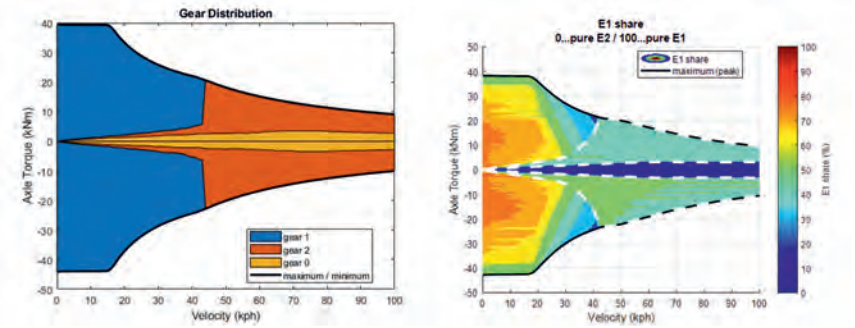

Fig. 12: Gear map and torque split map for maximum efficiency

Simulation showed that, even at 42 tons, it is possible to drive on just e-motor 2 for almost half the time, resulting in overall efficiency gains in the VECTO-LongHaul Cycle of up to 3% depending on the actual vehicle weight. Also, for efficiency reasons, the e-axle will assign a higher portion of the torque to EM2 whenever possible, as the transmission efficiency is about a third higher, as less gears are involved. The resulting gear and torque distribution can be seen in Fig. 12.

Especially with heavy vehicles, this strategy will put significantly more load on e-motor 2 and the transmission parts associated with this e-motor, leading to a decreased lifetime expectation

for this powertrain path. With a 50/50 torque split whenever both e-motors are engaged, this lifetime problem can be significantly reduced. However, this is at the expense of efficiency when the vehicle is used in less demanding working cycles.

To get a possible compromise, fitting for each vehicle and its usage, AVL has applied for a patent for an adaptable operation strategy. This takes into account the actual history of the vehicle and its current damage vs. the damage that would be expected if the vehicle had been operating under the original dimensioning cycles. This does not have to be done for every single part of the axle, but for the parts that have the highest risk of failing over different load cases in the cycle. When a vehicle has to operate in high power modes for a higher time share than expected, that torque split can be adjusted to compensate.

If the data about the current damage state is relayed via connected vehicle features to the fleet management, the data can also be used for predictive maintenance purposes. It would even be possible to assign a vehicle with a high damage state to a less demanding route, to further increase the achievable lifetime.

Future Outlook

An A-Sample hardware prototype of this e-axle is currently being built. Testing will start in 2021. For the test program, it is planned to execute functional tests as well as load and short durability tests on AVL's HD e-axle test bed. Furthermore, it is planned to mount an e-axle prototype on a prototype vehicle and to also demonstrate the e-axle performance in the vehicle in 2022.

Based on the findings of this AVL research program, specific e-axle design solutions and technology building blocks can be carried over into AVL's customer engineering projects. Re-using such proven design solutions and building on the findings of this AVL-internal research program will ensure the most effective realization of a specific customer e-axle project in the future.

References

[1] Döbereiner, R.; Linderl, J.; Mayr, J.; Riedler, S.: In-vehicle integration of fuel cell systems for commercial vehicles, MOBEX ,Webinar

[2] Tochtermann, J.: Innovative Electric Axle for Heavy Duty Long Haul Trucks, CTI Symposium 2019, Berlin, Germany

[3] Bohr A., v. Petery, G.: Bearing Development for Electric High Speed Drives and Hybrid Applications, VDI “Getriebe in Fahrzeugen” 2013, Friedrichshafen, Germany

[4] Bayer, F.: Shifting Strategy and Optimization for Multi-Mode E-Axles, CTI Symposium 2020, Berlin, Germany/Online

eTransport

Application of axle-integrated e-drive in urban LCV and MD trucks

Dr.-Ing. **Alexander Bagh**, Dr.-Ing. **Dirk Magnor**,
M.Sc. (WU) **Josha Kneiber**, Dipl.-Ing. (FH) **Frank Löhe**,
BPW Bergische Achsen KG, Wiehl

1. Abstract

Urban development, environmental pollution as well as legal conditions require alternatives for combustion engines within urban freight delivery. Cities will ban diesel vehicles by 2025, however, a scarcity of electric vehicles is obvious. BPW Bergische Achsen KG develops electric utility vehicles for urban logistics including rear axles with electric powertrain - eTransport. Electric powered axle, necessary power electronics, battery as well as control unit provide a complete drive system solution including the application for different types of vehicles. At an early stage BPW, in cooperation with development partners, is able of retrofitting existing trucks to provide local emission-free vehicles as well as to collect user experience and test kilometres. The drive system is characterized by compact design, high power density, improved manoeuvrability as well as payload neutral electrification. Core elements of the given presentation include the evaluation of axle drives in comparison to common electric powertrains for medium-heavy duty vehicles, the current development status based on extensive field trials as well as a discussion of certain technical aspects of axle drive, e.g. mounting space, efficiency and vehicle dynamics. Concluding, an outlook of the transfer of the concept to heavy-duty vehicles will be given.

2. Introduction of BPW KG and BPW Group

BPW Bergische Achsen KG is the parent company of the BPW Group. With around 1,500 employees, including around 100 trainees, the family-run company has been developing and producing complete running gear systems for truck trailers and semi-trailers at its headquarters in Wiehl since 1898. BPW's technologies include axle systems, brake technology, suspensions and bearings. BPW's trailer axles and running gear systems are in use in millions of vehicles around the world. An extensive range of services also provides vehicle manufacturers and

vehicle operators with the opportunity to increase economic efficiency in their production and transport processes. [1]

Fig. 1: Core competences BPW Group

The BPW Group researches, develops and manufactures everything needed to ensure that transport keeps moving and is safe, illuminated, intelligent and digitally connected. With its brands BPW, Ermax, HBN, HESTAL and idem telematics shown in Fig. 1, the company group is a preferred system partner of the commercial vehicle industry around the globe for running gears, brakes, lighting, fasteners and superstructure technology, telematics and other key components for trucks, trailers and buses. The BPW Group offers comprehensive mobility services for transport businesses, ranging from a global service network to spare parts supply and intelligent networking of vehicles, driver and freight. The owner-operated company group currently employs 7,000 staff in more than 50 countries and achieved consolidated sales of 1.41 billion euros in 2019. [1]

The mission of BPW is to ensure the safe and reliable transport from point A to point B. In BPW´s strategy process focussing on the mobility partnership for fleet operators was clear that customers were not able to be accompanied by BPW products since BPW´s core products were not covering the urban transportation. Due to this BPW decided to invest in a new strategic business segment – fully integrated electric drive trains (electric axles) for light commercial vehicles (LCV) and medium duty (MD) trucks. As newcomer in the area of driven axles it was decided to enter the market in a consistent reassuring multi step approach. The

first step was to publish the electric drive train concept at IAA 2016 in order to get a first market feedback. Since the feedback was positive, the first phase of retro fitting was started, see Fig. 2. The retrofitting phase was a crucial step to get relevant field data as well as structured market feedback. In that phase BPW partnered with Paul Nutzfahrzeuge GmbH also a well-known specialist of truck modification. Currently 37 trucks are running in customer hand with approximately 250,000 kilometres driven.

Fig. 2: Roadmap Electromobility & InnerCity Solutions

Based on the technical experience from retrofit solutions and field data collected BPW decided in 2019 to enter the next phase "electrification of glider chassis" and utilize a specific glider chassis from a global truck OEM. The goal is to develop a state-of-the-art electric truck for the urban transportation sector with all relevant driver-assistance systems. This truck was developed together with fleet operators in order to enable them to get their job done. The truck got double the charging power and 50 % higher range in comparison to the retrofitted truck.
The first two elements of the strategy are short term goals with up to 4 years of relevance for the business unit. The long-term goal is to utilize the gained knowledge from the field and own experiences to become a tier-one supplier to truck OEM providing development ability and field experience. BPW already started the development of the modular drive train kit and will present a drive train for a 40 t long haul truck to be tested by a leading global OEM in 2022.

3. Introduction eTransport

Basic functionalities of an electromechanical drive system for commercial vehicles are the conversion of electrical energy stored in a high-voltage battery from direct to alternating current by power electronics on the one hand and driving a required number of wheels by a certain number of electrical motors combined or not combined either with shiftable or non-shiftable gear transmissions on the other hand. The definition of a powertrain concept out of this range of possible solutions has strong influence on packaging space, payload, performance and product cost. Fig. 3 shows three basically different powertrain concepts for light commercial vehicles that provide individual advantages and disadvantages to the customers.

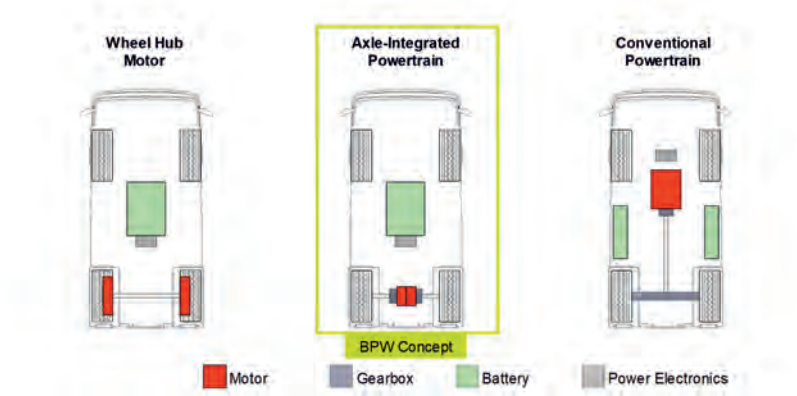

Fig. 3: Powertrain concepts for commercial vehicles

Due to the gear transmission ratio the concept "axle-integrated powertrain" allows the application of small electrical motors with regards to the diameter in comparison to both the concepts "wheel hub motor" and "conventional powertrain". Since the ratio of installation space between the wheels and drive performance requirements is moderate for light commercial vehicles and medium duty trucks in comparison to heavy duty trucks, the concept "axle integrated powertrain" offers the advantage of more space in the vehicle for batteries and other components. Furthermore, this integrational approach leads to payload capacity that equals payloads of internal-combustion-engine (ICE) driven commercial vehicles. Another benefit for the customer of an “axle-integrated powertrain” is the potential to increase the efficiency in comparison to technical solutions including differential gear with high friction losses. In addition

to this the single wheel drive provides the opportunity of traction control functions that, if needed, can be realized by corresponding software design.

The BPW concept eTransport 7.5 t realizes the single wheel drive using two electrical motors and two transmission gearboxes with output drive shafts integrated in one rigid axle, see Fig. 4. The beforementioned customer benefits of the BPW eTransport 7.5 t e-axle are listed on the left side of the picture.

Fig. 4: Concept, benefits and challenges

Fig. 4 shows technical challenges on the right side of the picture. In the first instance, limited installation space with regards to both diameter and length leads to high power density requirements for the powertrain sub systems electrical motor and gear transmission. High power density is attended by local power loss that must be dissipating by an adequate and highly integrated thermal management for the axle that should be. In addition to this the powertrain must meet mechanical specification requirements depending on the axle acceleration on the one hand and on the axle deformation on the other hand. In total these challenges require a compact and reliable powertrain design.

Fig. 5 shows an overview of all powertrain sub systems of the current state of the development beginning with a double inverter (1) that supplies both electrical machines in the drive axle with alternating current at a system voltage of U_{DC} = 400 V. Torque is provided by two oil cooled electrical motors (2), (3) that are integrated in one cast iron motor housing. The maximum operating speed of the motors amounts to $n_{M,max}$ = 10.000 1/min while the maximum operating torque is limited to approximately $T_{M,max}$ = 230 Nm. Two two-staged splash lubricated planetary gear boxes (4), (5) with a total transmission ratio of approximately i_{total} = 15 transfer the torque to two drive shafts (6) in the axle body that are connected to the wheel ends. The motor oil

cooling system is provided by a chassis mounted cooling system that is not shown in the picture.

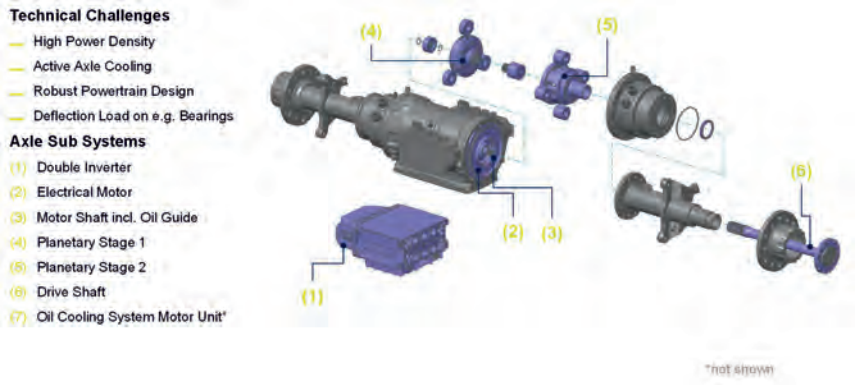

Fig. 5: Powertrain

For eTransport retrofit solutions BPW provides not only drive axle and inverter but the entire drive system, see Fig. 6. For the target vehicle Mercedes-Benz Vario the scope of supply besides e-axle, inverter and motor oil cooling system includes a charger with controller (1), two HV-Batteries (2), HV- and LV-wires and a logic box with vehicle control unit (VCU), safety control unit (SCU), battery management system (BMS) and DC converter. For all technical solutions the traction software is programmed by BPW.

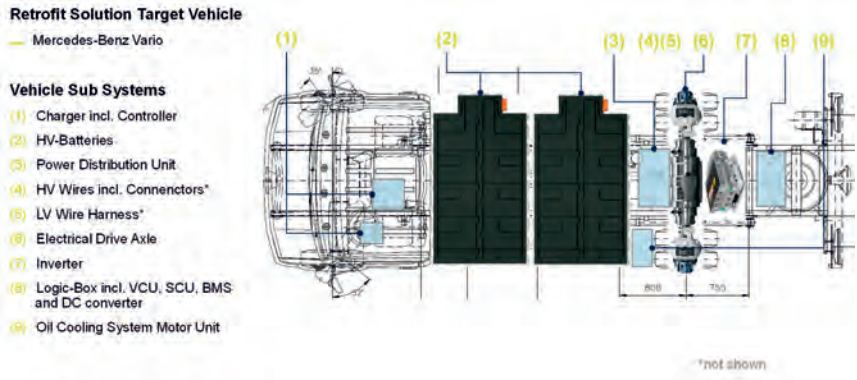

Fig. 6: Drive System

4. Perfomance and Field Data Analysis

Fig. 7 shows four customer examples for the eTransport 7.5 t retrofit target vehicle Mercedes-Benz Vario. At the time of publication 37 vehicles are running in the field. BPW is using data loggers to collect field data of some of these vehicles in order to review and optimize the design for the drive system depending on the application requirements, the operational area and the environmental conditions.

The retrofitted Mercedes-Benz Vario is driven by a continuous mechanical power of $P_{mech,cont}$ = 50 kW with a maximum nominal torque per driven wheel of T_{max} = 3,290 Nm. The system voltage amounts to U_{DC} = 400 V and two high voltage batteries provide a total nominal energy of $E_{tot,nom}$ = 84 kWh. Top speed of the vehicle is limited to v_{max} = 86 km/h and the effective range amounts to R > 120 km for most of the applications being tested. The fully laden vehicle takes a slope of G = 20 %. The target value for service life of the vehicle is L = 450.000 km.

Fig. 7: Technical Data of Retrofit Solution

The functional safety development and evaluation of the eTransport 7.5 t drive system is done in accordance with ISO 26262 [2]. In the concept phase BPW has carried out a hazard analysis and risk assessment (HARA) where all relevant operating situations of the vehicle have been reviewed and potential hazards of the given application have been derived. For electric vehicles one of the most hazardous events to be considered result from the torque path of the

electric drive system. Fig. 8 lists different specific hazards with respect to the torque path that have been derived for the drive system eTransport.

The system setup of the retrofitted Mercedes-Benz Varios contained a redundant safety control unit (SCU) supervising the plausibility of the torque command generated by the vehicle control unit (VCU). The effectiveness of this approach has been proven by fault injection test where the safe state of the electric drive system has been triggered by the SCU after detecting an implausible torque request of the VCU that would have led to an unintended launch of the vehicle. For the electrification of glider chassis additional optimisations and further developments have been undertaken to improve the functional safety of the electric drive system.

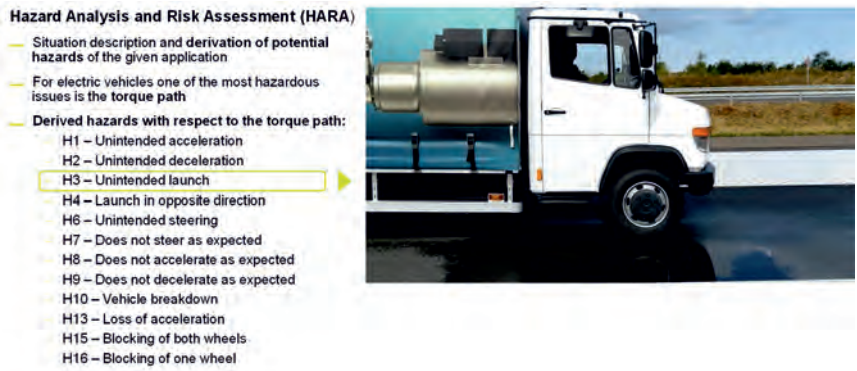

Fig. 8: Functional Safety (ISO 26262)

Until today, retrofitted Mercedes-Benz Vario vehicles have performed approximately 250,000 kilometres in different applications. BPW has been collecting and analysing field data from relevant applications, part of which is described hereinafter. Fig. 9 shows the three main application categories for urban transportation: “customer goods transportation”, “courier / express / parcel (CEP) service” and “municipal service”. BPW has analysed data for one vehicle in each of these application categories for at least one year on regular bases. A thorough analysis of the data revealed that the vehicles under consideration showed only small day-to-day variations in their respective use profiles. The detail information regarding the specific vehicle application and the route description show qualitative parallels and differences between the analysed use cases. All vehicles run in central European major cities and both

the CEP vehicle and the municipal service vehicle move in urban traffic with a high number of stops. The customer goods transportation vehicle shows a high share of highway route and the average daily driven distance is twice as long as for the other two vehicles. Furthermore, the average speed without stops is about twice as high for this application in comparison to the other two applications. The number of stops per 100 km is remarkably high for the CEP application and leads to a very low average speed (with stops) for this application.

	Consumer Goods Transportation	Courier / Express / Parcel Service	Municipal Service
Application Detail	Suburban Warehouse to City Center (up to twice a day)	Parcel Delivery in Major City	Cleaning Operation in Suburbs
Decription	High Share of Highway Drive, Last Mile Delivery	High Number of Stops, Urban Traffic	High Number of Stops, Urban Traffic
Map / City	Vienna, AUT	Cologne, GER	Berlin, GER
Daily Driven Distance	80 – 170 km	30 – 80 km	15 – 70 km
Average Daily Driven Distance	Ø 101 km	Ø 49 km	Ø 48 km
Average Speed	Ø 27,5 km/h	Ø 4 km/h	Ø 15,6 km/h
Average Speed w/o Stop	Ø 47 km/h	Ø 18 km/h	Ø 24 km/h
Number of Stops	Ø 64 Stopps/ 100 km	Ø 450 Stopps/ 100 km	Ø 239 Stopps/ 100 km
Vehicle Speed Profile (Example)			
Energy Consumption (Traction)	Ø 58,3 kWh/100 km = 100%	Ø 39,9 kWh/100 km = 70%	Ø 28,9 kWh/100 km = 50%
Recuperation Savings (Traction)	Ø - 8 %	Ø - 17 %	Ø - 19 %
Energy Consumption Auxiliary Epqipment (Heater, AC, Servo, Compr.)	Ø 7,4 kWh per day	Ø 29,5 kWh per day	Ø 17 kWh per day
	Heater and AC only active while driving	Heater and AC continuously active	Heater and AC only active while break time

Fig. 9: Field Data Analysis

The comparatively high energy consumption of the customer good transportation can be explained by the high power needed for high vehicle speeds as shown in the vehicle speed profile. Even though the other two applications show comparable recuperation savings the energy consumption by traction is considerably higher for the CEP application. The very high energy consumption of the auxiliaries in the CEP vehicle is another important finding of the

field data analysis that shows the importance of an efficient vehicle thermal management for this application.

5. Powertrain Efficiency

Powertrain efficiency measurements have been carried out during load carrying capacity tests on a special axle test rig. In the test cycle applied in the tests the nominal power limits of the drive system have been exceeded in order to decrease the duration of the test. Fig. 10 shows the setup of the axle test rig with indication of the virtual driving direction. The axle test rig allows load application in the form of a quasi-static variation of the vertical load F_V as well as a dynamic variation of wheel speed n_{wheel} and wheel torque M_{wheel}. The specimen includes the axle sub systems electrical machines (EM), gearboxes (GB), power electronics (PE) and VCU.

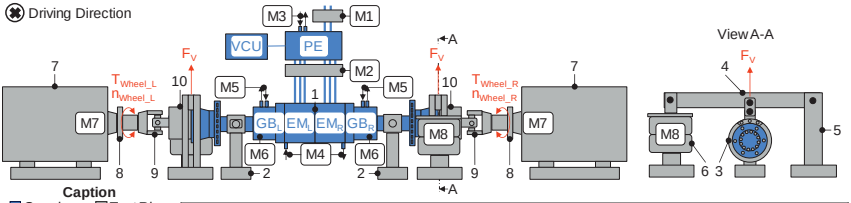

Measurement Points			
M1	Current, Voltage, Wire Temperature DC	M2	Current, Voltage, Wire Temperature AC
M3	Temperature, Flow Rate Coolant PE	M4	Temperature, Flow Rate Coolant EM
M5	Temperature, Flow Rate Coolant GB	M6	Structure-Born Sound, Condition Monitoring
M7	Torque, Rotational Speed Wheel Machine	M8	Pressure Air Suspension Bellow Vertical Load

Fig. 10: Efficiency Measurement: Axle Test Rig

For the connection between vehicle control unit (VCU), power electronics (PE) and electrical machine (EM) identical cables are used as in the vehicle. The cables between constant voltage source and power electronics are adapted to a larger cross-section in order to allow higher power values for a time accelerated testing procedure. The adjustment of specific loads with regards to speed and torque is carried out on the axle test rig according to the electrical tensioning principle. As in real driving mode in the vehicle, the VCU transfers one target torque per electric machine to the power electronics, which converts them by powering the electrical machines in the axle. The wheel machines are speed-controlled and generate a counter-torque. For overrun modethe wheel machines are motoring.

The electric drive axle (1) is mounted on two supports (2) attached to the test field at the axle connection. The right-hand support is designed as a fixed bearing, the left-hand support is

designed as a floating bearing. At the wheel connection, the vertical load on both sides of the axle is exerted on the hub using an additional rolling bearing (3) so that the wheel hub can rotate under vertical load. The rolling bearing is connected to the deflection lever (4), which is mounted in the support (5). The vertical load is applied by air spring bellows (6). The left and right wheel machines (7) are each connected to the wheel hub via a torque measuring flange (8), a constant velocity joint shaft (9) and an adapter flange (10). For efficiency analysis data from measurement points M1, M2 and M7 are used to calculate electrical and mechanical power values.

From the results obtained during the operation of the test rig four use cases with specific characteristics have been derived and analysed in more detail in terms of efficiency. The use cases are short sequences taken from the overall test profile and are characterised as follows (data given per wheel):

a) Inner City
   Representing inner city drive operation with low to medium speeds including motoring and regenerative operating modes.
   Profile Duration: 111 s
   Motor speeds: 48 rpm ≤ n_{EM} ≤ 5,824 rpm
   Motor Torques: -86 Nm ≤ T_{EM} ≤ 203 Nm

b) Country Road
   Representing a country road drive operation with medium to high speeds including motoring and regenerative operating modes.
   Profile Duration: 360 s
   Motor speeds: 395 rpm ≤ n_{EM} ≤ 8,387 rpm
   Motor Torques: -109 Nm ≤ T_{EM} ≤ 223 Nm

c) Autobahn
   Representing a drive on the Autobahn with top speed and varying motoring torques:
   Profile Duration: 120 s
   Motor speeds: 0 rpm ≤ n_{EM} ≤ 9,900 rpm
   Motor Torques: 15 Nm ≤ T_{EM} ≤ 108 Nm

d) Ramp

Representing an acceleration of the fully laden vehicle from standstill up to a speed of 20 kph at ramp with a slope of 20 %.

Profile Duration: 25 s

Motor speeds: 170 rpm ≤ n_{EM} ≤ 2,284 rpm

Motor Torques: 0 Nm ≤ T_{EM} ≤ 223 Nm

The respective torque-speed-diagrams of the four described use cases are shown in Fig. 11. The time axes are according to the duration of the respective use case profile and do not have the same scale over the different use cases.

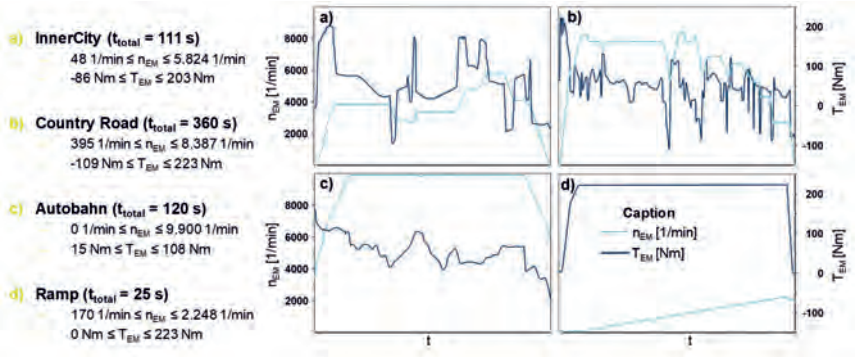

Fig. 11: Efficiency Measurement: Use Cases

The described use case profiles have been analysed with respect to inverter efficiency and efficiency of the axle, where the latter includes the electric efficiency of the electric machines as well as the mechanical efficiencies of the drive system and test rig. Fig. 12 shows the relative shares of inverter losses and axle losses for the four use cases in comparison with the overall test cycle that has been applied for lifecycle testing (“total cycle”). In addition, the deviations of overall efficiencies in %P compared to “total cycle” are given.

The efficiencies are within 1 %P for use cases a) to c) and in the same range as for “total cycle”. In use case Autobahn c) the inverter shows a high efficiency in comparison to use cases a) and b) but the efficiency of the axle is lower due to higher mechanical and electrical motor losses at high rotational speed. For the ramp use case d), the efficiency drops significantly. This can be explained by the demand of maximum torque over most of the time at relatively

low speeds during this profile. As the torque is proportional to the AC currents, the electrical power losses of both inverter and electrical machines increase while the output power remains relatively low, leading to a decreased efficiency. This is backed also by the high share of inverter losses in this specific use case, as most mechanical losses are proportional to the low rotation speed, leading to a shift of losses from axle to inverter. The overall efficiency of the electric drive system is highest at its intended operating conditions represented by use cases “innercity” a) and “country road” b).

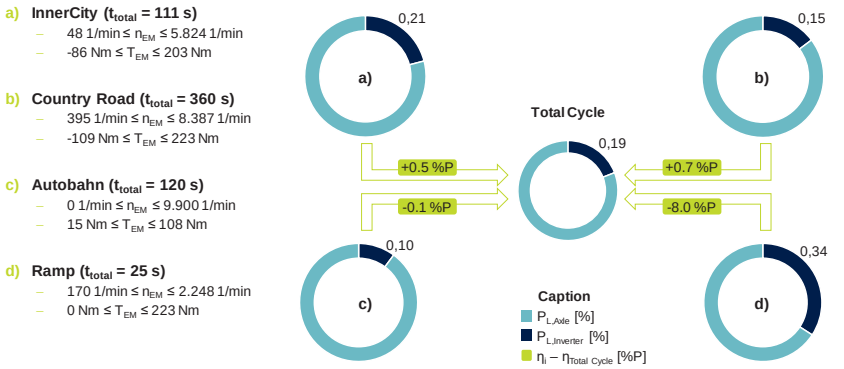

Fig. 12: Efficiency Measurement: Results

In order to reduce mechanical losses in the axle, BPW has taken, among others, the approach to optimize the oil volume in the planetary gear box. To achieve this without risk of insufficient lubrication of tribological loaded components such as bearings or sealings, functional tests are carried out on a spinning test rig with output driven gearbox without load torque. The test gearbox is assembled with transparent housing and ring gear components to visualize the oil flow within the gearbox depending on rotational speed and oil volume. Fig. 13 shows photographical pictures of the oil distribution for oil volumes of V_{oil} = 800 ml (A) and V_{oil} = 500 ml (B) for an input rotational speed of n_{in} = 4,000 1/min.

The test results show the potential of reducing the oil displacement in the planetary gearbox with the oil volume. For an oil volume of V_{oil} = 500 ml all bearings and sealings show a sufficient oil supply. Current development activities are focussed on the influence of the oil volume reduction on the wear behaviour of the oil and corresponding oil-change intervals.

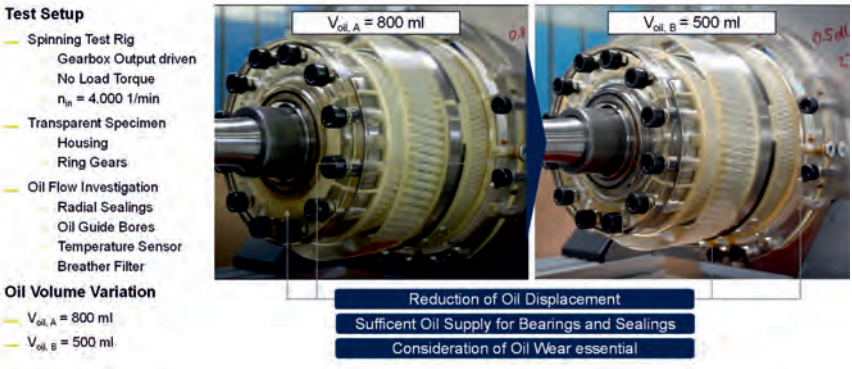

Fig. 13: Efficiency Optimization: Oil Level Reduction

6. Summary and Outlook

BPW develops all-electric commercial vehicles for urban logistics. Core of the development are entire drive systems including traction software in accordance with ISO 26262, E/E-system, batteries, power electronics and e-axle. The eTransport 7.5 t e-axle provides important advantages for end-customers like more space in the vehicle and high range due to high powertrain efficiency at intended operating conditions. The efficiency of the e-axle has been analysed and optimized in terms of mechanical losses in the transmission gearbox.

With regards to the electrification of heavy duty trucks, BPW is member of the project consortium of the research project "SeLv" that is funded by Bundesministerium für Verkehr und digitale Infrastruktur (BMVI) and managed by the Institute for Production Engineering of E-Mobility Components (PEM) of RWTH Aachen University, see Fig. 14. Aim of the SeLv project is the development of a modular drive train that enables application-specific powertrain configurations for fuel cell electrical driven heavy-duty trucks. [3]

Fig. 14: Transfer to heavy duty trucks

[1] https://newsroom-en.bpw.de/pressreleases/bpw-remains-the-first-choice-for-transport-professionals-3117700

[2] ISO 26262:2018 Road vehicles – Functional Safety

[3] www.pem.rwth-aachen.de

Advanced design of electric machines for trailers with electric axles

Optimal design and operation strategy for eDrive System

Dr. **Felix Müller-Deile**, ZF Commercial Vehicle Control Systems, Hannover

Abstract

Truck manufacturers are taking actions to lower the fuel consumption and the emissions of the vehicles. Approaches will be realized on different areas: more efficient diesel engines and reducing the losses of the drivetrain, reducing rolling resistance and air drag, predictive driver assistance energy management systems and last but not least electrification of the drivetrain meaning hybridization or full electric vehicles. As an alternative to the local hybridization of the truck, ZF presented its eTrailer concept in 2018 for hybridization of the entire tractor-trailer combination. It was the industry first solution integrating a powerful electric drive in a semi-trailer and embedding the control of the e-Drive system in the combined control systems of truck and trailer. The vehicles brake energy is stored in a battery and reused for auxiliaries or traction support leading to 16% diesel savings of the towing vehicle in a typical delivery cycle with maximum payload.

For the future series realization of the e-Drive and its components it is essential to find a balance between lightweight, cost efficient design, recuperation power and the efficiency improvement of the system. The characteristics and the dimensioning of the e-Drive system will be discussed in this paper along with the requirements derived from the eTrailer usecase. In addition, a recuperation and a traction support strategy will be presented to maximize the fuel savings of the hybrid vehicle (conventional truck with eTrailer).

eTrailer concept

A major advantage of hybrid vehicles over purely electrical propulsion is the elimination of range issues. While ranges of around 500 km can be achieved in everyday use for electric passenger cars, a significant improvement in energy storage density and cost is still required for the conventional 40 t truck. However, if the electric drive is used as an add-on as part of a hybrid concept, the energy storage system doesn't have to be designed for the entire distance to be covered. The typical power requirement of a truck-trailer combination with a total weight of 40 tons is approximately 140 kWh/100 km. Therefore, a storage capacity of about 280 kWh

would be required for a range of 200 km. On the other hand, a 5 km long downhill gradient of 5% at 80 km/h requires a constant braking power of 300 kW, ignoring roll and wind resistance. An accumulator with 20 kWh of (free) capacity would be sufficiently large to store this amount of energy, i.e. roughly 15 times smaller.

The challenge for a hybrid concept is therefore not to be able to drive as long as possible under purely electrical power, but to achieve high fuel savings using the fewest possible resources and the lowest initial investment costs. Additionally, the electric drive has to be integrated as an auxiliary driveline unit in the vehicle, regardless of whether this is a passenger car, a truck or a trailer. However, in the commercial vehicle sector, the EURO6 exhaust emission standard is increasing the space requirement for exhaust gas after-treatment in the towing vehicle and is also reducing the already very limited space available for the battery, inverter and electric motor.

The approach of hybridizing commercial vehicles by electrifying the trailer may seem surprising at first sight. Yet, it makes perfect sense to install the e-Drive system in the trailer: While the space in the towing vehicle is limited, the trailer can easily be fitted with such a system. All it takes is the installation of a few standardized modular components, whereas the towing vehicle would need complex modifications with expensive components. At a first sight there are more trailers than tractors in use, which leads to a business disadvantage from an invest perspective. This is partially compensated by the fact of longer lifespans of a trailer. Thus, together with the more easy system integration, the eTrailer is a competitive solution from an economic point of view.

The basic function of the eTrailer is to recuperate kinetic and potential energy during braking. This energy is temporarily stored in a battery in the trailer to reuse it for traction support. To ensure optimal and safe integration of the eTrailer control system, the electronic controlled brake system in the Truck (EBS) and Trailer (TEBS) manage together the e-Drive system in the trailer interacting via ISO11992-2 truck-trailer CAN- interface. In order to enable the maximal recuperation potential, the electric drive is prioritized in the brake management system of the truck EBS. The other endurance brakes of the truck and the friction brakes are only activated if the e-Drive system of the trailer cannot fulfill the demand deceleration.

The EBS in the towing vehicle represents the interface to the driver or to a future autonomous driving computer, as well as to the conventional drive and additional ADAS (Advanced Driver Assistance System) and stability control systems such as the ABS and ESC of the towing vehicle. The TEBS forms the trailer side interface to the electric drive and the trailer-specific comfort and safety functions. It is also responsible for the positive and negative torque control

of the e-Drive based on torque demands form the truck EBS and other local parameters such as the battery charge status and component temperatures. Fig. 1 below illustrates the system and communication layout of the ZF eTrailer concept.

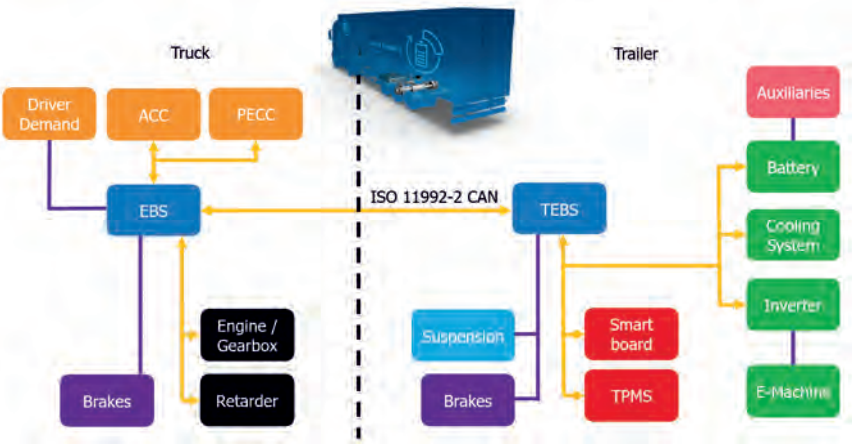

Fig. 1: Schematic diagram of system and communication layout of the ZF eTrailer concept

This deep integration of the electric drive's energy recovery capabilities into the overall vehicle deceleration control by the EBS systems in the towing vehicle and the TEBS in the trailer enables maximum recuperation while always maintaining vehicle stability at the same time. Both systems have all of the relevant vehicle status information like vehicle (part) masses, wheel and vehicle speeds, accelerator pedal position, steering angle, drive torque and braking torque to safely control lateral and longitudinal vehicle motion.

For the integration of the electric drive into the deceleration control, an existing function, the so-called endurance brake integration of the truck EBS is modified. According to the state of the art, this function is used to apply wear-free endurance braking preferably for vehicle deceleration, when the brake pedal is activated, or an external braking requirement arises. Fig. 2 illustrates the principle being applied.

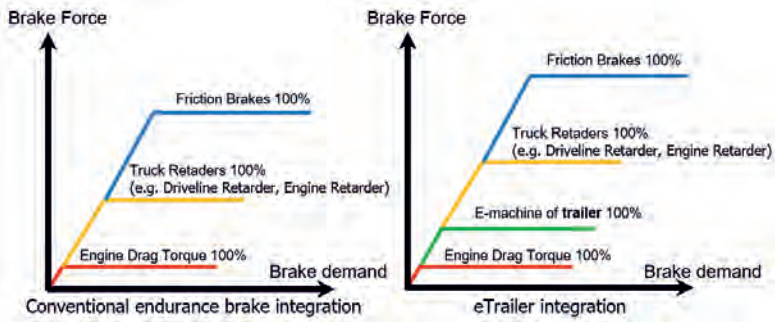

Fig. 2: Schematic integration of the electrical drive into the vehicle deceleration control

In future, the truck EBS will be informed by the TEBS via the ISO-11992-2 interface of the presence of the electrical machine in the trailer, as well as its reference performance and the actual produced torque. Using this information, the EBS in the towing vehicle can send a braking torque request (and thus energy recovery) to the e-Drive System of the trailer to achieve the deceleration request of the driver. This forms a closed loop torque control of the trailers e-Drive seen from the truck's perspective. The local energy management in TEBS then decides on the absolute level of the braking torque actually applied. If, for example, the battery charge status prohibits further recuperation of electrical power, no deceleration torque is applied and this is fed back to the EBS in the towing vehicle. In such a case, the wear-free endurance brakes in the towing vehicle or the friction brake system can then produce the desired deceleration. The outcome of the deceleration control is therefore not affected and the vehicle behavior remains stable and calculable. Incidentally, the same applies if a vehicle stability system such as ABS intervenes. In this case, both EBS systems have the necessary information to switch off the energy recovery system in such a way that the function in truck and trailer is not affected. By suitable control of the traction drive in the trailer it is also achieved that the trailer does not push the truck and the trailer remains a towed vehicle in all the operational cases where the previously stored energy is taken out of the battery in order to reduce usage of diesel fuel. As a result, additional mechanical stress on kingpin is avoided. The major benefit of this integration concept is the prioritization of the e-Drive System. Without the integration into the endurance brake control of the towing vehicle, a very significant proportion of the deceleration would be produced by the endurance brake system of the truck, which is generally not able to recuperate energy.

The recuperated energy can be used for two different usecases. On the one hand, a single-phase or three-phase isolated grid can be operated via an additional inverter to supply, for

example, a cooling compressor on refrigeration trailers. On the other hand, the stored energy can also be used by the e-Drive System to produce traction support for the ICE of the truck.

Dimensioning of e-Drive system

The challenge for a hybrid concept is to achieve high fuel savings using the fewest possible resources and the lowest initial investment costs. Therefore, it is essential to find a balance between lightweight, cost efficient design, recuperation power and the efficiency of the e-Drive system and its components. To identify the required power of the e-Drive system different driving cycles and driving scenarios were analyzed.

Keeping a fully laden truck-trailer combination with 40 t at a speed of 80 km/h while going downhill with a 2% road slope requires about 150kW continuous brake power. This typically event on a highway is a good indication to define the required continuous power of the e-Drive system.

For further analysis the VECTO regional delivery driving cycle (see Fig. 3) was used to identify the required peak power and torque of the e-Drive system for different payloads.

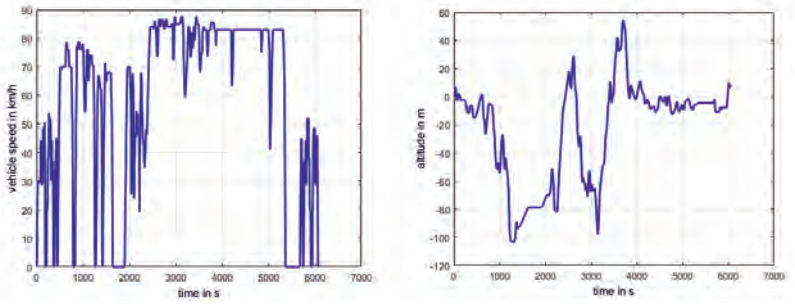

Fig. 3: Velocity and altitude of VECTO regional delivery cycle

The left diagram of Fig. 4 shows all braking operation points during the VECTO cycle with a partly laden trailer (vehicle weight 25t). The maximum axle torque is 12 kNm and the maximal power is about 300 kW. The right diagram of Fig. 4 shows the axle braking torque during the VECTO cycle with a fully laden trailer. The maximum axle torque and power increase to 20 kNm and 500 kW. In both scenarios the maximum braking torques only occur at vehicle speeds below 45 km/h. That is why the maximum torque of the e-Drive system should be available up to 45 km/h and the maximum possible recuperation power should be available in the speed range of 45-90 km/h.

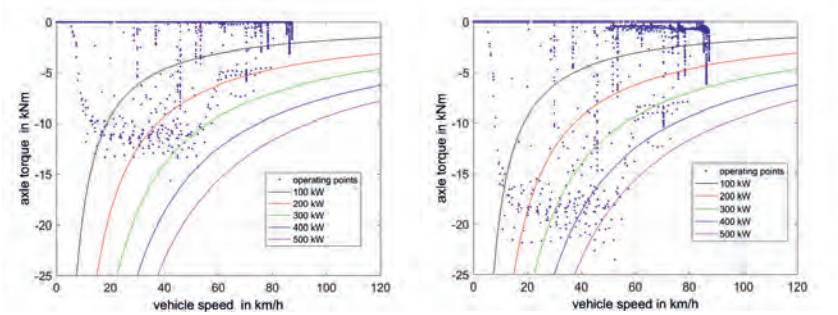

Fig. 4: Braking torque and power with 25t and 40t during VECTO regional delivery cycle

In addition, the total duration of braking events with higher power than 300 kW is very small (Fig. 5). Braking torques higher than 16 kNm are also very rare. The duration of a single braking event varies between 1-30 seconds.

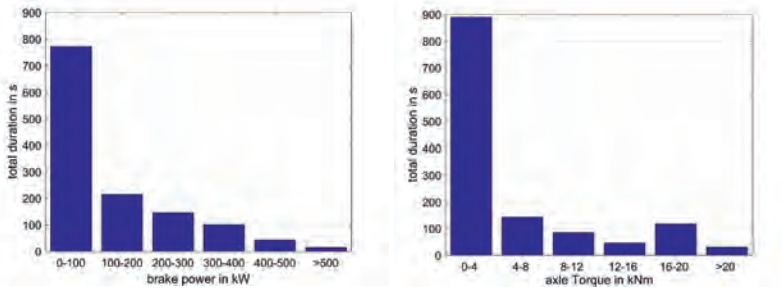

Fig. 5: Duration of braking power and torque during VECTO regional delivery cycle with 40t

Based on this driving cycle the recuperated potential using e-Drives Systems with different power and torque characteristic were analyzed. Fig. 6 shows the possible recuperated energy for e-Drive Systems with different power assuming an overall system efficiency of 83% (gearbox, e-machine, inverter, battery).

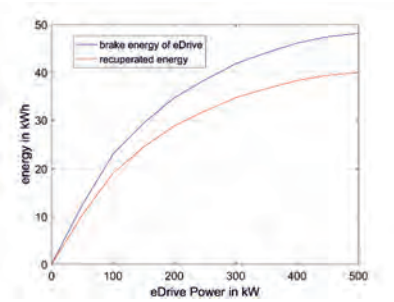

Fig. 6: Brake energy of eTrailer with different system power

The total amount of mechanical brake energy in the cycle is about 55 kWh. While the vehicle is braking and the driveline is engaged the ICE produces a drag torque. This drag torque leads to a brake energy of 6 kWh. This is why the available mechanical brake energy for the e-Drive is reduced to 49 kWh. Using a 500kW e-Drive system with 16kNm all the remaining mechanical brake energy of 49 kWh could be covered by the e-Drive alone. Due to the losses of the e-Drive system finally 40.5 kWh are then recuperated and stored in the battery. The retarder and friction brakes are not used in this scenario.With a smaller e-Drive system (300 kW and 12 kNm) 83% of the available mechanical brake energy can be used for recuperation leading to 34 kWh of recuperated electric energy. With this e-Drive system the retarder and friction brakes are only used to produce 15% of the total mechanical brake energy.

Due to the fact that the system costs rise with its torque and power capability an optimum for cost-efficiency was identified with a system power of 300 kW and an axle torque of 12 kNm. This optimum is based on different vehicle weights, driving cycles, system powers and system torques. Fig. 7 shows the brake energy charts of the VECTO delivery cycle for a conventional truck trailer combination and the eTrailer with a 300 kW e-Drive system. The total weight of the e-Drive system including the battery is in the range of 800 kg.

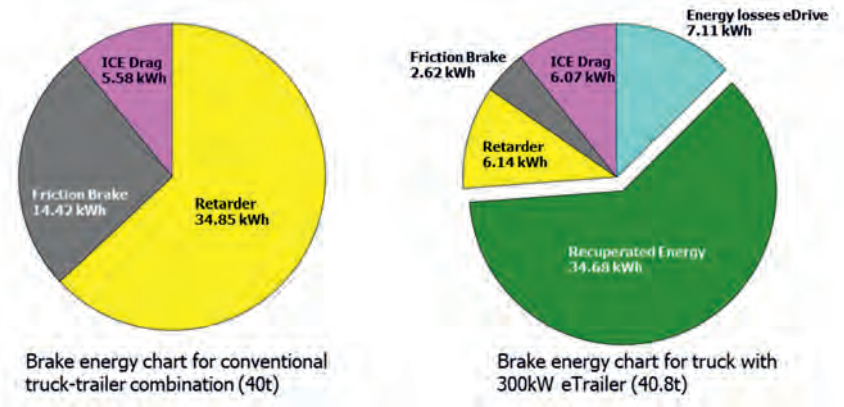

Fig. 7: Brake energy charts

The recuperated energy is stored in a battery and can be reused for traction support leading to 16% (6.5 l/100km) diesel and CO2 savings of the towing vehicle. If the energy is used to power e.g. a reefer, then the truck will not save fuel. But then the benefits change: the reefer unit becomes full electric using the recuperated energy without consuming fuel for the todays used diesel generator of the refrigeration unit.

Installation of the e-Drive System on the trailer

In general, there are two different concepts for installing an e-Drive System on a trailer. One option is to mount the e-machine on the frame using a cardan shaft to connect the e-machine with the differential of the driven axle (Fig. 8). Without an additional speed reducer, a transmission ratio of 1:5 can be achieved leading to a high torque and low speed e-machine (M_{max} = 2400 Nm, n_{max} = 3000 rpm) with a weight of about 300 kg. Due to the lack of installation space the e-machine is mounted at the back of the trailer leading to a non-optimal weight distribution.

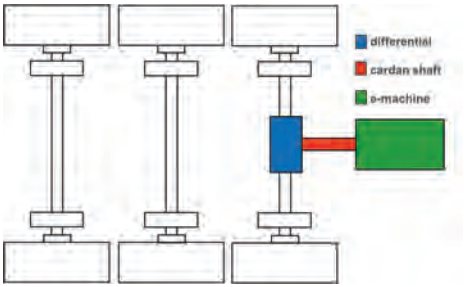

Fig. 8: Frame mounted e-machine

A high-speed electric motor concept directly mounted on the trailer axle (Fig. 9) has more advantages regarding weight and size compared to a high torque solution with a cardan shaft and a frame mounted e-machine. The combined gear ratio of 1:20 (differential and speed reducer) leads to an e-machine speed range of 0-12000 rpm (typical in the automotive sector) and a maximum required e-machine torque of 600 Nm. This high-speed e-machine has a weight of less than 100 kg. Even with the additional weight of the speed reducer the total weight of the system can be reduced compared to a frame mounted e-machine. The weight distribution of this concept is also good because the e-machine can be mounted on the middle axle of the trailer. Therefore, the serialized eTrailer will have an axle mounted concept.

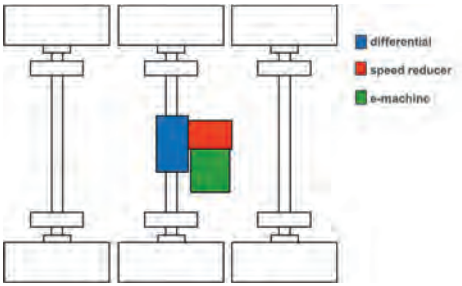

Fig. 9: Axle mounted e-machine

Battery

The required battery capacity and the maximum charging power are critical parameters for choosing the right battery technology. The ratio of maximum charging power vs. installed capacity is defined as the C-rate of the battery. As described in the chapters before the selected e-Drive System has a maximal mechanical power of 300 kW. Assuming a system efficiency of 91% (e-machine 94% and inverter 97%) at the maximum mechanical power of 300 kW, a DC-charging power of 275 kW is required. Since the eTrailer is a hybrid system and not a pure electric vehicle the required battery capacity is very low. In general, a deceleration event of the vehicle lasts for less than 30s. Assuming a maximum electric charging power of 275 kW during the braking event only results in a recuperated energy of 2.3 kWh.

In order to define the minimum required battery capacity another driving event was used. If the vehicle is driving downhill (rote slope of 2%) with a constant speed of 80 km/h for 10 km the battery will be charge with a constant charging power of about 135 kW leading to a recuperated energy of 17 kWh. This event demonstrates that a battery capacity of only 20 kWh is sufficient for the eTrailer, leading to the first conclusion that a battery with a very high power density and a high C-rate is required.

One option is to use a high-power batterie (e.g. LTO) with a low battery capacity (~ 25 kWh) and a high C-rate. This technology is expensive and has only a moderate energy density leading to a relative high battery weight even with a small battery capacity. Another option is to increase the installed capacity and use a high-energy-density battery (e.g. NMC) with a lower C-rate and a relatively high battery capacity (~ 55 kWh). Due to the higher energy density the total weight of such a high-energy battery is comparable to the weight of the proposed high-power battery.

During standstill in a traffic jam, it is not possible to recuperate energy. Therefore, a higher battery capacity is beneficial to extend the operating time for the auxiliaries (e.g. electrified reefer unit). For the eTrailer a high-energy battery was selected.

Traction strategy of the hybrid vehicle

An integration of the traction control into the brake system is also helpful, as both driving status information from the towing vehicle and trailer are available. Regarding vehicle stability it is beneficial that the trailer remains a towed vehicle and does not push the truck. The traction support provided by the e-Drive System leads to a torque and fuel reduction of the internal combustion engine (ICE). In order to optimize the operating strategy and achieve maximum fuel savings, the efficiency map of the e-Drive and ICE must be taken into account.

The left side of Fig. 10 shows an efficiency map of an ICE and the right side of the Fig. shows the efficiency map of the e-Drive System. The efficiency of both components depends on the speed and the torque.

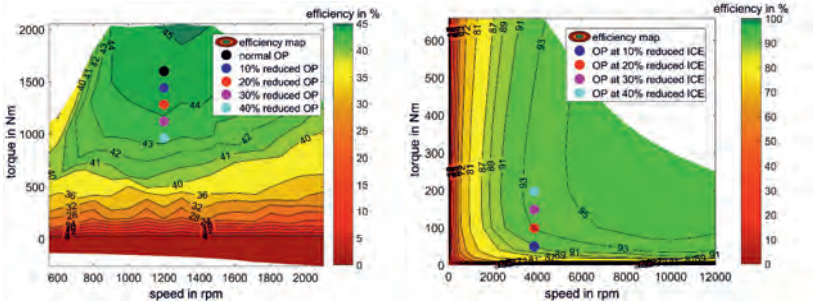

Fig. 10: Efficiency map of ICE and e-Drive System

The traction support of the e-Drive system leads to a torque reduction of the ICE. The marked operation points in the efficiency maps show examples for different amounts of torque reduction and traction support. The black point represents the operation point without any support of the trailer. The combination of the operating points that are marked in the same color results in the same axle torque as the black operating point of the ICE. If the torque reduction of the ICE increases the efficiency of the ICE is reduced but the efficiency of the e-Drive System increases.

For further analysis the fuel and power consumption of both components have to be considered. The left side of Fig. 11 shows the fuel consumption map of the ICE. The fuel consumption is given in l/h and depends on the speed and the torque of the ICE. A torque reduction leads to a lower fuel consumption. The right side of the Fig. 11 shows the achieved fuel savings for different amounts of torque reduction compared to the black operation point. The fuel savings seems to have a linear characteristic, but further analysis will show that this is not the case.

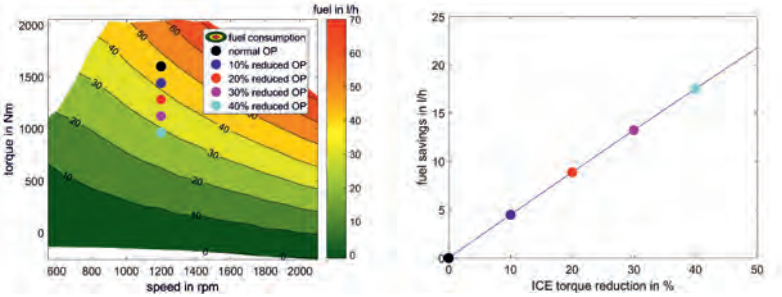

Fig. 11: Fuel consumption map and potential fuel savings of ICE

The torque reduction of the ICE leads to an increased torque and power consumption of the e-Drive (Fig. 12). The power consumption of the e-Drive also looks like it has a linear behavior.

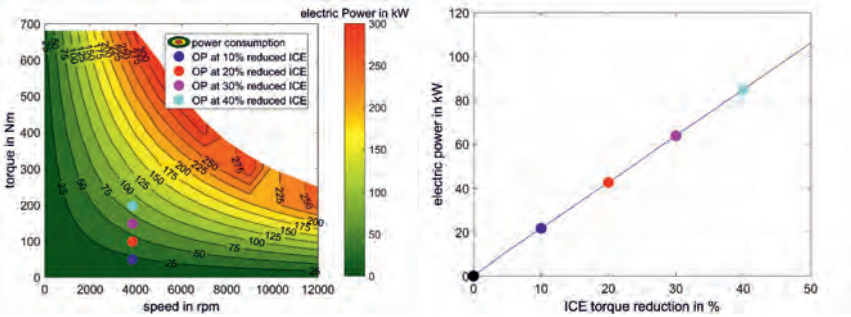

Fig. 12: Power consumption of e-Drive System

The goal is to find the optimal ratio of fuel savings vs. electric power consumption. Therefore, the fuel savings of the ICE are divided by the power consumption of the e-Drive as shown in

Fig. 13. This ratio stands for the achievable fuel savings while spending 1 kWh of electric energy and can be interpreted as a fuel conversion rate.

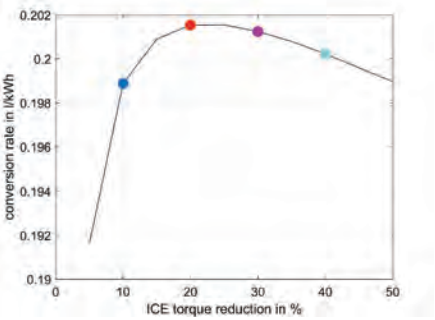

Fig. 13: Fuel conversion rate

For the black operation point a maximum fuel conversion rate of 0.202 l/kWh can be found at an ICE torque reduction of about 25%. In order to save as much fuel as possible it is very important to know the optimal amount of traction support for all operating points of the ICE.
Fig. 14 shows the optimal fuel conversion rate for all ICE operating points and the corresponding amount of torque reduction.

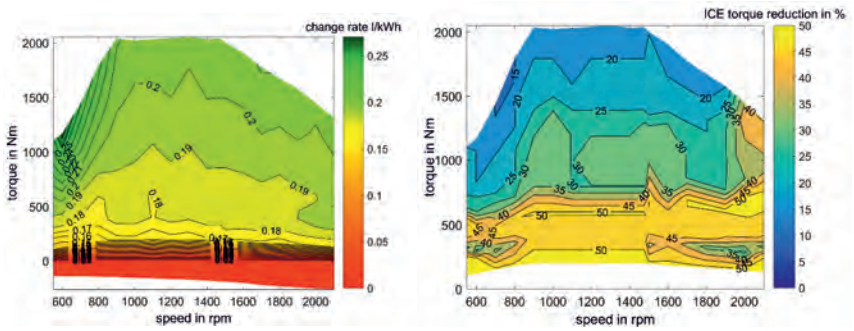

Fig. 14: Fuel conversion rate and torque reduction map of ICE

The optimal conversion rate is about 0.21 l/kwh and can only be achieved at high torques of the ICE. To optimize the fuel savings traction support during partial load of the ICE should be avoided. The efficiency of the e-Drive system at low speed is not good (see Fig. 10). To further optimize the fuel savings the traction support is only activated above a minimum vehicle speed.

Using the recuperated energy during the VECTO regional delivery cycle in combination with the presented traction strategy it is possible to achieve fuel savings of 6.5 l/100km (16%). Fig. 15 shows the energy charts of the VECTO delivery cycle for a conventional truck trailer combination and the eTrailer with a 300 kW e-Drive system. The total weight of the e-Drive system including the battery will not exceed 800 kg.

Using the explained traction support strategy, the maximal traction power of the e-Drive system is only about 130 kW. Nevertheless, a system power of 300 kW is required to recuperate all of the consumed electric energy and sustain the state of charge of the battery.

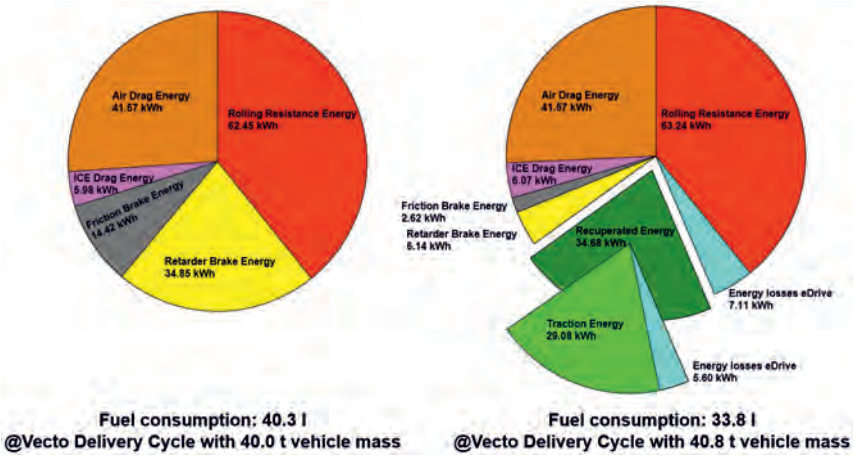

Fig. 15: Energy charts of the VECTO delivery cycle

E-machine type selection

In order to identity the right e-machine type for the eTrailer use case the efficiency map of two different axle mounted high-speed e-machine types were analyzed. An induction machine (IM) has relatively low no load losses and a high efficiency at high speed but only a moderate efficiency at high torques. A permanent magnet synchronous machine (PSM) has relative high no load losses but also a high efficiency at high torques.

The Fig. 16 below shows the area where the PSM has a higher efficiency than the IM. The blue points are the operating points during the VECTO reginal delivery cycle with a 40 t truck trailer combination. Some operating points are in the area where the PSM has a higher efficiency but there are also lots of points in the area where the IM has a higher efficiency.

The PSM has a lower efficiency at roughly 50% of the traction operating points. That means that both e-machine types require nearly the same total energy for the traction support. The PSM has a higher efficiency at high recuperation power, leading to higher amount of recuperated energy during the VECTO reginal delivery cycle. That is why the possible fuel savings using a PSM are a little bit higher than using an IM.

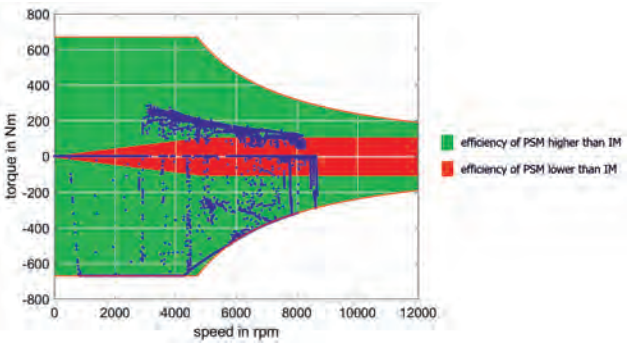

Fig. 16: Efficiency comparison of IM and PSM

First eTrailer prototype

The first Prototype was built up to validate the simulation and allow a validation in function of the general concept of the eTrailer. Therefore, available components of the shelf where used. The prototype has a frame mounted 270 kW induction machine with a maximal torque of 1400 Nm (Fig. 17). The optimal gear ratio for this e-machine would be 1:8. Since such gear ratio was not available, a differential gear with a gear ratio of 1:5 was used, leading to a maximum axle torque of 7000 Nm which is far lower than the required 12000 Nm. In addition, the

maximum recuperation power of the e-Drive System (270 kW) can only be reached in the speed range of 65-80 km/h.

Using the components of the first prototype in the simulation tool, fuel savings of 4.8 l/km were calculated. On the test track fuel savings of 4.5 l/100km were measured. That means that the simulation could be validated.

For the next Prototype a high-speed axle mounted PSM with a maximum recuperation power about around 300 kW in a speed range of 45-80 km/h is planned to increase the achievable fuel savings to an expected value of 6.5 l/100km.

Fig. 17: First eTrailer Prototype

Conclusion

Using the integrated endurance brake management of the EBS and TEBS to control the eTrailer maximizes the potential for recuperation. The eTrailer should have an e-Drive system power of about 300 kW to recuperate as much energy as possible while avoiding oversizing in the interest of cost optimization. Even though the eTrailer requires a high charging power and only a small battery capacity it can be more beneficial to use a high-energy battery than using a high-power battery. An axle mounted high-speed permanent magnet synchronous machine has more advantages than a high-torque frame mounted solution. The traction support of the e-Drive should be optimized based on efficiency characteristic of e-Drive system and ICE. Overall, using the eTrailer fuel savings of 16% can be achieved in the VECTO delivery cycle. In this layout the eTrailer can be a powerful and economic solution for hybridization of conventional ICE tractors – however, in the long term eTrailer technology has additional potential as enabler for long-haul BEV CV.

Alternative drivetrains for sustainable commercial vehicles

Dipl.-Ing. **Rico Resch**, Dr. **Christoph Danzer**, **Alexander Poppitz**, **Tommy Pirkl**, IAV GmbH Stollberg

Abstract

Ecological awareness among customers and the industry as well as legislative regulations in key markets will drive the demand for sustainable commercial vehicles (CV). In a techno-economical study IAV proved that electrically driven CVs are the most efficient option for a sustainable mobility. To propose a well-suited powertrain concept that fulfils the market requirements, IAV utilizes its “Powertrain Synthesis” methodology. The results from this systematic process are used to make data driven design decisions. Within the boundaries of this investigation, IAV developed a 2-E-Motor 3-speed E-Drive Unit (EDU) as a concept that can be utilized for various applications ranging from 18t rigid trucks up to 40 t long haul tractors. The concept uses electrical sub-systems, which have characteristic properties that are typical for light vehicle applications. Advantageously, this may facilitate a scaling potential of these components regarding production volumes, thus enabling lower prices for these components. Depending on the vehicles load profile the EDU may be used in a 4 x 2 or a 6 x 4 axle configuration to provide appropriate drive torque in all driving situations.

Introduction

Future commercial vehicles have to meet diverse and at the same time conflicting boundaries, Fig. 1. Two main driving factors for future development originate mainly from legislative regulations: harmful emissions and entry bans to city centers. The map in Fig. 2 provides a rough overview about CO_2-regulations that are in place or will be intensified in leading markets around the globe. In connection with the Paris climate goals this means that one of the dominating targets of future truck development will be carbon neutrality. Furthermore it is expected that entry bans into certain urban areas will come in the future, may it be 24/7 bans or maybe only during certain time frames. In such cases transport companies will demand Zero Emission Vehicles (ZEV) to be able to provide goods to their customers. Besides the environmental and regulatory targets, also the market attractiveness of products and the financial potential are main influences for a successful commercialization of future truck platforms. A main challenge in regard to this topic is to realize lowest total costs of ownership. To provide a cost effective vehicle to the customer, OEM’s may be using highly flexible and modular systems with potential for global scalability. In order to achieve low running costs,

these systems furthermore need highly efficient drivetrain solutions that are perfectly balanced with other vehicle and performance requirements. Various analyses show that alternative powertrains will have the potential to overcome conflicting targets in future, e. g.: [1].

Fig. 1: Conflicting boundaries for future commercial vehicles

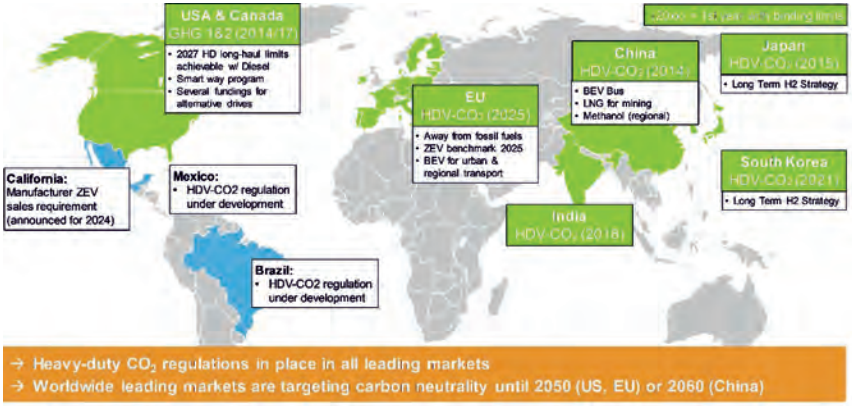

Fig. 2: Exemplary regions with CO_2 regulations in place or under development

In order to develop the right powertrain technology to meet regulatory and market requirements, IAV employs a standardized development process that covers everything from overall requirements to the optimally balanced vehicle concept, Fig. 3. An optimal result regarding multiple criteria like efficiency, costs and sustainability may be found by using

computer aided methods that are part of IAV's digital development tool chain. After a high level concept approach, systems engineering loops are carried out with deep dives into the component layout and dimensioning for hardware and software. Based on that vehicle, cost and lifecycle simulations lead to a systematical improvement of the concepts. The final result of this process is an optimally balanced vehicle and powertrain concept whose specific parameters can be traced back to data-driven decisions with a maximum of transparency.

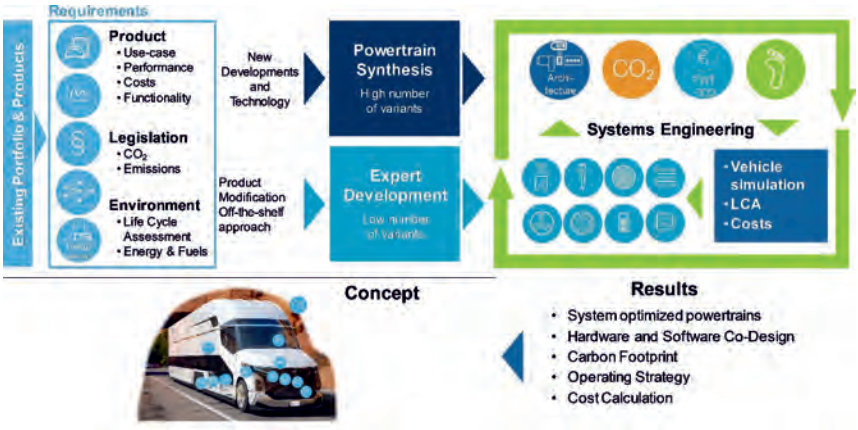

Fig. 3: Holistic development process from requirements to optimized concept

Evaluation of alternative powertrains in comparison with fossil-fueled powertrains

General requirements for a newly developed powertrain, like energy source and energy conversion principle, can be derived from a techno-economical study, carried out by IAV, [1]. The complete study covers passenger cars, light and heavy commercial vehicles. For these vehicles optimized powertrain layouts were determined for hydrogen (H_2-ICE, H_2-Fuel Cell) as energy source as well as for battery electric vehicles (BEV) and for conventional diesel ICE.

In order to assess more than the Tank-to-Wheel (TtW) balance of the different technologies, as it is the case under current regulations, the entire life cycle is considered, including various energy pathways and also the vehicle production, Fig. 4. The original study provides information on the Total Cost of Ownership (TCO) and the Global Warming Potential (GWP) for different stage lengths in a product life cycle, where CO_2e emissions are generated [TtW, Well-to-Wheel (WtW), Cradle-to-Grave (CtG)].

Fig. 4: Overview of H_2-Production paths, energy supply, vehicle segments and powertrain types [1]

This contribution focuses solely on the assessment of the TCO and CtG-results of a heavy duty long haul tractor trailer combination simulated in the standardized VECTO Long Haul Cycle. A few results and boundaries for the TCO and CtG calculations are shown in Fig. 5.

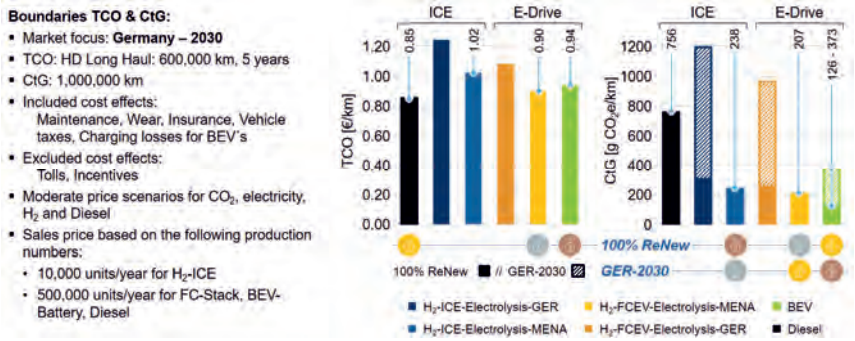

Fig. 5: TCO and CtG results for a heavy-duty long haul truck

For the Germany-2030 scenario (Fig. 5, left) considered, it is predicted that a conventional diesel powertrain will have the best TCO values. The calculations also show that the TCO disadvantage of vehicles powered either by 100% renewable energy generated in Germany (100% ReNew) or by imported green hydrogen from Middle East and North Africa (MENA) is not very high. It is in a range between 0.05 € to 0.17 € which corresponds to about 6 % to 20%. The fully filled bars in the diagram on the very right side of Fig. 5 show the CtG-CO_2e emissions

that are generated by long haul trucks equipped with the powertrains under consideration over the entire life cycle with 100% ReNew energy. It becomes obvious that a BEV truck is the best option. Second and third best options are MENA-hydrogen-powered trucks using either a fuel cell combined with an electric drivetrain (FCEV) or a hydrogen-ICE with a 12-speed DCT (H_2-ICE). This reverses if electric energy is used to power the BEV trucks, which is not completely generated by renewable sources, as currently predicted for Germany in 2030. This can be seen, when the green diagonally dashed bar for the BEV is compared to the fully filled bars for the MENA-hydrogen-powered trucks. Either way, the CtG-CO_2e emissions of a conventional diesel truck are about 600 % compared to a BEV truck powered by 100 % renewable energy or still 365 % compared to the MENA-hydrogen-powered truck. At the same time, it must be pointed out that hydrogen production by means of electrolysis and using the energy mix predicted for 2030 in Germany is worse than a diesel powertrain running on fossil fuels. Such a use case must be prevented. As a consequence of the previous investigations, it is essential to move away from fossil diesel as a fuel to alternative drive systems that are powered by energy from sustainable sources. In addition, the truck should be equipped with an electric drive system for maximum efficiency.

Systematic development of alternative powertrains

The high potential of alternative powertrains regarding sustainability brings new challenges for the vehicle design. This is due to the new energy carriers that need to be fitted in the available package space in a safe manner. This challenge is visualized at the example of a Fuel Cell Truck in Fig. 6. At the same time the picture lists components that are required in a heavy duty long haul truck for a target range of 800 km (according to the simulation results in [1] for 2030).

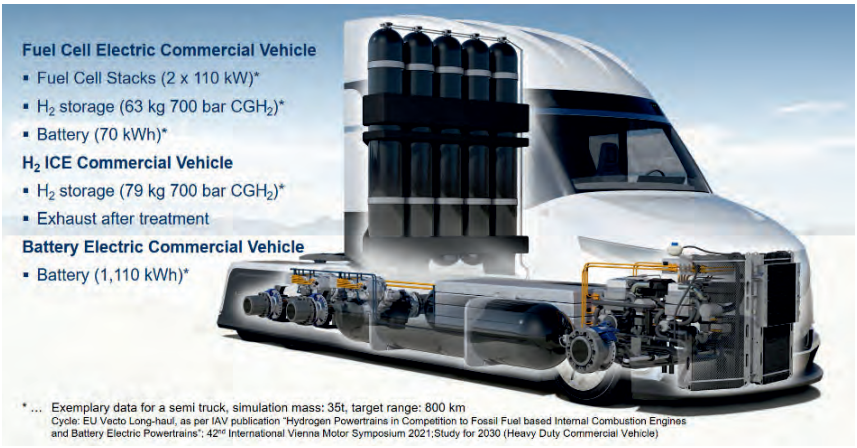

Fig. 6: Packaging challenges for alternative powertrains

Depending on the powertrain choice it might be sufficient to integrate hydrogen tanks and a hydrogen combustion engine with an appropriate exhaust after treatment to deal with emissions that are not allowed by legal regulations, e. g. NO_x. In this case the powertrain package may be comparable to current diesel trucks. If the powertrain should provide a higher overall efficiency making use of an electric drive system it is either necessary to integrate a significantly large battery pack or a more complex fuel cell system with its stacks, the hydrogen storage and an additional battery, that is much smaller than that of a comparable BEV.

Since electrically powered vehicles, whether FCEVs or BEVs, are more efficient, it is important that adequate drive systems are available in the future.

For the exemplary target vehicles shown in the upper part of Fig. 7, representing trucks with a possible combined weight of up to 40 t, different powertrain topologies were investigated in regard of their specific advantages. The classical central drive on the very left of Fig. 7 has significant advantages in regard of using or implementing carryover parts from current powertrains like rear axles or PTOs. Additionally, there is a high flexibility for the E-transmission design as there is a significant amount of axial packaging space in the current powertrain area. On the downside this topology limits the available package space for the energy storage. That's the big advantage of the other three powertrains, starting with wheel individual electric motors or axle drives where the E-transmission is arranged either transverse or longitudinal on the very right of Fig. 7.

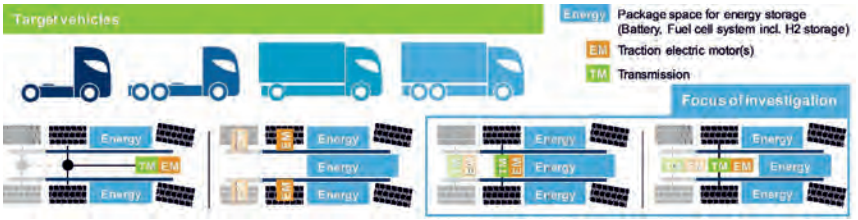

Fig. 7: Powertrain and energy storage installation options in heavy-duty on-road trucks

Drive systems where the electric motor is directly integrated in the wheel do have an extremely high mechanical efficiency. But these solutions typically do not have a multi speed connection between the motor and the wheel and therefore are limited in optimizing the electrical path during operation. In addition to that, the electric motors required for these drives need to provide a large torque and also a wide range of speeds to cover all requirements regarding vehicle start, gradeability and also maximum vehicle speed. Both properties are the big advantages of integrated axle drives, where electric motors are connected to a multi speed transmission. There, the electrical efficiency can be optimized at the expense of a slightly lower mechanical efficiency. Previous IAV-internal investigations have shown that this advantage is key for drive systems that are used in applications that need to cover a wide range from high launch torques up to high vehicle speeds.

Although the package is a challenge for the E-Transmission, the current investigation focuses on an integrated axles drive system as the basis for the concept of a new e-drive for commercial vehicles.

The decision for an integrated axle drive does not clearly define the arrangement of the electric motors and the gear set in relation to the drive shafts. Transverse EDU arrangements, as shown in the topologies on the left side of Fig. 8, have the advantage of using helical gears down to the differential. These are simple to manufacture and may realize a high efficiency during operation. This study identified gear set arrangements with up to 3 speeds that could fit into the tight package. Advantageously, longitudinal arrangements, such as those shown on the right side of this Fig. allow more axial installation space and thus more speeds for the E-Transmission. Disadvantageously, these layouts require the implementation of a bevel gear to change the direction of rotation. In order to cover a wide range of investigated parameters, this study considers topologies with up to 3 speeds in a transverse arrangement and for more than 3 speeds in a longitudinal layout.

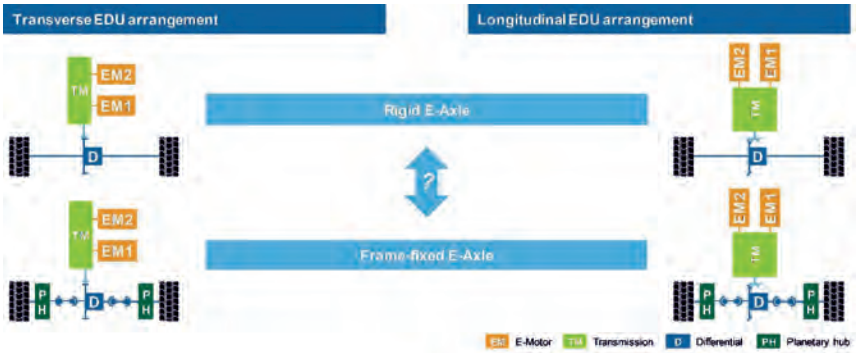

Fig. 8: Topology options for axle drives in heavy-duty on-road trucks

A final fundamental design decision must be made about the positioning of the EDU, either integrated directly into a rigid axle or fixed to the frame. A rigid axle has the advantage that the complete gear set may be integrated in one housing and that the complete torque build up is realized within the EDU. The disadvantage of this powertrain layout is that higher vibration loads at the E-axle might be challenging, given the required operating times of the electrical components. In addition, this topology leads to higher unsprung masses. Both of these issues can be improved by implementing a frame-mounted EDU. One disadvantage of this layout is, that the torque needs to be transferred via drive shafts that are flexibly connected to the drive unit and the wheels via universal joints. The required maximum axle torque is considered critical for the u-joints. A possible solution could be an additional planetary hub in the wheel.
To be able to use standard axle parts that can be found in current heavy duty applications the new concept shall be realized as a rigid axle concept.
After the definition of the most principal design boundaries, it is necessary to identify, how many speeds are beneficial for an EDU-concept for commercial vehicles. The decision about the most important powertrain parameters may be supported by IAV's unique Powertrain Synthesis methodology that was established about 8 years ago. A main reason, why this methodology was developed is the demand for objective and transparent, data driven decisions. This tool enables the generation of the relevant data within defined investigation boundaries. The innovation of this method is rooted in the systematical cross-combination of all theoretically possible system parameters without ignoring any combination, Fig. 9.

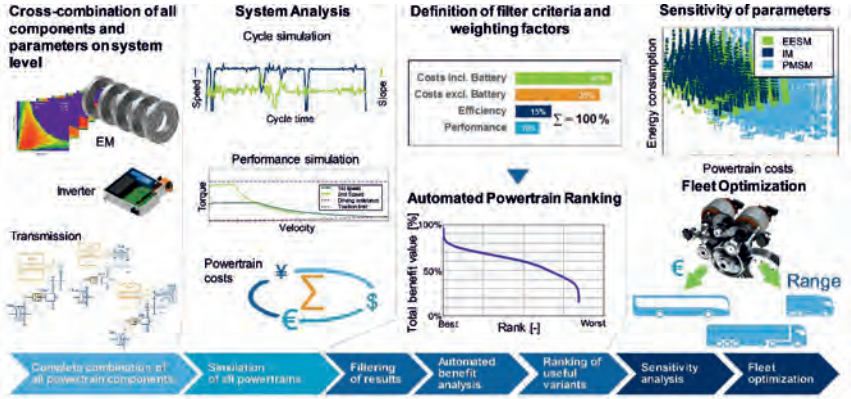

Fig. 9: Process overview of IAV‘s Powertrain Synthesis

In the first phase of the process millions of system configurations are often generated, which are then systematically investigated for their efficiency behavior, performance characteristics and costs. Based on the vehicle requirements a set of filters is applied to identify the valid powertrain configurations. After that, an objective ranking is generated by a benefit analysis, where the most important properties are assessed with different weighting factors. To define the right filter values and weighting factors it is important that the overall system properties are taken into account. In a next step the whole solution set or only a part of it may be investigated regarding the effects that arise from different powertrain parameters. The results may be investigated on the basis of the pure data or with an appropriate visualization that shows up to several million different powertrain configurations in one diagram. In the end IAV’s or IAV’s customers engineers have all the information in hand to make the right decision based on objective data.

The process described above was implemented for the development of the new e-drive concept. The aim of this study is to optimize an EV powertrain for European requirements. The main application is a typical heavy duty long haul vehicle with a maximum weight of 40 t. For cost reasons, it is important to develop a solution that can be used flexibly and has the potential for global scalability. Therefore, the specifics of the US market are also taken into account. This enables a worldwide use of the drive system. The most important parameters of the study are shown in Fig. 10.

Fig. 10: Boundaries for Powertrain Synthesis study to determine optimized and valid powertrain topologies

As previously described, in the powertrain synthesis process sensitivity charts are generated to get information about effects, different powertrain parameters do have. On the left side of Fig. 11 some exemplary diagrams are shown, where one is enlarged to explain this approach a bit more in detail.

In the large diagram on the upper right side of Fig. 11 more than 10 million valid powertrain solutions are plotted with its total benefit value versus the cycle energy consumption in the VECTO long haul cycle. The total benefit value assesses each single solution regarding multiple criteria from the area of efficiency, cost and performance. From the diagram a general tendency becomes obvious. Even in EV-drives an increasing number of speeds may provide a better overall system. This can be determined from the maximum total benefit value of the solutions in each group. Due to the weighting the high total benefit values are significantly associated with a low energy consumption throughout the drive cycle. An important relation shown in the diagram is the fact that a drive system with more gears does not generally have better characteristics. Depending on the powertrain layout and the parameters of the powertrain, it may also be the case that a system with a lower number of speeds is the better compromise. The powertrain synthesis methodology aims at precisely this aspect - finding a drive system with the lowest mechanical, electrical and cost effort to achieve the best overall benefit.

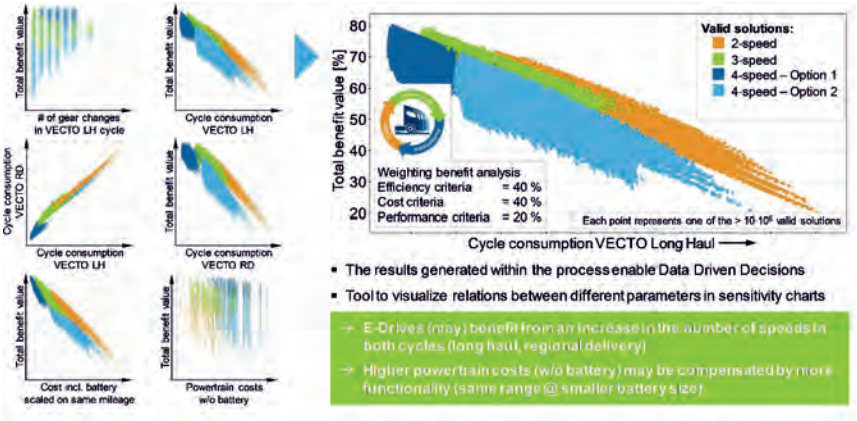

Fig. 11: Exemplary results of the Powertrain Synthesis study with focus on different topologies

Based on the large number of solutions in Fig. 11, it can be seen that the range of solutions can be further restricted. As a result, solutions are to be identified which also offer advantages from a cost perspective. Therefore, the next step is to identify preferred solutions that meet the additional requirements shown in Fig. 12. These requirements take into account that the use of electric motors, which can also be found in high-volume markets for light vehicles, offers further cost potential. In addition, such electric motors can be built smaller, making it possible that the multi-speed drive unit fits into the limited packaging space within the frame.

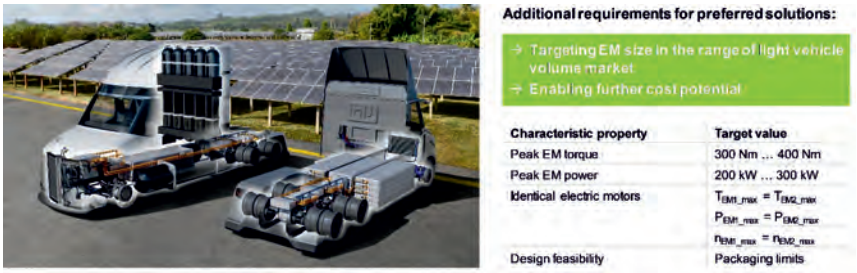

Fig. 12: Additional requirements for preferred solutions with focus on cost potential on EM-side

The sensitivity chart on the upper right side of Fig. 13 shows the impact of the additional requirements. All the powertrain variants shown as a grey dots are removed under the new boundaries. Only the colored solutions are fulfilling the additional requirements. The previously

highest ranked 4-speed drive system is removed from the solution amount and so the best three speed solution is the best balanced compromise on system level. The exemplary diagram on the left side shows one reason, why the three speed variant is the best compromise in this group. It has the lowest summarized mechanical and electrical losses.

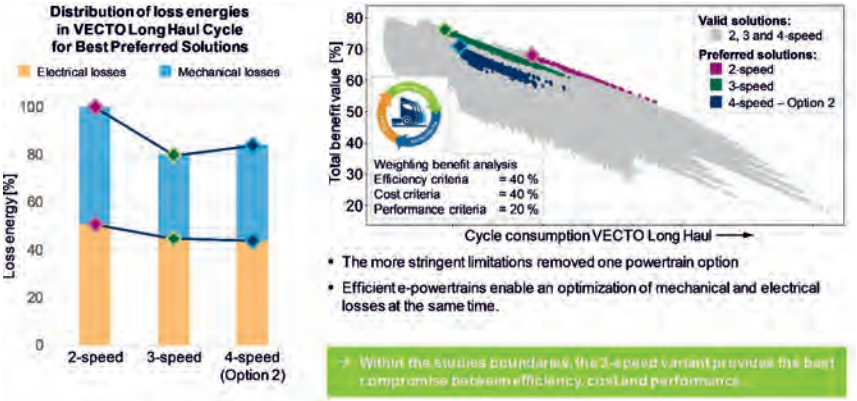

Fig. 13: Exemplary results for preferred solutions of the Powertrain Synthesis Study

IAV's new 3-speed E-Drive concept

Based on the previous investigations the E-Drive concept that is shown in Fig. 14 has been identified as a well-suited solution.

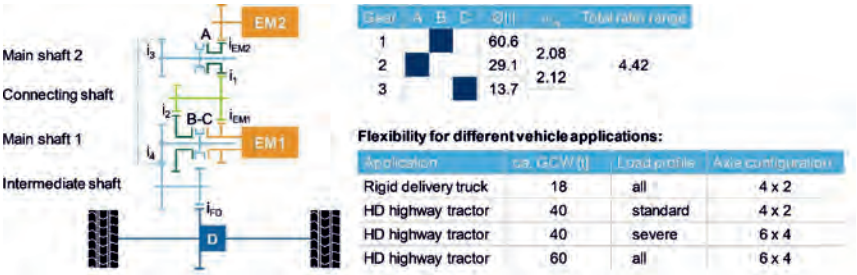

Fig. 14: Topology, shift logic, EDU ratios and configuration options for different applications of the new 3-speed E-Drive concept

The drive system is developed as a rigid axle concept, solely based on helical gear sets and dog clutches as shift elements. The main mechanical elements – gear set and also shift elements – are arranged in 4 main levels. Combined with the relatively small electric motors,

it is possible to fit the system into current packages. The small electric motors are a core element of this EDU concept. Besides the previously mentioned possibility to be compatible with components from the volume market, this EM size may fulfil the torque and speed requirements within the available package. Due to the low maximum torque of the EM it is necessary to achieve a high mechanical ratio of about 60 within the gear set in the first gear. The E-transmission realizes a total ratio range of 4.4. For a low energy consumption the efficiency optimized design uses locating floating bearings for the majority of the shafts and an electric oil pump to realize an on-demand supply for the lubrication needs.

Another important item for a commercial vehicle EDU is its versatility. Used in a 4 x 2 or 6 x 2 configuration it provides sufficient drive power for 18 t rigid pick-up & delivery trucks or heavy-duty highway tractor-trailer combinations being used within a lighter load profile. For more severe load profiles or heavier vehicles with up to and more than 60 t gross combined weight the truck should be set up in a 6 x 4 axle configuration.

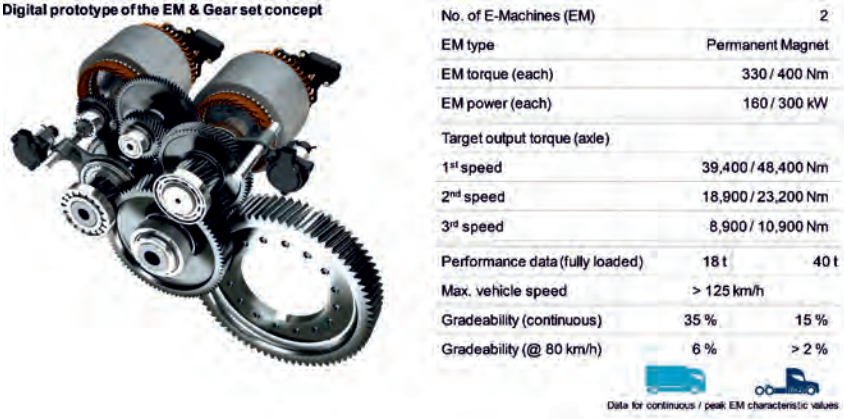

Fig. 15: Digital prototype and core performance data of the new 3-speed E-Drive concept

On the left side of Fig. 15 a digital prototype of the new E-Drive unit's gear set and electric motors is shown. IAV's e-Drive concept makes use of two relatively small permanent magnet synchronous electric motors, each with a continuous torque of about 330 Nm and a continuous power of 160 kW. The electric motors used in this concept have been developed using IAV's development tool chain for dimensioning and designing electric motors. In order to speed up the overall development process towards series maturity and to achieve further cost potentials it is also possible to acquire motors with comparable characteristic properties from the volume

market of light vehicles. If doing so, it is necessary to consider the specific durability requirements and how to handle these by using off-the-shelf components.
The two motors are combined with a 3-speed E-Transmission to provide a peak axle torque of more than 48,000 Nm in the first speed. With the continuous torque in first speed a gradeability of 15 % is possible for a heavy-duty tractor trailer combination with a gross combined weight of 40 t and more than 30 % for an exemplary rigid truck weighing 18 t. With the other two speeds the E-Drive-Unit offers sufficient drive torque in situations for up to 125 km/h. Due to the maximum power of the drive unit the two previously named vehicles have a gradeability of 2 % respectively 6 % at a vehicle speed of 80 km/h. In case that this isn't sufficient, the system may be used in a 6 x 4 axle configuration to double the drive torque. Additionally to the positive impact on drive torque it is also possible to increase the overall vehicle efficiency in real world drive cycles as the efficiency map of the electric motors may be used in better areas.

Key takeaways

A global need for carbon neutrality leads to a necessary change in commercial vehicle powertrains towards alternative powertrains. Electrically driven commercial vehicles provide the highest potential regarding Cradle-to-Grave CO_2-equivalent emissions. Either with an energy storage in a battery or in hydrogen that is produced with renewable energy.
IAV's systematical methodology to identify optimal powertrains may be applied to heavy duty commercial vehicles.
In this study, IAV shows that it is possible to develop a well-suited multi-speed E-Drive unit for commercial vehicles with motors that have characteristic properties, which are in the range of vehicles with high production volumes. The drive concept that was developed may enable a top vehicle performance in single or dual axle drive systems. Additionally it provides cost potentials for fleet operators due to low energy consumption that should be achievable in real world operation. Finally it offers scalability of production volumes on the one hand through a flexible use in different applications and on the other hand by optional making use of components that are also a good match in volume market applications.

Closing remarks

The author likes to thank everybody who was involved in the development activities that led to this new 3-speed E-Drive concept.
For more details about the techno-economical study the authors recommend to review the original resource [1].

References

[1] Sens, M.; von Essen, C.; Dr.-Ing. Brauer, M.; Wascheck, R.; Dr.-Ing. Seebode, J; Kratzsch, M: Hydrogen Powertrains in Competition to Fossil Fuel based Internal Combustion Engines and Battery Electric Powertrains; 42nd International Vienna Motor Symposium 2021
also available at (state of September 16th 2021):
https://www.iav.com/app/uploads/2021/04/210422_Paper_Vienna_IAV.pdf

Holistic system design and operation of a fuel cell truck based on an innovative energy management

Dr. **Christoph Schörghuber**, Dipl.-Ing. **Markus Ortner**,
Dipl.-Ing. **Johannes Pell**, Dipl.-Ing. **Sabine Pretsch**,
AVL List GmbH, Steyr, Austria

Abstract

The powertrain of a fuel cell truck consists of several systems, the most important ones are the fuel cell, the battery, the e-axle and the cooling system. All systems have to operate together in an optimal way which is controlled on high level by the energy management. Due to the special properties of the components and the limited installation space in the vehicle the system design is challenging. The focus for system design is on fuel efficiency optimization on a defined driving cycle under consideration of all system limitations. Especially for fuel cell and battery system these limitations are changing over lifetime due to aging effects. In this paper a model-based approach is described where overall vehicle simulations are used to support system design. Standard energy management as well as predictive energy management are investigated. Furthermore, the energy split between the involved powertrain sub systems is analyzed. Based on parameter variations and analysis of the resulting energy split the well dimensioned powertrain configuration is confirmed.

Introduction

Global climate change and the resulting stricter emissions legislations are pushing the automotive industry to develop new clean powertrain technologies, refer to e.g. [1]. Especially in the field of heavy duty commercial vehicles this is quite challenging. In addition to the zero emission target, the powertrain must be operated with highest efficiencies. Important vehicle requirements such as driving range, weight, product cost and installation space lead to conflicting goals. Hydrogen in combination with proton exchange membrane fuel cell (PEMFC) technology can be one solution for a future zero emission propulsion technology for heavy-duty trucks, especially in long-haul application. Thereby hydrogen is stored within high pressure tanks in gaseous or liquid state. The relatively fast refilling possibility of hydrogen is representing an important advantage of this technology. On the other hand, the overall powertrain efficiency decreases slightly over time due to aging effects of the fuel cells and battery cells. The resulting cooling demand leads to a significantly higher complexity of the

thermal management system compared to other technologies which furthermore presents a challenge for vehicle integration [2]. However, these difficulties can be overcome by optimizing the powertrain systems and their dimensioning for the considered vehicle application in a holistic approach. The presented methodology for model-based system design takes into account all relevant systems and their characteristics, including energy management, from the beginning of development.

System overview and design approach

The considered vehicle application is a typical European 4x2 heavy-duty long-haul semi-trailer tractor with a possible gross combination weight (GCW) of 42 tons (i.e. 40t + 2t due to European new energy legislation). The main components of the powertrain are the hydrogen tank system, the fuel cell system, the battery system, the e-axle system, the thermal management system, the brake resistors, the auxiliaries (e.g. steering pump, brake air compressor, air conditioning) and the control units incl. energy management, see Fig. 1.

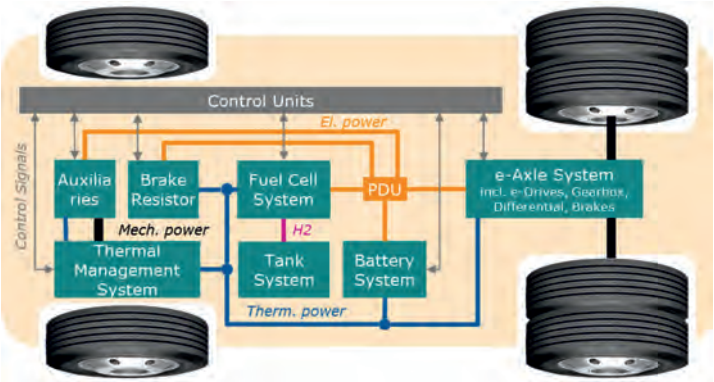

Fig. 1: Powertrain overview of a fuel cell powered long-haul truck

The fuel cell system contains the fuel cell stack including a certain number of fuel cells in series, the balance-of-plant (BOP) components including pumps, air blower, valves, etc. as well as the DC/DC converter to adapt the voltage level of the fuel cell stacks (410 - 520 V) to that of the DC-link defined by the battery system (530 – 720 V), refer to [3]. The fully integrated e-axle contains two e-motors, a shiftable two speed gearbox, a differential drive and the mechanical brakes, while the inverters are integrated into the vehicle chassis [4]. The power

of the e-axle of 400 kW continuous and 540 kW peak is selected to permanently enable vehicle inclination requirements of 2.5 to 3% (depending on vehicle resistance) at 80 kph. The required electric energy for vehicle propulsion and auxiliary supply is provided by the fuel cell and battery system. The battery is used to store energy and to cover high dynamic power requests. During vehicle braking, electric energy is recuperated into the battery or, if the battery is fully charged, dissipated via brake resistors. The waste heat of fuel cell, battery, e-drives (i.e. e-motors and inverters), brake resistors and auxiliaries (e.g. air conditioning) is discharged via the thermal management system to the surroundings. Thereby several cooling circuits including appropriate heat exchanger areas and fan power have to be considered. The target of the energy management is to control the electric and thermal energy flow in order to achieve highest powertrain efficiencies under consideration of all system limitations and aging effects [3].

For system dimensioning the general idea is to develop a powertrain with hydrogen as main power source where only the hydrogen tanks have to be refilled and no external battery charging is required. Thus, the resulting fuel cell system has to provide at least the average power required for vehicle propulsion on the representative driving cycle. According to the typical efficiency characteristics of a fuel cell, the efficiency is lower at maximum power, whereas the highest efficiency is achieved at relatively small power values, see Fig. 2Fig. 1.

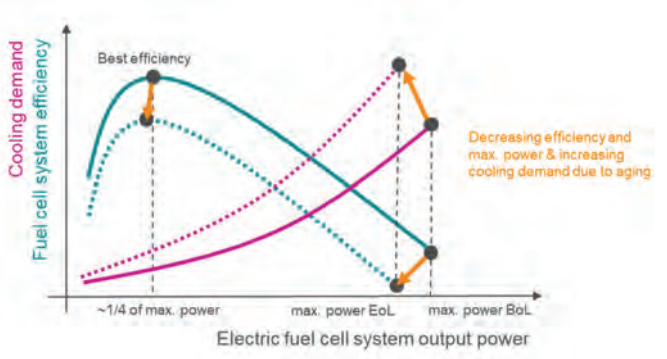

Fig. *2*: Efficiency characteristics and principle cooling demand of a fuel cell system depending on power and aging

If the fuel cell system is dimensioned in order to achieve the best efficiency at average power of about 100 to 150 kW of a typical long-haul truck driving cycle, it is currently hardly possible to integrate the resulting fuel cell system (resulting in 400 to 600 kW max. power) into the

available installation space of a standard truck. So of course also the available installation space has to be considered when doing an optimized system dimensioning. Furthermore, the efficiency curve and the maximum provided power of a fuel cell is decreasing over lifetime due to degradation effects. Consequently, also the required cooling demand is increasing. Also the availability of the BOP components plays a decisive role for fuel cell system dimensioning. In accordance with the above-mentioned interrelationships, the fuel cell system must be designed as large as possible in order to maximize the efficiency, but taking into account all the boundaries. The potential of regenerative braking is mainly limited by the power capabilities of the e-axle and the available battery capacity and charging power, influenced also by the aging of the battery cells over lifetime.

The dimensioning of the fuel cell and battery system is done within overall vehicle simulations on a defined driving cycle. To achieve the optimum solution, all influencing factors such as energy management and component aging as well as possible installation space and costs have to be considered. To exploit the full recuperation potential, predictive energy management must be used in order to avoid reaching preventable battery state of charge (SOC) limitations of the battery.

Aging behaviour of fuel cell and battery systems

Fuel cells are essentially used to convert the chemical energy of a fuel like hydrogen directly into electricity through electrochemical reactions. A proton-exchange membrane fuel cell mainly consists of an anode surrounded by hydrogen and a cathode surrounded by oxygen. The two electrodes are typically made of carbon coated with platinum and are separated by the cell membrane allowing protons to pass. As a result out of an exothermal chemical reaction water is generated and an electric current flows between the two electrodes. In order to increase the voltage level, several fuel cells are connected in series to a fuel cell stack. Due to different degradation mechanisms the performance of a fuel cell is generally decreasing during operating time. This is reflected by a decreasing cell voltage and cell efficiency, see Fig. 2. As described in [4], the main degradation effects in a fuel cell are mechanical and chemical degradation of the cell membrane, platinum oxidation and dissolution as well as carbon corrosion. These degradation effects are mainly triggered by fuel cell operation with high temperatures, high dynamic load changes, low power operation (idle mode) and during shut-down and start-up processes. Thus, the aging of a fuel cell is strongly depending on the available cooling power and the operating strategy which is also influenced by the fuel cell dimensioning and the limitations of the battery system. To reduce fuel cell degradation basically the battery has to support the e-motor power supply for dynamic load changes which

are depending on the application specific driving cycle. Thus, the battery power dimensioning is important and has to be adapted to the vehicle application.

Furthermore, also typical lithium-ion (Li-Ion) cells are underlying degradation effects over operation life. This degradation depends on the chemical type of the Li-Ion cells and is increasing during operation at high temperatures, over-charging, over-discharging and too high power gradients [4]. The physical effect of battery aging can essentially be described by a decrease of capacity and an increase of impedance resulting in higher losses and reduced power.

Thus, it is important to analyze the aging behavior of both systems and to consider begin of life (BOL) but also end of life (EOL) performance (achieved after typical vehicle lifetime) during system dimensioning. For this reason, aging models are used to predict end of life performance of fuel cell and battery systems.

Energy management

The overall energy management is typically placed within the vehicle control unit and considers electrical as well as thermal energy flow. For thermal energy management the temperatures of the different cooling circuits have to be controlled via the available actuators in order to keep them within required limits and to minimize the required energy for the fans. The fuel cells, (where most of the waste heat is generated) and the designated cooling circuit(s) have a rather low thermal capacity. Therefore, the potential for thermal energy management optimization regarding optimized fan power strategy and subsequently regarding overall powertrain efficiency increase is quite small.

The situation is different for the electrical energy management where two main measures for increase of fuel efficiency are available. The first one is to define an optimum power-split between fuel cell and battery system in order to achieve highest overall efficiency and the second one is to utilize the whole potential of brake energy recuperation. Due to the generally higher efficiency of the battery and the lower amount of energy conducted through the battery, the focus of the efficiency optimization is on the fuel cell system. However, the potential of brake energy recuperation via the defined e-motors is mainly depending on the battery power limitations and SOC. If battery is fully charged also the brake resistors have to be considered within the energy management, especially during continuous braking events. A further potential for electric energy flow optimization is seen in the operating strategy of the electrical auxiliaries.

The main outer influence factor for potential fuel savings is given by the driving cycle and especially the road inclination profile. Via using predictive energy management the power-split

between fuel cell and battery system can be planned on long term by defining an optimized SOC trajectory for the battery over the upcoming route. The optimized SOC trajectory defines an efficient power split, avoids full depletion of the battery and enables to utilize the whole recuperation potential before reaching a fully charged battery. Furthermore, situations can be avoided where the truck has maybe too less traction power because of an empty battery at uphill driving sections, which forces the vehicle to slow down. In Fig. 3, the planned battery SOC trajectory for a given road height profile can be seen in a schematic way.

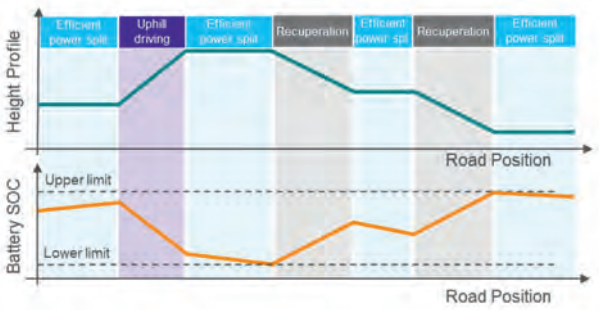

Fig. 3: Schematic diagram of predictive battery SOC planning, depending on the road height profile

Thereby different driving situations are highlighted: Before uphill sections the SOC should achieve a high level to have enough battery power and energy available during uphill driving. Thereby, the target for the energy management is more on providing the required power than on efficient driving. Before downhill sections the SOC should be at a low level to enable full brake energy recuperation. The target for driving sections with a moderate road profile without significant inclination is to split the power between fuel cell and battery system in order to achieve highest possible system efficiencies.

Without predictive controls the general idea is to control the battery SOC via the fuel cell system power to a defined target value. In Fig. 4 this operating strategy is depicted in a graphical way. As can be seen, the fuel cell system power is depending on the requested e-motor power and on the battery SOC. If the SOC of the battery is close to the target SOC, the power of the fuel cell system is equal to the requested power of the e-motor. In order to achieve highest fuel efficiency, the fuel cell system power is limited to a maximum value and is shut off below a defined minimum power level. If the battery SOC is below the target value, the fuel cell power is increased and vice versa. If battery SOC is exceeding certain minimum and

maximum limits the fuel cell power is further adapted. A certain number of calibration parameters have to be tuned during simulation loops on a defined drive cycle.

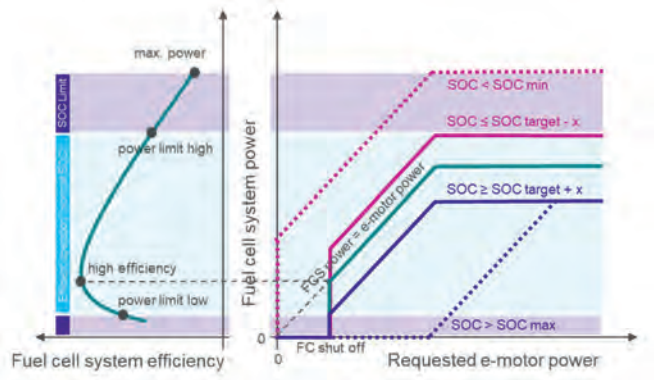

Fig. 4: Standard (non-predictive) operating strategy of the fuel cell system depending on the requested e-motor power and battery SOC with focus on fuel cell efficiency

Vehicle simulation on defined driving cycle

In order to do the calibration of the energy management, to perform the component dimensioning and to evaluate the resulting vehicle behavior as well as the energy consumption, a vehicle model is developed and overall vehicle simulations are performed. Therefore the described long haul truck and all relevant powertrain sub systems are modeled within the tool AVL Cruise M [6]. For this purpose the sub systems are considered as shown in Fig. 5, using simplified component models from Cruise M library.

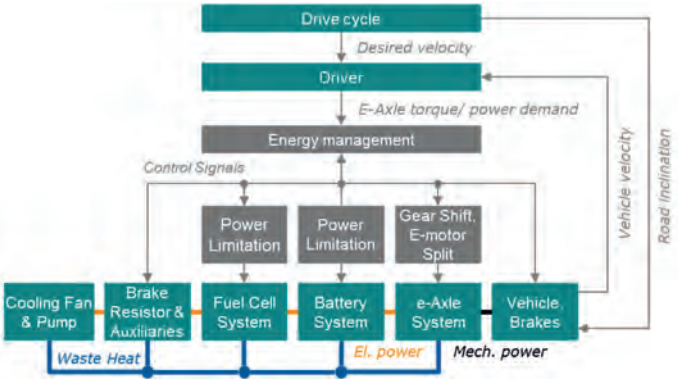

Fig. 5: Structure of the developed Cruise M simulation model for the fuel cell truck

The fuel cell system model is based on the efficiency characteristics and considers power as well as power gradient limitations. The battery system is represented by an equivalent circuit model and a power limitation. The e-axle system is modeled via efficiency maps of the e-drives as well as gear ratios and efficiency values for all gears. Gear shifting and e-motor torque split is controlled via appropriate maps. Furthermore, thermal derating based on peak and continuous power capabilities is considered for both, battery and e-drives via simplified thermal models. The cooling fan power is depending on the waste heat of all components being dissipated to the coolant and the thermic inertias and modeled via a map. The cooling pumps are considered as constant power values. The vehicle model is based on a longitudinal dynamic approach and is represented by the vehicle mass and driving resistances, simplified tire models and the mechanical brakes. The brake resistor power is controlled via the energy management. Typical constant power values are assumed for the vehicle auxiliary units.

Two driving cycles are considered for simulation. The first one, called “GWG”, driving in Austria from Graz to Wiener Neustadt and back to Graz mainly on the A2 highway is considered as dimensioning driving cycle. The second one, called “UTU”, driving from Ulm (Germany) to Trient (Italy) over the Brenner pass in the Alps and back is considered as extreme case. The speed profiles are based on the allowed legal speed limits and are furthermore processed to represent a typical truck resistance with the considered vehicle weight and maximum 330 kW wheel power respectively. In the result plots in Fig. 6 and Fig. 7 the speed as well as the road profiles are depicted. The route GWG is representing a medium challenging driving cycle where a typical conventional truck (40t GCW) achieves 35,5 liter Diesel per 100 km average fuel consumption. The UTU driving cycle is more challenging due to higher and longer

inclination phases, but total fuel consumption is at the same magnitude. The fuel cell and battery system dimensioning is done based on simulation loops on GWG driving cycle. Together with two identical defined fuel cell systems, each providing 150 kW maximum electric power, a battery capacity of 52 kWh is finally selected. These dimensioning values are based on a compromise between simulation results and the availability of commercially available components.

In Fig. 6 the results of the vehicle simulation with final parametrization on GWG driving cycle are depicted. Here a scenario with 42 tons GCW, BOL parametrization of battery and fuel cells and standard energy management (without predictive functions) is considered. As can be seen in the first diagram the demanded driving cycle velocity can be followed quite well by the simulated vehicle velocity. The velocity deviation is most of the time below one kph. In the following three diagrams the electric power load point distribution and the respective overall energy of e-axle, fuel cell and battery systems are depicted. The last diagram shows the battery SOC over time. As can be seen in the e-Axle diagram, about 540 kWh electric energy is required for vehicle traction and 100 kWh are recuperated. The battery is charged with 130 kWh in overall. Thus, 30 kWh of the battery charging energy is provided via the fuel cell system which in overall generates 530 kWh electric energy. Subsequently, 500 kWh from the fuel cell system and 115 kWh battery discharge energy are used mainly for vehicle traction (540 kWh) and to supply vehicle as well as cooling auxiliaries, resulting in 75 kWh. The electric power distribution of the fuel cell system is strongly influenced by the energy management and its parametrization. Because of the demanding driving cycle the fuel cell system is operated often at high power levels but also at lower power, when the battery SOC is close to the target SOC, or switched off.

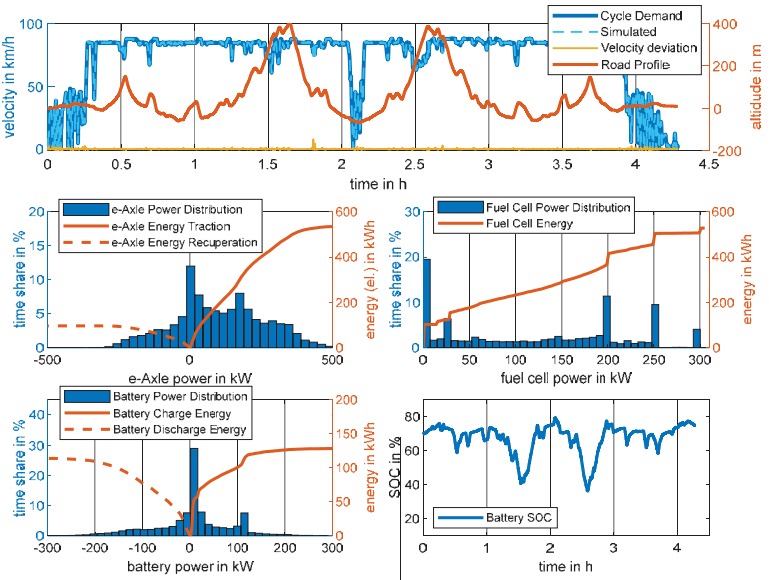

Fig. 6: Simulation results of the fuel cell truck with 42 tons GCW driving on GWG driving cycle

In Fig. 7 the results of the vehicle simulation with same parametrization on UTU driving cycle are depicted. Again a scenario with 42 tons GCW, BOL parametrization of battery and fuel cells and standard energy management (without predictive functions) is considered. The velocity deviation is getting significantly higher for some sections. This is mainly resulting due to battery SOC limitation at a minimum of 15%. Compared to the GWG results the fuel cell power distribution is shifted to more extreme power values, i.e. the time share for fuel cell shut off and maximum power is increased. Nevertheless, the quite demanding drive cycle over the Brenner pass can be driven with satisfactory performance.

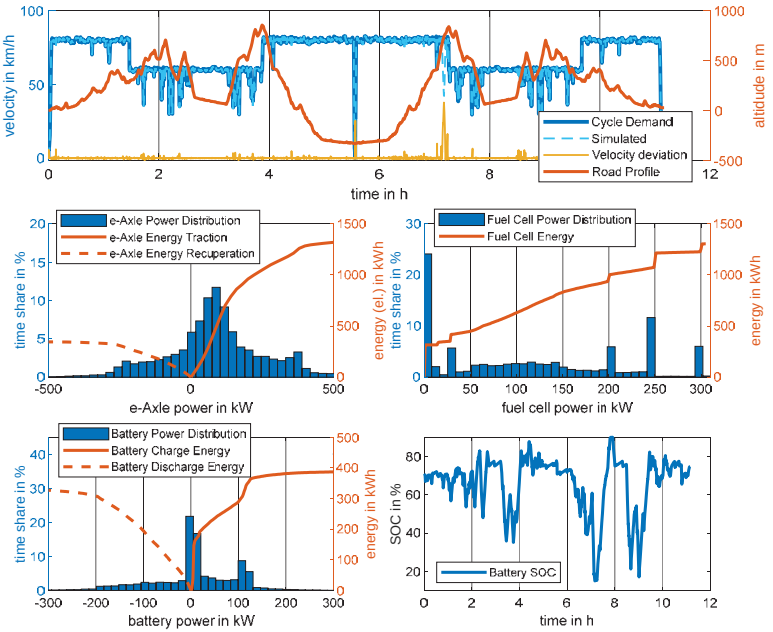

Fig. 7: Simulation results of the fuel cell truck with 42 tons GCW driving on UTU driving cycle

Resulting energy split of all powertrain systems and sensitivity analysis

For detailed analysis of the energy consumption and the respective powertrain losses, the consumed energy of all powertrain systems is calculated in kWh per 100 km and relatively compared. Furthermore, some parameters are varied in order to show their impact on the resulting energy split. In Fig. 8 the results are shown.

The first diagram indicates the energy split of the truck with 42 tons GCW driving on GWG driving cycle, representing the situation depicted in Fig. 6. The base (100%) for the relative representation in this diagram is the consumed hydrogen fuel on the overall driving cycle. As can be seen, 36 % of this fuel amount is used for vehicle traction representing the energy required for overcoming the vehicle resistance. No potential energy is included in vehicle traction because start and end location of the driving cycle and thus also start and end altitude are identical. The remaining part of the overall energy is lost in the powertrain systems, where the major part of 49 % is lost in the fuel cell system for conversion of chemical power into electrical power. Only 1% is lost in the battery during charging and discharging. About 8 % is

lost in the e-axle system, split into 5 % e-drive losses and 3 % mechanic gear losses. 5 % of the consumed hydrogen energy is used for operation of the auxiliaries including typical vehicle auxiliaries (e.g. steering pump, brake air compressor, air conditioning) as well as cooling auxiliaries (e.g. pumps and fans). Only 1 % of the consumed energy is lost in mechanical brakes or in the brake resistor during vehicle braking events mainly caused by reduced power limits due to e-motor or battery derating. This confirms the well dimensioned powertrain for the GWG driving cycle.

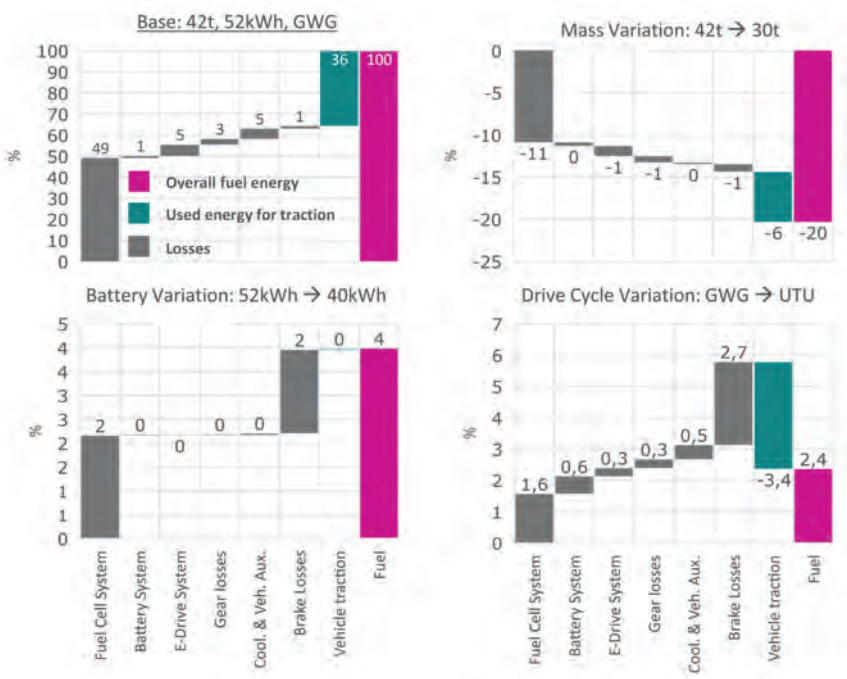

Fig. 8: Resulting energy split of the fuel cell truck with 42 tons GCW, BOL parametrization of battery and fuel cells, driving on GWG driving cycle (base) and relative comparison of the energy split for some parameter variations

In the following three diagrams the impact on the fuel consumption and the respective energy split is shown as a relative comparison to the described base energy split. If the vehicle mass is changed from 42 to 30 tons, the fuel consumption is reduced by 20 %. It is remarkable that

only 6% of this reduction is coming from the reduced vehicle resistance. The major part of 11% fuel reduction is coming from fuel cell system operation at lower power values resulting in higher efficiencies. Except the auxiliary systems, the energy consumption of all other powertrain systems is reduced by about 1 %. If the battery capacity is reduced from 52 to 40 kWh the fuel consumption is increased by 4 %. Due to the consequent decrease of battery charge and discharge power limits (considering a battery with same C-rates), the power demand for the fuel cell system is increasing and the recuperation potential is decreasing. Thus, the energy losses in the fuel cell system and due to braking are increased by 2% respectively. Furthermore, the battery is operated longer at high power values resulting in higher cell degradation. For comparison of the energy split on GWG driving cycle with UTU, it is especially important to use a distance neutral energy consideration in kWh per 100 km. Compared to GWG, the fuel consumption on UTU is increased by 2.4 %, although the required energy for vehicle traction is reduced by 3.4 %. This reduction is mainly caused by lower vehicle resistance due to lower velocity. The nevertheless increased fuel consumption is a result of worse system operating points (mainly of the fuel cell system) and increasing losses in the service brakes and brake resistor. These effects are mainly caused by the challenging road height profile with high and long-lasting road inclinations at the Brenner pass. Because of resulting e-motor and battery power derating and consequent reduction of power limitations it is not possible to recuperate all the braking energy resulting in 2.7 % increased losses in the service brakes and brake resistor.

With the help of predictive energy management the powertrain can be pre-conditioned before upcoming events to optimize brake energy recuperation as well as availability of system performance. The potential for increasing brake energy recuperation on GWG driving cycle is rather low compared to UTU. However, with predictive energy management an optimized power distribution in terms of efficiency with less shut offs and thus reduced aging can be achieved, also for GWG driving cycle. By changing the fuel cell parametrization from BOL to estimated EOL parameters, the hydrogen consumption is generally increasing. This is influenced directly by the decreasing fuel cell efficiency but furthermore also by a worse power distribution due to less maximum available fuel cell power. Knowing these interrelations, predictive energy management is the lever to optimize and to balance aging of both systems, fuel cell and battery. Thus, 1.5 million kilometers lifetime and durability of fuel cell electric heavy duty trucks is achievable without exchange of the battery or fuel cell system. This is as well one contributor to reduce total cost of ownership (TCO).

Summary and Conclusion

The powertrain of a fuel cell truck consists of various systems. To optimize the overall vehicle performance as well as the fuel efficiency, it is important to consider all powertrain systems and their limitations already within concept phase during system dimensioning. Thereby, also the energy management as well as component aging effects have to be taken into account. In combination with the optimization targets it is needed to consider the component availability, the product cost and the limited installation space as boundaries. Via system engineering as well as simulations the system dimensioning can be performed in an optimal way. With the help of the presented energy split diagrams, the remaining potential for energy optimization is clearly shown and the key drivers for improvement of the overall powertrain efficiency can be identified. Furthermore, the impact of parameter variation on the energy split is easy to be analyzed.

Unlike Diesel engines, fuel cell systems offer best efficiency not at maximum but partial load. Thus, hydrogen consumption increases on challenging driving cycles with extreme road gradients. In general, it can be said that the fuel efficiency of a fuel cell powered truck is quite sensitive on system limitations and on the performed power split between fuel cell and battery system and their power distribution. A holistic system design is mandatory to challenge today's standard Diesel trucks, that are already in a very good position in terms of efficiency, lifetime and TCO. To gain market acceptance, fuel cell electric heavy duty trucks rely on an innovative energy management. It enables low TCO by taking care of lifetime and durability of fuel cell and battery system, being the most cost intensive systems of the vehicle. At the same time, vehicle performance is optimized.

References

[1] COMMISSION REGULATION (EU) 2017/2400. (12 2017). Implementing Regulation (EC) No 595/2009 of the European Parliament and of the Council as regards the determination of the CO_2 emissions and fuel consumption of heavy-duty vehicles and amending Directive 2007/46/EC of the European Parliament and of the Council and Commission Regulation (EU) No 582/2011. Official Journal of the European Union.

[2] Linderl, J.; Doebereiner, R.; Mayr, J.; Riedler, S. (06 2021). In-vehicle integration of fuel cell systems for commercial vehicles, MOBEX ,Webinar

[3] Pell, J.; Müller, I.; Gruber, W.; Schilk, A. (09 2021). E/E architecture and operating strategy for fuel-cell trucks. 16th international VDI conference Commercial vehicles 2021.

[4] Bayer, F.; Tochtermann, J. (10 2021). Development of a Heavy-Duty E-Axle. 7th international VDI conference Drivetrain Solutions for Commercial Vehicles 2021.

[5] Schörghuber, C.; Pell, J.; Schubert, T.; Ozli, S. (04 2020). Energy and Lifetime Management for Fuel Cell Powered Trucks. *ATZ heavy duty*.

[6] AVL CRUISE™ M. Multi-disciplinary vehicle system simulation tool. https://www.avl.com/cruise-m

Heavy Duty Vehicles with Electric Drive Train and Hydrogen Fuel Cells as Range Extender

Dipl.-Ing. **Georg Sandkühler**, M.Eng.,
Faun Umwelttechnik GmbH & Co. KG, Osterholz-Scharmbeck

Already 2006 FAUN started with the development of electrified vehicles for the refuse collection based on standard diesel chassis. The electric drive train was designed for low speed operation up to 30 km/h only, for high speed transportation the original diesel engine was kept in place. The electric power was supplied by a small diesel generator at 30 kW in combination with super capacitors; this project was handled under the name DUALPOWER, closer information to this is available on different public pages, e.g. https://www.youtube.com/watch?v=k5MoUsI95so .

Based on the learnings and collected data of these 20 vehicles delivered to customers between 2007 and 2009 the current project BLUEPOWER was started. The vehicles available under this name are completely electrified, no ICE is on board any longer.

The drive train comprises an electric asynchronous motor (P_{const} = 240 kW, P_{peak} = 550 kW, T_{peak} = 4.200 Nm) driving the rear axle via a conventional shaft, no gears in between. The motor inverter is supplied by the HV link at 680 VDC nominal. Different from many other application this drive motor is equipped with a disc brake directly on the shaft; this disc brake is used as a comfort feature for the driver during the refuse collection to keep the vehicle in place without using the air brakes to save energy. The brake callipers are operated by hydraulic pressure derived from the hydraulic supply circuit for the rear axle.

Electric power is supplied by a Lithium NMC battery with 85 kWh usable energy EoL (End of Life). This battery capacity was calculated from the energy needs of the former DUALPOWER vehicles; the data showed that for a standard refuse collection day 150 kWh are necessary just for driving from bin to bin, dumping the refuse and compacting it. With an intermediate high power charging during lunch break the vehicle with just the pure battery can do the daily job if there are no long distance transports required. For charging the vehicles are equipped with CCS 2 inlets for DC- and/or AC-charging depending on customer's choice. The maximum charging power is theoretically limited to 150 kW; tests showed that due to the thermal management the best results / shortest charging time could be achieved starting with 85 kW.

With higher power at the start the thermally caused limitation reduce the charge power very soon to lower rates which results in longer charge times in total.

For all other applications fuel cells and hydrogen tanks can be added to the vehicles, either during production or via refurbishment after delivery; this refurbishment opportunity is important because the mission profile of a refuse collection vehicle can change dramatically during its lifetime.

The fuel cells deliver up to 30 kW constant power each, maximum three of them can be applied to each vehicle. Data show, that for pure urban traffic constant power of 30 kW is sufficient, peaks are covered by the battery. For rural traffic at higher speeds 60 kW are sufficient, for highway use 90 kW are required.

Additionally to the fuel cells the hydrogen tanks can be ordered form production line or refurbished later, the vehicles can carry up to four hydrogen vessels with approximately 4 kg usable hydrogen each.

To answer the questions concerning the range of the vehicles a tool was set up to simulate driving according to the WHVC (Worldwide harmonized Heavy duty Vehicle Cycle). This cycle was selected because no other possibility to compare vehicle range is commonly available. The maximum range in this simulation is 240 km pure driving according to WHVC, no refuse collection taken into account in this approach. Very important is to stress that the vehicles in any configuration with any available rear loaded refuse collection body will still have more than 10 Mg payload, which is strongly required by customers to fulfil their daily operations.

Of course the chassis comprise much more than just the described elements, namely the auxiliaries for pressurised air supply and the two hydraulic steering pumps for front and rear axle.

During the development a strong focus was set to the thermal situation: The main power electronics (drive inverter, drive motor, auxiliary inverter and auxiliary motors) are connected to an air over water heat exchanger to dissipate the thermal energy created in the power electronics. The heat exchanger is calculated to be sufficient at 40°C ambient temperature with an intake at up to 85°C and an outlet of 55°C. The total power of the heat exchanger in this scenario is up to 52 kW.

The same heat exchanger type and size is used for the fuel cells, too. The heat from the fuel cells is transferred to the external, secondary cooling circuit by a plate heat exchanger, the primary cooling circuit is due to this separation very small in terms of volume, it contains only 4,2 litres of de-ionized cooling water, where the secondary cooling circuit is at approximately 70 litres per fuel cell.

ZF E-Mobility Software Functions for Commercial Vehicles

Dr. **Daniel Morgenweck**, M.Sc. **Michael Großmann**,
Dr. **Winfried Fakler**, Dr. **Martin Lamke**, Dr. **Franz Bitzer**,
ZF Friedrichshafen AG, Friedrichshafen

Abstract

E-Mobility has been one of the top-priority subjects for the past few years and will remain so in the future. OEM und suppliers have been struggling to find the ideal, yet equally commercial and technical solution. So far there seems to be not one solution, but many, ranging from Hybrid, Plug-in Hybrid, BEV and FCEV. It is vital to meet the needs of the respective segments with components that can be used in as many applications as possible. This article describes one element of the ZF commercial technology approach: A kit that consists of electrical, mechanical and software components. One major problem with electrified powertrains is the lack of electric range. ZF tackles the challenge by developing energy saving strategies that are tailored to the degree of electrification. They cover aspects comprising intelligent control of auxiliary units, thermal management, as well as charge control. Together with functionalities like prevision, it is possible to push energy efficiency even further. The development of an energy management system relies strongly on the use of their ZF owned development vehicles. Integrated in the series software ZF provides a portfolio which covers all important aspects of E-Mobility software.

Introduction

Since the market development of the various E-Mobility solutions for commercial vehicles (CV) is still unclear, a flexible approach is necessary. To be able to fulfil both the commercial demands as well as technical demands for E-Mobility driveline for CV, it is important to supply the respective segments with components that can be used in as many applications as possible. In the sections below a compilation of current ZF E-Mobility solutions are presented with special focus on software.

It is now understood that for low daily mileage applications, the electrification of BEV will become ubiquitous in almost all vehicle segments, from LCV up to HCV. For high daily mileages exceeding 400 km/day, however, it would not be possible to install the battery capacity needed for BEV in the vehicle due to installation space and weight limitations. In this area of application fuel cell technology offers promising solutions.

Regardless of the energy storage capacity the importance of the factor range is evident in all segments. To increase the mileage of a vehicle with a fixed amount energy installed it is necessary to have an overall view on the vehicle. Only in that way energy saving potentials could be identified and utilised. ZF tackles the challenge with the development of an energy management that implements strategies to save valuable energy to increase the range of commercial vehicles.

ZF E-Mobility Solutions

Table 1 introduces the first generation of ZF CV E-Mobility products. They have been released over the last few years and are already in volume production or are in various stages of development. Beyond the depicted hardware, there are software products of various kinds complementing the hardware or extending the control to higher levels.

Table 1: ZF E-Mobility CV products, first generation.

	CeTrax	CeTrax lite	AxTrax AVE	eTrailer
				
CV segment	Bus, MCV 26 t	LCV < 7,5 t	Bus 26 t	Semi-Trailer 40t
Type	BEV Central drive	BEV Central drive	BEV Axle drive	e-Trailer Hybrid / Range-Extender
Electric motor type	Induction motor	Induction motor	Induction motor	PSM
Power peak	300 kW	125 kW	2 x 125 kW	~ 270 kW
Power continuous	200 kW S2 = 30 min	80 kW S2 = 30 min	2 x 87 kW S2 = 30 min	~ 180 kW S1
Nominal voltage level	650 V DC	420 V DC	650 V DC	650 V DC
Torque Peak	1,350 Nm	390 Nm	2 x 485 Nm	~ 600 Nm
Max. rpm	8,500 rpm	13,000 rpm	10,300 rpm	13,000 rpm

CeTrax is the ZF central drive solution for buses and HCV . It consists of an induction motor with 200 kW continuous power and a one-stage planetary gear set. SOP has been in 2020. There are different models for the Chinese market that have the same design concept but are developed according to local requirements.
AxTrax AVE is the ZF electrical portal axle for low-floor buses where the complete drivetrain is integrated into the wheel hubs. It consists of two 125 kW induction motors with two gear sets and a fixed gear ratio. AxTrax AVE is a volume-production product.
CeTrax lite is the ZF central drive for LCV. This product features an induction motor rated at 80 kW continuous power and a fixed ratio gear set. The electric components come from the ZF volume-produced product Electric Axle Drive of the ZF E-Mobility-Division for passenger car market.
ETrailer is a product of the former WABCO and now ZF company . It consists of an electric drive system, a battery, and a cooling system attached to a trailer. There are several fields of application. One is hybridizing the tractor and trailer combination to a cost efficient HEV variant. The fuel savings are estimated with 7 to 16 percent. Another opportunity lies in utilizing the electrified trailer as range extender for BEV tractor units. With an increased battery capacity and an additional charging system this amounts also to higher costs for the range extending trailer. Thinking of a PHEV variant, it could also be used in applications where there is another power consumer on the trailer like in reefers. Thus, the recuperation energy can be used to supply those auxiliary units.

ZF E-Mobility software products comprise among others, functions for the drive software, gearbox and, energy management. Especially the drive software has a high degree of maturity and is part of serial products. All software components are under constant development and are subject to quality processes.

ZF E-Mobility Hardware Kit

The following part describes in detail the key components for successful kit products. These include the electric machines, transmissions, cooling systems, shifting actuator and, power electronics. Wherever possible, synergy effects between the various E-Mobility products were used as well as synergy effects from already existing ZF volume-production products in the AT segment. The carry-over of components and parts as well as proven design features in hardware has a major impact on development time, robustness, quality, and predictability.

Electric motors

As key components, the used electric motors are described in greater detail. To meet various requirements regarding drivability, installation space and total costs of ownership (TCO), different induction motor (IM) sizes and types are used for the vehicle segments. All IM are developed by ZF in-house for optimum performance and durability and since its development is from one source, synergies can be used in an ideal way.

For the LCV segment up to 7,5 t, the already existing induction motor used in the ZF passenger car series application represents a great opportunity because the 400 V level appears to be a good solution for those applications in terms of short-term availability and economic advantages. Lifetime requirements in this segment can be met without restrictions.

For MCV or even HCV, a higher voltage level of 650 V to 800 V is desirable due to the higher power levels required for up to 400 kW. ZF uses mainly induction motors for traction applications because they are robust, cost effective and their efficiency is very good even when compared with PSM (permanent magnet synchronous machine) applications. ZF was even able to prove this in internal testing with an equivalent competitor product.

Since these systems will be continually developed and the requirements regarding full integration (weight, space) and efficiency will constantly evolve, PSM technology, which was already included in different ZF projects, will be considered in future developments. PSM technology allows for various technical design approaches like wave winding or hair-pin systems.

The CeTrax induction motor is rated 300 kW peak power @ 650 V and 8,500 rpm. Since space restrictions are not an issue for state-of-the-art central drive bus applications, the CeTrax installation space meets the ZF AT Ecolife series while remaining compact. AxTrax AVE is a volume-produced product for buses and also uses induction motor technology. Peak power is 2 x 125 kW @ 650 V / 10.300 rpm.

Power Electronics

For power electronics, ZF uses products supplied by its cooperation partner Zapi / InMotion for drives with a DC nominal voltage of 650 V. The power electronics are also designed according to a modular principle which enables the expensive power semiconductor components to be variably adjusted. This makes it possible to match the power electronics precisely to the requirements of the electric motor.

Software functions can be split between the inverter control and a central electronic control unit, i.e. the ZF drive control unit. The split can be flexibly represented. Functions with high demand torque dynamics can be performed on the inverter control unit. In contrast, low

dynamic functions such as temperature calculations can be moved from the inverter to the ZF control unit. The ratio may vary depending on the project and ECU resources.

When it comes to power electronics, numerous projects show that two inverter variants enable most projects to be optimally operated in terms of cost, installation space and weight. The two variants feature identical customer interfaces for high-voltage, low-voltage, and cooling connections. This also makes it easier to integrate the different drive variants from the modular system.

The interface between the ZF control unit and the inverter is also identical for all inverter power classes. Therefore, the vehicle control unit can be combined with different inverters without additional effort. This makes it very easy to build single- and multi-motor drives. The inverters and functions are designed so that induction and PSM motors can be operated. Fig. 1 shows the characteristic data of the two inverter variants, which have proven to exhibit low installation space and weight costs. Both power electronic systems allow a DC voltage up to 750 V without derating and without loss of lifetime. At higher DC voltages, these factors entirely depend on the driving profile and other customer requirements as to whether the lifetime is affected or not. The smaller of the two inverters has a 20 second peak current of 340 A (RMS). The larger version can hold up to 530 A (RMS). The S1 continuous current is 225 A (RMS) or 375 A (RMS).

	ACH65M30	ACH65L50
Manufacturer	InMotion	
Type	3-phase drive inverter	
Performance data		
Nominal DC voltage	650 V	
Maximum DC voltage	750 V (without derating)	
Current (peak, 20 s)	Up to 340 A_{rms}	Up to 530 A_{rms}
Current (duration, S1)	225 A_{rms}	375 A_{rms}
Insulation resistance	> 20 MΩ (new hardware)	
Dimensions, weight		
L x W x H (mm)	421 x 362 x 122	583 x 362 x 122
Weight (kg)	20	25
Highlights	• Efficiency > 98 % (nominal value) • Robust design with IP6K9K • Liquid cooling	

Fig. 1: Inverters.

Mechanical components: transmission and cooling systems

The ratio between the reuse of components from already existing products and new components was a key point in different E-Mobility systems. ZF, as a driveline specialist , views the gear set and, especially, planetary gear sets, as key E-Mobility components in terms of

power density and the required lifetime in the CV sector with strict requirements. Another important component is the oil used, which is what ZF is focusing on together with established suppliers. The oil types used are familiar from other ZF products, impacting durability and serviceability.

	CeTrax	CeTrax lite	AxTrax AVE
Transmission type, ratio	Planetary gear set, i = 3,4	Two-stage spur gear set, i = 5,9	Two-stage ratio i = 22,7
Cooling / lubrication system	Stator: water cooled T/M: oil injection	Stator: water cooled T/M: oil injection	Stator:water and air cooled T/M: splash
Pump type	electric	electric	-

Fig. 2: Transmission and cooling.

Since CeTrax is ZF's forerunner central drive for BEVs, as many carry-over parts from the ZF AT Ecolife were used as possible. These parts include one planetary gear set to reduce the input speed of 8,500 rpm as well as both the complete output bearing concept and the output shaft. Since city bus applications have extremely high requirements regarding lifetime and reliability in general, the possibility of having well-proven carry-over components from volume-produced AT products can be regarded as a big advantage. For optimized performance and overall efficiency, ZF decided to use a normal water-cooled stator system combined with an oil circuit for transmission cooling, including an electrical oil pump. Furthermore, some induction motor applications require, under certain conditions like a standstill after high power passages, thorough cooling of the rotor, the corresponding bearing and the sealing components. CeTrax lite is the perfect example of an effective carry-over from the existing ZF passenger car volume-produced product, the Electric Axle Drive. This creates high confidence levels right at the development start because off-the-shelf components can be used, thus ensuring cost effective engineering. CeTrax lite features a two-stage spur gear set to reduce the electric machine speed of 13,000 rpm and uses two ratios currently taking into account the same design space. Also, the transfer of the power electronic and parking lock concept from the passenger car product and integration into new packaging variants can be achieved. The stator remains water cooled, whereas the rotor shaft, stator windings as well as the transmission are additionally cooled by an electric oil pump, combined with an extra oil cooler. Thus, the continuous power of CeTrax lite can be considerably increased by some 10 kW.

Mechanical component: electric actuators

ZF considers electric actuators as a strategic component for the next generation of E-Mobility products since they are easily adaptable for different applications and allow precise and smooth gear shifting without the need of a pneumatic or hydraulic system supply. The actuators feature one BLDC motor with an integrated planetary gear set and position sensors. Kits with various motor sizes and additional components such as an actuator brake are considered to cover every aspect of future product development.

E-Mobility Software Functions

In conventional vehicles, many driving and assistance functions are implemented in the combustion engine control unit. For electric vehicles, these functions must be executed elsewhere. The ZF control unit can take over the functions as a central vehicle / drive control unit. As there are numerous different application variants in commercial vehicles this poses challenges not only to the hardware but also to the software. To meet these demands and yet supporting a common base a platform software is used that is adapted and applied accordingly. Moreover, the opportunity is offered to provide customers a custom interface which suits their specific needs. The communication interface between the central ZF control unit and the vehicle is identical for all drive variants. This also applies to variants with and without multispeed transmission. This makes it very easy for customers to integrate different electric drive systems into their vehicles. The software is split into four major components. The EV-Drive functions are controlling the drive system, the EV-Control is managing start up and shut down of all delegated ECUs, the EV-Energy is controlling the power distribution of all high voltage components and the EV-Gearbox controls the transmission. All components are functional software and share the same abstraction layer and the same basic software (see Fig. 3).

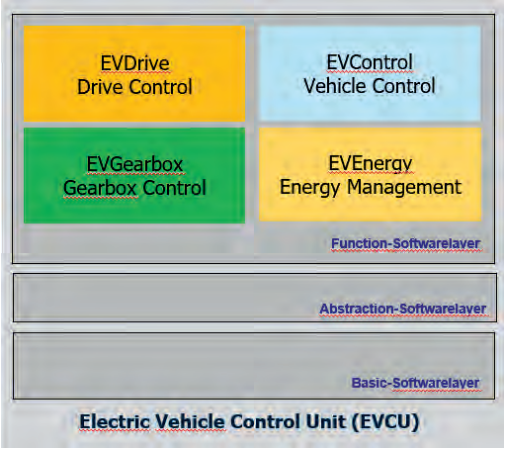

Fig. 2: Architecture of e-mobility software.

Depending on customer wishes individual software components can be switched on or off. The development of the four functional parts is highly quality oriented with project management, supplier monitoring, configuration management, change request management, quality assurance, problem resolution management, functional safety and thorough testing. In the following the EV-Drive and the EV-Energy software components are depicted in more detail. Both components are running at the same ECU.

EV-Drive Software Component

The drive software controls the electric drive. It handles, verifies, and brings together various torque demands. On one hand it provides a unified interface to the inverter whereas on the other hand it supports numerous variants and several interfaces to the customer. The EV-Drive software has a high degree of maturity and proofed itself in various volume-production projects.

The job of the drive software comprises interpreting the accelerator pedal, determining the driving conditions, and distributing torque and power including recuperation. The software platform can handle central drive architecture or axle drive architecture with multiple axles.

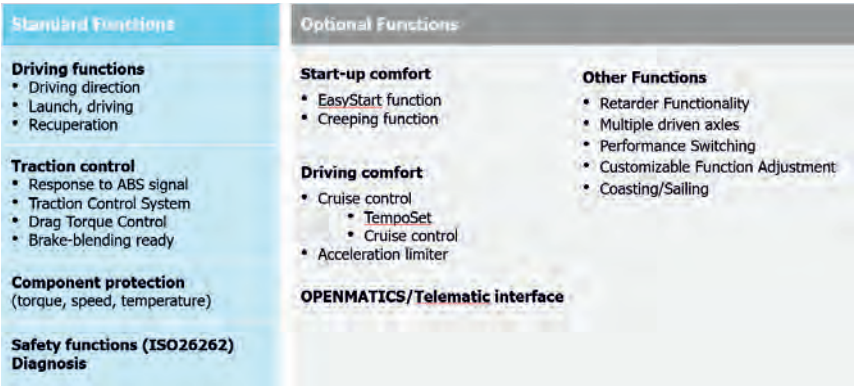

Fig. 3: Function of EV-Drive.

The drive control functions are separated into standard and optional functions. Basic functions essentially include the basic driving and driving dynamics functions, the component protection functions, and the safety functions developed according to ISO26262. Fig. 4 lists the driving functions for a single-axle drive. The software modules are divided into operational and strategic functions. The strategic functions aim to essentially determine the driving torque, the torque distribution and recognize the driving condition. The operative functions process the desired torques and convert these into the drive torques considering the component protection. In that way recuperation is handled as negative torque request which can be controlled either by the retarder lever or is part of a one pedal drive strategy and is controlled by the acceleration pedal. One example for standard functions is the electronic traction control. It not only supports traction on slippery surfaces it also prevents the axle gear stage from being exposed to so-called ice plate impacts. These heavy torque impacts occur abruptly when the driven wheels are spinning and then return to a high friction surface like asphalt. The resulting torque peaks can damage the mechanical drive components so that they fail prematurely. In that sense electronic traction control also comprises component protection. It is essentially the duty of the drive software to assure that the hardware runs in its operational boundaries. That is torque, voltage, current, and temperature limits are not violated. Especially monitoring the temperature means to provide a temperature model for mechanical parts that cannot be measured directly.

An example for optional functions of the drive software is the easy start capability. It ensures at start up that a vehicle does not unintentionally roll back down a slope when the driver switches from brake to accelerator pedal. Other functions like cruise control and tempo-set

functions assist the driver. For city buses, limiting the acceleration is important so that standing passengers are not injured during a high-start acceleration. When combined with a telematics system (i.e. ZF Openmatics), additional functions, such as power or acceleration limits that depend on vehicle position can be used. The GPS-based power limitation, for example, is usually used in city buses. On one hand, the power is limited to save energy in inner city traffic and on the other hand, full power is released when the bus is traveling on a city highway.

EV-Energy Software Component

It is a well-known fact that with E-Mobility arises the problem of driving range. Especially BEV based commercial vehicle lack the necessary energy storage capacity to prove themselves in every long-haul scenario. Moreover, the total costs of ownership increase tremendously with the installed battery capacity. Also, the construction space for battery packs in semitrailer tractors is an issue. Hence, there are strong arguments that necessitate a high-power consumption efficiency to gain the maximum range with the installed amount of energy.

In conventional commercial vehicles the internal combustion engine is the heart of the vehicle. Aside from delivering the drive power it also provides power to several other auxiliary units like air compressor, alternator, air condition, etc. In a BEV those units must be electrified. It is favourable to connect the great power consuming units directly to the high voltage electrical system. This results in higher efficiency and the stability of the low voltage electrical system is sustained.

Both aspects energy efficiency and the management of other ECUs are covered by the ZF energy management system so called ZF-EMS. ZF-EMS is essentially a standalone software that controls and coordinates all units connected to the high voltage circuit (Fig. 5). It currently manages the high voltage battery with the battery management system as control unit. Furthermore, auxiliary units like electric power steering, air compressor and air condition are managed by EV-Energy Software. In a BEV the low voltage electrical system is supplied with energy from the high voltage circuit via a DCDC converter that is itself supervised by the energy

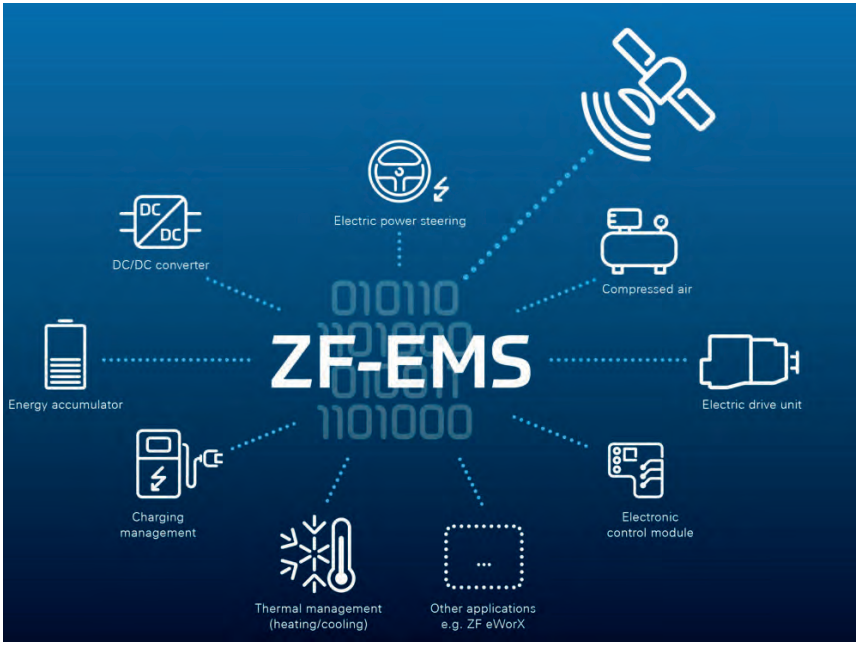

Fig. 4: Energy management software and controlled HV components.

management. Of course, the EMS is also responsible for limiting the consumed power and the delivered power of the drive system. ZF-EMS distributes the available power to all high voltage components. It monitors that the current limits of the battery are maintained. Furthermore, the EV-Energy software incorporates the thermal management. The cooling system of BEVs is typically divided into separate cooling circuits. For the thermal management of the battery active cooling and heating is mandatory which is done in a low temperature circuit. Other components like electric motors and inverters are normally passively cooled. However, in situations of extensive power demand also active cooling is used. It is a matter of the cooling system's layout how much the different circuits can interchange heat with each other. Having energy efficiency in mind it offers a great potential to use for example the waste heat of the drive system to heat up the battery or the cabin. That holds especially true in the winter season. Another part of the EV-Energy software comprises charge management. ZF-EMS supports both AC charging and DC charging. AC charging uses an on-board charging unit which converts AC current of lower voltage to DC current of the vehicle's high voltage. In contrast to that, DC charging does not need any power conversion. The charge plug is directly connected

to the vehicle's high voltage circuit. However, the process must comply the safety regulations of ISO 15118 / DIN 70121 due to the high charging power. A sequence of checks and prerequisites is run through before power delivery can start. As ZF-EMS is on top of several other control units it extensively uses CAN communication to manage the different components. Therefore, extra CAN networks are setup besides the vehicle's conventional ones that are exclusively used by the additional units. As supervising ECU, the energy management also handles errors of other components. It is in the responsibility of the energy management to assess the impact of a failure of a single unit to the operating conditions of the overall system. For example, considering a defect of the DCDC converter if it occurs during start-up it is appropriate to shut down the vehicle again and warn the driver whereas if it occurs in driving situations a shutdown could be dangerous and thus the driver is only warned.

Efficiency Functions

The heart of energy management is dedicated to energy saving strategies which increase the driving range of the vehicle. There are several possibilities to do that. Some of them are easy to implement because only a single component is involved others have greater potential but incorporate the interaction between different components. An easy to implement efficiency function is the speed dependent support of the steering pump. At standstill the steering pump is switched off, at low speed the support is maximised, and with increasing vehicle speed it is decreased again. In contrast to that a smart thermal management offers greater potential. However, it concerns not only the interaction of different components but also the design of the cooling system. Exploiting the full operational temperature range of the components leads to less cooling and heating and the pump speed can be reduced, too. With that, a fair amount of energy can be saved. Moreover, if the design of the cooling system enables to interchange heat between different circuits waste heat from the passive circuit could be used to heat the cabin and the battery. Another important issue of energy management is the prioritisation of components concerning the power distribution. This becomes important if the high voltage battery is low on energy. In that situation the assignment of power to the drive system and cabin air condition is reduced. Further on, if the energy level drops below a lower threshold the drive system will not gain any power and the cabin air condition is switched off.

The above-given energy management functions represent only a few examples. There are a lot more worth of mentioning but this would take far too long. Energy efficiency is not only restricted to the state of driving but also parking and charging benefit from smart strategies.

ZF Test and development facilities

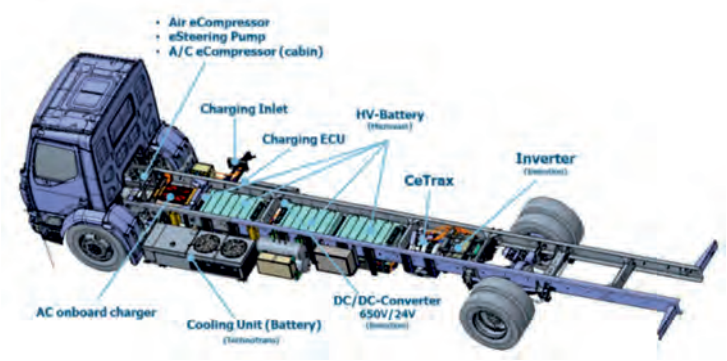

Fig. 5: ZF test vehicle for developing energy management functions.

The development of an energy management functions relies on an overall view on the vehicle in various situations. The complex interaction between the different components and their energy saving potential is analysed best under real test conditions. Therefore, ZF has built up a test truck which serves as platform to develop the energy management system. Fig. 6 shows a schematic overview of the vehicle. The positions of the aforementioned high voltage components are marked. Furthermore, MiL, SiL and, HiL simulations are utilised to support the development. There are several reasons why simulations are considered in the development process. One is to ensure the software has reached the necessary degree of maturity before it is used in the truck. Another one lies in the possibility to conduct various automated tests that cannot simply be done in a vehicle.

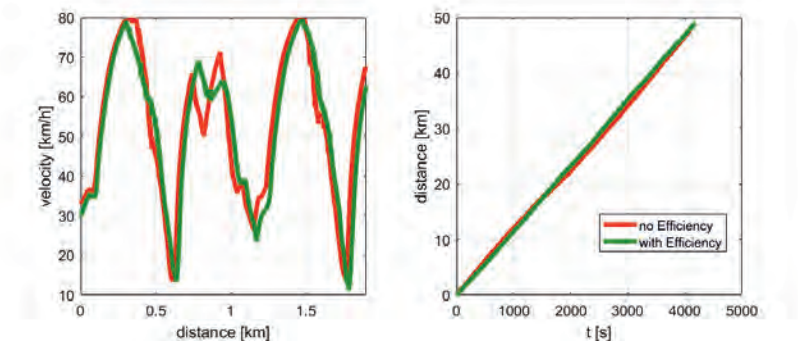

Fig. 6: Velocity and distances of test drives with and without energy management.

Having the ability to test energy management right on the track offers the opportunity to assess the potential of various functions. Below, a test-driven survey is presented and the conclusions that are derived from it. The left diagram of Fig. 7 shows the velocity profiles of some test drives. It illustrates quite aggressive driving sequences those consist of cycles of strong acceleration and deaccelerations. The test drives were carried out on ZF's own test track. They

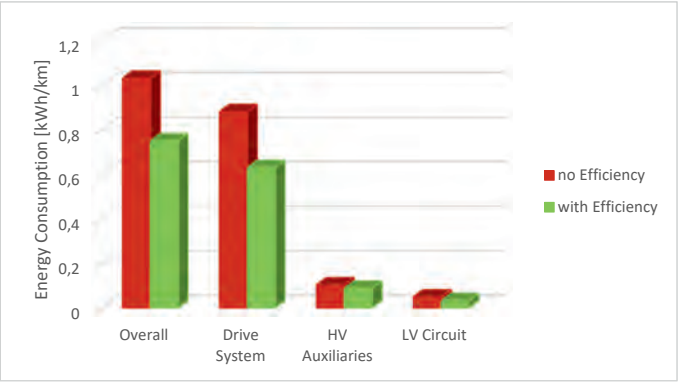

Fig. 7: Energy consumption of test drives with and without efficiency functions.

were done with non-active and active energy efficiency functions. As Fig. 8 shows ZF-EMS clearly has an impact. The test drive carried out without efficiency functions active has an average energy consumption of about 1 kWh/km whereas with efficiency functions it reduces to 0.78 kWh/km. The major portion of the savings is achieved by limiting the maximum available power of the drive system and enforce strong recuperation. This could be also recognised in the velocity profile (left diagram of Fig. 7). The maximum velocity is hardly achieved in the case of active efficiency functions. However, this does not lead to a slower average speed as it could be deduced from the right diagram of Fig. 7. The 45 km mark is reached almost within the same amount of time. Fig. 8 also shows the energy savings from the other high voltage auxiliary units which is about 0.015 kWh/km. This is mainly achieved by adapting the power to the driving conditions and allowing the temperature of the battery to vary in a wider range. Also, the low voltage circuit benefits from these measures. Its savings amounts to approximately 0.01 kWh/km. Although, the results can only be evaluated in the context of route and velocity profile the difference between an active, well-adapted energy management and the absence of any energy management becomes very clear.

Further development in EV software

ZF-PreVision was already applied in conventional vehicles for adapting the gearshift strategy which led to a reduction of fuel consumption. Future efforts aim for the usage in connection with ZF-EMS. This further increases the ability to save energy. Knowing parameters from the route and topology ahead enables the energy management to precondition the vehicle in advance. For example, storage systems (like compressed air tank) could be driven to low before the vehicle enters a long downhill passage where recuperation refills them. Furthermore, improvements concerning the component protection of the drive system are possible if the derating strategy also accounts for temperature prediction on the base of topological information. There are a lot more opportunities one can think of if prevision is available. Common to all of them is the usage of prediction models that must be developed and linked to route information.

Summary and Outlook

The ZF E-Mobility kit represents one approach that will meet customer cost, efficiency, robustness, and versatility requirements for all products in almost all CV segments. For customers as well as for ZF, the modular ZF E-Mobility kit approach will result in significantly shorter development times, more robust products, improved serviceability, and a broader field of applications to cover. Also, modifications based on specific customer requirements can be implemented comparatively easily.

Nowadays, the increasing importance of software products becomes even more evident. This holds true for software functions related to specific hardware like the drive software and the gearbox software as well as for software focusing on the overall vehicle like the energy management. Especially, the later one plays an underestimated role in the electrification process of the drive system. But however, it is a matter of energy management that with a certain amount of installed battery capacity a maximum amount of electrical range can be achieved.

Next generation ZF E-Mobility products are already undergoing further development since costs, compactness and efficiency requirements will increase drastically when volumes rise starting in 2025. For the next generation, even more elaborate electric motors, power electronics and a higher level of sophisticated transmission knowledge will be required, nevertheless, first-generation E-Mobility products will be needed. To achieve ZF's goal as a market leader, we are introducing two completely new products/ product lines.

References

[1] J. Witzig, M. Wenger and R. Januschevski, "Electric Central Drive for Commercial Vehicles," *MTZ,* no. 10, 2018.

[2] A. Grossl, H. Krojer and H. Wendl, "Portal Axle AVE 130 for Electric Urban Buses," *ATZ,* no. 12, 2015.

[3] F. Müller-Deile, J. Heseding, G. Schünemann and T. Dieckmann, "Fuel Savings of an Electrified Semi-trailer in Driving Tests," *ATZ Worldw,* no. 122, pp. 54-59, 2020.

[4] S. Gohl, F. Tenbrock, L. van Rooij, D. Williams and G. Gumpoltsberger, "ZF Innovation Truck," in *VDI Commercial Vehicles Conference*, Baden-Baden, Germany, 2016.

[5] A. Banerjee, M. Würthner and C. Tudosie, "Prevision GPS — The Anticipatory Gearshift Strategy for the Traxon Transmission System," *ATZ worldwide,* no. 6, 2013.

Possibilities of a modern Powertrainmanagement

How can the futures Powertrain complexity be dealt?

Dipl. Ing. (FH) **Norbert Scharlach**, MAN Truck& Bus SE, Munich

Abstract

With the new Truck Generation TG3, MAN launched a centralized EE - Architecture. By that architecture approach MAN gets new possibilities for handling the variance of the different propulsion systems. On the one hand side electrified propulsion system needs to be integrated in a given vehicles architecture, but also classic combustion systems needs to be further developed for fulfilling new legislations.

The lecture shows, how MAN handles the variety of propulsion systems by a modern and modular Powertrainmanagement.

1. Introduction

The facts, described in the Abstract, will be explained in the next chapters.

The paper starts with the challenges of our engineers business with the goal to develop a truck, followed by the principals for the centralized EE Architecture of the latest MAN Truck Generation 3 and finally gives an overview of different Powertrain configurations.

2. Challenges

2.1 Challenges given by the Market

A driver for the product development is the market. The market gives us challenges, which affect our daily business and the next truck generations.

Some of them are plannable / predictable. But there are also highly dynamic impacts, which forcing us to react and to keep the pace.

Currently for the Powertrain function development the market asks:

- Driven by the CO2 legislation, what is the futures propulsion system?
  - Hydrogen ICE
  - Fuel Cell
  - BEV
  - Hybridization
  - …

- How can the Total Costs of Ownership ~~be further reduced~~?
  - Efficiency
  - Digital Services
  - FOTA / OTA
  - ....

- What does the Truck transformation to autonomous driven vehicle look like?

- And so on

All these market related questions - they are for sure not complete - are important impacts for the product development. They need to be taken into account when designing a EE architecture and finally engineering Powertrain functions.

2.2 Challenges for the Engineering / Development

Beside the markets requirements, which are thematically outlined in the chapter above, the product benefits also from the engineers ideas and creativity.
While we used to use our creativity to simplify complex algorithms to get them running on the ECUs, modern automotive µCs performance allows us to bring complex and computing intensive approaches to life.
In addition, the latest µC families allow to transform the EE domain architecture, which could be seen as state of the art, to a centralized EE architecture with an central vehicle computer.
That trend shows the following Fig., which was published by presentation “AUTOSAR Introduction / October 2020” [1].

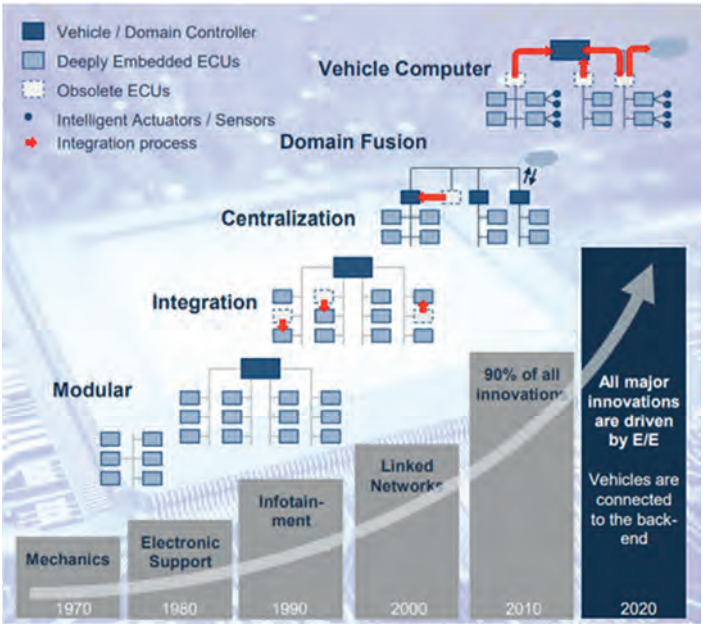

Fig. 1: Development of the EE-Architectures / “AUTOSAR Introduction / October 2020”.

From the beginning of the development of the MAN **T**ruck **G**eneration **3**, which started in 2015 and was launched in spring 2020, the EE Engineering @MAN was convinced, that only a centralized EE architecture with a centralized vehicle computer is future proven.

Why?

The next bullet points are / were our motivation and main drivers:

- cost optimization by minimizing the ECU number
- scalability of the EE architecture
- modularity of the function architecture
- reduced complexity by reduced Network activities
- reusable function and SW modules
- highly performing integration platform
- easy maintenance
- generate customer values, because of a high level in-house development
- …

But beside all these technical advantages, there was also an impact in our way of daily working and development. That impact was also a challenge for the engineering, but we found simple and efficient solutions for being successful to finalize the project.

3. EE Architecture @MAN

3.1 The big picture

By the decision to equip the new MAN Truck Generation 3 with a central EE architecture and central vehicle computer, additional and mandatory components, subsystems, … needed to be partly redesigned or revised.
For the identification, what needs to be done and what's the effort, the following principals § were defined on the highest level:

§ Central Vehicle Computer

- The central vehicle computer, which is called **C**entral **V**ehicle **M**anager, is the heart of the EE Architecture and is a multi domain controller.
- Functions, ~~which are~~ influencing the vehicles behaviour, should be allocated on the **C**entral **V**ehicle **M**anager
- All strategic and management functions should be allocated on the **C**entral **V**ehicle **M**anager.
-

That means for the Powertrain, that functions for efficiency and driveability should be allocated on the CVM.

§ Additional components and subsystems

- Hardware protection functions should be allocated there.
- Operation functions and low level management functions should be allocated there
- All these components and subsystems are intelligent and operational ECUs. On vehicle level, they are seen as enhanced I/O modules.

All additional component are intelligent subsystem and/or smart actuators.

§ Network / Interfaces between **C**entral **V**ehicle **M**anager and intelligent subsystems and smart actuators

- The interface should be lean.
- Redundancy should be avoided.
- The interface should be safe & secure
- Exchanged signals should be physical based

The network communication and the exchange of the information can be seen as a smart interface

Derived from these high level principals $, the next Fig. shows an overview of the centralized EE Architecture.

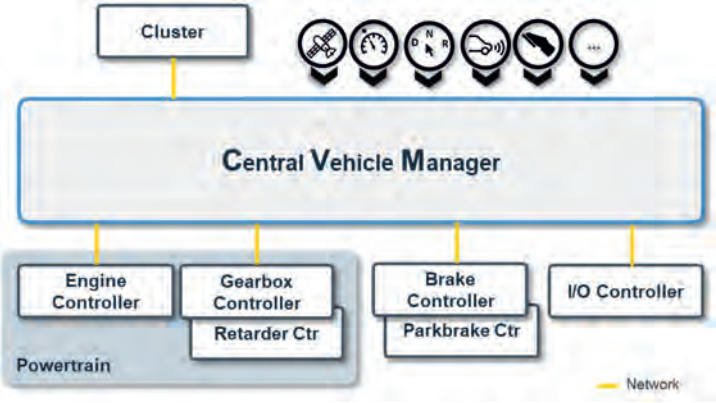

Fig. 2: Structure of the new Truck Generations EE architecture @MAN

3.2 Functional Architecture of the Central Vehicle Manager

Because of the multi domain controller approach, a further challenge was to integrate many functions on the Central Vehicle Manger.
This was only possible by using the powerful tool **eese**, a MAN in-house development. But in addition, the Central Vehicle Manager Software architecture needs to be structured in different layers. These layers are comparable with a company's structure. The layers of the Central Vehicle Manager are shown in the next Fig..

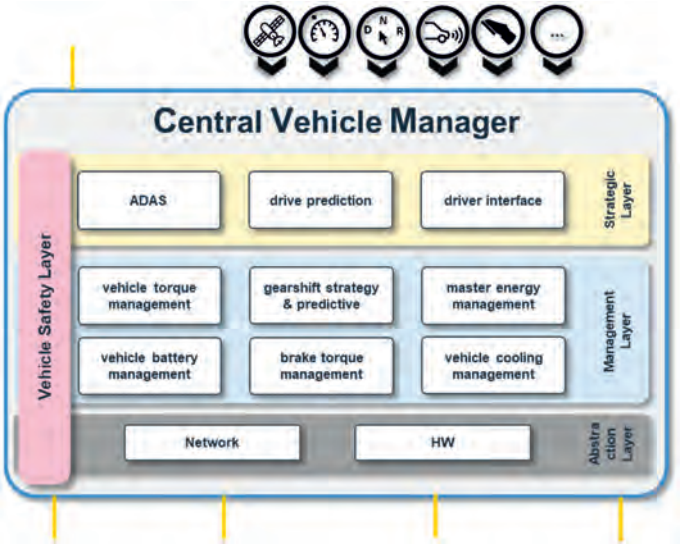

Fig. 3: Software layers and structure of the Central Vehicle Manger

The highest layer is the Strategic Layer:

- The Strategic Layer defines the vehicles behaviour.
  There are allocated higher level predictive algorithms, ADAS functions and also the driver interface.
- Powertrain examples:
  - Accelerator Pedal
  - DNR-Shifter
  - Map / Route Data

From top to down, the next layer is the Management Layer

- By the input of the Strategic Layer and the physical properties of the components and subsystems (Operational Layer), the Management Layers task is to coordinate the interaction between them and to generate control commands for the Operational Layer.
- Algorithms in the Management Layer should be adaptive and physically based, so there is a reduced application & calibration effort.
- Powertrain examples:

- Traction Torque Management incl. drive off strategy
- Gearshift strategy incl. ECO Roll (classic & predictive)
- Brake Torque Management (wearless braking & foundation brake)

One of the lower layers of the Central Vehicle Manager is the Abstraction Layer

- The Abstraction Layer is used for the signal mapping, in order to supply the higher level functions with physically based information.
  By that approach, the signals are independent of the technical solution.
- Powertrain examples:
  - Actual traction torque or actual available propulsion torque
  - brake torque
  - vehicle acceleration (calculated or measured)

The Safety Layer is designed as a cross functional layer

- Safety relevant functions, which are classified greater than ASIL QM are allocated in the Safety Layer.
  These functions are mainly designed as an observer, which brings the vehicle in a safe state, when a safety goal is violated.
- Powertrain examples:
  - Unintended acceleration (positive and negative)
  - Drive off in the wrong direction
  - Blocked traction axle

For the data & information exchange between the different layers to be given, the signals should be physically based.
This technical requirement makes it easier to extend the existing function architectures.
It's also an advantage for the modular kit / modularity, because systems can be purposive tailored, reused and integrated/allocated on successive platforms.

A further advantage of a central vehicle computer is the unique data/signal backbone. Functions have direct access to all signals and can provide the results directly.
In comparison to a distributed or domain EE architecture, all that information doesn't need to be exchanged via the Network (CAN, Flexray, …) , the signals are consistent and don't need to be complex synchronized.

Also redundant calculations, like mass and traction force estimations, can be reduced a minimum.

3.3 Functional Architecture of the components and subsystems

To complete the centralized EE architecture, the intelligent subsystems, smart actuators and enhanced I/O modules are also structured in functional layers.
The physical layer is the lowest one and represents the HW, e.g. the ICE, exhaust treatment, retarder, … .

The physical layer is driven by the operational layer, where HW protecting functions, fast loop controllers, HW specific functions, … are allocated.
To pick up here the example of the companies structure, the operational layer is executing the commands of the management layer.

Powertrain examples are:

- ICE Controller
  - fuel injection / fuel quantity controller to adjust the on vehicle level arbitrated torque
- Gearbox Controller
  - engaging the requested gear, which is calculated by the vehicles shifting strategy
- Retarder Controller
  - Adjusting the requested brake torque, which is given by the vehicles brake management.

Because safety goals can be violated by the components and/or subsystems, they have also a safety layer.
The safety layer is observing the actual states / situations and if necessary, brings about the safe state.

Powertrain examples are mostly the same as on vehicle level, but the realisation to detect them is different:

- Unintended acceleration (positive and negative)
- Drive off in the wrong direction

Fig. 4 shows different layers on component / subsystem level.

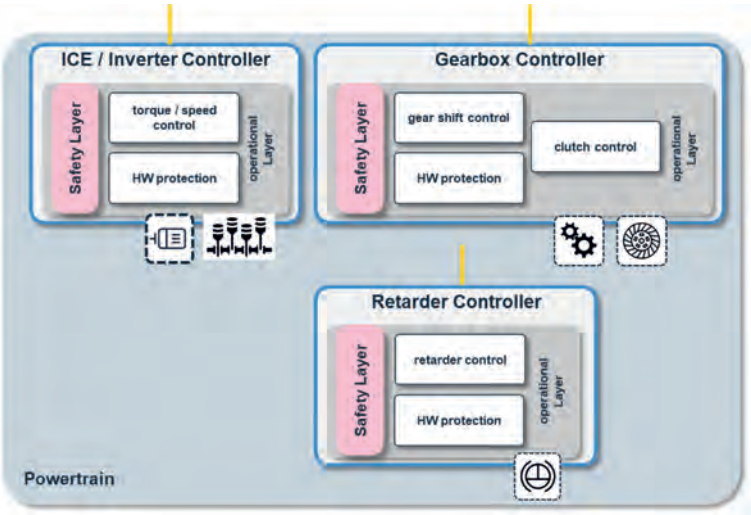

Fig. 4: Layers on component / subsystem level.

4. Examples of Powertrain Configurations

sIn the previous chapters the drivers for and principals of the centralized EE Architecture in our latest MAN Truck Generation 3 are shown, the goal of the following that chapter is to illustrate actual examples of powertrain configurations.
But also an outlook to new technologies should be given.

4.1 Combustion Powertrain

With only one Central Vehicle Manger Software release, the variance of different powertrain configurations and performance steps is supported.
The torque management, shifting strategy (classic or predictive), brake management, … are allocated on the Central Vehicle Manager and need to be developed only once.

The ICE, gearbox, retarder, … are controlled on their physical characteristics and can be easily exchanged.

The strategic and management functions on the Central Vehicle Manager get the physical characteristics of the components / subsystems via Network (CAN) or EOL parametrization.

The following Fig. shows the different Combustion Powertrain configurations @MAN.

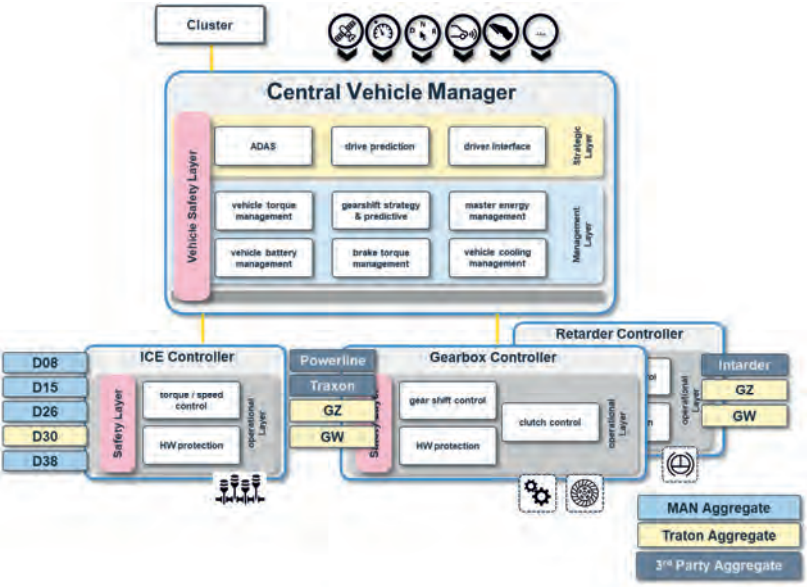

Fig. 5: Combustion Powertrin Configuration @MAN

4.2 Electrified Powertrain + Fuel Cell

Even though there is an electrified Powertrain, from the vehicle point of view the propulsion unit is a torque source and the gearbox is transforming the torque by different gear ratios.

This view is valid for an electrified central drive system or an electrified axle.

The management functions, like shifting strategy, torque management, brake management, … can be reused, because they are physically based.

And because of the different layers and the modularity, new functions (e.g. for the Battery Management, Energy Management) can scalable allocated on the Central Vehicle Manger.

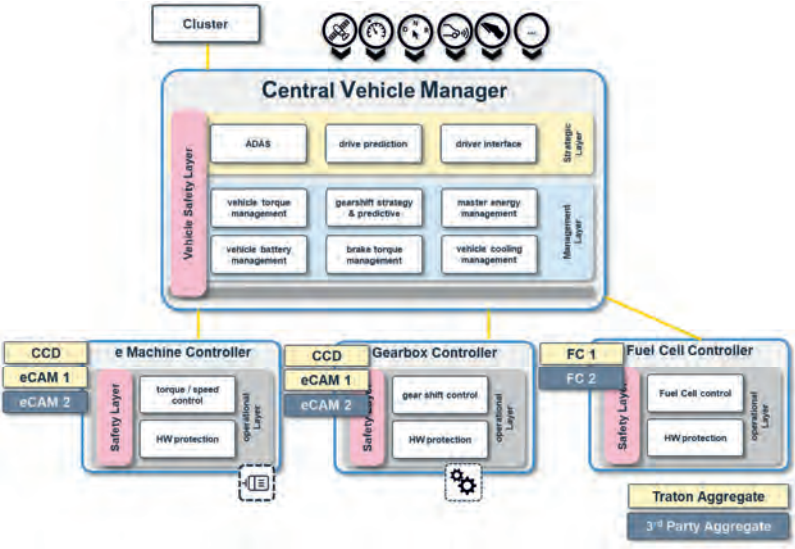

Fig. 6: Electrified Powertrain + Fuel Cell

4.3 Outlook Autonomous Truck

Even if it is a highly automated Truck / Level 4 / 5, the efficiency of the powertrain is very important, no matter it is an electrified or combustion powertrain.

Because of that, functions of the management layer, e.g. shifting strategy, torque management, … can be reused.

For sure, there will be new approaches in the strategy layer and changes in safety layer, but that's the headline for a new paper.

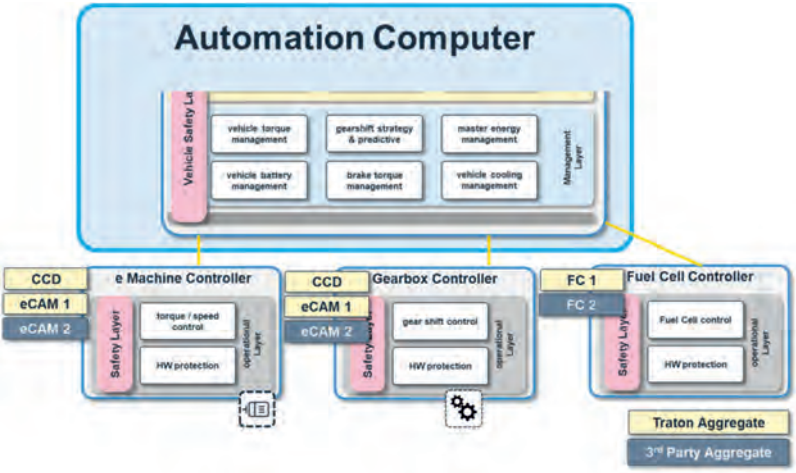

Fig. 7: Powertrain configuration + Fuel Cell in an Autonomous Truck

5. Conclusion

By the centralized EE architecture, which was launched with the latest MAN Truck Generation 3, MAN has a scalable and very effective solution to handle different Powertrain configurations.

A modular function architecture in combination with different function layers and physical interfaces is the success factor for that approach.

The new MAN EE architecture is future proven.

6. References

[1] AUTOSAR Introduction / October 2020

INGENIEUR.de
TECHNIK - KARRIERE - NEWS

powered by VDI Verlag

Starten Sie durch – auf INGENIEUR.de!

Das TechnikKarriereNews-Portal für Ingenieure und IT-Ingenieure.

Was immer Sie für Ihre Karriere brauchen – Sie finden es auf ingenieur.de: Auf Sie zugeschnittene Infos und Services, Stellenangebote in der Jobbörse, Firmenprofile, Fachartikel, Gehaltstest, Bewerbungstipps, Newsletter und alles zu den VDI nachrichten Recruiting Tagen.

VDI Wissensforum

Dritev

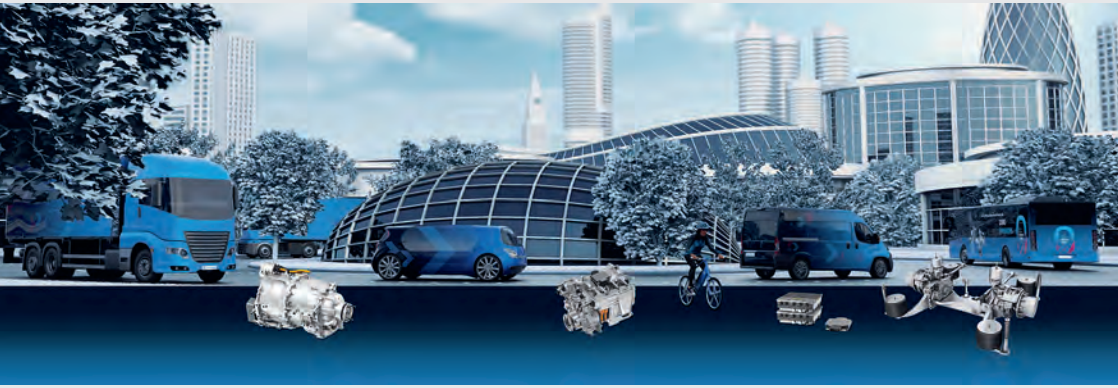

Image credits: ©ZF Friedrichshafen AG

ISBN 978-3-18-092381-9